ADVANCES IN PROSTATE CANCER: MODEL SYSTEMS, MOLECULAR AND CELLULAR MECHANISMS, EARLY DETECTION, AND THERAPIES

EDITED BY: Tanya I. Stoyanova, Antonina Mitrofanova and Andrew Goldstein

PUBLISHED IN: Frontiers in Oncology

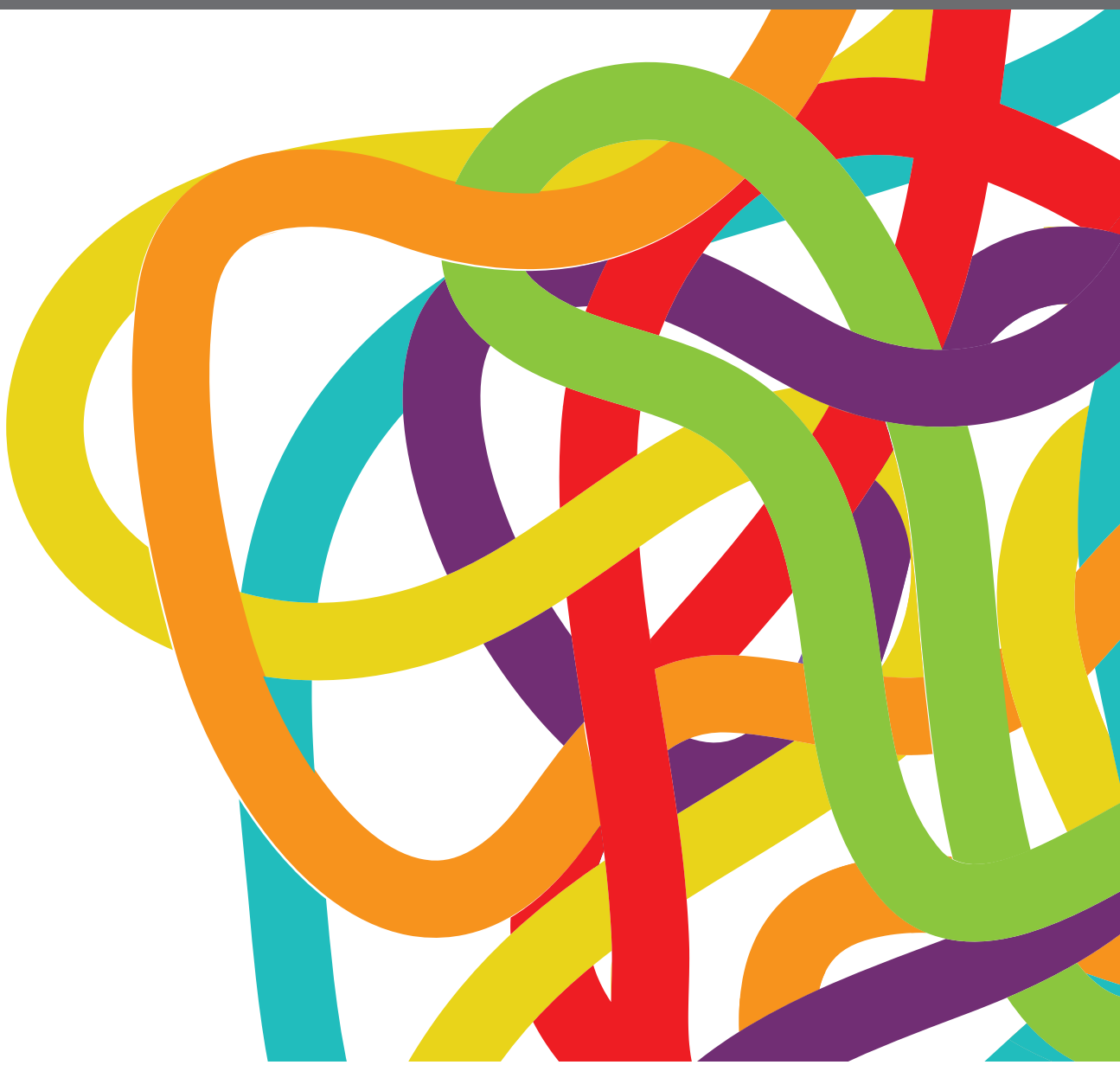

frontiers Research Topics

frontiers

Frontiers eBook Copyright Statement

The copyright in the text of individual articles in this eBook is the property of their respective authors or their respective institutions or funders. The copyright in graphics and images within each article may be subject to copyright of other parties. In both cases this is subject to a license granted to Frontiers.

The compilation of articles constituting this eBook is the property of Frontiers.

Each article within this eBook, and the eBook itself, are published under the most recent version of the Creative Commons CC-BY licence. The version current at the date of publication of this eBook is CC-BY 4.0. If the CC-BY licence is updated, the licence granted by Frontiers is automatically updated to the new version.

When exercising any right under the CC-BY licence, Frontiers must be attributed as the original publisher of the article or eBook, as applicable.

Authors have the responsibility of ensuring that any graphics or other materials which are the property of others may be included in the CC-BY licence, but this should be checked before relying on the CC-BY licence to reproduce those materials. Any copyright notices relating to those materials must be complied with.

Copyright and source acknowledgement notices may not be removed and must be displayed in any copy, derivative work or partial copy which includes the elements in question.

All copyright, and all rights therein, are protected by national and international copyright laws. The above represents a summary only. For further information please read Frontiers' Conditions for Website Use and Copyright Statement, and the applicable CC-BY licence.

ISSN 1664-8714
ISBN 978-2-88976-739-7
DOI 10.3389/978-2-88976-739-7

About Frontiers

Frontiers is more than just an open-access publisher of scholarly articles: it is a pioneering approach to the world of academia, radically improving the way scholarly research is managed. The grand vision of Frontiers is a world where all people have an equal opportunity to seek, share and generate knowledge. Frontiers provides immediate and permanent online open access to all its publications, but this alone is not enough to realize our grand goals.

Frontiers Journal Series

The Frontiers Journal Series is a multi-tier and interdisciplinary set of open-access, online journals, promising a paradigm shift from the current review, selection and dissemination processes in academic publishing. All Frontiers journals are driven by researchers for researchers; therefore, they constitute a service to the scholarly community. At the same time, the Frontiers Journal Series operates on a revolutionary invention, the tiered publishing system, initially addressing specific communities of scholars, and gradually climbing up to broader public understanding, thus serving the interests of the lay society, too.

Dedication to Quality

Each Frontiers article is a landmark of the highest quality, thanks to genuinely collaborative interactions between authors and review editors, who include some of the world's best academicians. Research must be certified by peers before entering a stream of knowledge that may eventually reach the public - and shape society; therefore, Frontiers only applies the most rigorous and unbiased reviews.
Frontiers revolutionizes research publishing by freely delivering the most outstanding research, evaluated with no bias from both the academic and social point of view. By applying the most advanced information technologies, Frontiers is catapulting scholarly publishing into a new generation.

What are Frontiers Research Topics?

Frontiers Research Topics are very popular trademarks of the Frontiers Journals Series: they are collections of at least ten articles, all centered on a particular subject. With their unique mix of varied contributions from Original Research to Review Articles, Frontiers Research Topics unify the most influential researchers, the latest key findings and historical advances in a hot research area! Find out more on how to host your own Frontiers Research Topic or contribute to one as an author by contacting the Frontiers Editorial Office: frontiersin.org/about/contact

ADVANCES IN PROSTATE CANCER: MODEL SYSTEMS, MOLECULAR AND CELLULAR MECHANISMS, EARLY DETECTION, AND THERAPIES

Topic Editors:
Tanya I. Stoyanova, Stanford University, United States
Antonina Mitrofanova, Rutgers, The State University of New Jersey, United States
Andrew Goldstein, University of California, Los Angeles, United States

Citation: Stoyanova, T. I., Mitrofanova, A., Goldstein, A., eds. (2022). Advances in Prostate Cancer: Model Systems, Molecular and Cellular Mechanisms, Early Detection, and Therapies. Lausanne: Frontiers Media SA.
doi: 10.3389/978-2-88976-739-7

Table of Contents

frontiers in Oncology

ORIGINAL RESEARCH
published: 26 January 2021
doi: 10.3389/fonc.2020.584280

Age and Tumor Differentiation-Associated Gene Expression Based Analysis of Non-Familial Prostate Cancers

Shashwat Sharad[1,2†], Travis C. Allemang[1†], Hua Li[1,2], Darryl Nousome[1,2], Anson Tai Ku[3], Nichelle C. Whitlock[3], Adam G. Sowalsky[3], Jennifer Cullen[1], Isabell A. Sesterhenn[4], David G. McLeod[1], Shiv Srivastava[1] and Albert Dobi[1,2*]*

[1] Center for Prostate Disease Research, John P. Murtha Cancer Center Research Program, Department of Surgery, Uniformed Services University of the Health Sciences and Walter Reed National Military Medical Center, Bethesda, MD, United States, [2] Henry M. Jackson Foundation for the Advancement of Military Medicine, Bethesda, MD, United States, [3] Laboratory of Genitourinary Cancer Pathogenesis, National Cancer Institute, NIH, Bethesda, MD, United States, [4] Pathology Center, Joint Pathology Center, Silver Spring, MD, United States

Prostate cancer incidence in young men has increased. Patients diagnosed at an earlier age are likely to have aggressive prostate cancer and treatment decisions are continuing to be weighted by patient age and life expectancy. Identification of age-associated gene-expression signatures hold great potential to augment current and future treatment modalities. To investigate age-specific tumor associated gene signatures and their potential biomarkers for disease aggressiveness, this study was designed and stratified into well and poorly differentiated tumor types of young (42–58 years) and old (66–73 years) prostate cancer patients. The differentially expressed genes related to tumor-normal differences between non-familial prostate cancer patients were identified and several genes uniquely associated with the age and tumor differentiation are markedly polarized. Overexpressed genes known to be associated with somatic genomic alterations was predominantly found in young men, such as TMPRESS2-ERG and c-MYC. On the other hand, old men have mostly down-regulated gene expressions indicating the loss of protective genes and reduced cell mediated immunity indicated by decreased HLA-A and HLA-B expression. The normalization for the benign signatures between the age groups indicates a significant age and tumor dependent heterogeneity exists among the patients with a great potential for age-specific and tumor differentiation-based therapeutic stratification of prostate cancer.

Keywords: age-associated gene expression, microarray, prostate cancer, tumor differentiation, laser captured microdissection, tumor-associate gene

OPEN ACCESS

Edited by:
Fabio Grizzi,
Humanitas Research Hospital, Italy

Reviewed by:
Leena Latonen,
University of Eastern Finland, Finland
Wei-de Zhong,
Guangzhou First People's Hospital, China

***Correspondence:**
Shashwat Sharad
ssharad@cpdr.org
Albert Dobi
adobi@cpdr.org

†These authors have contributed equally to this work and share first authorship

Specialty section:
This article was submitted to Genitourinary Oncology, a section of the journal Frontiers in Oncology

Received: *16 July 2020*
Accepted: *03 December 2020*
Published: *26 January 2021*

Citation:
Sharad S, Allemang TC, Li H, Nousome D, Ku AT, Whitlock NC, Sowalsky AG, Cullen J, Sesterhenn IA, McLeod DG, Srivastava S and Dobi A (2021) Age and Tumor Differentiation-Associated Gene Expression Based Analysis of Non-Familial Prostate Cancers. Front. Oncol. 10:584280. doi: 10.3389/fonc.2020.584280

INTRODUCTION

Prostate cancer is known as a disease of old men and age is the greatest risk factor for cancer development. In the United States, the median age of diagnosis for men with prostate cancer is >75 years and only 10% of men young than 55 years are diagnosed with prostate cancer (1). However, the incidence of prostate cancers with poorly differentiated tumors is increasing in young men (2, 3). The prostate cancer associated mortality among young men with high grade tumor is much higher as compared to old men (4, 5). This suggests a distinct biology of prostate cancer development and the potential roles of unique oncogenic process between young and old men. Recently, it was shown that young prostate cancer patients had significantly higher inflammatory and immune responses to tumor development as compared to the old patients (6). Gene expression differences in early and late onset prostate cancer may influence early detection and treatment of prostate cancer. Prostate cancer incident rate and severity vary substantially by race, ethnicity, and geography. The understanding and identification of risk factors will assist in the development of more consistent screening parameters. It was also noted that men who develop prostate cancer before 50 years of age, are more likely to have a family history of prostate cancer. These men were also found to have worse clinicopathologic features, higher incidence of biochemical recurrence after radical prostatectomy, and lower survival probability (4, 7). Men who develop prostate cancer after 70 years of age had better clinicopathologic features, lower incidence of biochemical recurrence, and greater overall survival (8). These findings suggest a clinically relevant age-associated difference among men with prostate cancer.

Several other studies have linked prostate cancer to diet and altered metabolic conditions, such as obesity and diabetes. There is a contradictory report on young men with a family history of prostate cancer were less likely to have high-grade disease (9). To date, very few studies have focused specifically on aging and prostate cancer to better explain the genetic differences between young and old men with prostate cancer. Several disease-specific factors: tumor stage, tumor grade, prostate-specific antigen (PSA) level; and patient-specific factors: age, co-morbidity and functional status need to be considered in the decision-making process for the diagnosis and management of prostate cancer. To incorporate these important factors to select optimal treatment for individuals, several decision models have been published, yet their utility in clinical practice remains poorly understood. In general, prostate cancer is considered as a cancer of the elderly and the median age for prostate cancer diagnosis is around 66 years (between 65 and 74 years old). They men diagnosed before age 55 years were defined as early-onset prostate cancer. The recommendation of age specific prostate cancer management guidelines needs to be taken in account. There is a clear need to improve our understanding of the complex interrelationships between aging, tumor types, co-morbidities, and their impacts on expected outcomes. In this study, using laser capture microdissection of prostate cancer tumor cells and patient matched non-adjacent "non-malignant" prostate epithelial cells, we evaluated the genome-wide expression profiles in Caucasian men with no known family history of prostate cancer. The gene expression profiles were assessed in cells with well and poorly differentiated tumor cells morphology among old and young prostate cancer patients. for identification and validation of uniquely expressed genes. The goal of this study was to carefully identify and evaluate the comparative gene expression signatures from young and old prostate cancer patients stratified for similar clinicopathological features presented with tumor differentiation and recurring PSA (rPSA) at the time of radical prostatectomy.

MATERIALS AND METHODS

Patient Cohort Selection and Study Design

The prostatic adenocarcinoma patients treated at the Walter Reed National Military Medical Center (WRNMMC) were enrolled at the Center for Prostate Disease Research (CPDR) from 1997 to 2010 under institutional review board approved protocol of WRNMMC 20405 and Uniformed Services University of the Health Sciences (USUHS) 20311. Prostate tissue specimens and clinical data used in this study were obtained under above IRB-approved protocol and informed consent was obtained from each subject. Prostate tumor samples and adjacent histologically normal tissues were obtained from patients that underwent radical prostatectomy (RP). The tissue sections were frozen and stored in optimal cutting temperature (OCT) compound at -80^{0}C. Over 300 radical prostatectomy tumor and adjacent benign specimens of a PSA-screened patient with no prior androgen ablation treatment were evaluated and eligible for selection into the study. Forty unique patients met the inclusion criteria of race (Caucasian American), age (young and old), and tumor differentiation (well and poorly) from the initial cohort. Well differentiated tumor cells were obtained from specimens with Gleason sum 6–7 with no seminal vesicle invasion and with no PSA recurrence (rPSA) and poorly differentiated tumors were defined with a Gleason sum 8-9 with PSA recurrence in 65% of cases. PSA recurrence was defined as two consecutive times of PSA > 0.2 ng/ml with follow up from surgery. Laser capture microdissection (LCM) was performed on 80 specimens from 40 patients and were sub grouped based on the age and tumor differentiation (**Table 1** and **Figure 1**). The criteria for the inclusion of "young (42–58 years)" and "old (66–73 years)" patients with minimum average age difference of at least ~10 years (~9.9 years to ~14.2 years) were normalized for natural aging related gene signatures and also to define the true young (≤ age 58) and old (≥ age 66) age in the context of prostate cancer (**Table 1** and **Figure 1**). Also, this study is a longitudinal cohort of military health-care beneficiaries and this setting reduces disparity in socioeconomic status, health-care access, and lifestyle factors that potentially influence prostate cancer progression.

Laser Capture Microdissection and RNA Extraction

The selection of both the benign prostate epithelial cells with normal morphological appearance (N) and prostate tumor epithelial cells (T) from hematoxylin and eosin stained frozen

TABLE 1 | Patient selection clinical data.

	Tumor Differentiation			
Patient Group	**Well Differentiated "WD"**	**Poorly Differentiated "PD"**	**Balanced (WD & PD)**	**Recurrent PSA**
Number (n)	12	12	16	09
Age Range [Young], [Old]	[Young], [Old] (n=6), (n=6) [42–58], [66–73]	[Young], [Old] (n=6), (n=6) [50–62], [68–72]	[Young], [Old] (n=8), (n=8) [42–59], [65–73]	[Young], [Old] (n=5), (n=4) [56–63], [68–70]
Average Age Difference	12.7 years	11.5 years	14.2 years	9.9 years
Family History	None	None	None	None

"WD", well differentiated; "PD", poorly differentiated; "Balanced", balanced differentiation; "rPSA", recurrent PSA.

tissue sections was performed by using the PixCell II Laser Capture Microdissection System (LCM, Arcturus, Mountain View, CA, USA). Approximately 5000 cells from morphologically normal fields of nonadjacent prostate epithelial cells and poorly/well differentiated morphology were captured and collected from tumor foci. All captured normal benign and tumor epithelial cells were further processed for RNA extraction by using Arcturus Paradis RNA extraction and isolation kit. The isolated RNA was quantified by using RiboGreen dye (Molecular Probes, Eugene, OR, USA) and Versa-Fluor fluorimeter (BioRad, Hercules, CA, USA).

RNA Labeling, Hybridization, and Gene Expression

The linear amplification of the RNA was done by using the Arcturus Paradise RNA amplification kit as per the manufactures protocol. Two nanograms of total RNA was used for the cDNA synthesis and biotinylation steps. The biotinylation of poly (A) RNA was carried out by using MEGA script T7 *in vitro* Transcription Kit (Ambion, Austin, TX, USA). After biotinylation step the RNA was further purified by QIAGEN RNeasy spin columns (Qiagen, Germantown, MD, USA) as per manufacturer's protocol. Linearly amplified biotin labeled RNA samples were hybridized to a high-density oligonucleotide human genome array HG-U133A Affymetrix GeneChip Arrays at 42°C for 16 h and prepared according to previously described methods (10, 11). The hybridized GeneChip arrays were washed, stained and scanned with the HP GeneArray Scanner (Hewlett-Packard, Santa Clara, CA, USA) controlled by GeneChip 3.1 Software (Affymetrix, Thermo Fisher Scientific, Waltham, MA, USA).

GeneChip Expression Data Analysis

Schematic bioinformatic data analysis workflow of the raw gene expression data output (CEL files) of 80 GeneChip analysis (HG U133A array, Affymetrix, Santa Clara, CA, USA) are presented in **Figure 2**. The probe intensity of Microarray GeneChip images were captured and analyzed by Affymetrix GeneChip® Microarray Analysis Software, version 3.1 and Affymetrix Micro DB and Data Mining Tool version 2.0 (Affymetrix,

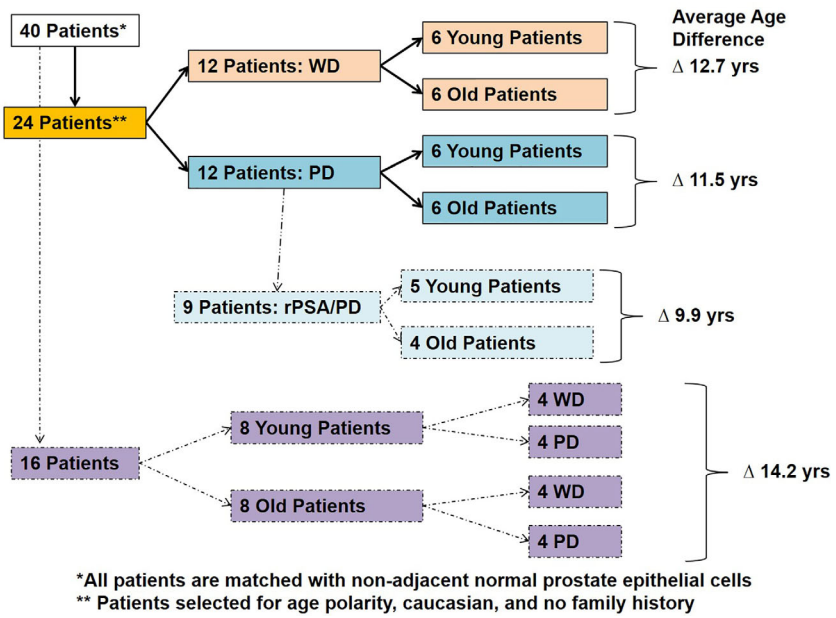

FIGURE 1 | Patient selection and study design. Forty Caucasian American patients with well differentiated (WD) and poorly differentiated (PD) tumors with or without PSA recurrence (rPSA) were selected and divided into two groups based on age with an average age difference of 9.9–14.2 years; 1) Young and 2) Old.

Thermo Fisher Scientific, Waltham, MA, USA), and Statistica version 4.1 (Stat Soft, Inc., Tulsa, OK, USA). Further, the CEL files of raw gene expression data were processed by statistical computing language R (Bioconductor package). The background subtraction and normalization were done by Robust Multi-array Analysis (RMA, http://rmaexpress.bmbolstad.com) and by the ChipInspector a single-probe analysis approach (Genomatix GmbH, Munich, Germany; http://www.genomatix.de). To improve the signal-to noise ratio, increase the statistical stringency, and to eliminate probe mismatches or multiple matches, the single probes matching to the transcripts and normalization of total intensities was performed by the Significance Analysis of Microarrays (SAMs) and enrichment of significantly altered signal intensities approach (12). The signal of probe intensities which met both RMA and ChipInspector normalization criteria with a false discovery rate of p 0.05% yielded significantly up and down regulated probes. The signal intensities below 30 were excluded from both the tumor and corresponding normal probe for further analyses. The normalized data were then used to calculate the fold changes dividing gene expression signal value of Tumor over Normal (T/N), and then applying 2, 2.5 (data not shown) and 3 cut-offs. Probes were then matched to genes. In this study high stringent criteria were used and the genes with fold change T/N > 3 and T/N < 0.33 were differentially expressed as up or down regulated genes. The Genomatix-GePS and DAVID (NAÏVE-DAVID) software were used for the functional gene ontology and venn diagram analysis (13). The gene network analysis for the selected genes was performed by using Genomatix pathway edition of Bibliosphere (Genomatix GmbH, Munich, Germany, www.genomatix.de) as previously described methods (12–14). The network and pathway analysis as previously described methods (15).

Gene Ontology and Pathway

The unique age associated genes of young and old prostate cancer patients in well differentiated, poorly differentiated, balanced differentiated and recurred prostate-specific antigen in poorly differentiated tumors (rPSA-PD) were queried into the Genomatix Pathway System (GePS) which utilize the expert-curated GO information from public and proprietary databases (Genomatix GmbH). Independently, these age and tumor type associated genes were also queried by the Database for Annotation, Visualization and Integrated Discovery (DAVID) software (http://david.abcc.ncifcrf.gov) (13). The DAVID software runs the clustering algorithm to classify highly related genes into functionally related groups used to reveal the tight association of genes associated with age, tumor type and rPSA. The gene IDs of all the differentially expressed genes with their corresponding fold change values of the studied group of young and old prostate cancer patients were entered the BiblioSphere knowledge-based pathway analysis software (Genomatix GmbH) for functional network, canonical pathway and gene ontology analysis (10). The functional Classification Tool was utilized to evaluate the functional similarity between queried input genes (10, 16). The software generates the interaction between genes and connects by co-citation within one sentence at abstract levels. The significance of enriched genes mapped to different canonical pathways was calculated by the Fischer's exact test (p-value). The color code in the network is related to fold changes (red indicating up-regulation and blue downregulation). Genes with the highest number of interactions forming the central node in the network were considered as most significant and were further analyzed to evaluate significant probe-signal intensities individually in tumor and benign samples. Canonical pathways and gene ontology terms were ranked by log (p-value) (10, 16).

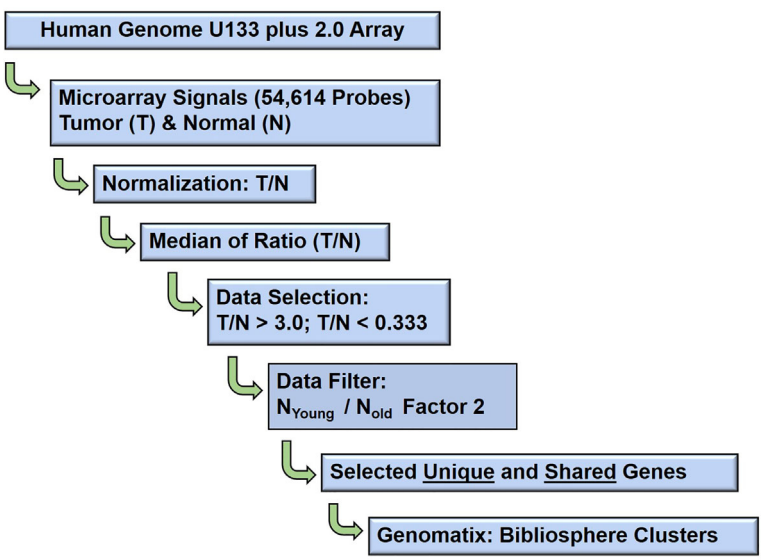

FIGURE 2 | Schematic diagram: Microarray data analysis workflow. The bioinformatics data analysis of age (young and old) associated gene expression responses in well, poorly, balanced differentiated tumors and biochemical (PSA) recurrence in prostate cancer patients.

RNA Seq Expression Data Analysis From the Publicly Available Human Gene Samples

Publicly available RNA-Seq from the Cancer Genome Atlas (TCGA) and associated clinical processed data were downloaded from the recount2 project for 319 cases (https://jhubiostatistics.shinyapps.io/recount/) of Caucasian men. Only cases matching primary tumors and within the age threshold (42–58 and 66–73) were retained for analysis. The DESeq2 R/Bioconductor package was used to read and perform analysis of the RNA-seq count data. Differential expression tests were used to compare the differences between young and old patients adjusting for Gleason score (≤3 + 4 and ≥4 + 3). Unsupervised hierarchical clustering was used after a variance stabilizing transformation of the raw count data.

Furthermore, 46 pairs of paired-end RNA-Seq data from TCGA(https://gdc.cancer.gov) corresponding to prostate tumor (n=23) and matching normal tissue (n=23) from 23 patients were selected based on race (Caucasian) and age (young: 42–58, old: 66–73). Briefly, reads were filtered by quality and complexity prior to alignment to human reference genome (hg19) using Star and aggregated by featureCounts. Genes with less than five counts in at least 50% of the samples were filtered out. Differential expression analysis between tumor and normal samples was performed using DESeq2 after stratifying the dataset by age (young and old) and Gleason score (well differentiated: Gleason score ≤3 + 4, poorly differentiated: Gleason score ≥4 + 3). Differentially expressed genes were filtered by false-discovery rate of 0.05 and a log2 fold change less than -1 or greater than 1.

RESULTS

Selection of Young and Old Gene Patients

In this experiment, we evaluated tumor samples from 40 Caucasian American (CA) prostate cancer patients who underwent radical prostatectomy from a common and homogenous tumor subtype, and recurrent PSA from 40 Caucasian American (CA) prostate cancer patients. The old and young prostate cancer patients were selected based on their age, race, cellular differentiation status, and by no indication of family history of prostate cancer (**Table 1**). The patient age referenced is the age at which the patient underwent radical prostatectomy surgery. In this study, a patient was said to have no family history if he did not have any known first or second-degree relatives with a history of prostate cancer. None of these patients underwent neoadjuvant chemotherapy or radiation therapy prior to date of prostatectomy. The Laser Captured Microdissection (LCM)-selected individual tumor and normal cells from RP specimens were matched by the histological cellular differentiation status. The Gleason score of the patients within the Well Differentiated "WD" group was equal to 7 (≤3 + 4) or less, whereas the Gleason score of the patients in the Poorly Differentiated "PD" group was equal to 7 (≥4 + 3) or greater. The 16 patients within the balanced differentiation "Balanced" subset and the nine patients within the recurrent prostate specific antigen "rPSA" subset were selected from the 24 patients which make up the two primary groups WD and PD (**Figure 1**). The average age difference between young and old prostate cancer patients' groups were 12.7 years (Well Differentiated "WD"), 11.5 years (Poorly Differentiated "PD"), 14.2 years (Balanced-WD & PD), and 9.9 years (Recurrent PSA "rPSA"). The tumor and matching histologically normal prostate epithelial cells from each specimen, were isolated and total RNA were extracted to measure the gene expression levels by microarray analysis (10, 17–19). The clinical, histopathological and demographic characteristics of the study population stratified by age and differentiation are summarized in **Supplementary Table 1**; PD (1A), WD (1B), Balanced (1C) and rPSA (1D).

Identification of Differentially Expressed Prostate Cancer Gene Signature of Young and Old Gene Patients

The gene expression features were normalized using the RMAExpress and ChipInspector software's. The gene expression signals were calculated using their patient patched tumor over normal (T/N) expression ratio and the median signal values calculated. A stringent factor of 3X cut off was applied to enrich gene expression signatures to determine the significantly expressed genes. Young and old age group unique gene expression features were further analyzed based on their tumor histological differentiation and rPSA. The tumor signature was also normalized for the benign signature to minimize the normal aging caused differences. A Venn-Diagram was performed to evaluate the shared and unique signatures among the groups, WD, PD, Balanced Differentiation, and rPSA. The unique gene expression features of the young age group were matched to 520 up-regulated and 28 down-regulated genes. Of these gene expressions unique to young men, the majority of unique gene expressions were found to be upregulated within the WD, PD, balanced and rPSA groups respectively, 79% (64 genes), 97.5% (78 genes), 98.3% (236 genes), and 97.5% (142 genes). In the old group, 27 genes were up-regulated and 99 genes down-regulated, respectively (**Figure 4**). Of these gene expressions unique to old men, most unique gene expressions were found to be downregulated within the WD, PD, balanced and rPSA groups respectively, 57.9% (11 genes), 94.7% (18 genes), 100% (43 genes), and 60% (27 genes). These results suggest the existence of strong age-tumor associated difference in gene expression profile. Young men with prostate cancer tend to have more up-regulated genes whereas in the old men are mostly down regulated (**Figure 3**).

Gene Signature Unique to Well-Differentiated Tumors of Young and Old Prostate Cancer Patients

To identify unique pathway/network of genes associated with WD tumor in old/young prostate cancer patients, 12 WD (six old and six young) patients were identified with 12.73 years age

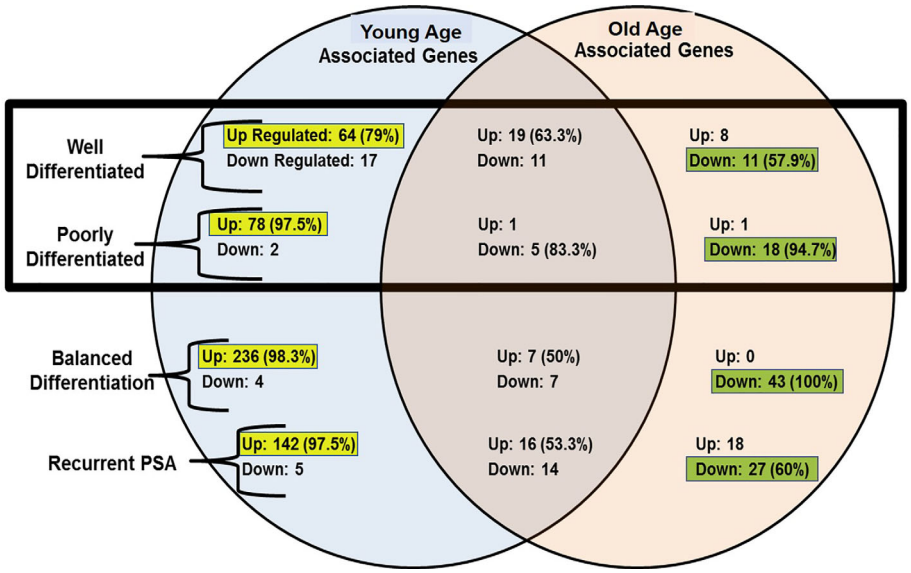

FIGURE 3 | Venn-diagram summary of gene expression results; "Up", Up-Regulated Gene Expression; "Down", Down-Regulated Gene Expression; "-Associated Genes" Genes with expression levels that surpass the factor 3 inclusion criteria. The up-regulated genes are more common in young prostate cancer patients whereas old patient's gene profile carry mostly down-regulated genes.

difference. The mean age for the WD-Young and WD-old patients were ~53.9 and ~66.6 years respectively. All the differentially expressed genes for both the groups were queried for Genomatix Network and Pathway Analysis (GePS). The 81 genes were uniquely expressed in young patient's-WD tumor and 19 genes in Old-WD tumors. Interestingly, 79% (64 genes) were up regulated in young-WD tumor and 58% (11 genes) were down regulated in old-WD tumor (**Figure 4A**). To further evaluate the impacted signaling pathways, we constructed the pathway/network system of all the differentially expressed genes unique to old/young-WD tumors with cut-off over 3-fold change (**Figures 4B, C**). This analysis revealed Vascular Endothelial Growth Factor A (VEGFA), which is down regulated in young patients with well differentiated tumors as a central node based on the gene score (score represents numerous interactions of a gene). Further, Neuropeptide Y (NPY) gene was found to be upregulated in old patients with well differentiated tumors as a central node. A list of all the unique and shared gene for the well differentiated (WD) are tabulated in **Supplementary Figures 1A–C**.

Gene Signature Unique to Poorly Differentiated Tumors of Young and Old Prostate Cancer Patients

The unique genes associated with PD tumor of old and young prostate cancer patients, 12 PD (six old and six young) prostate cancer patients were identified with 11.52 years age difference. The mean age for the PD-Young and PD-old patients were ~57.2 and ~68.8 years respectively. All the differentially expressed genes for the age groups were queried for Genomatix Network and Pathway Analysis (GePS). It was found that 80 genes were uniquely expressed in young-PD tumor cohort and 19 genes in old-PD tumor cohort. Remarkably, 97.5% (78 genes) were up-regulated in young-PD tumor and 94.7% (18 genes) were down-regulated in old-PD tumor (**Figure 5A**). To further understand the significantly altered signaling pathways, the pathway/network were constructed for all the differentially expressed genes unique to old/young-PD tumors with cut-off of 3-fold change (**Figures 5B, C**). This analysis revealed the MYC Proto-Oncogene, BHLH Transcription Factor (*MYC*) and ETS Transcription Factor ERG (*ERG*) were upregulated in young patients with poorly differentiated tumors as the central node based on the gene score (score represents numerous interactions of a gene). Further, Annexin A2 (*ANXA2*) gene was found to be down-regulated in old patients with poorly differentiated tumors as a central node, and inhibitor of Differentiation (*ID4*), human leukocyte antigens (*HLA)-A/B* were down regulated in old patients. A list of all the unique and shared genes for the poorly differentiated (PD) group are tabulated in **Supplementary Figures 2A–C**.

Gene Signature Unique to Balanced Diffrentited Tumors of Young and Old Prostate Cancer Patients

The unique genes and their network associated with balanced differentiation (WD and PD) tumor in young and old prostate cancer patients, eight young and eight old prostate cancer patients were identified with WD and PD tumor (four young and four old men in each group) patients were identified The mean age difference between young and old group was 14.2 years. The uniquely expressed genes for the groups were queried with Genomatix Network and Pathway Analysis (GePS). The 240 genes were uniquely expressed in young group and 43 genes in old group. Interestingly, all the 43 (100%) genes were

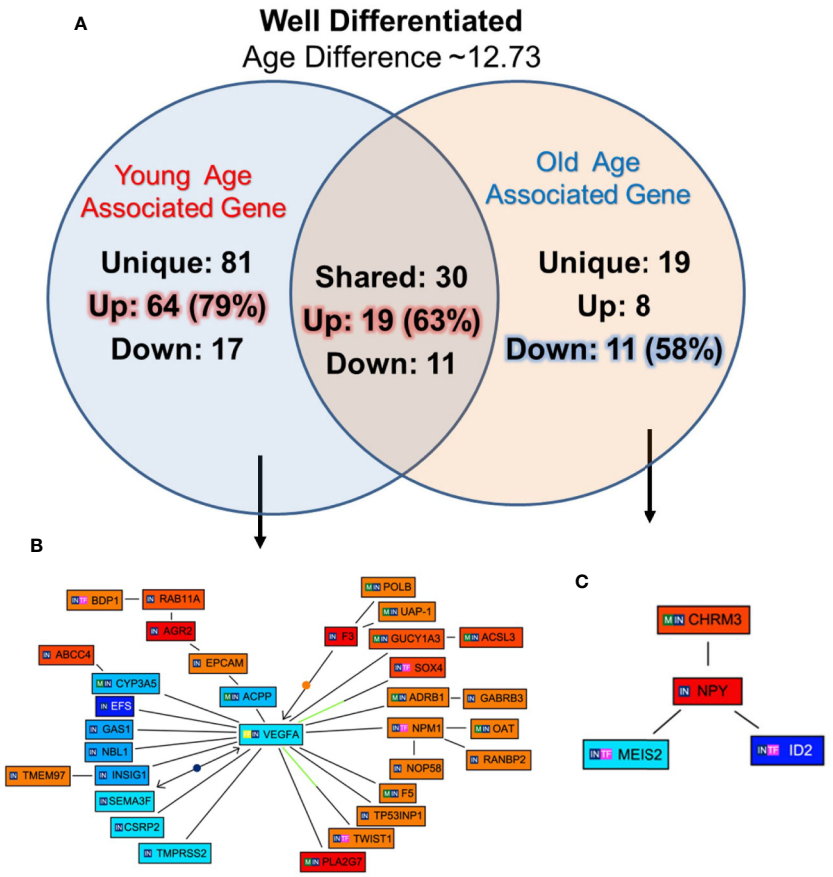

FIGURE 4 | Functional analysis of differentially expressed genes in well differentiated tumors of young and old prostate cancer patients by GePS system. **(A)** The total 81 genes were uniquely associated with young age [64 (79%) genes up-regulated and 17 (21%) genes down-regulated] and 19 genes with old age [8 (42%) up-regulated and 11 (58%) down-regulated]. There are 30 genes [19 (63%) up-regulated and 11 (37%) down-regulated were common between the both the groups. **(B, C)** The Venn diagram analysis represents significant genes with at least 3-fold expression. The hierarchical cluster showing the expression levels of the 32 significant genes associated with WD-young group **(B)** and 04 genes with WD-old group **(C)**. The unique genes associated with WD young and old group were imported into GePS. Orange/red color shows up-regulation and blue color shows down-regulation. The intensity of blue and red colors indicates the degree of up or down-regulation, respectively. A solid line represents an expert curated association between the two gene products and a dotted line means there is an association by co-citation. Expert level filter settings were used to generate the network, which contains interactions curated by experts (Genomatix and NetPro) based on literature and genes without any interactions were filtered out.

down-regulated in old group, whereas 98.3% (236 genes) were up-regulated in young prostate cancer patients (**Figure 6A**). Among the genes shared among the young and old patients, seven (50%) were upregulated and seven (50%) were down regulated. Further signaling pathways/network were constructed of all the uniquely expressed genes with cut-off over 3-fold change (**Figures 6B, C**). *MYC* Proto-Oncogene, *HDAC1* (Histone Deacetylase 1) and *HSPD1* [Heat Shock Protein Family D (*Hsp60*) Member 1] were upregulated in young patients forming central node with several gene. The *RASA1* (RAS P21 Protein Activator 1) inhibitory regulator of the Ras-cyclic AMP pathway and suppressor of RAS function and CAPN2 (*Calpain 2*), muscle-specific proteins were also found to be up-regulated. Among the old patients, *VEGFA* (Vascular Endothelial Growth Factor A) was found to be down regulated forming a central node. The *HLA* (human leukocyte antigen), *LDHB* (Lactate Dehydrogenase B), lipocortin I (Annexin A1, *ANAX1*), *ANAX2* (Annexin A2), *MEIS1* (Meis Homeobox 1), developmental genes such as *SLC40A1* (Solute Carrier Family 40 Member 1), *FOXQ1* (Forkhead Box Q1), DNA binding protein *SOX9* [SRY- Sex Determining Region Y)-Box 9], *ID2* (Inhibitor Of DNA Binding 2), immune system and developmental biology related gene, *CEBPD* (CCAAT Enhancer Binding Protein Delta), and *LDHB* (Lactate Dehydrogenase B) previously described as hypermethylated in prostate cancer were down-regulated in old prostate cancer patients.

Gene Signature Unique to Biochemical Recurrence and Age

In this cohort of prostate cancer patients 22.5% (nine out of 40) patients reported PSA recurrence after a follow-up, we further analyzed the unique genes associated with biochemical recurrence (rPSA) and age by creating subgroup of the five young patients and the 4 old patients with rPSA. The mean age

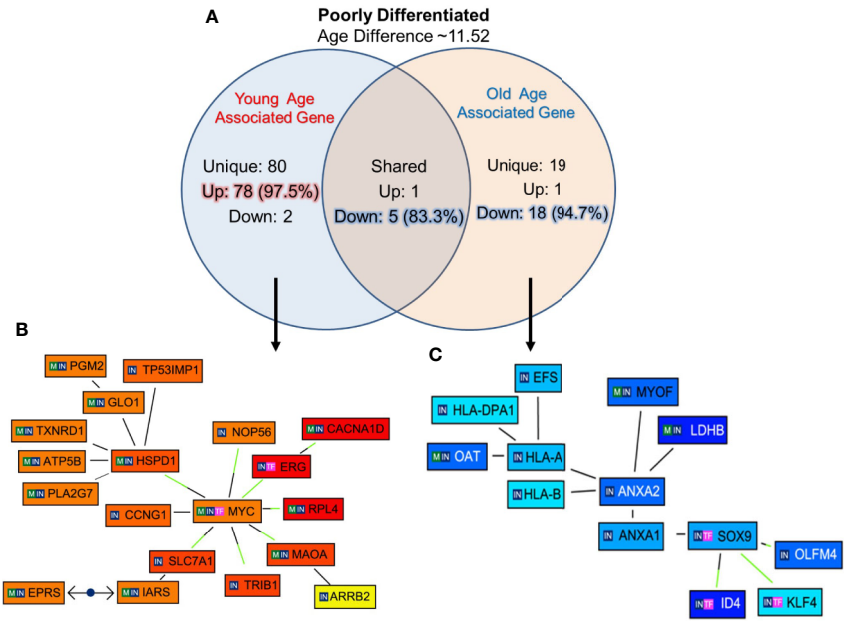

FIGURE 5 | Functional analysis of uniquely expressed genes in poorly differentiated tumors of young and old prostate cancer patients by GePS system. **(A)** The total 80 genes were uniquely associated with young age [78 (97.5%) genes up-regulated and 02 (2.5%) genes down-regulated] and 19 genes with old age [01 (2.3%) up-regulated and 18 (94.7%) down-regulated]. There are six genes [01 (16.7%) up-regulated and 05 (83.3%) down-regulated were common between the both the groups. **(B, C)** The Venn diagram analysis represents significant genes with at least 3-fold expression. The hierarchical cluster showing the expression levels of the significant genes associated with Poorly Differentiated (PD)-young group **(B)** and PD-old group **(C)**. The unique genes associated with PD young and old group were imported into GePS. Orange/red color shows up-regulation and blue color shows down-regulation. The intensity of blue and red colors indicates the degree of up or down-regulation, respectively. A solid line represents an expert curated association between the two gene products and a dotted line means there is an association by co-citation. Expert level filter settings were used to generate the network, which contains interactions curated by experts (Genomatix and NetPro) based on literature and genes without any interactions were filtered out.

difference between the young and old patients was 9.93 years. The uniquely expressed genes for both groups were queried for Genomatix Network and Pathway Analysis (GePS). Among the young men with rPSA, 147 genes were uniquely expressed with 142 genes (96.5%) up-regulated. Among the old men with rPSA, 45 genes (60%) were down-regulated (**Figure 7A**). The uniquely expressed genes that were common between the young and old men with rPSA were found to have nearly equal proportion upregulated (53%) vs down regulated (47%).

Further signaling pathways/network were constructed of all the uniquely expressed genes with cut-off over 3-fold change (**Figures 7B, C**). In young-rPSA group, *MYC* Proto-Oncogene and in old-rPSA group *JUN* (Jun Proto-Oncogene, *AP-1* Transcription Factor Subunit), *Wnt* signaling pathway associated gene were populated as central node. The gene network analysis showed *HDAC1* (Histone Deacetylase 1), *RASA1* (RAS P21 Protein Activator 1), and Prostatitis and urethral stricture associated and coregulator of androgen receptor activity *KLK3*/(PSA) (Kallikrein Related Peptidase 3) gene tightly associated with *MYC* transcription factor in young-rPSA group. On the other hand in old-rPSA group he network of genes such as lipocortin I (Annexin A1, *ANAX1*), mTOR signaling pathway associated gene *NPRL3* (NPR3 Like, GATOR1 Complex Subunit), bladder urothelial carcinoma and Breast disease associated gene *SATB1* (SATB Homeobox 1), body mass index and metabolism associated gene *UCP2* (Uncoupling Protein 2) and *DHRS4* (Dehydrogenase/Reductase 4), NOD-like receptor signaling pathway associated gene *CTSB* (Cathepsin B), developmental biology and butyrophilin (*BTN*) family interactions associated gene *PPL* (Periplakin), Down Syndrome and Alzheimer Disease associated gene *BACE2* (Beta-Secretase 2) and hereditary, colorectal cancer, mismatch repair cancer syndrome associated TP53 activity regulator *MLH1* (MutL Homolog 1) gene was found to be associated with JUN transcription factor.

Validation of Gene Signature Unique to Poorly and Well Differentiated Tumors of Young and Old Prostate Cancer Patients in The Cancer Genome Atlas Database

To validate our findings, we first analyzed RNA-seq gene expression along with clinical data from the recount2 project for 319 cases Caucasian men. The matching primary tumors within the age threshold were analyzed (**Figure 8**) for age (young and old) and Gleason score ≤3 + 4 (WD) and ≥4 + 3 (PD). The gene signature profile of young PD and WD tumors (**Figure 8A**), old PD and WD tumors (**Figure 8B**) and gene signatures for the young (42–58 years) and old (66–73 years) (**Figure 8C**) were consistent with our discovery cohort. All the up and down

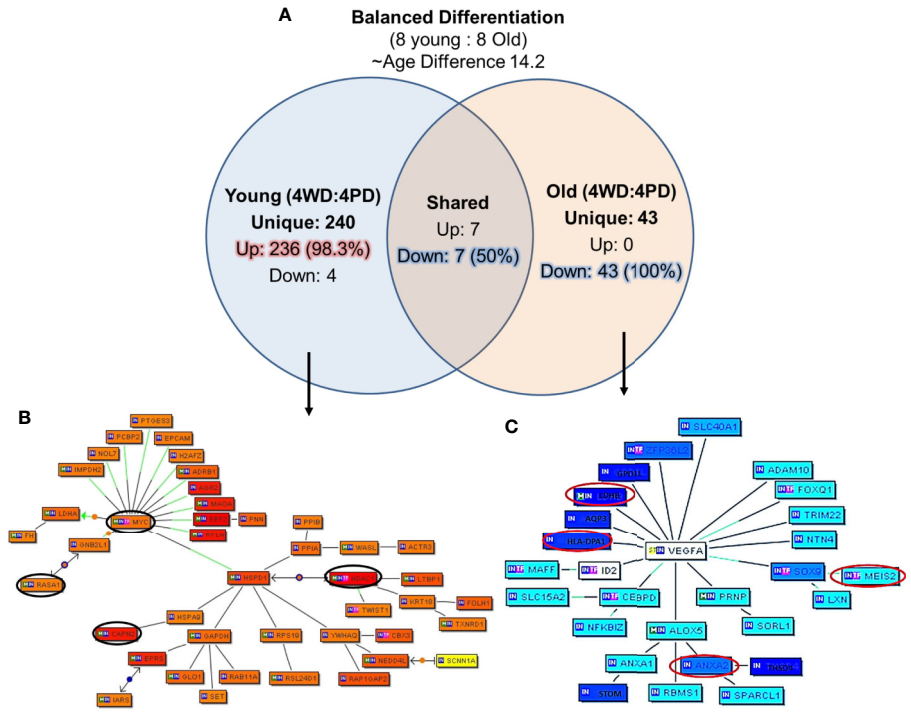

FIGURE 6 | Uniquely expressed genes in balanced differentiated tumors of young and old prostate cancer patients. **(A)** 240 genes were uniquely associated with young age and 98.3% genes are upregulated. All uniquely expressed genes among the old patients were down regulated. Marked age-associated differences in gene expression signatures have been identified in prostate tumors **(B)** *MYC/HDAC1/RASA1*, *CAPN2* genes were elevated in young patients, and **(C)** *VEGFA/MEIS2/HLA/LDHB/ANXA2* genes were down-regulated in old patients. The Venn diagram analysis represents significant genes with at least 3-fold expression. The hierarchical cluster showing the expression levels of the significant genes. Orange/red color shows up-regulation and blue color shows down-regulation. The intensity of blue and red colors indicates the degree of up or down-regulation, respectively. A solid line represents an expert curated association between the two gene products and a dotted line means there is an association by co-citation. Expert level filter settings were used to generate the network, which contains interactions curated by experts (Genomatix and NetPro) based on literature and genes without any interactions were filtered out.

regulated gene panel of WD-old/young and PD-old/young present in our initial findings are validated in this cohort.

To further confirm these findings, we accessed 46 samples from the prostate TCGA cohort consisting of prostate tumor (n=23) and matching normal tissue (n = 23) from 23 patients were stratified by age (young: 42-58, old: 66-73), Gleason score (well differentiated: Gleason score ≤3 + 4, poorly differentiated: Gleason score ≥4 + 3) and race (Caucasian American). Clinicopathological features and clinical data such as patient ID, race, family history, Gleason score, PSA at diagnosis, clinical stage, pathological stage, and biochemical recurrence for the old WD, young WD, old PD, and young PD used for the TCGA analysis were summarized in the **Supplementary Tables 2A, B**. The differentially expressed genes (DEGs) of interest were validated and presented in the table and heatmap (present/absent and up/down regulated) (**Figure 8D**). The *ERG/MYC* was up and *ANXA2* was down regulated in Young-WD whereas *FOLH1/PSMA* was up regulated in both young-WD and old-PD group. The genes *NPY/NEDD4L/MAOA/TWIST1* were up regulated and ID4 down regulated in old-PD group. The gene *LDHB* was down regulated in both WD-young and PD-old group of patients (**Figure 8D**).

DISCUSSION

Prostate cancer is an age-associated disease and behaves very heterogeneously in clinical aggressiveness. An increased incidence of prostate cancer in young men has been reported. The biological difference of prostate cancer development between young and old men is not clearly understood. This study describes the results of transcriptome profiling of clinically localized and lymph node-negative prostate cancer. Through gene expression profiling, we investigated the men diagnosed with prostate cancer and treated with radical prostatectomy at young and old ages with well and poorly differentiated tumors, as well as those that developed PSA recurrence. The individual cellular differentiation classified as well differentiated (WD) or poorly differentiated (PD) was determined histologically. Several genes have been identified that are potentially associated with the unfavorable prognosis of the tumors. We found that most of the unique genes expressed in young patients are upregulated in in all the tumor types and rPSA group, whereas in old patients all the uniquely expressed genes were predominantly down regulated, suggesting the fundamental tumor development biology differences associated with patient age. This tumor and

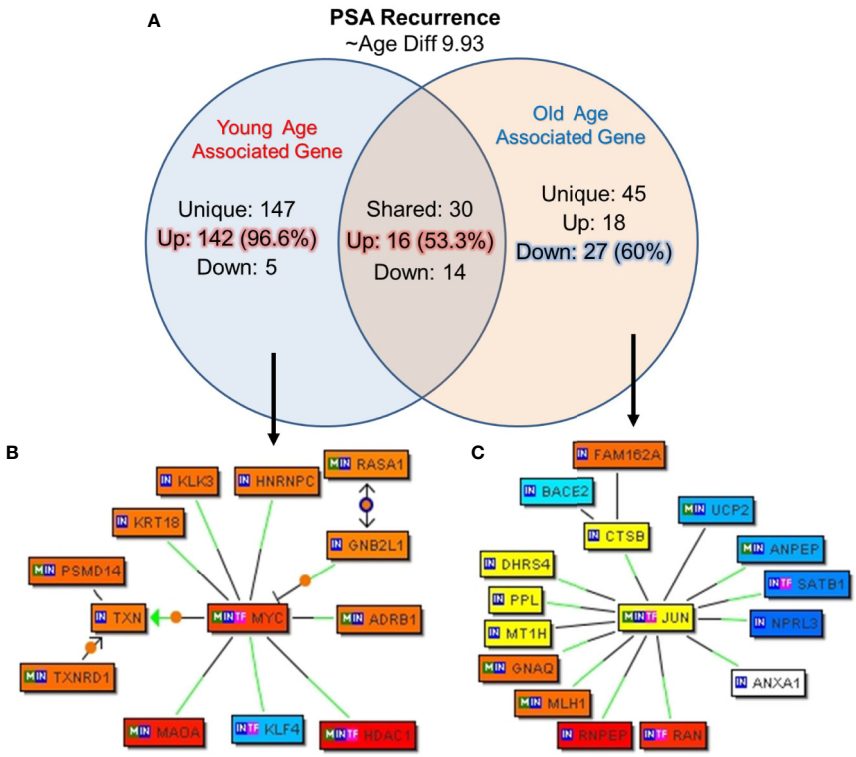

FIGURE 7 | Uniquely expressed genes in PSA recurrence group of young and old prostate cancer patients. **(A)** 147 genes were uniquely associated and 96.6% (142) genes were up-regulated in rPSA-young prostate cancer group. In old group 45 genes were uniquely expressed and 60% (27) genes were down regulated. Thirty genes were found to be co-expressed in both the groups. ~53% (N=16) were up-regulated and ~47% (N=14) genes were down-regulated. rPSA and marked age-associated differences in gene expression signatures were identified in prostate tumors **(B)** *MYC* form a central node with *HDAC1, RASA1*, and *KLK3*/PSA genes and were down-regulated in young-rPSA patients, and **(C)** *JUN* form a central node with *ANAX1, NPRL3, SATB1, UCP2, DHRS4, CTSB, PPL, BACE2*, and *MLH1* in old-rPSA patients. The Venn diagram analysis represents significant genes with at least 3-fold expression. The hierarchical cluster showing the expression levels of the significant genes. Orange/red color shows up-regulation and blue color shows down-regulation. The intensity of green and red colors indicates the degree of up or down-regulation, respectively. A solid line represents an expert curated association between the two gene products and a dotted line means there is an association by co-citation. Expert level filter settings were used to generate the network, which contains interactions curated by experts (Genomatix and NetPro) based on literature and genes without any interactions were filtered out.

age associated gene expression difference was seen across all the subgroups that we evaluated in young/old men with WD/PD/Balanced and rPSA. In well differentiated tumor type the up regulation of *VEGFA* was identified as a key central node in young prostate cancer patients and down regulation of *NPY* in old men. *VEGF* is a sub-family of growth factors and the key mediator of angiogenesis in cancer for cancer development and growth. NPY is a secretary plasma protein mostly over expressed in prostate cancers. The upregulation of *VEGF* and down regulation of *NPY* can serve as potential prognostic and diagnostic markers for the well differentiated tumor type of young and old men.

c-MYC is often upregulated leading to increased expression of several genes involved in cell proliferation and cancer development such as carcinoma of the cervix, colon, breast, lung, and stomach (20). In this study, we found the up regulation of *MYC* proto oncogene in only poorly differentiated tumor of young prostate cancer men. Interestingly, instead of *MYC*, calcium-dependent phospholipid-binding protein *ANXA2* was downregulated in PD tumor of old men forming a key central node. The main function of ANXA2 is to establish exocytosis of intracellular proteins to the extracellular domain and interferes with various cellular processes. In cancers, *ANXA2* plays a role in disease progression and down regulation of mRNA expression correlates with resistance to treatment, binding to the bone marrow, histological grade and type, TNM-stage and shortened overall survival. The regulation of Annexin A2 (*ANXA2*) is one of the potential targets for cancer management and treatment (21). In prostate cancer, *ANXA2* module inversely correlated with ERG in its network and can be used for biological stratification and therapeutic targeting of ERG based stratification of prostate cancers (22). Immunotherapy works by activating the patient's own immune system to fight cancer. Human leukocyte antigen class I (HLA-I) molecules are important for effective tumor killing. CD8+ T cells recognize tumor peptides presented by major *HLA-I* genes (*HLA-A*, *HLA-B*, and *HLA-C*). Here we found that HLA-A/B decreases in old patients. The down regulation of *HLA-A/B* genotypes can

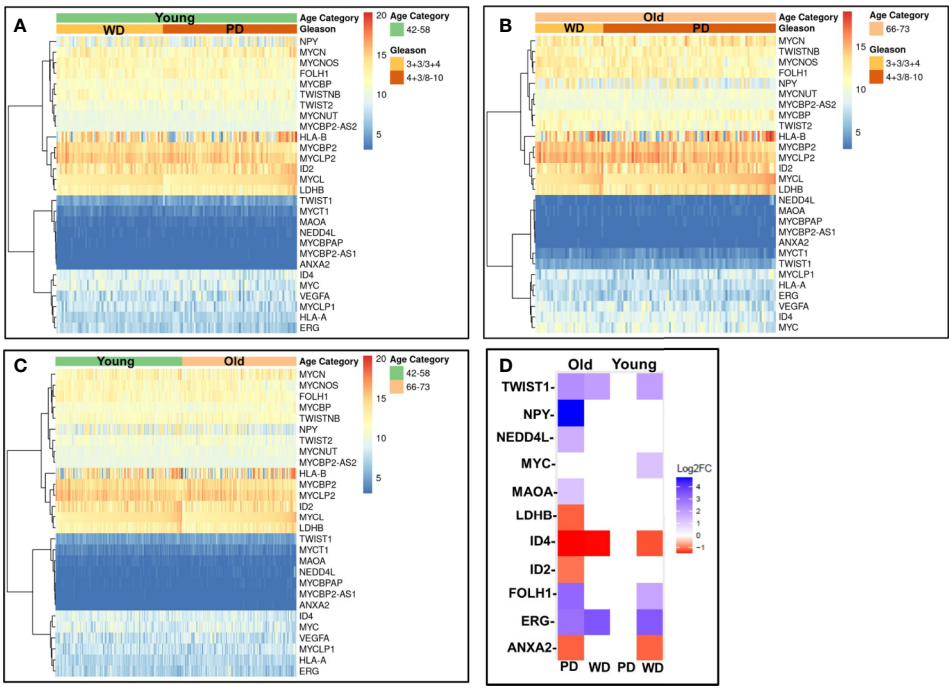

FIGURE 8 | Validation of gene expression signatures. Gene profile of old/young age-associated well/poorly differentiated prostate tumors were cross-referenced using RNA-seq gene expression data from recount2 project **(A–C)** and prostate cancer TCGA cohort **(D)**. The differentially expressed genes (DEGs) of interest were investigated for age (young and old) and Gleason/Differentiation (Well (and Poorly). **(A)** The gene of interest signature of young poorly differentiated (PD) and well differentiated (WD) tumors; **(B)** old PD and WD tumors, and **(C)** the young (42–58 years) and old (66–73 years) are presented in heatmap form. **(D)** DEGs of interest are presented in the table and heatmap.

influence the responsiveness of the old men to immunotherapy (23). Down-regulation of immune-related pathways, and especially the pathway involved in immuno-suppression, may be a common mechanism related to prostate cancer onset in old men.

In the balanced differentiated group of young and old prostate cancer patients, *MYC and HDAC1* genes were emerged as a central node and uniquely upregulated in young men whereas *VEGFA is* the key node in old men and found to be down regulated along with *HLA* and *ANXA2* genes in old patients. This set of genes can also serve as the potential age differentiated marker for prostate cancer development and progression in old and young men.

We have also evaluated PSA recurrence in old and young men as disease progression parameter. Our results propose new age specific gene signatures unique to biochemical recurrence of prostate cancer. Interestingly, both the young and old prostate cancer men with PSA recurrence bear poorly differentiated tumor only that could be due to the small sample size. The up-regulation of proto-oncogene *MYC* and down-regulation of *JUN* transcription factor have been populated as central node forming gene in young and old men with PD tumor respectively with PSA recurrence (24).

The genes identified as central regulatory nodes were *ANXA2* which was down-regulated in old patients with poorly differentiated tumor type, *VEGFA* which was down regulated in young patients with well differentiated tumors, and *NPY* which was up-regulated in old patients with well differentiated tumors. *FOLH1(PSMA)* a male reproductive organ cancer associated gene was up-regulated in young patients with well differentiated tumors, potential target of toxin-based immunotherapy. The other significant findings were *RARRES1* was down regulated in old patients, implicated in retinoid therapy and found to be as a tumor suppressor for multiple cancers such as prostate, breast, gastric, leukemia (25, 26). It has been shown that prostate-specific membrane antigen (PSMA) has potential for the management of prostate cancer chemoprevention by phytochemicals which is emerging as a potential adjunctive approach for the treatment of early carcinogenic processes (27). Further, several other genes such as *LDH-B* described as hypermethylated in prostate cancer; *ID4*, potential tumor suppressor gene in prostate cancer; *ANXA2* indicator of poor prognosis, recurrence, metastasis, high Gleason; *PSGR*, potential serum biomarker of prostate cancer; *ID2*, a p53 independent anti-apoptotic function in prostate cancer cells was found to be down regulated; and *MEIS2*, which act as putative tumor suppressor genes in prostate cancer; NPY, differentially expressed and up-regulated in 60% of "non-aggressive" tumors. *ERG* can fuse with *TMPRSS2* promoter to form an oncogenic fusion gene that is commonly found in human prostate cancer, especially in hormone-refractory prostate cancer. This gene encodes a member of the

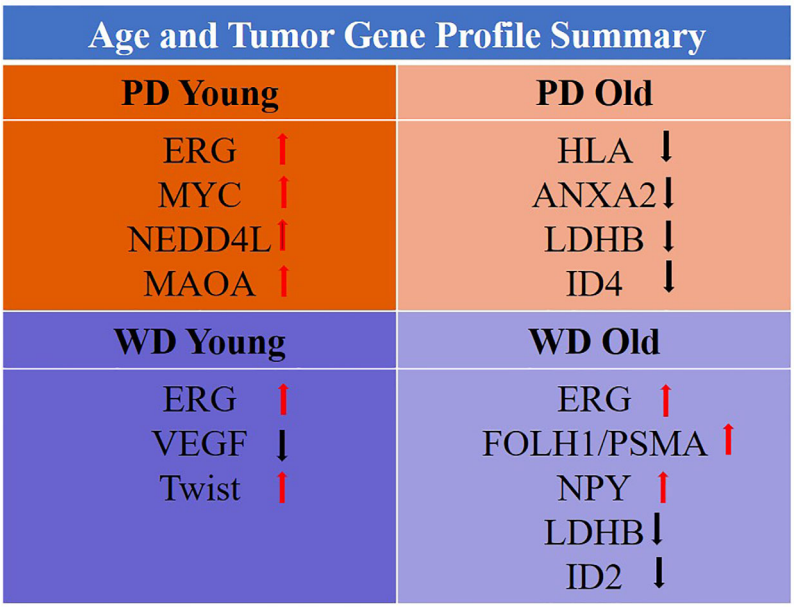

FIGURE 9 | Gene profile of old/young age-associated well/poorly differentiated tumors.

erythroblast transformation specific (ETS) family of transcriptions factors. All members of this family are key regulators of embryonic development, cell proliferation, differentiation, angiogenesis, inflammation, and apoptosis. *ERG* found to be up regulated in young patients with both well and poorly differentiated tumor and in old only in well differentiated tumor. Interestingly, *ERG* alterations were not found in old men with poorly differentiated tumor.

It is worth discussing the study limitations and strengths of the study. The small sample size, low power, in some extent the age difference between young and old (only ~9.9 to ~14.2 years) and lack of biological data currently are some of the limitations of the study. Additional sample sizes and with different ethnic backgrounds specifically African Americans are needed to further extent this study. The strengths of this study are 1) RNA from single malignant and normal epithelial cells from same patient, 2) high stringency of gene selection (T/N > Factor 3), 3) minimized normal cell aging variability, and 4) multiple known prostate cancer genes ID's which were common among the age groups. Our results are the first in the literature to suggest the existence of strong age disparateness in gene expression among old and young well and poorly differentiated tumors. The unique feature of this study is the robust enrichment of age-associated prostate tumor gene expression signature achieved by subtraction of normal aging signature of prostate epithelial cells of non-familial prostate cancer patients. The differential gene expression levels appear to be very polarized; tumors of young prostate cancer patients bear more oncogenic expressions as compared to old men and old men have more loss of tumor suppressor as when compared to young group. The gene profile of old and young age-associated well and poorly differentiated tumors are summarized in **Figure 9** and age-associated differences in gene expression signatures in poorly differentiated prostate tumors were presented in **Supplementary Figures 3A, B**. Further we have extended our work to confirm and validate these findings in a larger prostate cancer TCGA RNA-seq cohort. The RNA-seq gene expression signature along with clinical data within the age and differentiation threshold were consistent with our discovery cohort. It has been well established that alterations in various molecular genetic mechanisms, including mutations and epigenetic changes followed by perturbations in cell signaling and metabolic pathways are involved in prostate cancer development. Genes, which participate in these pathways, can serve as either diagnostic or prognostic biomarkers. As prostate cancer is a late onset disease and the genetic, ethnic and familial factors being responsible for this occurrence. A very limited information on early-onset of prostate cancer as well as its causes and trends are available. The main focus of this research study to develop only age and tumor differentiation associated gene signature of non-familial prostate cancers in Caucasian men. Further extension of this study is needed in other ethnic populations to develop global age and tumor specific biomarker panel for systemic progression, PSA Recurrence and prostate cancer therapy.

CONCLUSIONS

Age is a risk factor of cancers and age-associated differences in clinical outcome have been established in prostate cancer. Prostate cancer in young men appears to be composed predominantly of overexpressed genes known to be associated with somatic genomic alterations in prostate cancer. In contrast, prostate cancer of old men appears to have mostly down-regulated gene expressions indicating the loss of protective

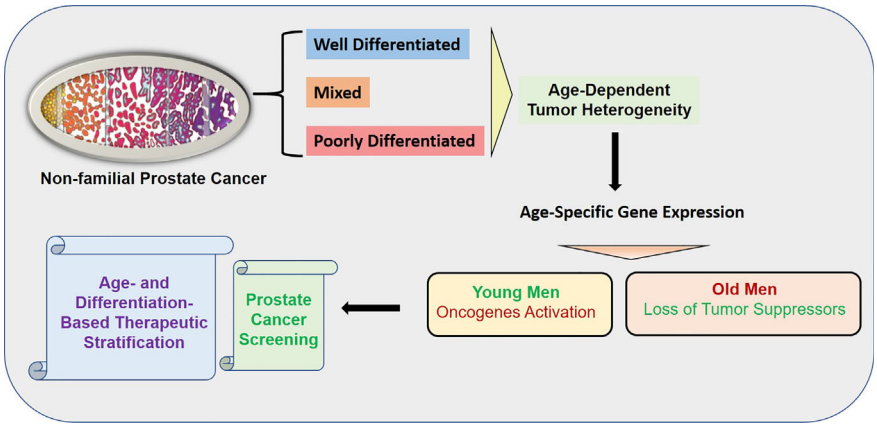

FIGURE 10 | Graphical Abstract: The overall summary of the findings is presented in the graphical abstract. The age-dependent heterogeneity was found to be associated with tumor differentiation. The activation of oncogenes was found in the young patients whereas loss of tumor suppressors was found in old patents. The uniqueness of the study is the robust enrichment of age-associated prostate tumor gene expression signature achieved by subtraction of normal aging signature of prostate epithelial cells of non-familial prostate cancer patients.

genes. The age-dependent heterogeneity was found to be associated with tumor differentiation. The overall summary of the findings is presented in the graphical abstract (**Figure 10**).

CLINICAL SIGNIFICANCE

The difference in prostate cancer of young and old men suggest a distinct biology among these groups. The unique age specific gene expression signature showed oncogenic activation in young and loss of tumor suppressors in old prostate cancer patients, which suggests fundamental differences in tumor development based on aging. This age dependent tumor heterogeneity of non-familial prostate cancer will not only establish prostate cancer screening but also will serve as age-and differentiation based therapeutic stratification of prostate cancer. In young-PD patients *ERG/MYC/NEDD4L/MAOA* oncogene panel was found to be activated whereas in old-PD patients *HLA-A/B/ANXA2/LDHB/ID4* tumor suppressor panel was down regulated. In WD-old group *ERG/FOLH1/PSMA/NPY* were up and LDHB/ID2 were down regulated however in WD-young *ERG/Twist* were up and *VEGF* was down regulated (**Figure 9**). These findings suggest some advantage of immunotherapy in old-PD patients and BET bromodomain inhibitors in young-PD, which block prostate cancer cell growth through c-MYC and androgen receptor (AR) suppression can be used in the prostate cancer subset of patients based on the age and tumor type.

DATA AVAILABILITY STATEMENT

The datasets presented in this study can be found in online repositories. The names of the repository/repositories and accession number(s) can be found below: https://www.ncbi.nlm.nih.gov/, GEO Accession: GSE32448; the recount2 project for 319 cases at https://jhubiostatistics.shinyapps.io/recount/; and https://portal.gdc.cancer.gov/projects/TCGA-PRAD.

ETHICS STATEMENT

The studies involving human participants were reviewed and approved by Walter Reed National Military Medical Center (WRNMMC) and Uniformed Services University of the Health Sciences (USUHS). Written informed consent for participation was not required for this study in accordance with the national legislation and the institutional requirements.

AUTHOR CONTRIBUTIONS

SSh, AD, and TA conceptualized the study. SSh and TA contributed to the methodology, SSh and TA provided the software. SSh and TA conduted the formal analysis. SSr, IS, and JC conducted the investigation.AD, JC, IS, DM, and SSr provided the resources. SSh and TA conducted the data curation. SSh and TA wrote and prepared the original draft. HL, SSh, and TA wrote, reviewed, and edited the manuscript. SSh and TA conducted the visualization. DM, AK, NW, and AS conducted the TCGA data analysis and validation. SSh and AD supervised the study. AD, HL, SSr, DM, ATK, NW, and AS revised the manuscript. SSh and TA conducted the project administration. DM and SSr acquired the funding. All authors contributed to the article and approved the submitted version.

FUNDING

This work has been supported by funding from Center for Prostate Disease Research, Uniformed Services University for

the Health Sciences (HU0001-17-2-2019, HU0001-10-2-0002 and HU001-004-c-1502 to DM, IR, and SSr) from the office of Congressionally Directed Medical Research Programs (CDMRP) of the US Army Medical Research and Materiel Command (USAMRMC) and the Intramural Research Program of the National Cancer Institute, National Institutes of Health.

ACKNOWLEDGMENTS

The authors thank the patients who participated in this study. The authors thank Dr. Gyorgy Petrovics at the Center for the Prostate Disease Research (CPDR), Department of Surgery, Uniformed Services, University of Health Sciences, Bethesda, for providing administrative, technical, material, and funding support. We also thank Ms. Shilpa Katta at CPDR for the initial bioinformatic analyses. The authors are grateful to all members of the CPDR, USU, HJF, and especially Chantal Falade for administrative support.

SUPPLEMENTARY MATERIAL

The Supplementary Material for this article can be found online at: https://www.frontiersin.org/articles/10.3389/fonc.2020.584280/full#supplementary-material

REFERENCES

1. Cynthia CS, Plymate SR, Reed MJ. Aging-related alterations in the extracellular matrix modulate the microenvironment and influence tumor progression. *Int J Cancer* (2010) 127:2739–48. doi: 10.1002/ijc.25615
2. Shelke AR, Mohile SG. Treating prostate cancer in elderly men: how does aging affect the outcome? *Curr Treat Options Oncol* (2011) 12:263–75. doi: 10.1007/s11864-011-0160-6
3. Salinas CA, Tsodikov A, Ishak-Howard M, Cooney KA. Prostate cancer in young men: an important clinical entity. *Nat Rev Urol* (2014) 11:317–23. doi: 10.1038/nrurol.2014.91
4. Li J, German R, King J, Joseph D, Thompson T, Wu XC, et al. Recent trends in prostate cancer testing and incidence among men under age of 50. *Cancer Epidemiol* (2012) 36:122–7. doi: 10.1016/j.canep.2011.10.014
5. Cetin K, Beebe-Dimmer JL, Fryzek JP, Markus R, Carducci MA. Recent time trends in the epidemiology of stage IV prostate cancer in the United States: analysis of data from the Surveillance, Epidemiology, and End Results Program. *Urology* (2010) 75:1396–404. doi: 10.1016/j.urology.2009.07.1360
6. Lin DW, Porter M, Montgomery B. Treatment and survival outcomes in young men diagnosed with prostate cancer: a Population-based Cohort Study. *Cancer* (2009) 115:2863–71. doi: 10.1002/cncr.24324
7. Merrill RM, Bird JS. Effect of young age on prostate cancer survival: a population-based assessment (United States). *Cancer Causes Control* (2002) 13:435–43. doi: 10.1023/a:1015764507609
8. Ding Y, Wu H, Warden C, Steele L, Liu X, Iterson MV, et al. Gene Expression Differences in Prostate Cancers between Young and Old Men. *PLoS Genet* (2016) 12:e1006477. doi: 10.1371/journal.pgen.1006477
9. Rohrmann S, Roberts WW, Walsh PC, Platz EA. Family history of prostate cancer and obesity in relation to high-grade disease and extraprostatic extension in young men with prostate cancer. *Prostate* (2003) 55:140–6. doi: 10.1002/pros.10211
10. Sharad S, Srivastava A, Ravulapalli S, Parker P, Chen Y, Li H, et al. Prostate cancer gene expression signature of patients with high body mass index. *Prostate Cancer Prostatic Dis* (2011) 14:22–9. doi: 10.1038/pcan.2010.44
11. Thangapazham RL, Shaheduzzaman S, Kim KH, Passi N, Tadese A, Vahey M, et al. Androgen responsive and refractory prostate cancer cells exhibit distinct curcumin regulated transcriptome. *Cancer Biol Ther* (2008) 7:1427–35. doi: 10.4161/cbt.7.9.6469
12. Cohen CD, Lindenmeyer MT, Eichinger F, Hahn A, Seifert M, Moll AG, et al. Improved elucidation of biological processes linked to diabetic nephropathy by single probe-based microarray data analysis. *PLoS One* (2008) 3:e2937. doi: 10.1371/journal.pone.0002937
13. Dennis GJr, Sherman BT, Hosack DA, Yang J, Gao W, Lane HC, et al. DAVID: Database for Annotation, Visualization, and Integrated Discovery. *Genome Biol* (2003) 4:P3. doi: 10.1186/gb-2003-4-9-r60
14. Katta S, Srivastava A, Thangapazham RL, Rosner IL, Cullen J, Li H, et al. Curcumin-Gene Expression Response in Hormone Dependent and Independent Metastatic Prostate Cancer Cells. *Int J Mol Sci* (2019) 20:19E4891. doi: 10.3390/ijms20194891
15. Scherf M, Epple A, Werner T. The next generation of literature analysis: integration of genomic analysis into text mining. *Brief Bioinform* (2005) 6:287–97. doi: 10.1093/bib/6.3.287
16. Kaaks R, Stattin P. Obesity, endogenous hormone metabolism, and prostate cancer risk: a conundrum of 'highs' and 'lows'. *Cancer Prev Res (Phila Pa)* (2010) 3:259–62. doi: 10.1158/1940-6207.CAPR-10-0014
17. Parker PM, Rice KR, Sterbis JR, Chen Y, Cullen J, McLeod DG, et al. Prostate cancer in men less than the age of 50: a comparison of race and outcomes. *Urology* (2011) 78:110–5. doi: 10.1016/j.urology.2010.12.046
18. Brassell SA, Rice KR, Parker PM, Chen Y, Farrell JS, Cullen J, et al. Prostate cancer in men 70 years old or old, indolent or aggressive: clinicopathological analysis and outcomes. *J Urol* (2011) 185:132–7. doi: 10.1016/j.juro.2010.09.014
19. Furusato B, Shaheduzzaman S, Petrovics G, Dobi A, Seifert M, Ravindranath L, et al. Transcriptome analyses of benign and malignant prostate epithelial cells in formalin-fixed paraffin-embedded whole-mounted radical prostatectomy specimens. *Prostate Cancer Prostatic Dis* (2008) 11:194–7. doi: 10.1038/sj.pcan.4501007
20. Sun C, Dobi A, Mohamed A, Li H, Thangapazham RL, Furusato B, et al. TMPRSS2-ERG fusion, a common genomic alteration in prostate cancer activates C-MYC and abrogates prostate epithelial differentiation. *Oncogene* (2008) 27:5348–53. doi: 10.1038/onc.2008.183
21. Takahashi S, Reddy SV, Chirgwin JM, Devlin R, Haipek C, Anderson J, et al. Cloning and identification of annexin II as an autocrine/paracrine factor that increases osteoclast formation and bone resorption. *J Biol Chem* (1994) 269:28696–701.
22. Griner NB, Young D, Chaudhary P, Mohamed AA, Huang W, Chen Y, et al. ERG oncoprotein inhibits ANXA2 expression and function in prostate cancer. *Mol Cancer Res* (2015) 13:368–79. doi: 10.1158/1541-7786.MCR-14-0275-T
23. Chowell D, Morris LGT, Grigg CM, Weber JK, Samstein RM, Makarov V, et al. Patient HLA class I genotype influences cancer response to checkpoint blockade immunotherapy. *Science* (2018) 359:582–7. doi: 10.1126/science.aao4572
24. Gollapudi K, Galet C, Grogan T, Zhang H, Said JW, Huang J, et al. Association between tumor-associated macrophage infiltration, high grade prostate cancer, and biochemical recurrence after radical prostatectomy. *Am J Cancer Res* (2013) 3:523–9.
25. Sahab ZJ, Hall MD, Me Sung Y, Dakshanamurthy S, Ji Y, Kumar D, et al. Tumor suppressor RARRES1 interacts with cytoplasmic carboxypeptidase AGBL2 to regulate the α-tubulin tyrosination cycle. *Cancer Res* (2011) 71:1219–28. doi: 10.1158/0008-5472.CAN-10-2294
26. Youssef EM, Lotan D, Issa JP, Wakasa K, Fan YH, Mao L, et al. Hypermethylation of the retinoic acid receptor-beta(2) gene in head and neck carcinogenesis. *Clin Cancer Res* (2004) 10:1733–42. doi: 10.1158/1078-0432.ccr-0989-3

27. Sanna V, Pintus G, Roggio AM, Punzoni S, Posadino AM, Arca A, et al. Targeted biocompatible nanoparticles for the delivery of (-)-epigallocatechin 3-gallate to prostate cancer cells. *J Med Chem* (2011) 54:1321–32. doi: 10.1021/jm1013715

Disclaimer: The contents of this publication are the sole responsibility of the author(s) and do not necessarily reflect the views, opinions, or policies of Uniformed Services University of the Health Sciences (USUHS), The Henry M. Jackson Foundation for the Advancement of Military Medicine, Inc., the Department of Defense (DoD), the Departments of the Army, Navy, or Air Force. Mention of trade names, commercial products, or organizations does not imply endorsement by the U.S. Government.

Conflict of Interest: The authors declare no conflict of interest. The funders had no role in the design of the study; in the collection, analyses, or interpretation of data; in the writing of the manuscript, or in the decision to publish the results.

Copyright © 2021 Sharad, Allemang, Li, Nousome, Ku, Whitlock, Sowalsky, Cullen, Sesterhenn, McLeod, Srivastava and Dobi. This is an open-access article distributed under the terms of the Creative Commons Attribution License (CC BY). The use, distribution or reproduction in other forums is permitted, provided the original author(s) and the copyright owner(s) are credited and that the original publication in this journal is cited, in accordance with accepted academic practice. No use, distribution or reproduction is permitted which does not comply with these terms.

frontiers in Oncology

REVIEW
published: 14 September 2021
doi: 10.3389/fonc.2021.746040

Potential Role of Exercise Induced Extracellular Vesicles in Prostate Cancer Suppression

Ying Zhang[1,2,3†], Jin-Soo Kim[2,3†], Tian-Zhen Wang[2,3,4], Robert U. Newton[2,3,5], Daniel A. Galvão[2,3], Robert A. Gardiner[2,6,7], Michelle M. Hill[6,8] and Dennis R. Taaffe[2,3]*

[1] Department of Physiology, Harbin Medical University, Harbin, China, [2] Exercise Medicine Research Institute, Edith Cowan University, Joondalup, WA, Australia, [3] School of Medical and Health Sciences, Edith Cowan University, Joondalup, WA, Australia, [4] Department of Pathology, Harbin Medical University, Harbin, China, [5] School of Human Movement and Nutrition Sciences, University of Queensland, Brisbane, QLD, Australia, [6] UQ Centre for Clinical Research, University of Queensland, Brisbane, QLD, Australia, [7] Department of Urology, Royal Brisbane and Women's Hospital, Brisbane, QLD, Australia, [8] QIMR Berghofer Medical Research Institute, Brisbane, QLD, Australia

OPEN ACCESS

Edited by:
Tanya I Stoyanova,
Stanford University, United States

Reviewed by:
Lucas Delmonico,
Federal University of Rio de Janeiro, Brazil
Avishay Sella,
Yitzhak Shamir Medical Center, Israel

***Correspondence:**
Dennis R. Taaffe
d.taaffe@ecu.edu.au

[†]These authors have contributed equally to work and share first authorship

Specialty section:
This article was submitted to Genitourinary Oncology, a section of the journal Frontiers in Oncology

Received: 23 July 2021
Accepted: 27 August 2021
Published: 14 September 2021

Citation:
Zhang Y, Kim J-S, Wang T-Z, Newton RU, Galvão DA, Gardiner RA, Hill MM and Taaffe DR (2021) Potential Role of Exercise Induced Extracellular Vesicles in Prostate Cancer Suppression. Front. Oncol. 11:746040. doi: 10.3389/fonc.2021.746040

Physical exercise is increasingly recognized as a valuable treatment strategy in managing prostate cancer, not only enhancing supportive care but potentially influencing disease outcomes. However, there are limited studies investigating mechanisms of the tumor-suppressive effect of exercise. Recently, extracellular vesicles (EVs) have been recognized as a therapeutic target for cancer as tumor-derived EVs have the potential to promote metastatic capacity by transferring oncogenic proteins, integrins, and microRNAs to other cells and EVs are also involved in developing drug resistance. Skeletal muscle has been identified as an endocrine organ, releasing EVs into the circulation, and levels of EV-containing factors have been shown to increase in response to exercise. Moreover, preclinical studies have demonstrated the tumor-suppressive effect of protein and microRNA contents in skeletal muscle-derived EVs in various cancers, including prostate cancer. Here we review current knowledge of the tumor-derived EVs in prostate cancer progression and metastasis, the role of exercise in skeletal muscle-derived EVs circulating levels and the alteration of their contents, and the potential tumor-suppressive effect of skeletal muscle-derived EV contents in prostate cancer. In addition, we review the proposed mechanism of exercise in the uptake of skeletal muscle-derived EVs in prostate cancer.

Keywords: prostate cancer, exercise oncology, extracellular vesicles, cancer physiology, exercise physiology

INTRODUCTION

Prostate cancer (PCa) is the most frequently diagnosed cancer in 112 countries with over 1.4 million new cases estimated in 2020, which is 14.1% of all new cancer diagnoses (1). Moreover, 370,000 men were estimated to die from prostate cancer in 2020 (6.8% of deaths caused by all cancer) (1). Early detection and advancement in treatments have improved survival for patients with PCa (1). However, these treatments can also have enduring adverse effects, such as the loss of lean mass and

bone mass, fat mass gain, post-surgery incontinence, metabolic imbalance, and reduced quality of life (2–4).

Exercise or physical activity has been receiving attention in patient care in the oncology setting (5) due to the increasing body of research in the field of exercise oncology. Multiple epidemiological studies (6, 7) and clinical trials (8–10) consistently report improvements in health-related outcomes for PCa patients. In addition, preclinical murine model studies have also demonstrated a reduced PCa tumor volume and delayed tumor growth with an exercise stimulus (11, 12), and provide a strong mechanistic case for clinical trials to be tested on cancer outcomes. However, while numerous hypotheses exist, the mechanisms by which exercise influences tumor biology are not fully understood (13).

As such, multiple studies have been conducted to reveal the mechanisms of exercise-induced benefits for cancer patients. Alteration in circulating factors, epigenetic modulation, gene expression modulation, immune function improvement, and systemic inflammation reduction have been suggested as potential mechanisms for exercise-induced tumor suppression (13, 14). For instance, serum levels of myokines, skeletal muscle secreted cytokines and peptides, are known to be altered with skeletal muscle stimulation, and multiple preclinical studies have shown the tumor-suppressive role of myokines with direct application in different cancer cell lines, including PCa (13). Although the beneficial role of exercise in reduced disease progression, increased survival, and patient care is promising, the mechanisms underlying how exercise-induced physiological changes provide tumor-suppressive effects are not clearly understood.

One potential mechanism proposed is the involvement of extracellular vesicles (EVs) (15, 16), as exercise-induced skeletal muscle-derived EVs may reduce cancer cell proliferation and metastasis (17). EVs are small membrane-surrounded structures released from various cells (18) that transfer bioactive molecules (including DNA, RNA, and proteins) from donor to acceptor cells (19). Two main types of EVs are defined based on their cellular route of release, exosomes and microvesicles or microparticles (18). The term 'exosome' refers to vesicles of the endosomal system that are released through the fusion of the multivesicular body delimiting membrane with the plasma membrane, while 'microvesicles' or 'microparticles' refer to vesicles that directly pinch off the cell surface (18).

During exercise, the release of EVs packaging cytokines and myokines plays a crucial role in the communication between muscle and other tissues (20). For instance, the skeletal muscle-derived EVs have been shown to increase in response to exercise, and increased uptake of skeletal muscle-derived EVs in the liver has been shown in animal models (21). Thus, the potential role of skeletal muscle-derived EVs in reducing cancer proliferation and migration by transporting anti-oncogenic proteins and microRNAs (miRNAs) has been proposed (20). This review will provide the current evidence for the role of exercise in skeletal muscle-derived EVs concentration in the circulatory system, the alteration of EV contents, and the potential role of exercise-induced skeletal muscle-derived EVs content in PCa. In addition, we propose a potential mechanism whereby exercise enhances skeletal muscle-derived EV uptake and delivery in PCa.

EXTRACELLULAR VESICLES IN PROSTATE CANCER

EV cargoes are considered to be biologically influential in cancer progression, metastasis, and development of drug resistance (22–24). Furthermore, particular miRNAs in EV cargoes have been considered as potential diagnostic, prognostic, and predictive markers for PCa (24–26) (**Figure 1**). For instance, miR-107, miR-130b, miR-141, miR-2110, miR-301a, miR-326, miR-331-3p, miR-432, miR-484, miR-574-3p, and miR-625 were shown to be substantially increased in circulating EVs from prostate cancer patients (n=78) compared to healthy individuals (n=28) ($P<0.05$) (27). Out of 11 miRNAs shown to increase in prostate cancer patients, miR-141 and miR-375 were significantly increased in patients with metastatic prostate cancer (n=16) compared to patients with localized prostate cancer (n=55) ($P<0.05$) (27), suggesting potential of circulating exosomes as prognostic markers for PCa. Furthermore, exosomal RNA analysis of plasma from 100 castration-resistant prostate cancer (CRPC) patients showed significantly shorter overall survival in patients with higher miR-375 and miR-1290 levels compared to those with lower miR-375 and miR-1290 levels ($P=0.0045$) (28). Although further validation will be required, this study also showed improved performance of predictive models for overall survival by incorporating miR-375 and miR-1290 levels with clinical prognostic factors (time to ADT failure and PSA level at the time of CRPC diagnosis) (28).

The study by Albino and colleagues (29) investigating the role of circulating miR-424 positive EVs in PCa patients demonstrated that metastatic PCa patients (metastatic castration-sensitive (mCSPC), n=16; metastatic castration-resistance (mCRPC), n=17) showed a higher frequency ($P<0.05$) of circulating miR-424 positive EVs compared to patients with primary tumors (n=25) and benign prostatic hyperplasia (BPH, n=6). Moreover, the application of EVs isolated from plasma of patients (n=17) in the *in vitro* environment showed increased tumor-sphere formation in the application of EVs from patients with mCSPC and mCRPC compared to primary or BPH patients ($P<0.02$) (29). In addition, the level of miR-424 containing EVs was positively associated with tumor growth in the 3D cell culture environment (tumor-sphere formation) ($P=0.003$) (29), suggesting a potential role of EV-contained miRNAs in PCa progression.

The study by Albino et al. (29) also generated a castration-resistant cell model using the LNCaP cell line by culturing in an androgen-depleted condition and showed significantly increased miR-424 in castration-resistant LNCaP-derived EVs compared to EVs derived from normal LNCaP cells ($P<0.005$), confirming the elevation in circulating miR-424 positive EVs in patients with advanced PCa (29). Furthermore, the application of EVs isolated from the castrate-resistant LNCaP-derived EVs to another PCa cell line, RWPE-1, showed increased tumor formation in a 3D

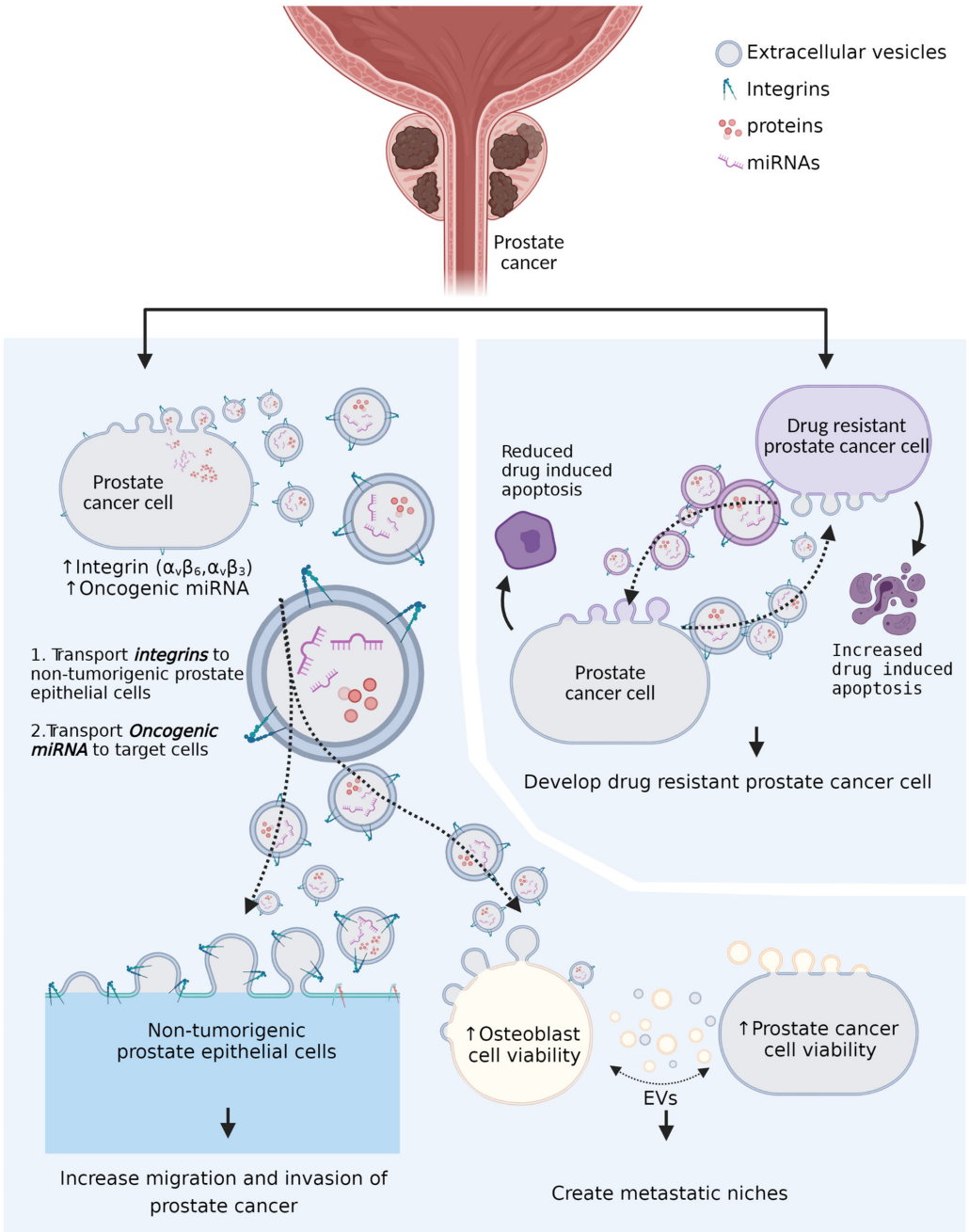

FIGURE 1 | The role of tumor-derived extracellular vesicles in prostate cancer progression and drug resistance. Tumor-derived extracellular vesicles (EVs) transport the integrins (α_V family integrins) to non-α_V family integrin presenting cells and promote cell-extracellular matrix communication to promote cancer growth. Tumor-derived extracellular vesicles also transport oncogenic microRNAs (miRNAs) to recipient cells and promote remodeling of metastatic niches. In addition, drug resistant prostate cancer cell-derived extracellular vesicles can reduce drug-induced apoptosis in non-drug resistant prostate cancer cells. Moreover, non-drug-resistant prostate cancer cell-derived extracellular vesicles can increase drug-induced apoptosis in drug-resistant prostate cancer cells.

cell culture model and cell migration compared to the application of normal LNCaP cell-derived EVs (P<0.005) (29), confirming the result by applying human plasma isolated EVs to cancer cell lines.

Preclinical studies involving PCa cell line-derived EVs and osteoblast cells also suggest a role for cancer cell-derived EVs in creating favorable niches for metastasis (30–32). In an *in vitro* study investigating the role of prostate cancer cell-induced EVs in osteoclastogensis and osteoblast proliferation, Inder and colleagues (30) demonstrated an increase in osteoclastogenesis of murine RAW264.7 pre-osteoclast cells (37 fold) and human primary-osteoblast proliferation (1.43 fold) with the presence of

EVs isolated from the human prostate cancer cell line PC3 compared with no PC3- induced EVs (P<0.005). However, secreted soluble factors from PC3 cells were not able to increase osteoclastogensis of RAW264.7 cells, indicating requirement for PCa-induced EVs in osteoclastogenesis (30).

Probert and colleagues (31) reported that culture of osteoblast cells with PC-3 (high metastasis capacity to bone), C4-2 (moderate metastasis capacity to bone), and C4-2-4B (a bone metastatic lineage of C4-2) PCa cell line-derived EVs resulted in a significant increase of osteoblast cell viability (*P*=0.004, *P*=0.032, and *P*=0.001, respectively). In addition, co-culture of the osteoblast cells preincubated with PCa derived-EVs with PC-3 and C4-2 cells showed a significant increase (*P*<0.001) in PCa cell line viability compared to PCa cell lines co-cultured with osteoblast cells precultured with non- PCa cell lines (31). This study also showed a significant increase of PCa abundant miRNA in osteoblast and induced functional changes of osteoblast *via* EVs transported miRNA, suggesting a role of PCa cell line-derived EVs in generating metastatic niches (31).

Similarly, there is also preclinical evidence for the role of EVs in transferring integrins to different subsets of PCa cell lines (33, 34). The integrins are a diverse family of glycoproteins that allows cells to interact with extracellular matrix (ECM) molecules and, in cancer, overexpression of the integrins in cancer cells contributes to migration and invasion by disrupting the ECM molecules (35). Studies have showed increased integrins (such as $\alpha_V\beta_6$ and $\alpha_V\beta_3$) in PCa cell lines (PC-3 and RWPE) and PCa cell line-derived exosomes (33, 34). Incubation of $\alpha_V\beta_6$ negative PCa cell line (DU145) or non-tumorigenic prostate epithelial cells with PCa cell line-derived exosomes results in *de novo* expression of these integrins in $\alpha_V\beta_6$ negative PCa cell and non-tumorigenic prostate epithelial cells (33, 34). These results suggest that tumor-derived EVs can transfer surface proteins, especially integrins, and enhance migration and invasion of tumor cells.

EVs have also been reported to be involved in PCa drug resistance (36). Panagopoulos and co-workers (37) showed increased camptothecin (CPT, chemotherapy drug) resistance in CPT sensitive DU145 cells when EVs isolated from CPT resistant RC1 PCa cell line conditioned growth media was applied. However, when RC1 cells were cultured with EVs isolated from DU145, CPT-induced apoptosis was increased in the RC1 cells. In addition, when PCa cell lines DU-145 and 22Rv1 cells were cultured with the presence of EVs isolated from docetaxel resistance, PCa cell lines demonstrated docetaxel resistance (38). Furthermore, application of exosomes isolated from docetaxel responding PCa patients (n=6) and non-responding PCa patients (n=2) to the DU145 PCa cell line showed increased docetaxel-resistance in DU145 cells cultured with exosomes isolated from docetaxel non-responders, suggesting the potential role of tumor-cell derived EVs in drug resistance (38).

EXERCISE AND PROSTATE CANCER

Multiple epidemiological studies in clinical oncology have consistently reported the positive impact of exercise in reducing PCa progression and enhancing survival. For instance, Kenfield and co-workers reported a 61% reduced risk (P=0.03) of PCa-related death (6) while Richman and co-workers reported a 57% reduction in disease progression (P=0.03) (7) in those with higher physical activity levels (≥3 hours/week) compared to those with lower physical activity levels. Furthermore, in preclinical studies, direct application of human serum obtained after exercise from healthy individuals to PCa cell line LNCaP showed a significant reduction in LNCaP cell growth (12). In addition, reduced tumor volume and delayed tumor growth was evident in a murine model injected with LNCaP cells exposed to human serum obtained after a bout of exercise compared with cells exposed to human serum acquired before exercise, suggesting a potential role for exercise in reducing tumor progression *in vivo* (12). Similar results were shown in the report by Hwang et al. (11), where human serum obtained after exercise from healthy older individuals (age > 60) was directly applied to PC-3 PCa cell lines. In addition, exercise increased blood delivery at the tumor site in a PCa animal model (R-3327 MatLyLu tumor cell orthotopically injected mice model) and reduced aggressiveness of PCa cells *via* reduced hypoxia at the tumor site (39) suggesting that exercise-induced physiological changes might have positive effects on cancer progression.

In addition, increased lean mass in PCa patients might also positively impact patient outcomes (10). In our recent systemic review and meta-analysis of the efficacy of exercise in improving supportive care outcomes in PCa patients with a range of treatments, improvements (P<0.001) in whole-body fat mass (-0.6 kg), lean mass (+0.5 kg), and appendicular lean mass (+0.4 kg) after exercise compared to usual care were noted (9). Furthermore, in our randomized controlled trial involving 57 PCa patients undergoing androgen deprivation therapy (ADT), 3 months of exercise significantly increased muscle strength, physical function, lean mass, and a number of patient-reported outcomes (8). Moreover, a recent retrospective report also showed that men with PCa exhibited increased prostate-specific antigen (PSA) progression-free survival and radiological progression-free survival in those with higher lean mass (P=0.03 and P<0.001, respectively) (10), providing a strong case for PCa patients to engage in exercise, especially of an anabolic nature to enhance or preserve lean mass.

SKELETAL MUSCLE DERIVED EVS DURING EXERCISE AND PROSTATE CANCER

Over the past decade, skeletal muscle has been identified as an important secretory organ producing a range of cytokines and peptides called myokines (40). In addition, in response to exercise training, skeletal muscle releases miRNAs into the circulation (41), and miRNAs, messenger RNAs (mRNAs), DNA, piwi-interacting RNAs (piRNAs), transfer RNAs (tRNAs), and myokines loaded into EVs for intercellular communication (20, 21). Moreover, clinical and preclinical studies have shown

alteration of skeletal muscle-derived EVs concentration in the circulatory system and their contained protein levels are also altered by exercise (21, 42–48) (**Table 1** and **Figure 2**).

Effect of an Exercise Bout on Skeletal Muscle-Derived EVs

Emerging clinical exercise trials are building our understanding of the effect of exercise bouts on exercise-derived EVs in both human and animal models (**Table 1** and **Figure 2**). Frühbeis and colleagues (44) showed that the level of small EVs of 100-130 nm that carry proteins characteristic of exosomes in plasma increased by an average of 5.2 times (Flot1, P=0.0021; Hsp/Hsc70, P=0.0021) in 12 healthy individuals in response to cycling or running until exhaustion. Similarly, another acute exhaustive exercise trial involving 16 healthy subjects also demonstrated a significant increase of EVs in serum at the peak exercise workload compared to at rest (P<0.05) (42), indicating an effect of exhaustive exercise in increasing circulating EVs concentration.

Elevation of serum EV concentrations and protein contents have also been shown after moderate-intensity aerobic exercise. Nielsen and colleagues demonstrated elevation of $CD36^+$ and $FATP4^+$ skeletal muscle-derived EVs in serum after 60 minutes of moderate-intensity aerobic exercise (70% VO_2max) in both healthy (n=14; $CD36^+$, 52%, P=0.019) and patients with metabolic disease (n=13; $CD36^+$, 55%, P=0.016; $FATP4^+$, 53%, P=0.007) compared to at rest (46). Moreover, Rigamonti and colleagues (48) showed a significant elevation of skeletal muscle-derived EVs (sarcoglycan-α^+EVs) in serum obtained immediately after 30 minutes of aerobic exercise (60% VO_2max) compared to at rest (P=0.016), whereas monocyte/macrophage ($CD14^+$EVs), endothelium ($CD62E^+$EVs), and adipose tissue ($FABP^+$EVs) derived EVs were unchanged. In addition, a study investigating the effect of 60 minutes of cycling exercise on circulating small vesicle concentrations and contents in 11 healthy subjects showed elevated circulating small vesicle levels with a significant alteration of 322 proteins after the exercise bout compared to pre-exercise (21).

Not only moderate-intensity aerobic exercise but high and low-intensity exercise also have been shown to increase serum EVs concentration and EVs protein content (45, 47). A clinical study involving a 40-minute bout of vigorous-intensity aerobic exercise (80%VO_2 max) in 22 healthy subjects reported the presence of skeletal muscle-derived EVs (sarcoglycan-α^+EV) in a cytofluorimetric analysis and level of muscle-specific mRNAs,

TABLE 1 | Effect of exercise on circulating extracellular vesicle concentration and contents.

Ref.	Subject	Subject number	Exercise protocol	Results
Frühbeis et al. (44)	Healthy human (male)	*Cycling*; n=8 *Treadmill*; n=4	Incremental cycling (increase power by 50 W every 3-min until exhaustion) Incremental treadmill (increase speed by 2 km/h every 3-min until exhaustion)	*Cycling*: 2.7 fold ↑ in small EVs; Flot1, Hsp/Hsc70, Tsg101 ↑ (average 5.2 fold) *Treadmill*: 1.5 fold ↑ in small EVs; significant ↑ Flot 1
Oliveira et al. (47)	Rats	*Non-ex*; n=4 *Low-ex*; n=5 *Mod-ex*; n=4 *High-ex*; n=5	Acute aerobic exercise (40 min) *Low-ex*: 14-16 m/min *Mod-ex*: 20-22 m/min *High-ex*: 24-26 m/min	Serum EVs concentration ↑ (non-ex, 1.1x10^9 unit/ml; low-ex, 3x10^9 unit/ml; mod-ex, 2.5x10^9 unit/ml; high-ex, 3.0x10^9 unit/ml); EVs protein concentration ↑ (non-ex, 0.935 mg/ml; low-ex, 4.33 mg/ml; mod-ex, 4.31 mg/ml; high-ex, 4.31 mg/ml); rno-miR330-5p, 10b-5p, 142-3p, and 410-3p ↑in exercise-EVs
Bei et al. (42)	Human, Mice	*Human*; n=16 *Mice*; n=4	*Human*: acute exercise stress test till exhaustion *Mice*: 5-90 min swimming, 2 day/week for 3 weeks	*Human*: EVs ↑ at peak exercise compared to rest *Mice*: 1.85-fold increase after 3-week swimming exercise
Bertoldi et al. (43)	Rat	*3-m-old*; n=12 (ex=6, con=6) *21-m-old*; n=12 (ex=6, con=6) *26-m-old*; n=10 (ex=5, con=5)	Daily 20 min treadmill running for 2 weeks	CD36 (exosome marker) ↑ after 18 hours following exercise cessation compared to the control group
Nielsen et al. (46)	Healthy human, T2DM patients	*Healthy subjects*; n=14 *T2DM patients*; n=13	Acute aerobic exercise (60min) 70% VO_2max	*Healthy subjects*: 52%↑$CD36^+$ SkM-EVs after exercise *T2DM patients*: 55% ↑$CD36^+$ SkM-EVs after exercise 53% ↑$FATP4^+$SkM-EVs after exercise
Rigamonti et al. (48)	Obese human, Healthy human	*Obese subject*; n=15 *Healthy subject*; n=8	Acute moderate constant workload exercise (30 min) 60% VO_2max	$SCGA^+$EVs ↑ immediately after exercise, $CD14^+$EVs ↔, $CD62^+$EVs ↔, $FABP^+$EVs ↔
Whitham et al. (21)	Healthy human	n=22	Acute cycling until exhaustion (~60 min) 30 min at 55% VO_2max, 20 min at 70% VO_2max, ~10 min (until exhaustion) at 80% VO_2max	Circulating small vesicle levels ↑ immediately after exercise, 322 EV protein contents altered

EV, Extracellular vesicle; Non-ex, non-exercise group; Low-ex, low-intensity exercise group; Mod-ex, moderate-intensity exercise group; High-ex, high-intensity exercise group; T2DM, type II diabetes; SkM-EVs, skeletal muscle-derived extracellular vesicle; FATP4, long-chain fatty acid transport protein 4; SCGA, sarcoglycan-α; FABP, fatty acid binding protein. ↑ indicate significant increase (p<0.05); ↔ indicate no change.

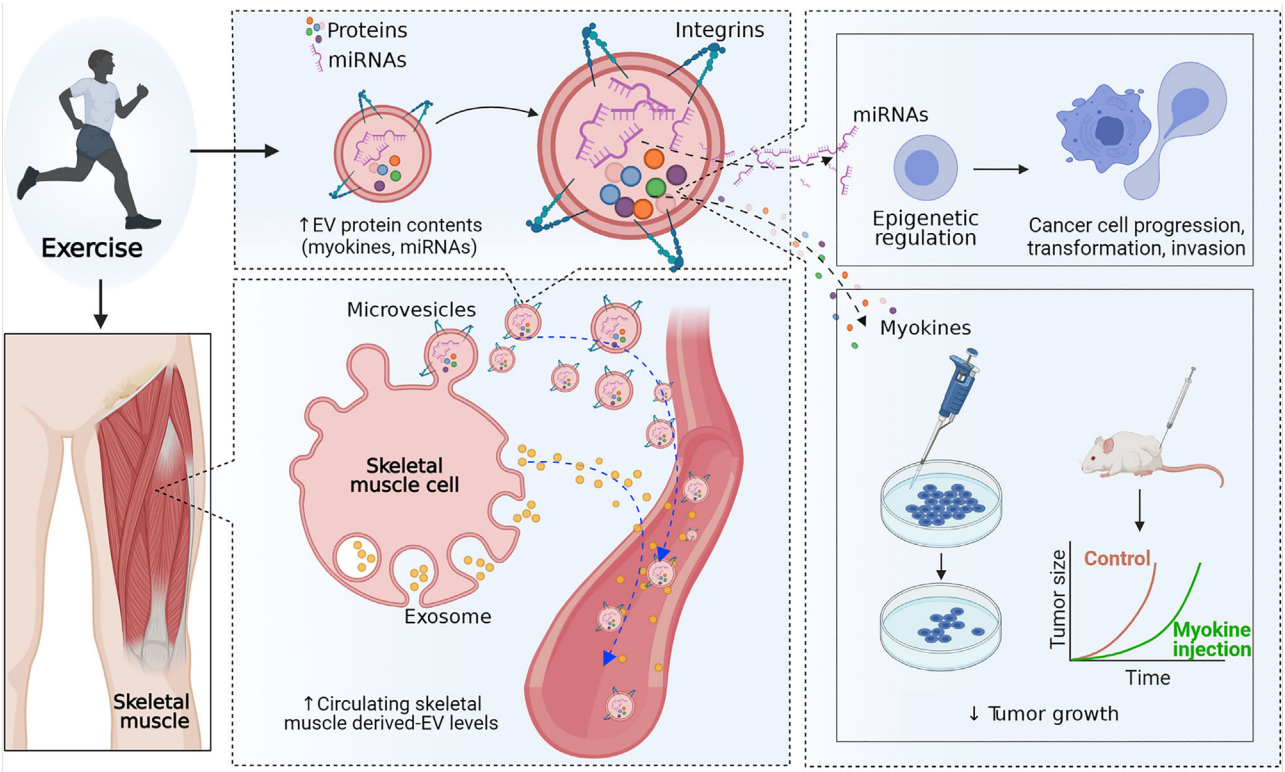

FIGURE 2 | Effect of exercise on extracellular vesicles. Exercise may increase the secretion of extracellular vesicles (EVs) into the circulatory system and alter the concentration of proteins and microRNAs (miRNAs) in skeletal muscle-derived extracellular vesicles. MicroRNAs in skeletal muscle-derived extracellular vesicles may induce epigenetic regulation in prostate cancer cells and reduce cell progression, transformation, and invasion. In addition, skeletal muscle-derived extracellular vesicles containing proteins, including myokines, have a direct tumor-suppressive effect.

such as miR-181a-5p and mi-133b, in sarcoglycan-α^+EVs to be significantly increased after exercise (P<0.05) (45). Furthermore, in a preclinical study, 18 mice were divided into 4 groups, non-exercise, low-intensity exercise, moderate-intensity exercise, and high-intensity exercise, and undertook 40 minutes of treadmill exercise at a speed of 14-16 m/min (20% below maximum lactate steady state (MLSS), 20-22 m/min (at MLSS), and 24-26 m/min (20% above MLSS) (47). Although there were no significant differences among exercise groups in serum EVs concentration, a significant difference in EVs concentration was shown in all exercise groups compared to the non-exercise group (low-ex *vs.* non-ex, P=0.014; mod-ex *vs.* non-ex, P=0.021; high-ex *vs.* non-ex, P=0.02) (47), whereas the size of EVs in the exercise groups was not changed compared to the non-exercise group. Similarly, EV protein concentrations were also significantly increased in all exercise groups compared to the non-exercise group (P=0.014) (47). In addition, 12 miRNAs in serum EVs (rno-miR-128-3p, 1033p, 330-5p, 148a-3p, 191a-5p, 10b-5p, 93-5p, 25-3p, 142-5p, 3068-3p, 142-3p, and 410-3p), predicted to target genes involved in the MAPK signal transduction pathway, were found to be differentially expressed after exercise in the animal model (47). These results suggest that low- and high-intensity exercise may also increase EV concentrations and protein content levels.

Effect of Chronic Exercise Training on Skeletal Muscle-Derived EVs

Due to the lack of clinical studies investigating the effect of chronic exercise training on circulating EVs concentration, insight into the effect of exercise training on resting circulating EVs concentration can only be derived from animal studies. However, positive associations between aerobic capacity (VO_2max) and EVs containing miRNAs (miR-1, R=0.58, P=0.01; miR-133b, R=0.54, P=0.02; miR-181a-5p, R=0.63, P=0.006; miR-206, R=0.5, P=0.003; miR-499, R=0.54, P=0.02) were found in the study by Guescini and colleagues (45) involving 18 healthy subjects suggesting that improvements in aerobic capacity due to chronic exercise might have a role in altering EV contents. Furthermore, a study by Bei and co-workers showed a 1.85-fold increase of circulating EVs after 3 weeks of swimming exercise in a mice model (42), and Bertoldi and colleagues demonstrated elevation of CD36 (exosome marker) in serum after 2 weeks of daily moderate-intensity exercise in a rat model at different ages (43). Although these studies suggest the elevation of circulating EVs concentration, the exercise period was short, and substantial exercise adaptation may not have occurred in the animals. Longer duration studies for exercise adaptation and investigation of the origin of these EV

responses to chronic training are required to enhance our understanding of the effect of chronic exercise on circulating skeletal muscle-derived EV resting concentrations.

Potential Role of Skeletal Muscle-Derived EV Cargoes in Prostate Cancer

Exercise can modify the biology of PCa *via* its effects on muscle hypertrophy, adipose tissue oxidation, increased insulin sensitivity, increased osteogenesis, reduced inflammation, and increased antitumor activity (49). Among the physiological alterations induced by exercise, the tumor-suppressive role of skeletal muscle secreted proteins (myokines) and miRNAs in PCa suggests a regulatory role of skeletal muscle-derived EV-containing proteins in PCa (**Figure 2**).

Myokines, such as IL-6, irisin/FNDC5, decorin, oncostatin M (OSM), and secreted protein acidic and rich in cysteine (SPARC), have shown the potential of a direct tumor-suppressive effect in different cancer cell lines, including PCa (13). For example, *in vitro* administration of IL-6 resulted in a reduction of hormone-sensitive PCa cell line proliferation by reducing androgen receptor expression (50), and application of irisin to PCa cell lines significantly reduced cell viability ($P<0.05$) (51). Moreover, direct application of SPARC and decorin significantly reduced PCa cell line growth by reduced Cyclin D1 and epidermal growth factor receptor (EGFR) activation, respectively (52, 53). Levels of myokines have also been shown to be altered in intercellular muscle protein and mRNA levels (13), supporting the analytic results of protein contents in skeletal muscle-derived EV contents by Whitham and co-workers, which showed alteration of protein contents in skeletal muscle-derived EVs (21).

The importance of epigenetics (including DNA methylation, histone modification, and miRNA *and* long non-coding RNA (lncRNA) regulation) in cellular transformation, tissue invasion, induction of angiogenesis, escape from immune surveillance, and metastasis is increasingly being recognized in cancer development and progression. In the pathogenesis of human PCa, somatic epigenetic alterations appear earlier than genetic changes, as well as more commonly and more consistently (54). Recent research has implicated EVs in epigenetic regulation of the cancer microenvironment to affect cancer progression (55). Bioinformatic analysis has indicated that many mRNAs and proteins contained in EVs are involved in epigenetic modulation (56). Proteins, mRNAs, microRNAs, and non-coding RNAs in EVs alter the phenotype of target cells by transferring mRNA, a transcriptional modulator, or degrading mRNA rapidly (57). Recently, it has been shown that aerobic exercise is a potential epigenetic modifier. Aerobic exercise induces epigenetic changes through several mechanisms, including chromatin methylation, histone acetylation, DNA methylation, and miR expression. MiRs secreted into the extracellular microenvironment *via* EVs may play an important role in epigenetic modulation (58).

Uptake of Skeletal Muscle-Derived EVs by Prostate Cancer Cells: Potential Myokine Involvement

Uptake of EVs by targeted cells is an important process to elicit the functional effects by initiating signaling events at the surface of recipient cells or transferring EV contents into recipient cells (59). Although the uptake of EVs by recipient cells is a critical process in cell-to-cell or ECM-to-cell communication *via* EVs, this process is poorly understood because the uptake of EVs depends on the specific properties of the recipient cells (60). However, the potential role of skeletal muscle-induced myokines, especially irisin, in skeletal muscle-derived EVs and cancer cell communication has been proposed in a recent review by Darkwah et al. (17) (**Figure 3**).

Fibronectin type III domain containing 5 (FNDC5), a type1 transmembrane glycoprotein embedded in the skeletal muscle cell membrane, is a precursor of irisin and with exercise stimulus not only does FNDC5 expression increase on the membrane of skeletal muscle cells but the fibronectin III domain is cleaved and released to the extracellular site as irisin (61, 62). Irisin has been shown to increase energy expenditure by inducing white adipocyte browning and helps to maintain metabolic homeostasis, reducing body weight, improving glucose metabolism, and improving insulin sensitivity (62–64). Furthermore, various preclinical studies have demonstrated a direct reduction of growth of various cancer cell lines after applying exogenous irisin including PCa (13).

The receptors of irisin were not identified until recently. However, irisin has been shown to have a high affinity to specific integrin families, α_V family, in bone and fat cells (65). Furthermore, previous studies have demonstrated high α_V family integrins (such as $\alpha_V\beta_6$ and $\alpha_V\beta_3$) expression in PCa cell lines, and these transmembrane proteins can be transferred to other recipient cells (33, 34), suggesting the potential role of irisin in increasing skeletal muscle-derived EVs and PCa cell communication. Although there is no research investigating the expression of FNDC5 in the membrane of skeletal muscle-derived EVs, the process of microvesicle biogenesis suggests the surface protein of the cell might be transferred to EVs (17). Taken together, it could be proposed that irisin-α_V family integrins interaction can directly induce a tumor-suppressive effect on PCa cells and possibly increase skeletal muscle-derived EVs-PCa cell communication through an extracellular domain of FNDC5 (irisin)-integrin interaction. This may increase the internalization of skeletal muscle-derived EVs into PCa cells to elicit the functional role of EV contents in PCa (17). Furthermore, circulating irisin may also interact with PCa cell-derived EV containing integrins and interfere with the delivery of PCa cell-derived EVs to the cells near PCa cells and contribute to remodeling the pre-metastatic environment (17). However, further investigation examining the role of irisin-integrin interaction in PCa is required to fully elucidate skeletal muscle-derived EVs uptake in PCa and involvement of myokines.

DISCUSSION

The importance of exercise oncology, the application of exercise medicine in cancer, has been well recognized in clinical oncology (5). Epidemiological (6, 7, 10) and clinical (8, 9) studies examining the effect of exercise in PCa patients have further

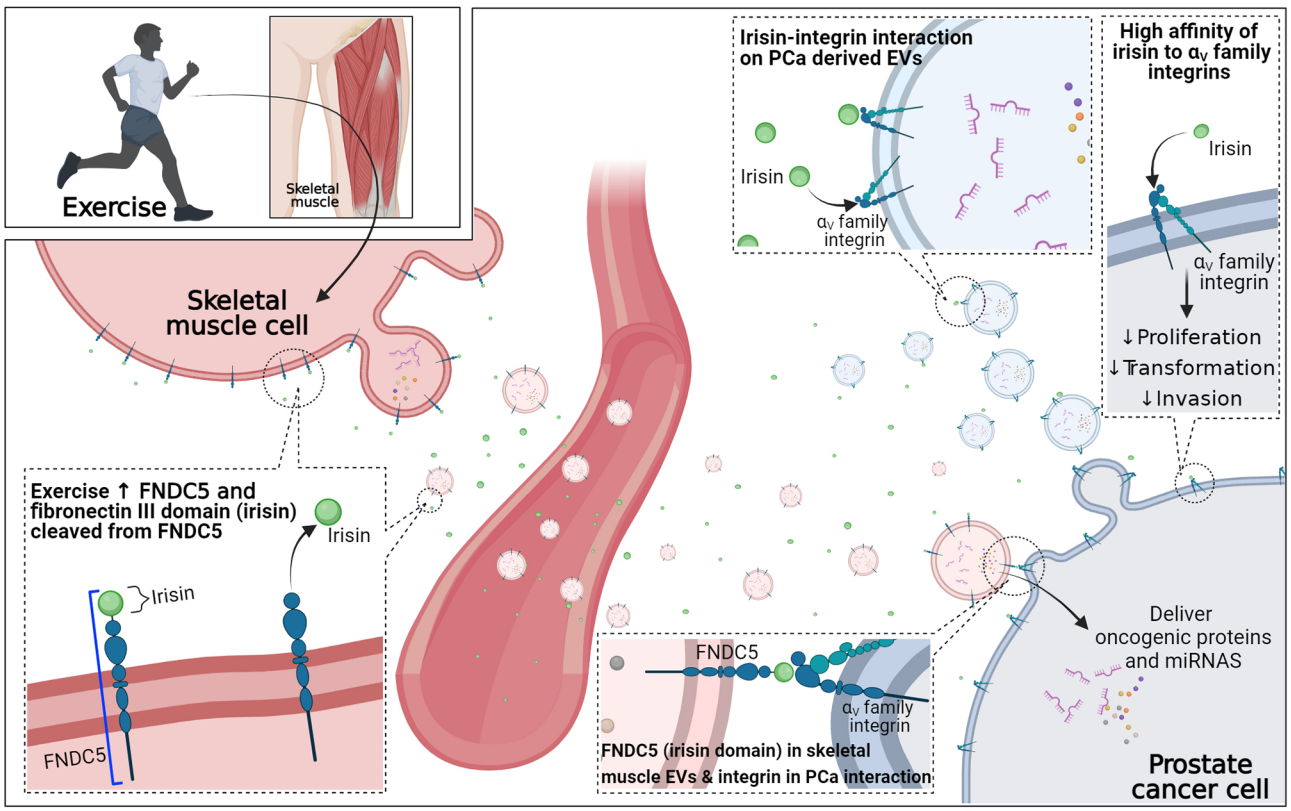

FIGURE 3 | Potential role of exercise-induced myokines in extracellular uptake in prostate cancer cells. Irisin has a high affinity to α_V family integrins, which is highly expressed in prostate cancer. FNDC5 is a precursor of irisin and with exercise stimulation FNDC5 is increased on the membrane, as is the secretion of irisin from skeletal muscle. Free irisin and skeletal muscle-derived extracellular vesicles (EVs) containing FNDC5 may travel to the prostate cancer site through the circulatory system. The high affinity of free irisin to α_V family integrins on the prostate cancer cell may directly induce irisin-integrin interaction to elicit the direct tumor-suppressive effect. Moreover, free irisin may also interact with α_V family integrins on tumor-derived extracellular vesicles to interfere with the remodeling of metastatic niches. Lastly, the irisin domain of FNDC5 on the membrane of skeletal muscle-derived extracellular vesicles may increase internalization of skeletal muscle-derived extracellular vesicles to prostate cancer cells through FNDC5 (irisin domain)- α_V family integrin interaction.

established the role of exercise in patient care for men with PCa. Moreover, exercise-induced circulating factor alteration, epigenetic modulation, and gene expression have been suggested as potential mechanisms whereby exercise may impact disease progression in men with PCa (13, 14).

Recently, extracellular vesicles have been highlighted in cell-to-cell and cell-to-extracellular matrix communications, and in PCa tumor-derived EVs have been suggested as a therapeutic target (24–26). Tumor-derived EVs have potential in delivering oncogenic proteins, surface proteins, and miRNAs to non-tumor cells and contribute to progression of PCa by initiating growth-promoting signal cascades or creating metastatic niches among non-tumoral cells near cancerous cells (29, 31, 33, 34). As such, multiple proteins, miRNAs, and surface proteins in tumor-derived EVs have been identified as potential predictable markers for PCa progression (22, 23, 26). However, a few clinical exercise trials demonstrating elevation of skeletal muscle-induced EVs after exercise and preclinical studies demonstrating a potential tumor-suppressive effect of skeletal muscle-derived factors (such as myokines and miRNAs) suggest EVs as a potential delivery mechanism for skeletal muscle induced proteins and miRNAs in PCa (13, 21, 42–48, 58). Furthermore, the potential role of myokines in the facilitation of skeletal muscle-derived EV uptake in cancer has been recently proposed in a review article by Darkwah and co-workers (17).

It is important to note that research into skeletal muscle-derived EVs in cancer is at an early stage; more research is required to fully elucidate the role of exercise in PCa. For instance, the clinical exercise trials investigating the alteration of skeletal muscle-derived EVs after exercise are limited to healthy populations, limiting the generalizability of these outcomes to cancer patients. Moreover, as common adverse effects of ADT, a widspread treatment in men with PCa, are a significant loss of skeletal muscle mass and gain of fat mass (4), physiology of skeletal muscle biogenesis may differ from that of healthy subjects (13). The lack of preclinical studies investigating the direct effect of skeletal muscle-derived EVs on PCa cells also prevents a clear understanding of the role of exercise-induced skeletal muscle-derived EVs. Although skeletal muscle secretomes, such as myokines and miRNAs, have been shown

to have potential in suppressing tumor growth (13, 49), the direct communication between skeletal muscle cells and PCa cells *via* EVs is yet to be reported.

CONCLUSIONS

Exercise-derived EVs have received increased attention as they provide an opportunity to understand the mechanistic benefit of exercise in cancer patients. Emerging evidence indicates that aerobic exercise affects circulating EV dynamics, including the size, morphology, and composition. Proteins, miRNAs, mRNAs, and DNAs packed in exercise-specific EVs may potentially play a role in preventing PCa development and disease progression. This review has summarized the preliminary evidence for an effect of exercise on circulatory levels of skeletal muscle-derived EV secretion, EV-containing protein or miRNA contents and the role of EV-containing factors in PCa progression, as well as the potential involvement of myokines in EV uptake in PCa. Given the speculative nature of the role of exercise-derived EVs to date, in the coming decade research will likely clarify the role of EVs with a focus on the dynamics of EVs in response to specific exercise modes and dosages, providing opportunities to enhance our understanding of the tailoring of exercise prescription on mediating possible cancer outcomes.

AUTHOR CONTRIBUTIONS

YZ and J-SK contributed equality to this work. YZ and T-ZW drafted the initial manuscript, and J-SK developed the manuscript. J-SK, RN, DG, RG, MH, and DT performed the revision. All authors contributed to the article and approved the submitted version.

FUNDING

J-SK is supported by National Health and Research Council Centre of Research Excellence (NHMRC-CRE) in Prostate Cancer Survivorship Scholarship. DG and RN are funded by an NHMRC-CRE in Prostate Cancer Survivorship (APP1116334).

REFERENCES

1. Sung H, Ferlay J, Siegel RL, Laversanne M, Soerjomataram I, Jemal A, et al. Global Cancer Statistics 2020: GLOBOCAN Estimates of Incidence and Mortality Worldwide for 36 Cancers in 185 Countries. *CA Cancer J Clin* (2021) 71:209–49. doi: 10.3322/caac.21660
2. Boorjian SA, Eastham JA, Graefen M, Guillonneau B, Karnes RJ, Moul JW, et al. A Critical Analysis of the Long-Term Impact of Radical Prostatectomy on Cancer Control and Function Outcomes. *Eur Urol* (2012) 61:664–75. doi: 10.1016/j.eururo.2011.11.053
3. Parsons BA, Evans S, Wright MP. Prostate Cancer and Urinary Incontinence. *Maturitas* (2009) 63:323–8. doi: 10.1016/j.maturitas.2009.06.005
4. Smith MR, Finkelstein JS, McGovern FJ, Zietman AL, Fallon MA, Schoenfeld DA, et al. Changes in Body Composition During Androgen Deprivation Therapy for Prostate Cancer. *J Clin Endocrinol Metab* (2002) 87:599–603. doi: 10.1210/jcem.87.2.8299
5. Schmitz KH, Campbell AM, Stuiver MM, Pinto BM, Schwartz AL, Morris GS, et al. Exercise is Medicine in Oncology: Engaging Clinicians to Help Patients Move Through Cancer. *CA Cancer J Clin* (2019) 69:468–84. doi: 10.3322/caac.21579
6. Kenfield SA, Stampfer MJ, Giovannucci E, Chan JM. Physical Activity and Survival After Prostate Cancer Diagnosis in the Health Professionals Follow-Up Study. *J Clin Oncol* (2011) 29:726–32. doi: 10.1200/JCO.2010.31.5226
7. Richman EL, Kenfield SA, Stampfer MJ, Paciorek A, Carroll PR, Chan JM. Physical Activity After Diagnosis and Risk of Prostate Cancer Progression: Data From the Cancer of the Prostate Strategic Urologic Research Endeavor. *Cancer Res* (2011) 71:3889–95. doi: 10.1158/0008-5472.CAN-10-3932
8. Galvão DA, Taaffe DR, Spry N, Joseph D, Newton RU. Combined Resistance and Aerobic Exercise Program Reverses Muscle Loss in Men Undergoing Androgen Suppression Therapy for Prostate Cancer Without Bone Metastases: A Randomized Controlled Trial. *J Clin Oncol* (2010) 28:340–7. doi: 10.1200/JCO.2009.23.2488
9. Lopez P, Taaffe DR, Newton RU, Galvao DA. Resistance Exercise Dosage in Men With Prostate Cancer: Systematic Review, Meta-Analysis, and Meta-Regression. *Med Sci Sports Exerc* (2020) 53:459–69. doi: 10.1249/MSS.0000000000002503
10. Pak S, Kim MS, Park EY, Kim SH, Lee KH, Joung JY. Association of Body Composition With Survival and Treatment Efficacy in Castration-Resistant Prostate Cancer. *Front Oncol* (2020) 10:558. doi: 10.3389/fonc.2020.00558
11. Hwang JH, McGovern J, Minett GM, Della Gatta PA, Roberts L, Harris JM, et al. Mobilizing Serum Factors and Immune Cells Through Exercise to Counteract Age-Related Changes in Cancer Risk. *Exerc Immunol Rev* (2020) 26:80–99.
12. Rundqvist H, Augsten M, Stromberg A, Rullman E, Mijwel S, Kharaziha P, et al. Effect of Acute Exercise on Prostate Cancer Cell Growth. *PloS One* (2013) 8:e67579. doi: 10.1371/journal.pone.0067579
13. Kim J-S, Galvão DA, Newton RU, Gray E, Taaffe DR. Exercise-Induced Myokines and Their Effect on Prostate Cancer. *Nat Rev Urol* (2021) 18:519–42. doi: 10.1038/s41585-021-00476-y
14. Galvao DA, Taaffe DR, Spry N, Gardiner RA, Taylor R, Risbridger GP, et al. Enhancing Active Surveillance of Prostate Cancer: The Potential of Exercise Medicine. *Nat Rev Urol* (2016) 13:258–65. doi: 10.1038/nrurol.2016.46
15. Becker A, Thakur BK, Weiss JM, Kim HS, Peinado H, Lyden D. Extracellular Vesicles in Cancer: Cell-to-Cell Mediators of Metastasis. *Cancer Cell* (2016) 30:836–48. doi: 10.1016/j.ccell.2016.10.009
16. Suchorska WM, Lach MS. The Role of Exosomes in Tumor Progression and Metastasis (Review). *Oncol Rep* (2016) 35:1237–44. doi: 10.3892/or.2015.4507
17. Darkwah S, Park EJ, Myint PK, Ito A, Appiah MG, Obeng G, et al. Potential Roles of Muscle-Derived Extracellular Vesicles in Remodeling Cellular Microenvironment: Proposed Implications of the Exercise-Induced Myokine, Irisin. *Front Cell Dev Biol* (2021) 9:634853. doi: 10.3389/fcell.2021.634853
18. Gyorgy B, Szabo TG, Pasztoi M, Pal Z, Misjak P, Aradi B, et al. Membrane Vesicles, Current State-of-the-Art: Emerging Role of Extracellular Vesicles. *Cell Mol Life Sci* (2011) 68:2667–88. doi: 10.1007/s00018-011-0689-3
19. Mathieu M, Martin-Jaular L, Lavieu G, Théry C. Specificities of Secretion and Uptake of Exosomes and Other Extracellular Vesicles for Cell-to-Cell Communication. *Nat Cell Biol* (2019) 21:9–17. doi: 10.1038/s41556-018-0250-9
20. Trovato E, Di Felice V, Barone R. Extracellular Vesicles: Delivery Vehicles of Myokines. *Front Physiol* (2019) 10:522. doi: 10.3389/fphys.2019.00522
21. Whitham M, Parker BL, Friedrichsen M, Hingst JR, Hjorth M, Hughes WE, et al. Extracellular Vesicles Provide a Means for Tissue Crosstalk During Exercise. *Cell Metab* (2018) 27:237–51. doi: 10.1016/j.cmet.2017.12.001
22. Fujita Y, Yoshioka Y, Ochiya T. Extracellular Vesicle Transfer of Cancer Pathogenic Components. *Cancer Sci* (2016) 107:385–90. doi: 10.1111/cas.12896
23. Jabalee J, Towle R, Garnis C. The Role of Extracellular Vesicles in Cancer: Cargo, Function, and Therapeutic Implications. *Cells* (2018) 7:93. doi: 10.3390/cells7080093

24. Ludwig M, Rajvansh R, Drake JM. Emerging Role of Extracellular Vesicles in Prostate Cancer. *Endocrinology* (2021) 162:bqab139. doi: 10.1210/endocr/bqab139
25. Linxweiler J, Junker K. Extracellular Vesicles in Urological Malignancies: An Update. *Nat Rev Urol* (2020) 17:11–27. doi: 10.1038/s41585-019-0261-8
26. Sita-Lumsden A, Dart DA, Waxman J, Bevan CL. Circulating microRNAs as Potential New Biomarkers for Prostate Cancer. *Br J Cancer* (2013) 108:1925–30. doi: 10.1038/bjc.2013.192
27. Bryant RJ, Pawlowski T, Catto JW, Marsden G, Vessella RL, Rhees B, et al. Changes in Circulating microRNA Levels Associated With Prostate Cancer. *Br J Cancer* (2012) 106:768–74. doi: 10.1038/bjc.2011.595
28. Huang X, Yuan T, Liang M, Du M, Xia S, Dittmar R, et al. Exosomal miR-1290 and miR-375 as Prognostic Markers in Castration-Resistant Prostate Cancer. *Eur Urol* (2015) 67:33–41. doi: 10.1016/j.eururo.2014.07.035
29. Albino D, Falcione M, Uboldi V, Temilola DO, Sandrini G, Merulla J, et al. Circulating Extracellular Vesicles Release Oncogenic miR-424 in Experimental Models and Patients With Aggressive Prostate Cancer. *Commun Biol* (2021) 4:119. doi: 10.1038/s42003-020-01642-5
30. Inder KL, Ruelcke JE, Petelin L, Moon H, Choi E, Rae J, et al. Cavin-1/PTRF Alters Prostate Cancer Cell-Derived Extracellular Vesicle Content and Internalization to Attenuate Extracellular Vesicle-Mediated Osteoclastogenesis and Osteoblast Proliferation. *J Extracell Vesicles* (2014) 3:23784. doi: 10.3402/jev.v3.23784
31. Probert C, Dottorini T, Speakman A, Hunt S, Nafee T, Fazeli A, et al. Communication of Prostate Cancer Cells With Bone Cells *via* Extracellular Vesicle RNA; A Potential Mechanism of Metastasis. *Oncogene* (2019) 38:1751–63. doi: 10.1038/s41388-018-0540-5
32. Robinson H, Ruelcke JE, Lewis A, Bond CS, Fox AH, Bharti V, et al. Caveolin-1-Driven Membrane Remodelling Regulates hnRNPK-Mediated Exosomal microRNA Sorting in Cancer. *Clin Transl Med* (2021) 11:e381. doi: 10.1002/ctm2.381
33. Fedele C, Singh A, Zerlanko BJ, Iozzo RV, Languino LR. The Alphavbeta6 Integrin Is Transferred Intercellularly *via* Exosomes. *J Biol Chem* (2015) 290:4545–51. doi: 10.1074/jbc.C114.617662
34. Singh A, Fedele C, Lu H, Nevalainen MT, Keen JH, Languino LR. Exosome-Mediated Transfer of Alphavbeta3 Integrin From Tumorigenic to Nontumorigenic Cells Promotes a Migratory Phenotype. *Mol Cancer Res* (2016) 14:1136–46. doi: 10.1158/1541-7786.MCR-16-0058
35. Hood JD, Cheresh DA. Role of Integrins in Cell Invasion and Migration. *Nat Rev Cancer* (2002) 2:91–100. doi: 10.1038/nrc727
36. Wang JQ, DeChalus A, Chatterjee DN, Keller ET, Mizokami A, Camussi G, et al. Extracellular Vesicle-Mediated Reversal of Paclitaxel Resistance in Prostate Cancer. *Crit Rev Oncog* (2015) 20:407–17. doi: 10.1615/CritRevOncog.v20.i5-6.120
37. Panagopoulos K, Cross-Knorr S, Dillard C, Pantazatos D, Del Tatto M, Mills D, et al. Reversal of Chemosensitivity and Induction of Cell Malignancy of a Non-Malignant Prostate Cancer Cell Line Upon Extracellular Vesicle Exposure. *Mol Cancer* (2013) 12:118. doi: 10.1186/1476-4598-12-118
38. Corcoran C, Rani S, O'Brien K, O'Neill A, Prencipe M, Sheikh R, et al. Docetaxel-Resistance in Prostate Cancer: Evaluating Associated Phenotypic Changes and Potential for Resistance Transfer *via* Exosomes. *PloS One* (2012) 7:e50999. doi: 10.1371/journal.pone.0050999
39. McCullough DJ, Stabley JN, Siemann DW, Behnke BJ. Modulation of Blood Flow, Hypoxia, and Vascular Function in Orthotopic Prostate Tumors During Exercise. *J Natl Cancer Inst* (2014) 106:dju036. doi: 10.1093/jnci/dju036
40. Pedersen BK, Febbraio MA. Muscles, Exercise and Obesity: Skeletal Muscle as a Secretory Organ. *Nat Rev Endocrinol* (2012) 8:457–65. doi: 10.1038/nrendo.2012.49
41. Baggish AL, Hale A, Weiner RB, Lewis GD, Systrom D, Wang F, et al. Dynamic Regulation of Circulating microRNA During Acute Exhaustive Exercise and Sustained Aerobic Exercise Training. *J Physiol* (2011) 589:3983–94. doi: 10.1113/jphysiol.2011.213363
42. Bei Y, Xu T, Lv D, Yu P, Xu J, Che L, et al. Exercise-Induced Circulating Extracellular Vesicles Protect Against Cardiac Ischemia-Reperfusion Injury. *Basic Res Cardiol* (2017) 112:38. doi: 10.1007/s00395-017-0628-z
43. Bertoldi K, Cechinel LR, Schallenberger B, Corssac GB, Davies S, Guerreiro ICK, et al. Circulating Extracellular Vesicles in the Aging Process: Impact of Aerobic Exercise. *Mol Cell Biochem* (2018) 440:115–25. doi: 10.1007/s11010-017-3160-4
44. Fruhbeis C, Helmig S, Tug S, Simon P, Kramer-Albers EM. Physical Exercise Induces Rapid Release of Small Extracellular Vesicles Into the Circulation. *J Extracell Vesicles* (2015) 4:28239. doi: 10.3402/jev.v4.28239
45. Guescini M, Canonico B, Lucertini F, Maggio S, Annibalini G, Barbieri E, et al. Muscle Releases Alpha-Sarcoglycan Positive Extracellular Vesicles Carrying miRNAs in the Bloodstream. *PloS One* (2015) 10:e0125094. doi: 10.1371/journal.pone.0125094
46. Nielsen MH, Sabaratnam R, Pedersen AJT, Hojlund K, Handberg A. Acute Exercise Increases Plasma Levels of Muscle-Derived Microvesicles Carrying Fatty Acid Transport Proteins. *J Clin Endocrinol Metab* (2019) 104:4804–14. doi: 10.1210/jc.2018-02547
47. Oliveira GPJr., Porto WF, Palu CC, Pereira LM, Petriz B, Almeida JA, et al. Effects of Acute Aerobic Exercise on Rats Serum Extracellular Vesicles Diameter, Concentration and Small RNAs Content. *Front Physiol* (2018) 9:532. doi: 10.3389/fphys.2018.00532
48. Rigamonti AE, Bollati V, Pergoli L, Iodice S, De Col A, Tamini S, et al. Effects of an Acute Bout of Exercise on Circulating Extracellular Vesicles: Tissue-, Sex-, and BMI-Related Differences. *Int J Obes (Lond)* (2020) 44:1108–18. doi: 10.1038/s41366-019-0460-7
49. Hayes BD, Brady L, Pollak M, Finn SP. Exercise and Prostate Cancer: Evidence and Proposed Mechanisms for Disease Modification. *Cancer Epidemiol Biomarkers Prev* (2016) 25:1281–8. doi: 10.1158/1055-9965.EPI-16-0223
50. Lee SO, Chun JY, Nadiminty N, Lou W, Gao AC. Interleukin-6 Undergoes Transition From Growth Inhibitor Associated With Neuroendocrine Differentiation to Stimulator Accompanied by Androgen Receptor Activation During LNCaP Prostate Cancer Cell Progression. *Prostate* (2007) 67:764–73. doi: 10.1002/pros.20553
51. Tekin S, Erden Y, Sandal S, Yilmaz B. Is Irisin an Anticarcinogenic Peptide? *Med-Science* (2015) 4:2172–80. doi: 10.5455/medscience.2014.03.8210
52. Hu Y, Sun H, Owens RT, Wu J, Chen YQ, Berquin IM, et al. Decorin Suppresses Prostate Tumor Growth Through Inhibition of Epidermal Growth Factor and Androgen Receptor Pathways. *Neoplasia* (2009) 11:1042–53. doi: 10.1593/neo.09760
53. Said N, Frierson HF Jr, Chernauskas D, Conaway M, Motamed K, Theodorescu D. The Role of SPARC in the TRAMP Model of Prostate Carcinogenesis and Progression. *Oncogene* (2009) 28:3487–98. doi: 10.1038/onc.2009.205
54. Nelson WG, Yegnasubramanian S, Agoston AT, Bastian PJ, Lee BH, Nakayama M, et al. Abnormal DNA Methylation, Epigenetics, and Prostate Cancer. *Front Biosci* (2007) 12:4254–66. doi: 10.2741/2385
55. Agnati LF, Fuxe K. Extracellular-Vesicle Type of Volume Transmission and Tunnelling-Nanotube Type of Wiring Transmission Add a New Dimension to Brain Neuro-Glial Networks. *Philos Trans R Soc Lond B Biol Sci* (2014) 369:20130505. doi: 10.1098/rstb.2013.0505
56. Sharma A. Bioinformatic Analysis Revealing Association of Exosomal mRNAs and Proteins in Epigenetic Inheritance. *J Theor Biol* (2014) 357:143–9. doi: 10.1016/j.jtbi.2014.05.019
57. Quesenberry PJ, Goldberg LR, Aliotta JM, Dooner MS, Pereira MG, Wen S, et al. Cellular Phenotype and Extracellular Vesicles: Basic and Clinical Considerations. *Stem Cells Dev* (2014) 23:1429–36. doi: 10.1089/scd.2013.0594
58. Masi LN, Serdan TD, Levada-Pires AC, Hatanaka E, Silveira LD, Cury-Boaventura MF, et al. Regulation of Gene Expression by Exercise-Related Micrornas. *Cell Physiol Biochem* (2016) 39:2381–97. doi: 10.1159/000452507
59. French KC, Antonyak MA, Cerione RA. Extracellular Vesicle Docking at the Cellular Port: Extracellular Vesicle Binding and Uptake. *Semin Cell Dev Biol* (2017) 67:48–55. doi: 10.1016/j.semcdb.2017.01.002
60. Lee TH, Chennakrishnaiah S, Meehan B, Montermini L, Garnier D, D'Asti E, et al. Barriers to Horizontal Cell Transformation by Extracellular Vesicles Containing Oncogenic H-Ras. *Oncotarget* (2016) 7:51991–2002. doi: 10.18632/oncotarget.10627
61. Huh JY, Panagiotou G, Mougios V, Brinkoetter M, Vamvini MT, Schneider BE, et al. FNDC5 and Irisin in Humans: I. Predictors of Circulating Concentrations in Serum and Plasma and II. mRNA Expression and Circulating Concentrations in Response to Weight Loss and Exercise. *Metabolism* (2012) 61:1725–38. doi: 10.1016/j.metabol.2012.09.002
62. Novelle MG, Contreras C, Romero-Pico A, Lopez M, Dieguez C. Irisin, Two Years Later. *Int J Endocrinol* (2013) 2013:746281. doi: 10.1155/2013/746281

63. Arhire LI, Mihalache L, Covasa M. Irisin: A Hope in Understanding and Managing Obesity and Metabolic Syndrome. *Front Endocrinol (Lausanne)* (2019) 10:524. doi: 10.3389/fendo.2019.00524
64. Reddy NL, Tan BK, Barber TM, Randeva HS. Brown Adipose Tissue: Endocrine Determinants of Function and Therapeutic Manipulation as a Novel Treatment Strategy for Obesity. *BMC Obes* (2014) 1:13. doi: 10.1186/s40608-014-0013-5
65. Kim H, Wrann CD, Jedrychowski M, Vidoni S, Kitase Y, Nagano K, et al. Irisin Mediates Effects on Bone and Fat *via* alphaV Integrin Receptors. *Cell* (2018) 175:1756–68.e17. doi: 10.1016/j.cell.2018.10.025

Conflict of Interest: The authors declare that the research was conducted in the absence of any commercial or financial relationships that could be construed as a potential conflict of interest.

Publisher's Note: All claims expressed in this article are solely those of the authors and do not necessarily represent those of their affiliated organizations, or those of the publisher, the editors and the reviewers. Any product that may be evaluated in this article, or claim that may be made by its manufacturer, is not guaranteed or endorsed by the publisher.

Copyright © 2021 Zhang, Kim, Wang, Newton, Galvão, Gardiner, Hill and Taaffe. This is an open-access article distributed under the terms of the Creative Commons Attribution License (CC BY). The use, distribution or reproduction in other forums is permitted, provided the original author(s) and the copyright owner(s) are credited and that the original publication in this journal is cited, in accordance with accepted academic practice. No use, distribution or reproduction is permitted which does not comply with these terms.

frontiers in Oncology

REVIEW
published: 14 September 2021
doi: 10.3389/fonc.2021.744679

Interaction Between Modern Radiotherapy and Immunotherapy for Metastatic Prostate Cancer

Luc Ollivier[1,2†], *Maureen Labbé*[2†], *Delphine Fradin*[2], *Vincent Potiron*[1,2] *and Stéphane Supiot*[1,2*]

[1] Institut de Cancérologie de l'Ouest, Nantes, France, [2] Université de Nantes, CNRS, Inserm, CRCINA, Nantes, France

Prostate cancer is the most frequently diagnosed cancer in men and a leading cause of cancer-related death. In recent decades, the development of immunotherapies has resulted in great promise to cure metastatic disease. However, prostate cancer has failed to show any significant response, presumably due to its immunosuppressive microenvironment. There is therefore growing interest in combining immunotherapy with other therapies able to relieve the immunosuppressive microenvironment. Radiation therapy remains the mainstay treatment for prostate cancer patients, is known to exhibit immunomodulatory effects, depending on the dose, and is a potent inducer of immunogenic tumor cell death. Optimal doses of radiotherapy are thus expected to unleash the full potential of immunotherapy, improving primary target destruction with further hope of inducing immune-cell-mediated elimination of metastases at distance from the irradiated site. In this review, we summarize the current knowledge on both the tumor immune microenvironment in prostate cancer and the effects of radiotherapy on it, as well as on the use of immunotherapy. In addition, we discuss the utility to combine immunotherapy and radiotherapy to treat oligometastatic metastatic prostate cancer.

Keywords: radiotherapy, immunotherapy, prostate cancer, metastasis, treatment combination

OPEN ACCESS

Edited by:
Andrew Goldstein, University of California, Los Angeles, United States

Reviewed by:
Gian Maria Busetto, University of Foggia, Italy
Asit K. Paul, Virginia Commonwealth University, United States

***Correspondence:**
Stéphane Supiot
Stephane.supiot@ico.unicancer.fr

†These authors have contributed equally to this work

Specialty section:
This article was submitted to Genitourinary Oncology, a section of the journal Frontiers in Oncology

Received: *20 July 2021*
Accepted: *24 August 2021*
Published: *14 September 2021*

Citation:
Ollivier L, Labbé M, Fradin D, Potiron V and Supiot S (2021) Interaction Between Modern Radiotherapy and Immunotherapy for Metastatic Prostate Cancer. Front. Oncol. 11:744679. doi: 10.3389/fonc.2021.744679

INTRODUCTION

Prostate cancer (PCa) is the most commonly diagnosed cancer in men and the second most common cancer worldwide (1). Despite the fact that more than 70% of cases of localized PCa are cured by local treatments [brachytherapy, (BT), surgery and/or external beam radiation therapy (EBRT)], or are under active surveillance before receiving treatment without altering the benefit of the latter, the median survival of metastatic patients is still less than 5 years (2). Oligometastatic disease (OMD) is first defined by Hellman and Weichselbaum as an intermediate state between local and systemic disease, but there are no validated biomarkers. The ESTRO-ASTRO consensus notes that there are currently no clinical studies showing a lack of benefit beyond a certain number of metastases to define OMD. It is thus a disease where all metastatic sites are treatable by radiotherapy with curative intent. Moreover, OMD can be split in two subtypes: i) synchronous when OMD is

detected at the time of the initial diagnosis, ii) metachronous or oligo-recurrent, when OMD is discovered during the course of the disease. Biologically, all metastases are synchronous but our ability to detect them makes them metachronous. Furthermore, metachronous metastases are known to have a better prognosis than synchronous metastases. Elimination of oligometastatic burden by radiation may prevent additional metastatic spread and improve overall survival (3–5). This approach may change the paradigm from palliative to potentially curable disease for oligometastatic PCa patients (6, 7). Indeed, the phase 2 SABR-COMET (Stereotactic ABlative Radiotherapy for the Comprehensive Treatment of OligoMETastases) trial recently evaluated the value of ablative stereotactic radiotherapy to metastatic sites in patients with 1 to 5 metastases (6). There was an overall survival benefit of 13 months (41 *vs* 28) (Hazard Ratio (HR) 0.57, 95% CI 0.3 - 1.1; p= 0.09) in favor of radiotherapy to all sites. Similarly, there was a randomized phase 2 study observation *vs* stereotactic ablative radiation for oligometastatic prostate cancer (ORIOLE) in which 54 patients with recurrent hormone-sensitive oligometastatic PCa were randomly assigned to stereotactic ablative radiotherapy (SABR) or observation in 2:1 ratio (8). At 6 months, disease progression was reported in 19% of patients receiving SABR *versus* 61% of patients undergoing observation (P=.005). The disease progression rate was 11% *vs* 50% (P=.005) and median progression-free survival was not reached *vs* 5.8 months (HR, 0.30; P=.002). Given progress in knowledge and treatments that allow some metastatic patients to be treated with a curative rather than a palliative objective, the concept of oligometastasis is also evolving. The European Society for Radiotherapy and Oncology (ESTRO) and European Organization for Research and Treatment of Cancer (EORTC) consensus seems to relate oligometastases less and less to their number and more to the possibilities of their treatment in terms of technical barriers to the volume and location of metastases (9).

Over the past decade, immunotherapy has revolutionized the treatment of metastatic cancer but has shown only modest efficacy in PCa patients. Nevertheless, recent advances in molecular diagnostics and understanding of immune mechanisms promise to improve the efficacy of immunotherapy in PCa as well. Immunomodulation induced by radiotherapy is a topic of current interest. Indeed, radiotherapy can promote immunogenic cell death and induce the immune response by enhancing antigen cross-presentation and CD8+ cytotoxic T cell response. However, radiation also enhances an immunosuppressive microenvironment by promoting myeloid cells infiltration and macrophage polarization toward an M2-like phenotype, as well as an increase of regulatory T cell subsets involved in the inhibition of naive T cell proliferation and activation (10). Therefore, the combination of radiotherapy and immunotherapy may induce synergistic effects to cure PCa (11). This review aims to highlight the advances in PCa physiopathology and summarize the state-of-the-art knowledge of radiotherapy and immunotherapy in oligo-recurrent PCa.

THE TUMOR IMMUNE MICROENVIRONMENT OF PCA

Induction of immune tolerance is a key process throughout tumor development to metastasis. Basically, tumor antigens, neo or not, must be processed and presented by antigen-presenting cells (APCs) such as dendritic cells (DCs). They then migrate to secondary lymphoid organs to activate specific T lymphocyte (T) cells. Conventional CD8α+ DCs appear to be critical APCs for cross-presentation of neoantigens for tumor rejection by T cells (12). Activation of APCs occurs in coordination with other innate immune cells, including natural killer (NK) cells, natural killer T (NKT) cells and γδ T cells in response to damage-associated molecular patterns (DAMPs).

Immunologically, tumors are classified as hot and cold tumors according to their immune infiltrate. Features of hot tumors include increased T cell and cytotoxic T lymphocyte (cTL) infiltration, primarily due to a high tumor mutational burden (TMB), and increased proteins that activate checkpoint proteins. In contrast, features of cold tumors include exhausted cTL cells in the tumor or their absence at the tumor margins, the presence of tumor-associated macrophages (TAM) polarized to an M2-like phenotype (pro-tumor), a low mutational load and poor antigen presentation. PCa can be considered as an immunologically cold tumor (13).

Cancer progression and response to immunotherapy may be strongly influenced by the tumor microenvironment (TME), including immune cells (14). In PCa, tumor-associated antigens (TAAs) are expressed both in normal and tumor cells, but at higher levels in cancer cells. These TAAs are, for example, prostate-specific antigen (PSA), prostate-specific membrane antigen (PSMA), prostatic acid phosphatase (PAP) or CD155. Nevertheless, no anti-tumor response can be triggered due to the immunosuppressive TME (15). Indeed, a lower density of immune cells has been observed in prostatic adenocarcinomas compared to benign nodular hyperplasia of the prostate (16). Anti-tumor CD8+ T cells are also suppressed by the depletion of arginase and tryptophan from the TME after upregulation of secretion of nitrous oxide synthase and indoleamine 2,3-dioxygenase (IDO) by myeloid-derived suppressor cells (MDSCs) (16), or by the presence of a large amount of regulatory T cells (Tregs) compared to other cancers (17), and other immunosuppressive cells

Abbreviations: APC, antigen-presenting cell; bsAb, bispecific antibodies; BT, brachytherapy; CAR, chimeric antigen receptor; CSF1, colony-stimulating factor 1; CTLA-4, cytotoxic T lymphocyte antigen; cTL, cytotoxic T lymphocyte; DC, dendritic cell; DHT, dihydrotestosterone; EBRT, external beam radiation therapy; EORTC, European Organization for Research and Treatment of Cancer; EMT, epithelial-mesenchymal transition; ESTRO, European Society for Radiotherapy and Oncology; EV, extracellular vesicle; HIF-1, hypoxia-inducible factor 1; HLA, human leukocyte antigen; HR, hazard ratio; ICI, immune checkpoint inhibitors; IFN, interferon; mCRPC, metastatic castration-resistant prostate cancer; MDSC, myeloid-derived suppressor cell; MHC, major histocompatibility complex; miRNA, microRNA; NK, natural killer; NKT, natural killer T; ORR, objective response rate; PAP, prostatic acid phosphatase; PCa, prostate cancer; PD-1, programmed cell death 1; PD-L1/2, programmed cell death-ligand 1/2; POLD1, DNA polymerase delta; POLE, polymerase epsilon; PSA, prostate-specific antigen; PSMA, prostate-specific membrane antigen; SABR, stereotactic ablative radiotherapy; SBRT, Stereotactic body radiation therapy; T, T lymphocyte; TAA, tumor associated antigen; TAM, tumor associated macrophage; TCR, t cell receptor; TEX, tumor exosome; TIL, tumor infiltrating lymphocyte; TMB, tumor mutational burden; TME, tumor microenvironment; T reg, regulatory T cell; TSA, tumor specific antigen; VSV, vesicular stomatitis virus.

such as M2 TAM or neutrophils, both associated with poor survival (18). This immunosuppressive environment is promoted by specific factors such as TGF-β (19) and CXCR2 (20) secreted under the TME. Then, inhibition of CXCR2 may be interesting to improve immunotherapy as tested in a current clinical trial (NCT03473925).

Focus on the Immune Particularities of the Most Common Metastatic Sites in PCa: Bones and Lymph Nodes

Bones represent 90% of the tumor registry in PCa (21) because they are fertile soil for metastases due to the high blood flow in red bone marrow, interactions between tumor cell and stromal cell, and the production of growth factors, angiogenic factors and bone resorbing factors by stromal cells which allow tumor growth (22). The tumor immune microenvironment is essential for the establishment and growth of PCa bone metastases (23). Disseminated tumor cells secrete IL-6, which attracts TAMs contributing to tumor cell proliferation and angiogenesis in bone sites in an *in vivo* mouse model. A significant concentration of TGF-β is also found in bone metastases that induce the polarization of CD4+ helpers into T reg and may explain the lack of efficiency of immunotherapies in metastatic castration-resistant prostate cancer (mCRPC) (24). Thus, targeting these secreted factors at preferential metastasis sites may be a promising target.

With regard to the lymph nodes, PCa cells build a pre-metastatic niche into them, changing their architecture and immune function (25). In fact, an immunosuppressive microenvironment is established. In PCa patients with pelvic lymph nodes, MDSCs, which include monocytes and granulocytes, exhibit immunosuppressive proteins such as programmed cell death-ligand 1/2 (PD-L1/L2) (26). These MDSCs have an immunosuppression activity and impair the proliferation of CD8 + T cells accumulated in pelvic lymph nodes, which express immune checkpoint proteins. The reactivity of anti-tumor T cells may also be altered since the density of antigens presenting DCs is reduced in the paracortical area (25). Tumor-derived extracellular vesicles (EVs) (discussed in more details in the following section) may be involved in establishing a pre-metastatic niche in lymph nodes by modulating T cells (27). Taking together, the TME cells in PCa metastatic sites favors immune escape and tumor growth (28). The use of immunotherapies to treat prostate metastases is promising to remodel the TME.

MECHANISMS OF IMMUNE ESCAPE TO PROMOTE PROSTATE CANCER DEVELOPMENT AND METASTASES

Prostate Tumor Cells Express Few Tumor Antigens

In cancer cells, various mutations, such as single nucleotide mutations, insertions or deletions, and gene fusions, alter the coding amino acid sequences and could generate new immunogenic antigens called neoantigens, specific for the tumor, so-called tumor-specific antigens (TSAs). Some of these mutant peptides may be presented on the surface of tumor cells and recognized by T cells, which could lead to an immune response. Some cancers are more predisposed to mutation than others and accordingly have a high TMB. PCa is associated with a low TMB (29) and is considered a poorly immunogenic cancer, as this lack of neoantigen formation reduces the ability of TILs (Tumor Infiltrated Lymphocytes) to kill or not to kill tumor cells after cross-priming by APCs (30). Nevertheless, TMB increases with age and tumor characteristics such as a higher Gleason score (31), but also due to the lack of DNA mismatch repair proteins (MSH2/6, MLH1 and PMS2) or proofreading/exonuclease domains such as polymerase epsilon (POLE) or DNA polymerase delta (POLD1) (32). Consequently, prostate tumors with high TMB display a stronger anti-tumor lymphocyte infiltration of memory CD4+ T cells, CD8+ T cells and follicular helper cells (18) (**Figure 1**).

Loss of HLA I Expression in Prostate Tumor Cells

Loss of HLA (Human Leukocyte Antigen) class I expression is observed in 34% in primary PCa and 80% in lymph node metastases (33). This leads to impaired cTLs response and tumor escape (34). This loss may be due to i) mutation or deletion of structural genes such as heavy chain gene or β2M (beta-2-microglobulin), ii) post-transcriptional and pre-transcriptional regulation of HLA genes especially by non-coding RNA, iii) post-translational mechanisms of HLA protein such as modification of amino acid residues in the peptide-binding groove impairing peptide binding, iv) signaling mechanisms and stimuli from the TME (35) Conversely, radiation therapy could increase HLA class I molecules for many days in a radiation dose-dependent manner (36).

Prostate Tumor Cells Express Immune Checkpoint Ligands

To escape the anti-tumor immune response, tumor cells increase their expression of immune checkpoint ligands, such as PD-L1. This molecule binds to its receptor, programmed cell death 1 (PD-1), which is expressed by T cells, leading to their anergy. Patients with expression of at least 1% of PD-L1 on tumor cells are associated with shorter metastasis-free survival than those with PD-L1 negative tumors (37). Furthermore, these patients have a fourfold higher risk of developing distant metastases. Another negative regulator of T cells is the cytotoxic T lymphocyte antigen 4 (CTLA-4), which is also upregulated in PCa (38).

Hypoxia and Epithelial-Mesenchymal Transition

In PCa tumors, pO2 measurements, using an Eppendorf pO2 microelectrodes, showed that increased levels of hypoxia are correlated to clinical stage of the disease (39), and the hypoxic prostate/muscle pO2 ratio predicts biochemical failure in patients (40). The hypoxia-inducible factor 1 (HIF-1), a transcription factor regulated by oxygen, is also overexpressed in PCa and metastases (41). Recurrent PCas are associated with increased expression stability and translocation of the androgen receptor which is also upregulated by hypoxia. Thus, tumor cells are more sensitized to the

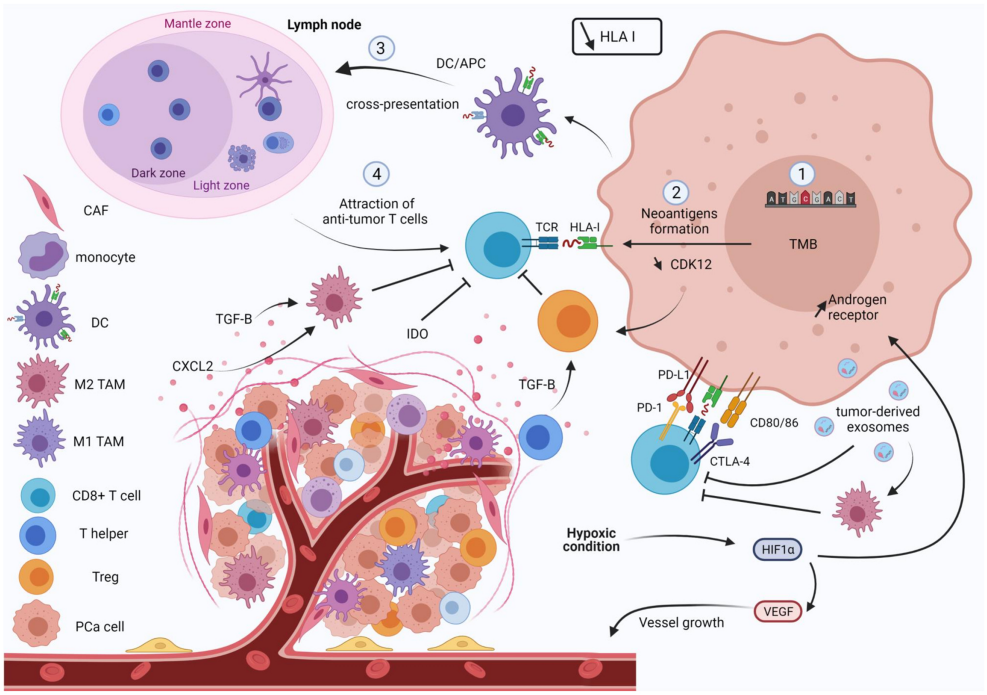

FIGURE 1 | Overview of the physiopathology of prostate cancer. A prostate tumor favors immune escape. Tumor cells harbor a low tumor mutational burden (TMB) and HLA I expression is lost, which decreases the anti-tumor response. Tumor cells also express immune checkpoint inhibitors (PD-L1) such as effector T cells (PD-1 and CTLA-4), leading to exhaustion of cytotoxic T cells. Promotion of immunosuppressive cells such as M2 tumor-associated macrophages or T reg, and suppression of effector T cell activity, are induced by immunosuppressive factors (IDO, CXCL2 and TGFβ). In lymph nodes, expression of PD-L1/L2 by MDSCs establishes a pre-metastatic niche that impairs proliferation of CD8+ T cells. Tumor-derived exosomes are also involved in this immunosuppressive environment by promoting M2 polarization and suppression of CD8+ T cells. Hypoxia molecule HIF-1 is also overexpressed. This induces the expression of the androgen receptor promoting tumor cell growth, notably through remodeling the vasculature. HLA I, human leukocyte antigen; CAF, cancer associated fibroblast; DC, dendritic cell; TAM, tumor-associated macrophage; PCa, prostate cancer.

growth-promoting effect of dihydrotestosterone (DHT) (42). DHT is also implicated in the stabilization of HIF-1a, strengthening the hypoxic response (43). Under hypoxic conditions, HIF-1 induces CD47, overexpressed in many cancers who can bind with SIRPα (signal regulatory protein alpha), an inhibitory receptor which is mostly located on macrophages. The binding of CD47-SIRPα transmits a "don't eat me" signal, which can prevent cancer cells from immune clearance. Subsequently, expression of CD47 allows tumor cells to increase their stemness and escape phagocytosis. This induces tumor cell progression and increased mortality. Thus, the induction of CD47 in hypoxic tumor cells leads to a disruption of macrophage signaling and does not allow phagocytosis of tumor cells (44). In addition, HIF-1 increases Nanog, which leads *via* TGF beta secretion to an increase in T reg and immunosuppressive macrophages and to a decrease in CD8 T lymphocyte infiltration. Inhibition of Nanog in a hypoxic tumor cell results in a decrease in TGF beta, an increase in CD8 T infiltration and a decrease in immunosuppressive cell infiltration (45).

Hypoxia can induce a certain plasticity in tumor cells, with epithelial cells that can acquire a mesenchymal phenotype, a process called epithelial-mesenchymal transition (EMT). Prostatic adenocarcinomas often show partial cell dissociation with destabilized junctions, corresponding to a grade 3 of 4 of the EMT (46). These grades are defined on three criteria: i) state of cell polarization, ii) stade of cell adhesiveness and iii) expression of intermediate filament proteins. EMT can play a part in immune escape, such as loss of cell-cell recognition, as a decrease in e-cadherin causes modulation of the T cells' synapse, a structure needed for an efficient immune response, and leads to an overexpression of the PD-L1 increasing immune tolerance (47). Mesenchymal cells also show a decrease of MHC1 expression but they express different factors promoting the differentiation and recruitment of Treg lymphocytes, the differentiation of DCs into immature DCs, and overall lead to immunosuppression in the tumor (47).

IMMUNOTHERAPY IN PROSTATE CANCER

Immune checkpoint inhibitors (ICIs) are antibodies designed to activate an effective immune response by targeting negative regulators of T cells such as PD-L1, PD-1 or CTLA-4 (48) (**Figure 2**). The use of a CTLA-4-targeted monotherapy, known as ipilimumab, was tested in PCa in an unselected population, but did not result in significant benefit (49). This

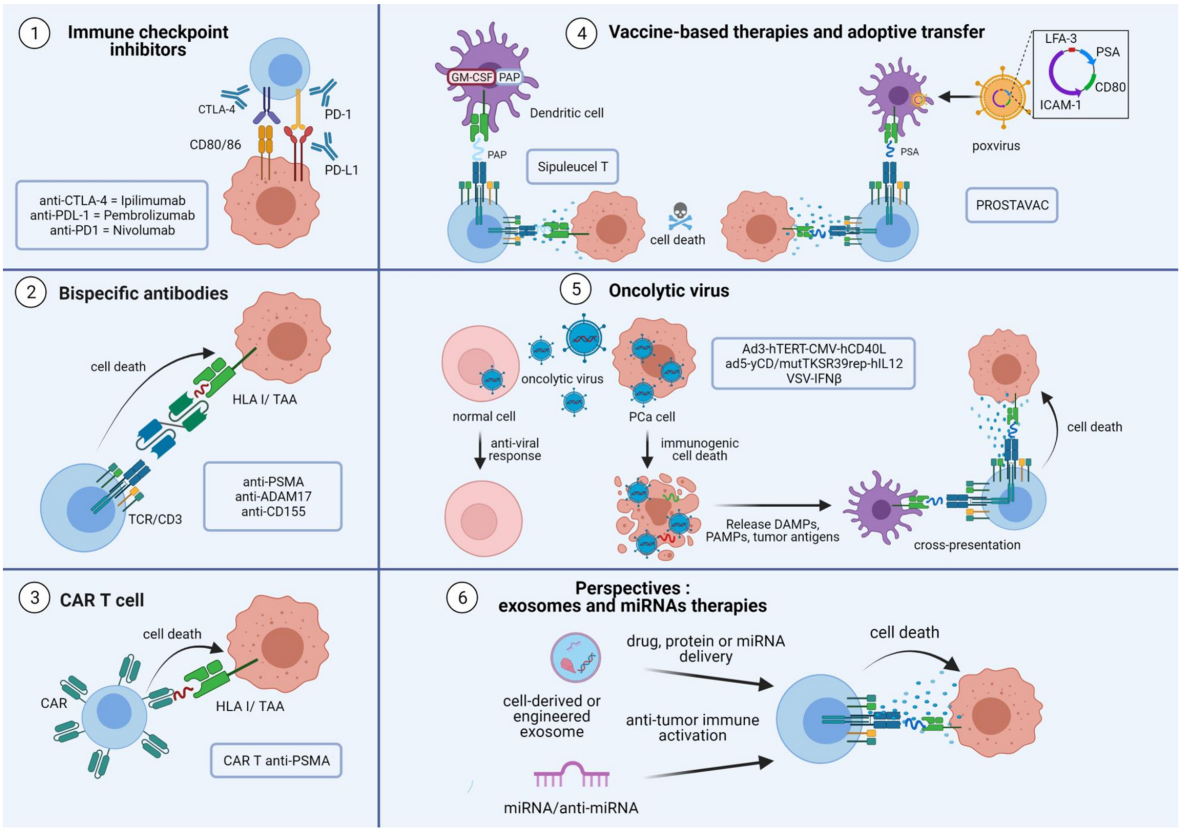

FIGURE 2 | Overview of immunotherapies and perspectives in prostate cancer. The aim of immunotherapies for prostate cancer is to activate tumor-specific CD8+ T cells to induce tumor cell death. The tumor microenvironment induces the expression of immune inhibitory signaling pathways to decrease the cytotoxic CD8+ T cell response. Immune checkpoint inhibitor antibodies directed against PD-L1, PD-1 and CTLA-4 are used to avoid T cell exhaustion. Bispecific antibodies consist of an effective arm that targets the CD3 protein and a target arm that recognizes the tumor antigen. This technology helps CD8+ T cells interact with tumor cells to induce their death. Personalized therapies are also being developed. CD8+ T cells from patients could be manipulated to express a chimeric antigen receptor directed against a specific antigen, notably TAAs. The cells are then expanded and reinjected into the patient, to selectively destroy target cells harboring the surface epitope of interest. Viral and non-viral vectors are used to increase the antigen loading of dendritic cells, leading to an increase in CD8+ cytotoxic T cells in the tumor and response. Enhanced immunotherapy is achieved by the use of oncolytic viruses engineered to replicate only in tumor cells and kill them to induce immunogenic cell death. The use of exosome and microRNA therapies are promising approaches as exosomes and microRNAs are involved in tumor escape. The use of engineered exosomes to deliver proteins, drugs or miRNAs are options to improve anti-tumor response in prostate cancer. TAA, tumor-associated antigen; TCR, T cell receptor; PSMA, prostate specific membrane antigen; CAR, chimeric antigen receptor; PSA, prostate specific antigen; PAP, prostatic acid phosphatase; PCa, prostate cancer; DAMPs, damage-associated molecular patterns; PAMPs, pathogens associated molecular patterns; VSV, vesicular stomatitis virus; MVE, multivesicular endosome.

could be explained by increased expression of PD-1/PD-L1 as a compensatory mechanism that maintains inhibition of the T cell response (50). Alternatively, an anti-PD-1, pembrolizumab, has been commercialized for mCRPC with mismatch repair deficiency and/or microsatellite instability (51), although the relevance of this ICI is still debated. Indeed, the Keynote 19 trial demonstrated that pembrolizumab monotherapy induced antitumor activity in only a small number of mCRPC patients, with an objective response rate (ORR) up to 5% (52). However, in a phase 2 trial (Checkmate 650), double-blockade immunotherapy with nivolumab and ipilimumab showed an ORR of 26% in asymptomatic or minimally symptomatic patients with mCRPC (26). Therefore, determining the subpopulations that might benefit from ICIs' immunotherapy appears essential.

A promising new approach uses bispecific antibodies (bsAb), also known as bispecific T cell engager (BiTE®), to mobilize T cells against tumor cells (53) (**Figure 2**). BsAbs are designed to recognize a TAA with their target arm and to stimulate the T cell receptor (TCR)/CD3 complex with their effector arm (54). Once BsAbs target tumor cells and activate T cells, they induce T cell proliferation and production of cytokines, perforins and granzymes, thereby killing surrounding tumor cells. Various combinations of bispecific conjugates have been tested in PCa. One of the most studied combinations uses PSMA, a specific-prostate antigen whose expression increases with disease progression, and an anti-CD3. Preclinical data demonstrated its efficacy to induce an anti-tumor CD8 T cell response *in vitro, ex vivo* and *in vivo* (55, 56). Several clinical trials with PSMA-targeted T cell engagers (NCT03792841; NCT03577028; NCT03926013) are

currently running, particularly for patients with mCRPC (NCT04104607). Furthermore, other TAAs, such as A-disintegrin and metalloprotease 17 (ADAM17) (57) and CD155 (58), are being evaluated as targets of bsAbs in PCa. Interestingly, such therapy may not need to be personalized for each patient.

Chimeric antigen receptor (CAR) T cells are also an interesting tool to fight PCa (**Figure 2**). These therapies are based on re-engineering patients' T cells to express a TCR directed against a specific tumor antigen. Cells are then expanded and reinjected into the patient to selectively destroy target cells harboring the epitope of interest. Several studies are currently underway with CAR T cells directed specifically against PSMA (NCT04053062; NCT03089203; NCT03873805). Initial results for NCT03089203 demonstrated that adoptive cell transfer of CAR-PSMA-TGFβRdn is safe and feasible in mCRPC patients (59).

Vaccine-based therapies are also being developed to treat PCa (**Figure 2**). In 2010, the Food and Drug Administration approved Sipuleucel-T for the treatment of castration-resistant PCa. Sipuleucel-T is a vaccine based on the transfer of autologous DC to cross-present prostatic acid phosphatase (PAP), a specific prostate antigen, to T cells and active adaptive immune cells (60). Another vaccine therapy evaluated in PCa is PROSTVAC, which uses a genetically engineered poxvirus encoding prostate specific antigen (PSA) to generate a T cell response. It also contained three co-stimulatory molecules: CD80, intercellular adhesion molecule 1 (ICAM-1) and lymphocyte function-associated antigen 3 (LFA-3). However, a phase III study showed no effect on overall survival in mCRPC (61). Combination therapy with a monoclonal antibody directed against PD-L1 and a recombinant vaccine of Avipoxvirus is currently in use (NCT03315871).

A new class of immunotherapy is oncolytic viruses (62, 63) (**Figure 2**). Oncolytic viruses selectively replicate in tumor cells, and induce an immunogenic cell death. The subsequent release of TAAs is thought to trigger an anti-tumor immune response by recruiting DCs and activating T cells. A recent study by Zafar et al. indicated that oncolytic adenoviruses expressing CD40L (Ad3-hTERT-CMV-hCD40L) can effectively stimulate DCs in the immunosuppressive microenvironment of PCa (64). Another genetically engineered oncolytic virus, Ad5-yCD/mutTKSR39rep-hIL12 shows promising effects in preclinical model of PCa through the enhancement of anti-tumor response by cytotoxic immune cells (NK and cTL) (65). In a phase I clinical trial (NCT02555397), improvement in local and metastatic tumor control resulted in significant prolongation of survival.

Extracellular vesicles and microRNA-based therapies represent future perspectives in immunotherapy (66, 67) (**Figure 2**), as they are involved in immunomodulation and tumor progression (68, 69). Exosomes are small extracellular vesicles (50-150nm) formed inside cells (70) and secreted by almost all cell types, including tumor cells. They appear as an interesting tool in cancer immunotherapy due to their low immunogenicity and toxicity (71). However, caution should be taken when targeting exosomes as they are involved in many physiological pathways. They play a role in intercellular communication through a specific interaction between transmembrane proteins of exosomes and receptors on the plasma membrane of recipient cells, and influence physiological and pathological functions in the recipient cell. In PCa, exosomes from cell lines expressing various regulatory proteins such as FAS ligand (FASL) or PD-L1, lead to suppression of T or NK cell responses (19, 72, 73).

Of note, exosomes are naturally enriched with non-coding RNAs such as microRNAs (miRNAs) (74), which are readily transferred to recipient cells (75). miRNAs are a subset of small non-coding RNAs with a length of 19 to 22 nucleotides that regulate gene expression at the post-transcriptional level by translational repression or degradation of the target mRNA. miRNAs included into tumor exosomes (TEX) can participate in tumor immune escape by reducing the CD8+ T cell response (69). Thus, the use of engineered EVs containing miRNA mimic or miRNA antagonists may be a promising therapy to enhance the anti-tumoral response (76–78).

RADIATION THERAPY AND THE IMMUNE MICROENVIRONMENT OF PROSTATE CANCER

Irradiation induces immunogenic cell death leading to the release of tumor antigens, including miRNA patterns (79) or DNA breaks. Radiation therapy also affects the TME, inducing immune cell recruitment and vascular changes (**Figure 3**). Of interest, irradiation of the vasculature may promote infiltration of immune-inflammatory cells [reviewed in (80)]. Conventional 2 Gy dose fractions, a single large dose fraction, or high dose hypofractionated radiotherapy are effective in tumor control. Recent preclinical studies have shown that tumor-resident T cells may be relatively radioresistant and can be amplified to control irradiated tumors (81). The main question remains to determine the dose or fractionation regimen that can transform an immunocompromised tumor into a highly immunogenic one (11). In that regard, stereotactic body radiation therapies (SBRT) can be divided into three categories based on their effects on the immune system or the TME: immunogenic ablative (15-35 Gy fractions), immunomodulatory sub-ablative (8-12Gy), and modulatory low-dose fractions (≈ 2 Gy). Ablative doses lead to profound cell death with concomitant depletion of radioresistant immune suppressor cells in the TME. They may also increase levels of fibrosis and chronic inflammatory/immunosuppressive pathways. However, high ablative fractionation is not considered due to normal tissue tolerance (82). Hypofractionated radiotherapy is considered the most suitable with the goal of immunomodulation, whereas ablative or sub-ablative doses remain more controversial. Preclinical data on fractionation showed that immunomodulatory fractionation of 3 x 8 Gy was more effective than a single ablative dose of 20-30 Gy (83). While modulatory doses (e.g. three x 8 Gy) can produce similar effects to standard fractionation, they resulted in a strong type I interferon (IFN) response (84, 85). On the other hand, low doses of irradiation also have profound effects, leading to remodeling of vessels, reprogramming of macrophages or increased lymphocyte infiltration (86).

Recently, a prospective observational study compared the effects of internal irradiation BT followed by EBRT (15 Gy high-dose rate BT, followed 2 weeks later by 46 Gy in 23

fractions the entire pelvis) with EBRT alone (46 Gy in 23 fractions to the entire pelvis followed by 32 Gy in 16 fractions to the prostate) on immunological cells in PCa patients with Gleason score 9 (87). An enhancement of cTL response was observed in patients receiving BT + EBRT compared to patients receiving EBRT alone, which was associated with IL-2 and granzyme B secretion. In addition, a reduction in CD4+ T cells was observed 3 months after treatment. The authors observed an increase in PD-1 expression by CD4+ and CD8+ cells following radiotherapy. Thus, it might be useful to combine anti-PD-1 checkpoint inhibitors with BT/EBRT to obtain a reliable immunological response.

Effects of Radiation Therapy on Immunogenic Cell Death and Immune Anti-Tumor Response

Radiation therapy increases DNA damage and leads to activation of IFN I response with pro-inflammatory effects and activation of T cells (11). Radiotherapy also increases antigen presentation (**Figure 3**). Indeed, radiotherapy induces immunogenic cell death, which allows the formation of TAA (88). These TAAs are captured by APCs such as DCs and presented to T cells *via* the major histocompatibility complex (MHC)-I complex, with co-stimulatory signals such as CD80 (89, 90). One of these TAA is the oncofetal tumor antigen 5T4, which is increased by irradiation. This leads to an enhancement of phagocytosis of irradiated tumor cells by DC and thus to an increase in cross-presentation of the 5T4 antigen to CD8+ T cells (91). The number of tumor-specific T cells is increased by radiotherapy in patients (92). In the ORIOLE study, significant clonotypic expansion after SABR was detected by sequencing the T cell receptor (8). A study by Berstein et al. investigated the effects of single dose EBRT on the modulation of costimulatory and co-inhibitory T cell molecules in PCa cell lines (93). The authors observed that irradiation increased the expression of OX40L (OX40 ligand), 4-1BBL (4-1BB ligand) and ICOSL (inducible costimulator-ligand), some of the T cell costimulatory molecules. Furthermore, 72h after irradiation, a decrease in PD-L1 and CTLA-4 expression were observed, as well as an increase in CD8+ T cell activity after their interaction

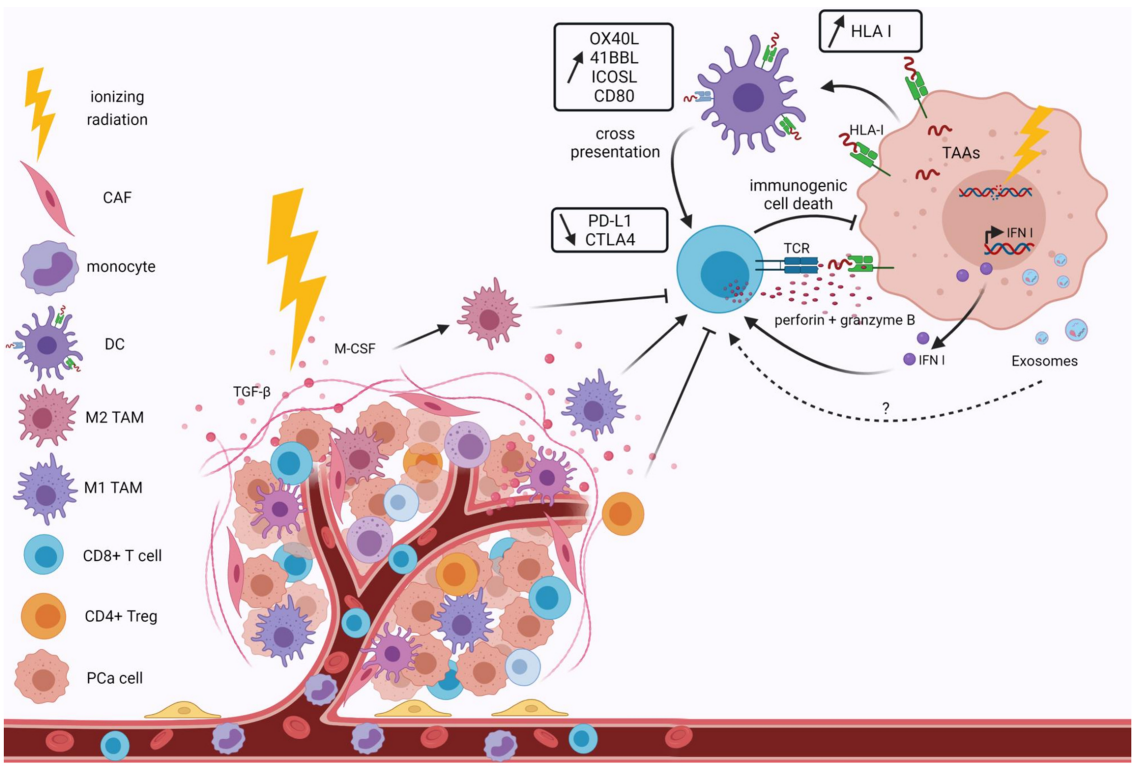

FIGURE 3 | Effects of ionizing radiation on the tumor immune microenvironment. Ionizing radiation modifies the tumor immune microenvironment by recruiting anti-tumor cells. Irradiation remodels the irradiated vasculature to enhance lymphocyte infiltration at the tumor site and macrophage polarization. Irradiation induces DNA damage, leading to the release of tumor-associated antigens, enhanced HLA I expression and type I IFN. An increase in T cell costimulatory molecules and a decrease in inhibitory proteins are also observed after irradiation. This results in immunogenic cell death of tumor cells. Immunosuppressive cells, such as M2 TAM or T reg, are also induced by irradiation due to their more radioresistant phenotypes. They induce suppression of the CD8+ cytotoxic T cell response. All these effects are dependent on the doses and fractionation of irradiation. Extracellular vesicle secretions and contents, notably in miRNAs, are affected by ionizing radiation. Exosomes are involved in tumor immune escape, but the irradiation effects on the promotion of the anti-tumor immune microenvironment of PCa through Evs remain to be addressed. HLA I, human leukocyte antigen; TAA, tumor-associated antigen; IFN I, Type I interferon; TCR, T cell receptor; CAF, cancer associated fibroblast; DC, dendritic cell; TAM, tumor-associated macrophage; PCa, prostate cancer.

with tumor cells. Thus, irradiation leads to an increase in the expression of co-stimulatory molecules and a decrease of co-inhibitory molecules.

Irradiation Enhances the Immunosuppressive Environment

After irradiation, an increased amount of immunosuppressive cells (TAM, myeloid derived suppressor cells and Tregs) is also found among the TME, as these cells are more radioresistant than the other immune subtypes (**Figure 3**). A recent study by Lin et al. showed in an allograft PCa model that high-dose radiotherapy induces both immunosuppressive and anti-tumor responses against prostate tumors (94). They observed an increase in MDSCs, followed by an increase in CD8+ TILs. Nevertheless, the response of CD8+ T cells is blocked by Treg. In an *in vivo* model, a systemic increase of MDSCs is observed after irradiation of primary tumor sites (95). The authors showed that the cytokine macrophage colony-stimulating factor 1 (CSF1), also known as M-CSF, increases in irradiated tumors, and in the serum of PCa patients after radiotherapy. This cytokine is involved in M2-like polarization. Therefore, the use of a CFS1 inhibitor in combination with radiotherapy might be interesting. Radiation doses also modulate macrophage phenotypes. Indeed, TAMs can be directed either towards a classical active M1 phenotype by doses below 2 Gy or towards an M2 phenotype with doses higher than 2 Gy. Hypofractionated radiotherapy causes an increase in bone marrow-derived suppressor cells, which are responsible for immune escape from pathogens and tumor malignancy by inducing NK cell and T cell anergy and blocking DC maturation (96). This is problematic because DCs are the main APCs that trigger a T cell response and regulate innate and adaptive immunity. T reg infiltration is also increased in tumors after stereotactic radiotherapy, which correlates with relapse and worsens survival by inhibiting effector T cells, B cells and NK cells (97). Low doses of radiotherapy increase IL-2 and IFN-gamma production, which promotes NK cytotoxicity, while high doses of radiation decrease IL-12 secretion by DCs, which impairs NK cell function. High doses also induce the decrease of Ki67 expression, a proliferative marker, in NK cells within the tumor (96). Finally, tumor-associated neutrophils are certainly a first line of defense against infection and inflammation, but also have pro-tumor effects. Radiation-induced signaling *via* TGF beta leads to the recruitment of these tumor-associated neutrophils, inducing NK anergy.

The interaction between the immune system and the cancer cells is weak and finding the optimal dose and fractionation of radiotherapy to achieve immunogenic results depends on the unique immune properties of each tumor and its TME (11). Thus, the combination of immunotherapy and radiotherapy may be a promising approach to increase the anti-tumor response and avoid immune escape.

HORMONE THERAPY AND RADIOTHERAPY

In the 1940s, prostate cancers (PCa) were found to have a dependence on androgens. This discovery led to the approach to treat PCa using androgen deprivation therapy (ADT) (98). Moreover, the addition of RT to ADT appears to improve outcomes by enhancing both local and distant disease control (99). Mechanisms of synergy are partially understood, but are likely mediated by the androgen receptor (AR) (100). The AR is a nuclear hormone receptor activated by engagement of its ligands, testosterone and dihydrotestosterone (DHT). Ligand binding exposes the AR in the nucleus, the receptor dimerizes and binds to androgen response elements in the promoter regions of target genes like the PSA (101). Additional co-regulatory proteins are recruited to allow transcription, leading to downstream cellular responses such as growth and survival (102). Thus, androgen ablation therapies repress transcription of AR target genes, which causes activation of tumor cell apoptosis and the eradication of most of the androgen-dependent cancer cells (103) Thus, inhibiting the tumor cell's ability to repair double-stranded DNA damage by ADT can act as a "radiosensitizer" (104). Combined treatment also induces permanent cell cycle arrest or apoptosis (105). Also, ADT reduces intraprostatic hypoxia which is an important risk factor for poor locoregional disease control and biochemical failure after RT (106, 107).

Finally, enhanced immune responses have also been reported after the association between ADT and RT (108). In addition, change has been also observed in ADT-treated mice CRPC following RT with more TILs associated and an attenuated MDSC recruitment (109). In fact, RT promotes T cell priming by the release of tumor antigens and pro-inflammatory soluble mediators. On the other hand, ADT promotes lymphopoiesis, immune cell trafficking and tumor infiltration (110). Associating immunotherapy to this combination may enhance these processes. Also, there is the question about the precisely timing of immune modulation and depends on many factors, such as the type of ADT, the RT strategy used as a drug (11). In a clinical report, ADT promoted strong adaptive anti-tumor T- and B-cell responses; however, peripheral TH1 and TH17 effector memory subsets decreased after 2 years of treatment (111).

HORMONE THERAPY AND IMMUNOTHERAPY IN PROSTATE CANCER

Both preclinical and clinical data showed that androgen-depriving therapy (ADT) synergizes with prostate cancer radiotherapy (100, 112). The impact of testosterone on tumor immune response is ambiguous (113). On the one hand, hormone-naive prostate cancer may respond better to immunotherapy than castration-resistant prostate cancer. In mice, orchiectomy synergizes with immunotherapy, whereas androgen receptor (AR) antagonists suppress the effects of immunotherapy by impairing the adaptive immune responses through interference with initial T cell priming (114). On the other hand, ADT induces T cell infiltration of the prostate (115). Neoadjuvant ADT promotes immune infiltration with proinflammatory effects, but the anti-tumor cells (CD8+ T) are

counterbalanced by local pro-tumor cells (TAMs and T reg) (116). ADT also does not increase or diminish PDL1 expression (117). Following ADT and vaccination, prostate cancer-specific T cells expand and develop effector functions (118), suggesting that neoadjuvant ADT may increase the efficacy of immunotherapy. Indeed, the androgen receptor antagonist, enzalutamide, has been tested in phase 2 in combination with immunotherapy and has shown interesting results with a 20% objective response rate (ORR) in patients with mCRPC treated with abiraterone naive chemotherapy (119).

Association of Immunotherapy and Radiation Therapy in Prostate Cancer

In preclinical data, high dose rate brachytherapy (HDBRT) induced a conversion of 80% of cold prostate tumors into intermediate or warm tumors (120). An increase in survival was also observed in a mouse model of CRPC treated with radiotherapy and either anti PD-1 or anti PD-L1 compared to immunotherapy alone (121, 122) (**Table 1**). In a preclinical model of metastatic PCa, combined irradiation of metastases and anti-CTLA-4 efficiently induced response of T cells and improved both local anti-tumor effects and also distant response, suggesting an abscopal effect (125). Other immunotherapy strategies have shown interesting results when combined with radiotherapy in PCa. A recent preclinical study (*in vitro* and *in vivo* models) used radiotherapy to enhance the activity of a vesicular stomatitis virus (VSV) engineered to express IFNβ (126). IFNβ was expressed by the VSV to reduce viral mediated toxicity to non-transformed cells. Amplification of tumor killing by VSV-IFNβ was observed with the combination of radiotherapy. Also, an increase in adaptive anti-tumor response occurred with the rise in CD8+ T cell numbers.

Despite encouraging preclinical experiments, clinical trials in patients combining immunotherapy and radiotherapy failed to improve survival in unselected patients (**Table 2**). Early phase clinical trials showed that the combination of any kind of immunotherapy with radiotherapy to the prostate or to metastases was safe. In some patients, the combination showed encouraging results: increased CD8+ T-cell response to prostate antigens (127, 129), and high complete response rates (131). In this sense a benefit was found in phase I in 3 patients, and good tolerance with HDRBT, androgen-deprivation therapy and nivolumab (127). Local injection of vaccine to the prostate was specifically able to increase PSA-specific T cells (130, 132) but disappointingly did not increase tumor responses in a randomized phase 2 trial (133). Similarly, CTLA-4 blockade using ipilimumab combined with irradiation induced very interesting biochemical responses (134) but failed to improve survival (135). In metastatic castration- and docetaxel-resistant PCa, the CA184-043 phase 3 study comparing ipilimumab *versus* placebo after palliative bone irradiation (8 Gy in 1 fraction) (135) failed to meet its primary endpoint and did not show improvement in overall survival. However, an updated analysis of the study with an additional 2.4 years of follow-up showed that ipilimumab potentially conferred a survival benefit at later stages (136), suggesting that a small subset of patients benefited significantly from ipilimumab. A second study (CA184-095) in patients with mCRPC naïve to chemotherapy showed that ipilimumab was associated with longer median progression-free survival, but unfortunately no survival benefit was shown (49). This negative result may suggest that there is a small subset of patients with mCRPC who are sensitive to ipilimumab, but only after treatment with radiation therapy. Based on preclinical work, these negative results could be interpreted in different ways: irradiation dose too low, too long time between SBRT and ipilimumab, and too few SBRT fractions (137). Interestingly, establishing antitumor immunity against melanoma is enhanced when elimination of regulatory T cells by anti-CTLA-4 antibody precedes radiotherapy (82).

TABLE 1 | Radiotherapy and immunotherapy in mouse models of prostate cancer: Effect on tumor volume and survival.

Authors, years	Cancer model	Therapeutic protocol	Efficacy parameters	Outcomes
Philippou BJ Cancer 2020 (116)	Murine PCa	3 x 5 Gy with or without anti PDL1	Tumor growth delay	No benefit to add anti PDL1 in tumor delay Rt increase CD8(+) T-cell, dendritic cell but also TAM and regulatory T-cell genes, upregulate PD-1/ PDL1,
Dudzinski J immunother Cancer 2019 (92)	Murine castration resistant PCa	Anti PD1 or Anti PDL1 with or without 20 Gy/2 fractions	Overall survival Abscopal response	Anti-PD-1 or anti-PD-L1 + Rt improved survival Anti PD L1 *vs* Anti PD-L1+RT: 13 days *vs* 30 days (p=0.0003) Anti PD1 *vs* Anti PD1+RT: 21 days *vs* 36 Days(p=0.0009) *Anti CD8 antibody blocked the survival effect*
Hannan Cancer Immunol Immunother 2012 (123)	Murine PCa	RT 10 Gy + *Lm* based PSA vaccine ADXS31-142	Tumor growth delay	Benefit of combination therapy in tumor growth delay (p<0.0001)
Guo Mol Cancer Ther 2012 (124)	Murine PCa	RT 30 Gy/10 Gy fractions during 3 consecutive days + Intratumoral modified dendritic cells (DC)	Tumor growth delay	Benefit of the combination in both tumor growth delay and metastases

Lm, Listeria monocytogenes; PCa, prostate cancer; RT, radiation therapy.

TABLE 2 | Clinical studies reporting radiotherapy and immunotherapy in patients with prostate cancer.

Authors, years	Cancer model	Design & pts	Therapeutic protocol	Efficacy parameters	Outcomes
Finkelstein Immunotherapy 2012 (119)	Localized prostate cancer	Non-randomized open label pilot study: 5 pts	EBRT + ADT 28 months +DC injections after fractions 5, 15 and 25	Assessment of immune reaction on biopsy and blood analysis	Increased CD8+ T-cell response
Rodriguez-Ruiz Ann Oncol 2018 (121)	Advanced Cancer	Two cohort pilot study phase I:17 pts, 2 mCRPC	Cyclophosphamide + intradermal monocyte derived dendritic cells (preload with Hiltonol, TNF Alpha and IFN alpha)+ Hiltonol + SABR 24 Gy/3 fractions	Safety	Safe combination; DC local reaction; abscopal effect in one pt
Lilleby, Cancer Immunol Immunother 2017 (122)	Metastatic hormone naive prostate cancer	Dose escalation trial; phase I/IIa: 22 pts, 21 patients received RT	hTERT vaccine UV1 + GM -CSF + EBRT	Safety PSA	Pruritus G1 CR 10 pts (45%) PSA decline 14 pts (64%)
Slovin Ann Oncol 2013 (127)	mCRPC with disease progression after interruption of ADT having received less than 1 chemotherapy	Non-randomized open label phase I/II: 50 pts	Ipilimumab monotherapy or Ipilimumab + EBRT	PSA evolution	PSA CR: 1 pt PSA decline >50%: 8 pts Stable disease: 6 pts
Yuan Prostate Cancer Prostatic Dis 2020 (120)	Localized prostate cancer	Open label single group assignment Phase I/II: 6 pts	ADT+ nivolumab and brachytherapy HDR 11.5 Gy x 2 applications + EBRT 40-50Gy 1.8-2Gy fractions	Safety PFS interval biopsy	G3 toxicity: 1 pt Response: 3 pts Tissue increase in CD8+ and FOXP3 +/CD4+ T cells increased circulating CD4+ effector T cells in responders
Twardowski Cancer Treat Res commun 2019 (128)	mCRPC	Randomized phase II: 51 pts	Sipuleucel T alone or sipuleucel T after EBRT to metastatic site 30 Gy/3Gy fractions	Systemic immune response	RT did not enhance humoral or cellular response
Gulley Clin Cancer Res 2005 (125)	Localized prostate cancer	Phase II: 30 pts	EBRT 70 Gy with or without vaccine (rV-PSA +rV B7.1) + GM CSF + IL-2	Safety	Safe combination; PSA-specific cellular immune response to vaccine
Lechleider Clin Cancer Res (126)	Localized prostate cancer	Phase II: 36 pts	EBRT + priming dose of vaccinia PSA and vaccinia B7.1 +GM CSF + IL-2 post vaccination	Safety	Safe combination; increase in PSA-specific T cells
Kamrava Prostate Cancer Prostatic Dis 2012 (129)	Localized prostate cancer	Randomized phase II: 36 pts	EBRT + ADT with or without vaccine (two recombinant vectors expressing PSA or human T cell costimulatory molecule B7.1)+Il2	PSA	No difference in PSA control with vaccine *versus* standard treatment
Fizazi, Eur Urol 2020 (130)	mCRPC in progression after docetaxel	Randomized phase III: 799 pts	8 Gy on bone metastases + ipilimumab or placebo	Overall Survival rate	RT + Ipilimumab *versus* Placebo OS rate: 2 yr: 25.2% *vs* 16.6% 3 yr: 15.3% *vs* 7.9% 4 yr: 10.1% *vs* 3.3% 5 yr: 7.9% *vs* 2.7%

Pts, patients; G, Grade; CR, Complete response; yr, year; mCRPC, metastatic castration-resistant prostate; EBRT, external beam radiation therapy; SABR, stereotactic ablative radiation therapy.

It is now recommended that immunomodulatory drugs be started before high dose fractional SBRT for future radioimmunotherapy strategies.

Patient selection might be the key for successful combinations. In patients with early-stage PCa, several studies have evaluated PD-1/PD-L1 as a prognostic marker. High expression of PD-L1 correlated with significantly shorter biochemical recurrence-free survival regardless of tumor stage, PSA, Gleason score and surgical margins (138). Likewise, methylation of PD-1 (123) and PD-L1 (124) promoters has been shown to independently predict biochemical progression-free survival in two independent cohorts. In another cohort of patients receiving salvage radiotherapy after a biochemical relapse, T cells infiltrating the PD-1 expressing tumor predicted relapse (128). A recent study showed that up to 25% of cases of localized PCa express PD-L1, which is correlated with increased density of $CD8^+$ T cells and *RB1* and *BRCA2* losses, and deletions of *CHD1* (139), suggesting that a subset of localized PCa is able to stimulate immune responses. **Table 3** summarizes ongoing clinical studies in both localized and metastatic PCa populations. Several studies combine anti PD-1/PD-L1 inhibitors with irradiation, mostly in unselected metastatic patients. Future studies combining immune checkpoint inhibitors and radiotherapy should therefore probably focus on biomarker-selected, especially immune-related and DNA repair gene-deficient, subpopulations of PCa patients.

Abscopal Effect in Prostate Cancer

The abscopal effect is a rare phenomenon commonly defined by the observation of an objective response at distance from the treated tumor site. Since its initial description in 1953 by Dr. RJ Mole (140) only 46 cases of abscopal responses have been reported until 2016 (141), although many studies have been performed to reproduce this phenomenon with disappointing results. Abscopal response remains one of the most active areas of research in oncology (142).

In a mouse model of castration resistant prostate cancer, an abscopal effect was observed after combining radiotherapy with an anti-PD-1 or an anti-PD-L1 antibodies (121). The authors observed an increase survival and a reduction in tumor graft growth after combining therapies compared with immunotherapy alone. An abscopal response is also observed in clinical trials (143). One patient with mCRPC showed a reduction in non-irradiated metastases after the combination of SABR and DC vaccine. Increased infiltration of CD3+ and CD8+ T cells was also observed.

The combination of radiotherapy with immunotherapy may enhanced frequency of the abscopal response. However, few studies have reported this effect. Therefore, further investigations need to be conducted on the optimal dose/fractionation of RT and the optimal schedule for the administration of RT with immunotherapy elicit the best abscopal response. These studies need to be addressed in future preclinical and clinical trials.

CONCLUSION

There is growing evidence that combination of immunotherapy and radiotherapy is a promising strategy to achieve overall survival benefits for patients. Radiation therapy of the primary tumor and/or metastases in combination with immunotherapy increases overall survival in preclinical models of prostate cancer. However, despite clinical evidence of increased immune response, clinical studies have failed to show improved survival

TABLE 3 | Ongoing radiation therapy and immunotherapy in prostate cancer.

Study Number	Study	Number of Patients	Primary outcome
NCT04569461	Trimodality Approach to Unfavorable Localized Prostate Cancer: a Prospective Trial of Neoadjuvant Pembrolizumab, ADT, and Prostate SBRT Followed by Radical Prostatectomy	39	Percentage of subjects who achieve biochemical progression-free survival (BPFS) at 24 months (2 years)
NCT04262154	SAABR: Single Arm Phase II Study of Abiraterone + Atezolizumab + GnRH Analog and Stereotactic Body Radiotherapy (SBRT) to the Prostate in Men with Newly Diagnosed Hormone-sensitive Metastatic Prostate Cancer	44	Failure-free rate at 2 years
NCT03795207	A Randomized Phase II Trial of Stereotactic Body Radiation Therapy (SBRT) With or Without Durvalumab (MEDI4736) in Oligometastatic Recurrent Hormone Sensitive Prostate Cancer Patients	96	Two-year progression-free survival
ACTRN 12619000097145	A phase II, open-label study of durvalumab in combination with stereotactic body radiotherapy in androgen-intact patients with oligometastatic prostate cancer.	30	Freedom from biochemical failure and toxicity
NCT03649841	Radiation Enhancement of Local and Systemic Anti-Prostate Cancer Immune Responses	30	Percent change in peripheral blood effector T-cells (CCR7-/CD45RO)
NCT03543189	Combination of Nivolumab Immunotherapy with Radiation Therapy and Androgen Deprivation Therapy in the Management of Gleason Group 5 Prostate Cancer	34	Phase 1: Safety Run In - Rate of Dose Limiting Toxicity (CTCAE V5.0)/Phase II: Relapse Free Survival Rate
NCT03007732	Phase II Trial Pembrolizumab or Pembrolizumab in Combination with Intratumoral SD-101 Therapy in Patients With Hormone-Naïve Oligometastatic Prostate Cancer Receiving Stereotactic Body Radiation Therapy and Intermittent Androgen Deprivation Therapy	42	Change Rate of prostate-specific antigen (PSA) < nadir + 2 ng/mL from first day of treatment to 15 months (Cohort 2)

ADT, Androgen deprivation therapy; DC, dendritic cells; EBRT, external beam radiotherapy; mCRPC, metastatic castration-resistant prostate cancer.

following combined immunotherapy and radiotherapy. It appears essential to better understand the mechanisms of metastases and notably the communication between tumor cells and immune cells. These may open up the development of new therapeutic approaches.

AUTHOR CONTRIBUTIONS

SS initiated the study. LO and ML performed the scientific literature search and wrote the manuscript. LO designed the tables. ML designed the figures. DF, VP and SS supervised, helped to revise and edit the manuscript. All authors contributed to the article and approved the submitted version.

FUNDING

ML was supported by a regional grant (EpiSAVMEN), and by Ms. Suzanne Saulnier. ML and DF were recipients of grant "Ligue contre le Cancer, comités 16, 22, 29, 35, 44, 49 and 56". ML and DF were also recipients of "Cancéropôle Grand Ouest AO Structurant ExomiR". SS and VP were recipients of grant "Ligue contre le cancer", transports Loizeau, De Graet consulting, Astra- Zeneca and Ms. Suzanne Saulnier. This study received funding from Astra Zeneca. The funder was not involved in the study design, collection, analysis, interpretation of data, the writing of this article or the decision to submit it for publication. LO was supported by an institutional grant from CHRU Brest. The POSTCARD F-GETUG P13 study received funding from Astra Zeneca.

REFERENCES

1. Bray F, Ferlay J, Soerjomataram I, Siegel RL, Torre LA, Jemal A. Global Cancer Statistics 2018: GLOBOCAN Estimates of Incidence and Mortality Worldwide for 36 Cancers in 185 Countries. *CA Cancer J Clin* (2018) 68(6):394–424. doi: 10.3322/caac.21492
2. Sartor O, de Bono JS. Metastatic Prostate Cancer. *N Engl J Med* (2018) 378 (7):645–57. doi: 10.1056/NEJMra1701695
3. Gundem G, Van Loo P, Kremeyer B, Alexandrov LB, Tubio JMC, Papaemmanuil E, et al. The Evolutionary History of Lethal Metastatic Prostate Cancer. *Nature* (2015) 520(7547):353–7. doi: 10.1038/nature14347
4. Hellman S, Weichselbaum RR. Oligometastases. *J Clin Oncol Off J Am Soc Clin Oncol* (1995) 13(1):8–10. doi: 10.1200/JCO.1995.13.1.8
5. Lievens Y, Guckenberger M, Gomez D, Hoyer M, Iyengar P, Kindts I, et al. Defining Oligometastatic Disease From a Radiation Oncology Perspective: An ESTRO-ASTRO Consensus Document. *Radiother Oncol J Eur Soc Ther Radiol Oncol* (2020) 148:157–66. doi: 10.1016/j.radonc.2020.04.003
6. Palma DA, Olson R, Harrow S, Gaede S, Louie AV, Haasbeek C, et al. Stereotactic Ablative Radiotherapy *Versus* Standard of Care Palliative Treatment in Patients With Oligometastatic Cancers (SABR-COMET): A Randomised, Phase 2, Open-Label Trial. *Lancet Lond Engl* (2019) 393 (10185):2051–8. doi: 10.1016/S0140-6736(18)32487-5
7. Ost P, Reynders D, Decaestecker K, Fonteyne V, Lumen N, De Bruycker A, et al. Surveillance or Metastasis-Directed Therapy for Oligometastatic Prostate Cancer Recurrence: A Prospective, Randomized, Multicenter Phase II Trial. *J Clin Oncol Off J Am Soc Clin Oncol* (2018) 36(5):446–53. doi: 10.1200/JCO.2017.75.4853
8. Phillips R, Shi WY, Deek M, Radwan N, Lim SJ, Antonarakis ES, et al. Outcomes of Observation *vs* Stereotactic Ablative Radiation for Oligometastatic Prostate Cancer: The ORIOLE Phase 2 Randomized Clinical Trial. *JAMA Oncol* (2020) 6(5):650–9. doi: 10.1001/jamaoncol.2020.0147
9. Guckenberger M, Lievens Y, Bouma AB, Collette L, Dekker A, deSouza NM, et al. Characterisation and Classification of Oligometastatic Disease: A European Society for Radiotherapy and Oncology and European Organisation for Research and Treatment of Cancer Consensus Recommendation. *Lancet Oncol* (2020) 21(1):e18–28. doi: 10.1016/S1470-2045(19)30718-1
10. Venkatachalam S, McFarland TR, Agarwal N, Swami U. Immune Checkpoint Inhibitors in Prostate Cancer. *Cancers* (2021) 13(9):2187. doi: 10.3390/cancers13092187
11. Demaria S, Guha C, Schoenfeld J, Morris Z, Monjazeb A, Sikora A, et al. Radiation Dose and Fraction in Immunotherapy: One-Size Regimen Does Not Fit All Settings, So How Does One Choose? *J Immunother Cancer* (2021) 9(4):e002038. doi: 10.1136/jitc-2020-002038
12. Hildner K, Edelson BT, Purtha WE, Diamond M, Matsushita H, Kohyama M, et al. Batf3 Deficiency Reveals a Critical Role for CD8alpha+ Dendritic Cells in Cytotoxic T Cell Immunity. *Science* (2008) 322(5904):1097–100. doi: 10.1126/science.1164206
13. Galon J, Bruni D. Approaches to Treat Immune Hot, Altered and Cold Tumours With Combination Immunotherapies. *Nat Rev Drug Discov* (2019) 18(3):197–218. doi: 10.1038/s41573-018-0007-y
14. Gasser S, Lim LHK, Cheung FSG. The Role of the Tumour Microenvironment in Immunotherapy. *Endocr Relat Cancer* (2017) 24 (12):T283–95. doi: 10.1530/ERC-17-0146
15. Westdorp H, Sköld AE, Snijer BA, Franik S, Mulder SF, Major PP, et al. Immunotherapy for Prostate Cancer: Lessons From Responses to Tumor-Associated Antigens. *Front Immunol* (2014) 5:191. doi: 10.3389/fimmu.2014.00191
16. Stultz J, Fong L. How to Turn Up the Heat on the Cold Immune Microenvironment of Metastatic Prostate Cancer. *Prostate Cancer Prostatic Dis* (2021) 5:1–21. doi: 10.1038/s41391-021-00340-5
17. Kiniwa Y, Miyahara Y, Wang HY, Peng W, Peng G, Wheeler TM, et al. CD8+ Foxp3+ Regulatory T Cells Mediate Immunosuppression in Prostate Cancer. *Clin Cancer Res* (2007) 13(23):6947–58. doi: 10.1158/1078-0432.CCR-07-0842
18. Wu Z, Chen H, Luo W, Zhang H, Li G, Zeng F, et al. The Landscape of Immune Cells Infiltrating in Prostate Cancer. *Front Oncol* (2020) 10:517637. doi: 10.3389/fonc.2020.517637
19. Lundholm M, Hägglöf C, Wikberg ML, Stattin P, Egevad L, Bergh A, et al. Secreted Factors From Colorectal and Prostate Cancer Cells Skew the Immune Response in Opposite Directions. *Sci Rep* (2015) 5:15651. doi: 10.1038/srep15651
20. Di Mitri D, Mirenda M, Vasilevska J, Calcinotto A, Delaleu N, Revandkar A, et al. Re-Education of Tumor-Associated Macrophages by CXCR2 Blockade Drives Senescence and Tumor Inhibition in Advanced Prostate Cancer. *Cell Rep* (2019) 28(8):2156–2168.e5. doi: 10.1016/j.celrep.2019.07.068
21. Hess KR, Varadhachary GR, Taylor SH, Wei W, Raber MN, Lenzi R, et al. Metastatic Patterns in Adenocarcinoma. *Cancer* (2006) 106(7):1624–33. doi: 10.1002/cncr.21778
22. Xiang L, Gilkes DM. The Contribution of the Immune System in Bone Metastasis Pathogenesis. *Int J Mol Sci* (2019) 20(4):999. doi: 10.3390/ijms20040999
23. Kim SW, Kim JS, Papadopoulos J, Choi HJ, He J, Maya M, et al. Consistent Interactions Between Tumor Cell IL-6 and Macrophage TNF-α Enhance the Growth of Human Prostate Cancer Cells in the Bone of Nude Mouse. *Int Immunopharmacol* (2011) 11(7):862–72. doi: 10.1016/j.intimp.2011.01.004
24. Jiao S, Subudhi SK, Aparicio A, Ge Z, Guan B, Miura Y, et al. Differences in Tumor Microenvironment Dictate T Helper Lineage Polarization and Response to Immune Checkpoint Therapy. *Cell* (2019) 179(5):1177–1190.e13. doi: 10.1016/j.cell.2019.10.029
25. Sleeman JP. The Lymph Node Pre-Metastatic Niche. *J Mol Med Berl Ger* (2015) 93(11):1173–84. doi: 10.1007/s00109-015-1351-6
26. Sharma V, Dong H, Kwon E, Karnes RJ. Positive Pelvic Lymph Nodes in Prostate Cancer Harbor Immune Suppressor Cells To Impair Tumor-Reactive T Cells. *Eur Urol Focus* (2018) 4(1):75–9. doi: 10.1016/j.euf.2016.09.003
27. Chen S, Zhu G, Yang Y, Wang F, Xiao Y-T, Zhang N, et al. Single-Cell Analysis Reveals Transcriptomic Remodellings in Distinct Cell Types That Contribute to Human Prostate Cancer Progression. *Nat Cell Biol* (2021) 23 (1):87–98. doi: 10.1038/s41556-020-00613-6

28. Klusa D, Lohaus F, Furesi G, Rauner M, Benešová M, Krause M, et al. Metastatic Spread in Prostate Cancer Patients Influencing Radiotherapy Response. *Front Oncol* (2021) 10:627379. doi: 10.3389/fonc.2020.627379/full
29. Lawrence MS, Stojanov P, Polak P, Kryukov GV, Cibulskis K, Sivachenko A, et al. Mutational Heterogeneity in Cancer and the Search for New Cancer-Associated Genes. *Nature* (2013) 499(7457):214–8. doi: 10.1038/nature12213
30. Coulie PG, Van den Eynde BJ, van der Bruggen P, Boon T. Tumour Antigens Recognized by T Lymphocytes: At the Core of Cancer Immunotherapy. *Nat Rev Cancer* (2014) 14(2):135–46. doi: 10.1038/nrc3670
31. Ryan MJ, Bose R. Genomic Alteration Burden in Advanced Prostate Cancer and Therapeutic Implications. *Front Oncol* (2019) 9:1287. doi: 10.3389/fonc.2019.01287
32. Salem ME, Bodor JN, Puccini A, Xiu J, Goldberg RM, Grothey A, et al. Relationship Between MLH1, PMS2, MSH2 and MSH6 Gene-Specific Alterations and Tumor Mutational Burden in 1057 Microsatellite Instability-High Solid Tumors. *Int J Cancer* (2020) 147(10):2948–56. doi: 10.1002/ijc.33115
33. Blades RA, Keating PJ, McWilliam LJ, George NJ, Stern PL. Loss of HLA Class I Expression in Prostate Cancer: Implications for Immunotherapy. *Urology* (1995) 46(5):681–6; discussion 686–687. doi: 10.1016/S0090-4295(99)80301-X
34. Schrörs B, Lübcke S, Lennerz V, Fatho M, Bicker A, Wölfel C, et al. HLA Class I Loss in Metachronous Metastases Prevents Continuous T Cell Recognition of Mutated Neoantigens in a Human Melanoma Model. *Oncotarget* (2017) 8(17):28312–27. doi: 10.18632/oncotarget.16048
35. Dhatchinamoorthy K, Colbert JD, Rock KL. Cancer Immune Evasion Through Loss of MHC Class I Antigen Presentation. *Front Immunol* (2021) 12:636568. doi: 10.3389/fimmu.2021.636568/full
36. Reits EA, Hodge JW, Herberts CA, Groothuis TA, Chakraborty M, Wansley EK, et al. Radiation Modulates the Peptide Repertoire, Enhances MHC Class I Expression, and Induces Successful Antitumor Immunotherapy. *J Exp Med* (2006) 203(5):1259–71. doi: 10.1084/jem.20052494
37. Petitprez F, Fossati N, Vano Y, Freschi M, Becht E, Lucianò R, et al. PD-L1 Expression and CD8+ T-Cell Infiltrate are Associated With Clinical Progression in Patients With Node-Positive Prostate Cancer. *Eur Urol Focus* (2019) 5(2):192–6. doi: 10.1016/j.euf.2017.05.013
38. Bou-Dargham MJ, Sha L, Sang Q-XA, Zhang J. Immune Landscape of Human Prostate Cancer: Immune Evasion Mechanisms and Biomarkers for Personalized Immunotherapy. *BMC Cancer* (2020) 20(1):572. doi: 10.1186/s12885-020-07058-y
39. Movsas B, Chapman JD, Greenberg RE, Hanlon AL, Horwitz EM, Pinover WH, et al. Increasing Levels of Hypoxia in Prostate Carcinoma Correlate Significantly With Increasing Clinical Stage and Patient Age: An Eppendorf Po(2) Study. *Cancer* (2000) 89(9):2018–24. doi: 10.1097/00000421-200110000-00009
40. Movsas B, Chapman JD, Hanlon AL, Horwitz EM, Greenberg RE, Stobbe C, et al. Hypoxic Prostate/Muscle Po2 Ratio Predicts for Biochemical Failure in Patients With Prostate Cancer: Preliminary Findings. *Urology* (2002) 60(4):634–9. doi: 10.1016/S0090-4295(02)01858-7
41. Lekas A, Lazaris A, Deliveliotis C, Chrisofos M, Zoubouli C, Lapas D, et al. The Expression of Hypoxia-Inducible Factor-1α (HIF-1α) and Angiogenesis Markers in Hyperplastic and Malignant Prostate Tissue. *Anticancer Res* (2006) 26:2989–93.
42. Bakin RE, Gioeli D, Sikes RA, Bissonette EA, Weber MJ. Constitutive Activation of the Ras/Mitogen-Activated Protein Kinase Signaling Pathway Promotes Androgen Hypersensitivity in LNCaP Prostate Cancer Cells. *Cancer Res* (2003) 63(8):1981–9.
43. Mabjeesh NJ, Willard MT, Frederickson CE, Zhong H, Simons JW. Androgens Stimulate Hypoxia-Inducible Factor 1 Activation via Autocrine Loop of Tyrosine Kinase Receptor/Phosphatidylinositol 3′-Kinase/Protein Kinase B in Prostate Cancer Cells. *Clin Cancer Res* (2003) 9(7):2416–25.
44. Huang C-Y, Ye Z-H, Huang M-Y, Lu J-J. Regulation of CD47 Expression in Cancer Cells. *Transl Oncol* (2020) 13(12):100862. doi: 10.1016/j.tranon.2020.100862
45. Hasmim M, Noman MZ, Messai Y, Bordereaux D, Gros G, Baud V, et al. Cutting Edge: Hypoxia-Induced Nanog Favors the Intratumoral Infiltration of Regulatory T Cells and Macrophages via Direct Regulation of TGF-β1. *J Immunol* (2013) 191(12):5802–6. doi: 10.4049/jimmunol.1302140
46. Klymkowsky MW, Savagner P. Epithelial-Mesenchymal Transition: A Cancer Researcher's Conceptual Friend and Foe. *Am J Pathol* (2009) 174(5):1588–93. doi: 10.2353/ajpath.2009.080545
47. Terry S, Savagner P, Ortiz-Cuaran S, Mahjoubi L, Saintigny P, Thiery J-P, et al. New Insights Into the Role of EMT in Tumor Immune Escape. *Mol Oncol* (2017) 11(7):824–46. doi: 10.1002/1878-0261.12093
48. Waldman AD, Fritz JM, Lenardo MJ. A Guide to Cancer Immunotherapy: From T Cell Basic Science to Clinical Practice. *Nat Rev Immunol* (2020) 20(11):651–68. doi: 10.1038/s41577-020-0306-5
49. Beer TM, Kwon ED, Drake CG, Fizazi K, Logothetis C, Gravis G, et al. Randomized, Double-Blind, Phase III Trial of Ipilimumab *Versus* Placebo in Asymptomatic or Minimally Symptomatic Patients With Metastatic Chemotherapy-Naive Castration-Resistant Prostate Cancer. *J Clin Oncol Off J Am Soc Clin Oncol* (2017) 35(1):40–7. doi: 10.1200/JCO.2016.69.1584
50. Gao J, Ward JF, Pettaway CA, Shi LZ, Subudhi SK, Vence LM, et al. VISTA is an Inhibitory Immune Checkpoint That is Increased After Ipilimumab Therapy in Patients With Prostate Cancer. *Nat Med* (2017) 23(5):551–5. doi: 10.1038/nm.4308
51. Marcus L, Lemery SJ, Keegan P, Pazdur R. FDA Approval Summary: Pembrolizumab for the Treatment of Microsatellite Instability-High Solid Tumors. *Clin Cancer Res* (2019) 25(13):3753–8. doi: 10.1158/1078-0432.CCR-18-4070
52. Antonarakis ES, Piulats JM, Gross-Goupil M, Goh J, Ojamaa K, Hoimes CJ, et al. Pembrolizumab for Treatment-Refractory Metastatic Castration-Resistant Prostate Cancer: Multicohort, Open-Label Phase II KEYNOTE-199 Study. *J Clin Oncol Off J Am Soc Clin Oncol* (2020) 38(5):395–405. doi: 10.1200/JCO.19.01638
53. Labrijn AF, Janmaat ML, Reichert JM, Parren PWHI. Bispecific Antibodies: A Mechanistic Review of the Pipeline. *Nat Rev Drug Discovery* (2019) 18(8):585–608. doi: 10.1038/s41573-019-0028-1
54. Heitmann JS, Pfluegler M, Jung G, Salih HR. Bispecific Antibodies in Prostate Cancer Therapy: Current Status and Perspectives. *Cancers* (2021) 13(3):549. doi: 10.3390/cancers13030549
55. Zekri L, Vogt F, Osburg L, Müller S, Kauer J, Manz T, et al. An IgG-Based Bispecific Antibody for Improved Dual Targeting in PSMA-Positive Cancer. *EMBO Mol Med* (2021) 13(2):e11902. doi: 10.15252/emmm.201911902
56. Buelow B, Avanzino B, Balasubramani A, Boudreau A, Davison L, Ganesan P, et al. A CD3 X Frα T-Cell Engaging Bispecific Antibody for Efficient Killing of Ovarian Cancer Cells With Minimal Cytokine Release. *J Clin Oncol* (2020) 38(15_suppl):e18050–e18050. doi: 10.1200/jco.2020.38.15_suppl.e18050
57. Yamamoto K, Trad A, Baumgart A, Hüske L, Lorenzen I, Chalaris A, et al. A Novel Bispecific Single-Chain Antibody for ADAM17 and CD3 Induces T-Cell-Mediated Lysis of Prostate Cancer Cells. *Biochem J* (2012) 445(1):135–44. doi: 10.1042/BJ20120433
58. Zhao H, Ma J, Lei T, Ma W, Zhang M. The Bispecific Anti-CD3 × anti-CD155 Antibody Mediates T Cell Immunotherapy for Human Prostate Cancer. *Invest New Drugs* (2019) 37(5):810–7. doi: 10.1007/s10637-018-0683-9
59. Narayan V, Barber-Rotenberg J, Fraietta J, Hwang W-T, Lacey SF, Plesa G, et alA Phase I Clinical Trial of PSMA-Directed/Tgfβ-Insensitive CAR-T Cells in Metastatic Castration-Resistant Prostate Cancer. *J Clin Oncol* (2021) 39:6_suppl, 125–125. doi: 10.1200/JCO.2021.39.6_suppl.125
60. Kantoff PW, Higano CS, Shore ND, Berger ER, Small EJ, Penson DF, et al. Sipuleucel-T Immunotherapy for Castration-Resistant Prostate Cancer. *N Engl J Med* (2010) 363(5):411–22. doi: 10.1056/NEJMoa1001294
61. Gulley JL, Borre M, Vogelzang NJ, Ng S, Agarwal N, Parker CC, et al. Phase III Trial of PROSTVAC in Asymptomatic or Minimally Symptomatic Metastatic Castration-Resistant Prostate Cancer. *J Clin Oncol Off J Am Soc Clin Oncol* (2019) 37(13):1051–61. doi: 10.1200/JCO.18.02031
62. Bommareddy PK, Shettigar M, Kaufman HL. Integrating Oncolytic Viruses in Combination Cancer Immunotherapy. *Nat Rev* (2018) 18(8):498–513. doi: 10.1038/s41577-018-0014-6
63. Kaufman HL, Kohlhapp FJ, Zloza A. Oncolytic Viruses: A New Class of Immunotherapy Drugs. *Nat Rev Drug Discovery* (2015) 14(9):642–62. doi: 10.1038/nrd4663

64. Zafar S, Basnet S, Launonen I-M, Quixabeira DCA, Santos J, Hemminki O, et al. Oncolytic Adenovirus Type 3 Coding for CD40L Facilitates Dendritic Cell Therapy of Prostate Cancer in Humanized Mice and Patient Samples. *Hum Gene Ther* (2021) 32(3–4):192–202. doi: 10.1089/hum.2020.222
65. Freytag SO, Barton KN, Zhang Y. Efficacy of Oncolytic Adenovirus Expressing Suicide Genes and Interleukin-12 in Preclinical Model of Prostate Cancer. *Gene Ther* (2013) 20(12):1131–9. doi: 10.1038/gt.2013.40
66. Syn NL, Wang L, Chow EK-H, Lim CT, Goh B-C. Exosomes in Cancer Nanomedicine and Immunotherapy: Prospects and Challenges. *Trends Biotechnol* (2017) 35(7):665–76. doi: 10.1016/j.tibtech.2017.03.004
67. Xu J, Shao T, Song M, Xie Y, Zhou J, Yin J, et al. MIR22HG Acts as a Tumor Suppressor via Tgfβ/SMAD Signaling and Facilitates Immunotherapy in Colorectal Cancer. *Mol Cancer* (2020) 19(1):51. doi: 10.1186/s12943-020-01174-w
68. Marar C, Starich B, Wirtz D. Extracellular Vesicles in Immunomodulation and Tumor Progression. *Nat Immunol* (2021) 22(5):560–70. doi: 10.1038/s41590-021-00899-0
69. Vignard V, Labbé M, Marec N, André-Grégoire G, Jouand N, Fonteneau J-F, et al. MicroRNAs in Tumor Exosomes Drive Immune Escape in Melanoma. *Cancer Immunol Res* (2020) 8(2):255–67. doi: 10.1158/2326-6066.CIR-19-0522
70. van Niel G, D'Angelo G, Raposo G. Shedding Light on the Cell Biology of Extracellular Vesicles. *Nat Rev Mol Cell Biol* (2018) 19(4):213–28. doi: 10.1038/nrm.2017.125
71. Zhu X, Badawi M, Pomeroy S, Sutaria DS, Xie Z, Baek A, et al. Comprehensive Toxicity and Immunogenicity Studies Reveal Minimal Effects in Mice Following Sustained Dosing of Extracellular Vesicles Derived From HEK293T Cells. *J Extracell Vesicles* (2017) 6:1. doi: 10.1080/20013078.2017.1324730
72. Abusamra AJ, Zhong Z, Zheng X, Li M, Ichim TE, Chin JL, et al. Tumor Exosomes Expressing Fas Ligand Mediate CD8+ T-Cell Apoptosis. *Blood Cells Mol Dis* (2005) 35(2):169–73. doi: 10.1016/j.bcmd.2005.07.001
73. Poggio M, Hu T, Pai C-C, Chu B, Belair CD, Chang A, et al. Suppression of Exosomal PD-L1 Induces Systemic Anti-Tumor Immunity and Memory. *Cell* (2019) 177(2):414–427.e13. doi: 10.1016/j.cell.2019.02.016
74. Guduric-Fuchs J, O'Connor A, Camp B, O'Neill CL, Medina RJ, Simpson DA. Selective Extracellular Vesicle-Mediated Export of an Overlapping Set of microRNAs From Multiple Cell Types. *BMC Genomics* (2012) 13(1):357. doi: 10.1186/1471-2164-13-357
75. Valadi H, Ekström K, Bossios A, Sjöstrand M, Lee JJ, Lötvall JO. Exosome-Mediated Transfer of mRNAs and microRNAs is a Novel Mechanism of Genetic Exchange Between Cells. *Nat Cell Biol* (2007) 9(6):654–9. doi: 10.1038/ncb1596
76. Cortez MA, Anfossi S, Ramapriyan R, Menon H, Atalar SC, Aliru M, et al. Role of miRNAs in Immune Responses and Immunotherapy in Cancer. *Genes Chromosomes Cancer* (2019) 58(4):244–53. doi: 10.1002/gcc.22725
77. Nishimura M, Jung E-J, Shah MY, Lu C, Spizzo R, Shimizu M, et al. Therapeutic Synergy Between microRNA and siRNA in Ovarian Cancer Treatment. *Cancer Discovery* (2013) 3(11):1302–15. doi: 10.1158/2159-8290.CD-13-0159
78. Baumann V, Winkler J. miRNA-Based Therapies: Strategies and Delivery Platforms for Oligonucleotide and non-Oligonucleotide Agents. *Future Med Chem* (2014) 6(17):1967–84. doi: 10.4155/fmc.14.116
79. Labbé M, Hoey C, Ray J, Potiron V, Supiot S, Liu SK, et al. microRNAs Identified in Prostate Cancer: Correlative Studies on Response to Ionizing Radiation. *Mol Cancer* (2020) 19(1):63. doi: 10.1186/s12943-020-01186-6
80. Guipaud O, Jaillet C, Clément-Colmou K, François A, Supiot S, Milliat F. The Importance of the Vascular Endothelial Barrier in the Immune-Inflammatory Response Induced by Radiotherapy. *Br J Radiol* (2018) 91:1089. doi: 10.1259/bjr.20170762
81. Arina A, Beckett M, Fernandez C, Zheng W, Pitroda S, Chmura SJ, et al. Tumor-Reprogrammed Resident T Cells Resist Radiation to Control Tumors. *Nat Commun* (2019) 10(1):3959. doi: 10.1038/s41467-019-11906-2
82. Dewan MZ, Galloway AE, Kawashima N, Dewyngaert JK, Babb JS, Formenti SC, et al. Fractionated But Not Single-Dose Radiotherapy Induces an Immune-Mediated Abscopal Effect When Combined With Anti-CTLA-4 Antibody. *Clin Cancer Res Off J Am Assoc Cancer Res* (2009) 15(17):5379–88. doi: 10.1158/1078-0432.CCR-09-0265
83. Vanpouille-Box C, Alard A, Aryankalayil MJ, Sarfraz Y, Diamond JM, Schneider RJ, et al. DNA Exonuclease Trex1 Regulates Radiotherapy-Induced Tumour Immunogenicity. *Nat Commun* (2017) 8:15618. doi: 10.1038/ncomms15618
84. Klug F, Prakash H, Huber PE, Seibel T, Bender N, Halama N, et al. Low-Dose Irradiation Programs Macrophage Differentiation to an iNOS$^+$/M1 Phenotype That Orchestrates Effective T Cell Immunotherapy. *Cancer Cell* (2013) 24(5):589–602. doi: 10.1016/j.ccr.2013.09.014
85. Monjazeb AM, Schalper KA, Villarroel-Espindola F, Nguyen A, Shiao SL, Young K. Effects of Radiation on the Tumor Microenvironment. *Semin Radiat Oncol* (2020) 30(2):145–57. doi: 10.1016/j.semradonc.2019.12.004
86. Clément-Colmou K, Potiron V, Pietri M, Guillonneau M, Jouglar E, Chiavassa S, et al. Influence of Radiotherapy Fractionation Schedule on the Tumor Vascular Microenvironment in Prostate and Lung Cancer Models. *Cancers* (2020) 12(1):121. doi: 10.3390/cancers12010121
87. Wang H, Mendez LC, Morton G, Loblaw A, Mesci A, Chung HT, et al. Immune Cell Profiling in Gleason 9 Prostate Cancer Patients Treated With Brachytherapy *Versus* External Beam Radiotherapy: An Exploratory Study. *Radiother Oncol J Eur Soc Ther Radiol Oncol* (2021) 155:80–5. doi: 10.1016/j.radonc.2020.10.029
88. Ko EC, Formenti SC. Radiotherapy and Checkpoint Inhibitors: A Winning New Combination? *Ther Adv Med Oncol* (2018) 10:1758835918768240. doi: 10.1177/1758835918768240
89. Lhuillier C, Rudqvist N-P, Elemento O, Formenti SC, Demaria S. Radiation Therapy and Anti-Tumor Immunity: Exposing Immunogenic Mutations to the Immune System. *Genome Med* (2019) 11(1):40. doi: 10.1186/s13073-019-0653-7
90. Liechtenstein T, Dufait I, Lanna A, Breckpot K, Escors D. Modulating Co-Stimulation During Antigen Presentation To Enhance Cancer Immunotherapy. *Immunol Endocr Metab Agents Med Chem* (2012) 12 (3):224–35. doi: 10.2174/187152212802001875
91. Salimu J, Spary LK, Al-Taei S, Clayton A, Mason MD, Staffurth J, et al. Cross-Presentation of the Oncofetal Tumor Antigen 5T4 From Irradiated Prostate Cancer Cells—A Key Role for Heat-Shock Protein 70 and Receptor Cd91. *Cancer Immunol Res* (2015) 3(6):678–88. doi: 10.1158/2326-6066.CIR-14-0079
92. Tabi Z, Spary LK, Coleman S, Clayton A, Mason MD, Staffurth J. Resistance of CD45RA– T Cells to Apoptosis and Functional Impairment, and Activation of Tumor-Antigen Specific T Cells During Radiation Therapy of Prostate Cancer. *J Immunol* (2010) 185(2):1330–9. doi: 10.4049/jimmunol.1000488
93. Bernstein MB, Garnett CT, Zhang H, Velcich A, Wattenberg MM, Gameiro SR, et al. Radiation-Induced Modulation of Costimulatory and Coinhibitory T-Cell Signaling Molecules on Human Prostate Carcinoma Cells Promotes Productive Antitumor Immune Interactions. *Cancer Biother Radiopharm* (2014) 29(4):153–61. doi: 10.1089/cbr.2013.1578
94. Lin L, Kane N, Kobayashi N, Kono EA, Yamashiro JM, Nickols NG, et al. High-Dose Per Fraction Radiotherapy Induces Both Antitumor Immunity and Immunosuppressive Responses in Prostate Tumors. *Clin Cancer Res Off J Am Assoc Cancer Res* (2021) 27(5):1505–15. doi: 10.1158/1078-0432.CCR-20-2293
95. Xu J, Escamilla J, Mok S, David J, Priceman S, West B, et al. CSF1R Signaling Blockade Stanches Tumor-Infiltrating Myeloid Cells and Improves the Efficacy of Radiotherapy in Prostate Cancer. *Cancer Res* (2013) 73(9):2782–94. doi: 10.1158/0008-5472.CAN-12-3981
96. Chen J, Liu X, Zeng Z, Li J, Luo Y, Sun W, et al. Immunomodulation of NK Cells by Ionizing Radiation. *Front Oncol* (2020) 10:874. doi: 10.3389/fonc.2020.00874/full
97. Muroyama Y, Nirschl TR, Kochel CM, Lopez-Bujanda Z, Theodros D, Mao W, et al. Stereotactic Radiotherapy Increases Functionally Suppressive Regulatory T Cells in the Tumor Microenvironment. *Cancer Immunol Res* (2017) 5(11):992–1004. doi: 10.1158/2326-6066.CIR-17-0040
98. Huggins C. Effect Of Orchiectomy And Irradiation On Cancer Of The Prostate. *Ann Surg* (1942) 115(6):1192–200. doi: 10.1097/00000658-194206000-00030
99. Bolla M, Van Tienhoven G, Warde P, Dubois JB, Mirimanoff R-O, Storme G, et al. External Irradiation With or Without Long-Term Androgen Suppression for Prostate Cancer With High Metastatic Risk: 10-Year

Results of an EORTC Randomised Study. *Lancet Oncol* (2010) 11(11):1066–73. doi: 10.1016/S1470-2045(10)70223-0
100. Martin JM, Supiot S, Berthold DR. Pharmacotherapeutic Management of Locally Advanced Prostate Cancer: Current Status. *Drugs* (2011) 71(8):1019–41. doi: 10.2165/11591500-000000000-00000
101. Lu NZ, Wardell SE, Burnstein KL, Defranco D, Fuller PJ, Giguere V, et al. International Union of Pharmacology. LXV. The Pharmacology and Classification of the Nuclear Receptor Superfamily: Glucocorticoid, Mineralocorticoid, Progesterone, and Androgen Receptors. *Pharmacol Rev* (2006) 58(4):782–97. doi: 10.1124/pr.58.4.9
102. Tan MHE, Li J, Xu HE, Melcher K, Yong E. Androgen Receptor: Structure, Role in Prostate Cancer and Drug Discovery. *Acta Pharmacol Sin* (2015) 36 (1):3–23. doi: 10.1038/aps.2014.18
103. Gao AC, Lou W, Sleeman JP, Isaacs JT. Metastasis Suppression by the Standard CD44 Isoform Does Not Require the Binding of Prostate Cancer Cells to Hyaluronate. *Cancer Res* (1998) 58(11):2350–2.
104. Polkinghorn WR, Parker JS, Lee MX, Kass EM, Spratt DE, Iaquinta PJ, et al. Androgen Receptor Signaling Regulates DNA Repair in Prostate Cancers. *Cancer Discovery* (2013) 3(11):1245–53. doi: 10.1158/2159-8290.CD-13-0172
105. Isaacs JT, Lundmo PI, Berges R, Martikainen P, Kyprianou N, English HF. Androgen Regulation of Programmed Death of Normal and Malignant Prostatic Cells. *J Androl* (1992) 13(6):457–64.
106. Ragnum HB, Røe K, Holm R, Vlatkovic L, Nesland JM, Aarnes E-K, et al. Hypoxia-Independent Downregulation of Hypoxia-Inducible Factor 1 Targets by Androgen Deprivation Therapy in Prostate Cancer. *Int J Radiat Oncol Biol Phys* (2013) 87(4):753–60. doi: 10.1016/j.ijrobp.2013.07.023
107. Milosevic M, Warde P, Ménard C, Chung P, Toi A, Ishkanian A, et al. Tumor Hypoxia Predicts Biochemical Failure Following Radiotherapy for Clinically Localized Prostate Cancer. *Clin Cancer Res Off J Am Assoc Cancer Res* (2012) 18(7):2108–14. doi: 10.1158/1078-0432.CCR-11-2711
108. Drake CG. Prostate Cancer as a Model for Tumour Immunotherapy. *Nat Rev Immunol* (2010) 10(8):580–93. doi: 10.1038/nri2817
109. Wu C-T, Chen W-C, Chen M-F. The Response of Prostate Cancer to Androgen Deprivation and Irradiation Due to Immune Modulation. *Cancers* (2018) 11(1):20. doi: 10.3390/cancers11010020
110. Kalina JL, Neilson DS, Comber AP, Rauw JM, Alexander AS, Vergidis J, et al. Immune Modulation by Androgen Deprivation and Radiation Therapy: Implications for Prostate Cancer Immunotherapy. *Cancers* (2017) 9(2):13. doi: 10.3390/cancers9020013
111. Morse MD, McNeel DG. Prostate Cancer Patients Treated With Androgen Deprivation Therapy Develop Persistent Changes in Adaptive Immune Responses. *Hum Immunol* (2010) 71(5):496–504. doi: 10.1016/j.humimm.2010.02.007
112. Locke JA, Dal Pra A, Supiot S, Warde P, Bristow RG. Synergistic Action of Image-Guided Radiotherapy and Androgen Deprivation Therapy. *Nat Rev Urol* (2015) 12(4):193–204. doi: 10.1038/nrurol.2015.50
113. Tang S, Moore ML, Grayson JM, Dubey P. Increased CD8+ T-Cell Function Following Castration and Immunization is Countered by Parallel Expansion of Regulatory T Cells. *Cancer Res* (2012) 72(8):1975–85. doi: 10.1158/0008-5472.CAN-11-2499
114. Pu Y, Xu M, Liang Y, Yang K, Guo Y, Yang X, et al. Androgen Receptor Antagonists Compromise T Cell Response Against Prostate Cancer Leading to Early Tumor Relapse. *Sci Transl Med* (2016) 8(333):333ra47. doi: 10.1126/scitranslmed.aad5659
115. Mercader M, Bodner BK, Moser MT, Kwon PS, Park ES, Manecke RG, et al. T Cell Infiltration of the Prostate Induced by Androgen Withdrawal in Patients With Prostate Cancer. *Proc Natl Acad Sci U S A* (2001) 98(25):14565–70. doi: 10.1073/pnas.251140998
116. Obradovic AZ, Dallos MC, Zahurak ML, Partin AW, Schaeffer EM, Ross AE, et al. T-Cell Infiltration and Adaptive Treg Resistance in Response to Androgen Deprivation With or Without Vaccination in Localized Prostate Cancer. *Clin Cancer Res* (2020) 26(13):3182–92. doi: 10.1158/1078-0432.CCR-19-3372
117. Calagua C, Russo J, Sun Y, Schaefer R, Lis R, Zhang Z, et al. Expression of PD-L1 in Hormone-Naïve and Treated Prostate Cancer Patients Receiving Neoadjuvant Abiraterone Acetate Plus Prednisone and Leuprolide. *Clin Cancer Res* (2017) 23(22):6812–22. doi: 10.1158/1078-0432.CCR-17-0807
118. Drake CG, Doody ADH, Mihalyo MA, Huang C-T, Kelleher E, Ravi S, et al. Androgen Ablation Mitigates Tolerance to a Prostate/Prostate Cancer-Restricted Antigen. *Cancer Cell* (2005) 7(3):239–49. doi: 10.1016/j.ccr.2005.01.027
119. Fong PCC, Retz M, Drakaki A, Massard C, Berry WR, Romano E, et al. Keynote-365 Cohort C: Pembrolizumab (Pembro) Plus Enzalutamide (Enza) in Abiraterone (Abi)-Pretreated Patients (Pts) With Metastatic Castrate Resistant Prostate Cancer (mCRPC). *J Clin Oncol* (2019) 37(7_suppl):171–171. doi: 10.1200/JCO.2019.37.7_suppl.171
120. Keam SP, Halse H, Nguyen T, Wang M, Van Kooten Losio N, Mitchell C, et al. High Dose-Rate Brachytherapy of Localized Prostate Cancer Converts Tumors From Cold to Hot. *J Immunother Cancer* (2020) 8:e000792. doi: 10.1136/jitc-2020-000792
121. Dudzinski SO, Cameron BD, Wang J, Rathmell JC, Giorgio TD, Kirschner AN. Combination Immunotherapy and Radiotherapy Causes an Abscopal Treatment Response in a Mouse Model of Castration Resistant Prostate Cancer. *J Immunother Cancer* (2019) 7(1):218. doi: 10.1186/s40425-019-0704-z
122. Philippou Y, Sjoberg HT, Murphy E, Alyacoubi S, Jones KI, Gordon-Weeks AN, et al. Impacts of Combining Anti-PD-L1 Immunotherapy and Radiotherapy on the Tumour Immune Microenvironment in a Murine Prostate Cancer Model. *Br J Cancer* (2020) 123(7):1089–100. doi: 10.1038/s41416-020-0956-x
123. Goltz D, Gevensleben H, Dietrich J, Ellinger J, Landsberg J, Kristiansen G, et al. Promoter Methylation of the Immune Checkpoint Receptor PD-1 (PDCD1) is an Independent Prognostic Biomarker for Biochemical Recurrence-Free Survival in Prostate Cancer Patients Following Radical Prostatectomy. *Oncoimmunology* (2016) 5(10):e1221555. doi: 10.1080/2162402X.2016.1221555
124. Gevensleben H, Holmes EE, Goltz D, Dietrich J, Sailer V, Ellinger J, et al. PD-L1 Promoter Methylation is a Prognostic Biomarker for Biochemical Recurrence-Free Survival in Prostate Cancer Patients Following Radical Prostatectomy. *Oncotarget* (2016) 7(48):79943–55. doi: 10.18632/oncotarget.13161
125. Hurwitz AA, Foster BA, Kwon ED, Truong T, Choi EM, Greenberg NM, et al. Combination Immunotherapy of Primary Prostate Cancer in a Transgenic Mouse Model Using CTLA-4 Blockade. *Cancer Res* (2000) 60 (9):2444–8.
126. Udayakumar TS, Betancourt DM, Ahmad A, Tao W, Totiger TM, Patel M, et al. Radiation Attenuates Prostate Tumor Antiviral Responses to Vesicular Stomatitis Virus Containing Ifnβ, Resulting in Pronounced Antitumor Systemic Immune Responses. *Mol Cancer Res* (2020) 18(8):1232–43. doi: 10.1158/1541-7786.MCR-19-0836
127. Yuan Z, Fernandez D, Dhillon J, Abraham-Miranda J, Awasthi S, Kim Y, et al. Proof-Of-Principle Phase I Results of Combining Nivolumab With Brachytherapy and External Beam Radiation Therapy for Grade Group 5 Prostate Cancer: Safety, Feasibility, and Exploratory Analysis. *Prostate Cancer Prostatic Dis* (2021) 24(1):140–9. doi: 10.1038/s41391-020-0254-y
128. Nardone V, Botta C, Caraglia M, Martino EC, Ambrosio MR, Carfagno T, et al. Tumor Infiltrating T Lymphocytes Expressing FoxP3, CCR7 or PD-1 Predict the Outcome of Prostate Cancer Patients Subjected to Salvage Radiotherapy After Biochemical Relapse. *Cancer Biol Ther* (2016) 17 (11):1213–20. doi: 10.1080/15384047.2016.1235666
129. Finkelstein SE, Rodriguez F, Dunn M, Farmello M-J, Smilee R, Janssen W, et al. Serial Assessment of Lymphocytes and Apoptosis in the Prostate During Coordinated Intraprostatic Dendritic Cell Injection and Radiotherapy. *Immunotherapy* (2012) 4(4):373–82. doi: 10.2217/imt.12.24
130. Gulley JL, Arlen PM, Bastian A, Morin S, Marte J, Beetham P, et al. Combining a Recombinant Cancer Vaccine With Standard Definitive Radiotherapy in Patients With Localized Prostate Cancer. *Clin Cancer Res Off J Am Assoc Cancer Res* (2005) 11(9):3353–62. doi: 10.1158/1078-0432.CCR-04-2062
131. Lilleby W, Gaudernack G, Brunsvig PF, Vlatkovic L, Schulz M, Mills K, et al. Phase I/IIa Clinical Trial of a Novel hTERT Peptide Vaccine in Men With Metastatic Hormone-Naive Prostate Cancer. *Cancer Immunol Immunother CII* (2017) 66(7):891–901. doi: 10.1007/s00262-017-1994-y
132. Lechleider RJ, Arlen PM, Tsang K-Y, Steinberg SM, Yokokawa J, Cereda V, et al. Safety and Immunologic Response of a Viral Vaccine to Prostate-Specific Antigen in Combination With Radiation Therapy When Metronomic-Dose

Interleukin 2 is Used as an Adjuvant. *Clin Cancer Res Off J Am Assoc Cancer Res* (2008) 14(16):5284–91. doi: 10.1158/1078-0432.CCR-07-5162
133. Kamrava M, Kesarwala AH, Madan RA, Lita E, Kaushal A, Tsang K-Y, et al. Long-Term Follow-Up of Prostate Cancer Patients Treated With Vaccine and Definitive Radiation Therapy. *Prostate Cancer Prostatic Dis* (2012) 15 (3):289–95. doi: 10.1038/pcan.2012.7
134. Slovin SF, Higano CS, Hamid O, Tejwani S, Harzstark A, Alumkal JJ, et al. Ipilimumab Alone or in Combination With Radiotherapy in Metastatic Castration-Resistant Prostate Cancer: Results From an Open-Label, Multicenter Phase I/II Study. *Ann Oncol* (2013) 24(7):1813–21. doi: 10.1093/annonc/mdt107
135. Kwon ED, Drake CG, Scher HI, Fizazi K, Bossi A, van den Eertwegh AJM, et al. Ipilimumab *Versus* Placebo After Radiotherapy in Patients With Metastatic Castration-Resistant Prostate Cancer That had Progressed After Docetaxel Chemotherapy (CA184-043): A Multicentre, Randomised, Double-Blind, Phase 3 Trial. *Lancet Oncol* (2014) 15(7):700–12. doi: 10.1016/S1470-2045(14)70189-5
136. Fizazi K, Drake CG, Beer TM, Kwon ED, Scher HI, Gerritsen WR, et al. Final Analysis of the Ipilimumab *Versus* Placebo Following Radiotherapy Phase III Trial in Postdocetaxel Metastatic Castration-Resistant Prostate Cancer Identifies an Excess of Long-Term Survivors. *Eur Urol* (2020) 78(6):822 –30. doi: 10.1016/j.eururo.2020.07.032
137. Golden EB, Formenti SC. Radiation Therapy and Immunotherapy: Growing Pains. *Int J Radiat Oncol* (2015) 91(2):252–4. doi: 10.1016/j.ijrobp. 2014.09.018
138. Gevensleben H, Dietrich D, Golletz C, Steiner S, Jung M, Thiesler T, et al. The Immune Checkpoint Regulator PD-L1 Is Highly Expressed in Aggressive Primary Prostate Cancer. *Clin Cancer Res Off J Am Assoc Cancer Res* (2016) 22(8):1969–77. doi: 10.1158/1078-0432.CCR-15-2042
139. Calagua C, Ficial M, Jansen CS, Hirz T, Del Balzo L, Wilkinson S, et al. A Subset of Localized Prostate Cancer Displays an Immunogenic Phenotype Associated With Losses of Key Tumor Suppressor Genes. *Clin Cancer Res Off J Am Assoc Cancer Res* (2021) 27(17):4836–47. doi: 10.1158/1078-0432.CCR-21-0121
140. Mole RH. Whole Body Irradiation; Radiobiology or Medicine? *Br J Radiol* (1953) 26(305):234–41. doi: 10.1259/0007-1285-26-305-234
141. Abuodeh Y, Venkat P, Kim S. Systematic Review of Case Reports on the Abscopal Effect. *Curr Probl Cancer* (2016) 40(1):25–37. doi: 10.1016/j.currproblcancer.2015.10.001
142. Ngwa W, Irabor OC, Schoenfeld JD, Hesser J, Demaria S, Formenti SC. Using Immunotherapy to Boost the Abscopal Effect. *Nat Rev Cancer* (2018) 18(5):313–22. doi: 10.1038/nrc.2018.6
143. Rodríguez-Ruiz ME, Perez-Gracia JL, Rodríguez I, Alfaro C, Oñate C, Pérez G, et al. Combined Immunotherapy Encompassing Intratumoral Poly-ICLC, Dendritic-Cell Vaccination and Radiotherapy in Advanced Cancer Patients. *Ann Oncol Off J Eur Soc Med Oncol* (2018) 29(5):1312–9. doi: 10.1158/1538-7445.AM2018-CT017

Conflict of Interest: The authors declare that the research was conducted in the absence of any commercial or financial relationships that could be construed as a potential conflict of interest.

Publisher's Note: All claims expressed in this article are solely those of the authors and do not necessarily represent those of their affiliated organizations, or those of the publisher, the editors and the reviewers. Any product that may be evaluated in this article, or claim that may be made by its manufacturer, is not guaranteed or endorsed by the publisher.

Copyright © 2021 Ollivier, Labbé, Fradin, Potiron and Supiot. This is an open-access article distributed under the terms of the Creative Commons Attribution License (CC BY). The use, distribution or reproduction in other forums is permitted, provided the original author(s) and the copyright owner(s) are credited and that the original publication in this journal is cited, in accordance with accepted academic practice. No use, distribution or reproduction is permitted which does not comply with these terms.

frontiers in Oncology

REVIEW
published: 27 September 2021
doi: 10.3389/fonc.2021.736431

Application of Organoid Models in Prostate Cancer Research

Ligui Zhou[1,2], *Caiqin Zhang*[2], *Yongbin Zhang*[1*] and *Changhong Shi*[2*]

[1] Animal Experiment Center, Guangzhou University of Chinese Medicine, Guangzhou, China, [2] Division of Cancer Biology, Laboratory Animal Center, The Fourth Military Medical University, Xi'an, China

Complex heterogeneity is an important characteristic in the development of prostate cancer (PCa), which further leads to the failure of known therapeutic options. PCa research has been hampered by the current *in vitro* model systems that cannot fully reflect the biological characteristics and clinical diversity of PCa. The tumor organoid model in three-dimensional culture retains the heterogeneity of primary tumor tissues *in vitro* well and enables high-throughput screening and genome editing. Therefore, the establishment of a PCa organoid model that recapitulates the diverse heterogeneity observed in clinical settings is of great significance for the study of PCa. In this review, we summarize the culture conditions, establishments, and limitations of PCa organoids and further review their application for the study of pathogenesis, drug screening, mechanism of drug resistance, and individualized treatment for PCa. Additionally, we look forward to other potential developmental directions of PCa organoids, such as the interaction between prostate cancer tumor cells and their microenvironment, clinical individualized treatments, heterogeneous transformation model, tumor immunotherapy, and organoid models combined with liquid biopsy. Through this, we provide more effective preclinical experimental schemes using the PCa organoid model.

Keywords: prostate cancer (PCa), organoid model, heterogeneity, pathogenesis, drug screening, individualized treatment

OPEN ACCESS

Edited by:
Andrew Goldstein, University of California, Los Angeles, United States

Reviewed by:
Larisa Nonn, University of Illinois at Chicago, United States
Leigh Ellis, Cedars-Sinai Medical Center, United States
Wassim Abou-Kheir, American University of Beirut, Lebanon
Jung Wook Park, Duke University, United States

***Correspondence:**
Changhong Shi
changhong@fmmu.edu.cn
Yongbin Zhang
yongbinzhang@gzucm.edu.cn

Specialty section:
This article was submitted to Genitourinary Oncology, a section of the journal Frontiers in Oncology

Received: *05 July 2021*
Accepted: *09 September 2021*
Published: *27 September 2021*

Citation:
Zhou L, Zhang C, Zhang Y and Shi C (2021) Application of Organoid Models in Prostate Cancer Research. Front. Oncol. 11:736431. doi: 10.3389/fonc.2021.736431

INTRODUCTION

Prostate cancer (PCa) is one of the most common malignancies among men worldwide (1). In 2020, the incidence of prostate cancer in men was as high as 7.3%, second only to lung cancer. At the same time, the mortality rate reached 3.8% which led PCa to become the fifth major cause of cancer death in men (2). Since most PCa cases are androgen-driven adenocarcinomas, androgen deprivation

Abbreviations: PCa, prostate cancer; ADT, androgen deprivation therapy; PSA, prostate-specific antigen; AR, androgen receptor; CRPC, castration-resistant prostate cancer; NEPC, neuroendocrine prostate cancer; CRC, conditional reprogramming cells; PDX, patient-derived xenografts; GEMM, genetically engineered mouse models; 3D, three-dimensional; EGF, epidermal growth factor; ALK, anaplastic lymphoma kinase; DHT, dihydrotestosterone; FGF10, fibroblast growth factor-10; FGF2, fibroblast growth factor-2; PGE2, prostaglandin E2; CTC, circulating tumor cells; ESCs, embryonic stem cells; iPSCs, induced pluripotent stem cells; BMP, bone morphogenetic protein; TGF-β, transforming growth factor-beta; mCRPC, metastatic castration-resistant prostate cancer; BMPC, bone metastatic prostate cancer; RNA-Seq, RNA Sequencing; KRT13, Keratin 13; LY6D, Lymphocyte Antigen 6D; PSCA, prostate stem cell antigen; CSCs, cancer stem cells; CARNs, castration-resistant Nkx3.1-expressing cells; CRPC-NE, CRPC-neuroendocrine; CRPC-Aden, CRPC-adenocarcinoma; PDO, patient-derived organoids; BRD4, bromodomain-containing protein 4.

therapy (ADT) is the main clinical treatment for early-stage PCa (3, 4). Most patients can benefit from treatment at an early stage through a rapid decrease in prostate-specific antigen (PSA) and a reduction in tumor volume. However, after a period of treatment, castration resistance ultimately ensues and the disease may develop into androgen receptor (AR)-castration-resistant prostate cancer (CRPC) or even neuroendocrine prostate cancer (NEPC), an AR-negative small cell neuroendocrine carcinoma (5, 6). The treatment for PCa is challenging due to its complex spatial, morphological, and genetic heterogeneity. Additionally, the oncologic transformation mechanism that results in clinical heterogeneity remains unclear. Therefore, there is an urgent need for prostate cancer preclinical models that can fully reflect the heterogeneity of PCa.

The research models used for the study of PCa mainly include traditional cell lines, conditional reprogramming cells (CRC), organoid models, patient-derived xenografts (PDX), and genetically engineered mouse models (GEMM). Different models have different advantages and disadvantages (**Table 1**). Traditional PCa cell lines, including LNCaP, VCaP, PC3, 22RV1, DU145, C4-2, and NCI-H660, are widely available and inexpensive. These cell lines show infinity growth, amenability to high-throughput screening and easy genome editing, but a lack of tumor heterogeneity and tumor microenvironment (7–9). In the CRC culture system, the combination of Rho kinase inhibitor Y-27632 and irradiated mouse fibroblast feeder cells enables primary cancer cells to acquire partial stem cell characteristics and the ability to indefinitely proliferate *in vitro* (10). However, androgen responsiveness of PCa is limited in this system and CRC is susceptible to contamination by feeder cells (11, 12). PDX, an important preclinical model *in vivo*, recapitulates tumor heterogeneity with high fidelity and correlates highly with patient responses (13). However, PDX is expansive and need a long time to establish (14). Most importantly, PDX is not amenable to high-throughput screening and genome editing (15). GEMM is spontaneous animal model that has been generated to emulate the expected functional consequences of key genomic alterations and has their own complete tumor microenvironment and immune system (16, 17). However, it is not only expensive and time consuming, but also only contains one or two genomic alterations by gene editing and is prone to induce multisystem tumors (18).

Therefore, a suitable model system, which can compensate for the shortcomings of the above-mentioned models, is particularly significant for PCa research. The organoid model might be such a compensatory model. Organoids in three-dimensional (3D) culture are derived from pluripotent stem cells or isolated organ progenitor cells to form organlike structures like the organs *in vivo* (19). Organoids encapsulate the diverse heterogeneity observed in clinical medicine (13, 14). More importantly, organoids are convenient for genetic manipulation and high-throughput drug screening *in vitro* (15, 16). Furthermore, they have a high correlation with the drug response of primary tumors in patients. On the other hand, PCa organoids also have some disadvantages, such as low efficiency of establishing organoids (particularly primary PCa), lack of microenvironment and immune system and the contamination of normal cells (17, 18). However, their unique advantages allow PCa organoids to be a great potential *in vitro* preclinical model, allowing for in-depth analyses of tumor heterogeneity.

In the present review, we review the culture conditions, establishments and limitations of PCa organoids and their applications in pathogenesis, drug screening, mechanism of drug resistance and individualized treatment for PCa. In

TABLE 1 | Comparison of different prostate cancer model systems.

	Traditional cell lines (7–9)	CRC (10–12)	Organoid (20–25)	PDX (13–15)	GEMM (6–18)
Advantage	✧ Infinity growth ✧ Enable to High-throughput screening ✧ High availability and cheap ✧ Sample to genome editing	✧ High success rate of primary culture ✧ Enable to High-throughput screening ✧ Applied to PDX model ✧ Sample to genome editing	✧ Retain heterogeneity ✧ High-throughput screening ✧ Applied to PDX model ✧ Sample to genome editing ✧ Correlate with patient responses	✧ Retain heterogeneity ✧ Correlate with patient responses ✧ Low contamination of normal cell ✧ Include tumor microenvironment	✧ Spontaneous tumor ✧ Complete tumor microenvironment and immune system ✧ Generated nicely emulate the expected functional consequences of key genomic alterations ✧ Ease of genetic manipulation
Disadvantage	• Lack of heterogeneity • Lack of tumor microenvironment and immune system • Low success rate	• Lack of AR responsiveness • Contamination of Feeder cells and normal cells	• Low success rate of PCa culture • No tumor microenvironment and immune system • Contamination of normal cells • Hard to long-term propagation • Contamination of and normal cells	• Expensive and Time consuming • Lack of immune system • Low-throughput screening • Low success rate of PCa culture • Contamination of mouse cells	• Expensive and Time consuming • Murine PCa tumor • Only one or two genomic alterations • Induction of multisystem tumors

CRC, conditional reprogramming cells; PDX, patient-derived xenografts; GEMM, genetically engineered mouse models.

addition, we further discuss the potential developmental directions of PCa organoids.

PROSTATE CANCER ORGANOID CULTURES

Culture Conditions for the Development of PCa Organoid Models

The organoid model is a 3D culture of isolated pluripotent stem cells or organ progenitor cells in a matrix such as Matrigel. It provides a similar environment *in vitro* for cells or tissues to develop into micro-organs. The culture method of PCa has been described. **Figure 1** shows the general process of organoid culture for PCa. Sato et al. (26) first developed the universal organoid medium that contains advanced DMEM/F12 medium with epidermal growth factor (EGF), Noggin, and Wnt agonist R-spondin-1. On this basis, Drost et al. (27) continued to add different compounds and growth factors, including anaplastic lymphoma kinase (ALK) 3/4/5 inhibitor A83-01, dihydrotestosterone (DHT), fibroblast growth factor-10 (FGF10), fibroblast growth factor-2 (FGF2), prostaglandin E2 (PGE2), nicotinamide, and p38 inhibitor SB202190, N-acetylcysteine, B27 supplement and Rho kinase inhibitor Y-27632 to culture PCa organoids successfully (**Table 2**). Among them, growth factors FGF10, FGF2, PGE2, nicotinamide and SB202190 are not required when murine-derived PCa organoids are cultured. These organoids form a glandular structure, have a stable karyotype similar to that of the prostate *in vivo*, and complete AR signal transduction (28). In this culture system, PCa organoids can be successfully cultured within 2 weeks with an average split ratio of 1:2 every 2 weeks (27). Additionally, it can be applied to the PDX model, maintaining the heterogeneity of PCa (17). Based on these culture conditions, PCa organoids have been successfully established from normal tissues, tumor biopsy samples, circulating tumor cells (CTC), PCa cell lines, PDX models of PCa, human embryonic stem cells (ESCs) and induced pluripotent stem cells (iPSCs) (17, 27–32).

Different growth factors play different roles in the culture of PCa organoids. R-spondin-1 and Noggin enhance the formation and expansion of organoids by promoting Wnt signaling and regulating the bone morphogenetic protein (BMP) signaling pathway, respectively (33, 34). Elimination of R-spondin-1 or Noggin will result in the inhibition of AR expression (28). Due to the high dosage and cost of R-spondin-1 and Noggin, the preparation methods of conditioned medium using modified cells for these factors are sorted in **Table 3** (27, 35, 36). EGF has been shown to be essential for prostate epithelial cell line growth derived from organoids, which vastly strengthens cell viability and proliferation (37). The absence of EGF upregulates AR signal transduction at the transcription and translation levels and also increases PSA expression (28). Previous research has suggested

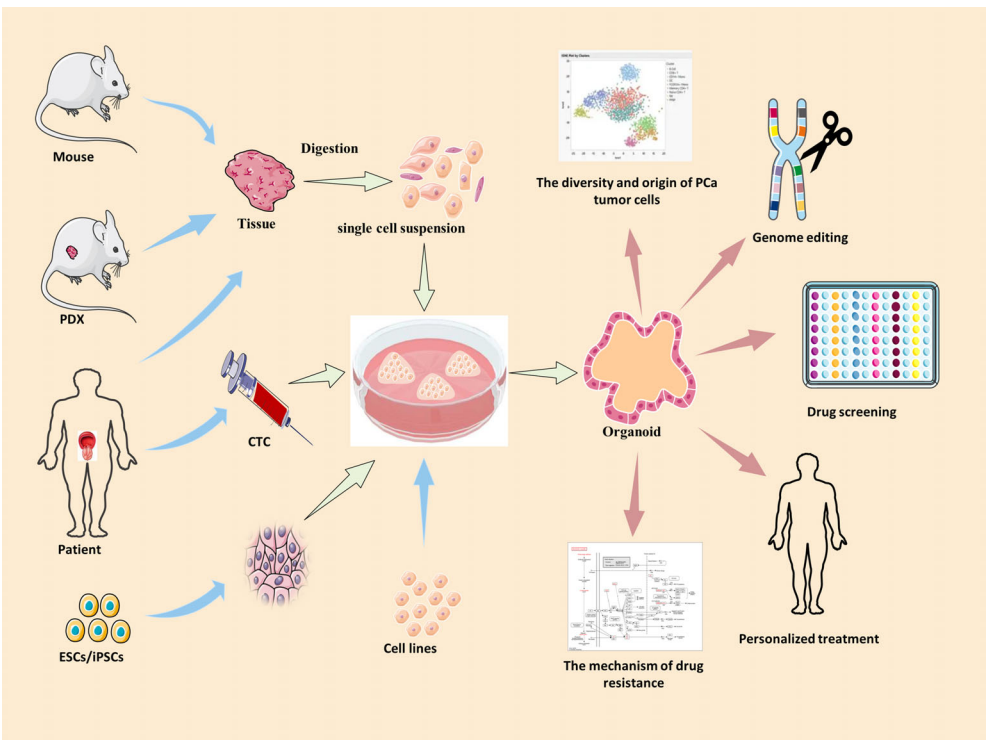

FIGURE 1 | The summary of culture and applications of PCa organoid. Blue arrow →, the specimen source of PCa organoid. Red arrow →, the applications of PCa organoid. PDX, patient-derived xenografts; ESCs, human embryonic stem cells; iPSCs, induced pluripotent stem cells; CTC, circulating tumor cells.

TABLE 2 | Summary of culture medium components for mouse and human prostate organoids (27, 28).

Factor	Mouse organoids	Human organoids
Advanced DMEM/F12	pure	pure
HEPES	10 mM	10 mM
Glutamax	1x	1x
Penicillin/streptomycin	1x	1x
B27	1x	1x
Human epidermal growth factor	50 ng/ml	5 ng/ml
Human Noggin	100 ng/ml or 10% Noggin-conditioned medium	100 ng/ml or 10% Noggin-conditioned medium
Human R-spondin-1	500 ng/ml or 10% R-spondin-1-conditioned medium	500 ng/ml or 10% R-spondin-1-conditioned medium
A83-01	200 nM	500 nM
DHT	1 nM	1 nM
FGF10	–	10 ng/ml
FGF2	–	5 ng/ml
PGE2	–	1 μM
Nicotinamide	–	10 mM
SB202190	–	10 μM
N-acetylcysteine	1.25 mM	1.25 mM
Y-27632 dihydrochloride*	10 μM	10 μM

**Y-27632 dihydrochloride is only required in the culture medium after initial plating and passaging of the organoid using TrypLE.*
DHT, dihydrotestosterone; FGF-10, fibroblast growth factor-10; FGF2, fibroblast growth factor-2; PGE2, prostaglandin E2.

that EGF in culture medium could significantly reduce the sensitivity of PCa organoids to androgen resistance (38); thus, it is necessary to eliminate EGF during the pharmacological response of sensitivity to anti-androgen drugs. FGF2, PGE2, nicotinamide, B27 supplement, and transforming growth factor-beta (TGF-β) inhibitor A83-01 promote the proliferation of prostate cells to maintain the long-term growth of organoids (39–41). P38 kinase inhibitor SB202190 inhibits the histological keratinization phenomenon that may be increased by pressure signal transduction (28). DHT and FGF10 improve the efficiency of organoid formation (28). Rho kinase inhibitor Y-27632 can promote the proliferation of epithelial cells (42). It is worth noting that Y-27632 is only added to the medium during establishment of the first generation of organoids, after which there is no need to add it to the subsequent generations, and added when using TrypLE to digest organoids (27). N-acetylcysteine promotes organoid proliferation by inhibiting cell oxidation (43). These growth factors and hormones constitute the basic conditions to support the survival and long-term culture of PCa cells in the 3D culture system. These studies highlight the importance of media modification in culturing organoids. Required additive components differ depending on cell types, gene mutations and phenotypes of PCa. For instance, the addition of 10% FBS helps to promote the proliferation of PCa organoids for patients with bone metastases (44).

The culture of PCa organoids is still under continuous exploration and improvement. It has evolved from a separate organoid culture to a co-culture of organoid and cells related to the tumor microenvironment (45). For example, Richards et al. (46) co-cultured PCa epithelial cells with primary prostate stromal cells to study the direct interaction between epithelial and stromal cells. They found that the addition of stromal cells not only improved the ability to generalize tissue characteristics, but also improved the survival rate and formation efficiency of tumor organs. This indicates that organoid technology can successfully simulate the growth environment, *in vivo*, for tumor cells through co-culture with the tumor microenvironment. It can also provide a new platform for the study of the interaction of cancer cells with the microenvironment. Unfortunately, only the co-culture of PCa organoids with stromal cells has been studied, and co-culture studies with other tumor microenvironment cells have been reported.

Establishment of Heterogeneous Organoid Models for Prostate Cancer

The specimen for organoid culture can be derived from any stage of tumor development and only a small piece of tissue or few cells are required to culture *in vitro* (47). Thus, different phenotypes of PCa organoids have been successfully cultivated. Karthaus et al. (28) used mouse prostate epithelial cells and human prostate specimens to cultivate normal prostate organoids composed of fully differentiated $CK5^+$ basal cells and $CK8^+$ luminal cells. It was found that such organoids retained the expression of AR signaling factors, prostate-specific transcription factor Nkx3.1, basal cell markers p63 and CK5, and luminal cell marker CK8. At the same time, the original tissues of mouse with *PTEN* knockout and *TMPRSS2-ERG* fusion gene were cultured in organoids, and the phenotypes were consistent. Additionally, Gao et al. (17) successfully cultivated seven metastatic castration-resistant prostate cancer (mCRPC)-type organoids from biopsy tissue

TABLE 3 | Preparation of Noggin-conditioned medium and R-spondin-1-conditioned medium for organoids (27, 35, 36).

Medium	Cell line	Source	Preparation of culture medium
R-spondin-1-conditioned medium	293T-HA-Rspo-Fc cell line	Calvin Kuo Laboratory, Stanford University	Cells are cultured at ~75% confluence. Subsequently, the medium is replaced with advanced DMEM/F12 + 1 M HEPES + 1x Glutamax + 1x penicillin/streptomycin (AdDMEM/F12 +/+/+) for 1 week to create the conditioned medium.
Noggin-conditioned medium	293T/17 cell line	ATCC	pcDNA3.1-based mammalian expression vector containing mouse Noggin cDNA* is transiently transfected into a 293T/17 cell line. After transfection, the cells were cultured in AdDMEM/F12 +/+/+ for 1 week.

**pcDNA3.1-based mammalian expression vector containing mouse Noggin cDNA can be obtained from Hans Clevers Laboratory.*

specimens and CTC in patients with metastatic PCa. These organoids capsulate the molecular diversity and clinical heterogeneity of PCa subtypes, including *TMPRSS2-ERG* fusion, *ETS* translocation, *SPOP* mutation, *SPINK1* overexpression, *FOXA1* and *PIK3R1* mutation, *CHD1* deletion, *PTEN* deletion, and AR expression, and retain the genomic characteristics of primary tumors. These organoids reproduce a large repertoire of patient-derived CRPC lines with different genomic alterations to research PCa.

NEPC, a subtype of PCa with a poor prognosis, easily develops therapeutic resistance (48). Currently, there are only a few effective models for the study of neuroendocrine tumors. Puca et al. (49) successfully cultured four neuroendocrine-like PCa organoids from metastatic biopsy specimens, including simple small cell carcinoma and high-grade carcinoma with extensive neuroendocrine differentiation. They reported that the organoid model is a good tool for further understanding the characteristics of NEPC. Currently, androgen-sensitive and hormone-insensitive CRPC organoid models have been established, and CRPC transformation models have also been reported. Additionally, PCa cell lines LNCaP, C4-2B, and single luminal epithelial progenitors can also produce PCa organoids (29, 50). LNCaP produces androgen-dependent models while C4-2B produces a non-androgen-dependent model, each representing different clinical characteristics.

Recently, a novel *in vitro* modeling system combining the advantages of organoids and PDX has been reported (51). The PDX-organoid model takes less time and costs less than the PDX model and provides an adequate source of tissue for the establishment of organoid models. The LuCap PDX series used surgical specimens from metastatic PCa, successfully producing 21 PDX models (52). Beshiri et al. (30) produced PDX-organoid models with mCRPC characteristics similar to the LuCaP series. These PDX-organoid models retained the genomic heterogeneity of mCRPC and AR-dependent signaling, thus providing a good platform for the study of the pathogenesis, therapeutic options, and individualized treatment for mCRPC. Furthermore, bone metastatic prostate cancer (BMPC) organoid models derived from patients have been successfully established (44).

Limitations of the Method in PCa Organoids

There are several limitations in the establishment of PCa organoids. Firstly, the overall success rate of PCa organoids is only 15-20% (17), limiting the extensive development of clinically diversified PCa models. A study produced statistics on organoids from 81 PCa specimens with diverse pathological and clinical features (53). The success rate of organoid development from metastatic prostatectomy reached 4/9 while that of organoid development from transurethral resection of the prostate was only 4/14. Another study reported a success rate of 16% (4/25) for organoids cultured from patients with metastatic PCa (49). This indicates that the key to the success of PCa organoids depends on the source and intrinsic characteristics of the sample. Therefore, it is necessary to improve the culture conditions for different origins or phenotypes of PCa specimens to obtain a high success rate. Secondly, the organoids from patients with primary PCa have not been successfully cultured to date. This is probably because tumor cells do not have a selective advantage over normal cells in the current culture medium (27). The optimal combination of culture factors still needs to be explored and verified repeatedly. Thirdly, the lack of availability of clinical samples of mCRPC patients hampers the establishment of a biological resource bank of PCa organoids that includes a wide variety of clinical phenotypes. Fourthly, it is still challenging to maintain the growth of organoids for a long time. Fifthly, PCa organoids contained only epithelial cells and/or stromal cells, and lacked some tumor microenvironment components, such as immune cells and vascular components. PCa organoids with an immune compatible microenvironment have not been developed. Therefore, they cannot be used for immunotherapy research.

APPLICATION OF ORGANOID MODELS IN PROSTATE CANCER RESEARCH

As a major technological breakthrough, organoids have been recognized as an important tool for biomedical research. An existing study has shown that PCa organoids can not only recapitulate *in situ* histology *in vitro*, but also have a genetic mutational landscape similar to that of prostate cancer (17). This suggests that organoids provide a very representative *in vitro* model for the study of prostate cancer. Organoids allow research on disease tissue biology, mechanism of disease occurrence and development, drug screening, and personalized treatment in an environment that simulates endogenous cell tissue and organ structure (**Figure 1**). Therefore, we summarize the applications of prostate cancer organoids with respect to these aspects.

Revealing the Diversity and Origin of Prostate Cancer Tumor Cells

In vitro models provide valuable insights into prostate biology, but current *in vitro* modeling systems are not representative of the cellular structure of the prostate. The organoid model better mimics prostate epithelial glands by recapitulating epithelial differentiation and cell polarity (50). Single-cell RNA Sequencing (RNA-Seq) analysis of patient-derived prostate epithelial cells revealed that compared to monolayer cultures, organoid cultures contained more distinct cell populations (54, 55). Ten cell types were identified *in vitro*, including a rare population of putative stem cells marked by high Keratin 13 (*KRT13*), Lymphocyte Antigen 6D (*LY6D*) and prostate stem cell antigen (*PSCA*). These results demonstrated that organoid culture condition has contribute to the survival and proliferation of different cell populations. It has allowed a deeper understanding of the cells present in prostate model systems and the creation of an in-depth atlas of the cellular population.

The origin cell of PCa remains a subject of debate. According to previous studies (56), PCa has two types of origin cells: basal cells and luminal cells. In tissue recombination models, only basal cells reconstitute a complete prostate gland (57, 58). However, it has been shown that luminal cells can generate basal cells through murine lineage-tracing experiments (59). Additionally, in the human prostate, only basal cells have been shown to be effectively transformed by select oncogenes (60). Organoid culture provides a unique model to solve this problem. After the organoid culture of basal and luminal cells of mouse/human prostate tissue were separated by fluorescence-activated cell sorting, both formed prostate-like organoids that retained both basal and luminal epithelial layers and preserved androgen-responsiveness in culture (28). This suggests that both basal and luminal cells have stem-like potential, and organoid culture can maintain stem cell characteristics of PCa. Another study (61) reported that c-MYC/myrAKT1-transduced human prostate basal- and luminal-derived organoids represented histological and molecular features of human PCa. These studies confirm that both human primary basal cells and luminal cells are the origin cells of PCa. Organoids can monitor the early development of PCa *in vitro* in real-time and directly compare the transformation of basal and luminal cells.

As is well-known, organoids are originally derived from cancer stem cells (CSCs) residing within the tumor bulk of the samples. PCa is a highly heterogeneous tumor harboring multiple cancer cell types. Different from the cell-of-origin that undergoes tumorigenic transformation due to gene mutation, CSCs are a cell population with self-renewal and pluripotent properties driving clonal tumor evolution (62). The existence of CSCs provides theoretical explanations for many molecular characteristics, cancer recurrence, metastasis and treatment resistance of PCa (63). Studies on CSCs have been hampered by the lack of suitable *in vitro* models. Here, organoids can be used as a good model *in vitro* for CSCs. Therapies targeting CSCs may lead to more effective cancer treatments for PCa. Therefore, organoid models can help us further understand the composition of normal stem cells and CSCs, which will be important in studying the occurrence and development of prostate cancer.

Exploring the Key Genes Driving the Development of Prostate Cancer

The mechanisms that drive the pathogenesis of PCa and the series of clinical transformations are not well understood. Gene editing at the organoid level can simulate the effects of different gene mutations on the occurrence, development, and heterogeneous transformation of PCa *in vitro*. The easy handling of PCa organoid cultures *in vitro* also facilitates the editing of specific genes related to human diseases using lentivirus transfection, plasmid transformation, or the CRISPR/Cas9 gene-editing system (64, 65). Chua et al. (50) demonstrated that combined *PTEN* deletion and $Kras^{G12D}$ activation in organoids derived from CARNs (castration-resistant Nkx3.1-expressing cells) produced similar phenotypes to donor tumors of PCa *in vivo*. This proved that the deletion of *PTEN* and the routine mutation of *KRAS* are important in the induction of prostate tumors. The tumor origin cells and the chronological sequence of oncogenic events play an important role in defining the disease status. Using PCa organoids, Pietrzak et al. (66) proved that loss of the TIP5 transcription factor could trigger *PTEN*-loss mediated oncogenic transformation in prostate luminal cells, but becomes dispensable once the transformation is established. This suggests that TIP5-mediated chromatin states can control key developmental pathways and tumor suppressor genes, which could drive the development of cancer. In summary, transforming normal prostate organoids into cancerous organoids *in vitro* provides the optimal tool to identify the molecular subtypes of PCa in the genomic analysis of primary tumors.

Considering the heterogeneity of PCa, it is difficult to identify the true driver mutations. However, organoid technology displays a unique advantage. Because normal tissue-derived and tumor tissue-derived organoids from the same patient can be established simultaneously, the discrepancy in gene expression between the two can be compared to identify possible driver mutations. Furthermore, organoid modeling and gene editing can verify the screened mutant genes to study their influence on PCa. Normal tissue-derived organoid has relatively stable genetic information and can be used as a control model for studying tumor mutations.

Drug Screening

Since PCa organoids can maintain genetic stability and heterogeneity, coupled with its easy high-throughput screening, it has become an ideal model for drug toxicity and efficacy evaluation (67). To explore whether CRPC-derived organoids were suitable for drug testing, they were used to determine the sensitivity to enzalutamide, everolimus, and BKM-120 (17). It was found that AR-amplified MSK-PCa2 organoid was extremely sensitive to enzalutamide and resistant to other drugs. Moreover, MSK-PCa2 organoid with *PTEN* loss and *PIK3R1* mutation was sensitive to everolimus and BKM-120, consistent with the results *in vivo*. This result demonstrates the utility of CRPC-derived organoids in assessing drug sensitivity, similar to findings in clinical trials. Further, these results suggest that organoids can be used for drug screening and modeling individualized treatment. Four CRPC-neuroendocrine (CRPC-NE) organoids and two CRPC-adenocarcinoma (CRPC-Aden) organoids were established for high-throughput sequencing of 129 chemotherapeutics and targeted drugs (49). The results demonstrated that the AR antagonist, enzalutamide and taxane chemotherapies, cabazitaxel and docetaxel were effective for CRPC-Aden organoids. A small number of drugs, such as pozotinib and vandetanib, were found to have significant activity in CRPC-NE organoids.

Organoid models are effective *in vitro* drug testing platforms for identifying potential pharmacological treatments and screening inhibitors targeting different phenotypes of PCa. For instance, Jansson et al. (68) screened 110 drugs from CRPC LuCaP PDX-derived organoids and showed that HSP90 inhibitors had a significant inhibitory effect on CRPC. Further

studies have demonstrated that the HSP90 inhibitor, ganetespib, decreased tumor growth by inhibiting multiple targets including the factors involved in AR and PI3K pathways. Using established PTEN/TP53 null LuCaP 136 tumors, they found that compared with any single therapy, the combination of ganetespib and castration significantly inhibited tumor growth and led to a delay in castration resistance.

Studying the Mechanism of Drug Resistance

Gene mutation, chromosome amplification, and chromosome rearrangement are the main reasons for the development of drug resistance in tumors (69). Patient-derived organoids (PDO) of drug resistance can be established according to the different mutations in patients to explore targets for improving the prognosis of patients with PCa, which is incomparable with existing PCa cell lines. It has been confirmed that there are at least three general mechanisms for the development of resistance in CRPC (38). First, genetic mutations, such as *AR*, *ETS*, *TP53*, and *PTEN* gene mutations, lead to the activation of the AR signaling pathway (70). Second, the activation of bypass signals, such as the glucocorticoid receptor pathway, compensates for the loss of the AR signal (71). Third, during treatment, tumor cells acquire resistance by switching lineages from a cell type, dependent on the drug target, to another, which is not. This may be represented by cases of PCa that are AR-negative or neuroendocrine specific (72, 73). The corresponding heterogeneous organoid models will represent their respective resistance mechanisms. Moreover, to clarify the molecular mechanism of PCa resistance, some groups have used PCa organoids as a platform for rapid detection of the effects of different mutations on anti-tumor drugs using CRISPR/Cas9 or lentivirus transfection technology for gene editing. For instance, Pappas et al. (38) used the PCa organoid model to demonstrate that the loss of *p53* did not induce resistance to androgenic molecules but *Pten* deficiency increased resistance to androgenic drugs. However, the dual loss of *p53* and *Pten* resulted in complete resistance to the second generation of anti-androgen drugs. Dai et al. (74) found that PCa-associated *SPOP* mutations conferred resistance to bromodomain and extra-terminal (BET) inhibitors by stabilizing bromodomain-containing protein 4 (BRD4). The development of resistance and relapse in CRPC tumor cells is a major problem in the field of PCa research. Since 3D organoid cultures simulate the emergence of treatment-resistant residual tumors, it provides a more effective platform for study. Dhimolea et al. (75) reported that treatment-resistant residual tumor cells in organoids, xenografts, and cancer patients entered a dormant diapause-like adaptation to reduce apoptosis priming by suppressing *MYC* activity or inhibiting *MYC* transcriptional co-activator *BRD4*, which could weaken drug cytotoxicity and induce the tumor to be resistant to treatment. Therefore, organoid culture can be useful in constructing a heterogeneous PCa model *in vitro* to study the influence of specific genes on PCa resistance with the help of gene-editing technology. It is beneficial for developing first-line therapeutic drugs or screening new therapeutic targets.

Personalized Treatment

Organoids, as preclinical cancer models, can be used to achieve precision medicine through *in vitro* therapeutic screening of individual patient samples. Several studies have demonstrated that drug response to organoids may predict clinical outcomes (76, 77). Although many clinical trials related to PDO models are carried out, there are limited reports about PCa. Beltran H's team cultured CRPC-NE samples from patients into organoids for high-throughput drug screening. One CRPC-NE organoid, OWCM155, showed significant sensitivity to aurora kinase inhibitor alisertib (49), a result concordant with what was being observed from the clinical response of corresponding patients in the phase II trial of alisertib for CRPC-NE (NCT01482962) (78). On the other hand, the CRPC-NE organoid, OWCM154, did not react to alisertib *in vitro*, nor did the patient in phase II clinical trial. In additional, Beshiri et al. (30) found that LuCaP-derived organoids with *BRCA2* deficiency were sensitive to olaparib, which was consistent with the response observed in clinical setting (79). These data indicate that organoids may be useful tools as patient 'avatars' for clinical trials and applied to develop new strategies for precision medicine in cancer. However, not all drug responses of organoids are consistent with clinical responses. Karkampouna at al. (80). cultured PDOs for drug screening. The organoids from an advanced PCa patient (case P82) as well as from a primary PCa patient (case P134) were both resistant to enzalutamide *in vitro*, while cases P82 and P134, were sensitive and resistant, respectively, to enzalutamide. The correlation between drug responses of organoids and clinical responses may depend on the size or site of the patient sample. Larger sample sizes would be needed to increase the confidence level in the data. The high heterogeneity of PCa and the drug profiles correlated with disease stage, sometimes leads to incompatibility between the results of the drug response in organoids and the clinical response of the patient.

DISCUSSION

As a novel *in vitro* preclinical disease model, the PCa organoid has potential for broad applications. This model is not only convenient for *in vitro* applications, but also demonstrates genetic stability and heterogeneity. Not only can it be applied for multi-model verification of PCa pathogenesis and drug screening combined with the PDX animal model, but also for observing the growth and development of tumor cells or tissues *in vitro* and studying the effects of different mutations on the occurrence and development of diseases. This model provides effective guidance for studying the heterogeneous transformation mechanism of PCa, especially to understand the molecular mechanisms underlying androgen resistance and to screen potential therapeutic targets. From the perspective of drug screening and individualized treatment, different primary or metastatic PCa organoids can be established using PCa samples from different sources. Combined with high-throughput screening technology, anti-PCa drugs can be assessed in batches. The response of patients with PCa to

different drugs can be predicted effectively, which will accelerate the development of therapeutic regimens for heterogeneous characteristics of PCa. In PCa organoids, CRISPR/Cas9 and shRNA techniques have been used to study the mechanism of drug resistance. This will allow the study of the functions of drug resistance genes, and will ultimately enable the improvement of first-line therapeutic drugs and the development of novel individualized drugs. Inevitably, PCa organoids still have some challenges including low efficiency of establishing organoids (particularly primary PCa) from human samples, the optimal combination of medium factors that need to be added and the maintenance of culturing those organoids for a long time. Additionally, there are new application directions for PCa organoids.

Exploring the Interaction Between Prostate Cancer Tumor Cells and Their Microenvironment

Exploring the interaction between the tumor and its microenvironment is an important aspect of oncology research. Organoid culture of the vascular system *in vitro* simulates the interaction between tumor cells and the vascular system while that of the nervous system revealed the interaction between cells and the nervous system. Immunocytes are co-cultured with tumor organoids to reveal the relationship between tumor cells and immune infiltrating cells (81). It is necessary to further study the role of fibroblasts, immune cells, and endothelial cells in the tumor microenvironment so that the structure of PCa organoids can better represent the composition of PCa *in vivo*.

Clinical Individualized Treatments for Patients With Prostate Cancer

The lack of *in vitro* tumor models maintaining the characteristics of tumor cells *in vivo* has become a bottleneck in the realization of personalized therapy and precision therapy for patients with cancer. Organoids are an ideal model for drug testing and screening because of their ability to be cultured *in vitro* for a long time to maximize the characterization of tumor cells *in vivo*. Therefore, to better reflect the clinical heterogeneity of PCa, it is necessary to improve the culture conditions in the future to better support the growth of different types of PCa cells. In 2014, world's first prostate tumor organ bank was established (18). These organoids were used to test a variety of experimental drugs and cancer drugs, finding that tumor organs with different genetic backgrounds had different sensitivities to these drugs.

Heterogeneous Transformation Model

Patients with CRPC that have high treatment selection pressure can lead to a significant increase in PCa heterogeneity (82), such as changes in AR and PSA expression levels, AR mutations, and the occurrence of the NEPC phenotype. Therefore, more CRPC models are needed to represent different resistance mechanisms, especially dynamic models to reflect their transformation characteristics. The existing organoid models only reflect the static characteristics of a patient at a certain stage and are insufficient in simulating the diversity and disease progression of PCa. Therefore, it is inevitable to develop a model based on the same specimen that can be induced to reflect the whole process of PCa transformation, including the development of CRPC, the transformation from adenocarcinoma to NEPC, and the occurrence of metastasis. This aids tremendously in investigating progression from pre-neoplastic to neoplastic to metastatic states. Additionally, a paired comparison model can be generated through organoid culture to compare genotypes and phenotypes and explore the mechanism of their heterogeneity.

Tumor Immunotherapy

The application of tumor organoids in tumor immunology offers researchers another attractive preclinical option. Studies (83–85) have found that tumor organoids can be co-cultured with immune cells isolated from autologous tumor tissues or peripheral blood of healthy donors. Further studies on different immune cells should be performed, including amplification of tumor organoids *in vitro* to explore the interaction between the immune system and tumors. In the model of tumor immunotherapy, compared with immortalized tumor cell lines and humanized immune-oncology models (86, 87), the co-culture of tumor organoids and immune cells from tumor tissues better represents the response of patients to immunotherapy. The co-culture system of tumor organoids and immune cells has a short experimental cycle and does not have the problem of human-mouse immune compatibility, which is expected for an ideal model for tumor immunotherapy.

Organoid Models Combined With Liquid Biopsy

The patient derived PDX model of PCa was established using a specimen from surgical resection or autopsy, highlighting the need for more specimens. At the same time, the heterogeneity within the tumor is one of the challenges of traditional tissue biopsy. Liquid biopsy is expected to overcome these issues. CTC can be used as an alternative to invasive biopsies to study the heterogeneity of tumors (88). However, liquid biopsy has disadvantages in the detection and enrichment of CTC since only a few CTC can usually be obtained. Tumor organoids can be grown from only limited amounts of specimens to solve this problem. Gao et al. (17) confirmed the feasibility of using a small amount of CTC from peripheral blood of patients with PCa to culture tumor organoids. Exome sequencing showed that PCa organoids derived from CTC retained molecular diversity consistent with primary tumors, including *TMPRSS2-ERG* fusion, *SPOP* mutation, *SPINK1* overexpression, and *CHD1* loss. This is the only successful case of derivation of organoids from blood samples reported thus far. Liquid biopsy combined with tumor organoids may create new opportunities for minimally invasive studies and may facilitate the inclusion of PDO in personalized medical procedures for cancers.

In conclusion, it is necessary to continuously optimize the culture conditions of PCa organoids, constructing a tumor microenvironment more suitable for the different mutations in PCa. Further improving the success rate of PCa organoids is beneficial for obtaining a wider range of phenotypes and genotypes. This will allow the construction of models for

hormone naïve PCa, CRPC, and mCRPC to fully demonstrate the clinical heterogeneity of PCa. This will also allow the formation of a PCa organoid bank to maximize its utility in mirroring clinical characteristics and become the preferred preclinical disease model of PCa.

AUTHOR CONTRIBUTIONS

LZ, YZ, and CS: conceptualization. LZ, CZ, and CS: writing. LZ, CZ, and CS: revising. All authors contributed to the article and approved the submitted version.

FUNDING

This study was funded by the National Natural Science Foundation Program of China (No. 31772546 and 32070532) and Laboratory Animal Foundation Program No. SYDW [2017]-02.

ACKNOWLEDGMENTS

We would like to thank Editage (www.editage.cn) for English language editing.

REFERENCES

1. Siegel RL, Miller KD, Fuchs HE, Jemal A. Cancer Statistics, 2021. *CA Cancer J Clin* (2021) 71:7–33. doi: 10.3322/caac.21654
2. Sung H, Ferlay J, Siegel RL, Laversanne M, Soerjomataram I, Jemal A, et al. Global Cancer Statistics 2020: GLOBOCAN Estimates of Incidence and Mortality Worldwide for 36 Cancers in 185 Countries. *CA Cancer J Clin* (2021) 71:209–49. doi: 10.3322/caac.21660
3. Mottet N, van den Bergh RCN, Briers E, Van den Broeck T, Cumberbatch MG, De Santis M, et al. EAU-EANM-ESTRO-ESUR-SIOG Guidelines on Prostate Cancer-2020 Update. Part 1: Screening, Diagnosis, and Local Treatment With Curative Intent. *Eur Urol* (2021) 79:243–62. doi: 10.1016/j.eururo.2020.09.042
4. Cornford P, van den Bergh RCN, Briers E, Van den Broeck T, Cumberbatch MG, De Santis M, et al. EAU-EANM-ESTRO-ESUR-SIOG Guidelines on Prostate Cancer. Part II-2020 Update: Treatment of Relapsing and Metastatic Prostate Cancer. *Eur Urol* (2021) 79:263–82. doi: 10.1016/j.eururo.2020.09.046
5. Karantanos T, Corn PG, Thompson TC. Prostate Cancer Progression After Androgen Deprivation Therapy: Mechanisms of Castrate Resistance and Novel Therapeutic Approaches. *Oncogene* (2013) 32:5501–11. doi: 10.1038/onc.2013.206
6. Ma T, Bai S, Qi Y, Zhan Y, Ungerleider N, Zhang DY, et al. Increased Transcription and High Translation Efficiency Lead to Accumulation of Androgen Receptor Splice Variant After Androgen Deprivation Therapy. *Cancer Lett* (2021) 504:37–48. doi: 10.1016/j.canlet.2020.12.037
7. Sobel RE, Sadar MD. Cell Lines Used in Prostate Cancer Research: A Compendium of Old and New Lines–Part 1. *J Urol* (2005) 173:342–59. doi: 10.1097/01.ju.0000141580.30910.57
8. van Bokhoven A, Varella-Garcia M, Korch C, Johannes WU, Smith EE, Miller HL, et al. Molecular Characterization of Human Prostate Carcinoma Cell Lines. *Prostate* (2003) 57:205–25. doi: 10.1002/pros.10290
9. Namekawa T, Ikeda K, Horie-Inoue K, Inoue S. Application of Prostate Cancer Models for Preclinical Study: Advantages and Limitations of Cell Lines, Patient-Derived Xenografts, and Three-Dimensional Culture of Patient-Derived Cells. *Cells* (2019) 8:74. doi: 10.3390/cells8010074
10. Palechor-Ceron N, Krawczyk E, Dakic A, Simic V, Yuan H, Blancato J, et al. Conditional Reprogramming for Patient-Derived Cancer Models and Next-Generation Living Biobanks. *Cells* (2019) 8:1327. doi: 10.3390/cells8111327
11. Timofeeva OA, Palechor-Ceron N, Li G, Yuan H, Krawczyk E, Zhong X, et al. Conditionally Reprogrammed Normal and Primary Tumor Prostate Epithelial Cells: A Novel Patient-Derived Cell Model for Studies of Human Prostate Cancer. *Oncotarget* (2017) 8:22741–58. doi: 10.18632/oncotarget.13937
12. Wu X, Wang S, Li M, Li J, Shen J, Zhao Y, et al. Conditional Reprogramming: Next Generation Cell Culture. *Acta Pharm Sin B* (2020) 10:1360–81. doi: 10.1016/j.apsb.2020.01.011
13. Jacob F, Salinas RD, Zhang DY, Nguyen PTT, Schnoll JG, Wong SZH, et al. A Patient-Derived Glioblastoma Organoid Model and Biobank Recapitulates Inter- and Intra-Tumoral Heterogeneity. *Cell* (2020) 180:188–204.e22. doi: 10.1016/j.cell.2019.11.036
14. Kopper O, de Witte CJ, Lõhmussaar K, Valle-Inclan JE, Hami N, Kester L, et al. An Organoid Platform for Ovarian Cancer Captures Intra- and Interpatient Heterogeneity. *Nat Med* (2019) 25:838–49. doi: 10.1038/s41591-019-0422-6
15. Kondo J, Inoue M. Application of Cancer Organoid Model for Drug Screening and Personalized Therapy. *Cells* (2019) 8:470. doi: 10.3390/cells8050470
16. Mazzocchi A, Soker S, Skardal A. 3D Bioprinting for High-Throughput Screening: Drug Screening, Disease Modeling, and Precision Medicine Applications. *Appl Phys Rev* (2019) 6:011302. doi: 10.1063/1.5056188
17. Gao D, Vela I, Sboner A, Iaquinta PJ, Karthaus WR, Gopalan A, et al. Organoid Cultures Derived From Patients With Advanced Prostate Cancer. *Cell* (2014) 159:176–87. doi: 10.1016/j.cell.2014.08.016
18. Bahmad HF, Cheaito K, Chalhoub RM, Hadadeh O, Monzer A, Ballout F, et al. Sphere-Formation Assay: Three-Dimensional *In Vitro* Culturing of Prostate Cancer Stem/Progenitor Sphere-Forming Cells. *Front Oncol* (2018) 8:347. doi: 10.3389/fonc.2018.00347
19. Vela I, Chen Y. Prostate Cancer Organoids: A Potential New Tool for Testing Drug Sensitivity. *Expert Rev Anticancer Ther* (2015) 15:261–3. doi: 10.1586/14737140.2015.1003046
20. Okada S, Vaeteewoottacharn K, Kariya R. Application of Highly Immunocompromised Mice for the Establishment of Patient-Derived Xenograft (PDX) Models. *Cells* (2019) 8:889. doi: 10.3390/cells8080889
21. Arriaga JM, Abate-Shen C. Genetically Engineered Mouse Models of Prostate Cancer in the Postgenomic Era. *Cold Spring Harb Perspect Med* (2019) 9:a030528. doi: 10.1101/cshperspect.a030528
22. Walrath JC, Hawes JJ, Van Dyke T, Reilly KM. Genetically Engineered Mouse Models in Cancer Research. *Adv Cancer Res* (2010) 106:113–64. doi: 10.1016/S0065-230X(10)06004-5
23. Parisotto M, Metzger D. Genetically Engineered Mouse Models of Prostate Cancer. *Mol Oncol* (2013) 7:190–205. doi: 10.1016/j.molonc.2013.02.005
24. Lancaster MA, Knoblich JA. Organogenesis in a Dish: Modeling Development and Disease Using Organoid Technologies. *Science* (2014) 345:1247125. doi: 10.1126/science.1247125
25. Lin D, Wyatt AW, Xue H, Wang Y, Dong X, Haegert A, et al. High Fidelity Patient-Derived Xenografts for Accelerating Prostate Cancer Discovery and Drug Development. *Cancer Res* (2014) 74:1272–83. doi: 10.1158/0008-5472.CAN-13-2921-T
26. Sato T, Vries RG, Snippert HJ, van de Wetering M, Barker N, Stange DE, et al. Single Lgr5 Stem Cells Build Crypt-Villus Structures *In Vitro* Without a Mesenchymal Niche. *Nature* (2009) 459:262–5. doi: 10.1038/nature07935
27. Drost J, Karthaus WR, Gao D, Driehuis E, Sawyers CL, Chen Y, et al. Organoid Culture Systems for Prostate Epithelial and Cancer Tissue. *Nat Protoc* (2016) 11:347–58. doi: 10.1038/nprot.2016.006
28. Karthaus WR, Iaquinta PJ, Drost J, Gracanin A, van Boxtel R, Wongvipat J, et al. Identification of Multipotent Luminal Progenitor Cells in Human Prostate Organoid Cultures. *Cell* (2014) 159:163–75. doi: 10.1016/j.cell.2014.08.017
29. Ma L, Li J, Nie Q, Zhang Q, Liu S, Ge D, et al. Organoid Culture of Human Prostate Cancer Cell Lines Lncap and C4-2B. *Am J Clin Exp Urol* (2017) 5:25–33.
30. Beshiri ML, Tice CM, Tran C, Nguyen HM, Sowalsky AG, Agarwal S, et al. A PDX/Organoid Biobank of Advanced Prostate Cancers Captures Genomic and Phenotypic Heterogeneity for Disease Modeling and Therapeutic Screening. *Clin Cancer Res* (2018) 24:4332–45. doi: 10.1158/1078-0432.CCR-18-0409

31. Calderon-Gierszal EL, Prins GS. Directed Differentiation of Human Embryonic Stem Cells Into Prostate Organoids In Vitro and Its Perturbation by Low-Dose Bisphenol a Exposure. *PloS One* (2015) 10: e0133238. doi: 10.1371/journal.pone.0133238
32. Hepburn AC, Curry EL, Moad M, Steele RE, Franco OE, Wilson L, et al. Propagation of Human Prostate Tissue From Induced Pluripotent Stem Cells. *Stem Cells Transl Med* (2020) 9:734–45. doi: 10.1002/sctm.19-0286
33. Carmon KS, Gong X, Lin Q, Thomas A, Liu Q. R-Spondins Function as Ligands of the Orphan Receptors LGR4 and LGR5 to Regulate Wnt/Beta-Catenin Signaling. *Proc Natl Acad Sci USA* (2011) 108:11452–7. doi: 10.1073/pnas.1106083108
34. Cook C, Vezina CM, Allgeier SH, Shaw A, Yu M, Peterson RE, et al. Noggin Is Required for Normal Lobe Patterning and Ductal Budding in the Mouse Prostate. *Dev Biol* (2007) 312:217–30. doi: 10.1016/j.ydbio.2007.09.038
35. Broutier L, Andersson-Rolf A, Hindley CJ, Boj SF, Clevers H, Koo BK, et al. Culture and Establishment of Self-Renewing Human and Mouse Adult Liver and Pancreas 3D Organoids and Their Genetic Manipulation. *Nat Protoc* (2016) 11:1724–43. doi: 10.1038/nprot.2016.097
36. Yan HHN, Siu HC, Law S, Ho SL, Yue SSK, Tsui WY, et al. A Comprehensive Human Gastric Cancer Organoid Biobank Captures Tumor Subtype Heterogeneity and Enables Therapeutic Screening. *Cell Stem Cell* (2018) 23:882–897.e11. doi: 10.1016/j.stem.2018.09.016
37. Cheaito K, Bahmad HF, Jalloul H, Hadadeh O, Msheik H, El-Hajj A, et al. Epidermal Growth Factor Is Essential for the Maintenance of Novel Prostate Epithelial Cells Isolated From Patient-Derived Organoids. *Front Cell Dev Biol* (2020) 8:571677. doi: 10.3389/fcell.2020.571677
38. Pappas KJ, Choi D, Sawyers CL, Karthaus WR. Prostate Organoid Cultures as Tools to Translate Genotypes and Mutational Profiles to Pharmacological Responses. *J Vis Exp* (2019) 152:e60346. doi: 10.3791/60346
39. Kato M, Ishii K, Iwamoto Y, Sasaki T, Kanda H, Yamada Y, et al. Activation of FGF2-FGFR Signaling in the Castrated Mouse Prostate Stimulates the Proliferation of Basal Epithelial Cells. *Biol Reprod* (2013) 89:81. doi: 10.1095/biolreprod.112.107516
40. Sato T, Stange DE, Ferrante M, Vries RG, Van Es JH, Van den Brink S, et al. Long-Term Expansion of Epithelial Organoids From Human Colon, Adenoma, Adenocarcinoma, and Barrett's Epithelium. *Gastroenterology* (2011) 141:1762–72. doi: 10.1053/j.gastro.2011.07.050
41. Vo BT, Morton DJr, Komaragiri S, Millena AC, Leath C, Khan SA. Tgf-β Effects on Prostate Cancer Cell Migration and Invasion Are Mediated by PGE2 Through Activation of PI3K/AKT/Mtor Pathway. *Endocrinology* (2013) 154:1768–79. doi: 10.1210/en.2012-2074
42. Liu X, Ory V, Chapman S, Yuan H, Albanese C, Kallakury B, et al. ROCK Inhibitor and Feeder Cells Induce the Conditional Reprogramming of Epithelial Cells. *Am J Pathol* (2012) 180:599–607. doi: 10.1016/j.ajpath.2011.10.036
43. Khanna S, Mitra S, Lakhera PC, Khandelwal S. N-Acetylcysteine Effectively Mitigates Cadmium-Induced Oxidative Damage and Cell Death in Leydig Cells *In Vitro*. *Drug Chem Toxicol* (2016) 39:74–80. doi: 10.3109/01480545.2015.1028068
44. Lee S, Burner DN, Mendoza TR, Muldong MT, Arreola C, Wu CN, et al. Establishment and Analysis of Three-Dimensional (3D) Organoids Derived From Patient Prostate Cancer Bone Metastasis Specimens and Their Xenografts. *J Vis Exp* (2020) 156:e60367. doi: 10.3791/60367
45. Eder T, Eder IE. 3D Hanging Drop Culture to Establish Prostate Cancer Organoids. *Methods Mol Biol* (2017) 1612:167–75. doi: 10.1007/978-1-4939-7021-6_12
46. Richards Z, McCray T, Marsili J, Zenner ML, Manlucu JT, Garcia J, et al. Prostate Stroma Increases the Viability and Maintains the Branching Phenotype of Human Prostate Organoids. *iScience* (2019) 12:304–17. doi: 10.1016/j.isci.2019.01.028
47. Xia X, Li F, He J, Aji R, Gao D. Organoid Technology in Cancer Precision Medicine. *Cancer Lett* (2019) 457:20–7. doi: 10.1016/j.canlet.2019.04.039
48. Wang HT, Yao YH, Li BG, Tang Y, Chang JW, Zhang J. Neuroendocrine Prostate Cancer (NEPC) Progressing From Conventional Prostatic Adenocarcinoma: Factors Associated With Time to Development of NEPC and Survival From NEPC Diagnosis-a Systematic Review and Pooled Analysis. *J Clin Oncol* (2014) 32:3383–90. doi: 10.1200/JCO.2013.54.3553
49. Puca L, Bareja R, Prandi D, Shaw R, Benelli M, Karthaus WR, et al. Patient Derived Organoids to Model Rare Prostate Cancer Phenotypes. *Nat Commun* (2018) 9:2404. doi: 10.1038/s41467-018-04495-z
50. Chua CW, Shibata M, Lei M, Toivanen R, Barlow LJ, Bergren SK, et al. Single Luminal Epithelial Progenitors can Generate Prostate Organoids in Culture. *Nat Cell Biol* (2014) 16:951–61. doi: 10.1038/ncb3047
51. Huang L, Bockorny B, Paul I, Akshinthala D, Frappart PO, Gandarilla O, et al. PDX-Derived Organoids Model *In Vivo* Drug Response and Secrete Biomarkers. *JCI Insight* (2020) 5:e135544. doi: 10.1172/jci.insight.135544
52. Nguyen HM, Vessella RL, Morrissey C, Brown LG, Coleman IM, Higano CS, et al. Lucap Prostate Cancer Patient-Derived Xenografts Reflect the Molecular Heterogeneity of Advanced Disease and Serve as Models for Evaluating Cancer Therapeutics. *Prostate* (2017) 77:654–71. doi: 10.1002/pros.23313
53. Servant R, Garioni M, Vlajnic T, Blind M, Pueschel H, Müller DC, et al. Prostate Cancer Patient-Derived Organoids: Detailed Outcome From a Prospective Cohort of 81 Clinical Specimens. *J Pathol* (2021) 254:543–55. doi: 10.1002/path.5698
54. McCray T, Moline D, Baumann B, Vander Griend DJ, Nonn L. Single-Cell RNA-Seq Analysis Identifies a Putative Epithelial Stem Cell Population in Human Primary Prostate Cells in Monolayer and Organoid Culture Conditions. *Am J Clin Exp Urol* (2019) 7:123–38.
55. Henry GH, Malewska A, Joseph DB, Malladi VS, Lee J, Torrealba J, et al. A Cellular Anatomy of the Normal Adult Human Prostate and Prostatic Urethra. *Cell Rep* (2018) 25:3530–3542.e5. doi: 10.1016/j.celrep.2018.11.086
56. Packer JR, Maitland NJ. The Molecular and Cellular Origin of Human Prostate Cancer. *Biochim Biophys Acta* (2016) 1863:1238–60. doi: 10.1016/j.bbamcr.2016.02.016
57. Goldstein AS, Lawson DA, Cheng D, Sun W, Garraway IP, Witte ON. Trop2 Identifies a Subpopulation of Murine and Human Prostate Basal Cells With Stem Cell Characteristics. *Proc Natl Acad Sci USA* (2008) 105:20882–7. doi: 10.1073/pnas.0811411106
58. Garraway IP, Sun W, Tran CP, Perner S, Zhang B, Goldstein AS, et al. Human Prostate Sphere-Forming Cells Represent a Subset of Basal Epithelial Cells Capable of Glandular Regeneration In Vivo. *Prostate* (2010) 70:491–501. doi: 10.1002/pros.21083
59. Wang ZA, Mitrofanova A, Bergren SK, Abate-Shen C, Cardiff RD, Califano A, et al. Lineage Analysis of Basal Epithelial Cells Reveals Their Unexpected Plasticity and Supports a Cell-of-Origin Model for Prostate Cancer Heterogeneity. *Nat Cell Biol* (2013) 15:274–83. doi: 10.1038/ncb2697
60. Stoyanova T, Cooper AR, Drake JM, Liu X, Armstrong AJ, Pienta KJ, et al. Prostate Cancer Originating in Basal Cells Progresses to Adenocarcinoma Propagated by Luminal-Like Cells. *Proc Natl Acad Sci USA* (2013) 110:20111–6. doi: 10.1073/pnas.1320565110
61. Park JW, Lee JK, Phillips JW, Huang P, Cheng D, Huang J, et al. Prostate Epithelial Cell of Origin Determines Cancer Differentiation State in an Organoid Transformation Assay. *Proc Natl Acad Sci USA* (2016) 113:4482–7. doi: 10.1073/pnas.1603645113
62. Rycaj K, Tang DG. Cell-of-Origin of Cancer Versus Cancer Stem Cells: Assays and Interpretations. *Cancer Res* (2015) 75:4003–11. doi: 10.1158/0008-5472.CAN-15-0798
63. Skvortsov S, Skvortsova II, Tang DG, Dubrovska A. Concise Review: Prostate Cancer Stem Cells: Current Understanding. *Stem Cells* (2018) 36:1457–74. doi: 10.1002/stem.2859
64. Koo BK, Stange DE, Sato T, Karthaus W, Farin HF, Huch M, et al. Controlled Gene Expression in Primary Lgr5 Organoid Cultures. *Nat Methods* (2011) 9:81–3. doi: 10.1038/nmeth.1802
65. Nie J, Hashino E. Organoid Technologies Meet Genome Engineering. *EMBO Rep* (2017) 18:367–76. doi: 10.15252/embr.201643732
66. Pietrzak K, Kuzyakiv R, Simon R, Bolis M, Bär D, Aprigliano R, et al. TIP5 Primes Prostate Luminal Cells for the Oncogenic Transformation Mediated by PTEN-Loss. *Proc Natl Acad Sci USA* (2020) 117:3637–47. doi: 10.1073/pnas.1911673117
67. Weeber F, Ooft SN, Dijkstra KK, Voest EE. Tumor Organoids as a Pre-Clinical Cancer Model for Drug Discovery. *Cell Chem Biol* (2017) 24:1092–100. doi: 10.1016/j.chembiol.2017.06.012
68. Jansson KH, Tucker JB, Stahl LE, Simmons JK, Fuller C, Beshiri ML, et al. High-Throughput Screens Identify HSP90 Inhibitors as Potent Therapeutics That Target Inter-Related Growth and Survival Pathways in Advanced Prostate Cancer. *Sci Rep* (2018) 8:17239. doi: 10.1038/s41598-018-35417-0
69. Fojo T. Multiple Paths to a Drug Resistance Phenotype: Mutations, Translocations, Deletions and Amplification of Coding Genes or Promoter

Regions, Epigenetic Changes and Micrornas. *Drug Resist Update* (2007) 10:59–67. doi: 10.1016/j.drup.2007.02.002
70. Robinson D, Van Allen EM, Wu YM, Schultz N, Lonigro RJ, Mosquera JM, et al. Integrative Clinical Genomics of Advanced Prostate Cancer. *Cell* (2015) 161:1215–28. doi: 10.1016/j.cell.2015.06.053
71. Arora VK, Schenkein E, Murali R, Subudhi SK, Wongvipat J, Balbas MD, et al. Glucocorticoid Receptor Confers Resistance to Antiandrogens by Bypassing Androgen Receptor Blockade. *Cell* (2013) 155:1309–22. doi: 10.1016/j.cell.2013.11.012
72. Ku SY, Rosario S, Wang Y, Mu P, Seshadri M, Goodrich ZW, et al. Rb1 and Trp53 Cooperate to Suppress Prostate Cancer Lineage Plasticity, Metastasis, and Antiandrogen Resistance. *Science* (2017) 355:78–83. doi: 10.1126/science.aah4199
73. Mu P, Zhang Z, Benelli M, Karthaus WR, Hoover E, Chen CC, et al. SOX2 Promotes Lineage Plasticity and Antiandrogen Resistance in TP53- and RB1-Deficient Prostate Cancer. *Science* (2017) 355:84–8. doi: 10.1126/science.aah4307
74. Dai X, Gan W, Li X, Wang S, Zhang W, Huang L, et al. Prostate Cancer-Associated SPOP Mutations Confer Resistance to BET Inhibitors Through Stabilization of BRD4. *Nat Med* (2017) 23:1063–71. doi: 10.1038/nm.4378
75. Dhimolea E, de Matos Simoes R, Kansara D, Al'Khafaji A, Bouyssou J, Weng X, et al. An Embryonic Diapause-Like Adaptation With Suppressed Myc Activity Enables Tumor Treatment Persistence. *Cancer Cell* (2021) 39:240–256.e11. doi: 10.1016/j.ccell.2020.12.002
76. Pauli C, Hopkins BD, Prandi D, Shaw R, Fedrizzi T, Sboner A, et al. Personalized In Vitro and In Vivo Cancer Models to Guide Precision Medicine. *Cancer Discovery* (2017) 7:462–77. doi: 10.1158/2159-8290.CD-16-1154
77. Vlachogiannis G, Hedayat S, Vatsiou A, Jamin Y, Fernández-Mateos J, Khan K, et al. Patient-Derived Organoids Model Treatment Response of Metastatic Gastrointestinal Cancers. *Science* (2018) 359:920–6. doi: 10.1126/science.aao2774
78. Beltran H, Oromendia C, Danila DC, Montgomery B, Hoimes C, Szmulewitz RZ, et al. A Phase II Trial of the Aurora Kinase a Inhibitor Alisertib for Patients With Castration-Resistant and Neuroendocrine Prostate Cancer: Efficacy and Biomarkers. *Clin Cancer Res* (2019) 25:43–51. doi: 10.1158/1078-0432.CCR-18-1912
79. Mateo J, Carreira S, Sandhu S, Miranda S, Mossop H, Perez-Lopez R, et al. DNA-Repair Defects and Olaparib in Metastatic Prostate Cancer. *N Engl J Med* (2015) 373:1697–708. doi: 10.1056/NEJMoa1506859
80. Karkampouna S, La Manna F, Benjak A, Kiener M, De Menna M, Zoni E, et al. Patient-Derived Xenografts and Organoids Model Therapy Response in Prostate Cancer. *Nat Commun* (2021) 12:1117. doi: 10.1038/s41467-021-21300-6
81. Xu R, Zhou X, Wang S, Trinkle C. Tumor Organoid Models in Precision Medicine and Investigating Cancer-Stromal Interactions. *Pharmacol Ther* (2021) 218:107668. doi: 10.1016/j.pharmthera.2020.107668
82. Grasso CS, Wu YM, Robinson DR, Cao X, Dhanasekaran SM, Khan AP, et al. The Mutational Landscape of Lethal Castration-Resistant Prostate Cancer. *Nature* (2012) 487:239–43. doi: 10.1038/nature11125
83. Dijkstra KK, Cattaneo CM, Weeber F, Chalabi M, van de Haar J, Fanchi LF, et al. Generation of Tumor-Reactive T Cells by Co-Culture of Peripheral Blood Lymphocytes and Tumor Organoids. *Cell* (2018) 174:1586–1598.e12. doi: 10.1016/j.cell.2018.07.009
84. Cattaneo CM, Dijkstra KK, Fanchi LF, Kelderman S, Kaing S, van Rooij N, et al. Tumor Organoid-T-Cell Coculture Systems. *Nat Protoc* (2020) 15:15–39. doi: 10.1038/s41596-019-0232-9
85. Neal JT, Li X, Zhu J, Giangarra V, Grzeskowiak CL, Ju J, et al. Organoid Modeling of the Tumor Immune Microenvironment. *Cell* (2018) 175:1972–1988.e16. doi: 10.1016/j.cell.2018.11.021
86. Yuki K, Cheng N, Nakano M, Kuo CJ. Organoid Models of Tumor Immunology. *Trends Immunol* (2020) 41:652–64. doi: 10.1016/j.it.2020.06.010
87. Guo W, Zhang C, Qiao T, Zhao J, Shi C. Strategies for the Construction of Mouse Models With Humanized Immune System and Evaluation of Tumor Immune Checkpoint Inhibitor Therapy. *Front Oncol* (2021) 11:673199. doi: 10.3389/fonc.2021.673199
88. Praharaj PP, Bhutia SK, Nagrath S, Bitting RL, Deep G. Circulating Tumor Cell-Derived Organoids: Current Challenges and Promises in Medical Research and Precision Medicine. *Biochim Biophys Acta Rev Cancer* (2018) 1869:117–27. doi: 10.1016/j.bbcan.2017.12.005

Conflict of Interest: The authors declare that the research was conducted in the absence of any commercial or financial relationships that could be construed as a potential conflict of interest.

Publisher's Note: All claims expressed in this article are solely those of the authors and do not necessarily represent those of their affiliated organizations, or those of the publisher, the editors and the reviewers. Any product that may be evaluated in this article, or claim that may be made by its manufacturer, is not guaranteed or endorsed by the publisher.

Copyright © 2021 Zhou, Zhang, Zhang and Shi. This is an open-access article distributed under the terms of the Creative Commons Attribution License (CC BY). The use, distribution or reproduction in other forums is permitted, provided the original author(s) and the copyright owner(s) are credited and that the original publication in this journal is cited, in accordance with accepted academic practice. No use, distribution or reproduction is permitted which does not comply with these terms.

frontiers in Oncology

CASE REPORT
published: 27 September 2021
doi: 10.3389/fonc.2021.732071

Case Report: Systemic Treatment and Serial Genomic Sequencing of Metastatic Prostate Adenocarcinoma Progressing to Small Cell Carcinoma

XiaoJun Lu[1†], Wenwen Gao[2†], Yu Zhang[3†], Tao Wang[4], Hongliang Gao[1], Qing Chen[1], Xiaolei Shi[1], Bijun Lian[5], Wenhui Zhang[1], Xu Gao[1*] and Jing Li[3*]*

[1] Department of Urology, Shanghai Changhai Hospital, Second Military Medical University, Shanghai, China, [2] Department of Oncology, Shidong Hospital, Affiliated to University of Shanghai for Science and Technology, Shanghai, China, [3] Department of Bioinformatics, Center for Translational Medicine, Second Military Medical University, Shanghai, China, [4] Department of Urology, The First Affiliated Hospital of Zhengzhou University, Zhengzhou, China, [5] Department of Urology, The 903th PLA Hospital, Hangzhou, China

OPEN ACCESS

Edited by:
Tanya I. Stoyanova, Stanford University, United States

Reviewed by:
Shaolong Cao, University of Texas MD Anderson Cancer Center, United States
Baijun Dong, Shanghai JiaoTong University, China

***Correspondence:**
Jing Li
drljing@163.com
Xu Gao
gaoxu.changhai@foxmail.com
Wenhui Zhang
daring_wh@smmu.edu.cn

[†]These authors have contributed equally to this work

Specialty section:
This article was submitted to Genitourinary Oncology, a section of the journal Frontiers in Oncology

Received: *28 June 2021*
Accepted: *06 September 2021*
Published: *27 September 2021*

Citation:
Lu X, Gao W, Zhang Y, Wang T, Gao H, Chen Q, Shi X, Lian B, Zhang W, Gao X and Li J (2021) Case Report: Systemic Treatment and Serial Genomic Sequencing of Metastatic Prostate Adenocarcinoma Progressing to Small Cell Carcinoma. Front. Oncol. 11:732071. doi: 10.3389/fonc.2021.732071

Small cell carcinoma (SCC)/neuroendocrine prostate cancer (NEPC) is a rare and highly aggressive subtype of prostate cancer associated with an AR(androgen receptor)-null phenotype and visceral metastases. This study presents a 44-year-old man originally diagnosed with metastatic hormone-sensitive prostatic adenocarcinoma. After 6-month androgen deprivation therapy (ADT) combined with docetaxel, the patient developed paraplegia. Laminectomy was performed, and a thoracic vertebral biopsy revealed neuroendocrine differentiation and mixed adenocarcinoma. The patient developed liver metastases and experienced stable disease for 4 months following etoposide combined with cisplatin and pembrolizumab. Seminal vesicle biopsy after chemotherapy revealed small-cell cancer. The prostate biopsy specimen also indicated pure SCC. We witnessed the dynamic evolution from pure adenocarcinoma to fully differentiated SCC, leading to obstruction and death. In addition, whole-exome sequencing was performed on both biopsy specimens of the thoracic vertebra at the beginning of castration resistance and that of seminal vesicle after multiple lines of treatment failure. Utilizing phylogenetic reconstruction, we observed that both samples shared a common ancestor clone harboring aberrations in the *TP53*, *RB1*, and *NF2* genes. We also discovered that driver events in the private subclones of both samples, such as alterations in *CDC27* and *RUNX1*, might have played a significant role in tumor progression or even neuroendocrine differentiation. Tumor biopsy and IHC assessment must be repeated at different stages of progression, because of intrapatient spatial and temporal heterogeneity of adenocarcinoma *versus* SCC/NEPC. Although, typical treatments including ADT, docetaxel, etoposide, cisplatin, and pembrolizumab provided temporary response, the patient still had a poor prognosis.

Keywords: neuroendocrine differentiation, small cell carcinoma, whole-exome sequencing, neuroendocrine prostate cancer, clonal evolution

INTRODUCTION

The androgen receptor (AR) regulates of growth and proliferation of prostate cancer (1). Androgen-deprivation or highly potent AR-targeted therapies, such as enzalutamide, remain the mainstay for the systematic treatment of metastatic hormone-sensitive prostate cancer (mHSPC). However, majority of the mHSPC cases eventually develop to metastatic castration-resistant prostate cancer (mCRPC) after long-term androgen deprivation therapy (ADT). An important mechanism in treatment-resistant prostate cancer development might be associated with neuroendocrine differentiation. Neuroendocrine prostate cancer (NEPC) is an aggressive variant of prostate cancer, characterized by pure or mixed neuroendocrine differentiation. Histologically, small cell neuroendocrine carcinoma is among the highest-grade and poorly differentiated neuroendocrine tumors. Small cell carcinoma constitutes 0.5–2% of prostate cancer cases, whereas 10–20% of CRPC cases; however, the current prevalence of SCC/NEPC after intense therapeutic pressures designed to inhibit AR signaling might be higher (2). Using molecular classifiers some studies have supported the clonal evolution trajectory of NEPC from adenocarcinoma (3).

Here, we present a case that shows the transformation process from adenocarcinoma to neuroendocrine cells and small cell prostate cancer at a very late stage. We found the coexistence of heterogeneous subtypes in the whole body during treatment, which elicited different reactions to different treatments. Furthermore, we performed serial molecular profiling and explored the clonal evolution pattern of NEPC to small cell carcinoma in this patient after treatment to help understand the potential mechanism of this evolutionary path.

CASE DESCRIPTION

In June 2018, a 44-year-old man was originally diagnosed with prostate cancer (PCa) confirmed using prostate biopsy, which indicated a Gleason score of 4 + 5 = 9 prostate adenocarcinomas involving all 15 cores (**Figure 1A**). From June 2018 to December 2020, the patient presented with three stages of prostate cancer, according to treatment, mHSPC, mCRPC, and small cell. Immunohistochemical (IHC) assessment demonstrated tumors to be positive for prostate-specific membrane antigen (PSMA), P504s, and P501s (**Table 1**). Prostate-specific antigen (PSA) levels were initially elevated at 147.7 ng/mL. Whole-body magnetic resonance imaging (WB-MRI) indicated metastases involving the prostate capsule, bilateral seminal vesicles, pelvic lymph nodes, and extensive osteosclerotic lesions (**Figure 1C**). Hence, the patient was diagnosed with cT3bN1M1b stage cancer. Because of the high tumor burden, we began treatment for mHSPC with ADT plus docetaxel at 75 mg/m^2 for six cycles. Following this, the PSA levels showed a rapid and significant improvement, dropping to 0.004 ng/mL in December 2018. Both WB-MRI and a bone scan showed no obvious active lesions in the prostate, pelvic lymph nodes, and bones (**Supplementary Figure 1**).

Although ADT plus docetaxel therapy achieved periodic results in the treatment of mHSPC, his levels of PSA increased continuously with ADT therapy alone over 5 months after stopping chemotherapy, reaching 0.132 ng/mL in May 2019. Meanwhile, PSMA positron emission tomography (PET)/computed tomography (CT) revealed the presence of metabolically active lesions in multiple bones, but not in the prostate (**Figure 1C**). Therefore, we assumed that the mHSPC had progressed to mCRPC. In July 2019, we treated the patient with ADT and abiraterone for over 3 months. However, his levels of PSA continued to increase, and a severe complication of paraplegia occurred in October 2019. The patient underwent laminectomy in November 2019, which led to improved motor capacity. The posttreatment thoracic vertebral biopsy specimen revealed metastatic prostate adenocarcinoma with neuroendocrine differentiation (**Figure 1B**). IHC assessment demonstrated tumors to be positive for PSMA, P504s, NKX3.1, synaptophysin (Syn), CD56, chromogranin A (CgA), AR(+, 80%), and KI67(+, 40%) (**Table 1**). A fresh portion of the vertebral specimen was sent for tumor sequencing.

One month later, the patient had elevated levels of transaminases. Magnetic resonance imaging (MRI) revealed new lesions in the liver (**Figure 2A**). Neuron-specific enolase (NSE) levels were elevated at 36.23 ng/mL (**Figure 1A**). Based on the pathology and clinical features, we initiated etoposide at 80 mg/m^2 combined with cisplatin at 25 mg/m^2, and continued ADT therapy plus pembrolizumab specific for NEPC. After two cycles, an MRI showed that the liver lesions had almost disappeared (**Figure 2B**).

Following four cycles of etoposide combined with cisplatin plus pembrolizumab, the patient experienced severe general bone pain and blurred vision. His levels of PSA were transiently decreased, but increased again to 1.826 ng/mL in the last four cycles, whereas his levels of NSE decreased to 10.53 ng/mL. A new MRI revealed metastases involving the clivus and adjacent right sphenoid bone (**Figure 2C**). Hence, we hypothesized the coexistence of mixed adenocarcinoma and neuroendocrine components. In particular, we considered that the NSE signal showed the efficiency, while the levels of PSA represented the growth of adenocarcinoma components. Therefore, we attempted treatment with docetaxel at 75 mg/m^2, cisplatin at 25 mg/m^2, and continued ADT therapy plus pembrolizumab. Notably, the patient recovered his vision and experienced pain relief. After four cycles, his symptoms improved significantly. However, PSMA-PET/CT revealed metabolically active lesions on the left seminal vesicle, liver, and multiple bones, indicating cancer progression (**Figure 1C**). In addition, a seminal vesicle biopsy in July 2020 revealed small cell carcinoma. IHC assessment demonstrated tumors to be positive for CAM5.2, Syn, CD56, CgA, AR (+, 30%), and Ki-67(+, 100%), but negative for NKX3.1 and P501s (**Table 1**). A fresh portion of this seminal vesicle specimen was sent for tumor sequencing. Three months later, the patient underwent palliative transurethral resection of prostate (TURP) for dysuria. The prostate biopsy specimen indicated small cell carcinoma. IHC assessment demonstrated tumors to be positive for P504s,

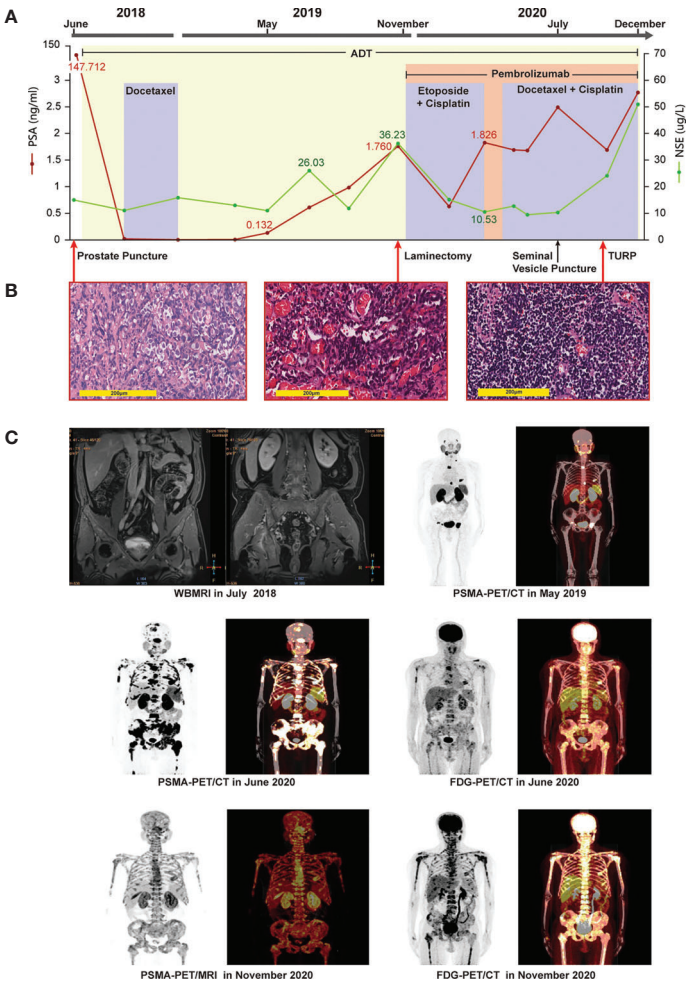

FIGURE 1 | Clinical timeline, systemic therapy, imaging data, and pathologic diagnosis. **(A)** systemic therapy: continuous adjusted treatment protocols in disease progression and changes in the levels of PSA and NSE during the treatment course. **(B)** pathologic diagnosis: (left picture) HE staining revealing prostate adenocarcinomas in the prostate puncture tissue; (middle picture) HE staining revealing metastatic prostate adenocarcinoma with neuroendocrine differentiation in the thoracic vertebral tissue; (right picture) HE staining revealing small-cell cancer in the tissue after TURP surgery. Magnification: ×200. **(C)** Imaging data: whole-body magnetic imaging resonance showing changes in the prostate lesion before treatment in July 2018. PSMA-PET/CT showing multiple bone lesions in May 2019, after termination of docetaxel chemotherapy, and elevation of the levels of the patient's PSA to 0.132 ng/mL. PSMA-PET/CT in June 2020 showing metastases in the left seminal vesicle, liver, and multiple bones. FDG-PET/CT in June 2020 showing metastases in the left seminal vesicle, liver, and multiple bones. PSMA-PET/MRI in November 2020 showing a metastasis in the posterior wall of the bladder, diffuse bone metastases, bilateral pleural effusion liquid, and a chronic subdural hematoma in bilateral brain. FDG-PET/CT in November 2020 showing multiple metastases in the bones and liver, and bilateral pleural effusion liquid, but no abnormalities in brain.

CAM5.2, Syn, CD56, CgA, ERG, PTEN, and Ki-67(+, 100%), but negative for NKX3.1 and PSMA.

MOLECULAR TUMOR BOARD

Pathology and Molecular Evolution From Adenocarcinoma to NEPC to SCC

Neuroendocrine differentiation in adenocarcinoma should be detected in a timely manner. Both the elevation of serum NSE levels and the presence of visceral metastases indicate the development of neuroendocrine differentiation in prostate cancer. Despite their high sensitivity, the CgA and NSE serum neuroendocrine markers lack specificity for SCC/NEPC (2, 4, 5). Pathological diagnosis is the most reliable diagnosis, and the acquisition of reliable biopsy specimens usually depends on good compliance of the patient and the puncture technique of the doctor (6). We obtained four pre- and posttreatment biopsy specimens, which revealed the histological progression of tumors (**Table 1**) (**Supplementary Figure 2**). PSMA, P504s, and NKX3.1 were expressed in nearly all prostatic adenocarcinomas. Only these markers were expressed at initial diagnosis, indicating the adenocarcinoma origin of the tumor. The CgA, Syn, and CD56

TABLE 1 | Immunohistochemical (IHC) assessment of puncture tissue of prostate, thoracic vertebral biopsy specimen, seminal vesicle tissue, and prostate after transurethral resection of prostate (TURP).

IHC Assessment	mHSPC Puncture Tissue	mCRPC Thoracic Vertebra	Small Cell Seminal Vesicle	Small Cell Prostate Tissue
NKX3.1	(+)	(+)	(-)	(-)
PSMA	(+)	(+)		(-)
ERG	(-)	(-)		(+)
AR		80%	30%	
CgA		(+)	(+)	(+)
CD56		(+)	(+)	(+)
Syn		(+)	(+)	(+)
NSE		(-)		
CK20		(-)		
P504s	(+)	(+)		(+)
P501s	(+)	(+)	(-)	/
CAM5.2		(+)	(+)	(+)
Pten				(+)
PD-1		(-)		
PDL-1		(-)		
KI-67	40%	40%	100%	100%

(+) represents positive assessment. (-) represents negative assessment. Blank indicates no protein staining.

markers are expressed in nearly all prostate cancers with neuroendocrine differentiation (7). Following its progression to mCRPC, IHC assessment of the thoracic vertebral biopsy specimen revealed positive signals for PSMA, P504s, NKX3.1, Syn, CD56, and CgA, which indicated adenocarcinoma admixed with NEPC after intense therapeutic pressures of ADT therapy. Likewise, IHC assessment of the seminal vesicle biopsy specimen showed positive signals for CAM5.2, Syn, CD56, and CgA, but negative for NKX3.1 and P501s, indicating the predominance of SCC/NEPC in the patient during this period. Under the pressure of treatment, NEPC transformed into a poorly differentiated small cell phenotype, losing the expression of adenocarcinoma origin-specific markers, such as PSMA and NKX3.1.

Functional and Clinical Significance of Specific Mutations in This Case

As the special genetic pattern of NEPC reflects its cellular origin, the genetic alterations in two samples collected at different stages were investigated using whole-exome sequencing. The first was a mixed adenocarcinoma and neuroendocrine cancer sample (M-sample) at CRPC, whereas the second was a pure SCC/NEPC (S-sample) at the last stage. We described the mutational landscape and applied phylogenetic reconstruction to analyze the dynamic clonal progression. We estimated and clustered the cancer cell fraction (CCF) to track and visualize the clonal evolution of each tumor using PyClone (8).

We observed that both samples shared the most recent common ancestor (MRCA) encompassing 23 mutations and an exon1-exon13 truncation of the neurofibromin 2 (*NF2*) gene, indicating their common origin (**Figure 3**). Notably, a double deletion of *TP53* and *RB1* was identified at the initiation of neuroendocrine stages, while a truncation of *NF2* resulted in sensitivity to platinum chemotherapy (9). A specific subclone harboring 37 mutated genes and an AR amplification was observed in the M-sample. We integrated the mutation frequency of all mutated genes in different types of prostate cancer in this patient, according to the existing data using "cBioPortal" (http://www.cbioportal.org) as previously described (10) (**Figure 3A**). We observed that the *CDC27* oncogene was frequently mutated in NEPC samples (7.4%, 4/54 public samples). *CDC27* has been recognized as either a tumor suppressor gene or an oncogene in different neoplasms. Furthermore, *CDC27* increases the stemness of cancer stem cells in colorectal cancer (11). A private subclone harboring three copy number alterations and five mutations was detected in the S-sample. Among them, the *RUNX1* gene, a transcription factor playing key roles in the regulation of stem cell fate, might be driving the neuroendocrine progression of tumor (12). Although Beltran et al. observed that the *RUNX1* copy number deletion was meaningful in NEPC, a *RUNX1* amplification could also occur, further supporting the key role of *RUNX1* in neuroendocrine-differentiated tumors (13). Consequently, the two samples obtained individual subclones after MRCA in the clonal evolutionary tree (**Figures 3C, D**). Some driving events in these subclones might have played a key role in tumor progression or even in promoting neuroendocrine differentiation.

DISCUSSION

Potential Strategies to Target the Pathway and Implications for Clinical Practice

Precision oncology is based on tumor biopsies and sequencing to identify therapeutic targets. Here, two posttreatment biopsy specimens with histologic progression were analyzed using whole-exome sequencing. An AR amplification was detected in the first mixed tumor sample but not in the second pure SCC/NEPC sample, indicating the downregulation of AR in NEPC compared with that in adenocarcinoma (5, 13). In addition, the inactivation of *RB1* and *TP53* tumor suppressor genes is frequently associated with small cell cancer (14, 15), and is a key mechanism of resistance to antiandrogen therapy and lineage plasticity (16, 17). Identical mutations in the DNA-

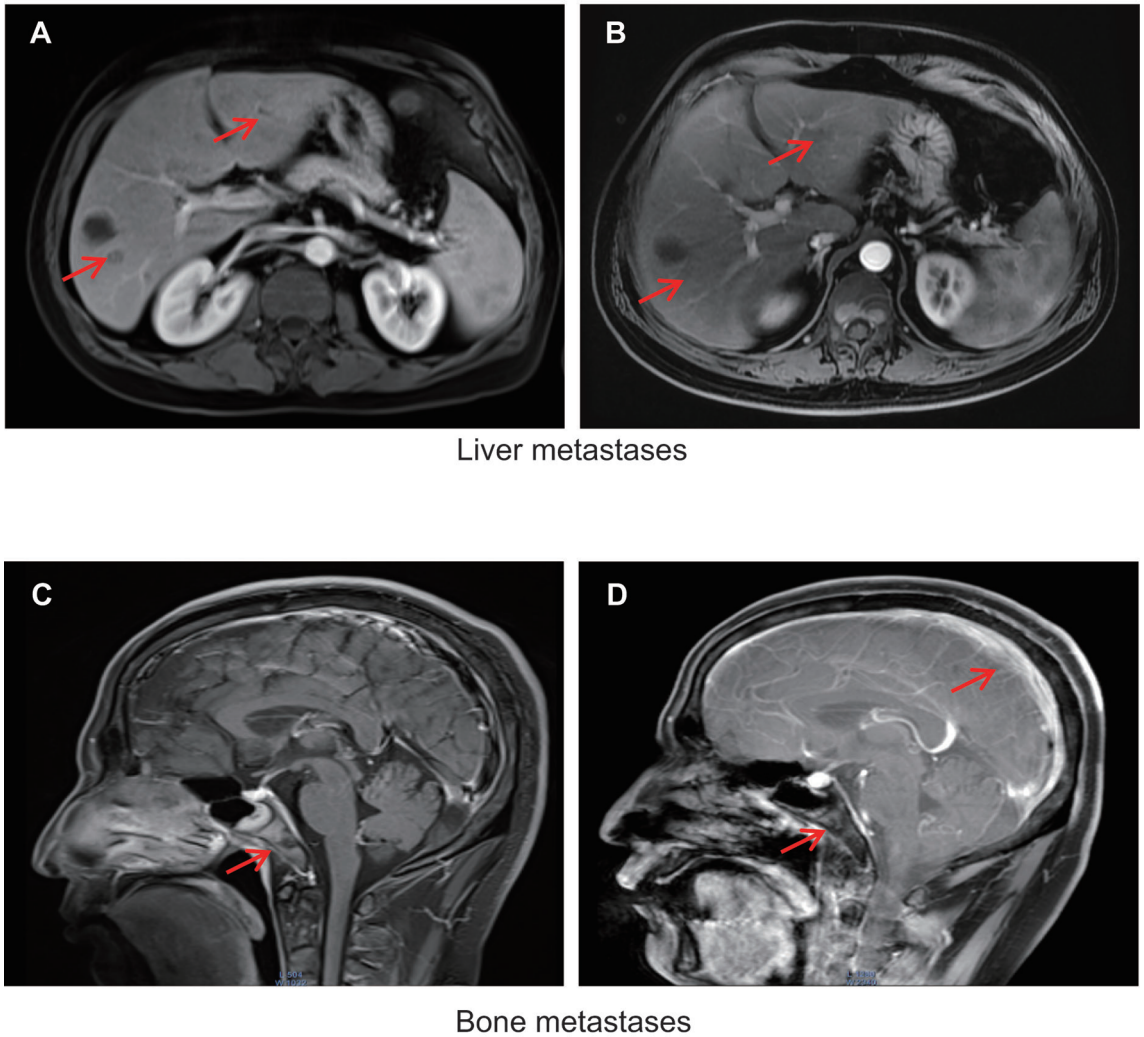

FIGURE 2 | **(A)** Liver metastases detected using magnetic resonance imaging (MRI) in November 2019. **(B)** Response of liver metastases detected using MRI in January 2020 after treatment with etoposide combined with cisplatin and continued ADT plus pembrolizumab. Metastases are indicated by red arrows. **(C)** Clivus and adjacent right sphenoid bone metastases detected by MRI in April 2020. **(D)** Meningeal clivus and adjacent right sphenoid metastases in November 2020. Metastases are indicated by red arrows.

binding domains of TP53, RB1, and MYC have also been observed in both NGS profiles, indicating the possible derivation of NEPC from adenocarcinoma (18–20). We attempted to identify therapeutic targets, such as DNA damage repair (DDR) pathway genes (*BRCA1*, *BRCA2*, *ATM*, and *CDK12*), which could be paired with poly ADP-ribose polymerase (PARP) inhibitors (6, 21). However, we did not detect any alterations in DDR pathway genes in the NGS profiling. Similarly, other studies have also shown the rare occurrence of alterations in DDR pathway genes in SCC/NEPC (2). We observed alterations in *PIK3CA* and *NF2*, which could be associated with the phosphatidylinositol-3-kinase/mammalian target of rapamycin (PI3K/mTOR) pathway. However, the curative effect of mTOR inhibitors in prostate cancer remains uncertain (22, 23). Considering the uncertain curative effect and the poor physical condition of the patient, we elected the regimen recommended by the guidelines (6, 24).

Prostate cancer with neuroendocrine differentiation shows remarkable clinical heterogeneity, as revealed by the constantly changing clinical symptoms, such as bone pain, liver metastases, and meningeal metastases. We deduced that adenocarcinoma and SCC/NEPC alternately dominated the shift in the process of disease. We elected ADT combined with docetaxel as the initial treatment, but changed to etoposide combined with cisplatin and pembrolizumab after the detection of neuroendocrine differentiation. In this case, the key advantage of the approach used is the timely correction of treatment strategy according to the pathological type and the construction of tumor subclone structures using sequential sampling. In addition, we advanced chemotherapy at the initial diagnosis based on the NCCN

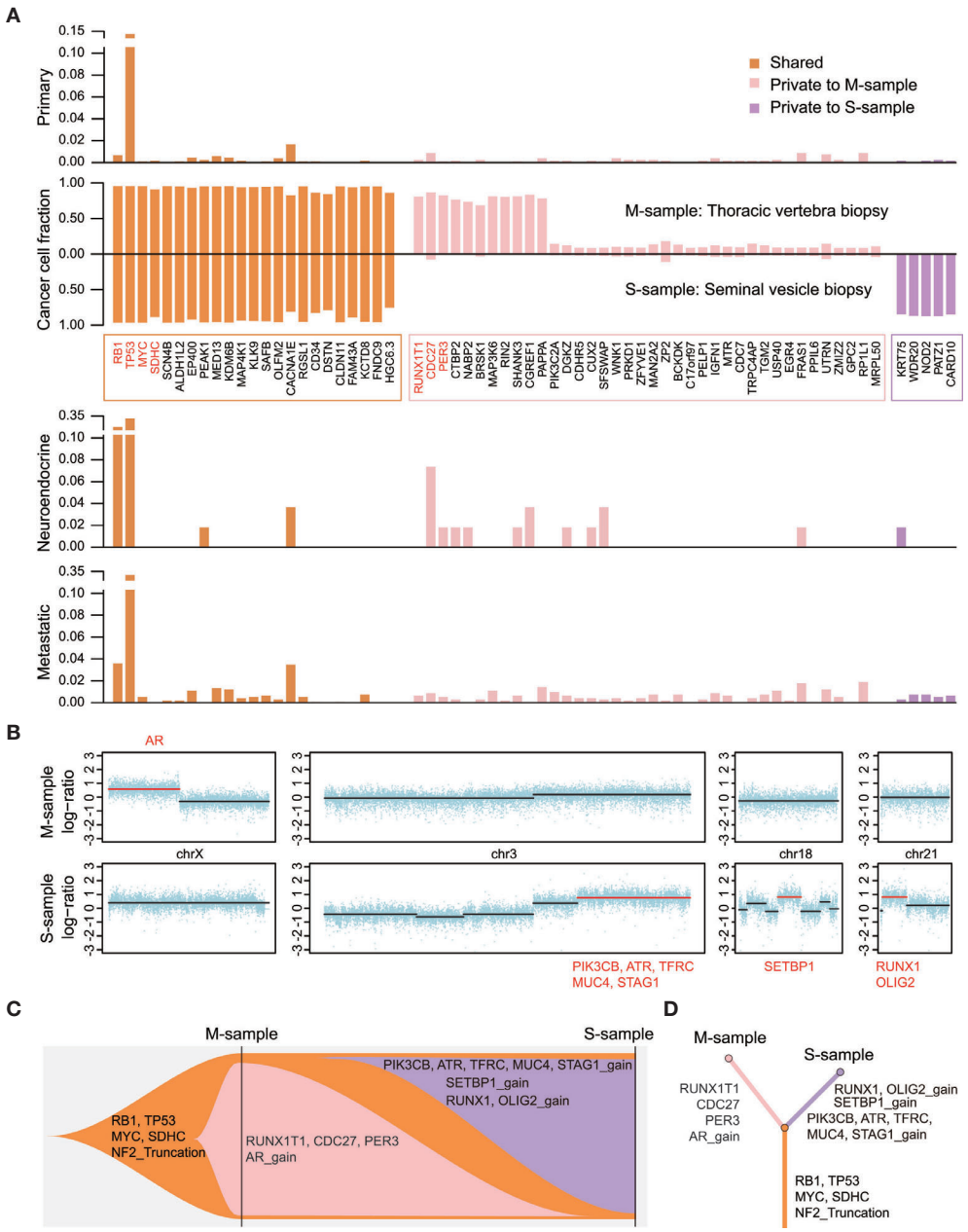

FIGURE 3 | The altered landscape and phylogenetic reconstruction of the two samples. **(A)** The second panel shows the cancer cell fraction estimated by using PyClone and calculated using the read depth of mutations, copy numbers, and purity of tumors. Other panels are showing the frequency of mutations in three types of prostate cancer using public data from the cBioPortal (1400 primary tumors, 54 NEPC samples, and 880 mCRPC samples). Important functional cancer genes are marked in red. **(B)** Overview of copy number alterations and cancer genes encompassed in segments are shown in red. **(C, D)** Fishplot indicating the dynamic clonal progression of the tumor, and clonal evolution tree showing the phylogenetic relationship between the two samples.

guidelines (6), and timely chose the regimen with etoposide and platinum (EP) + PD1 when the tumor was revealed to be neuroendocrine differentiation and mixed adenocarcinoma. Despite accomplishing a temporary response, regrettably, we could not find a regimen that could ideally control both adenocarcinoma and SCC/NEPC to improve the prognosis. We have also supplemented our report with the research on the origin of SCC/NEPC from the perspective of clonal evolution. Previous studies have reported the transdifferentiation phenomenon of NEPC and its molecular changes, that is, prostate adenocarcinoma cells could transform into a neuroendocrine phenotype (25, 26). We described here the clonal evolution from mixed adenocarcinoma and neuroendocrine cancer to pure SCC/NEPC. Meanwhile, some

molecular alterations have also been provided, which could hopefully be used to monitor the progress of SCC/NEPC in the future.

Notably, this case study has some limitations. While longitudinal sampling combined with bulk sequencing could distinguish tumor subclones and monitor tumor progression, for the special tumor type observed in this case—with higher heterogeneity and more complex cellular components—single-cell sequencing may be a better and more accurate solution (27). Alternatively, in a previous report, transcription factors have been utilized for the molecular subtyping of small cell lung cancer; however, this has not been applied in clinical practice (28). Accordingly, further research is required to explore the value of transcription factor typing to guide clinical treatment.

Patient Update

Despite a periodic clinical response, the patient died from respiratory failure, severe anemia, infection, and brain edema in December 2020. The last MRI showed metastases of the meninges, clivus, skull, and sphenoid bone (**Figure 2D**).

Key Points

If the IHC assessment of the initial puncture biopsy tissue detects potential neuroendocrine differentiation, doctors should offer patients more frequent imaging examination and analyses of serum markers.

Tumor biopsy and IHC assessment must be repeated at different stages of the disease to judge the progress of neuroendocrine differentiation and adjust the treatment regimen.

Tumor sequencing remains necessary even though changes might not be necessarily detected, as it could help clinicians better understand the genomic changes during neuroendocrine differentiation.

DATA AVAILABILITY STATEMENT

The original contributions presented in the study are included in the article/**Supplementary Material**. Further inquiries can be directed to the corresponding authors.

AUTHOR CONTRIBUTIONS

Conception/design: JL and WZ. Provision of study material or patients: TW and HG. Collection and/or assembly of data: YZ and XS. Data analysis and interpretation: WZ and QC. Manuscript writing: XL and WG. Manuscript revision: XG. Final approval of manuscript: BL and JL. All authors contributed to the article and approved the submitted version.

FUNDING

This study was supported by the Shanghai Rising-Star Program (20QA1411800) and National Natural Science Foundation of China (82022055).

ACKNOWLEDGMENTS

We also would like to thank Shanghai OrigiMed Clinical Laboratory Co., Ltd. for Whole-exome sequencing service and Editage (https://www.editage.com/) for English language editing.

SUPPLEMENTARY MATERIAL

The Supplementary Material for this article can be found online at: https://www.frontiersin.org/articles/10.3389/fonc.2021.732071/full#supplementary-material

Supplementary Figure 1 | Figure WB-MRI shows there were no obvious active lesions in prostate, pelvis lymph nodes, and bones all over the body in January 2019 after six chemotherapy cycles of docetaxel along with ADT therapy.

Supplementary Figure 2 | Positive IHC assessment of puncture tissue of prostate, thoracic vertebra biopsy specimen, seminal vesicle tissue, and prostate after TURP.

Supplementary Table 1 | Summary whole exome sequencing findings from the thoracic vertebra biopsy specimen and the seminal vesicle specimen. Variants were identified including single nucleotide variants(SNV), small insertion-deletions, and copy number alterations. The cancer cell fractions(CCF) and clusters of each mutations are also indicated.

REFERENCES

1. C. Global Burden of Disease Cancer, Fitzmaurice C, Dicker D, Pain A, Hamavid H, Moradi-Lakeh M, et al. The Global Burden of Cancer 2013. *JAMA Oncol* (2015) 1:505–27. doi: 10.1001/jamaoncol.2015.0735
2. Aggarwal R, Huang J, Alumkal JJ, Zhang L, Feng FY, Thomas GV, et al. Clinical and Genomic Characterization of Treatment-Emergent Small-Cell Neuroendocrine Prostate Cancer: A Multi-Institutional Prospective Study. *J Clin Oncol* (2018) 36:2492–503. doi: 10.1200/JCO.2017.77.6880
3. Beltran H, Tagawa ST, Park K, MacDonald T, Milowsky MI, Mosquera JM, et al. Challenges in Recognizing Treatment-Related Neuroendocrine Prostate Cancer. *J Clin Oncol* (2012) 30:e386–389. doi: 10.1200/JCO.2011.41.5166
4. Beltran H, Jendrisak A, Landers M, Mosquera JM, Kossai M, Louw J, et al. The Initial Detection and Partial Characterization of Circulating Tumor Cells in Neuroendocrine Prostate Cancer. *Clin Cancer Res* (2016) 22:1510–9. doi: 10.1158/1078-0432.CCR-15-0137
5. Aggarwal RR, Quigley DA, Huang J, Zhang L, Beer TM, Rettig MB, et al. Whole-Genome and Transcriptional Analysis of Treatment-Emergent Small-Cell Neuroendocrine Prostate Cancer Demonstrates Intraclass Heterogeneity. *Mol Cancer Res* (2019) 17:1235–40. doi: 10.1158/1541-7786.MCR-18-1101
6. Schaeffer E, Srinivas S, Antonarakis ES, Armstrong AJ, Bekelman JE, Cheng H, et al. NCCN Guidelines Insights: Prostate Cancer, Version 1.2021. *J Natl Compr Canc Netw* (2021) 19:134–43. doi: 10.6004/jnccn.2021.0008
7. Shariff AH, Ather MH. Neuroendocrine Differentiation in Prostate Cancer. *Urology* (2006) 68:2–8. doi: 10.1016/j.urology.2006.02.002
8. Roth A, Khattra J, Yap D, Wan A, Laks E, Biele J, et al. PyClone: Statistical Inference of Clonal Population Structure in Cancer. *Nat Methods* (2014) 11:396–8. doi: 10.1038/nmeth.2883
9. Achkar T, Ali SM, Welsh A, Dhir R, Gollin SM, Parikh RA. A Prolonged Response to Platinum-Based Therapy in a Patient With Metastatic Urothelial Carcinoma Harboring a Single Rearranged and Truncated NF2 Gene. *Genes Chromosomes Cancer* (2018) 57:430–3. doi: 10.1002/gcc.22537

10. Li J, Xu C, Lee HJ, Ren S, Zi X, Zhang Z, et al. A Genomic and Epigenomic Atlas of Prostate Cancer in Asian Populations. *Nature* (2020) 580:93–9. doi: 10.1038/s41586-020-2135-x
11. Kazemi-Sefat GE, Keramatipour M, Talebi S, Kavousi K, Sajed R, Kazemi-Sefat NA, et al. The Importance of CDC27 in Cancer: Molecular Pathology and Clinical Aspects. *Cancer Cell Int* (2021) 21:160. doi: 10.1186/s12935-021-01860-9
12. Deltcheva E, Nimmo R. RUNX Transcription Factors at the Interface of Stem Cells and Cancer. *Biochem J* (2017) 474:1755–68. doi: 10.1042/BCJ20160632
13. Beltran H, Prandi D, Mosquera JM, Benelli M, Puca L, Cyrta J, et al. Divergent Clonal Evolution of Castration-Resistant Neuroendocrine Prostate Cancer. *Nat Med* (2016) 22:298–305. doi: 10.1038/nm.4045
14. Aparicio AM, Shen L, Tapia EL, Lu JF, Chen HC, Zhang J, et al. Combined Tumor Suppressor Defects Characterize Clinically Defined Aggressive Variant Prostate Cancers. *Clin Cancer Res* (2016) 22:1520–30. doi: 10.1158/1078-0432.CCR-15-1259
15. Kumar A, Coleman I, Morrissey C, Zhang X, True LD, Gulati R, et al. Substantial Interindividual and Limited Intraindividual Genomic Diversity Among Tumors From Men With Metastatic Prostate Cancer. *Nat Med* (2016) 22:369–78. doi: 10.1038/nm.4053
16. Ku SY, Rosario S, Wang Y, Mu P, Seshadri M, Goodrich ZW, et al. Rb1 and Trp53 Cooperate to Suppress Prostate Cancer Lineage Plasticity, Metastasis, and Antiandrogen Resistance. *Science* (2017) 355:78–83. doi: 10.1126/science.aah4199
17. Park JW, Lee JK, Sheu KM, Wang L, Balanis NG, Nguyen K, et al. Reprogramming Normal Human Epithelial Tissues to a Common, Lethal Neuroendocrine Cancer Lineage. *Science* (2018) 362:91–5. doi: 10.1126/science.aat5749
18. Nadal R, Schweizer M, Kryvenko ON, Epstein JI, Eisenberger MA. Small Cell Carcinoma of the Prostate. *Nat Rev Urol* (2014) 11:213–9. doi: 10.1038/nrurol.2014.21
19. Aparicio AM, Harzstark AL, Corn PG, Wen S, Araujo JC, Tu SM, et al. Platinum-Based Chemotherapy for Variant Castrate-Resistant Prostate Cancer. *Clin Cancer Res* (2013) 19:3621–30. doi: 10.1158/1078-0432.CCR-12-3791
20. Beltran H, Rickman DS, Park K, Chae SS, Sboner A, MacDonald TY, et al. Molecular Characterization of Neuroendocrine Prostate Cancer and Identification of New Drug Targets. *Cancer Discovery* (2011) 1:487–95. doi: 10.1158/2159-8290.CD-11-0130
21. Loeb S, Giri VN. Clinical Implications of Germline Testing in Newly Diagnosed Prostate Cancer. *Eur Urol Oncol* (2021) 4:1–9. doi: 10.1016/j.euo.2020.11.011
22. de Bono JS, De Giorgi U, Rodrigues DN, Massard C, Bracarda S, Font A, et al. Randomized Phase II Study Evaluating Akt Blockade With Ipatasertib, in Combination With Abiraterone, in Patients With Metastatic Prostate Cancer With and Without PTEN Loss. *Clin Cancer Res* (2019) 25:928–36. doi: 10.1158/1078-0432.CCR-18-0981
23. Statz CM, Patterson SE, Mockus SM. mTOR Inhibitors in Castration-Resistant Prostate Cancer: A Systematic Review. *Target Oncol* (2017) 12:47–59. doi: 10.1007/s11523-016-0453-6
24. Wu Y, Gao Y, Dou X, Yue J. Metastatic Castration-Resistant Prostate Cancer With Neuroendocrine Transformation and BRCA 1 Germ-Line Mutation: A Case Report and Literature Review. *Onco Targets Ther* (2020) 13:8049–54. doi: 10.2147/OTT.S264347
25. Kadakia KC, Tomlins SA, Sanghvi SK, Cani AK, Omata K, Hovelson DH, et al. Comprehensive Serial Molecular Profiling of an "N of 1" Exceptional non-Responder With Metastatic Prostate Cancer Progressing to Small Cell Carcinoma on Treatment. *J Hematol Oncol* (2015) 8:109. doi: 10.1186/s13045-015-0204-7
26. Terry S, Beltran H. The Many Faces of Neuroendocrine Differentiation in Prostate Cancer Progression. *Front Oncol* (2014) 4:60. doi: 10.3389/fonc.2014.00060
27. Dong B, Miao J, Wang Y, Luo W, Ji Z, Lai H, et al. Single-Cell Analysis Supports a Luminal-Neuroendocrine Transdifferentiation in Human Prostate Cancer. *Commun Biol* (2020) 3:778. doi: 10.1038/s42003-020-01476-1
28. George J, Lim JS, Jang SJ, Cun Y, Ozretic L, Kong G, et al. Comprehensive Genomic Profiles of Small Cell Lung Cancer. *Nature* (2015) 524:47–53. doi: 10.1038/nature14664

Conflict of Interest: The authors declare that the research was conducted in the absence of any commercial or financial relationships that could be construed as a potential conflict of interest.

Publisher's Note: All claims expressed in this article are solely those of the authors and do not necessarily represent those of their affiliated organizations, or those of the publisher, the editors and the reviewers. Any product that may be evaluated in this article, or claim that may be made by its manufacturer, is not guaranteed or endorsed by the publisher.

Copyright © 2021 Lu, Gao, Zhang, Wang, Gao, Chen, Shi, Lian, Zhang, Gao and Li. This is an open-access article distributed under the terms of the Creative Commons Attribution License (CC BY). The use, distribution or reproduction in other forums is permitted, provided the original author(s) and the copyright owner(s) are credited and that the original publication in this journal is cited, in accordance with accepted academic practice. No use, distribution or reproduction is permitted which does not comply with these terms.

frontiers in Oncology

ORIGINAL RESEARCH
published: 30 September 2021
doi: 10.3389/fonc.2021.745530

Prediction of Biochemical Recurrence After Radical Prostatectomy Based on Preoperative ^{68}Ga-PSMA-11 PET/CT

Xuefeng Qiu[1,2†], Mengxia Chen[1,2†], Haoli Yin[1,2†], Qing Zhang[1,2,3], Haoyang Li[4], Suhan Guo[5], Yao Fu[6], Shiming Zang[7], Shuyue Ai[7], Feng Wang[7] and Hongqian Guo[1,2*]*

[1] Department of Urology, Affiliated Drum Tower Hospital, Medical School of Nanjing University, Nanjing, China, [2] Institute of Urology, Nanjing University, Nanjing, China, [3] Department of Radiology, Affiliated Drum Tower Hospital, Medical School of Nanjing University, Nanjing, China, [4] Department of Applied Mathematics, X2017 École Polytechnique, Palaiseau, France, [5] School of Artificial Intelligence, Nanjing University, Nanjing, China, [6] Department of Pathology, Affiliated Drum Tower hospital, Medical School of Nanjing University, Nanjing, China, [7] Department of Nuclear Medicine, Nanjing First Hospital, Nanjing Medical University, Nanjing, China

OPEN ACCESS

Edited by:
Antonina Mitrofanova, The State University of New Jersey, United States

Reviewed by:
Vikas Prasad, Universitätsklinikum Ulm, Germany
Naoya Nagaya, Juntendo University, Japan

****Correspondence:***
Hongqian Guo
dr.ghq@nju.edu.cn
Feng Wang
fengwangcn@hotmail.com

[†]These authors have contributed equally to this work

Specialty section:
This article was submitted to Genitourinary Oncology, a section of the journal Frontiers in Oncology

Received: *22 July 2021*
Accepted: *14 September 2021*
Published: *30 September 2021*

Citation:
Qiu X, Chen M, Yin H, Zhang Q, Li H, Guo S, Fu Y, Zang S, Ai S, Wang F and Guo H (2021) Prediction of Biochemical Recurrence After Radical Prostatectomy Based on Preoperative ^{68}Ga-PSMA-11 PET/CT. Front. Oncol. 11:745530. doi: 10.3389/fonc.2021.745530

Purpose: This study was designed to investigate the prognostic role of preoperative ^{68}Ga-PSMA-11 PET/CT in predicting biochemical recurrence (BCR) of localized prostate cancer (PCa) after radical prostatectomy (RP).

Methods: A total of 77 biopsy-confirmed PCa patients with ^{68}Ga-PSMA-11 PET/CT prior to RP were included. A PSMA-ligand PET/CT-based risk model with SUV_{max}, maximum diameter of the index tumor and T stage was developed for prediction of 2-year BCR using Cox regression analysis. Also, the efficacy of the developed risk model was compared with European Association of Urology risk stratification (D'Amico) and the Cancer of the Prostate Risk Assessment (CAPRA) score. C-index and calibration plot were used to assess discrimination and calibration with internal validation.

Results: With a median follow-up of 25 months, 23 (29.9%) patients experienced BCR within 2 years after RP. Patients experienced BCR had a significant higher PSA at diagnosis ($p<0.001$), a higher ISUP grade of biopsy ($p=0.044$), as well as a higher ISUP grade ($p=0.001$), a higher possibility of T3 diseases ($p=0.001$) and positive margin ($p=0.008$) on postoperative pathology. SUV_{max}, maximum diameter of the index tumor and T stage on preoperative PSMA-ligand PET/CT were significantly associated with BCR (all $p<0.01$). PSMA-ligand PET/CT-based risk model had a superior discrimination (c-index 78.5%) and good calibration at internal validation. The efficacy of this model in predicting 2-year BCR after RP was better, compared with CAPRA (c-index 66.3%) and D'Amico (c-index 66.2%). The addition of the PSMA-ligand PET/CT-derived variables also improved the efficacy of the existing models in predicting 2-year BCR (C-index of 78.9% for modified CAPRA and 79.3% for modified D'Amico, respectively).

Conclusion: A PSMA-ligand PET/CT-based risk model showed good efficacy in predicting 2-year BCR after RP, which needed to be validated by further prospective studies.

Keywords: prostate cancer, PSMA - prostate specific membrane antigen, radical prostatectomy, biochemical recurrence (BCR), prediction

INTRODUCTION

Radical prostatectomy (RP) is a widely adopted definitive option for men with localized prostate cancer (PCa) (1, 2). However, up to 40% of patients experienced biochemical recurrence (BCR) after RP (3). Several clinical models, such as D'Amico risk stratification scheme (4), and the University of California, San Francisco, Cancer of the Prostate Risk Assessment (CAPRA) score, have been developed to predict BCR (5). Preoperative variables such as prostate-specific antigen (PSA), clinical T staging, and Gleason score of systematic biopsy are used as prognostic factors in these models. However, the efficacy of these nomograms are far from excellent, with the prediction accuracy of 5-year BCR less than 70% (6, 7).

Prostate specific membrane antigen (PSMA)-ligand positron emission tomography/computed tomography (PET/CT) is currently a promising technique for recurrent PCa imaging (8, 9), as well as primary staging (10, 11). Our previous study indicates improved sensitivity of PSMA-ligand PET/CT in describing intraprostatic tumor lesions compared with multiparametric magnetic resonance Imaging (mpMRI) (12). In addition, increased PSMA uptake on PSMA-ligand PET/CT has been indicated to be positively correlates with prostate cancer aggressiveness and adverse pathologic features in our previous studies (13, 14), making PSMA-ligand PET/CT a potential tool to predict BCR following RP. Nonetheless, current models for prediction of BCR are mostly based on clinical and pathologic variables. The predictive role of PSMA-ligand PET/CT in this setting has been rarely investigated (15). Furthermore, the added value of PSMA-ligand PET/CT over the pre-existing models has not been evaluated.

Therefore, this study was designed to assess the potential role of PSMA-ligand PET/CT as a biomarker to predict early BCR after RP. We developed a PSMA-ligand PET/CT-based risk model for the prediction of BCR. The added value of PSMA-ligand PET/CT to the commonly used clinical models to predict BCR was also evaluated.

PATIENTS AND METHODS

Study Population

We retrospectively included 138 consecutive patients with biopsy-confirmed prostate cancer who underwent ^{68}Ga-PSMA-11 PET/CT before radical prostatectomy (RP) between January 2017 and June 2019. We excluded the patients with suspicious pelvic lymph nodes (n=11) or distant metastases (n=5). Patients who received treatment before RP (TURP, n=2; hormone therapy, n=35) were also excluded. Patients with inadequate clinical or pathological information (n=3) or incomplete follow-up information were also excluded (n=5). Finally, 77 patients were eligible for the analysis. This study was approved by the Ethics Committee of the Drum Tower Hospital (2017-147-01).

PSMA-Ligand PET/CT Scanning and Image Evaluation

^{68}Ga-PSMA-11 PET/CT was acquired as previously described (12). ^{68}Ga-PSMA-11 was synthesized using an ITG semiautomated module and were injected intravenously one hour before scanning. All PET/CT scans were performed in an uMI 780 PET/CT scanner (United Imaging Healthcare (UIH), Shanghai, China). A CT scan (130 keV, 80 mAs) and a static emission scans, corrected for dead time, scatter and decay, were acquired from the vertex to the proximal legs. PSMA-ligand PET/CT imaging were double reviewed by two experienced nuclear medicine physicians (SZ and SA). Lesions were delineate by higher uptake than background or blood pool. Semi-quantitative analysis of PSMA intensity was evaluated by an automated standard maximum uptake value (SUV_{max}) in the delineated lesion. For patients with multiple lesions, the one with highest SUV_{max} was recognized as the index tumor. The maximum diameter of the index tumor was also measured based on the delineate lesions previous recognized by nuclear medicine physicians on PET imaging as primary tumor is not distinctly visible on CT alone. For the assessment of T stage on PSMA-ligand PET/CT, all the assessment were based on the fusion image of PET and CT. PET image with angulated contour of the prostate gland or obliteration of the recto-prostatic angle accordant with the shape on CT were recognized as extracapsular extension (T3a) while seminal vesicle invasion (T3b) was diagnosed if there is a focal or diffuse ^{68}Ga-PSMA-11 accumulation above the background (16).

Covariates, Endpoints, and Model Development

Clinical information including age, PSA level at diagnosis and clinical stage assessed by digital rectal examination (DRE) were included. Transperineal systematic prostate biopsy were performed, with additional fusion targeted biopsies if suspicious lesions (PI-RADS 3-5) were detected on multiparametric magnetic resonance imaging (mpMRI). For preoperative parameters of biopsy, Gleason score and percentage of positive cores were collected. For, PSMA-ligand PET/CT-derived parameters, we included SUV_{max}, maximum diameter of the index tumor, and T stage. Postoperative BCR was defined as three successive rises in PSA level of >0.1 ng/ml at least 6 weeks postoperatively with final PSA >0.2 ng/ml (n=19), or administration of secondary therapy for evidence of detectable PSA >0.1 ng/ml at least 6 weeks postoperatively (n=10) (17).

PSMA-ligand PET/CT-based model was developed by inputting PSMA-ligand PET/CT-derived variables (SUV_{max}, maximum diameter of the index tumor, and T stage). For the existing clinical models, D'Amico and CAPRA scores were collected according to the established D'Amico and CAPRA risk stratification scheme (5), by inputting clinical variables such as patient age, PSA level at diagnosis, Gleason score at biopsy, percentage of positive cores at biopsy, and clinical T stage assessed by DRE. To investigate the added value of PSMA-ligand PET/CT-derived parameters to the existing clinical models, modified D'Amico and modified CAPRA were developed. D'Amico score or CAPRA score was integrated with SUV_{max}, maximum diameter and T stage and re-assessed by Cox regression analyses.

Statistical Analysis

Mann-Whitney U test was performed for continuous variables and the Fisher exact test/chi-square test for categorical variables to compare the characteristics between the patients who

underwent BCR and those free from BCR at 2-year follow-up. The risk of BCR was predicted using Cox regression model. By plotting the observed versus predicted cumulative incidences within 2 years after RP, we also assessed the calibration of our risk model. The discrimination of our risk model and modified D'Amico or CAPRA models was assessed by the concordance index (C-Index). The C-index and calibration plots were produced using the predicted probabilities after a validation with bootstrap by 1000 iterations. A significance level of 5% was used. All analyses were performed using SPSS software, version 22.0 (IBM Corp.) and R statistical package v.3.0.2 (R Project for Statistical Computing, www.r-project.org).

RESULTS

Patient Characteristics and Survival Analysis

Table 1 showed the clinical, preoperative and postoperative pathological characteristics as well as the PSMA-ligand PET/CT-derived features of the 77 patients, with a median age of 69 (interquartile range [IQR]: 62–73 years and median PSA 13.30 ng/ml (IQR: 7.89-28.70) at diagnosis. The median (IQR) follow-up time were 25 (19-27) months for all patients, 25 (21.5-26.8) months for BCR patients and 26 (17.5-27) months for BCR-free patients. Twenty-nine (37.7%) and 23 (29.9%) patients experienced BCR overall and within 24 months after RP. The patients were divided into two groups according to the status of BCR at 2-year follow-up. All clinical, pathological, and imaging variables were compared between the two groups.

At the time point of 24-month follow-up, 23 (29.9%) had experienced BCR while the other 54 (70.1%) are free from BCR. **Table 1** showed summary characteristics of the two groups. The BCR group had a significantly higher PSA level at diagnosis (32.25 versus 10.89 ng/ml), a higher ISUP grade of biopsy (p=0.044), as well as a higher ISUP grade (p=0.001), a higher possibility of T3 diseases (p=0.001) and positive margin (p=0.008) on postoperative pathology. For parameters on PSMA-ligand PET/CT, patients with BCR had a higher SUV_{max}, a larger maximum diameters and a higher T stage than BCR-free patients.

TABLE 1 | Characteristics of prostate cancer patients with ^{68}Ga-PSMA PET/CT scanning prior to radical prostatectomy.

Characteristics	Total (n = 77)	Median (IQR) or n (%)		p
		BCR Free (n = 54)	BCR (n = 23)	
Preoperative characteristics				
Age	69 (65-75)	69 (65-74)	68 (65.5-75.5)	0.993
PSA	13.30 (7.89-28.70)	10.89 (6.61-16.00)	32.25 (14.05-71.43)	**0.000**
Clinical T stage by DRE				0.356
T2	71 (92.2)	51 (94.4)	20 (87.0)	
T3	6 (7.8)	3 (5.6)	3 (13.0)	
ISUP at Biopsy				**0.044**
1	14 (18.2)	13 (24.1)	1 (4.3)	
2	18 (23.4)	13 (24.1)	5 (21.7)	
3	16 (20.8)	13 (24.1)	3 (13.0)	
4	21 (27.3)	10 (18.5)	11 (47.8)	
5	8 (10.4)	5 (9.3)	3 (13.0)	
Percent of positive cores on biopsy	35.71 (21.42-55.91)	30.0 (21.4-51.6)	42.9 (28.1-57.64)	0.130
Postoperative characteristics				
Post-operative ISUP				**0.001**
1	5 (6.5)	5 (9.3)	0 (0)	
2	25 (32.5)	22 (40.7)	3 (13.0)	
3	18 (23.4)	15 (27.8)	3 (13.0)	
4	16 (20.8)	7 (13.0)	9 (39.1)	
5	13 (16.9)	5 (9.3)	8 (34.8)	
Pathological T stage, n (%)				**0.001**
T2	27 (35.5)	23 (43.4)	4 (17.4)	
T3a	35 (46.1)	26 (49.1)	9 (39.1)	
T3b	14 (18.4)	4 (7.5)	10 (43.5)	
Positive margin				**0.008**
Absent	56 (72.7)	12 (52.2)	44 (81.5)	
Present	21 (27.3)	11 (47.8)	10 (18.5)	
Preoperative PET/CT features				
SUV_{max}	13.04 (7.76-21.60)	10.70 (6.83-17.00)	22.90 (15.74-31.01)	**0.000**
Maximum diameter (cm)	1.19 (0.76-2.27)	1.09 (0.74-1.80)	1.93 (1.13-2.44)	**0.008**
PET-detected T stage				**0.002**
T2	46 (59.7)	39 (72.2)	7 (30.4)	
T3a	23 (29.9)	12 (22.2)	11 (47.8)	
T3b	8 (10.4)	3 (5.6)	5 (21.7)	

PSMA, prostate specific membrane antigen; PET/CT, positron emission computed tomography; IQR, interquartile range; BCR, biochemical recurrence; PSA, prostate specific antigen; DRE, digital rectal examination; SUV, standard uptake value; ISUP, International Society of Urological Pathology; cm, centimeter.
Significant P values were presented in bold text.

Multivariable Models Predicting BCR

In Cox regression, PSMA-ligand PET/CT-based model with input of SUV_{max}, maximum diameters, and T stage on PSMA-ligand PET/CT achieved a superior discrimination of BCR during the 2-year follow-up than CAPRA [C-Index: 78.5% (70.3-86.7%) *versus* 66.3 (76.5-56.1)] and D'Amico [C-Index: 78.5% (70.3-86.7%) *versus* 66.2 (75.0-57.4)] (**Table 2**). This model was also characterized by a good calibration at internal validation (**Figure 1**). The inclusion of the PSMA-ligand PET/CT-derived variables also improved the efficacy of the existing models in predicting post-surgery BCR (C-Index: 66.3 versus 78.9% for CAPRA and modified CAPRA; C-Index: 66.2 versus 79.3 for D'Amico and modified D'Amico) (**Table 2**).

DISCUSSION

The newly developed risk model based on ^{68}Ga-PSMA-11 PET/CT-derived parameters (SUV_{max}, maximal diameter of index tumor, and T staging) showed better performance in predicting 2-year BCR, compared with that of D'Amico and CAPRA models. Furthermore, we found that addition of parameters obtained from PSMA-ligand PET/CT outperformed models based on clinical and biopsy variables. To the best of our knowledge, this was the first study to develop a PSMA-ligand PET/CT-based model for prediction of BCR after RP.

The evidence investigating the role of PSMA-ligand PET/CT in predicting BCR after RP was very limited. Roberts et al. showed that intraprostatic ^{68}Ga-PSMA-11 intensity (SUV_{max}) was one of the significant pre-operative predictors of progression-free survival after RP. Sub-analysis indicated that SUV_{max} was the most significant predictor of progression-free survival in patients with biopsy Gleason score ≤ 4 + 3 (15). Our study developed a new risk model only based on parameters derived from PSMA-ligand PET/CT, which was different from Roberts's study that SUV_{max} was added to clinical and pathological variables for Cox regression analysis. In addition, the comparison of the efficacy to the existing clinical models was not performed in Roberts's study.

In the present study, our risk model showed better performance compared to the commonly used D'Amico and CAPRA models (**Table 2**), although only three parameters (SUV_{max}, T staging, and tumor size described on PSMA PET/CT) were included. This result might be explained by the better performance of PSMA-ligand PET/CT-derived parameters in indicating histopathological features compared with clinical parameters. The most commonly used clinical variable reflecting tumor aggressiveness was PSA. However, PSA was an organ-specific biomarker instead of a disease-specific biomarker (18), as it could be induced to be released by several benign diseases such as benign prostatic hyperplasia (BPH), and prostatitis (19). In contrast, PSMA could be considered as PCa-specific marker, as it was highly expressed on the surface of PCa cells (20, 21). The other clinical variable that reflected tumor aggressiveness was histopathology obtained from prostate biopsy. However, Gleason score of prostate biopsy was always related with underestimation of tumor aggressiveness, as Gleason score upgrading from systematic biopsy to RP was commonly reported (22). Though MRI-targeted biopsy increased the detection rate of clinical significant PCa, it was associated with a 30.9% upgrading of cancer group (23). It might be due to the relatively low sensitivity of mpMRI in detecting intraprostatic lesions, especially for small lesions with low grade (24). Moreover, only small part of tissue was obtained from targeted biopsy, which was difficult to reflect the tumor grade of the whole lesion. It has been demonstrated that the detection rate was improved when the number of targeted biopsy increased (25). Different from biopsy, preoperative PSMA-ligand PET/CT was more informative for tumor grade reporting. Previous studies had revealed that SUV derived from PSMA PET/CT was positively correlated with tumor Gleason score (26, 27).

T staging on PSMA-ligand PET/CT is another contributor for better performance of our risk model in predicting of BCR compared with clinical models (**Table 2**). Clinically, tumor staging is assessed by DRE. Apparently, PSMA-ligand PET/CT provides more precise information regarding tumor size and

TABLE 2 | Cox regression analyses assessing the prediction models of biochemical recurrence in prostate cancer patients treated with radical prostatectomy.

Parameters	PET/CT based risk model		D'Amico		CAPRA		Modified D'Amico		Modified CAPRA	
	HR (95% CI)	p	HR (95% CI)	p	HR (95% CI)	p	HR (95% CI)	p	HR (95% CI)	p
PET/CT T stage										
T2	1 (ref)		-	-	-	-	1 (ref)		1 (ref)	
T3a	2.92 (1.08-7.87)	**.034**	-	-	-	-	2.64 (0.38-7.15)	.055	2.76 (1.02-7.47)	.045
T3b	2.29 (0.54-9.72)	.260	-	-	-	-	1.74 (0.57-7.29)	.449	1.99 (0.50-8.61)	.358
SUV_{max}	1.04 (1.02-1.07)	**.002**	-	-	-	-	1.04 (0.96-1.07)	**.003**	1.04 (1.01-1.07)	**.004**
Maximum diameter on PET	0.97 (0.58-1.61)	.905	-	-	-	-	0.88 (1.14-1.51)	.632	0.90 (0.59-1.56)	.686
D'Amico score	-	-	2.71 (1.37-5.38)	**0.004**	-	-	2.01 (0.50-4.41)	.083	-	-
CAPRA score	-	-	-	-	1.30 (1.09-1.56)	**0.004**	-	-	1.11 (0.90-1.38)	.363
C-Index	78.5 (70.3-86.7)		66.2 (57.4-75.0)		66.3 (56.1-76.5)		79.3 (70.1-88.5)		78.9 (70.4-87.3)	

PET/CT, positron emission computed tomography; HR, hazard ratio; CI, confidence intervals; SUV, standard uptake value.
Significant p values were presented in bold text.

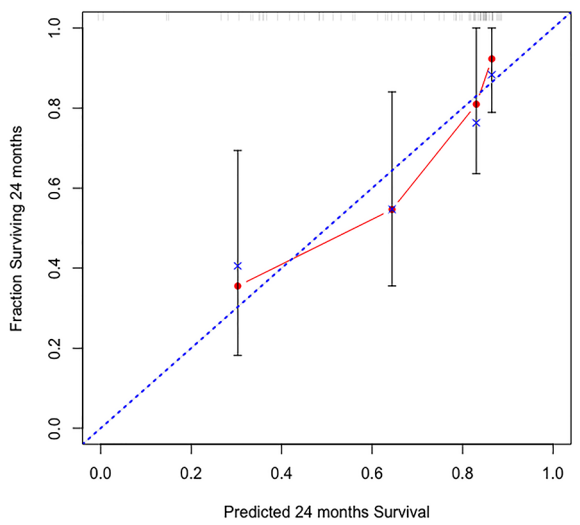

FIGURE 1 | Calibration plot of observed proportion versus predicted probability of 2-year biochemical recurrence after radical prostatectomy by the PSMA-ligand PET/CT-based risk model.

tumor location compared with DRE, improving the efficacy of PSMA-ligand PET/CT in evaluating clinical staging of T1 and T2. Recently, accumulative evidence shows the equivalent and even improved efficacy of PSMA-ligand PET/CT in detecting extraprostatic extension (EPE) and seminal vesical invasion (SVI) compared with mpMRI (16, 28), which could explain the significantly improved efficacy of PSMA-ligand PET/CT in providing tumor information regarding T3 staging. As shown in **Table 2**, T3a on PSMA-ligand PET/CT was significantly associated with the higher BCR after RP. However, this was not observed in patients with T3b, which has been reported to be a strong risk factor for BCR. It might be due to the smaller sample size in this polit study. Only 8 patients (10.4%) (**Table 1**) with T3b staging on PSMA-ligand PET/CT were included in the present study.

In our study, about 30% (23/77) patients experienced BCR within 2-year follow-up post PR, which was higher than the published results (29). Since tumor grade had been well demonstrated to be an independent predictor for early BCR after RP (5), our results could be explained by more cases with higher Gleason score (preoperative ISUP>2: 58.5% versus 36%) (30). Also, the median PSA level in the present study was much higher compared with that in the published study (13.30 versus 7.49 ng/ml) (30). Different from the United States, PCa screening was less pervasive in China, resulting in much higher percentage of high/very high risk and even metastatic patients at initial diagnosis (31). Therefore, the efficacy of our risk model for low-to-intermediate risk cases needed to be further validated with external data.

Regarding limitations, our study was a single-center retrospective study with relatively small sample and the median follow-up was only 25 months for patients without BCR. Therefore, our model needed to be further validated on patients with a longer follow-up procedure, as they might experience BCR after maintaining BCR-free survival within this period. To avoid selection bias, our risk model needed to be validated by further prospective studies before clinical application, as patients with pelvic lymph nodes and distant metastases were not included. However, our study aimed to propose the perspective that PSMA-ligand-based risk model might have great potential for risk stratification and prediction of BCR after RP, as it could provide noninvasive and prospective information regarding tumor aggressiveness and prognosis. In our established model, the weight of maximal tumor diameters seemed to be limited compared with T stage and SUVmax, though there was a significant difference between the BCR-free patients and BCT patients. In addition, the measurement of the maximal diameters on PET/CT is tricky though all measurements in the present study were performed by the same team with the same methods. Therefore, the value of maximal tumor diameters needs to be further verified and optimized in the following study.

In conclusion, a PSMA-ligand PET/CT-based risk model was developed for the BCR prediction following RP. Our newly developed risk model was shown to have better efficacy in predicting 2-year BCR after RP than the current D'Amico and CAPRA nomograms. Furthermore, the efficacy of the existing models were significantly improved by the additions of the parameters derived from PSMA-ligand PET/CT. PSMA-ligand PET/CT-based risk model showed great potential for the risk stratification and prediction of BCR of localized PCa after RP, which needed to be further validation by prospective studies.

CONCLUSION

This study demonstrated that a PSMA-ligand PET/CT based model had a good efficacy in predicting 2-year BCR after RP and the efficacy of the existing models were significantly improved by the additions of the parameters derived from PSMA-ligand PET/CT.

DATA AVAILABILITY STATEMENT

The original contributions presented in the study are included in the article/supplementary material. Further inquiries can be directed to the corresponding authors.

ETHICS STATEMENT

The studies involving human participants were reviewed and approved by 2017-147-01. The patients/participants provided their written informed consent to participate in this study. Written informed consent was obtained from the individual(s)

for the publication of any potentially identifiable images or data included in this article.

AUTHOR CONTRIBUTIONS

All authors listed have made a substantial, direct, and intellectual contribution to the work and approved it for publication.

FUNDING

This study was supported by grants from the National Natural Science Foundation of China (81602232, 81802535), Nanjing Medical Science and technique Development Foundation (QRX17128), and Nanjing Health Distinguished Youth Fund (JQX16025). All the funding supported equally in the design of the study and collection, analysis, and interpretation of data and in writing the manuscript.

REFERENCES

1. Mohler JL, Antonarakis ES, Armstrong AJ, D'Amico AV, Davis BJ, Dorff T, et al. Prostate Cancer, Version 2.2019, NCCN Clinical Practice Guidelines in Oncology. *J Natl Compr Cancer Network JNCCN* (2019) 17:479–505. doi: 10.6004/jnccn.2019.0023
2. Mottet N, Bellmunt J, Bolla M, Briers E, Cumberbatch MG, De Santis M, et al. EAU-ESTRO-SIOG Guidelines on Prostate Cancer. Part 1: Screening, Diagnosis, and Local Treatment With Curative Intent. *Eur Urol* (2017) 71:618–29. doi: 10.1016/j.eururo.2016.08.003
3. Babaian RJ, Troncoso P, Bhadkamkar VA, Johnston DA. Analysis of Clinicopathologic Factors Predicting Outcome After Radical Prostatectomy. *Cancer* (2001) 91:1414–22. doi: 10.1002/1097-0142(20010415)91:8<1414::AID-CNCR1147>3.0.CO;2-G
4. D'Amico AV, Whittington R, Malkowicz SB, Schultz D, Blank K, Broderick GA, et al. Biochemical Outcome After Radical Prostatectomy, External Beam Radiation Therapy, or Interstitial Radiation Therapy for Clinically Localized Prostate Cancer. *JAMA* (1998) 280:969–74. doi: 10.1001/jama.280.11.969
5. Cooperberg MR, Pasta DJ, Elkin EP, Litwin MS, Latini DM, Du Chane J, et al. The University of California, San Francisco Cancer of the Prostate Risk Assessment Score: A Straightforward and Reliable Preoperative Predictor of Disease Recurrence After Radical Prostatectomy. *J Urol* (2005) 173:1938–42. doi: 10.1097/01.ju.0000158155.33890.e7
6. Lughezzani G, Budäus L, Isbarn H, Sun M, Perrotte P, Haese A, et al. Head-To-Head Comparison of the Three Most Commonly Used Preoperative Models for Prediction of Biochemical Recurrence After Radical Prostatectomy. *Eur Urol* (2010) 57:562–8. doi: 10.1016/j.eururo.2009.12.003
7. Morote J, Del Amo J, Borque A, Ars E, Hernández C, Herranz F, et al. Improved Prediction of Biochemical Recurrence After Radical Prostatectomy by Genetic Polymorphisms. *J Urol* (2010) 184:506–11. doi: 10.1016/j.juro.2010.03.144
8. Afshar-Oromieh A, Holland-Letz T, Giesel FL, Kratochwil C, Mier W, Haufe S, et al. Diagnostic Performance of (68)Ga-PSMA-11 (HBED-CC) PET/CT in Patients With Recurrent Prostate Cancer: Evaluation in 1007 Patients. *Eur J Nucl Med Mol Imaging* (2017) 44:1258–68. doi: 10.1007/s00259-017-3711-7
9. Rauscher I, Düwel C, Haller B, Rischpler C, Heck MM, Gschwend JE, et al. Efficacy, Predictive Factors, and Prediction Nomograms for (68)Ga-Labeled Prostate-Specific Membrane Antigen-Ligand Positron-Emission Tomography/Computed Tomography in Early Biochemical Recurrent Prostate Cancer After Radical Prostatectomy. *Eur Urol* (2018) 73:656–61. doi: 10.1016/j.eururo.2018.01.006
10. Herlemann A, Wenter V, Kretschmer A, Thierfelder KM, Bartenstein P, Faber C, et al. (68)Ga-PSMA Positron Emission Tomography/Computed Tomography Provides Accurate Staging of Lymph Node Regions Prior to Lymph Node Dissection in Patients With Prostate Cancer. *Eur Urol* (2016) 70:553–7. doi: 10.1016/j.eururo.2015.12.051
11. Hofman MS, Lawrentschuk N, Francis RJ, Tang C, Vela I, Thomas P, et al. Prostate-Specific Membrane Antigen PET-CT in Patients With High-Risk Prostate Cancer Before Curative-Intent Surgery or Radiotherapy (proPSMA): A Prospective, Randomised, Multicentre Study. *Lancet (Lond Engl)* (2020) 395:1208–16. doi: 10.1016/S0140-6736(20)30314-7
12. Chen M, Zhang Q, Zhang C, Zhao X, Marra G, Gao J, et al. Combination of (68)Ga-PSMA PET/CT and Multiparametric MRI Improves the Detection of Clinically Significant Prostate Cancer: A Lesion-By-Lesion Analysis. *J Nucl Med Off Publication Soc Nucl Med* (2019) 60:944–9. doi: 10.2967/jnumed.118.221010
13. Chen M, Qiu X, Zhang Q, Zhang C, Zhou Y, Zhao X, et al. PSMA Uptake on [68Ga]-PSMA-11-PET/CT Positively Corrects With Prostate Cancer Aggressiveness. *Q J Nucl Med Off Publ Ital Assoc Nucl Med (AIMN) Int Assoc Radiopharm (IAR)* (2019). doi: 10.1097/01.JU.0000557493.33637.42
14. Chen M, Zhang Q, Zhang C, Zhou YH, Zhao X, Fu Y, et al. Comparison of (68)Ga-Prostate-Specific Membrane Antigen (PSMA) Positron Emission Tomography/Computed Tomography (PET/CT) and Multi-Parametric Magnetic Resonance Imaging (MRI) in the Evaluation of Tumor Extension of Primary Prostate Cancer. *Trans Androl Urol* (2020) 9:382–90. doi: 10.21037/tau.2020.03.06
15. Roberts MJ, Morton A, Donato P, Kyle S, Pattison DA, Thomas P, et al. (68)Ga-PSMA PET/CT Tumour Intensity Pre-Operatively Predicts Adverse Pathological Outcomes and Progression-Free Survival in Localised Prostate Cancer. *Eur J Nucl Med Mol Imaging* (2021) 48(2):477–82. doi: 10.1007/s00259-020-04983-9
16. von Klot CJ, Merseburger AS, Böker A, Schmuck S, Ross TL, Bengel FM, et al. (68)Ga-PSMA PET/CT Imaging Predicting Intraprostatic Tumor Extent, Extracapsular Extension and Seminal Vesicle Invasion Prior to Radical Prostatectomy in Patients With Prostate Cancer. *Nucl Med Mol Imaging* (2017) 51:314–22. doi: 10.1007/s13139-017-0476-7
17. Brockman JA, Alanee S, Vickers AJ, Scardino PT, Wood DP, Kibel AS, et al. Nomogram Predicting Prostate Cancer-Specific Mortality for Men With Biochemical Recurrence After Radical Prostatectomy. *Eur Urol* (2015) 67:1160–7. doi: 10.1016/j.eururo.2014.09.019
18. Balk SP, Ko YJ, Bubley GJ. Biology of Prostate-Specific Antigen. *J Clin Oncol Off J Am Soc Clin Oncol* (2003) 21:383–91. doi: 10.1200/JCO.2003.02.083
19. Gjertson CK, Albertsen PC. Use and Assessment of PSA in Prostate Cancer. *Med Clinics North America* (2011) 95:191–200. doi: 10.1016/j.mcna.2010.08.024
20. Silver DA, Pellicer I, Fair WR, Heston WD, Cordon-Cardo C. Prostate-Specific Membrane Antigen Expression in Normal and Malignant Human Tissues. *Clin Cancer Res an Off J Am Assoc Cancer Res* (1997) 3:81–5.
21. Bostwick DG, Pacelli A, Blute M, Roche P, Murphy GP. Prostate Specific Membrane Antigen Expression in Prostatic Intraepithelial Neoplasia and Adenocarcinoma: A Study of 184 Cases. *Cancer* (1998) 82:2256–61. doi: 10.1002/(SICI)1097-0142(19980601)82:11<2256::AID-CNCR22>3.0.CO;2-S
22. Hsieh TF, Chang CH, Chen WC, Chou CL, Chen CC, Wu HC. Correlation of Gleason Scores Between Needle-Core Biopsy and Radical Prostatectomy Specimens in Patients With Prostate Cancer. *J Chin Med Assoc JCMA* (2005) 68:167–71. doi: 10.1016/S1726-4901(09)70243-6
23. Ahdoot M, Wilbur AR, Reese SE, Lebastchi AH, Mehralivand S, Gomella PT, et al. MRI-Targeted, Systematic, and Combined Biopsy for Prostate Cancer Diagnosis. *New Engl J Med* (2020) 382:917–28. doi: 10.1056/NEJMoa1910038
24. Schouten MG, van der Leest M, Pokorny M, Hoogenboom M, Barentsz JO, Thompson LC, et al. Why and Where do We Miss Significant Prostate Cancer With Multi-Parametric Magnetic Resonance Imaging Followed by Magnetic Resonance-Guided and Transrectal Ultrasound-Guided Biopsy in Biopsy-Naïve Men? *Eur Urol* (2017) 71:896–903. doi: 10.1016/j.eururo.2016.12.006
25. Stewart CS, Leibovich BC, Weaver AL, Lieber MM. Prostate Cancer Diagnosis Using a Saturation Needle Biopsy Technique After Previous Negative Sextant Biopsies. *J Urol* (2001) 166:86–91; discussion -2. doi: 10.1016/S0022-5347(05)66083-1

26. Uprimny C, Kroiss AS, Decristoforo C, Fritz J, von Guggenberg E, Kendler D, et al. (68)Ga-PSMA-11 PET/CT in Primary Staging of Prostate Cancer: PSA and Gleason Score Predict the Intensity of Tracer Accumulation in the Primary Tumour. *Eur J Nucl Med Mol Imaging* (2017) 44:941–9. doi: 10.1007/s00259-017-3631-6
27. Koerber SA, Utzinger MT, Kratochwil C, Kesch C, Haefner MF, Katayama S, et al. (68)Ga-PSMA-11 PET/CT in Newly Diagnosed Carcinoma of the Prostate: Correlation of Intraprostatic PSMA Uptake With Several Clinical Parameters. *J Nucl Med Off Publication Soc Nucl Med* (2017) 58:1943–8. doi: 10.2967/jnumed.117.190314
28. Grubmüller B, Baltzer P, Hartenbach S, D'Andrea D, Helbich TH, Haug AR, et al. PSMA Ligand PET/MRI for Primary Prostate Cancer: Staging Performance and Clinical Impact. *Clin Cancer Res* (2018) 24:6300–7. doi: 10.1158/1078-0432.CCR-18-0768
29. Coughlin GD, Yaxley JW, Chambers SK, Occhipinti S, Samaratunga H, Zajdlewicz L, et al. Robot-Assisted Laparoscopic Prostatectomy Versus Open Radical Retropubic Prostatectomy: 24-Month Outcomes From a Randomised Controlled Study. *Lancet Oncol* (2018) 19:1051–60. doi: 10.1016/S1470-2045(18)30357-7
30. Yaxley JW, Coughlin GD, Chambers SK, Occhipinti S, Samaratunga H, Zajdlewicz L, et al. Robot-Assisted Laparoscopic Prostatectomy Versus Open Radical Retropubic Prostatectomy: Early Outcomes From a Randomised Controlled Phase 3 Study. *Lancet (Lond Engl)* (2016) 388:1057–66. doi: 10.1016/S0140-6736(16)30592-X
31. Chen W, Zheng R, Baade PD, Zhang S, Zeng H, Bray F, et al. Cancer Statistics in China, 2015. *CA: Cancer J Clin* (2016) 66:115–32. doi: 10.3322/caac.21338

Conflict of Interest: The authors declare that the research was conducted in the absence of any commercial or financial relationships that could be construed as a potential conflict of interest.

Publisher's Note: All claims expressed in this article are solely those of the authors and do not necessarily represent those of their affiliated organizations, or those of the publisher, the editors and the reviewers. Any product that may be evaluated in this article, or claim that may be made by its manufacturer, is not guaranteed or endorsed by the publisher.

Copyright © 2021 Qiu, Chen, Yin, Zhang, Li, Guo, Fu, Zang, Ai, Wang and Guo. This is an open-access article distributed under the terms of the Creative Commons Attribution License (CC BY). The use, distribution or reproduction in other forums is permitted, provided the original author(s) and the copyright owner(s) are credited and that the original publication in this journal is cited, in accordance with accepted academic practice. No use, distribution or reproduction is permitted which does not comply with these terms.

frontiers in Oncology

ORIGINAL RESEARCH
published: 22 November 2021
doi: 10.3389/fonc.2021.742354

Alpha-L-Fucosidase Has Diagnostic Value in Prostate Cancer With "Gray-Zone PSA" and Inhibits Cancer Progression *via* Regulating Glycosylation

Cong Zhang[1], Jikai Liu[2], Fan Chao[1], Shiyu Wang[1], Dawei Li[2], Dunsheng Han[1], Zhonghua Xu[2], Guoxiong Xu[3] and Gang Chen[1]**

[1] Department of Urology, Jinshan Hospital, Fudan University, Shanghai, China, [2] Department of Urology, Qilu Hospital, Shandong University, Jinan, China, [3] Research Center for Clinical Medicine, Jinshan Hospital, Fudan University, Shanghai, China

OPEN ACCESS

Edited by:
Tanya I. Stoyanova, Stanford University, United States

Reviewed by:
En-Chi Hsu, Stanford University, United States
Koji Hatano, Osaka University, Japan

***Correspondence:**
Gang Chen
chgan365@126.com
Zhonghua Xu
xuzhonghua1963@163.com

Specialty section:
This article was submitted to Genitourinary Oncology, a section of the journal Frontiers in Oncology

Received: *16 July 2021*
Accepted: *29 October 2021*
Published: *22 November 2021*

Citation:
Zhang C, Liu J, Chao F, Wang S, Li D, Han D, Xu Z, Xu G and Chen G (2021) Alpha-L-Fucosidase Has Diagnostic Value in Prostate Cancer With "Gray-Zone PSA" and Inhibits Cancer Progression via Regulating Glycosylation. Front. Oncol. 11:742354. doi: 10.3389/fonc.2021.742354

Background: This study aimed to explore the diagnostic value of alpha-l-fucosidase (AFU) in prostate cancer (PCa) patients with "gray-zone PSA" and to investigate the correlation between AFU expression and clinicopathological characteristics of PCa patients.

Methods: The level of AFU and other necessary clinicopathological variables of patients were retrieved from electronic medical records. The transcriptome profiling and clinical information of PCa patients were obtained from The Cancer Genome Atlas (TCGA) database. The protein level of AFU in tissue was assessed by immunohistochemistry (IHC). All the data were processed by appropriate analysis methods. The p-value of <0.05 was considered statistically significant.

Results: AFU showed ideal diagnostic value for PCa with prostate-specific antigen (PSA) levels ranging from 4 to 10 ng/ml, and its optimal cutoffs were 19.5 U/L. Beyond this, low AFU expression was associated with high pathological grade, T stage and N stage, more postoperative residual tumors, and poor primary therapy outcome, as well as shorter progression-free interval. The Kyoto Encyclopedia of Genes and Genomes (KEGG) analysis illustrated that FUCA1/FUCA2 exerted tumor-suppressive function by regulating the glycosylation.

Conclusions: AFU (<19.5 U/L) could effectively distinguish the PCa from the patients with "gray-zone PSA", and low expression of AFU was an independent unfavorable predictor for the clinicopathological characteristics of PCa patients.

Keywords: prostate cancer, AFU, diagnosis, tumor progression, progression-free interval

INTRODUCTION

Prostate cancer (PCa) is an epithelial malignancy with a high incidence that occurs in the male genitourinary system (1). In recent years, the morbidity and mortality of PCa have increased dramatically worldwide. Based on the last data, the morbidity of PCa ranks no. 1, and the mortality ranks no. 2 among male malignant tumors in 112 countries (2). In 2020, there were 1.4 million new PCa cases and 370,000 deaths globally (2). The treatment options of PCa vary based on cancer grade and stage. For example, surgery is the standard treatment for early PCa, and it can lead to a favorable prognosis. Therefore, early and accurate diagnosis is crucial for the treatment of PCa patients. Although the prostate-specific antigen (PSA) screening has made great contributions to the early diagnosis of PCa, some limitations are readily apparent. It is well established that the "diagnostic gray zone" existed in PSA screening due to the poor specificity (3). A prostate biopsy can provide an accurate diagnosis, but it is a time-consuming and expensive method that requires an experienced urologist and causes great suffering for patients. Therefore, the identification of effective and practical biomarkers for early and accurate diagnosis of PCa (especially men with a PSA of 4–10 ng/ml) is urgent and important.

AFU containing two isoforms, AFU1 and AFU2, is an enzyme that is capable of clearing the terminal α-l-fucose residues from glycoproteins (4, 5). AFU1 and AFU2 are encoded by *FUCA1* gene and *FUCA2* gene, respectively. Interestingly, high α-l-fucose expression has been reported to be correlated with many cancers, such as breast, thyroid, and colorectal cancers (6–10). Therefore, it is reasonable to speculate that AFU with the function of hydrolyzing α-l-fucose may imply tumor-suppressive function. Previous studies have confirmed that AFU is indeed lowly expressed in a variety of cancers, including colon cancer, colorectal cancer, and breast cancer (11–13). Other than that, low expression of AFU usually predicts a worse prognosis in cancer patients (12–14).

However, the possible correlations between AFU and PCa have not yet been explored. Consequently, the current study is conducted to investigate the relationship between AFU expression and PCa. We hope that the current research can identify a promising early diagnostic and effective prognostic biomarker for PCa.

MATERIALS AND METHODS

Patients

Patients' clinicopathological information was collected and analyzed through retrospective chart reviews of electronic medical records of Qilu Hospital of Shandong University between 2013 and 2020. Following inclusion and exclusion criteria, a total of 106 PCa patients with PSA levels between 4 and 10 ng/ml met the requirements. Those patients all accepted prostate biopsy and were confirmed as PCa by biopsy pathological results. Meanwhile, 113 benign prostatic hyperplasia (BPH) patients whose PSA levels ranged from 4 to 10 ng/ml were included as a control in this retrospective study. Beyond that, in order to further investigate the relationship between AFU expression and clinicopathological features of PCa patients, 196 eligible PCa patients who were treated with radical prostatectomy at Qilu Hospital were integrated into the current study.

The inclusion criteria were the following:

1) Necessary information was available, such as important test records, clinicopathological variables, and other necessary data.
2) The postoperation pathological outcomes indicated benign prostatic hyperplasia or prostatic adenocarcinoma.

The exclusion criteria were the following:

1) Coexisting other malignant diseases or history of tumor or cancer
2) Suffering from immune system disease or hematologic disorders
3) Taking procoagulant or anticoagulant or other medicine interfering with lab test within the past 2 weeks

Data Collection

Essential demographic information, important laboratory results, and clinicopathological data were retrieved from electronic patient records. The pathological grade was evaluated using the Gleason system. It was divided into two groups: high-pathological grade group (Gleason scores ≥8) and low-pathological grade group (Gleason scores <8) as described by a previous study (15). The stage was judged by the 2002 TNM classification (16).

Alpha-l-Fucosidase Measurement

After 12-h fasting, 5 ml of venous blood was drawn from each patient before he received any clinical treatment in the early morning. Blood was stored in the blood-sampling tubes containing procoagulant. Subsequently, samples were centrifuged at 2,000 rpm for 10 min, and the serum was separated to determine the activity of AFU by The Roche Cobas 8000 automatic analyzer (Roche, Switzerland) according to the standard operating procedure.

Extraction and Analysis of The Cancer Genome Atlas Datasets

The transcriptome profiling and clinical information of PCa patients were obtained from The Cancer Genome Atlas (TCGA) database (https://www.cancer.gov/tcga). The expression of *FUCA1*/*FUCA2* and important clinicopathological variables of PCa patients, such as pathological grade, stage, and survival data, were extracted and analyzed.

Abbreviations: PCa, prostate cancer; BPH, benign prostatic hyperplasia; AFU, alpha-l-fucosidase; PSA, prostate-specific antigen; SA, serum sialic acid; LDH, lactate dehydrogenase; AKP, alkaline phosphatase; HR, hazard ratios; PFI, progression-free interval.

Immunohistochemistry Analysis Based on The Human Protein Atlas

The protein expression of AFU in PCa tissue was evaluated under the support of the online website The Human Protein Atlas (https://www.proteinatlas.org/).

Statistical Analysis

The expression of AFU in each group was shown as mean and SD. The correlations between AFU levels and variables were assessed by Student's t-test if the data followed a normal distribution, and if not, using the Mann–Whitney test. The data were obtained from TCGA by employing chi-square test, Fisher's exact test, or Wilcoxon rank-sum test. Kaplan–Meier and Cox regression methods were used to evaluate the survival data from TCGA. The hazard ratio (HR) and 95% CI were calculated by logistic regression or Cox regression model. A two-sided p-value was set in the current study, and a p-value of <0.05 was regarded as statistically significant. Statistical analysis was performed by the Statistical Package for Social Sciences version 20.0 (SPSS Inc., Chicago, IL, USA), GraphPad Prism 8 software (GraphPad Software Inc., San Diego, CA, USA), and R (version 3.6.3; R Foundation, Vienna, Austria).

RESULTS

Baseline Clinicopathological Characteristics

A total of 219 patients with PSA between 4 and 10 ng/ml were enrolled in the present study. Based on the pathological results after a needle biopsy, 113 patients were diagnosed with BPH, and 106 patients were confirmed to have PCa. Surprisingly, the mean level of PSA in the BPH was higher than that in the PCa, although no statistical differences were presented (7.84 ± 2.55 vs. 7.48 ± 2.58 ng/ml, $p = 0.675$). It was meaningful that we found that the free/total (F/T) PSA and AFU levels in the BPH patients were higher than in the PCa patients (F/T PSA: 0.22 ± 0.24 vs. 0.18 ± 0.19, $p = 0.008$; AFU: 20.16 ± 6.17 U/L vs. 18.21 ± 6.66 U/L, $p = 0.049$) (**Table 1** and **Figures 1A, B**), but there was no line correlation between them (**Figure 1E**). Then, the receiver operating characteristic (ROC) analysis indicated that AFU had a better value for PCa diagnosis than F/T PSA especially in specificity (the area under the ROC curve (AUC): 0.630 vs. 0.612) (**Figures 1C, D**), and the AFU optimal cutoffs for PCa was 19.5 U/L. Logistic regression analysis was employed to further validate the AFU cutoffs' diagnostic value for PCa, and the results indicated that AFU cutoffs showed ideal diagnostic performance for PCa (≥19.5 vs. <19.5 U/L: HR = 0.513, $p = 0.044$) (**Figure 1F**).

Associations Between Alpha-l-Fucosidase Expression and Clinicopathological Variables of 196 Prostate Cancer Patients

A total of 196 PCa patients who underwent radical prostatectomy, with the PSA average of 30.30 ng/ml (ranking 0.04 to 343 ng/ml), were analyzed in the present study. The results indicated that AFU expression was inversely correlated with PSA. The PCa patients with higher PSA levels (PSA ≥ 4 ng/ml) indicated lower AFU expression (15.89 ± 5.01 U/L) and vice versa ($p = 0.043$) (**Table 2** and **Figure 2A**). Importantly, non-localized PCa (pT3 and pT4) showed lower AFU expression than localized PCa (pT1 and pT2) ($p = 0.05$) (**Table 2** and **Figure 2B**). Likewise, the advanced PCa with lymph node metastasis had a lower AFU level than that without lymphatic metastasis ($p = 0.017$) (**Table 2** and **Figure 2C**). Although differences were not statistically significant, we found that the high pathological grade group had lower AFU levels than the low pathological grade group (**Table 2**). The results of the ROC analyses indicated good predictive power of AFU for PCa pathological T stage and N stage especially for N stage (**Table 2** and **Figures 2D, E**). However, no linear relationship was observed among AFU levels and age, lactate dehydrogenase (LDH), serum sialic acid (SA), alkaline phosphatase (AKP), and PSA (**Figures 2F–J**).

FUCA1 and *FUCA2* Expression in Prostate Cancer Based on The Cancer Genome Atlas Database

The expression of *FUCA1*/*FUCA2* and clinicopathological data of 499 PCa patients were extracted from TCGA database and presented in **Tables 3**, **4**, respectively. *FUCA1* expression was lower in the older group ($p = 0.0006$) compared with the younger group (**Table 3** and **Figure 3A**), but *FUCA2* expression had no notable difference between the two groups ($p = 0.896$) (**Table 4**). Notably, lower *FUCA1*/*FUCA2* expression predicted both higher pathological grade group and stage, more residual tumors, and worse therapeutic effect (**Figures 3A**, **4A**). In parallel, the ROC analysis confirmed that low *FUCA1* and *FUCA2* indeed

TABLE 1 | Clinical characteristics of PCa and BPH patients.

Characteristics	BPH	PCa	*p*-Value
Patients (n; %)	113 (51.6%)	106 (48.4%)	
Age (years)	68.08 ± 8.99	69.97 ± 8.43	0.149*
PSA (ng/ml)	7.84 ± 2.55	7.48 ± 2.58	0.675*
F/T PSA	0.22 ± 0.24	0.18 ± 0.19	0.008*
AFU (U/L)	20.16 ± 6.17	18.21 ± 6.66	0.049*

p < 0.05 is considered as statistically significant.

PCa, prostate cancer; BPH, benign prostatic hyperplasia; PSA, prostate-specific antigen; F/T PSA, free/total prostate-specific antigen; AFU, alpha-L-fucosidase.

**p: Mann–Whitney U-test.*

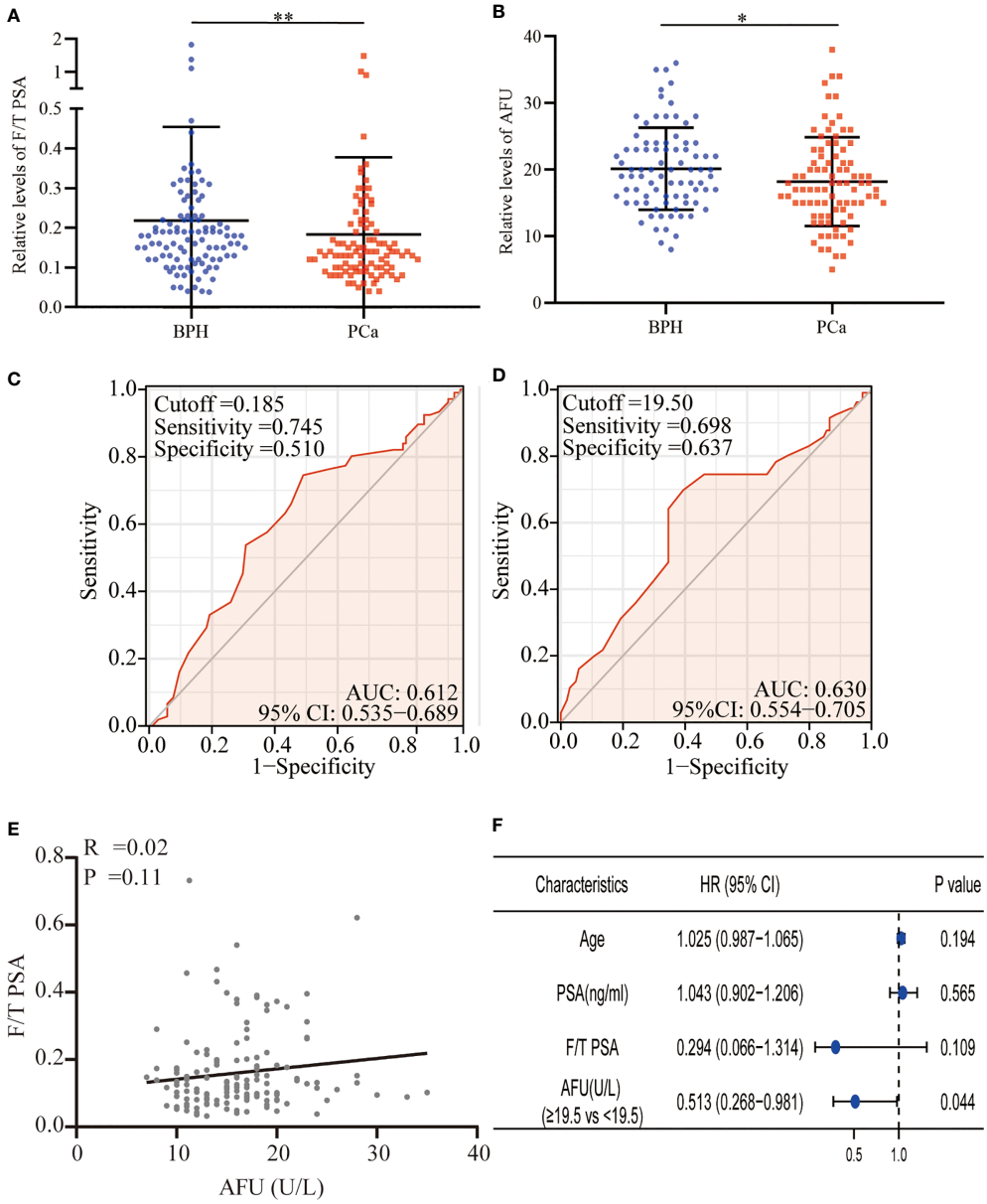

FIGURE 1 | F/T PSA and AFU level in BPH and PCa. **(A)** F/T PSA level. **(B)** AFU level. **(C)** The diagnostic value of F/T PSA for PCa. **(D)** The diagnostic value of AFU for PCa. **(E)** The line correlation between F/T PSA and AFU. **(F)** Logistic analysis of AFU expression for the PCa diagnosis; *$p < 0.05$, **$p < 0.01$. F/T PSA, free/total prostate-specific antigen; AFU, alpha-L-fucosidase; BPH, benign prostatic hyperplasia; PCa, prostate cancer.

promoted PCa progression, metastasis, and drug resistance (**Figures 3B**, **4B**). All the above results were further validated by logistic regression analysis (**Figures 3C**, **4C**).

Immunohistochemistry Staining of Alpha-l-Fucosidase

AFU protein levels in PCa tissue were further measured by immunohistochemistry (IHC) staining based on the online website, The Human Protein Atlas (https://www.proteinatlas.org/). As may be immediately apparent, the expression of AFU1 and AFU2 were much lower in high-grade PCa tissue compared with low-grade tissue (**Figures 3D, E** and **4D, E**).

Low Expression of *FUCA1/FUCA2* Predicted Worse Prognosis of Prostate Cancer Patients

Log-rank analysis indicated that the lower level of *FUCA1/FUCA2* indicated shorter progression-free interval (PFI) of

TABLE 2 | Correlations between preoperative AFU levels and clinicopathological parameters of PCa patients.

Characteristics	N (%)	AFU levels (U/L, mean ± SD)	*p*-Value
Patients[a]	196 (100%)	16.35 ± 5.20	
Age			0.144*
<69	92 (46.9%)	16.92 ± 5.87	
≥69	104 (53.1%)	15.59 ± 4.29	
PSA (ng/ml)			**0.043***
<4	49 (25%)	17.63 ± 5.41	
≥4	116 (59.2%)	15.89 ± 5.01	
Missing data	31 (15.8%)	–	
LDH[a]			0.585*
<197	102 (52.0%)	16.47 ± 5.42	
≥197	80 (40.8%)	16.41 ± 4.60	
Missing data	14 (7.1%)	–	
SA[a]			0.954*
<56	110 (56.1%)	16.38 ± 4.83	
≥56	71 (36.2%)	16.62 ± 5.44	
Missing data	15 (7.7%)	–	
AKP[a]			0.364*
<75	114 (58.2%)	16.34 ± 5.58	
≥75	71 (36.2%)	16.42 ± 4.11	
Missing data	11 (5.6%)	–	
Pathological grade group			
Low-grade group (<8)	107 (54.6%)	16.45 ± 5.31	0.531*
High-grade group (≥8)	89 (45.4%)	15.93 ± 4.90	
T stage			**0.050***
T1 and T2	141 (71.9%)	16.73 ± 5.32	
T3 and T4	55 (28.1%)	14.89 ± 4.35	
N stage			**0.017***
N0	185 (94.4%)	16.41 ± 5.13	
N1	11 (5.6%)	12.91 ± 3.81	
Bone metastasis			0.105[a]*
No	99 (50.5%)	16.74 ± 5.36	0.924[b]*
Yes	14 (7.1%)	14.21 ± 4.14	
Suspicion	23 (11.7%)	16.30 ± 4.70	
Missing data	60 (30.6%)	–	

Pathological grade falls into high grade and low grade using the GS. Pathological stage is assessed by postoperative pathology results (not biopsy) in accordance with 2002 TNM classification; $p < 0.05$ is considered as statistically significant.

PCa, prostate cancer; BPH, benign prostate hyperplasia; AFU, alpha-L-fucosidase; PSA, prostate-specific antigen; LDH, lactate dehydrogenase; SA, serum sialic acid; AKP, alkaline phosphatase; GS, Gleason system.

[a]*Continuous variables are expressed as median.*

[a]*p: no bone metastases versus bone metastases.*

[b]*p: no bone metastases versus suspicion.*

**p: Mann–Whitney U-test.*

Bold values was used for emphasis, means $p \leq 0.05$.

PCa patients (**Figures 5A, B**). Cox regression model illustrated that low *FUCA1* expression was a reliable indicator for PCa patients' poor prognosis (**Figures 5C, E**), but the prognostic performance of *FUCA2* was susceptible to other factors (**Figures 5D, F**).

Kyoto Encyclopedia of Genes and Genomes Analysis Indicated *FUCA1*/*FUCA2* Exerted Biological Function Through Regulating Glycosylation

In order to probe the underlying mechanism through which *FUCA1*/*FUCA2* exerted its functional role, the Kyoto Encyclopedia of Genes and Genomes (KEGG) analysis was applied. The analysis results indicated that *FUCA1* and *FUCA2* both played an essential role in the regulation of glycosylation, especially in the protein glycosylation (**Figures 6A, B**).

DISCUSSION

The present study indicates, for the first time, that AFU can effectively distinguish PCa from patients with PSA levels ranging from 4 to 10 ng/ml. We find that compared with the BPH patients, the PCa patients have lower serum AFU expression and smaller values of F/T PSA, both with gray-zone PSA level. We are aware that PSA is secreted by prostate epithelial cells, and its level will be elevated in PCa and BPH (17). Therefore, it is difficult to distinguish early PCa from BPH solely dependent on the PSA expression. In line with a previous study (18), our results indicated that no meaningful difference in PSA levels was observed between BPH and PCa patients with "gray-zone PSA". To validate and further test the diagnostic reliability of F/T PSA and AFU, the logistic regression analysis was applied. However, the results illustrated that only AFU but not F/T PSA still exhibited a robust and independent diagnostic value for PCa.

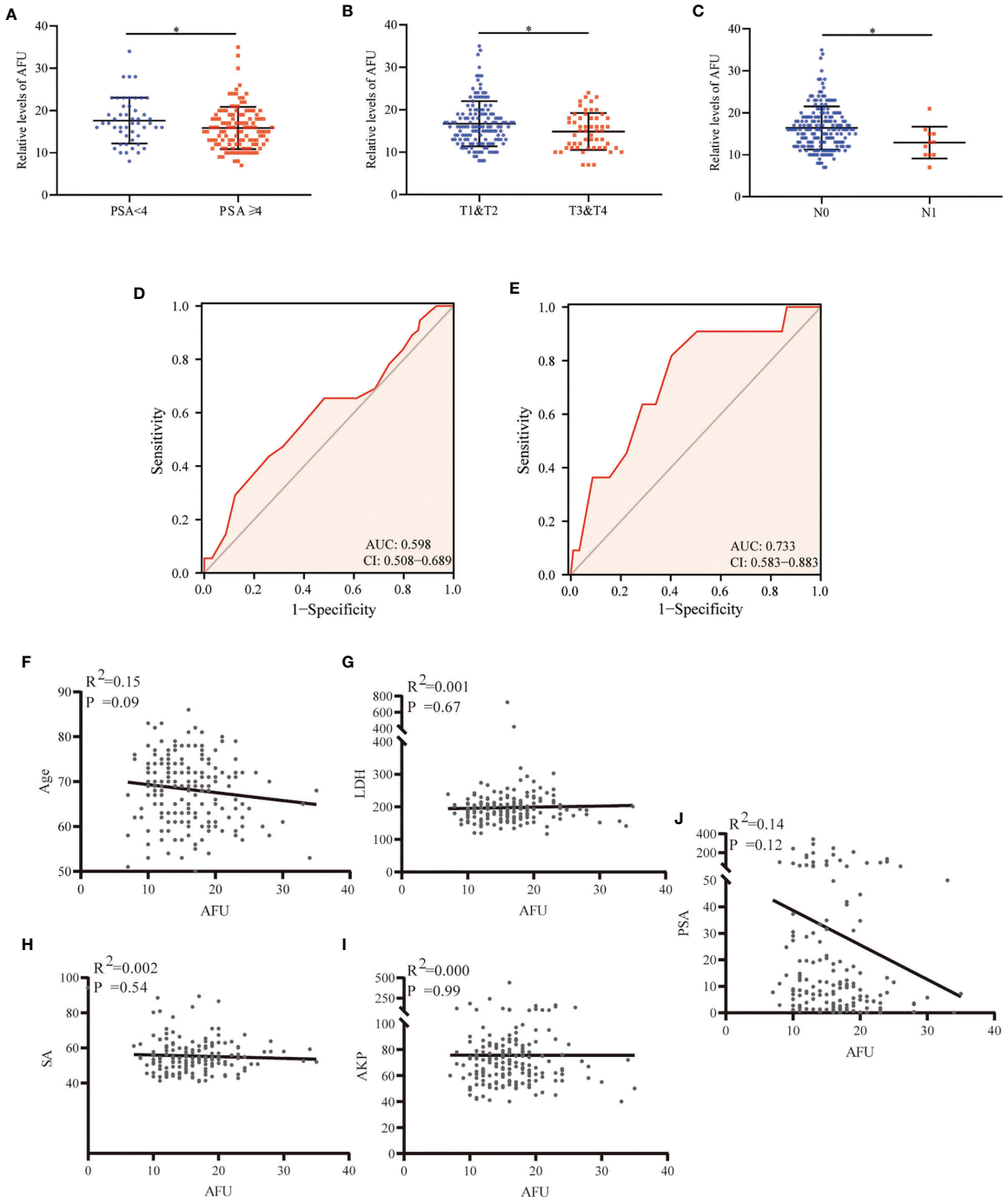

FIGURE 2 | AFU expression in PCa subgroups. **(A)** PSA. **(B)** T stage. **(C)** N stage. **(D)** The diagnostic value of AFU for advanced T stage. **(E)** The diagnostic value of AFU for lymph node metastasis. Line correlations among AFU and PCa patient's variables: **(F)** age; **(G)** LDH; **(H)** SA; **(I)** AKP; and **(J)** PSA. *$p < 0.05$. AFU, alpha-L-fucosidase; PCa, prostate cancer; PSA, prostate-specific antigen; LDH, lactate dehydrogenase; SA, serum sialic acid; AKP, alkaline phosphatase.

Likewise, the ROC analysis indicated that the diagnostic efficiency of F/T PSA was inferior compared with that of AFU. These data indicated that the diagnostic value of F/T PSA was more vulnerable to be interfered with other factors such as age and PSA level; for this reason, F/T PSA was not a reliable indicator for PCa patients with gray-zone PSA level. After confirmation of the diagnostic value of AFU for PCa, the possible correlations between AFU expression and PCa patients' clinicopathological varies, which were further explored. Consistent with the above conclusion, lower

TABLE 3 | Correlations between FUCA1 expression and clinicopathological parameters of PCa patients.

Characteristic	Low expression of FUCA1 n (%)	High expression of FUCA1 n (%)	*p*-Value
Patients	249 (40.9%)	250 (50.1%)	
Age			0.006***
≤60	96 (19.2%)	128 (25.7%)	
>60	153 (30.7%)	122 (24.4%)	
PSA (ng/ml)			0.092*
<4	199 (45%)	216 (48.9%)	
≥4	18 (4.1%)	9 (2%)	
Pathological grade group			<0.001*
Low-grade group (Gleason score < 8)	110 (22%)	183 (36.7%)	
High-grade group (Gleason score ≥ 8)	139 (31%)	67 (13.4%)	
T stage			<0.001*
T2	68 (13.8%)	121 (24.6%)	
T3 and T4	178 (36.2%)	125 (25.4%)	
N stage			0.004*
N0	168 (39.4%)	179 (42%)	
N1	53 (12.4%)	26 (6.1%)	
M stage			0.621**
M0	225 (49.1%)	230 (50.2%)	
M1	2 (0.4%)	1 (0.2%)	
Primary therapy outcome			<0.001*
PR and CR	171 (39.1%)	210 (48%)	
PD and SD	43 (9.9%)	14 (3.2%)	
Residual tumor			<0.001**
R0	140 (29.9%)	175 (37.4%)	
R1 and R2	92 (19.6%)	61 (13.1%)	
OS event, n (%)			0.063**
Alive	241 (48.3%)	248 (49.7%)	
Dead	8 (1.6%)	2 (0.4%)	
DSS event, n (%)			0.684**
Alive	244 (49.1%)	248 (49.9%)	
Dead	3 (0.6%)	2 (0.4%)	
PFI event, n (%)			<0.001*
Alive	184 (36.9%)	221 (44.3%)	
Dead	65 (13%)	29 (5.8%)	

p < 0.05 is considered as statistically significant.
PCa, prostate cancer; BPH, benign prostate hyperplasia; OS, overall survival; DSS, disease-specific survival; PFI, progression-free interval; PR, partial response; CR, complete response; PD, progressive disease; SD, stable disease.
**p: chi-square test.*
***p: Fisher's test.*
****p: Wilcoxon rank-sum test.*

TABLE 4 | Correlations between FUCA2 expression and clinicopathological parameters of PCa patients.

Characteristic	Low expression of FUCA2 n (%)	High expression of FUCA2 n (%)	*p*-Value
Patients	249 (40.9%)	250 (50.1%)	
Age			0.896***
≤60	113 (22.6%)	111 (22.2%)	
>60	136 (27.3%)	139 (27.9%)	
PSA (ng/ml)			0.112*
<4	203 (45.9%)	212 (48%)	
≥4	18 (4.1%)	9 (2%)	
Pathological grade group			0.001*
Low-grade group (Gleason score < 8)	126 (25.28%)	167 (33.5%)	
High-grade group (Gleason score ≥ 8)	123 (24.6%)	83 (16.6%)	
T stage			0.005*
T2	79 (16.1%)	110 (22.4%)	
T3 and T4	166 (33.7%)	137 (27.8%)	
N stage			0.007*
N0	167 (39.2%)	180 (42.3%)	
N1	52 (12.2%)	27 (6.3%)	
M stage			0.618**
M0	232 (50.7%)	223 (48.7%)	
M1	1 (0.2%)	2 (0.4%)	
Primary therapy outcome			0.008*
PR and CR	182 (41.6%)	199 (45.5%)	
PD and SD	38 (8.6%)	19 (4.4%)	
Residual tumor			0.023*
R0	145 (31%)	170 (36.3%)	
R1 and R2	88 (18.8%)	65 (13.9%)	
OS event			0.751**
Alive	245 (49.1%)	244 (48.9%)	
Dead	4 (0.8%)	6 (1.2%)	
DSS event			0.373**
Alive	246 (49.5%)	246 (49.5%)	
Dead	1 (0.2%)	4 (0.8%)	
PFI event			0.049*
Alive	193 (38.7%)	212 (42.5%)	
Dead	56 (11.2%)	38 (7.6%)	

p < 0.05 is considered as statistically significant.
PCa, prostate cancer; BPH, benign prostate hyperplasia; OS, overall survival; DSS, disease-specific survival; PFI, progression-free interval; PSA, prostate-specific antigen; PR, partial response; CR, complete response; PD, progressive disease; SD, stable disease.
**p: chi-square test.*
***p: Fisher's test.*
****p: Wilcoxon rank-sum test.*

expression of AFU implied a worse outcome. Compared with those of the early-stage group (pT1 and pT2 stages), the levels of AFU were markedly decreased in the advanced stage group (pT3 and pT4 stages). Furthermore, the patients with lymph node metastases had lower expression of AFU than those without lymph node metastases. The expression of AFU in prostate tissue was assessed using IHC. Similarly, it indicated the AFU expression was lower in high-grade PCa in contrast to low-grade PCa.

All the above analyses were conducted for AFU protein; next, the mRNA level of AFU was further evaluated based on TCGA database. Previous studies report AFU containing two subtypes, AFU1 and AFU2, which are encoded by genes *FUCA1* and *FUCA2*, respectively (5, 19, 20). Therefore, the relationships between *FUCA1*/*FUCA2* expression and PCa patients' clinicopathological characteristics were further assessed based on TCGA database. It has long been known that the incidence of malignant disease in human is rapidly increased with aging, while our result suggested that the *FUCA1* level was decreased with the increase of age. Beyond that, we found significant correlations among *FUCA1*/*FUCA2* expression and pathological grade, pathological stage, postoperative residual tumor numbers, and primary therapeutic effect. Although *FUCA1* and *FUCA2* both showed prognostic value for patients' PFI, the diagnostic performance of *FUCA1* is more accurate and stable than that of *FUCA2*. All of these results imply that *FUCA1*/*FUCA2* may be acting in a tumor-suppressive role, and

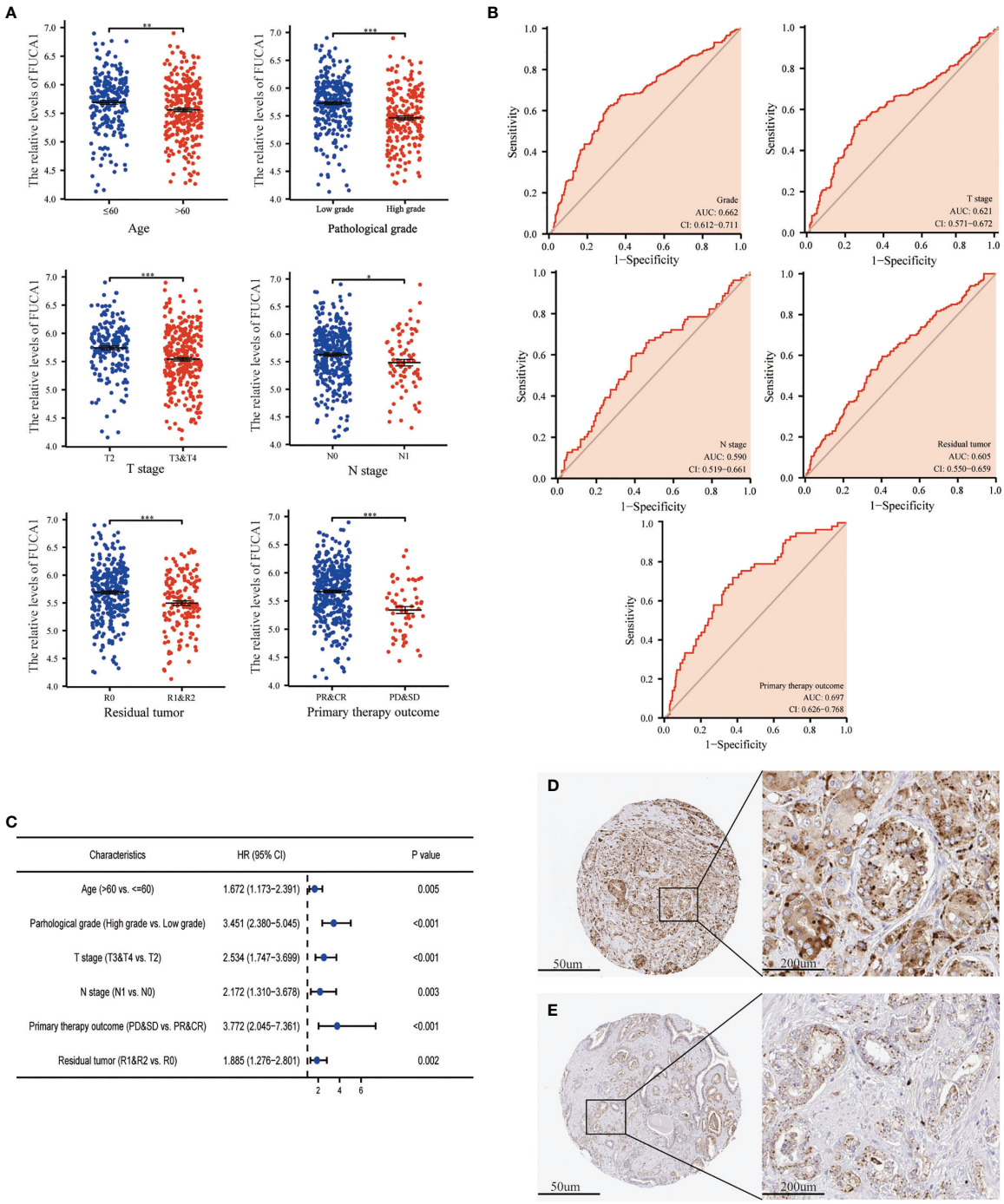

FIGURE 3 | The expression of *FUCA1* in PCa subgroups. **(A)** *FUCA1* mRNA expression in different PCa subgroups. **(B)** The diagnostic value of *FUCA1* for different PCa clinicopathological parameters. **(C)** Logical regression analysis of clinicopathological variables' effects on low *FUCA1* expression. IHC analysis of *FUCA1* in low- **(D)** and high-grade **(E)** PCa tissue. CR, complete response; PR, partial response; SD, stable disease; PD, progressive disease. $^{*}p < 0.05$, $^{**}p < 0.01$, $^{***}p < 0.01$. PCa, prostate cancer; IHC, immunohistochemistry.

lower expression of *FUCA1*/*FUCA2* prognosticates worse pathological results, less therapeutic effect, and shorter PFI. This finding is consistent with many previous studies, which further validate the reliability of our conclusion (12, 13, 21–23).

The KEGG analysis indicated the biological function of *FUCA1* and *FUCA2* mainly involved glycosylation, especially glycoprotein. Glycosylation plays an important role in the initiation and progression of human disease including

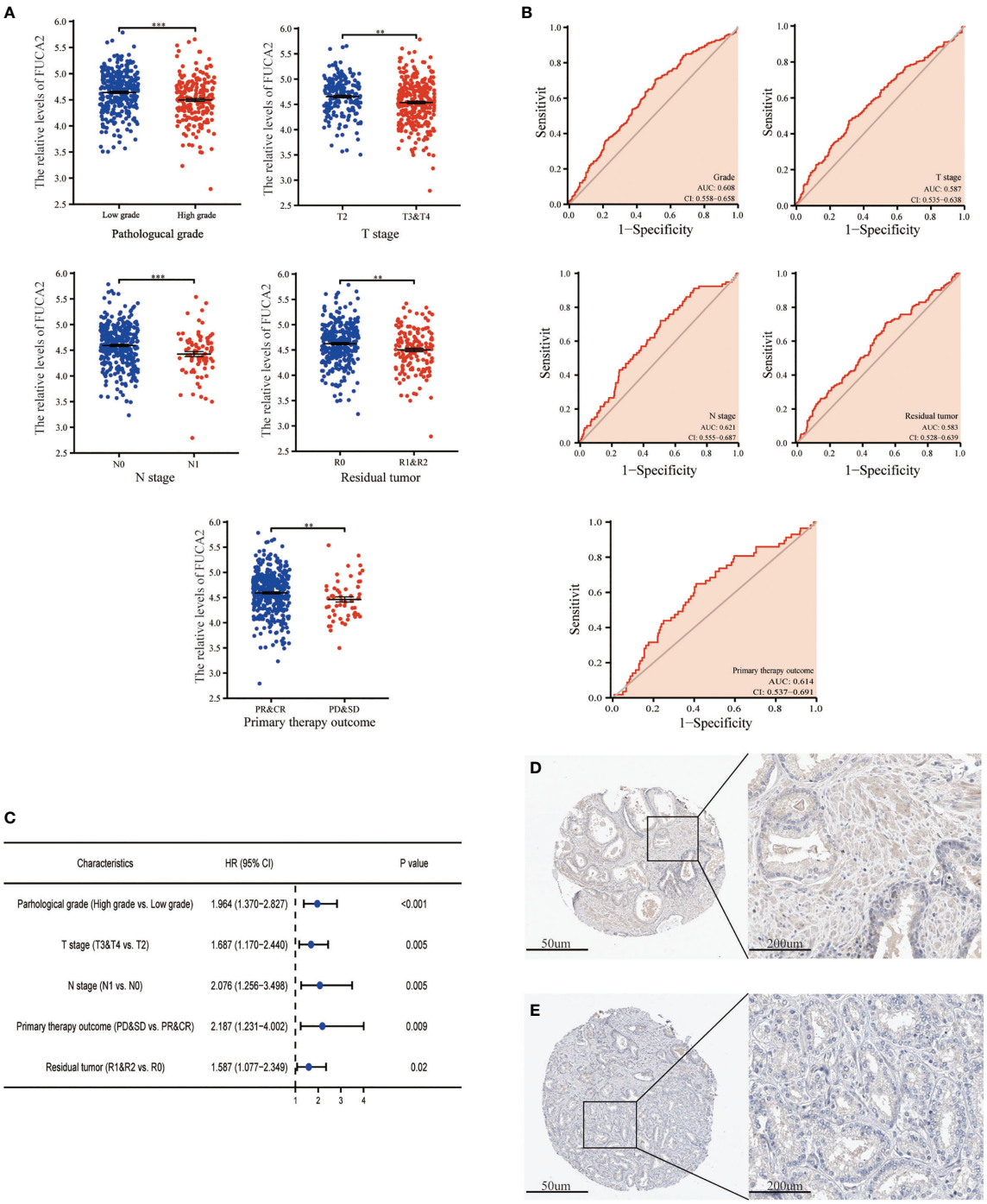

FIGURE 4 | The expression of *FUCA2* in PCa subgroups. **(A)** *FUCA2* mRNA expression in different PCa subgroups. **(B)** The diagnostic value of *FUCA2* for different PCa clinicopathological parameters. **(C)** Logical regression analysis of clinicopathological variables' effects on low *FUCA2* expression. IHC analysis of *FUCA2* in low- **(D)** and high-grade **(E)** PCa tissue. CR, complete response; PR, partial response; SD, stable disease; PD, progressive disease. $^{**}p < 0.01$, $^{***}p < 0.01$. PCa, prostate cancer; IHC, immunohistochemistry.

infection, inflammation, metabolism, and, of course, tumors (24–26). Some well-known tumor markers such as haptoglobin and CA 19-9 are fucosylated glycoproteins (27, 28). Apart from this, several key signal proteins, like integrin, E-cadherin, TGF-β receptors, and epidermal growth factor receptor (EGFR), are glycoproteins as well, which indicates that modification of glycosylation has a complex and crucial effect on their functions (29–32). Remarkably, many studies have revealed

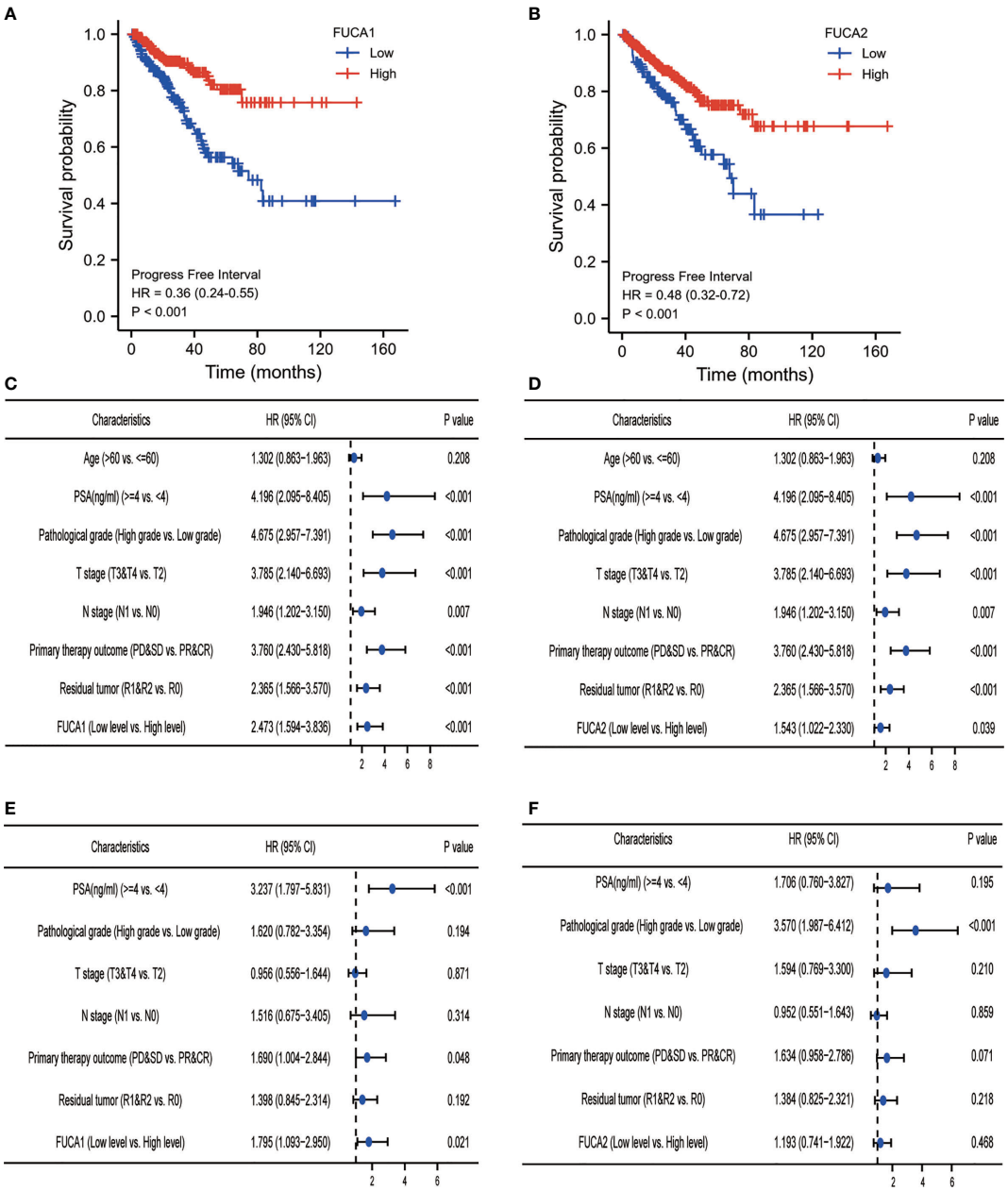

FIGURE 5 | Survival analysis of PCa patients with different *FUCA1*/*FUCA2* expression based on TCGA databases. The Kaplan–Meier curve analysis based on *FUCA1* **(A)** and *FUCA2* **(B)** expression effect for PFI. Univariate Cox regression analysis of *FUCA1* **(C)** and *FUCA2* **(D)** expression effect for PFI. Multivariate Cox regression analysis of *FUCA1* **(E)** and *FUCA2* **(F)** expression effect for PFI. PCa, prostate cancer; TCGA, The Cancer Genome Atlas; PFI, progress-free interval.

that abnormal glycosylation can lead to tumor onset and progression (33–36). AFU encoded by *FUCA1* or *FUCA2* can remove the terminal fucose residues from glycans and prevents aberrant accumulation of fucose-containing glycans (5, 26). Thus, the lack of AFU, which is responsible for the degradation of glycans, causes the overexpression of glycans and may prompt tumor initiation and development.

In this study, we first showed that AFU could be an effective diagnostic marker for PCa patients who had "gray-zone PSA". In addition, our study demonstrated that low expression of AFU portends a worse prognosis of PCa. However, some limitations that existed in the present study deserve special attention. First, our study is retrospective research, which only allows for speculation based on the available data. Second, in consideration of the longer survival time of PCa patients, the differences in survival among different subgroups are difficult to be analyzed. Third, by bioinformatics analysis, we speculated that AFU suppressed the progression of PCa *via*

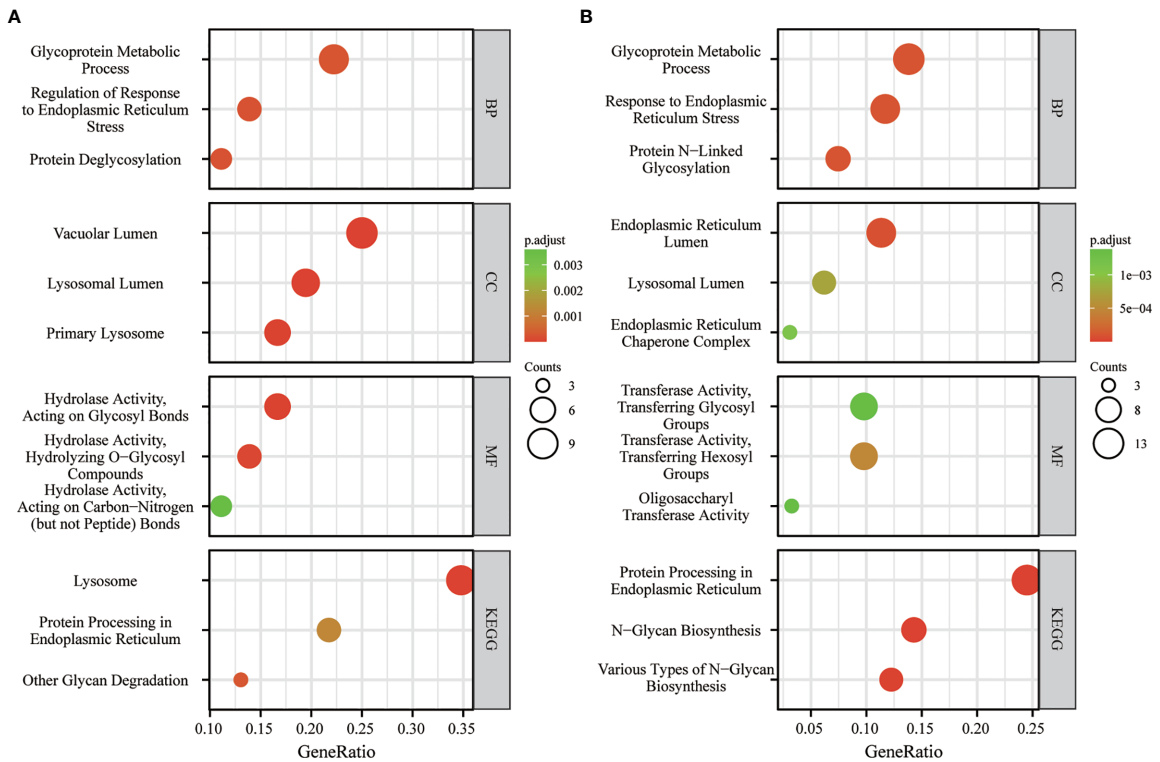

FIGURE 6 | The KEGG analysis of *FUCA1* **(A)** and *FUCA2* **(B)**. KEGG, The Kyoto Encyclopedia of Genes and Genomes.

regulation of glycosylation metabolism, which awaited further experimental validation.

CONCLUSION

AFU can effectively distinguish PCa from patients with gray-zone PSA levels; and lower AFU expression predicates advanced pathological results, poor therapeutic effect, more postoperative residual tumor numbers, and worse prognosis of PCa patients.

DATA AVAILABILITY STATEMENT

The original contributions presented in the study are included in the article/**Supplementary Material**. Further inquiries can be directed to the corresponding authors.

ETHICS STATEMENT

The studies involving human participants were reviewed and approved by the Research Ethics Committee of Qilu Hospital of Shandong University. The patients/participants provided their written informed consent to participate in this study.

AUTHOR CONTRIBUTIONS

Study design: GC and ZX. Data collection: CZ, JL, DL, and ZX. Writing: CZ, GX, and GC. Editing: CZ, FC, SW, and DH. All authors contributed to the article and approved the submitted version.

FUNDING

This work was supported by grants from the National Science Foundation of Shanghai (No. 18ZR1405800) and the Project for Key Medical Specialty Construction in Jinshan District (6th Period, Type A) (No. JSZK2019A03) to GC.

ACKNOWLEDGMENTS

I am thankful to my fiancee for her help and tolerance and I hope this work can act as a witness for our wedding.

SUPPLEMENTARY MATERIAL

The Supplementary Material for this article can be found online at: https://www.frontiersin.org/articles/10.3389/fonc.2021.742354/full#supplementary-material

REFERENCES

1. Deng ZH, Yu GS, Deng KL, Feng ZH, Huang Q, Pan B, et al. Hsa_circ_0088233 Alleviates Proliferation, Migration, and Invasion of Prostate Cancer by Targeting hsa-miR-185-3p. *Front Cell Dev Biol* (2020) 8:528155. doi: 10.3389/fcell.2020.528155
2. Sung H, Ferlay J, Siegel RL, Laversanne M, Soerjomataram I, Jemal A, et al. Global Cancer Statistics 2020: GLOBOCAN Estimates of Incidence and Mortality Worldwide for 36 Cancers in 185 Countries. *CA Cancer J Clin* (2021) 71(3):209–49. doi: 10.3322/caac.21660
3. Flores-Fraile MC, Padilla-Fernandez BY, Valverde-Martinez S, Marquez-Sanchez M, Garcia-Cenador MB, Lorenzo-Gomez MF, et al. The Association Between Prostate-Specific Antigen Velocity (PSAV), Value and Acceleration, and of the Free PSA/Total PSA Index or Ratio, With Prostate Conditions. *J Clin Med* (2020) 9(11):3400. doi: 10.3390/jcm9113400
4. Ishida S, Kayamori K, Sakamoto K, Yukimori A, Kugimoto T, Harada H, et al. Alpha-L-Fucosidase-1 Is a Diagnostic Marker That Distinguishes Mucoepidermoid Carcinoma From Squamous Cell Carcinoma. *Pathol Int* (2019) 69(2):76–85. doi: 10.1111/pin.12764
5. Zhang M, Wang L, Zhang H, Cong J, Zhang L. Serum Alpha-L-Fucosidase Activities are Significantly Increased in Patients With Preeclampsia. *Prog Mol Biol Transl Sci* (2019) 162:349–62. doi: 10.1016/bs.pmbts.2018.12.008
6. Herrera H, Dilday T, Uber A, Scott D, Zambrano JN, Wang M, et al. Core-Fucosylated Tetra-Antennary N-Glycan Containing A Single N-Acetyllactosamine Branch Is Associated With Poor Survival Outcome in Breast Cancer. *Int J Mol Sci* (2019) 20(10):2528. doi: 10.3390/ijms20102528
7. Listinsky JJ, Listinsky CM, Alapati V, Siegal GP. Cell Surface Fucose Ablation as a Therapeutic Strategy for Malignant Neoplasms. *Adv Anat Pathol* (2001) 8 (6):330–7. doi: 10.1097/00125480-200111000-00003
8. Huang W, Li X. [Significance of Fucose Expression in Lung Carcinoma and Their Brain Metastases]. *Zhonghua Bing Li Xue Za Zhi* (2000) 29(4):259–62.
9. Listinsky JJ, Siegal GP, Listinsky CM. The Emerging Importance of Alpha-L-Fucose in Human Breast Cancer: A Review. *Am J Transl Res* (2011) 3(4):292–322.
10. Fernandez-Rodriguez J, Paez de la Cadena M, Martinez-Zorzano VS, Rodriguez-Berrocal FJ. Fucose Levels in Sera and in Tumours of Colorectal Adenocarcinoma Patients. *Cancer Lett* (1997) 121(2):147–53. doi: 10.1016/s0304-3835(97)00343-1
11. Ayude D, Fernandez-Rodriguez J, Rodriguez-Berrocal FJ, Martinez-Zorzano VS, de Carlos A, Gil E, et al. Value of the Serum Alpha-L-Fucosidase Activity in the Diagnosis of Colorectal Cancer. *Oncology* (2000) 59(4):310–6. doi: 10.1159/000012188
12. Otero-Estevez O, Martinez-Fernandez M, Vazquez-Iglesias L, Paez de la Cadena M, Rodriguez-Berrocal FJ, Martinez-Zorzano VS. Decreased Expression of Alpha-L-Fucosidase Gene FUCA1 in Human Colorectal Tumors. *Int J Mol Sci* (2013) 14(8):16986–98. doi: 10.3390/ijms140816986
13. Ezawa I, Sawai Y, Kawase T, Okabe A, Tsutsumi S, Ichikawa H, et al. Novel P53 Target Gene FUCA1 Encodes a Fucosidase and Regulates Growth and Survival of Cancer Cells. *Cancer Sci* (2016) 107(6):734–45. doi: 10.1111/cas.12933
14. Shuang Z, Mao Y, Lin G, Wang J, Huang X, Chen J, et al. Alpha-L-Fucosidase Serves as a Prognostic Indicator for Intrahepatic Cholangiocarcinoma and Inhibits Its Invasion Capacity. *BioMed Res Int* (2018) 2018:8182575. doi: 10.1155/2018/8182575
15. Mazzone E, Dell'Oglio P, Rosiello G, Puliatti S, Brook N, Turri F, et al. Technical Refinements in Superextended Robot-Assisted Radical Prostatectomy for Locally Advanced Prostate Cancer Patients at Multiparametric Magnetic Resonance Imaging. *Eur Urol* (2021) 80(1):104–12. doi: 10.1016/j.eururo.2020.09.009
16. Wittekind C, Compton CC, Greene FL, Sobin LH. TNM Residual Tumor Classification Revisited. *Cancer* (2002) 94(9):2511–6. doi: 10.1002/cncr.10492
17. Inahara M, Suzuki H, Kojima S, Komiya A, Fukasawa S, Imamoto T, et al. Improved Prostate Cancer Detection Using Systematic 14-Core Biopsy for Large Prostate Glands With Normal Digital Rectal Examination Findings. *Urology* (2006) 68(4):815–9. doi: 10.1016/j.urology.2006.05.010
18. Liu J, Wang ZQ, Li M, Zhou MY, Yu YF, Zhan WW. Establishment of Two New Predictive Models for Prostate Cancer to Determine Whether to Require Prostate Biopsy When the PSA Level Is in the Diagnostic Gray Zone (4-10 Ng Ml(-1)). *Asian J Androl* (2020) 22(2):213–6. doi: 10.4103/aja.aja_46_19
19. Darby JK, Willems PJ, Nakashima P, Johnsen J, Ferrell RE, Wijsman EM, et al. Restriction Analysis of the Structural Alpha-L-Fucosidase Gene and Its Linkage to Fucosidosis. *Am J Hum Genet* (1988) 43(5):749–55.
20. Eiberg H, Mohr J, Nielsen LS. Linkage of Plasma Alpha-L-Fucosidase (FUCA2) and the Plasminogen (PLG) System. *Clin Genet* (1984) 26(1):23–9. doi: 10.1111/j.1399-0004.1984.tb00782.x
21. Milde-Langosch K, Karn T, Schmidt M, zu Eulenburg X, Oliveira-Ferrer L, Wirtz RM, et al. Prognostic Relevance of Glycosylation-Associated Genes in Breast Cancer. *Breast Cancer Res Treat* (2014) 145(2):295–305. doi: 10.1007/s10549-014-2949-z
22. Wang Y, Yan K, Lin J, Li J, Bi J. Macrophage M2 Co-Expression Factors Correlate With the Immune Microenvironment and Predict Outcome of Renal Clear Cell Carcinoma. *Front Genet* (2021) 12:615655. doi: 10.3389/fgene.2021.615655
23. Vecchio G, Parascandolo A, Allocca C, Ugolini C, Basolo F, Moracci M, et al. Human a-L-Fucosidase-1 Attenuates the Invasive Properties of Thyroid Cancer. *Oncotarget* (2017) 8(16):27075–92. doi: 10.18632/oncotarget.15635
24. Li J, Hsu HC, Mountz JD, Allen JG. Unmasking Fucosylation: From Cell Adhesion to Immune System Regulation and Diseases. *Cell Chem Biol* (2018) 25(5):499–512. doi: 10.1016/j.chembiol.2018.02.005
25. Lan Y, Hao C, Zeng X, He Y, Zeng P, Guo Z, et al. Serum Glycoprotein-Derived N- and O-Linked Glycans as Cancer Biomarkers. *Am J Cancer Res* (2016) 6(11):2390–415.
26. Darby JK, Johnsen J, Nakashima P, Willems PJ, O'Brien JS, Fowler ML, et al. Pvu II RFLP at the Human Chromosome 1 Alpha-L-Fucosidase Gene Locus (Fuca1). *Nucleic Acids Res* (1986) 14(23):9543. doi: 10.1093/nar/14.23.9543
27. Miyoshi E, Moriwaki K, Nakagawa T. Biological Function of Fucosylation in Cancer Biology. *J Biochem* (2008) 143(6):725–9. doi: 10.1093/jb/mvn011
28. Takeda Y, Shinzaki S, Okudo K, Moriwaki K, Murata K, Miyoshi E. Fucosylated Haptoglobin Is a Novel Type of Cancer Biomarker Linked to the Prognosis After an Operation in Colorectal Cancer. *Cancer* (2012) 118 (12):3036–43. doi: 10.1002/cncr.26490
29. Hu P, Shi B, Geng F, Zhang C, Wu W, Wu XZ. E-Cadherin Core Fucosylation Regulates Nuclear Beta-Catenin Accumulation in Lung Cancer Cells. *Glycoconj J* (2008) 25(9):843–50. doi: 10.1007/s10719-008-9144-6
30. Zhao Y, Itoh S, Wang X, Isaji T, Miyoshi E, Kariya Y, et al. Deletion of Core Fucosylation on Alpha3beta1 Integrin Down-Regulates Its Functions. *J Biol Chem* (2006) 281(50):38343–50. doi: 10.1074/jbc.M608764200
31. Lin H, Wang D, Wu T, Dong C, Shen N, Sun Y, et al. Blocking Core Fucosylation of TGF-Beta1 Receptors Downregulates Their Functions and Attenuates the Epithelial-Mesenchymal Transition of Renal Tubular Cells. *Am J Physiol Renal Physiol* (2011) 300(4):F1017–25. doi: 10.1152/ajprenal.00426.2010
32. Wang X, Gu J, Ihara H, Miyoshi E, Honke K, Taniguchi N. Core Fucosylation Regulates Epidermal Growth Factor Receptor-Mediated Intracellular Signaling. *J Biol Chem* (2006) 281(5):2572–7. doi: 10.1074/jbc.M510893200
33. Brockhausen I. Mucin-Type O-Glycans in Human Colon and Breast Cancer: Glycodynamics and Functions. *EMBO Rep* (2006) 7(6):599–604. doi: 10.1038/sj.embor.7400705
34. Dube DH, Bertozzi CR. Glycans in Cancer and Inflammation–Potential for Therapeutics and Diagnostics. *Nat Rev Drug Discov* (2005) 4(6):477–88. doi: 10.1038/nrd1751
35. Lau KS, Dennis JW. N-Glycans in Cancer Progression. *Glycobiology* (2008) 18 (10):750–60. doi: 10.1093/glycob/cwn071
36. Pinho SS, Reis CA. Glycosylation in Cancer: Mechanisms and Clinical Implications. *Nat Rev Cancer* (2015) 15(9):540–55. doi: 10.1038/nrc3982

Conflict of Interest: The authors declare that the research was conducted in the absence of any commercial or financial relationships that could be construed as a potential conflict of interest.

Publisher's Note: All claims expressed in this article are solely those of the authors and do not necessarily represent those of their affiliated organizations, or those of the publisher, the editors and the reviewers. Any product that may be evaluated in this article, or claim that may be made by its manufacturer, is not guaranteed or endorsed by the publisher.

Copyright © 2021 Zhang, Liu, Chao, Wang, Li, Han, Xu, Xu and Chen. This is an open-access article distributed under the terms of the Creative Commons Attribution License (CC BY). The use, distribution or reproduction in other forums is permitted, provided the original author(s) and the copyright owner(s) are credited and that the original publication in this journal is cited, in accordance with accepted academic practice. No use, distribution or reproduction is permitted which does not comply with these terms.

frontiers in Oncology

ORIGINAL RESEARCH
published: 24 November 2021
doi: 10.3389/fonc.2021.777684

A Multivariate Diagnostic Model Based on Urinary EpCAM-CD9-Positive Extracellular Vesicles for Prostate Cancer Diagnosis

Yibei Dai[1†], Yiyun Wang[2†], Ying Cao[1], Pan Yu[1], Lingyu Zhang[1], Zhenping Liu[3], Ying Ping[1], Danhua Wang[1], Gong Zhang[1], Yiwen Sang[1], Xuchu Wang[1] and Zhihua Tao[1*]*

[1] Department of Laboratory Medicine, The Second Affiliated Hospital of Zhejiang University School of Medicine, Hangzhou, China, [2] Zhejiang University School of Medicine, Hangzhou, China, [3] Department of Laboratory Medicine, The First People's Hospital of Yuhang District, Hangzhou, China

OPEN ACCESS

Edited by:
Antonina Mitrofanova, Rutgers, The State University of New Jersey, United States

Reviewed by:
Bilal A. Siddiqui, University of Texas MD Anderson Cancer Center, United States
Mariana Chantre Justino, Rio de Janeiro State University, Brazil

***Correspondence:**
Zhihua Tao
zrtzh@zju.edu.cn
Xuchu Wang
wangxc@zju.edu.cn

[†]These authors have contributed equally to this work

Specialty section:
This article was submitted to Genitourinary Oncology, a section of the journal Frontiers in Oncology

Received: *15 September 2021*
Accepted: *29 October 2021*
Published: *24 November 2021*

Citation:
Dai Y, Wang Y, Cao Y, Yu P, Zhang L, Liu Z, Ping Y, Wang D, Zhang G, Sang Y, Wang X and Tao Z (2021) A Multivariate Diagnostic Model Based on Urinary EpCAM-CD9-Positive Extracellular Vesicles for Prostate Cancer Diagnosis. Front. Oncol. 11:777684. doi: 10.3389/fonc.2021.777684

Introduction: Prostate cancer (PCa) is one of the most frequently diagnosed cancers and the leading cause of cancer death in males worldwide. Although prostate-specific antigen (PSA) screening has considerably improved the detection of PCa, it has also led to a dramatic increase in overdiagnosing indolent disease due to its low specificity. This study aimed to develop and validate a multivariate diagnostic model based on the urinary epithelial cell adhesion molecule (EpCAM)-CD9–positive extracellular vesicles (EVs) ($uEV_{EpCAM\text{-}CD9}$) to improve the diagnosis of PCa.

Methods: We investigated the performance of $uEV_{EpCAM\text{-}CD9}$ from urine samples of 193 participants (112 PCa patients, 55 benign prostatic hyperplasia patients, and 26 healthy donors) to diagnose PCa using our laboratory-developed chemiluminescent immunoassay. We applied machine learning to training sets and subsequently evaluated the multivariate diagnostic model based on $uEV_{EpCAM\text{-}CD9}$ in validation sets.

Results: Results showed that $uEV_{EpCAM\text{-}CD9}$ was able to distinguish PCa from controls, and a significant decrease of $uEV_{EpCAM\text{-}CD9}$ was observed after prostatectomy. We further used a training set (N = 116) and constructed an exclusive multivariate diagnostic model based on $uEV_{EpCAM\text{-}CD9}$, PSA, and other clinical parameters, which showed an enhanced diagnostic sensitivity and specificity and performed excellently to diagnose PCa [area under the curve (AUC) = 0.952, $P < 0.0001$]. When applied to a validation test (N = 77), the model achieved an AUC of 0.947 ($P < 0.0001$). Moreover, this diagnostic model also exhibited a superior diagnostic performance (AUC = 0.917, $P < 0.0001$) over PSA (AUC = 0.712, $P = 0.0018$) at the PSA gray zone.

Conclusions: The multivariate model based on $uEV_{EpCAM\text{-}CD9}$ achieved a notable diagnostic performance to diagnose PCa. In the future, this model may potentially be used to better select patients for prostate transrectal ultrasound (TRUS) biopsy.

Keywords: extracellular vesicle, EpCAM, chemiluminescent immunoassay, prostate cancer, multivariate diagnostic model

INTRODUCTION

Prostate cancer (PCa) is one of the most frequently diagnosed cancers and the leading cause of cancer death in males worldwide (1). Despite the widespread use of prostate-specific antigen (PSA) as a noninvasive screening tool for PCa, the low specificity of PSA has led to an increase in either overdiagnosis or unnecessary biopsies, especially when its value is within the PSA gray zone (4–10 ng/ml) (2, 3). Thus, it is urgently needed to explore new biomarkers for more accurate PCa diagnosis.

Urine is an ideal source of PCa biomarkers because the samples can be collected noninvasively in large amounts, and several urinary markers have been reported such as prostate cancer antigen-3 *(PCA3)*, transmembrane protease serine-2 *(TMPRSS2)*, and glutathione S-transferase P *(GSTP1)* gene (4–7). Recently, urinary extracellular vesicles (uEVs) have sparked interest as potential biomarkers (8, 9). uEVs are low-density membrane vesicles containing lipids, proteins, DNA, mRNAs, and microRNAs (10). A reproducible method for uEV isolation has been described by Pisitkun et al. (11) in 2004 and has been widely adopted for uEV analysis. Previous proteomic analysis of uEVs has revealed varieties of cancer-specific proteins in their cargoes (12, 13). However, the question remained whether there is a specific protein in uEVs that could provide diagnostic information for PCa and also be easily detected.

Epithelial cell adhesion molecule (EpCAM) is a transmembrane glycoprotein that plays an important role in Ca2+-independent hemophilic cell-to-cell adhesion, cell signaling, migration, proliferation, and differentiation of cancer cells (14, 15). It has thus gained considerable attraction as an appealing candidate biomarker for cancer diagnosis due to its strong expression in various carcinomas and their metastases compared with normal epithelia (16, 17). Recently, EpCAM on tumor-derived EV membrane was also employed as a promising tumor surface marker, while the tetraspanin family of proteins, such as CD63, CD9, and CD81, was mainly used as EV universal markers (18, 19). The use of these biomarkers to identify EVs from bodily fluids has garnered much interest as a non-invasive liquid biopsy for cancer.

Accordingly, we herein aimed to develop and validate a multivariate diagnostic model based on the urinary EpCAM-CD9-positive EVs ($uEV_{EpCAM\text{-}CD9}$) to improve the diagnosis of PCa. We first investigated the performance of $uEV_{EpCAM\text{-}CD9}$ for the diagnosis of PCa using a newly laboratory-developed chemiluminescent immunoassay (CLIA) (**Figure 1A**). Briefly, $uEV_{EpCAM\text{-}CD9}$ diffused in urine is bound with acridinium ester (ACE)-labeled anti-CD9 antibodies and captured by magnetic bead-labeled anti-EpCAM antibodies, followed by a thorough isolation under an external magnetic field. Consequently, the concentrations of EpCAM-CD9-positive EVs ($EV_{EpCAM\text{-}CD9}$) can be quantitatively determined by measuring the chemiluminescent signals. Results indicated that $EV_{EpCAM\text{-}CD9}$ from the culture supernatant of PCa cell lines were significantly elevated under the simulated tumor microenvironment. Moreover, preliminary results showed that $uEV_{EpCAM\text{-}CD9}$ could distinguish patients with PCa from control sets, indicating that $uEV_{EpCAM\text{-}CD9}$ may be a potential biomarker for PCa diagnosis. We then applied machine learning to training sets and subsequently evaluated the multivariate diagnostic model based on $uEV_{EpCAM\text{-}CD9}$ in validation sets.

MATERIALS AND METHODS

Cell Lines and Culture

Two human PCa cell lines (PC3 and LNCaP) and an immortalized prostate epithelial cell line (RWPE-1) were obtained from the American Type Culture Collection (Manassas, VA, USA). All cell lines were cultured in RPMI 1640 medium (Gibco Invitrogen, Carlsbad, CA, USA) supplemented with 10% fetal bovine serum (FBS; Thermo Fisher Scientific, MA, USA), 100 U/ml penicillin, and 100 μg/ml streptomycin in an incubator with 5% CO_2 at 37°C.

Urine Collection

Urine samples from 193 participants [112 PCa patients, 55 benign prostatic hyperplasia (BPH) patients, and 26 healthy donors (HDs)] were collected in the Second Affiliated Hospital of Zhejiang University School of Medicine. Approval was obtained from the Second Affiliated Hospital of Zhejiang University School of Medicine Ethical Committee before initiating the study. Detailed information on the patients is summarized in **Supplementary Table S1**. All methods were performed in accordance with the relevant guidelines and regulations. All the patients met the following inclusion criteria: (1) undergoing prostate biopsy for the first time, (2) three-dimensional size of the prostate available *via* transabdominal ultrasonography before biopsy, (3) blood tests performed within 1 week before biopsy, (4) complete clinical and pathological data available, (5) absence of acute prostatitis or systemic inflammatory disease, (6) absence of urinary tract infection, (7) no history of prostate surgery, (8) no history of

Abbreviations: EpCAM, epithelial cell adhesion molecule; PCa, prostate cancer; PSA, prostate-specific antigen; EVs, extracellular vesicles; $uEV_{EpCAM\text{-}CD9}$, urinary EpCAM-CD9-positive extracellular vesicles; AUC, area under the curve; TRUS, transrectal ultrasound; *PCA3*, prostate cancer antigen-3; *TMPRSS2*, transmembrane protease serine-2; *GSTP1*, glutathione S-transferase; uEVs, urinary extracellular vesicles; CLIA, chemiluminescent immunoassay; ACE, acridinium ester; $EV_{EpCAM\text{-}CD9}$, EpCAM-CD9-positive extracellular vesicles; FBS, fetal bovine serum; BPH, benign prostatic hyperplasia; HD, healthy donor; PBS, phosphate-buffered saline; TEM, transmission electron microscope; NTA, nanoparticle tracking analysis; RIPA, radioimmunoprecipitation assay; SDS-PAGE, sodium dodecyl sulfate-polyacrylamide gel electrophoresis; PVDF, polyvinylidene difluoride; TBST, Tris-buffered saline with Tween-20; WB, western blot; HRP, horseradish peroxidase; $Density_{EpCAM\text{-}CD9}$, EpCAM-CD9 protein density; BCA, bicinchoninic acid; SD, standard deviation; IQR, interquartile range; ROC, receiver operating characteristic; DCA, decision curve analysis; RCU, relative chemiluminescent unit; LOD, limit of detection; intra-CV, intra-assay coefficient of variation; inter-CV, inter-assay coefficient of variation; CI, confidence interval; OR, odds ratio; fPSA, free prostate-specific antigen; f/T PSA, free/total prostate-specific antigen; PV, prostate volume; PSAD, prostate-specific antigen density; BMI, body mass index; EMT, epithelial–mesenchymal transition; CRPC, castration-resistant prostate cancer.

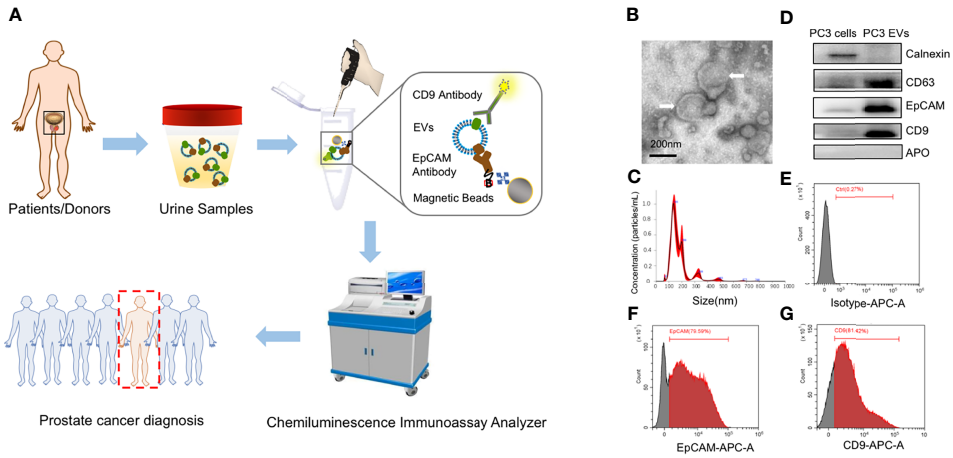

FIGURE 1 | The scheme of workflow for urinary EpCAM-CD9-positive extracellular vesicle ($uEV_{EpCAM-CD9}$) detection. **(A)** EpCAM-CD9-positive EVs diffused in urine are bound with acridinium ester (ACE)-labeled anti-CD9 antibodies and captured by magnetic microbeads labeled anti-EpCAM antibodies. After incubation for 60 min, $uEV_{EpCAM-CD9}$ binding with magnetic microbeads can be easily isolated under an external magnetic field and quantitatively analyzed by a chemiluminescent immunoassay analyzer to diagnose prostate cancer. **(B)** TEM images of EVs isolated by ultracentrifugation (white arrow). **(C)** EVs are characterized by NTA. **(D)** The expression of CD63, CD9, EpCAM, calnexin, and APO in PC3 cell lysates and the EV fraction from PC3 by WB analysis. **(E–G)** Flow cytometry assay identified that approximately 80% of EVs released by PC3 carried EpCAM and CD9. EpCAM, epithelial cell adhesion molecule; uEVEpCAM-CD9, urinary EpCAM-CD9-positive extracellular vesicles; EVs, extracellular vesicles; ACE, acridinium ester; TEM, transmission electron microscope; NTA, nanoparticle tracking analysis; WB, western blot.

5-alpha reductase inhibitor use, and (9) no anti-inflammatory drug use within 2 weeks before blood tests. Initial voided urine (5–10 ml) was prospectively collected from patients at the time of day most convenient to the person before prostate biopsy. Matched urine samples were collected from PCa patients prior to (n = 10) and a week after local treatment by radical prostatectomy (n = 10).

Extracellular Vesicle Isolation From Cell Culture Medium and Urine

EVs were isolated from cell culture medium by ultracentrifugation as previously described (20). Briefly, when 70%–80% confluency was reached, cells were washed twice with phosphate-buffered saline (PBS; pH7.0) and then incubated for 48 h in FBS-free medium. Cell culture medium was collected and subjected to consecutive centrifugation steps (300 × g for 10 min and 2,000 × g for 20 min) to remove dead cells and cellular debris. The supernatant was vacuum filtered using a 10-kDa centrifugal filter (Merck Millipore, Darmstadt, Germany), and EV concentrates were ultracentrifuged at 100,000 × g for 70 min at 4°C (Type 70 Ti Fixed-angle Titanium Rotor, k factor = 157.4) (Optima^{TM} XP ultracentrifuge; Beckman Coulter, Indianapolis, IN, USA). Pellets were washed with PBS followed by ultracentrifugation at the same speed and time. The supernatant was discarded, and the resulting EV pellets were suspended in PBS and stored at -80°C.

In order to obtain uEVs, urine samples from patients with PCa, BPH and HDs were centrifuged at 3,000 × g for 20 min at 4°C to remove debris and then ultracentrifuged at 200,000 × g for 2 h at 4°C. The supernatant was removed, and the uEV pellets were resuspended in PBS and stored at -80°C.

Transmission Electron Microscopy

Transmission electron microscope (TEM) was used to investigate the morphology of the EVs isolated by ultracentrifugation. Briefly, EVs at an optimal concentration were first placed on 400 mesh carbon/formvar-coated grids and allowed to be absorbed on formvar for a minimum of 10 min. Next, the grids (membrane side down) were transferred to a 50-µl drop of 2.5% glutaraldehyde for 5 min, after which they were transferred to a 100-µl drop of distilled water and were left to stand for 2 min. This process was repeated nine times for a total of 10 water washes. Then, the sample was loaded on the grid and stained by 4% uranyl acetate for 10 min and 1% methylcellulose for 5 min. The remaining water was removed using filter paper. Finally, the samples were viewed using a Tecnai Bio Twin TEM (FEI, Hillsboro, OR, USA), and images were obtained using an AMT CCD camera (Advanced Microscopy Techniques, Woburn, MA, USA).

Nanoparticle Tracking Analysis

The concentration and the size distribution of EVs were analyzed by nanoparticle tracking analysis (NTA) using a ZetaView instrument (Particle Metrix, Inning am Ammersee, Germany) and the NanoSight LM10 microscope (NanoSight Ltd., Amesbury, UK) configured with a 405-nm laser. Videos were collected and analyzed using the NTA software (version 2.3) with the default setting of the minimal expected particle size, minimum track length, and blur. Each EV sample was vortexed and diluted with particle-free PBS to obtain the recommended 25–100 particles/frame of the NTA system. Five videos of typically 60-s duration were recorded to generate replicate histograms that were averaged.

Western Blot Analysis

Cells and EVs were lysed in radioimmunoprecipitation assay (RIPA) Lysis Buffer (Beyotime Biotechnology, Shanghai, China) for 30 min on ice, and the protein concentration was measured by the Enhanced BCA Protein Assay Kit (Beyotime Biotechnology, Shanghai, China). And then, the lysates were mixed with loading buffer and heated to 100°C for 10 min. Subsequently, the samples were electrophoretically separated on an 8% sodium dodecyl sulfate–polyacrylamide gel electrophoresis (SDS-PAGE) and electro-transferred onto polyvinylidene difluoride (PVDF) membranes (Millipore, Carlsbad, CA). After blocking for 2 h at 25°C in Tris-buffered saline with 0.05% Tween-20 (TBST) and 5% non-fat dry milk, the membranes were incubated overnight at 4°C with the primary antibodies in TBST containing 5% BSA. The following antibodies were used for Western blot (WB) analysis, including anti-Alix antibody (1:1,000; ab88388; Abcam, Cambridge, MA, USA), anti-Calnexin antibody (1:200; ab238078; Abcam, Cambridge, MA, USA), anti-CD63 antibody (1:300; ab8219; Abcam, Cambridge, MA, USA), anti-EpCAM antibody (1:200; ab218448; Abcam, Cambridge, MA, USA), anti-CD9 antibody (1:300; sc-13118; Santa-Cruz Biotechnology, Santa Cruz, CA, USA), anti-beta Actin antibody (1:5,000; ab6276; Abcam, Cambridge, MA, USA), and anti-Apo antibody (1:500; ab66379; Abcam, Cambridge, MA, USA). Thereafter, the membrane was washed and immersed into horseradish peroxidase (HRP)-conjugated secondary antibodies (Jackson ImmunoResearch, Suffolk, UK) for 2 h at 25°C. Chemiluminescent detection of bands was performed using Clarity Western ECL Substrate Kit (Bio-Rad Laboratories, Inc., Hercules, CA, USA), and the signals were visualized using the Quantity One Imaging Software from Bio-Rad according to the manufacturer's instructions. In order to quantify the levels of EpCAM-CD9-positive EVs from WB analysis and investigate the association with the chemiluminescent signals by our immunoassay, we rationally defined the EpCAM-CD9 protein density ($Density_{EpCAM\text{-}CD9}$): $Density_{EpCAM\text{-}CD9} = Density_{EpCAM} \times Density_{CD9}$, where the value of $Density_{EpCAM}$ and $Density_{CD9}$ can be quantitatively obtained from WB images using Quantity One Imaging Software. This definition was based on the hypothesis that all the EVs expressing EpCAM and CD9 were sufficiently captured and detected by the antibody sets of our immunoassay, and the chemiluminescent signals of each EV captured by EpCAM antibody can be multiplied by CD9 antibody. Our results showed that $Density_{EpCAM\text{-}CD9}$ was correlated highly with chemiluminescent signals ($r = 0.8395$, 95% CI: 0.6317–0.9348, $P < 0.0001$) (**Supplementary Figure S2A**).

Flow Cytometry Analysis

The expression of CD9 and EpCAM on EVs were analyzed by flow cytometry as previously described (21). Briefly, EVs attached to 4 μm aldehyde/sulfate latex beads (Invitrogen, Carlsbad, CA, USA) were incubated with anti-CD9 antibodies (SAB4700092; Sigma-Aldrich, St. Louis, MO), anti-CD63 antibodies (ab1318; Abcam, Cambridge, MA, USA), anti-CD81 antibodies (ab79559; Abcam, Cambridge, MA, USA), or anti-EpCAM antibodies (ab187372; Abcam, Cambridge, MA, USA) for 30 min with rotation at 4°C followed by Alexa-488-tagged secondary antibodies (Life Technologies, Carlsbad, CA, USA) for 30 min with rotation at 4°C. Samples were detected using CytoFLEX Flow Cytometer (Beckman Coulter, Brea, CA, USA) and data were analyzed using CytExpert (Beckman Coulter, Brea, CA, USA).

Bicinchoninic Acid Assay

According to the manufacturer's instructions, the concentration and the protein amount of EVs were measured by bicinchoninic acid (BCA) assay using Enhanced BCA Protein Assay Kit (Beyotime Biotechnology, Shanghai, China) and a spectrophotometer (Bio-Rad Laboratories, Inc., Hercules, CA, USA) set to 562 nm.

Urinary Creatinine and Serum Prostate-Specific Antigen

The urinary creatinine was measured with Roche-developed assays for creatinine (CRE2U, ACN 8152) using a Roche Cobas 8000 Modular Analyzer (Roche, Woerden, Netherlands) according to the manufacturer's instructions. The automated chemiluminescent microparticle immunoassay analyzer ARCHITECT i2000 (Abbott Laboratories, Abbott Park, IL, USA) was used following the manufacturer's protocols to determine the concentrations of PSA protein in serum samples.

Serum Starvation and Hypoxia for Cells

Cells were seeded and cultured in RPMI 1640 medium, which contains glucose and amino acids for 24 h. The medium was discarded, and then cells were washed once with PBS to remove trace serum. The cells were further cultured in serum-free RPMI 1640 medium under normoxia (21% O_2) to suffer serum starvation or cultured in RPMI 1640 medium supplemented with 10% FBS under hypoxic conditions (1% O_2) to suffer hypoxia for the indicated time periods.

Chemiluminescent Immunoassay for Extracellular Vesicle Detection

EVs were detected by a newly developed paramagnetic particle-based sandwich CLIA (**Figure 1A**).

For EVs from the cell line supernatant, 100 μl EVs were mixed with 50 μl ACE-labeled anti-CD9 antibodies (1.320 μg/ml) and biotin-labeled anti-EpCAM antibodies (4.000 μg/ml). After incubation for 1 h at 25°C, the mixtures are incubated with 50 μl turbid liquid containing 4 mg/ml avidin-coated magnetic beads for another 30 min, followed by thorough washing of the magnetic beads under an external magnetic field. Finally, magnetic beads with ACE-labeled anti-CD9 antibodies are mixed with trigger solution for chemiluminescent signal excitation. All the measurements are performed in triplicate. $EV_{EpCAM\text{-}CD9}$ secretion index was calculated to describe the average amount of $EV_{EpCAM\text{-}CD9}$ secreted per PC3 cell. $EV_{EpCAM\text{-}CD9}$ secretion index $= V_s \times Con_{EV}/N_{cell}$, where V_s (μl) is the volume of the PC3 cell line supernatant, Con_{EV} (particles/μl) is the concentration of $EV_{EpCAM\text{-}CD9}$ derived by

PC3 cells in the supernatant, and N_{cell} corresponds to the number of the PC3 cells.

For EVs from the urine samples, each step was the same as the EVs from the cell line supernatant, except the concentration of the ACE-labeled anti-CD9 antibodies (0.132 μg/ml). To avoid urine sampling variance, $uEV_{EpCAM\text{-}CD9}$ concentrations were normalized by urinary creatinine. We herein rationally defined "n.u.": n.u. = Con EV/Cr, where Con EV (g/L) corresponds to the concentration of $EV_{EpCAM\text{-}CD9}$ in the urine samples and Cr (g/L) corresponds to the urinary creatinine of the urine samples, to compare $uEV_{EpCAM\text{-}CD9}$ concentrations between patients with PCa and without PCa better.

Statistical Analysis

Continuous variables were presented as mean ± standard deviation (SD) or median [interquartile range (IQR)] and compared with each other by Student's t-test or Mann–Whitney U test. Categorical variables are presented as rate and compared using the chi-square test or the Fisher's exact test. Receiver operating characteristic (ROC) curve was used to evaluate the diagnostic performance of EpCAM-CD9-positive EVs, PSA, and models. Decision curve analysis (DCA) was used to compare the diagnostic benefits of different biomarkers and models for PCa. P-values lower than 0.05 were considered statistically significant. All analyses were undertaken with GraphPad Prism version 8.0, SPSS Statistics 20, and R version 2.10.1 (R Foundation for Statistical Computing; http://www.R-project.org).

RESULTS

Characterization of Extracellular Vesicles From the Prostate Cell Line PC3

In this study, we used PC3-derived EVs to construct and optimize the CLIA. Standard characterization of EVs was performed using TEM, NTA, and WB analysis (**Figures 1B–D**). EVs showed characteristic cup-shaped morphology under TEM and showed a mean size of 175.9 ± 6.3 nm (standard error; SD: 78.6 ± 11.1 nm) by NTA. The EV fraction from PC3 was enriched in CD63, CD9, and ALIX, the common biomarkers of EVs, but did not contain calnexin and APO, the negative control of EVs, compared to the PC3 cell lysates (20). In addition, PC3-derived EVs were positive for EpCAM, an epithelial cell marker. Moreover, flow cytometry assay identified that approximately 80% of EVs released by PC3 carried EpCAM and CD9 (**Figures 1E–G**). These results indicated that EpCAM and CD9 were enriched on the membrane of EVs from the prostate cell line PC3 and EVs can be effectively captured by anti-EpCAM antibody-conjugated magnetic beads and successfully detected by ACE-labeled anti-CD9 antibodies.

Ultrasensitive Detection of EpCAM-CD9-Positive Extracellular Vesicles by Chemiluminescent Immunoassay

We performed an ultrasensitive CLIA to quantify $EV_{EpCAM\text{-}CD9}$ (**Figure 1A**). Noteworthy, although several conventional surface markers (e.g., CD9, CD63, and CD81) are used for EV analysis, we selected CD9 as our detection antibody for EVs. The expression of CD9, CD63, CD81, and EpCAM on PC3-derived EVs were analyzed by flow cytometry in our study, showing that EVs carrying CD9, CD63, CD81, and EpCAM accounted for 81.42%, 82.08%, 67.19%, and 79.59% of total PC3-derived EVs, respectively. Practically, the CLIA employing ACE-labeled anti-CD9 antibody exhibited a superior performance over ACE-labeled CD63 antibody or ACE-labeled CD81 antibody (data not shown). This assay exhibited remarkable chemiluminescent signals for PC3-derived EVs, while the four control groups (non-EVs, non-streptavidin-labeled magnetic beads, non-biotin-labeled anti-EpCAM antibodies, and non-ACE-labeled anti-CD9 antibodies) presented negligible chemiluminescent signals (**Figure 2A**). By contrast, a significant reduction in the relative chemiluminescent unit (RCU) was observed after the addition of Triton X-100, a detergent to lyse EVs (**Figure 2B**) (22). These results strongly demonstrated the feasibility of the assay for selectively detecting EVs.

Next, we systematically optimized the reaction conditions of the EV assay, including the concentration of streptavidin-labeled magnetic beads, biotin-labeled anti-EpCAM antibodies, ACE-labeled anti-CD9 antibodies, and reaction time (**Supplementary Figures S1A–D**). To further investigate the quantitative performance of the EV assay, isolated PC3-derived EVs by ultracentrifugation were quantified using the EV assay based on the concentrations obtained by NTA. As shown in **Figure 2C**, the RCU value was found to greatly depend on the concentration of EVs, with a good linearity range ranging from 5.50×10^4 to 8.80×10^5 particles/μl (R^2 = 0.9823). The limit of detection (LOD) calculated as three times of SD above the background (negative control) was 2.86×10^4 particles/μl. Moreover, PC3-derived EVs were quantified by a standard procedure of a recovery test to evaluate the accuracy of the EV assay. The recovery rates of low, medium, and high concentrations of EVs were 85.45%, 95.45%, and 101.65%, respectively (**Supplementary Table S2**, left panels). In addition, three different concentrations of EVs were tested to evaluate the repeatability of the EV assay. The intra-assay coefficient of variation (intra-CV) and the inter-assay coefficient of variation (inter-CV) were less than 10% and 20%, respectively (**Supplementary Table S2**, left panels). The above results suggested an excellent analytical performance of our EV assay.

Then, we asked whether the $EV_{EpCAM\text{-}CD9}$ could be used to infer the prostatic cell types, e.g., PCa cell lines (PC3 and LNCaP) and benign prostate epithelial cell line (RWPE-1). Hence, we obtained the EVs from the culture supernatant by ultracentrifugation and quantified the concentrations by our assay. As shown in **Figure 2D**, the concentrations of EVs derived from human PCa cell lines such as PC3 and LNCaP were significantly higher than that of the BPH cell line RWPE-1, which were consistent with the EV $Density_{EpCAM\text{-}CD9}$ from corresponding cell lines. Moreover, FBS-derived EVs exhibited negligible chemiluminescent signals in the assay. These results revealed that the concentration of $EV_{EpCAM\text{-}CD9}$ can be a potential indicator for distinguishing cancerous cells from normal ones.

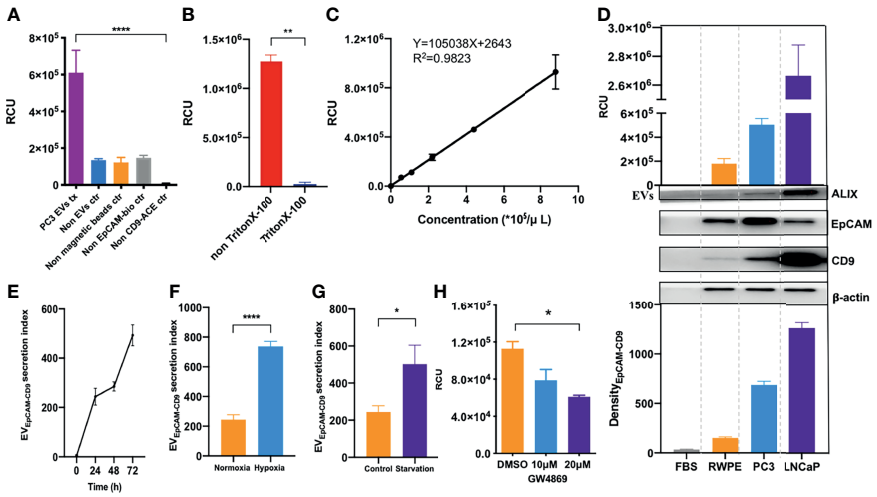

FIGURE 2 | $EV_{EpCAM\text{-}CD9}$ is ultrasensitively detected by chemiluminescent immunoassay and oversecreted under simulated tumor microenvironment. **(A)** Groups of PC3 EVs, non-EVs, non-streptavidin-labeled magnetic beads, non-biotin-labeled anti-EpCAM antibodies, and non-ACE-labeled anti-CD9 antibodies were detected by our assay. **(B)** EVs were penetrated by Triton X-100. **(C)** A standard curve was for EVs from cell line supernatant quantification using our EV assay. **(D)** EVs derived from FBS, BPH cell line RWPE-1, and human prostate cancer cell lines PC3 and LNCaP were detected by our EV assay and WB. **(E)** The changes of $EV_{EpCAM\text{-}CD9}$ secretion index during the growth of PC3 cells. **(F)** The changes of $EV_{EpCAM\text{-}CD9}$ secretion index when the PC3 cells were cultured under hypoxia. **(G)** The changes of $EV_{EpCAM\text{-}CD9}$ secretion index when the PC3 cells were cultured under serum starvation. **(H)** The changes of $EV_{EpCAM\text{-}CD9}$ secreted by PC3 cells with the treatment of 10 and 20 μM GW4869. RCU, relative chemiluminescent unit; EVs, extracellular vesicles; FBS, fetal bovine serum; EVEpCAM-CD9, EpCAM-CD9-positive extracellular vesicles. *P < 0.05,**P < 0.01,****P < 0.0001.

$EV_{EpCAM\text{-}CD9}$ Are Oversecreted by Prostate Cancer Cells Under Simulated Tumor Microenvironment

In the course of tumor expansion, cancer cells within the tumor microenvironment often have restricted access to nutrients and oxygen and thus were subjected to starvation and hypoxia (23). Previous reports have demonstrated that the levels of EVs carrying tumor-related proteins can be significantly elevated under such microenvironment, contributing to the regulation of tumor microenvironment, thus promoting tumor initiation, progression, and metastasis (24). However, $EV_{EpCAM\text{-}CD9}$ derived from PCa cells under tumor microenvironment, which may be diagnostically beneficial in reflecting the pathological stage during PCa development, remained unknown.

Herein, we defined $EV_{EpCAM\text{-}CD9}$ secretion index to describe the average amount of $EV_{EpCAM\text{-}CD9}$ secreted per PC3 cell. As shown in **Figure 2E**, the $EV_{EpCAM\text{-}CD9}$ secretion index was gradually elevated at the early stage of cell growth due to the initial activation of the cells in the latent phase. At 24–48 h, the PC3 cells entered the logarithmic growth phase, and the equative rate of increase between the amount of $EV_{EpCAM\text{-}CD9}$ and PC3 cells resulted in a constant $EV_{EpCAM\text{-}CD9}$ secretion index. Interestingly, however, when the cell reached the stationary phase after 48 h, the $EV_{EpCAM\text{-}CD9}$ secretion index started increasing again. This may be a result of the inadequate living conditions in the microenvironment. Accordingly, we investigated the impact of some conditions (e.g., hypoxia and serum starvation) involved in such microenvironment on the $EV_{EpCAM\text{-}CD9}$ secretion index. We observed higher $EV_{EpCAM\text{-}CD9}$ secretion indexes when the PC3 cells were cultured under hypoxia and serum starvation compared with the controls (**Figures 2F, G**). Additionally, this trend can be reversed upon the treatment of the EV biogenesis inhibitor, such as GW4869 (**Figure 2H**). These results strongly support our hypothesis that $EV_{EpCAM\text{-}CD9}$ can be a potential indicator in revealing the pathological status of PCa.

Urinary EpCAM-CD9-Positive Extracellular Vesicle Is a Biomarker for Prostate Cancer Diagnosis

Urine can harbor PCa cell-derived EVs, as mentioned above. We thus investigated whether the urinary EpCAM-CD9-positive EVs ($uEV_{EpCAM\text{-}CD9}$) can be detected using our EV assay. As shown in **Supplementary Figure S2B**, the protein profile from urine revealed the presence of EpCAM and CD9-positive EVs in PCa. Using a well-adopted EV protein assay, WB, $uEV_{EpCAM\text{-}CD9}$ from less than 2 ml of urine volume was almost undetectable (**Figure 3A**). However, the $uEV_{EpCAM\text{-}CD9}$ from even down to 125 μl of urine volume could be successfully detected by our CLIA, and the levels of $uEV_{EpCAM\text{-}CD9}$ in the same urine volume were statistically distinguishable between the pooled samples from PCa and healthy controls (**Figures 3B, C**). In view of the significant differences between the cell supernatant and urine in the concentration and proportion of $EV_{EpCAM\text{-}CD9}$, we optimized the methodology again. Additionally, in the clinical laboratory, it is not suitable to quantify EVs by NTA due to the requirement of

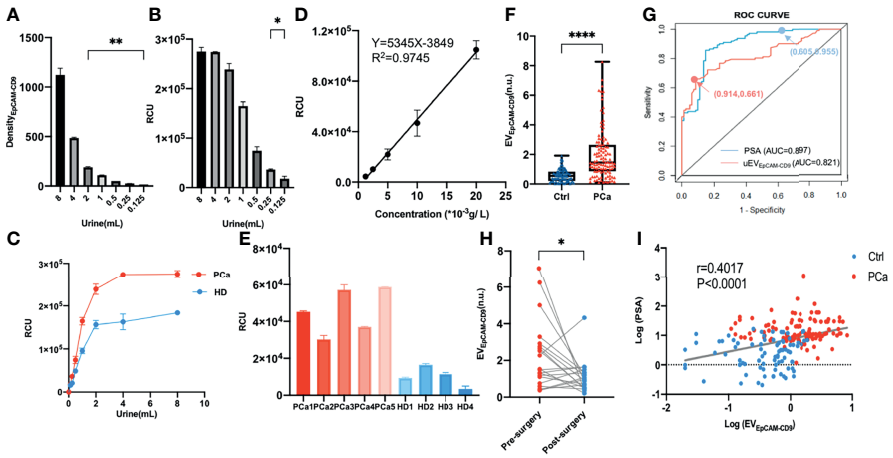

FIGURE 3 | Urinary EpCAM-CD9-positive EV is a potential biomarker for PCa diagnosis. **(A)** The $uEV_{EpCAM\text{-}CD9}$ in different urine volumes was detected by WB. **(B)** The $uEV_{EpCAM\text{-}CD9}$ from different urine volumes was detected by our chemiluminescent immunoassay. **(C)** The $uEV_{EpCAM\text{-}CD9}$ of the pooled samples from PCa and healthy controls were detected by EV assay. **(D)** A standard curve was for urinary EV quantification using our EV assay. **(E)** The $uEV_{EpCAM\text{-}CD9}$ from nine randomly selected donors including five PCa and four HDs was assayed by the chemiluminescent immunoassay. **(F)** The levels of $uEV_{EpCAM\text{-}CD9}$ was observed from men with PCa (n = 112) and without PCa (n = 81). **(G)** The ROC curve of $uEV_{EpCAM\text{-}CD9}$ and PSA. **(H)** The $uEV_{EpCAM\text{-}CD9}$ was detected before and after prostatectomy in 20 PCa patients. **(I)** The correlation between the $uEV_{EpCAM\text{-}CD9}$ and PSA. $Density_{EpCAM\text{-}CD9}$, EpCAM-CD9 protein density; RCU, relative chemiluminescent unit; $EV_{EpCAM\text{-}CD9}$, EpCAM-CD9-positive extracellular vesicles; Ctrl, control; PCa, prostate cancer; ROC, receiver operating characteristic; uEVEpCAM-CD9, urinary EpCAM-CD9-positive extracellular vesicles; PSA, prostate-specific antigen; AUC, area under the curve; HD, healthy donor. *P < 0.05,**P < 0.01,****P < 0.0001.

the specialized equipment. And NTA may be biased toward certain particle size ranges (especially 50–150 nm), and large EVs (>400 nm) and very small EVs (<50 nm) are not well quantified by NTA. We thus used a simple and low-cost protein assay, BCA, as an alternative for EV quantification (25). As described in the *Materials and Methods*, we optimized the concentration of CD9 antibody and restructured the standard curve and corresponding performance evaluation. As shown in **Figure 3D**, the RCU value was found to greatly depend on the concentration of EVs, with a good linearity range ranging from 1.25×10^{-3} to 20.00×10^{-3} g/L (R^2 = 0.9745) and a low detection limit, 0.60×10^{-3} g/L. The recovery test and repeatability test both performed excellently especially at the low level of $uEV_{EpCAM\text{-}CD9}$ (**Supplementary Table S2**, right panels). Furthermore, $uEV_{EpCAM\text{-}CD9}$ from nine randomly selected donors including five PCa and four HDs was assayed by the CLIA and WB, which suggested a significant elevation of $uEV_{EpCAM\text{-}CD9}$ in PCa compared with HD (**Figure 3E** and **Supplementary Figures S2C, D**).

In the validation experiment, urine samples from a total of 193 participants were further enrolled, including 112 PCa patients, 55 BPH patients, and 26 HDs. Complete datasets were available in 193 men who underwent the first transrectal ultrasound (TRUS)-guided prostate biopsy, and the histologic subtypes of all the 112 PCa patients were identified as prostate adenocarcinoma and without any metastatic sites confirmed by computed tomography examinations. The clinical characteristics of all the participants were listed in **Supplementary Table S1**. A remarkably higher level of $uEV_{EpCAM\text{-}CD9}$ was observed from men with PCa (1.46, IQR 0.86-2.66) than men without PCa (0.55, IQR 0.22-0.84) (**Figure 3F**). ROC curve showed that the diagnostic sensitivity and specificity of $uEV_{EpCAM\text{-}CD9}$ was 66.07% and 91.36%, respectively (cutoff value: 1.130), and the area under the curve (AUC) was 0.821 (P < 0.0001), while the diagnostic sensitivity and specificity of PSA was 95.54% and 60.49%, respectively (cutoff value: 4.015), and the AUC was 0.897 (P < 0.0001) (**Figure 3G**). Moreover, there was a statistically significant correlation between $uEV_{EpCAM\text{-}CD9}$ and Gleason grades in PCa patients (r = 0.215, 95% CI: 0.025–0.389, P = 0.023). Significant decreases of $uEV_{EpCAM\text{-}CD9}$ were observed after prostatectomy in 20 PCa patients (**Figure 3H**). It also showed that $uEV_{EpCAM\text{-}CD9}$ levels were positively associated with PSA (r = 0.402, 95% CI: 0.272–0.517, P < 0.0001), which was an important indicator for the diagnosis of PCa (**Figure 3I**).

A Multivariate Diagnostic Model Based on $uEV_{EpCAM\text{-}CD9}$ for Prostate Cancer

Due to the results that $uEV_{EpCAM\text{-}CD9}$ has high specificity and low sensitivity, while PSA is just the opposite (**Figure 3G**), we consider building a model combining $uEV_{EpCAM\text{-}CD9}$ and PSA to better diagnose PCa. The training dataset (n = 116) and validation dataset (n = 77) had an even distribution in patient characteristics (**Table 1**). The predictive value of the $uEV_{EpCAM\text{-}CD9}$ was analyzed using a logistic regression model. The odds ratio (OR) for each clinical factor and/or covariate in training sets was assessed by univariate logistic regression modeling. Age, $uEV_{EpCAM\text{-}CD9}$, PSA, fPSA, f/T PSA, prostate volume (PV), and prostate-specific antigen density (PSAD) were statistically significant predictors of PCa (P < 0.001) on univariate logistic regression analysis (**Table 2**, left panels). Then, we compared varieties of multivariate diagnostic models employing different

TABLE 1 | Baseline characteristics of the training and validation cohorts.

Variable	Training Set (n = 116)		P value	Validation Set (n = 77)		P value
	Men with PCa (n = 69) Median (IQR) or n (%)	Men without PCa (n = 47) Median (IQR) or n (%)		Men with PCa (n = 43) Median (IQR) or n (%)	Men without PCa (n = 34) Median (IQR) or n (%)	
Age (years)	72 (66–76)	64 (51–70)	<0.0001	71 (64–74)	64 (55–73)	0.018
Smoking			0.014			0.127
Yes	30 (43.5)	10 (21.3)		20 (46.5)	10 (29.4)	
No	39 (56.5)	37 (78.7)		23 (53.5)	24 (70.6)	
Drinking			0.026			0.229
Yes	30 (43.5)	11 (23.4)		17 (39.5)	9 (26.5)	
No	39 (56.5)	36 (76.6)		26 (60.5)	25 (73.5)	
Family history			0.167			0.428
Yes	8 (11.6)	2 (4.3)		3 (7.0)	1 (2.9)	
No	61 (88.4)	45 (95.7)		40 (93.0)	33 (97.1)	
BMI (kg/m^2)	23.88 (22.00–26.03)	22.23 (21.29–24.62)	0.012	23.30 (21.80–25.08)	22.78 (21.72–24.14)	0.538
Gleason score			<0.0001			<0.0001
6	12 (17.4)	NA		5 (11.6)	NA	
7	32 (46.4)	NA		17 (39.5)	NA	
8	12 (17.4)	NA		9 (20.9)	NA	
9–10	13 (18.8)	NA		12 (27.9)	NA	
CEA (ng/ml)	2.6 (2.1–3.5)	2.1 (1.4–3.0)	0.019	2.2 (1.8–3.2)	2.0 (1.5–3.0)	0.228
AFP (ng/ml)	2.6 (1.8–3.5)	2.5 (1.8–3.6)	0.833	2.8 (1.7–3.2)	2.5 (1.6–3.0)	0.285
CA125 (U/ml)	9.9 (7.1–12.8)	11.5 (7.1–13.9)	0.389	11.3 (9.1–14.5)	11.2 (5.5–12.8)	0.327
CA199 (U/ml)	7.4 (4.1–11.3)	7.1 (4.0–11.6)	0.884	6.2 (4.7–11.9)	5.9 (3.7–11.1)	0.432
EpCAM-CD9-positive EV concentration (n.u)	1.38 (0.56–2.48)	0.53 (0.31–0.84)	<0.0001	1.57 (1.15–3.08)	0.58 (0.16–0.91)	<0.0001
PSA (ng/ml)	10.9820 (7.3635–22.0090)	2.6780 (0.8072–5.5960)	<0.0001	14.8340 (9.5180–29.9020)	2.7025 (1.0583–8.3488)	<0.0001
fPSA (ng/ml)	1.5390 (1.0730–3.0710)	0.6777 (0.3045–1.1920)	<0.0001	2.1080 (0.8620–3.2330)	0.7826 (0.2259–1.6068)	<0.0001
f/T PSA	0.13 (0.09–0.20)	0.22 (0.18–0.34)	<0.0001	0.11 (0.08–0.19)	0.23 (0.19–0.29)	<0.0001
PV (cm^3)	63.00 (44.93–109.35)	66.58 (24.00–107.04)	0.556	54.71 (47.23–77.76)	50.34 (24.00–110.83)	0.785
PSAD (ng/ml^2)	0.17 (0.08–0.45)	0.04 (0.02–0.06)	<0.0001	0.31 (0.17–0.43)	0.05 (0.03–0.07)	<0.0001

BMI, body mass index; EV, extracellular vesicle; PSA, prostate-specific antigen; fPSA, free prostate-specific antigen; f/T PSA, free/total prostate-specific antigen; PV, prostate volume; PSAD, prostate-specific antigen density; PCa, prostate cancer; IQR, interquartile range; NA, not applicable.

combinations of the variables assessed by their AUC in ROC curve analysis variables (**Supplementary Table S3**). The optimal multivariate model for diagnosing PCa should be selected on the basis of the complexity (numbers of variables) and prediction efficiency (AUC); we rationally selected the multivariate model containing the variable age, smoking, drinking, family history, BMI, $uEV_{EpCAM\text{-}CD9}$, PSA, and PV as the final diagnostic model. The OR of each variable from the multivariate logistic regression analysis was presented in **Table 2** (right panels).

The nomogram was constructed according to the results of multivariate logistic regression (**Figure 4A**). In the ROC curve analysis, the AUC of the combined PCa diagnostic model was increased to 0.952 in the training set (**Figure 4B**). Moreover, the multivariate diagnostic model was perfectly in the internal validations, as the calibration curve showed good agreement between prediction and observation (**Figure 4C**). On DCA, by combining $uEV_{EpCAM\text{-}CD9}$ with other clinical parameters, the combination model to predict PCa added more clinical overall benefit than that of $uEV_{EpCAM\text{-}CD9}$ only (**Figure 4D**). When applied to the validation test, the model achieved an AUC of 0.947 ($P < 0.0001$) (**Figure 4B**). The AUC value revealed the high performance of PCa diagnosis using the combined nomogram. Additionally, in patients with PSA gray zone (4–10 ng/ml) including 23 PCa and 31 BPH, the model based on $uEV_{EpCAM\text{-}CD9}$ showed a better diagnostic performance (AUC = 0.917, $P < 0.0001$) than the $uEV_{EpCAM\text{-}CD9}$ only (AUC = 0.887, $P < 0.0001$) and the traditional biomarkers PSA (AUC = 0.712, $P = 0.0018$) (**Figure 4E**).

DISCUSSION

EVs represent a rich source of information in many liquid biopsy samples, including plasma, serum, and urine, since they are abundantly released by most tumors and are relatively stable in the biological fluids, whereas cell-free nucleic acids suffer rapid degradation and are always presented at low concentration (26). PCa cell-derived EVs in urine have been extensively studied recently and regarded as novel biomarkers for cancer diagnosis. However, the major concern about the use of EVs as biomarkers in the clinical laboratory is the difficulties in the characterization of EVs. Consequently, there will be essential interest in developing standardized sampling and analytical techniques for reliable and reproducible measurements. CLIA is

TABLE 2 | Univariate analysis and multivariate analysis of potential predictors of PCa.

Variable	Univariate analysis		Multivariate analysis	
	OR (95% CI)	P value	OR (95% CI)	P value
Age (years)	1.090 (1.053–1.129)	<0.001	1.019 (0.962–1.080)	0.515
Smoking	2.460 (1.313–4.607)	0.005	0.579 (0.148–2.268)	0.433
Drinking	2.205 (1.176–4.138)	0.014	1.690 (0.462–6.178)	0.428
Family history	2.832 (0.764–10.498)	0.119	4.386 (0.452–42.528)	0.202
BMI (≥24 kg/m² *vs*. <24 kg/m²)	2.186 (1.188–4.019)	0.012	1.312 (0.433–3.976)	0.631
CEA (ng/ml)	1.227 (0.988–1.523)	0.064		
AFP (ng/ml)	1.109 (0.937–1.313)	0.228		
CA125 (U/ml)	1.016 (0.965–1.069)	0.545		
CA199 (U/ml)	1.002 (0.980–1.025)	0.836		
Log EpCAM-CD9-positive EV concentration (n.u)	15.392 (6.377–37.149)	<0.001	28.745 (6.438–128.346)	<0.001
PSA (ng/ml)				
<4	Reference	<0.001	Reference	<0.001
4–10	15.200 (5.301–43.581)	<0.001	33.292 (6.105–181.543)	<0.001
>10	73.600 (23.220–233.284)	<0.001	169.450 (25.652–1119.355)	<0.001
fPSA (ng/ml)	2.007 (1.470–2.742)	<0.001		
f/T PSA	0.000 (0.000–0.003)	<0.001		
PV (cm³)				
<36	Reference	<0.001	Reference	0.001
36–48	6.462 (2.079–20.086)	0.001	1.384 (0.173–11.083)	0.760
48–72	9.333 (2.079–24.838)	<0.001	3.352 (0.489–22.973)	0.218
72–108	2.741 (0.981–7.661)	0.054	0.203 (0.025–1.636)	0.134
>108	2.234 (0.961–5.194)	0.062	0.088 (0.012–0.633)	0.016
PSAD (≥0.15 ng/ml² *vs*. <0.15 ng/ml²)	68.402 (15.964–293.082)	<0.001		

PCa, prostate cancer; BMI, body mass index; EV, extracellular vesicle; PSA, prostate-specific antigen; fPSA, free prostate-specific antigen; f/T PSA, free/total prostate-specific antigen; PV, prostate volume; PSAD, prostate-specific antigen density; OR, odds ratio; CI, confidence interval.

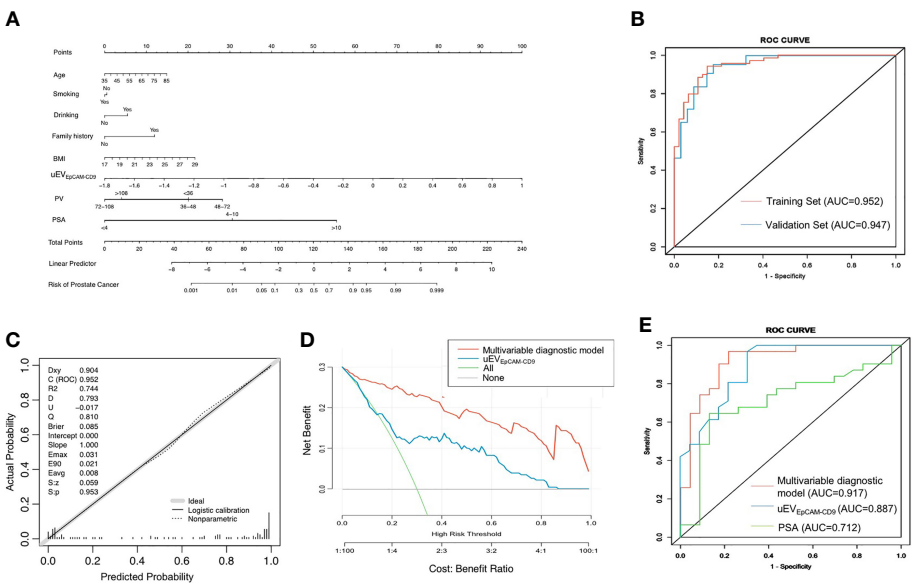

FIGURE 4 | A multivariate diagnostic model based on $uEV_{EpCAM\text{-}CD9}$ for PCa. **(A)** The nomogram was constructed according to the results of multivariate logistic regression. **(B)** The ROC curve analysis of the multivariable diagnostic model in the training set and validation set. **(C)** The multivariable diagnostic model was calibrated in the internal validations. **(D)** The decision curve analysis of the multivariable diagnostic model and $uEV_{EpCAM\text{-}CD9}$. **(E)** The diagnostic performance of the model, $uEV_{EpCAM\text{-}CD9}$, and PSA in patients with PSA gray zone (4–10 ng/ml) including 23 PCa and 31 BPH. BMI, body mass index; $uEV_{EpCAM\text{-}CD9}$, Log urinary EpCAM-CD9-positive extracellular vesicles concentration (n.u); PV, prostate volume; PSA, prostate-specific antigen; ROC, receiver operating characteristic; AUC, area under the curve.

a non-isotopic immunological technique that is increasingly used in ultramicroanalysis of biological substances owing to extreme sensitivity, high specificity, good reproducibility, and simplicity (27, 28). In this study, we proposed a chemiluminescent quantitative immunoassay of $uEV_{EpCAM\text{-}CD9}$, requiring only a small volume of urine (125 μl) to perform an EV analysis, which is superior to WB and flow cytometry (29). The extremely low LOD of EpCAM revealed that it was possible to detect other non-abundant proteins on EVs by employing multiple antibody sets. Furthermore, the use of CLIA embodies the superiority that could be fully automated to reduce operator errors and bias and enhance its potential for clinical translation.

EpCAM (also known as CD326) is deemed as a cancer-associated marker, as it is always overexpressed in many human adenocarcinomas and squamous cell carcinomas (30). Besides, this expression often closely correlates with the epithelial–mesenchymal transition (EMT)-regulating tumor invasion and metastasis (31, 32): the tumor cells have been observed to undergo loss of EpCAM expression during EMT and release a large number of EpCAM-enriched EVs simultaneously (32, 33). The source and the underlying functions of these EVs in PCa, however, remain unknown. It has been suggested that the cancerous cells will proliferate more rapidly due to the dysregulated cell cycle resulting in a state of oxygen and nutrient deprivation, and adaptation to such microenvironments is pivotal to tumor growth (34). There is good evidence that many signaling pathways are involved to help the cells escape from stresses such as hypoxia and nutrient deprivation and determine cell growth, promotion, metastasis, hormone-refractory progression, and treatment outcome (35, 36). Additionally, previous studies have reported that higher numbers of EVs were secreted by cancer cells to offer a survival advantage to cells and promote cancer progression under hypoxia and serum starvation (37, 38). These EVs usually promoted the PCa aggressiveness by adhesion junction proteins that could enhance invasiveness and induce microenvironment changes (39). Thus, such mechanisms may account for the elevated levels of PCa cell-derived $EV_{EpCAM\text{-}CD9}$ under simulated tumor microenvironment (such as hypoxia and serum starvation), as well as in PCa patients.

However, $uEV_{EpCAM\text{-}CD9}$ was not prostate-specific; that is, it may be over-released by other urogenital tumors such as bladder and kidney and other non-urological cancers. Recalling that the levels are commonly very low in HDs and patients with BPH, our multivariate model employing $uEV_{EpCAM\text{-}CD9}$, prostate tissue-specific protein (PSA), and other clinical parameters showed an enhanced diagnostic performance both in sensitivity and specificity. We also envision that by combining other cancer biomarkers, such as metabolites, RNAs or genetic signatures and medical imaging data could further provide more precise information regarding PCa diagnosis and localization.

Another limitation is the number of samples studied (n = 193). We only evaluated the diagnostic value of $uEV_{EpCAM\text{-}CD9}$ in PCa, and it has not been evaluated in depth in other aspects, e.g., as a predictor in the development of castration-resistant prostate cancer (CRPC), an indicator for successful radiotherapy and chemotherapy. Besides, while $EV_{EpCAM\text{-}CD9}$ can be released from different types of epithelial cancers and the diagnostic performance of $uEV_{EpCAM\text{-}CD9}$ in these cancers remains poorly investigated, further large-scale studies will be warranted to fully evaluate the potential applications of $uEV_{EpCAM\text{-}CD9}$ with regard to the diagnosis of varieties of cancers.

CONCLUSIONS

Urinary EpCAM-CD9-positive EVs were successfully quantified by our laboratory-developed CLIA, requiring only a small volume of urine (125 μl) to perform an EV analysis. Using this assay, we achieve a notable diagnostic performance by constructing a multivariate diagnostic model based on $uEV_{EpCAM\text{-}CD9}$ and a tissue-specific biomarker PSA. Further validation studies are warranted and should also investigate before its clinical value can be confidently affirmed. In the future, this model may potentially be used to better select patients for prostate TRUS biopsy.

DATA AVAILABILITY STATEMENT

The raw data supporting the conclusions of this article will be made available by the authors without undue reservation.

ETHICS STATEMENT

The studies involving human participants were reviewed and approved by the Second Affiliated Hospital of Zhejiang University School of Medicine Ethical Committee. The patients/participants provided their written informed consent to participate in this study.

AUTHOR CONTRIBUTIONS

YD, YW, XW, and ZT planned the project, performed the research, analyzed the data, and wrote the article. YC, YS, and DW collected clinical samples. PY and LZ performed statistical analysis. ZL, YP, and GZ collected patient information and analyzed the data. All authors contributed to the article and approved the submitted version.

FUNDING

This study was supported by grants from the National Natural Science Foundation of China Youth Science Foundation Project (Grant no. 81902156) and Zhejiang Provincial Natural Science Foundation of China (Grant no. LQ21H160016).

SUPPLEMENTARY MATERIAL

The Supplementary Material for this article can be found online at: https://www.frontiersin.org/articles/10.3389/fonc.2021.777684/full#supplementary-material

REFERENCES

1. Sung H, Ferlay J, Siegel RL, Laversanne M, Soerjomataram I, Jemal A, et al. Global Cancer Statistics 2020: GLOBOCAN Estimates of Incidence and Mortality Worldwide for 36 Cancers in 185 Countries. *CA Cancer J Clin* (2021) 71:209–49. doi: 10.3322/caac.21660
2. Martin R, Donovan J, Turner E, Metcalfe C, Young G, Walsh E, et al. Effect of a Low-Intensity PSA-Based Screening Intervention on Prostate Cancer Mortality: The CAP Randomized Clinical Trial. *JAMA* (2018) 319:883–95. doi: 10.1001/jama.2018.0154
3. Brassell SA, Kao TC, Sun L, Moul JW. Prostate-Specific Antigen Versus Prostate-Specific Antigen Density as Predictor of Tumor Volume, Margin Status, Pathologic Stage, and Biochemical Recurrence of Prostate Cancer. *Urology* (2005) 66:1229–33. doi: 10.1016/j.urology.2005.06.106
4. Sanda M, Feng Z, Howard D, Tomlins S, Sokoll L, Chan D, et al. Association Between Combined TMPRSS2:ERG and PCA3 RNA Urinary Testing and Detection of Aggressive Prostate Cancer. *JAMA Oncol* (2017) 3:1085–93. doi: 10.1001/jamaoncol.2017.0177
5. Crawford E, Rove K, Trabulsi E, Qian J, Drewnowska K, Kaminetsky J, et al. Diagnostic Performance of PCA3 to Detect Prostate Cancer in Men With Increased Prostate Specific Antigen: A Prospective Study of 1,962 Cases. *J Urol* (2012) 188:1726–31. doi: 10.1016/j.juro.2012.07.023
6. Laxman B, Tomlins S, Mehra R, Morris D, Wang L, Helgeson B, et al. Noninvasive Detection of TMPRSS2:ERG Fusion Transcripts in the Urine of Men With Prostate Cancer. *Neoplasia (New York NY)* (2006) 8:885–8. doi: 10.1593/neo.06625
7. Van Neste L, Partin A, Stewart G, Epstein J, Harrison D, Van Criekinge W. Risk Score Predicts High-Grade Prostate Cancer in DNA-Methylation Positive, Histopathologically Negative Biopsies. *Prostate* (2016) 76:1078–87. doi: 10.1002/pros.23191
8. Davey M, Benzina S, Savoie M, Breault G, Ghosh A, Ouellette R. Affinity Captured Urinary Extracellular Vesicles Provide mRNA and miRNA Biomarkers for Improved Accuracy of Prostate Cancer Detection: A Pilot Study. *Int J Mol Sci* (2020) 21:8330. doi: 10.3390/ijms21218330
9. Kohaar I, Chen Y, Banerjee S, Borbiev T, Kuo H, Ali A, et al. A Urine Exosome Gene Expression Panel Distinguishes Between Indolent and Aggressive Prostate Cancers at Biopsy. *J Urol* (2021) 205:420–5. doi: 10.1097/ju.0000000000001374
10. Merchant M, Rood I, Deegens J, Klein J. Isolation and Characterization of Urinary Extracellular Vesicles: Implications for Biomarker Discovery. *Nat Rev Nephrol* (2017) 13:731–49. doi: 10.1038/nrneph.2017.148
11. Pisitkun T, Shen R, Knepper M. Identification and Proteomic Profiling of Exosomes in Human Urine. *Proc Natl Acad Sci USA* (2004) 101:13368–73. doi: 10.1073/pnas.0403453101
12. Gonzales P, Pisitkun T, Hoffert J, Tchapyjnikov D, Star R, Kleta R, et al. Large-Scale Proteomics and Phosphoproteomics of Urinary Exosomes. *J Am Soc Nephrol: JASN* (2009) 20:363–79. doi: 10.1681/asn.2008040406
13. Moon P, You S, Lee J, Hwang D, Baek M. Urinary Exosomes and Proteomics. *Mass Spectromet Rev* (2011) 30:1185–202. doi: 10.1002/mas.20319
14. Gires O, Pan M, Schinke H, Canis M, Baeuerle P. Expression and Function of Epithelial Cell Adhesion Molecule EpCAM: Where Are We After 40 Years? *Cancer Metastasis Rev* (2020) 39:969–87. doi: 10.1007/s10555-020-09898-3
15. Fagotto F, Aslemarz A. EpCAM Cellular Functions in Adhesion and Migration, and Potential Impact on Invasion: A Critical Review. *Biochim Biophys Acta Rev Cancer* (2020) 1874:188436. doi: 10.1016/j.bbcan.2020.188436
16. Miller M, Doyle G, Terstappen L. Significance of Circulating Tumor Cells Detected by the CellSearch System in Patients With Metastatic Breast Colorectal and Prostate Cancer. *J Oncol* (2010) 2010:617421. doi: 10.1155/2010/617421
17. Pu K, Li C, Zhang N, Wang H, Shen W, Zhu Y. Epithelial Cell Adhesion Molecule Independent Capture of Non-Small Lung Carcinoma Cells With Peptide Modified Microfluidic Chip. *Biosensors Bioelectron* (2017) 89:927–31. doi: 10.1016/j.bios.2016.09.092
18. Wei P, Wu F, Kang B, Sun X, Heskia F, Pachot A, et al. Plasma Extracellular Vesicles Detected by Single Molecule Array Technology as a Liquid Biopsy for Colorectal Cancer. *J Extracell Vesicles* (2020) 9:1809765. doi: 10.1080/20013078.2020.1809765
19. Sunkara V, Kim C, Park J, Woo H, Kim D, Ha H, et al. Fully Automated, Label-Free Isolation of Extracellular Vesicles From Whole Blood for Cancer Diagnosis and Monitoring. *Theranostics* (2019) 9:1851–63. doi: 10.7150/thno.32438
20. Théry C, Witwer K, Aikawa E, Alcaraz M, Anderson J, Andriantsitohaina R, et al. Minimal Information for Studies of Extracellular Vesicles 2018 (MISEV2018): A Position Statement of the International Society for Extracellular Vesicles and Update of the MISEV2014 Guidelines. *J Extracell Vesicles* (2018) 7:1535750. doi: 10.1080/20013078.2018.1535750
21. Wang Y, Liu Z, Wang X, Dai Y, Li X, Gao S, et al. Rapid and Quantitative Analysis of Exosomes by a Chemiluminescence Immunoassay Using Superparamagnetic Iron Oxide Particles. *J BioMed Nanotechnol* (2019) 15:1792–800. doi: 10.1166/jbn.2019.2809
22. Osteikoetxea X, Sódar B, Németh A, Szabó-Taylor K, Pálóczi K, Vukman K, et al. Differential Detergent Sensitivity of Extracellular Vesicle Subpopulations. *Organic Biomol Chem* (2015) 13:9775–82. doi: 10.1039/c5ob01451d
23. Han L, Lam E, Sun Y. Extracellular Vesicles in the Tumor Microenvironment: Old Stories, But New Tales. *Mol Cancer* (2019) 18:59. doi: 10.1186/s12943-019-0980-8
24. Maacha S, Bhat A, Jimenez L, Raza A, Haris M, Uddin S, et al. Extracellular Vesicles-Mediated Intercellular Communication: Roles in the Tumor Microenvironment and Anti-Cancer Drug Resistance. *Mol Cancer* (2019) 18:55. doi: 10.1186/s12943-019-0965-7
25. Lötvall J, Hill A, Hochberg F, Buzás E, Di Vizio D, Gardiner C, et al. Minimal Experimental Requirements for Definition of Extracellular Vesicles and Their Functions: A Position Statement From the International Society for Extracellular Vesicles. *J Extracell Vesicles* (2014) 3:26913. doi: 10.3402/jev.v3.26913
26. Neumann M, Bender S, Krahn T, Schlange T. ctDNA and CTCs in Liquid Biopsy - Current Status and Where We Need to Progress. *Comput Struct Biotechnol J* (2018) 16:190–5. doi: 10.1016/j.csbj.2018.05.002
27. Zhao L, Sun L, Chu X. Chemiluminescence Immunoassay. *TrAC Trends Anal Chem* (2009) 28:404–15. doi: 10.1016/j.trac.2008.12.006
28. Akhavan-Tafti H, Binger DG, Blackwood JJ, Chen Y, Creager RS, de Silva R, et al. A Homogeneous Chemiluminescent Immunoassay Method. *J Am Chem Soc* (2013) 135:4191–4. doi: 10.1021/ja312039k
29. Campos-Silva C, Suárez H, Jara-Acevedo R, Linares-Espinós E, Martinez-Piñeiro L, Yáñez-Mó M, et al. High Sensitivity Detection of Extracellular Vesicles Immune-Captured From Urine by Conventional Flow Cytometry. *Sci Rep* (2019) 9:2042. doi: 10.1038/s41598-019-38516-8
30. Went P, Lugli A, Meier S, Bundi M, Mirlacher M, Sauter G, et al. Frequent EpCam Protein Expression in Human Carcinomas. *Hum Pathol* (2004) 35:122–8. doi: 10.1016/j.humpath.2003.08.026
31. Sankpal NV, Fleming TP, Sharma PK, Wiedner HJ, Gillanders WE. A Double-Negative Feedback Loop Between EpCAM and ERK Contributes to the Regulation of Epithelial-Mesenchymal Transition in Cancer. *Oncogene* (2017) 36:3706–17. doi: 10.1038/onc.2016.504
32. Gao J, Yan Q, Wang J, Liu S, Yang X. Epithelial-To-Mesenchymal Transition Induced by TGF-Beta1 Is Mediated by AP1-Dependent EpCAM Expression in MCF-7 Cells. *J Cell Physiol* (2015) 230:775–82. doi: 10.1002/jcp.24802
33. Ye X, Tam W, Shibue T, Kaygusuz Y, Reinhardt F, Ng Eaton E, et al. Distinct EMT Programs Control Normal Mammary Stem Cells and Tumour-Initiating Cells. *Nature* (2015) 525:256–60. doi: 10.1038/nature14897
34. Kalaany N, Sabatini D. Tumours With PI3K Activation Are Resistant to Dietary Restriction. *Nature* (2009) 458:725–31. doi: 10.1038/nature07782
35. Fraga A, Ribeiro R, Príncipe P, Lopes C, Medeiros R. Hypoxia and Prostate Cancer Aggressiveness: A Tale With Many Endings. *Clin Genitourin Cancer* (2015) 13:295–301. doi: 10.1016/j.clgc.2015.03.006
36. Li X, Lao Y, Zhang H, Wang X, Tan H, Lin Z, et al. The Natural Compound Guttiferone F Sensitizes Prostate Cancer to Starvation Induced Apoptosis *via* Calcium and JNK Elevation. *BMC Cancer* (2015) 15:254. doi: 10.1186/s12885-015-1292-z
37. Panigrahi GK, Praharaj PP, Peak TC, Long J, Singh R, Rhim JS, et al. Hypoxia-Induced Exosome Secretion Promotes Survival of African-American and Caucasian Prostate Cancer Cells. *Sci Rep* (2018) 8:3853. doi: 10.1038/s41598-018-22068-4
38. Umezu T, Tadokoro H, Azuma K, Yoshizawa S, Ohyashiki K, Ohyashiki J. Exosomal miR-135b Shed From Hypoxic Multiple Myeloma Cells Enhances Angiogenesis by Targeting Factor-Inhibiting HIF-1. *Blood* (2014) 124:3748–57. doi: 10.1182/blood-2014-05-576116

39. Ramteke A, Ting H, Agarwal C, Mateen S, Somasagara R, Hussain A, et al. Exosomes Secreted Under Hypoxia Enhance Invasiveness and Stemness of Prostate Cancer Cells by Targeting Adherens Junction Molecules. *Mol Carcinog* (2015) 54:554–65. doi: 10.1002/mc.22124

Conflict of Interest: The authors declare that the research was conducted in the absence of any commercial or financial relationships that could be construed as a potential conflict of interest.

Publisher's Note: All claims expressed in this article are solely those of the authors and do not necessarily represent those of their affiliated organizations, or those of the publisher, the editors and the reviewers. Any product that may be evaluated in this article, or claim that may be made by its manufacturer, is not guaranteed or endorsed by the publisher.

Copyright © 2021 Dai, Wang, Cao, Yu, Zhang, Liu, Ping, Wang, Zhang, Sang, Wang and Tao. This is an open-access article distributed under the terms of the Creative Commons Attribution License (CC BY). The use, distribution or reproduction in other forums is permitted, provided the original author(s) and the copyright owner(s) are credited and that the original publication in this journal is cited, in accordance with accepted academic practice. No use, distribution or reproduction is permitted which does not comply with these terms.

frontiers in Oncology

ORIGINAL RESEARCH
published: 21 December 2021
doi: 10.3389/fonc.2021.769068

Comparison of Abiraterone and Combined Androgen Blockade Therapy for High-Risk Metastatic Hormone-Sensitive Prostate Cancer: A Propensity Score-Matched Analysis

Naoki Matsumura[1], Kazutoshi Fujita[2], Mitsuhisa Nishimoto[2], Yutaka Yamamoto[3], Ken Kuwahara[4], Yasuharu Nagai[5], Takafumi Minami[2], Yuji Hatanaka[6], Masahiro Nozawa[2], Yasuhiro Morimoto[7], Hideo Tahara[1], Shigeya Uejima[5], Atsunobu Esa[4], Akihide Hirayama[3], Kazuhiro Yoshimura[2] and Hirotsugu Uemura[2]*

[1] Department of Urology, Mimihara General Hospital, Sakai Sakai-ku, Japan, [2] Department of Urology, Faculty of Medicine, Kindai University Hospital, Osakasayama, Japan, [3] Department of Urology, Faculty of Medicine, Kindai University Nara Hospital, Ikoma, Japan, [4] Department of Urology, Kaizuka City Hospital, Kaizuka, Japan, [5] Department of Urology, National Hospital Organization Osaka Minami Medical Center, Kawachinagano, Japan, [6] Department of Urology, Saiseikai Tondabayashi Hospital, Tondabayashi, Japan, [7] Department of Urology, Morimoto Urology Clinic, Sakai Minami-ku, Japan

OPEN ACCESS

Edited by:
Tanya I. Stoyanova, Stanford University, United States

Reviewed by:
Andrew Protheroe, Oxford University Hospitals NHS Trust, United Kingdom
Shiqin Liu, Stanford University, United States

***Correspondence:**
Kazutoshi Fujita
kazufujita@gmail.com

Specialty section:
This article was submitted to Genitourinary Oncology, a section of the journal Frontiers in Oncology

Received: *01 September 2021*
Accepted: *29 November 2021*
Published: *21 December 2021*

Citation:
Matsumura N, Fujita K, Nishimoto M, Yamamoto Y, Kuwahara K, Nagai Y, Minami T, Hatanaka Y, Nozawa M, Morimoto Y, Tahara H, Uejima S, Esa A, Hirayama A, Yoshimura K and Uemura H (2021) Comparison of Abiraterone and Combined Androgen Blockade Therapy for High-Risk Metastatic Hormone-Sensitive Prostate Cancer: A Propensity Score-Matched Analysis. Front. Oncol. 11:769068. doi: 10.3389/fonc.2021.769068

This study aimed to compare the effects of abiraterone acetate plus prednisone (AAP) with androgen deprivation therapy (ADT) with those of combined androgen blockade (CAB) therapy in patients with high-risk metastatic hormone-sensitive prostate cancer (mHSPC). This study retrospectively identified 163 patients with high-risk mHSPC at Kindai University and affiliated hospitals between January 2014 and December 2020. Kaplan-Meier analysis was used to summarize progression-free survival (PFS) and overall survival (OS). Multivariate Cox proportional hazard modeling was used to identify the prognostic factors in the overall cohort. Propensity score matching was used to adjust the clinical characteristics, and log-rank test was applied to these propensity score–matched cohorts. Seventy-four patients who received AAP with ADT and 89 patients who received CAB were included in this study. The median follow-up duration was 27 months (range, 2–89 months). The median PFS and OS were not reached by the AAP +ADT group and 15 and 79 months, respectively, in the CAB group. The Eastern Cooperative Oncology Group (ECOG) performance status (PS) score and AAP+ADT were significant prognostic factors for PFS, whereas ECOG PS score, visceral metastasis, and AAP+ADT were significant prognostic factors for OS. The 2-year PFS was 76.1% in the AAP+ADT group and 38.6% in the CAB group ($P < 0.0001$), and the 2-year OS was 90.2% in the AAP+ADT group and 84.8% in the CAB group ($P = 0.015$). In conclusion, AAP+ADT had better PFS and OS than CAB in patients with high-risk mHSPC.

Keywords: prostate cancer, metastatic hormone-sensitive prostate cancer, abiraterone acetate, combined androgen blockade, high risk prostate cancer

INTRODUCTION

Prostate cancer is the most common cancer and the second most common cause of death in the United States. The 5-year relative survival rate of patients with metastatic prostate cancer is 30% (1). The U.S. Preventive Services Task Force recommends individualized decision making, not blanked against prostate-specific antigen (PSA) screening for prostate cancer, but the incidence of metastatic prostate cancer has been increasing rapidly since 2012 (2). Metastatic hormone-sensitive prostate cancer (mHSPC) accounts for up to 5% of patients newly diagnosed with prostate cancer in the United States (3). Androgen deprivation therapy (ADT) with a luteinizing hormone-releasing hormone agonist or receptor antagonist or with bilateral orchiectomy has been the standard of care for men with mHSPC. Combined androgen blockade (CAB) therapy with a standard nonsteroidal antiandrogen drug (bicalutamide or flutamide) is not recommended with systemic therapy for castration-naïve disease according to the National Comprehensive Cancer Network clinical practice guidelines in oncology, but it is recommended as grade B in the Japanese Urological Association guidelines. CAB therapy may be superior to other hormone therapies for overall survival (OS) in patients with mHSPC in Japan (4). The rate of CAB therapy in primary hormone therapy is higher in Japan than in Western Europe, and the cancer-specific mortality rate is less than half that in the United States (5). The dosage of bicalutamide in Japan and Western Europe differs (80 and 50 mg, respectively).

In the LATITUDE trial, addition of abiraterone acetate plus prednisone (AAP) to ADT significantly prolonged progression-free survival (PFS) and OS compared with ADT in high-risk mHSPC, who were defined as having at least two of the following three high-risk factors: Gleason score ≥8, visceral metastasis, and ≥3 bone metastases (6). In the ENZAMET trial, addition of enzalutamide to ADT resulted in longer PFS and OS within 3 years than CAB therapy (7). However, whether the addition of AAP to ADT improves PFS and OS in patients with high-risk mHSPC compared with CAB therapy remains unknown. The aim of our study was to compare the effect of AAP+ADT with CAB therapy for upfront treatment in patients with high-risk mHSPC.

MATERIALS AND METHODS

This study retrospectively identified 166 patients with high-risk mHSPC at Kindai University and its affiliated hospitals from January 2014 to December 2020. All patients were adult men with pathologically diagnosed prostate adenocarcinomas and had not received prior hormonal therapy. Patients with high-risk HSPC were defined as having at least two of the following three high risk factors: Gleason score ≥8, visceral metastasis, and ≥3 bone metastases. Three patients with no prostate biopsy or unknown prognosis were excluded. The data of 163 patients were retrospectively analyzed. The metastasis burden was evaluated using computed tomography and diffusion-weighted whole-body imaging with background body signal or bone scan. Eligible patients had an Eastern Cooperative Oncology Group (ECOG) performance status (PS) score <3. Disease progression was assessed using the Prostate Cancer Working Group 2. PSA progression was defined as a confirmed relative increase in the PSA level from the nadir value by ≥25% and ≥2 ng/ml. The extent of disease (EOD) score was used to classify bone metastases. This study was approved by the institutional ethics committee of Kindai University (R02-247), and written informed consent was waived owing to the retrospective design.

Statistical Analysis

Clinical characteristics were analyzed using the Mann-Whitney U test and Fisher's exact test. Kaplan-Meier analysis was used to summarize PFS and OS. Differences in time events were compared using log-rank tests. Hazard ratios (HRs) and their 95% confidence intervals (CIs) were estimated using Cox proportional hazards regression to investigate the factors affecting PFS and OS. Variables included age, PSA, Gleason score, ECOG PS score, visceral metastasis, and AAP+ADT. Propensity score matching was used to adjust patient characteristics to a 1:1 ratio between the AAP+ADT and CAB groups. The propensity score was calculated using logistic regression models with age, PSA, Gleason score, ECOG PS score, visceral metastasis, and EOD score. The propensity scores were estimates of the probability of receiving AAP. With propensity score matching, one produces individual pairs of patients, one from each treatment, that were matched on an individual basis. A matched analysis that takes 105 individual pairing into account was carried out. Probability values (P) and CIs were two-sided, and a P value <0.05 was considered significant. All statistical analyses were performed with EZR (Saitama Medical Center, Jichi Medical University, Saitama, Japan), which is a modified version of the R packages designed to add statistical functions frequently used in biostatistics.

RESULTS

Patients, Treatment, and Safety

Among 163 patients with high-risk mHSPC, 74 patients (45.4%) received AAP (abiraterone acetate 1000 mg+ prednisone 5 mg daily) +ADT and 89 patients (54.6%) received CAB (bicalutamide 80 mg daily). The baseline characteristics are summarized in **Table 1**. The median follow-up duration was 27 months (range, 2–89 months). There was no significant difference in clinical characteristics between the two groups. Sixteen (21.6%) of 74 patients in the AAP+ADT group and 65 (73.0%) of 89 patients in the CAB group progressed to castration-resistant prostate cancer (CRPC). The secondary therapies were enzalutamide (58.3%) and docetaxel (25.0%) in the AAP+ADT group and flutamide (41.0%), abiraterone (19.7%), and docetaxel (18.0%) in the CAB group (**Supplementary Table 1**). The most frequently used subsequent therapy was enzalutamide (72.7%) in the AAP+ADT group and abiraterone (50.8%) in the CAB group (**Table 2**). Eight (72.7%) of 11 CPRC patients in the AAP+ADT group received

TABLE 1 | Characteristics of the patients at baseline.

Characteristic	AAP+ADT (n = 74)	CAB (n = 89)	P-value
Age (years), median (range)	74 (53-88)	74 (52-88)	0.54
PSA (ng/ml), median (range)	456 (4.6-11,507)	241 (8.8-11371)	0.279
ECOG PS score (no, %)			
0	46 (62.2)	54 (60.7)	0.873
≥1	28 (37.8)	35 (39.3)	
Gleason score (no, %)			
<8	0 (0)	1 (1.1)	1
≥8	74 (100)	88 (98.9)	
Metastasis site			
Lymph node	29 (39.2)	31 (34.8)	0.626
Bone	71 (96.0)	86 (96.6)	1
Visceral	20 (27.0)	20 (22.5)	0.584
EOD			
0	4 (5.4)	3 (3.4)	0.063
1	26 (35.1)	18 (20.2)	
≥2	44 (59.5)	68 (76.4)	
ALP (IU/ml), median (range)	395 (84-4,797)	431 (70-24,280)	0.794
LDH (IU/ml), median (range)	208 (137-4,220)	204 (135-1,334)	0.252

AAP, abiraterone acetate plus prednisone; ADT, androgen deprivation therapy; CAB, combined androgen blockade; PSA, prostate-specific antigen; ECOG PS, Eastern Cooperative Oncology Group performance status; EOD, extent of disease ; ALP, alkaline phosphatase; LDH, lactose dehydrogenase.

next-generation androgen receptor signaling inhibitor (ARSI) as subsequent therapy, whereas 45 (69.5%) of 61 CRPC patients in the CAB group received next-generation ARSI. There was no significant difference between the two groups regarding the use of the next-generation ARSI and taxane for CPRC (P = 1 and P = 0.31, respectively, Fisher's exact test). Treatment-emergent adverse events leading to treatment discontinuation were reported in 5 (6.8%) of 74 patients in the AAP+ADT group and in 1 (1.1%) of 89 patients in the CAB group. The details of serious adverse events are summarized in **Table 3**. There was no significant difference between 2 groups regarding the serious adverse events (Fisher's exact test, P=0.09). No treatment-emergent adverse events that led to death were reported in either group. No patient died within 30 days of prostate cancer treatment.

Progression-Free and Overall Survival

At the time of the analysis, 40 patients died. The median PFS and OS were not reached in the AAP+ADT group, but they were 15 and 79 months, respectively, in the CAB group. The 2-year PFS was 71.5% (95% CI, 55.2%) in the AAP+ADT group and 36.1% (95% CI, 25.8%–46.4%) in the CAB group, respectively (P < 0.0001; **Figure 1A**). The 2-year OS was 91.3% (95% CI, 80.1%–96.4%) in the AAP+ADT group and 80.8% (95% CI, 80.4%–90.4%) in the CAB group (P = 0.043; **Figure 1B**). In the univariate Cox proportional hazards analysis, the ECOG PS score and AAP +ADT were significantly associated with PFS. Multivariate analysis showed that ECOG PS score and AAP+ADT were significantly associated with PFS (**Table 4**). In the univariate Cox proportional hazards analysis, age, ECOG PS score, and AAP+ADT were significantly associated with OS. The multivariate analysis for the prediction of overall survival showed that the ECOG PS score, presence of visceral metastasis, and AAP+ADT were associated with OS (**Table 5**).

Propensity Score–Matched Analysis

Propensity score matching was used because a selection bias for the use of AAP could exist, resulting in matched cohorts of 63 patients with AAP+ADT and 63 patients with CAB. The clinical characteristics after matching are summarized in **Table 6**. The clinical characteristics were well adjusted between the two

TABLE 2 | Subsequent therapy for mHSPC patients who have progressedto mCRPC.

Summary of subsequent therapy, n (%)	AAP+ADT (n = 11)	CAB (n = 61)
Flutamide	0 (0)	23 (37.7)
Enzalutamide	8 (72.7)	19 (31.1)
Abiraterone	0 (0)	31 (50.8)
Apalutamide	1 (9.1)	2 (3.3)
Darolutamide	0 (0)	2 (3.3)
Docetaxei	6 (54.5)	21 (34.4)
Cabazitaxel	1 (9.1)	9 (14.8)
Radium-223 chloride	0 (0)	2 (3.3)
Dexamethasone	1 (9.1)	5 (8.2)
Etinolestridol	0 (0)	6 (9.8)

mHSPC, metastatic hormone-sensitive prostate cancer; mCRPC,metastatic castration-resistant prostate cancer; AAP, abiraterone acetate plus prednisone; ADT, androgen deprivation therapy; CAB, combined androgen blockade.

TABLE 3 | Treatment-emergent adverse eventsleading to treatment discontinuation.

Summary of TEAEs, n (%)	AAP+ADT (n = 74)	CAB (n = 8B)
AE leading to death	0	0
AE leading to treatment discontinuation	5 (6.8]	1 (1.1)
Grade 3 events		
Vertigo	1 (14]	0
Fatigue	1 (1.4)	0
Hypokalemia	2 (2.8)	0
ALT increased	1 (14]	1 (1.1)
AST increased	1 (14]	1 (1.1)
ALP increased	1 (14]	0

TEAEs. Treatment-emergent adverse events; AAP, abiraterone acetate plus prednisone, ADT. androgen deprivation therapy; CAB, combined androgen blockade; AE, adverse event; ALT, alanine aminotransferase; AST, aspartate aminotransferase: ALP, alkaline phosphatase.

groups. The 2-year PFS was 76.1% (95% CI, 60.3%) in the AAP +ADT group and 38.6% (95% CI, 26.7%–74.7%) in the CAB group (P < 0.0001; **Figure 2A**). The 2-year OS was 90.2% (95% CI, 77.9%–90.9%) in the AAP +ADT group and 84.8% (95% CI, 72.8%–90.8%) in the CAB group (P = 0.015; **Figure 2B**). AAP +ADT significantly improved OS and PFS compared with CAB, even in the propensity score–matched cohorts of patients with high-risk mHSPC.

DISCUSSION

This study retrospectively analyzed the efficacy of AAP+ADT in patients with high-risk mHSPC compared with CAB therapy and found that AAP+ADT significantly improved PFS and OS by propensity score–matched analysis. In the CHAARTED and STAMPEDE (arm C), addition of docetaxel to ADT resulted in beneficial effects on PFS and OS in patients with mHSPC (8, 9). In the LATITUDE and STAMPEDE (arm G) trial, AAP+ADT resulted in beneficial effects on PFS and OS in patients with high-risk mHSPC (6, 10). In the ENZAMET trial, addition of enzalutamide to CAB therapy resulted in beneficial effects on PFS and OS in patients with mHSPC (7). In the ARCHES trial, addition of enzalutamide to ADT resulted in a reduced risk of metastatic progression or death in patients with mHSPC, including after docetaxel chemotherapy (11). In the TITAN trial, addition of apalutamide to ADT resulted in beneficial effects on radiographic PFS and OS in patients with mHSPC (12).

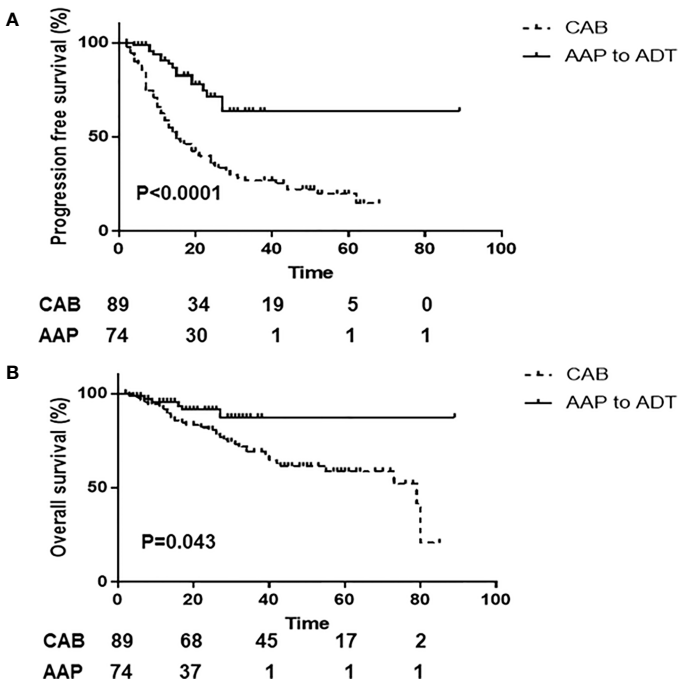

FIGURE 1 | Kaplan-Meier analysis of men with high-risk metastatic hormone-sensitive prostate cancer stratified by AAP+ADT and CAB therapy. Progression-free survival **(A)** and overall survival **(B)** in the overall population. AAP+ADT, addition of abiraterone acetate plus prednisone to androgen deprivation therapy; CAB, combined androgen blockade.

TABLE 4 | Cox regression analysis of progression free survival.

Variable	Univariate analysis			Multivariateanalysis		
	HR	95% CI	P-value	HR	95% CI	P-value
Age	1.05	0.99-1.09	0.056	1.04	0.99-1.09	0.096
PSA	0.99	0.99-1.00	0.312	0.99	0.99-1.00	0.264
Gleasonscore(≥8vs6-7)			0.997			0.996
ECOG PS score (1-3 vs O)	2.55	1.36-4.76	0.003	3.02	1.59-5.75	<0.001
Visceral metastasis (yes vs no)	1.53	0.77-3.00	0.222	2.00	0.99-4.02	0.051
AAP+ADT (yes vs no)	0.20	0.08-0.48	<0.001	0.09	0.07-0.40	<0.001

AAP, abiraterone acetate plus prednisone; ADT, androgen deprivation therapy; PSA, prostate-specific antigen; ECOG PS, Eastern Cooperative Oncology Group performance status; HR, hazards ratio; CI, confidence interval.

TABLE 5 | Cox regression analysis of overall survival.

Variable	Univariate analysis			Multivariate analysis		
	HR	95% CI	P-value	HR	95% CI	P-value
Age	1.05	1.00-1.11	0.042	1.05	0.99-1.11	0.069
PSA	0.99	0.99-1.00	0.408	0.99	0.99-1.00	0.285
Gleasanscore (≥8 vs6-7)			0.997			0.998
ECOG PS score (1 -3 vs 0)	2.77	1.47-5.21	0.002	2.94	1.53-5.64	0.001
Visceral metastasis (yes vs no)	1.85	0.94-3.67	0.077	2.49	1.21-5.09	0.013
AAP+ADT (yes vs no)	0.41	0.17-0,99	0.049	0.36	0.15-0.91	0.031

AAP, abiraterone acetate plus prednisone; ADT, androgen deprivation therapy; PSA, prostate-specific antigen; ECOG PS, Eastern Cooperative Oncology Group performance status; HR, hazards ratio; CI, confidence interval.

Based on these studies, docetaxel, AAP, enzalutamide, and apalutamide are recommended for patients with mHSPC. In the Japanese subgroup analyses of LATITUDE with high-risk mHSPC patients, a reduced risk of radiographic PFS and PSA-PFS in Japanese patients was observed in the AAP group compared with the ADT group and the AAP+ADT group had a favorable treatment effect on OS than the ADT group (13, 14).

Results from LATITUDE and STAMPEDE (arm G) showed that Gleason score, ECOG PS score, and nodal status were not prognostic factors for OS in mHSPC patients treated with AAP +ADT compared with those treated with ADT alone, but the benefit of AAP+ADT was greater in younger men (15). Miyazawa et al. (2021) reported that the prognostic factors for OS in high-risk mHSPC patients treated with CAB therapy were ECOG PS

TABLE 6 | Characteristicsofthe propensity scorematched patients at baseline.

Characteristic	AAP+ADT (n=63)	CAB (n=63)	P-value
Age (years), median (range)	75 (58-88)	73 (62-84)	0.40
PSA (ng/ml), median (range)	450 (4.6-11,507)	232 (11.0-11371)	0.373
ECOG PS score (no, %)			
0	41 (65.1)	42 (66.7)	1
≥1	22 (34.9)	21 (33.3)	
Gleason score (no, %)			
<8	0 (0)	0 (0)	1
≥8	63 (100|	63 (100|	
Metastasis site			
Lymph node	22 |34.9|	25 (39.7)	0.713
Bone	60 (95.2)	61 (96.8)	1
Visceral	18 (28.6)	17 (27.0)	1
EOD			
0	3 (4.8)	3 (4.8)	0.950
1	19 (30.1)	17 (26.9)	
≥2	41 (65.1)	43 (68.3)	
ALP (IU/ml), median (range)	402 (84-4,797)	377 (70-24,280)	0.S88
LDH (IU/ml), median (range)	208 (137-4,220)	214 (136-729)	0.246

AAP, abirateroiie acetate plus prednisone; ADT, androgen deprivation therapy; CAR. combined androgen blockade; PSA, pro state˙specific antigen; ECOG PS, Eastern Cooperative Oncology Group performance status, EOD. extent of disease', ALP, alkaline phosphatase; LDH, lactose dehydrogenase.

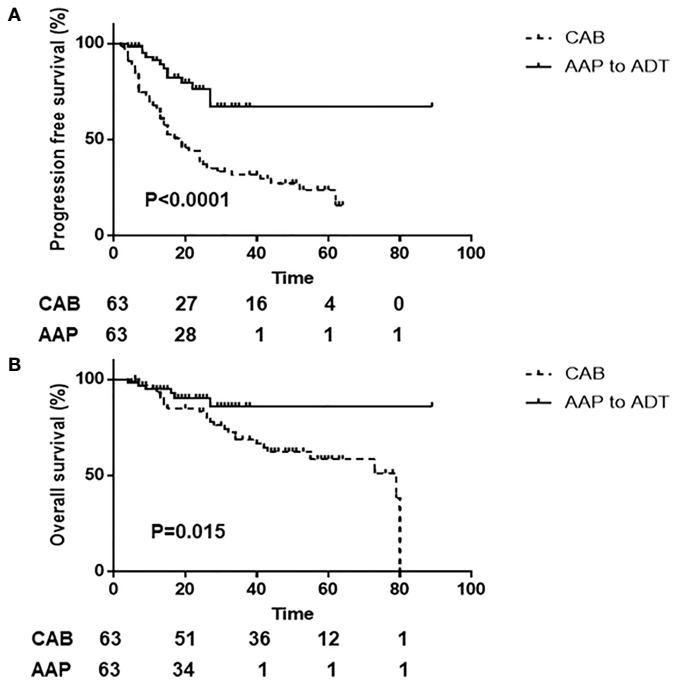

FIGURE 2 | Kaplan-Meier analysis of men with high-risk metastatic hormone-sensitive prostate cancer stratified by AAP+ADT and CAB therapy. Progression-free survival **(A)** and overall survival **(B)** in the propensity score–matched cohorts. AAP+ADT, addition of abiraterone acetate plus prednisone to androgen deprivation therapy; CAB, combined androgen blockade.

score, hemoglobin, and PSA response after 3 months (<97.0%) (16).

In our study, PFS and OS were significantly longer in the AAP+ADT group than in the CAB group. Ueda et al. retrospectively compared 50 high-risk mHSPC patients with AAP+ADT and 99 patients with CAB therapy, and showed the benefit of AAP+ADT for improvement of overall survival in Japanese patients with high-risk mHPSC (17). However, the sample size was small and further accumulation of evidence is necessary. In their study, LHRH antagonist were used as ADT, while LHRH agonists were used in our study. Our results confirmed the efficacy of AAP +ADT in 74 patients compared with CAB. While Ueda et al. reported that the prognostic factor for PSA-PFS in high-risk mHSPC patients was a high Gleason score, the ECOG PS score and visceral metastasis were poor prognostic factors for OS in our study. Docetaxel may be an alternative option for patients with these factors.

Since 2014, ARSI has been used for CPRC treatment in Japan, and the prognosis of patients with high-risk mHSPC treated with CAB has been prolonged. Our study included cases from 2014, who have received ARSI and taxane after the diagnosis of CRPC. Secondary therapy after progression to CRPC includes enzalutamide and docetaxel in the AAP+ADT group and flutamide, enzalutamide, and docetaxel in the CAB group. The subsequent therapies were docetaxel and ARSI in both groups. Bicalutamide did not improve the OS of patients with high-risk HSPC, regardless of whether most of the patients in the CAB group received ARSI (enzalutamide or abiraterone) after the diagnosis of CRPC. Our results suggest that the upfront use of AAP instead of bicalutamide followed by ARSI resulted in prolonged OS in patients with high-risk mHSPC.

The present study has several limitations. This was retrospective study with a small cohort and a short observation period. Further larger-scale studies should be performed to compare the effect of AAP+ADT with CAB therapy for upfront treatment in patients with high-risk mHSPC.

CONCLUSION

In this study, AAP+ADT provided better PFS and OS than CAB therapy in patients with high-risk mHSPC. Upfront AAP+ADT would be recommended for patients with high-risk mHSPC.

DATA AVAILABILITY STATEMENT

The original contributions presented in the study are included in the article/**Supplementary Material**. Further inquiries can be directed to the corresponding author.

ETHICS STATEMENT

The studies involving human participants were reviewed and approved by the institutional ethics committee of Kindai

University (R02-247). The patients/participants provided their written informed consent to participate in this study.

AUTHOR CONTRIBUTIONS

NM and KF performed concept and design of experiments. Acquisition of data was done by NM, MNi, YY, KK, YH, YM, and SU. NM performed manuscript writing and data analysis. KF performed manuscript editing and data analysis. YN, TM, MNo, HT, AE, AH, KY, and HU supervised the work. All authors contributed to the article and approved the submitted version.

SUPPLEMENTARY MATERIAL

The Supplementary Material for this article can be found online at: https://www.frontiersin.org/articles/10.3389/fonc.2021.769068/full#supplementary-material

REFERENCES

1. Siegel RL, Miller KDJemal. Cancer Statistics, 2019. *A Cancer J Clin* (2019) 69:7–34. doi: 10.3322/caac.21551
2. Magnani CJ, Li K, Seto T, McDonald KM, Blayney DW, Brooks JD, et al. PSA Testing Use and Prostate Cancer Diagnostic Stage After the 2012 U.S. Preventive Services Task Force Guideline Changes. *J Natl Compr Cancer Network* (2019) 17:795–803. doi: 10.6004/jnccn.2018.7274
3. Scher HI, Solo K, Valant J, Todd MB, Mehra M. Prevalence of Prostate Cancer Clinical States and Mortality in the United States: Estimates Using a Dynamic Progression Model. *PloS One* (2015) 10:0139440. doi: 10.1371/journal.pone.0139440
4. Hinotsu S, Akaza H, Usami M, Ogawa O, Kagawa S, Kitamura T, et al. Current Status of Endocrine Therapy for Prostate Cancer in Japan Analysis of Primary Androgen Deprivation Therapy on the Basis of Data Collected by J-CaP. *Jpn Japanese J Clin Oncol* (2007) 37:775–81. doi: 10.1093/jjco/hym098
5. Cooperberg MR, Hinotsu S, Namiki M, Carrol PR, Akaza H. Trans-Pacific Variation in Outcomes for Men Treated With Primary Androgen-Deprivation Therapy (ADT) for Prostate Cancer. *BJU Int* (2016) 117:102–9. doi: 10.1111/bju.12937
6. Fizazi K, Tran N, Fein L, Matsubara N, Rodriguez-Antolin A, Alekseev BY, et al. Abiraterone Plus Prednisone in Metastatic, Castration-Sensitive Prostate Cancer. *N Engl J Med* (2017) 377:352–60. doi: 10.1056/NEJMoa1704174
7. Davis ID, Martin AJ, Stockler MR, Begbie S, Chi KN, Chowdhury S, et al. Enzalutamide With Standard First-Line Therapy in Metastatic Prostate Cancer. *N Engl J Med* (2019) 381:121–31. doi: 10.1056/NEJMoa1903835
8. Sweeney CJ, Chen YH, Carducci M, Liu G, Jarrard DF, Eisenberger M, et al. Chemohormonal Therapy in Metastatic Hormone-Sensitive Prostate Cancer. *N Engl J Med* (2015) 373:737–46. doi: 10.1056/NEJMoa1503747
9. James ND, Sydes MR, Clarke NW, Mason MD, Dearnaley DP, Spears MR, et al. Addition of Docetaxel, Zoledronic Acid, or Both to First-Line Long-Term Hormone Therapy in Prostate Cancer (STAMPEDE): Survival Results From an Adaptive, Multiarm, Multistage, Platform Randomised Controlled Trial. The. *Lancet* (2016) 387:1163–77. doi: 10.1016/S0140-6736(15)01037-5
10. James ND, de Bono JS, Spears MR, Clarke NW, Mason MD, Dearnaley DP, et al. Abiraterone for Prostate Cancer Not Previously Treated With Hormone Therapy. *N Engl J Med* (2017) 377:338–51. doi: 10.1056/NEJMoa1702900
11. Armstrong AJ, Szmulewitz RZ, Petrylak DP, Holzbeierlein J, Villers A, Azad A, et al. A Randomized, Phase III Study of Androgen Deprivation Therapy With Enzalutamide or Placebo in Men With Metastatic Hormone Sensitive Prostate Cancer. *J Clin Oncol* (2019) 37:2974–86. doi: 10.1200/JCO.19.00799
12. Chi KN, Agarwal N, Bjartell A, Chung BH, Pereira de Santana Gomes AJ, Given R, et al. Apalutamide for Metastatic, Castration-Sensitive Prostate Cancer. *N Engl J Med* (2019) 381:13–24. doi: 10.1056/NEJMoa1903307
13. Fukasawa S, Suzuki H, Kawaguchi K, Noguchi H, Enjo K, Tran N, et al. Efficacy and Safety of Abiraterone Acetate Plus Prednisone in Japanese Patients With Newly Diagnosed, Metastatic Hormone-Naïve Prostate Cancer: A Subgroup Analysis of LATITUDE, a Randomized, Double-Blind, Placebo-Controlled Phase 3 Study. *Japanese J Clin Oncol* (2018) 48:1012–21. doi: 10.1093/jjco/hyy129
14. Suzuki H, Shin T, Fukasawa S, Hashine K, Kitani S, Ohtake N, et al. Efficacy and Safety of Abiraterone Acetate Plus Prednisone in Japanese Patients With Newly Diagnosed, Metastatic Hormone-Naïve Prostate Cancer: Final Subgroup Analysis of LATITUDE, a Randomized, Double-Blind, Placebo-Controlled Phase 3 Study. *Japanese J Clin Oncol* (2020) 50:810–20. doi: 10.1093/jjco/hyaa030
15. Rydzewska LHM, Burdett S, Vale CL, Clarke NW, Fizazi K, Kheoh T, et al. Adding Abiraterone to Androgen Deprivation Therapy in Men With Metastatic Hormone-Sensitive Prostate Cancer: A Systematic Review and Meta-Analysis. *Eur J Cancer* (2017) 84:88–101. doi: 10.1016/j.ejca.2017.07.003
16. Miyazawa Y, Sekine Y, Arai S, Oka D, Nakayama H, Syuto T, et al. Prognostic Factors in Hormone-Sensitive Prostate Cancer Patients Treated With Combined Androgen Blockade: A Consecutive 15-Year Study at a Single Japanese Institute. *In Vivo* (2021) 35:373–84. doi: 10.21873/invivo.12268
17. Ueda T, Shiraishi T, Ito S, Ohashi M, Matsugasumi T, Yamada Y, et al. Abiraterone Acetate Versus Bicalutamide in Combination With Gonadotropin Releasing Hormone Antagonist Therapy for High-Risk Metastatic Hormone Sensitive Prostate Cancer. *Sci Rep* (2021) 11:10094. doi: 10.1038/s41598-021-89609-2

Conflict of Interest: The authors declare that the research was conducted in the absence of any commercial or financial relationships that could be construed as a potential conflict of interest.

Publisher's Note: All claims expressed in this article are solely those of the authors and do not necessarily represent those of their affiliated organizations, or those of the publisher, the editors and the reviewers. Any product that may be evaluated in this article, or claim that may be made by its manufacturer, is not guaranteed or endorsed by the publisher.

Copyright © 2021 Matsumura, Fujita, Nishimoto, Yamamoto, Kuwahara, Nagai, Minami, Hatanaka, Nozawa, Morimoto, Tahara, Uejima, Esa, Hirayama, Yoshimura and Uemura. This is an open-access article distributed under the terms of the Creative Commons Attribution License (CC BY). The use, distribution or reproduction in other forums is permitted, provided the original author(s) and the copyright owner(s) are credited and that the original publication in this journal is cited, in accordance with accepted academic practice. No use, distribution or reproduction is permitted which does not comply with these terms.

frontiers in Oncology

REVIEW
published: 24 December 2021
doi: 10.3389/fonc.2021.809170

Glycosylation Changes in Prostate Cancer Progression

*William Butler and Jiaoti Huang**

Department of Pathology, Duke University School of Medicine, Durham, NC, United States

Prostate Cancer (PCa) is the most commonly diagnosed malignancy and second leading cause of cancer-related mortality in men. With the use of next generation sequencing and proteomic platforms, new biomarkers are constantly being developed to both improve diagnostic sensitivity and specificity and help stratify patients into different risk groups for optimal management. In recent years, it has become well accepted that altered glycosylation is a hallmark of cancer progression and that the glycan structures resulting from these mechanisms show tremendous promise as both diagnostic and prognostic biomarkers. In PCa, a wide range of structural alterations to glycans have been reported such as variations in sialylation and fucosylation, changes in branching, altered levels of Lewis and sialyl Lewis antigens, as well as the emergence of high mannose "cryptic" structures, which may be immunogenic and therapeutically relevant. Furthermore, aberrant expression of galectins, glycolipids, and proteoglycans have also been reported and associated with PCa cell survival and metastasis. In this review, we discuss the findings from various studies that have explored altered *N*- and *O*-linked glycosylation in PCa tissue and body fluids. We further discuss changes in *O*-GlcNAcylation as well as altered expression of galectins and glycoconjugates and their effects on PCa progression. Finally, we emphasize the clinical utility and potential impact of exploiting glycans as both biomarkers and therapeutic targets to improve our ability to diagnose clinically relevant tumors as well as expand treatment options for patients with advanced disease.

Keywords: prostate cancer, glycobiology, biomarker discovery, cancer biology, omics

OPEN ACCESS

Edited by:
Tanya I. Stoyanova,
Stanford University, United States

Reviewed by:
Sharon Pitteri,
Stanford University, United States
Jennifer Munkley,
Newcastle University, United Kingdom

***Correspondence:**
Jiaoti Huang
jiaoti.huang@duke.edu

Specialty section:
This article was submitted to Genitourinary Oncology, a section of the journal Frontiers in Oncology

Received: *04 November 2021*
Accepted: *07 December 2021*
Published: *24 December 2021*

Citation:
Butler W and Huang J (2021) Glycosylation Changes in Prostate Cancer Progression. Front. Oncol. 11:809170. doi: 10.3389/fonc.2021.809170

INTRODUCTION

Prostate Cancer (PCa) is the most common non-cutaneous malignancy and second leading cause of cancer-related mortality in men over the age of 50 (1). Although most men are diagnosed with low-grade or indolent tumors that are unlikely to metastasize and lead to death, a significant subset of patients develops recurrence of their tumor following local intervention or, more rarely, are diagnosed with distant metastases at clinical presentation (2, 3). Since the vast majority of PCa cells express high levels of androgen receptor (AR) (4), hormonal therapy (i.e. androgen ablation or AR inhibition) remains the mainstay of treatment for men diagnosed with recurrent or advanced disease (2). Unfortunately, the tumor eventually becomes resistant to treatment in all cases which is classified as castration-resistant prostate cancer (CRPC) (5). CRPC is associated with a poor prognosis as the tumor cells are more proliferative and display a higher capacity for metastasis (5).

Furthermore, treatment for CRPC remains very limited due to an overall lack of mechanistic understanding which in part is due to limited tissue resources as such tumors rarely undergo biopsy or resection.

Many studies have been performed to molecularly profile prostatic tumors to address two clinical situations: 1) Stratify patients with primary PCa into different risk groups for optimal management and 2) Elucidate the molecular features of CRPC to inform novel therapeutic strategies. In recent years, several studies with large patient cohorts (6–9) have been done to survey the molecular landscape in these contexts. Most of these involve the use of RNA or single-cell sequencing as well as proteomic analysis to study differential gene and protein expression amongst different disease stages. Whilst these studies provide powerful information on how the molecular landscape changes during PCa progression, it is becoming increasingly recognized that the glycome is also a significant source of biomarkers and therapeutic targets (10) that has remained relatively unexplored in many cancer settings including PCa. Aberrant glycosylation is a well-known hallmark of cancer and is known to have a significant effect on protein function and cell survival (10). Furthermore, the prostate is a major secretor of glycoproteins and significant changes in the structures of both cell surface and secreted glycans have been reported by several groups (11). In this review, we summarize the wide range of glycosylation changes observed as PCa progresses including changes in *N*- and *O*-linked glycans, *O*-GlcNacylation, as well as altered expression of galectins and glycoconjugates such as heparan and chondroitin sulfate proteoglycans (HSPGs and CSPGs) and glycolipids. Furthermore, we highlight new technological advances in studying glycobiology in human tissue and how this has been applied to PCa. By providing both historical context and modern perspective, this review hopes to emphasize how we may exploit glycans as biomarkers and therapeutic targets to advance the field of PCa biology.

N-LINKED GLYCOSYLATION IN PROSTATE CANCER

N-linked glycosylation is a process by which a pre-assembled group of 14 saccharides are co-translationally added to an asparagine (Asn) residue of a protein at a defined motif (Asn-X-Ser/Thr, where X is any amino acid besides proline) and then post-translationally modified in the Golgi apparatus by several glycosyltransferases and glycosidases which can result in a wide variety of unique structures (**Figure 1**) (13). Given the large number of glycosyltransferases/glycosidases that catalyze the addition or release of specific saccharide linkages (13), there is a large degree of structural heterogeneity that may be present in a given cell type. However, in most settings, the abundance of specific *N*-glycan structures is highly consistent in a given tissue type (13) and significant changes in the abundance of specific *N*-glycans is known to occur in cancer (10). This likely offers a survival benefit to cells and is thought to be due to mutations, changes in expression, epigenetic regulation, or posttranslational modifications to involved enzymes in *N*-glycan biosynthetic pathways (10, 11). In this section, we summarize the major reported changes in *N*-linked glycosylation derived from both broad profiling studies as well as targeted studies focusing on changes in glycosylation of select, common PCa biomarkers (PSA, PAP, PSMA). Furthermore, we highlight recent technological advances that have been made in studying the *N*-glycome and potential applications in the area of molecular histology.

Broad Changes in *N*-Glycosylation Associated With PCa

Gleason scoring is currently the most commonly used metric for predicting prognosis in men newly diagnosed with PCa (14). With this system, a pathologist renders a score (1-5) based on the most prevalent growth pattern and the second most prevalent

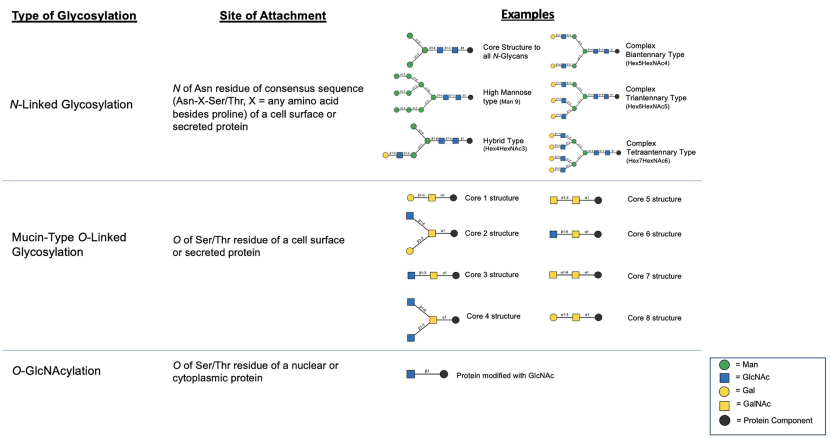

FIGURE 1 | Summary of major classes of glycosylation including examples of structural products resulting from the various mechanisms (12).

growth pattern (1 = well differentiated, 5 = poorly differentiated). The two scores are then added together with the first score listed being the most prevalent pattern (i.e. a score of 3 + 4 = 7 indicates that grade 3 pattern is more prevalent than grade 4). Men with higher Gleason scores (GS ≥ 8) are generally assumed to have a higher chance of disease recurrence followed by metastasis compared to men with lower scores (14). Despite the utility of Gleason scores in stratifying men into different risk groups, the disease course for a specific patient, particularly one with an intermediate score (i.e. GS = 3 + 4 or 4 + 3) can be unpredictable (14, 15). Therefore, many research efforts have been made to discover new biomarkers that can provide prognostic information independent of Gleason score.

Many studies characterized how the *N*-glycosylation profile changes correlate with PCa biology to discover new biomarkers often using the Gleason score system as a metric for disease aggressiveness. Many of these earlier studies, although insightful, did not characterize the glycan structures themselves but instead looked at changes in the levels of glycoproteins. For example, one of the earlier studies utilized OCT-embedded prostate tissues from patients with either non-aggressive PCa (GS = 6 or GS = 7 with no evidence of recurrence in 15 years) or aggressive PCa (GS = 7 with disease recurrence within 6 years or GS ≥ 8) and selected for *N*-glycans using a solid-phase extraction method followed by mass spectrometric (MS) analysis (16). From 350 formerly *N*-linked glycopeptides, 17 appeared to be differentially expressed between aggressive and non-aggressive PCa. In particular, an *N*-glycosite signature associated with aggressive PCa emerged from this approach where the expression of COMP and periostin was found to be increased and the expression of VAP-1 was decreased (16). Expanding on this work, a follow-up study was published by the same group with a larger cohort and wider variety of patient samples (17). Here, *N*-linked glycopeptides were isolated from tissue representing normal prostate (n = 10), non-aggressive PCa (n = 24), aggressive PCa (n = 16), and metastatic PCa (n = 25) and analyzed using SWATH mass spectrometry. In this study, 1430 *N*-glycosites were identified per sample and 220 showed significant quantitative changes associated with PCa progression and metastasis. Two glycoproteins in particular, N-acylethanolamine acid amidase and protein tyrosine kinase 7, were significantly associated with aggressive PCa and further validation in patient tissue showed the two markers to be highly predictive of advanced disease (17).

High throughput profiling of *N*-glycans on human PCa tissue has historically only been performed on small sample sizes, perhaps due to technological limitations and limited tissue resources. In 2014, Powers et al. utilized MALDI-imaging mass spectrometry (MALDI-IMS) to profile glycans directly on human PCa tissue (18). This powerful technology allows detected glycans to be spatially mapped to specific tissue regions. Here, a human PCa tissue block with both tumor and non-tumor regions was analyzed and it was shown that high mannose glycans (Man5-Man9) were particularly evident in the tumor regions compared to adjacent benign and stroma while multiple biantennary non-sialylated glycans were detected primarily in non-tumor regions (18). A recent study utilized MALDI-IMS to profile a tissue microarray containing prostate tumor tissue (n = 108) and benign tissue (n = 30) from 138 patients (19). Here, high mannose glycans were found to be abundant in tumor regions as well as increased tri- and tetraantennary glycans that increased proportionally with tumor grade (19). Furthermore, the triantennary glycan at 2,320 m/z was found to be highly abundant in patients with biochemical recurrence and was correlated with decreased survival by Kaplan-Meier analysis (19). Although not global approaches, several historical studies have utilized human PCa tissue to survey presence or absence of Lewis antigens which are highly associated with malignant transformation (20–24). These studies indicate reduction of the lewis A/B family of antigens in prostatic adenocarcinoma relative to benign prostate but the presence of sialyl lewis X and lewis Y in metastatic cancer. Furthermore, sialyl lewis X was shown to have a strong association with poor prognosis in men who have undergone hormonal therapy (24).

Although tissue studies remain limited, there is an abundance of studies that have profiled *N*-glycan structures from PCa patient serum. In a study comparing the serum from men with benign prostate hyperplasia (BPH) (n = 13) to men with PCa (n = 34), it was found that core-fucosylated biantennary glycans and α2-3 sialic acids were significantly increased in PCa relative to BPH (25). On the other hand, triantennary trigalactosylated glycans and tetraantennary tetrasialylated glycans with outer arm fucose showed a significant decrease compared to BPH (25). An earlier study attempted to profile the glycome in men receiving androgen deprivation therapy (ADT) using MALDI-MS of permethylated glycans released by PNGase F cleavage (26). Compared to healthy men (n = 10), men receiving ADT (n = 24) showed an overall decrease in smaller *N*-glycans and a significant increase in multiantennary glycans. Furthermore, overall fucosylation was increased in the ADT group (26). Interestingly, FUT8, the enzyme solely responsible for mammalian *N*-acetylglucosamine I core fucosylation, was found by another group to result in androgen-independent cell survival when overexpressed, potentially linking *N*-glycosylation to the CRPC phenotype (27). This was found to be associated with up-regulation of EGFR and downstream signaling, suggesting that core fucosylation may result in a "switch" from AR-driven signaling to EGFR-driven signaling in hormone-depleted conditions, allowing increased cell survival.

In a recent study, whole-serum glycome profiling was carried out on 117 PCa patients' serum using ultra-performance liquid chromatography (UPLC) to separate *N*-glycans released from serum glycoproteins (28). Results of this study indicated an increase in hybrid, high mannose, and biantennary digalactosylated monosialylated glycans (M5AG1S1, M8, and A2G2S1) with a decrease in triantennary trigalactosylated trisialylated glycans with and without core fucose (A3G3S3 and FA3G3S3) with PCa progression from indolent through significant/aggressive disease (28). Although insightful, none of the patients in the study received hormonal therapy and were categorized using Epstein's criteria post-prostatectomy. Another recent study examined serum *N*-glycans by glycoblotting from healthy volunteers (n = 80), BPH (n= 286), early-stage PCa (n = 258), PCa being treated with ADT (n = 46), and CRPC

(n = 68) (29). Similar to the results obtained by Kyselova et al. (26), this study found elevated levels of tri and tetra antennary glycans in CRPC serum and found this to also be predictive of developing CRPC in the ADT group (29). Collectively, the results of these studies suggest that increased branching of *N*-glycans may be an important mechanism for CRPC and is deserving of further study. However, it is important to note that the serum *N*-glycome does not necessarily indicate the glycans are derived directly from the prostate as this could be due to an effect on other tissue-types as a result of hormonal therapy. Further studies will be needed to elucidate whether these *N*-glycans are indeed prostate-derived.

Expressed prostatic secretions (EPS) and urine are also important sources of glycoconjugates (11). In addition to several proteomic studies that have shown an abundance of *N*- and *O*-linked glycoproteins in EPS (30–32), direct *N*-glycan analysis was performed on EPS-urine derived from men with negative biopsy (n = 10), low grade PCa (n = 10), and high grade PCa (n = 10) (33). Men were classified as having low versus high grade PCa by GS, where GS = 6 was considered low grade and GS = 8-10 was considered high grade. The most common glycan species detected in all samples was the biantennary complex glycan, NeuAc2Gal2N2M3N2, with and without core fucose, which is the most common glycan species found on PSA (**Figure 2**) (33). A global decrease in tri- and tetra-antennary glycans and an increase in bisecting *N*-acetylglucosamine was found to be correlated with disease severity. Interestingly, structures with bisecting *N*-acetylglucosamine prevent branching and therefore, metastasis, so their increased presence in EPS derived from high grade PCa is counterintuitive to what is currently reported in the literature (33).

As all these studies were performed on different sources (tissue, serum, EPS, EPS-urine), it is difficult to make definitive conclusions at the present time as to how *N*-glycosylation changes as PCa progresses. However, general trends observed from these collective studies suggest an increase in complex and high mannose *N*-glycans in PCa relative to benign prostate. In addition, increased branching may occur with disease progression and may be associated with CRPC. Furthermore, increased α2-3 sialylation as well as core fucosylation appear to be highly associated with PCa and the sialyl lewis X and lewis Y antigens appear correlated with metastatic disease.

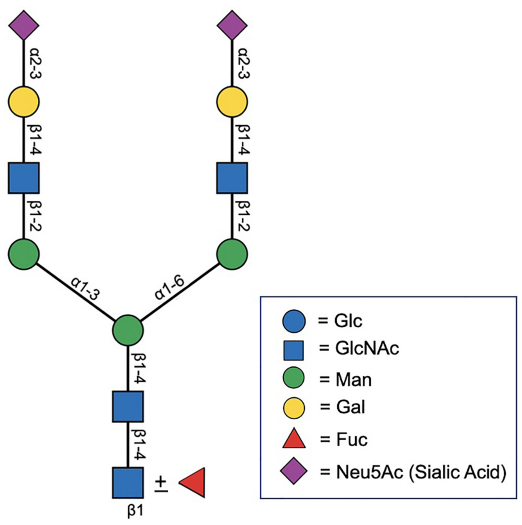

FIGURE 2 | Biantenarry *N*-glycan consisting of two terminally sialyted lactosamine groups with and without core fucose, representative of the most common glycoform found on PSA (12).

N-Glycosylation Changes of Common, PCa Markers

I. PSA

The most common screening test for PCa is serum PSA where levels > 4 ng/mL are considered to be abnormal (14). Although serum concentrations higher than 10 ng/mL are highly specific for PCa, most men with abnormal results are found to have only mild elevations on initial screening (i.e. 4-10 ng/mL) where only ~25% of men will be confirmed to have cancer on biopsy (14, 15). Furthermore, PSA levels alone cannot distinguish which tumors are favored to remain indolent versus progress to metastasis, often resulting in unnecessary treatment for men with cancer that would otherwise not affect quality of life or shorten life span (14, 15). Despite its limitations, PSA remains the most commonly used clinical test for PCa screening and monitoring treatment response (14). Importantly, PSA has a confirmed single site for *N*-glycosylation (Asn-69) and changes in this glycan structure is strongly associated with and quite specific for PCa (34).

Earlier studies have characterized the major *N*-glycan on PSA as a biantennary, disialylated structure of the *N*-acetylglucosamine type (**Figure 2**) (35). A subsequent study by a different group analyzed two isoforms of PSA derived from the seminal plasma of healthy donors (PSA-A and PSA-B) and found that both isoforms had mono- and biantennary *N*-glycans and found a prevalence of 3 outer chain moieties (Galβ1-4GlcNAcβ1-, GlcNAcβ1-, GalNAcβ1-4GlcNAcβ1-) (36). Interestingly, the GalNAcβ1-4GlcNAcβ1- linkage is only found on a limited number of glycoproteins and has been proposed by other authors to potentially have an immunosuppressive effect (37, 38). Another earlier study profiled the *N*-glycan signature on PSA present in the LNCaP cell line, which is derived from a patient with metastatic PCa without prior hormonal therapy (39). In this setting, triantennary structures were present and there was an observed overall decreased in sialic acid content and increase in fucosylation and *N*-acetylglucosamine (39). As PSA can be present in its free form (free-PSA) or complexed to alpha-1-antichymotrypsin (complexed PSA) (40), researchers have attempted to compare the *N*-glycans in these different molecular contexts in PCa (41, 42). Results of these studies showed no significant difference in the glycosylation profiles between free and complexed PSA and there was a high prevalence of fucosylated biantennary structures. High levels of sialylation was observed in the samples with a significant fraction found to be α2-3 linked. Although informative, most of these older studies were done on very small patient cohorts.

In 2009, White et al. utilized thiophilic absorption chromatography to enrich for PSA and prostate acid phosphatase (PAP) in seminal plasma followed by purification of each protein by SDS-PAGE (43). The seminal plasma used was derived from men with no disease (n = 65), BPH (n = 59), and PCa (n = 92). Following analysis by HPLC and MALDI-TOF, 40 glycoforms of PSA were discovered (21 for PAP) and these structures ranged from complex bi- and tetraantennary structures to hybrid and high mannose forms (43). Given the degree of variability, the authors were unable to determine disease-specific patterns and suggested that the use of pooled samples for analysis was a limiting factor in the experimental design (43). In 2016, Llop et al. utilized lectin-based assays to analyze the core fucosylation and sialylation of *N*-glycans on serum-derived PSA from men with BPH (n = 29) and PCa (n = 44) (44). Here, a significant increase in core fucose and α2-3 sialic acid PSA was found in patients with PCa. Furthermore, a cut-off value of 0.86 of the PSA core fucose ratio could distinguish between high-risk PCa (GS ≥ 8) and BPH with 90% sensitivity and 95% specificity (44). In the case of α2-3 sialic acid percentage of PSA, the cut off value of 30% distinguished between high risk PCa and the group of BPH, low risk PCa (GS ≤ 6, tPSA < 10 ng/mL, clinical stage ≤ pT2a), and intermediate risk PCa (GS = 6 with tPSA ≥ 10 ng/mL or clinical stage ≥ pT2a or GS = 7) with a sensitivity of 85.7% and specificity of 95.5% (44). The utility of α2-3 sialic acid PSA in discriminating high-risk PCa from benign or low-risk disease has been confirmed in subsequent studies and shows significant promise as a parameter for stratifying which patients require treatment and which are favored to have an indolent course (45, 46).

II. PAP

PAP is a 50 kDa glycoprotein which was one of the earliest biomarkers used for PCa screening before being replaced by the PSA test. In 1997, it was declared no longer clinically useful due to its lower sensitivity for detecting cancer (47%) compared to PSA (96%) (47). However, as PAP has three *N*-glycosylation sites (Asn-62, Asn-301, and Asn-188) (43, 48), there was significant interest in determining whether certain structural changes to glycans could improve sensitivity and specificity for PCa.

Asn-62 and Asn-301 have been historically characterized by X-ray crystallography as having primarily high mannose structures while Asn-188 had complex structures (48). An earlier study utilized lectin affinity chromatography to compare the *N*-glycans on PAP purified from homogenized human PCa tissue (n = 5) and BPH (n = 5) (49). Here, it was found that PCa-derived PAP had decreased high mannose structures compared to BPH with an increase in nonfucosylated hybrid structures (49). In the previously mentioned cohort studied by White et al. (43) utilizing thiophilic absorption chromatography for PSA and PAP enrichment, it was found that PAP contained 21 glycoforms. This study confirmed the presence of high mannose structures at Asn-301; however, Asn-62 was defined as having mostly sialylated complex bi and tri-antennary structures (43). Asn-188 was less characterized in this study but was thought to have a tetra-antennary structure with sialic acid and fucose content (43). A study in 2013 which analyzed expressed prostatic secretions representing different stages of prostate cancer further confirmed the presence of high mannose structures at Asn-301 with bi and tri-antennary structures present at Asn-62 and Asn-188 (33). The authors further suggested that increased bisecting *N*-acetylglucosamine, decreased branching, and the presence of Neu5GC on PAP glycans may be correlated with disease severity (33).

The cumulative studies that have examined the *N*-glycosylation status of PAP suggests that a combination of high mannose, bi, and tri-antennary structures are present between the 3 sites. Decreased branching and increased bisecting *N*-acetylglucosamine of these glycans may be associated with disease progression. Furthermore, the presence of Neu5GC on Asn-301 is significant as this sialic acid is only synthesized by non-humans due to irreversible mutation of the *CMAH* gene (50, 51). Therefore, if present on human cells, it is assumed to be obtained through dietary means and is considered immunogenic (50, 51). As PAP is highest in prostate tissue (52), this finding is deserving of further study to determine whether Neu5GC may be a target in PCa.

III. PSMA

Prostate-specific membrane antigen (PSMA) is a type II membrane glycoprotein (100-120 kDa) that is expressed highly in PCa and correlates with aggressiveness (53). In recent years, PSMA has received significant attention due to its important role in PCa imaging and therapy (53, 54). Despite its name, the protein is also expressed in other cell types where its enzymatic functions as a folate hydrolase and NAALADase have been widely characterized (55). In PCa, its exact function remains unclear but it is thought to be negatively regulated by androgens and has become a useful marker for hormone-refractory carcinomas and for the detection of metastases (56). Studies show that PSMA has 10 *N*-glycosylation sites, three of which are in the catalytic domain (Asn 336, Asn 459, and Asn 476) and it is predicted that 20-25% of the total molecular weight is due to carbohydrates (56). Despite having a high level of *N*-glycosylation, there are surprisingly very few studies have attempted to elucidate the specific glycan structures present on PSMA and how they are altered with disease progression. An early study used a series of exo and endoglycosidases, which target different glycan moieties, to determine what types of structures are present in LNCaP cells, patient tumor tissue lysate, and serum (57). Here, complex type glycans lacking polylactosamine were observed on PSMA derived from tissue and serum while primarily high mannose forms were observed in the LNCaP setting (57). The authors stated this discrepancy is likely due to a defect in one of the *N*-glycan biosynthetic steps where LNCaP cells are unable to convert the high mannose forms to the complex type that is observed *in vivo* (57).

Barinka et al. studied the enzymatic activity of PSMA as a consequence of glycosylation by mutating different *N*-glycosylation sites on the protein (58). The results of this study showed that mutations at Asn-76 (N76A), Asn-336 (N336A), and Asn-459 (N459A) caused an increase in activity exceeding 50% of the wild-type (58). Interestingly, Asn-336 and Asn-459

are within the catalytic domain and it was hypothesized these mutations would cause the opposite effect. For mutations at Asn-121 (N121A), Asn-140 (N140A), Asn-153 (N153A), Asn-195 (N195A), and Asn-638 (N638A), the exopeptidase activity was markedly compromised (58). In particular, N121A, N195A, and N638A caused nearly complete inactivity (58). Collectively, these studies show that PSMA is highly glycosylated and that *N*-glycosylation, particularly at distal sites, is critical to the function of the protein. Further studies are needed to characterize the specific glycan structures and what changes occur as disease progresses.

Advances in Studying *N*-Glycopathology

Historical studies that have characterized glycosylation changes associated with disease primarily relied on chemical reactions with monosaccharide constituents, metabolic labeling of glycoconjugates with radioactive sugars to help elucidate glycan composition, as well as lectin-based assays to characterize specific structural features of glycans [for a complete review of tools used for characterizing glycans, refer to Chapter 50 of (13)]. Although these methods have proven quite useful, most of these studies are unable to characterize the entire glycan species present which has caused slow progress in defining changes to carbohydrates that occur with disease progression. Many modern studies have utilized solid phase extraction techniques/chromatography to isolate N-glycans from total protein lysates and this has allowed specific glycans to be determined in various tissue homogenates. However, as many glycans are secreted into the extracellular matrix or stroma, spatial information is lost and whether or not a specific glycan is located within the tumor or stroma becomes a significant limiting factor in the interpretation of the data. The Drake lab, in collaboration with Anand Mehta, has developed an Imaging mass spectrometry (MALDI-IMS) technique for profiling N-glycans directly on formalin-fixed, paraffin-embedded (FFPE) tissue, which has been further applied to many disease settings including PCa (18, 59). The approach involves spraying a molecular coating of PNGase-F directly on the tissue to release the N-glycans. The reaction takes place in a humidified chamber so that there is little diffusion. Following the application of enzyme, chemical matrix is applied and glycans are analyzed by MALDI at each discrete tissue location in a rastered-grid format. Glycan abundances at each tissue location is then determined and visualized using intensity maps (similar to heat maps). This powerful technology adds significant advance to the fields of glycobiology and molecular histology and since it can be applied to formats such as tissue microarray, has the ability to profile the glycans across large patient cohorts.

MUCIN-TYPE *O*-LINKED GLYCOSYLATION AND PROSTATE CANCER PROGRESSION

Mucin-Type *O*-linked glycosylation is a post-translational process occurring in the Golgi apparatus where a GalNAc is added to the Ser/Thr residue of a protein followed by the step-wise addition of individual monosaccharides (13). The glycans resulting from this process, which may contain any of 8 core structures (**Figure 1**), are found on cell-surface and secreted proteins and are particularly prevalent on mucins which are further described subsequently. Unlike *N*-linked glycosylation, there is no pre-formed precursor and a consensus site has yet to be determined although predictive algorithms exist (13). There have been few historical studies that have attempted to characterize the *O*-glycome in PCa due to the high number of possible *O*-glycan modifications which remains incompletely characterized (60). However, due to advances in glycoproteomics in recent years, newer studies are emerging which provide insight into how mucin-type *O*-glycosylation is altered with PCa progression.

Broad Changes to Mucin-Type *O*-Glycosylation in PCa Progression

Studies attempting to characterize global changes to the mucin-type *O*-glycome as a function of PCa disease severity are currently very limited. In 2014, Chen et al. demonstrated that PCa has elevated levels of GCNT1, an enzyme catalyzing the formation of core-2 *O*-glycans (61). It was further shown that its increased expression was associated with increased levels of core-2 O-linked sialyl lewis X structures on PSA, MUC1, and PAP (61). Although the pathological significance of this structure on these proteins remains unknown, its presence was able to differentiate PCa from benign tissue with improved specificity compared to protein level alone (61). Interestingly, a subsequent study demonstrated that GCNT1-positive tumors were highly associated with extracapsular extension and that its detection in urine post digital rectal examination was an independent risk factor for biochemical recurrence (62). Future work is needed to determine the full utility of GCNT1 as a screening tool in predicting which tumors are favored to remain indolent versus metastasize as well as mechanisms as to how GCNT1 and its product contribute to PCa progression.

A recent study utilized surgically removed PCa tissue representing different histological grades (Grade 1-5, n = 10 cases per grade) as well as tissue from patients diagnosed with BPH (n = 5) (63). Here, 17 structures covering 13 compositions were observed and Core-1 and -2 structures were predominant across all samples (63). A significant reduction in sialylated core-1 and an increase in sialylated core-2 structures were observed as PCa progresses. Correlation analysis between the *O*-glycome and *O*-glycoproteome further revealed that the sialylated core-2 structure found to be elevated as PCa progressed was highly correlated with collagen IV and the glycoform was confidently identified at T1627 across all 54 replicates (63). Interestingly, Core-2 structures have been linked to evasion of natural killer (NK) cell immunity in the context of PCa which is deserving of further study (64).

Truncated *O*-glycans, such as Tn or sTn antigen, are commonly found in many tumor settings and linked to poor prognosis (10, 65–67). Furthermore, these carbohydrates are immunoreactive and several agents have been developed for therapeutic targeting (65). In PCa, there is conflicting data regarding the prevalence of these antigens. However, it is has

been reported that 4-26% of adenocarcinomas are positive for the Tn antigen and therefore, may qualify for Tn-targeted therapy (68). Interestingly, studies have shown that ST6GalNAC1, the enzyme that catalyzes the formation of sTn, is a direct and rapidly activated target gene of AR and transforms the cells to a more mesenchymal phenotype (69). Further studies are ultimately needed to determine the true prevalence of truncated *O*-glycans in PCa of different stages as well as the functional significance of their presence.

Mucins

Mucins are cell-surface or secreted glycoproteins containing clusters of *O*-glycans (13). They can be antiadhesive and repel cell-surface interactions or promote adhesion by recognizing glycan binding proteins *via* their *O*-GalNAc glycans (13). Furthermore, they are known to have multiple effects on the immune system and maintain cellular homeostasis through various signaling mechanisms (13). In 2005, Cozzi et al. characterized the expression of MUC1, MUC2, MUC4, MUC5AC, and MUC6 using tissue microarray (TMA) from 120 paraffin-embedded specimens derived from patients who underwent radical prostatectomy or transurethral resection of the prostate (TURP) (70). The cases included both non-metastatic primary PCa as well as 10 matched lymph node metastases. Here, MUC1 overexpression was found in 58% of primary PCa and 90% of lymph node metastases but not in normal adult or benign tissues (70). In addition, 86% of MUC1-positive tumors had GS scores > 7 (70). In another study, 57 biopsy specimens from PCa patients treated with hormone therapy as well as 10 normal cases were collected and stained for sialyl-Tn MUC-1 (71). Here, it was found that the level of sialyl-Tn MUC1 significantly correlated with progression-free and cause-specific survival and may predict prognosis for patients undergoing hormonal therapy (71).

Recently, Yasumizu et al. has shown that up-regulation of MUC1-C in hormone-sensitive PCa cells suppresses AR and induces neuroendocrine (NE) differentiation through up-regulation of the neural BRN2 transcription factor and suppression of the p53 pathway (72). Furthermore, another study has shown that MUC1-C directly binds to E2F1 resulting in activation of the BAF pathway and increased cancer stem cell (CSC) renewal in NE prostate cancer (NEPC) (73). These results only highlight the important role that *O*-glycans have in disease progression and the critical need for therapeutic targeting.

O-GlcNAcylation

The *O*-GlcNAc modification occurs in the nuclear and cytoplasmic compartments of the cell and does not elongate to form complex structures such as what is observed in other forms of glycosylation (13). Elevated levels of UDP-GlcNAc, derived from the hexosamine biosynthesis pathway (HBP), drive *O*-GlcNAcylation through activation of the enzyme, OGT (13, 74). Similar to phosphorylation, the residue is attached and removed several times in the lifetime of a polypeptide and the process is known to have significant effects on cellular processes such as transcription, signaling, and epigenetics (13, 75).

In 2014, Gu et al. performed immunostaining for *O*-GlcNAc on several PCa tissues (n = 55) as well as adjacent benign (n = 10) and BPH (n = 19) (76). Here, it was observed that *O*-GlcNAcylation was significantly increased in PCa tissue relative to benign disease (76). Furthermore, levels of *O*-GlcNAc are found to positively correlate with GS and be associated with reduced patient survival (77). Levels of OGT have been similarly found to be overexpressed in PCa and correlated with GS (78). Furthermore, its activity has been shown to be critical to c-MYC stability and MYC-driven proliferation of PCa cells (79). In addition to the effects on c-MYC, inhibition of OGT has been linked to decreased glucose consumption, decreased lactate secretion, and has been shown to lead to suppression of CDK1, whose expression predicts PCa recurrence (80). Effectively targeting aberrant *O*-GlcNAcylation through OGT inhibition may represent a good therapeutic strategy for targeting PCa cells. However, as *O*-GlcNAcylation is a critical process to every cell type, selectivity remains a limiting factor.

GALECTINS

Galectins are among the most widely expressed lectins in all organisms, typically recognizing β-galactose containing glycoconjugates (13). They have been reported to have a wide variety of biological functions including regulation of immune response, microbial recognition, as well as roles in development (13). Importantly, they are known to have roles in cancer progression and metastasis, likely through modulation of interactions between tumor cells and the surrounding microenvironment (endothelial cells, stromal cells, and immune cells) (81). In PCa, galectin-1 (Gal-1) was found to be the most abundant galectin expressed in PCa tissue with marked up-regulation as the disease progresses to CRPC (82). Interestingly, all other galectins were found to be expressed at lower levels with Gal-3, Gal-4, Gal-9, and Gal-12 becoming downregulated with disease evolution and Gal-8 remaining unchanged (82). Furthermore, Gal-1 has been shown to be highly associated with angiogenesis and use of an allosteric inhibitor (LLS30) resulted in significant growth inhibitory effects in human CRPC xenograft models (83).

In a study that examined galectin-3 (Gal-3) expression by tissue microarray constructed from 83 patients who underwent prostatectomy (83 tumor, 78 adjacent benign, and 75 benign tissues), it was shown that Gal-3 expression was significantly decreased in tumor tissue compared to benign (84). However, despite decreased expression, Gal-3 staining in tumor specimens was able to predict biochemical recurrence (PSA ≥ 0.2 ng/mL) with 91.3% sensitivity and 75% specificity, potentially implicating it as a prognostic marker (84). In 2018, Gao et al. determined that cleaved Gal-3, rather than intact Gal-3 (detected by older studies), is present in PCa tissue but completely absent in benign (85). Furthermore, cleaved Gal-3 was positively

associated with tumor progression and metastasis and its expression was closely related to PSA level (85). In addition, previous studies have shown that cleaved Gal-3 was crucial to bone remodeling in the metastatic niche implicating it as a potential therapeutic target for men with metastatic disease (86). Future studies are needed to further determine the pathological significance of cleaved Gal-3 and whether therapeutic targeting could be beneficial.

The role of other galectins in PCa progression remains controversial. Although Gal-4 was reported previously to have decreased expression with PCa progression (82), some authors have found that expression of both Gal-4 and C1GALT1 together predicts poor overall survival (87). Furthermore, Gal-4 was found to interact with C1GALT1-dependent *O*-glycans resulting in castration resistance through activation of receptor tyrosine kinase signaling and SOX9 (88). Gal-8, which remains stably expressed throughout PCa development and progression, was shown to contribute to metastasis through rearrangement of the cytoskeleton and modulation of E-Cadherin expression (89). Future studies are ultimately needed to determine the therapeutic benefit of targeting galectins in the context of PCa in relation to effects on patient survival as well as the toxicity of such an approach.

GLYCOCONJUGATES

Glycoconjugates are carbohydrates that are covalently linked to other biological molecules, such as proteins (glycoproteins) and lipids (glycolipids) (13). These molecules make up the majority of the cell surface (termed the "glycocalyx") and have significant effects on regulating cell-cell interactions, interactions with the extracellular matrix, as well as intracellular signaling to control a wide-variety of cellular functions (13). In this section, major studies are summarized that highlight the functional consequences of glycoconjugate expression in the context of PCa, both as potential tumor drivers and also tumor suppressors.

Proteoglycans

Proteoglycans are heavily glycosylated proteins, consisting of both a core protein and one or more glycosaminoglycan (GAG) chains, such as heparan sulfate, chondroitin sulfate, or dermatan sulfate (13). They can be located on the cell-surface or secreted into the extracellular matrix and have significant contributions to intracellular signaling and cell-cell interactions (13). Due to these functions, they have a high degree of control over proliferation and apoptosis and have been implicated in many tumor settings including PCa. For example, an earlier study showed that the CSPG, versican, was superior to tumor grade in predicting progression in patients with early stage PCa (90). Furthermore, the anti-adhesive properties of versican were observed to cause PCa cells to lose attachment to fibronectin, a major component of the stroma, which can increase the metastatic potential of cells (91). Subsequent studies have shown that versican contains AR-response elements and is positively regulated by AR, suggesting this may be a critical downstream mediator of AR-driven signaling (92). Biglycan, a proteoglycan of the extracellular matrix, was found to be expressed in 78% of 11,070 PCa tumors and was linked to the presence of TMPRSS2:ERG fusion and PTEN deletion (93). In addition, although not functionally proven, its expression was strongly linked to AR levels suggesting androgen regulation (93). Perlecan, a basement-membrane specific HSPG, has been shown to be up-regulated in PCa, positively correlating with Gleason score and Ki67 indices (94). Furthermore, its effects have been shown to be due to its ability to regulate sonic hedgehog (HH) signaling, which was found to occur independently of androgen (94). Other studies have shown that the HSPG, Syndecan-1, is an independent predictor of poor survival (95, 96), associated with the epithelial to mesenchymal transmission (97), and may be associated with resistance to docetaxel chemotherapy (98).

In addition to promoting tumor growth in certain settings, several proteoglycans have been reported as tumor suppressors. Glypican-5, a member of the HSPG family, was shown to be lowly expressed in PCa cell lines and its overexpression significantly inhibited cell proliferation and invasion through inhibition of EMT and Wnt/β-catenin signaling (99). Glypican-1 was shown by Quach et al. to suppress proliferation in DU-145 cells but promote it in PC-3 cells (100). Interestingly, when PC-3 was either grown *in vivo* or co-cultured with stromal cells, Glypican-1 was found to prevent tumor growth suggesting a cell-dependent role as well as highlighting the importance of the tumor environment in affecting the activity of proteoglycans (100). In addition to glypicans 1 and 5, decorin has been observed to be negatively associated with PCa (90, 101) and was shown to suppress tumor growth through inhibition of EGFR and AR phosphorylation, leading to inhibition of PI3K/AKT, a critical pathway in PCa (102). Lumican, a small leucine-rich proteoglycan of the extracellular matrix, has also been shown to inhibit PCa progression when present in the reactive stroma, potentially implicating it as a positive prognostic marker (103). Overall, the roles that various proteoglycans have on PCa progression is extremely complex and is significantly influenced by the tumor microenvironment. A combination of both *in vitro* and high quality *in vivo* models are needed to fully understand the role specific proteoglycans have in the evolution of PCa.

Glycosphingolipids

Glycosphingolipids (GSLs) are the major class of glycolipids found in animals (13). They consist of a hydrophobic ceramide backbone linked to a hydrophilic carbohydrate moiety and are responsible for maintaining the stability of cell membranes as well as regulating numerous cellular processes (proliferation, apoptosis, cell-cell-adhesion, migration, etc) (13, 104). An earlier study extracted the glycolipids from human prostate tissue surgically derived from six patients with BPH (105). Here, abundant neutral mono- to tetraglycosylceramides were obtained in addition to mono and disialylgangliosides (105). In a 2004 study, three AR-negative cell lines (PC-3, DU-145, and HH870) and two AR-positive cell lines (LNCaP-FGC, LNCaP-FGC 10) were used to characterize the gangliosides on both 2-D

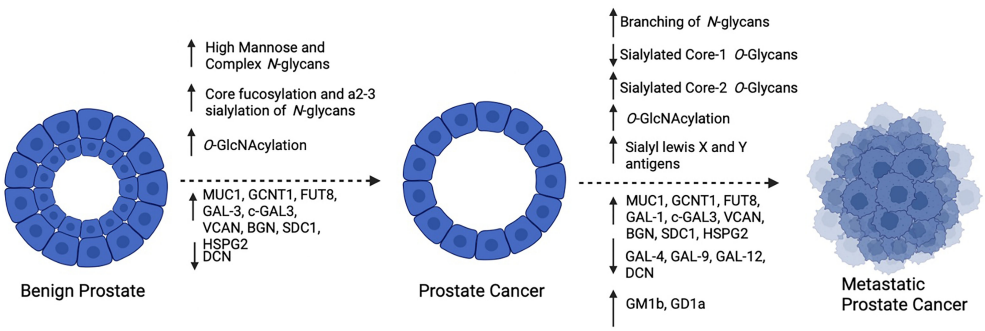

FIGURE 3 | Summary of reported changes in glycosylation as PCa progresses: As PCa develops, high mannose and complex biantennary *N*-glycans become prevalent, with frequent core fucosylation and a2-3 sialylation of complex forms, Furthermore, increased *O*-GlcNAcylation and altered expression of glycosyltransferases, glycoconjugates and galectins occurs. As PCa becomes metastatic, increased branching of *N*-Glycans and alterations in *O*-Glycans occurs with frequent expression of sialyl lewis X and Y antigens. In addition to changes in glycosyltransferases, glycoconjugates and galectin expression, glycolipids GM1b and GD1a have been reported to be increased. Created with BioRender.com.

chromatograms as well as by confocal fluorescent microscopy (106). It was found that AR-negative cells expressed higher levels of GM1b and GD1a relative to AR-positive cells. Furthermore, O-AcGD2 was specific to the AR-negative cell lines, PC-3 and HH870 (106). A follow-up study profiled the IgM responses to 8 gangliosides (GM3, GM2, GD3, GD2, GD1a, GM1a, GD1b, GT1b) in the sera of patients with BPH (n = 11), organ-confined PCa (T1/T2, n = 36), PCa with extra-prostatic extension (T3/T4, n = 27), and age-matched healthy controls (n = 11) (107). Patients with PCa showed increased titers against GD1a and decreased titers against GD3 (107). Interestingly, patients with organ-confined PCa showed increased titers against GD1a relative to unconfined PCa despite the previous study showing cell lines with more advanced phenotype (PC-3, DU-145, and HH870) showing elevated levels of the ganglioside. The authors conclude this may be due to B cells recognizing tumor-derived GD1a as a "danger signal", producing IgM to target GD1a-positive cells, contributing to the decline in GD1a as disease progresses (107). The specific role of GD1a in PCa remains unknown; however, its expression has been suggested to be controlled indirectly by NF-κB through transcriptional regulation of ST3GalI, II, and III, which are critical to its biosynthesis (108).

CONCLUSIONS AND PERSPECTIVES

It is well accepted that aberrant glycosylation is a hallmark of cancer and has a significant effect on tumor progression. As the prostate is a major producer of glycoproteins, it is not surprising that several structural changes to glycans and changes in the expression of glycoconjugates are observed throughout the evolution of PCa (**Figure 3**) and that these appear to be critical to disease progression. Furthermore, as shown by Munkley et al. (109), several enzymes involved in the synthesis and degradation of glycans are directly regulated by androgen stimulation, suggesting that downstream glycosylation is very likely an important mediator of PCa activity deserving of further study. Due to technological limitations, as well as small sample sizes used for glycan profiling in many of these studies, progress in defining changes to the PCa tumor glycome has been slow. There are many unanswered questions in the field of PCa including how to predict which patients will have indolent versus aggressive disease, why hormonally-treated tumors become resistant to therapy, how NE differentiation occurs, and why PCa tumors can evade immunosurveillance. Despite a surge in RNA-sequencing and proteomic studies that have included large cohorts of men with PCa in different disease stages, these questions remain unanswered and many of the molecular drivers that are discovered in these studies are "un-druggable". Therefore, there is a need to survey other molecular changes that occur as PCa progresses in addition to the products of gene expression. With greater realization of the contribution of carbohydrates to disease, the development of glycan-targeted therapy has become a high area of interest in the pharmaceutical community (110). These agents includes antibodies, enzyme inhibitors, as well as compounds that can disrupt glycan-protein interactions. In the field of PCa, it is of critical importance to thoroughly define the PCa glycome in different disease stages so that as these agents become widely available, they can be applied to patients with advanced PCa. A deeper understanding as to how glycosylation changes as PCa progresses may shed light on some of the major unanswered questions in the field and provide more opportunities for therapeutic intervention ultimately improving patient survival.

AUTHOR CONTRIBUTIONS

WB wrote the manuscript. JH supervised WB and edited the manuscript. All authors contributed to the article and approved the submitted version.

REFERENCES

1. Miller KD, Nogueira L, Mariotto AB, Rowland JH, Yabroff KR, Alfano CM, et al. Cancer Treatment and Survivorship Statistics, *2019*. *CA Cancer J Clin* (2019) 69(5):363–85. doi: 10.3322/caac.21565
2. Hussain A, Dawson N. Management of Advanced/Metastatic Prostate Cancer: 2000 Update. *Oncol (Williston Park)* (2000) 14(12):1677–88; discussion 1688, 1691-4.
3. Barry MJ, Nelson JB. Patients Present With More Advanced Prostate Cancer Since the USPSTF Screening Recommendations. *J Urol* (2015) 194(6):1534–6. doi: 10.1016/j.juro.2015.09.033
4. Culig Z, Santer FR. Androgen Receptor Signaling in Prostate Cancer. *Cancer Metastasis Rev* (2014) 33(2-3):413–27. doi: 10.1007/s10555-013-9474-0
5. Teo MY, Rathkopf DE, Kantoff P. Treatment of Advanced Prostate Cancer. *Annu Rev Med* (2019) 70:479–99. doi: 10.1146/annurev-med-051517-011947
6. Sinha A, Huang V, Livingstone J, Wang J, Fox NS, Kurganovs N, et al. The Proteogenomic Landscape of Curable Prostate Cancer. *Cancer Cell* (2019) 35(3):414–427 e6. doi: 10.1016/j.ccell.2019.02.005
7. Pritchard CC, Mateo J, Walsh MF, De Sarkar N, Abida W, Beltran H, et al. Inherited DNA-Repair Gene Mutations in Men With Metastatic Prostate Cancer. *N Engl J Med* (2016) 375(5):443–53. doi: 10.1056/NEJMoa1603144
8. Robinson D, Van Allen EM, Wu YM, Schultz N, Lonigro RJ, Mosquera JM, et al. Integrative Clinical Genomics of Advanced Prostate Cancer. *Cell* (2015) 161(5):1215–28. doi: 10.1016/j.cell.2015.05.001
9. Chen S, Zhu G, Yang Y, Wang F, Xiao YT, Zhang N, et al. Single-Cell Analysis Reveals Transcriptomic Remodellings in Distinct Cell Types That Contribute to Human Prostate Cancer Progression. *Nat Cell Biol* (2021) 23 (1):87–98. doi: 10.1038/s41556-020-00613-6
10. Pinho SS, Reis CA. Glycosylation in Cancer: Mechanisms and Clinical Implications. *Nat Rev Cancer* (2015) 15(9):540–55. doi: 10.1038/nrc3982
11. Drake RR, Jones EE, Powers TW, Nyalwidhe JO. Altered Glycosylation in Prostate Cancer. *Adv Cancer Res* (2015) 126:345–82. doi: 10.1016/bs.acr.2014.12.001
12. Mehta AY, Cummings RD. GlycoGlyph: A Glycan Visualizing, Drawing and Naming Application. *Bioinformatics* (2020) 36(11):3613–4.
13. Varki A, Cummings RD, Esko J, Stanley P, Hart GW, Aebi M, et al., editors *In Essentials of Glycobiology*. Cold Spring Harbor, NY: Cold Spring Harbor Laboratory Press (2015).
14. Schatten H. Brief Overview of Prostate Cancer Statistics, Grading, Diagnosis and Treatment Strategies. *Adv Exp Med Biol* (2018) 1095:1–14. doi: 10.1007/978-3-319-95693-0_1
15. Sehn JK. Prostate Cancer Pathology: Recent Updates and Controversies. *Mo Med* (2018) 115(2):151–5.
16. Chen J, Xi J, Tian Y, Bova GS, Zhang H. Identification, Prioritization, and Evaluation of Glycoproteins for Aggressive Prostate Cancer Using Quantitative Glycoproteomics and Antibody-Based Assays on Tissue Specimens. *Proteomics* (2013) 13(15):2268–77. doi: 10.1002/pmic.201200541
17. Liu Y, Chen J, Sethi A, Li QK, Chen L, Collins B, et al. Glycoproteomic Analysis of Prostate Cancer Tissues by SWATH Mass Spectrometry Discovers N-Acylethanolamine Acid Amidase and Protein Tyrosine Kinase 7 as Signatures for Tumor Aggressiveness. *Mol Cell Proteomics* (2014) 13(7):1753–68. doi: 10.1074/mcp.M114.038273
18. Powers TW, Neely BA, Shao Y, Tang H, Troyer DA, Mehta AS, et al. MALDI Imaging Mass Spectrometry Profiling of N-Glycans in Formalin-Fixed Paraffin Embedded Clinical Tissue Blocks and Tissue Microarrays. *PloS One* (2014) 9(9):e106255. doi: 10.1371/journal.pone.0106255
19. Conroy LR, Stanback AE, Young LEA, Clarke HA, Austin GL, Liu J, et al. In Situ Analysis of N-Linked Glycans as Potential Biomarkers of Clinical Course in Human Prostate Cancer. *Mol Cancer Res* (2021) 19(10):1727–38. doi: 10.1158/1541-7786.MCR-20-0967
20. Jørgensen T, Berner A, Kaalhus O, Tveter KJ, Danielsen HE, Bryne M. Up-Regulation of the Oligosaccharide Sialyl LewisX: A New Prognostic Parameter in Metastatic Prostate Cancer. *Cancer Res* (1995) 55(9):1817–9.
21. Culig Z, Hittmair A, Hobisch A, Bartsch G, Klocker H, Pai LH, et al. Expression of Lewis Carbohydrate Antigens in Metastatic Lesions From Human Prostatic Carcinoma. *Prostate* (1998) 36(3):162–7. doi: 10.1002/(SICI)1097-0045(19980801)36:3<162::AID-PROS3>3.0.CO;2-J
22. Martensson S, Bigler SA, Brown M, Lange PH, Brawer MK, Hakomori S. Sialyl-Lewis(x) and Related Carbohydrate Antigens in the Prostate. *Hum Pathol* (1995) 26(7):735–9. doi: 10.1016/0046-8177(95)90220-1
23. Walker PD, Karnik S, deKernion JB, Pramberg JC. Cell Surface Blood Group Antigens in Prostatic Carcinoma. *Am J Clin Pathol* (1984) 81(4):503–6. doi: 10.1093/ajcp/81.4.503
24. Young WW Jr, Mills SE, Lippert MC, Ahmed P, Lau SK. Deletion of Antigens of the Lewis a/B Blood Group Family in Human Prostatic Carcinoma. *Am J Pathol* (1988) 131(3):578–86.
25. Saldova R, Fan Y, Fitzpatrick JM, William R, Watson G, Rudd PM. Core Fucosylation and Alpha2-3 Sialylation in Serum N-Glycome Is Significantly Increased in Prostate Cancer Comparing to Benign Prostate Hyperplasia. *Glycobiology* (2011) 21(2):195–205. doi: 10.1093/glycob/cwq147
26. Kyselova Z, Mechref Y, Al Bataineh MM, Dobrolecki LE, Hickey RJ, Vinson J, et al. Alterations in the Serum Glycome Due to Metastatic Prostate Cancer. *J Proteome Res* (2007) 6(5):1822–32. doi: 10.1021/pr060664t
27. Hoti N, Lih TS, Pan J, Zhou Y, Yang G, Deng A, et al. A Comprehensive Analysis of FUT8 Overexpressing Prostate Cancer Cells Reveals the Role of EGFR in Castration Resistance. *Cancers (Basel)* (2020) 12(2). doi: 10.3390/cancers12020468
28. Gilgunn S, Murphy K, Stockmann H, Conroy PJ, Murphy TB, Watson RW, et al. Glycosylation in Indolent, Significant and Aggressive Prostate Cancer by Automated High-Throughput N-Glycan Profiling. *Int J Mol Sci* (2020) 21 (23). doi: 10.3390/ijms21239233
29. Ishibashi Y, Tobisawa Y, Hatakeyama S, Ohashi T, Tanaka M, Narita S, et al. Serum Tri- and Tetra-Antennary N-Glycan Is a Potential Predictive Biomarker for Castration-Resistant Prostate Cancer. *Prostate* (2014) 74 (15):1521–9. doi: 10.1002/pros.22869
30. Drake RR, Elschenbroich S, Lopez-Perez O, Kim Y, Ignatchenko V, Ignatchenko A, et al. In-Depth Proteomic Analyses of Direct Expressed Prostatic Secretions. *J Proteome Res* (2010) 9(5):2109–16. doi: 10.1021/pr1001498
31. Kim Y, Ignatchenko V, Yao CQ, Kalatskaya I, Nyalwidhe JO, Lance RS, et al. Identification of Differentially Expressed Proteins in Direct Expressed Prostatic Secretions of Men With Organ-Confined Versus Extracapsular Prostate Cancer. *Mol Cell Proteomics* (2012) 11(12):1870–84. doi: 10.1074/mcp.M112.017889
32. Principe S, Kim Y, Fontana S, Ignatchenko V, Nyalwidhe JO, Lance RS, et al. Identification of Prostate-Enriched Proteins by In-Depth Proteomic Analyses of Expressed Prostatic Secretions In Urine. *J Proteome Res* (2012) 11(4):2386–96. doi: 10.1021/pr2011236
33. Nyalwidhe JO, Betesh LR, Powers TW, Jones EE, White KY, Burch TC, et al. Increased Bisecting N-Acetylglucosamine and Decreased Branched Chain Glycans of N-Linked Glycoproteins in Expressed Prostatic Secretions Associated With Prostate Cancer Progression. *Proteomics Clin Appl* (2013) 7(9-10):677–89. doi: 10.1002/prca.201200134
34. Stura EA, Muller BH, Bossus M, Michel S, Jolivet-Reynaud C, Ducancel F. Crystal Structure of Human Prostate-Specific Antigen in a Sandwich Antibody Complex. *J Mol Biol* (2011) 414(4):530–44. doi: 10.1016/j.jmb.2011.10.007
35. Belanger A, van Halbeek H, Graves HC, Grandbois K, Stamey TA, Huang L, et al. Molecular Mass and Carbohydrate Structure of Prostate Specific Antigen: Studies for Establishment of an International PSA Standard. *Prostate* (1995) 27(4):187–97. doi: 10.1002/pros.2990270403
36. Okada T, Sato Y, Kobayashi N, Sumida K, Satomura S, Matsuura S, et al. Structural Characteristics of the N-Glycans of Two Isoforms of Prostate-Specific Antigens Purified From Human Seminal Fluid. *Biochim Biophys Acta* (2001) 1525(1-2):149–60. doi: 10.1016/S0304-4165(00)00182-3
37. Dell A, Morris HR, Easton RL, Panico M, Patankar M, Oehniger S, et al. Structural Analysis of the Oligosaccharides Derived From Glycodelin, a Human Glycoprotein With Potent Immunosuppressive and Contraceptive Activities. *J Biol Chem* (1995) 270(41):24116–26. doi: 10.1074/jbc.270.41.24116
38. Nimtz M, Grabenhorst E, Conradt HS, Sanz L, Calvete JJ. Structural Characterization of the Oligosaccharide Chains of Native and Crystallized Boar Seminal Plasma Spermadhesin PSP-I and PSP-II Glycoforms. *Eur J Biochem* (1999) 265(2):703–18. doi: 10.1046/j.1432-1327.1999.00766.x
39. Peracaula R, Tabares G, Royle L, Harvey DJ, Dwek RA, Rudd PM, et al. Altered Glycosylation Pattern Allows the Distinction Between Prostate-

Specific Antigen (PSA) From Normal and Tumor Origins. *Glycobiology* (2003) 13(6):457–70. doi: 10.1093/glycob/cwg041
40. Oesterling JE, Jacobsen SJ, Klee GG, Pettersson K, Piironen T, Abrahamsson PA, et al. Free, Complexed and Total Serum Prostate Specific Antigen: The Establishment of Appropriate Reference Ranges for Their Concentrations and Ratios. *J Urol* (1995) 154(3):1090–5. doi: 10.1016/S0022-5347(01)66984-2
41. Tabares G, Jung K, Reiche J, Stephan C, Lein M, Peracaula R, et al. Free PSA Forms in Prostatic Tissue and Sera of Prostate Cancer Patients: Analysis by 2-DE and Western Blotting of Immunopurified Samples. *Clin Biochem* (2007) 40(5-6):343–50. doi: 10.1016/j.clinbiochem.2006.12.006
42. Tajiri M, Ohyama C, Wada Y. Oligosaccharide Profiles of the Prostate Specific Antigen in Free and Complexed Forms From the Prostate Cancer Patient Serum and in Seminal Plasma: A Glycopeptide Approach. *Glycobiology* (2008) 18(1):2–8. doi: 10.1093/glycob/cwm117
43. White KY, Rodemich L, Nyalwidhe JO, Comunale MA, Clements MA, Lance RS, et al. Glycomic Characterization of Prostate-Specific Antigen and Prostatic Acid Phosphatase in Prostate Cancer and Benign Disease Seminal Plasma Fluids. *J Proteome Res* (2009) 8(2):620–30. doi: 10.1021/pr8007545
44. Llop E, Ferrer-Batalle M, Barrabes S, Guerrero PE, Ramirez M, Saldova R, et al. Improvement of Prostate Cancer Diagnosis by Detecting PSA Glycosylation-Specific Changes. *Theranostics* (2016) 6(8):1190–204. doi: 10.7150/thno.15226
45. Ferrer-Batalle M, Llop E, Ramirez M, Aleixandre RN, Saez M, Comet J, et al. Comparative Study of Blood-Based Biomarkers, Alpha2,3-Sialic Acid PSA and PHI, for High-Risk Prostate Cancer Detection. *Int J Mol Sci* (2017) 18 (4). doi: 10.3390/ijms18040845
46. Ishikawa T, Yoneyama T, Tobisawa Y, Hatakeyama S, Kurosawa T, Nakamura K, et al. An Automated Micro-Total Immunoassay System for Measuring Cancer-Associated Alpha2,3-Linked Sialyl N-Glycan-Carrying Prostate-Specific Antigen May Improve the Accuracy of Prostate Cancer Diagnosis. *Int J Mol Sci* (2017) 18(2). doi: 10.3390/ijms18020470
47. Stamey TA, Yang N, Hay AR, McNeal JE, Freiha FS, Redwine E. Prostate-Specific Antigen as a Serum Marker for Adenocarcinoma of the Prostate. *N Engl J Med* (1987) 317(15):909–16. doi: 10.1056/NEJM198710083171501
48. Jakob CG, Lewinski K, Kuciel R, Ostrowski W, Lebioda L. Crystal Structure of Human Prostatic Acid Phosphatase. *Prostate* (2000) 42(3):211–8. doi: 10.1002/(SICI)1097-0045(20000215)42:3<211::AID-PROS7>3.0.CO;2-U
49. Yoshida KI, Honda M, Arai K, Hosoya Y, Moriguchi H, Sumi S, et al. Serial Lectin Affinity Chromatography With Concavalin A and Wheat Germ Agglutinin Demonstrates Altered Asparagine-Linked Sugar-Chain Structures of Prostatic Acid Phosphatase in Human Prostate Carcinoma. *J Chromatogr B BioMed Sci Appl* (1997) 695(2):439–43. doi: 10.1016/S0378-4347(97)00186-2
50. Altman MO, Gagneux P. Absence of Neu5Gc and Presence of Anti-Neu5Gc Antibodies in Humans-An Evolutionary Perspective. *Front Immunol* (2019) 10:789. doi: 10.3389/fimmu.2019.00789
51. Yehuda S, Padler-Karavani V. Glycosylated Biotherapeutics: Immunological Effects of N-Glycolylneuraminic Acid. *Front Immunol* (2020) 11:21. doi: 10.3389/fimmu.2020.00021
52. Hassan MI, Aijaz A, Ahmad F. Structural and Functional Analysis of Human Prostatic Acid Phosphatase. *Expert Rev Anticancer Ther* (2010) 10(7):1055–68. doi: 10.1586/era.10.46
53. Bouchelouche K, Choyke PL, Capala J. Prostate Specific Membrane Antigen-a Target for Imaging and Therapy With Radionuclides. *Discov Med* (2010) 9 (44):55–61.
54. Czarniecki M, Mena E, Lindenberg L, Cacko M, Harmon S, Radtke JP, et al. Keeping Up With the Prostate-Specific Membrane Antigens (PSMAs): An Introduction to a New Class of Positron Emission Tomography (PET) Imaging Agents. *Transl Androl Urol* (2018) 7(5):831–43. doi: 10.21037/tau.2018.08.03
55. Ghosh A, Heston WD. Tumor Target Prostate Specific Membrane Antigen (PSMA) and its Regulation in Prostate Cancer. *J Cell Biochem* (2004) 91 (3):528–39. doi: 10.1002/jcb.10661
56. Ghosh A, Wang X, Klein E, Heston WDW. Novel Role of Prostate-Specific Membrane Antigen in Suppressing Prostate Cancer Invasiveness. *Cancer Res* (2005) 65(3):727–31.
57. Holmes EH, Greene TG, Tino WT, Boynton AL, Aldape HC, Misrock SL, et al. Analysis of Glycosylation of Prostate-Specific Membrane Antigen Derived From LNCaP Cells, Prostatic Carcinoma Tumors, and Serum From Prostate Cancer Patients. *Prostate Suppl* (1996) 7:25–9. doi: 10.1002/(SICI)1097-0045(1996)7+<25::AID-PROS3>3.0.CO;2-I
58. Barinka C, Sacha P, Sklenar J, Man P, Bezouska K, Slusher BS, et al. Identification of the N-Glycosylation Sites on Glutamate Carboxypeptidase II Necessary for Proteolytic Activity. *Protein Sci* (2004) 13(6):1627–35. doi: 10.1110/ps.04622104
59. Powers TW, Jones EE, Betesh LR, Romano PR, Gao P, Copland JA, et al. Matrix Assisted Laser Desorption Ionization Imaging Mass Spectrometry Workflow for Spatial Profiling Analysis of N-Linked Glycan Expression in Tissues. *Anal Chem* (2013) 85(20):9799–806. doi: 10.1021/ac402108x
60. Steentoft C, Vakhrushev SY, Joshi HJ, Kong Y, Vester-Christensen MB, Schjoldager KTBG, et al. Precision Mapping of the Human O-GalNAc Glycoproteome Through SimpleCell Technology. *EMBO J* (2013) 32 (10):1478–88. doi: 10.1038/emboj.2013.79
61. Chen Z, Gulzar ZG, St Hill CA, Walcheck B, Brooks JD. Increased Expression of GCNT1 is Associated With Altered O-Glycosylation of PSA, PAP, and MUC1 in Human Prostate Cancers. *Prostate* (2014) 74 (10):1059–67. doi: 10.1002/pros.22826
62. Kojima Y, Yoneyama T, Hatakeyama S, Mikami J, Sato T, Mori K, et al. Detection of Core2 Beta-1,6-N-Acetylglucosaminyltransferase in Post-Digital Rectal Examination Urine Is a Reliable Indicator for Extracapsular Extension of Prostate Cancer. *PloS One* (2015) 10(9):e0138520. doi: 10.1371/journal.pone.0138520
63. Kawahara R, Recuero S, Srougi M, Leite KRM, Thaysen-Andersen M, Palmisano G. The Complexity and Dynamics of the Tissue Glycoproteome Associated With Prostate Cancer Progression. *Mol Cell Proteomics* (2021) 20:100026. doi: 10.1074/mcp.RA120.002320
64. Okamoto T, Yoneyama MS, Hatakeyama S, Mori K, Yamamoto H, Koie T, et al. Core2 O-Glycan-Expressing Prostate Cancer Cells Are Resistant to NK Cell Immunity. *Mol Med Rep* (2013) 7(2):359–64. doi: 10.3892/mmr.2012.1189
65. Springer GF. Immunoreactive T and Tn Epitopes in Cancer Diagnosis, Prognosis, and Immunotherapy. *J Mol Med (Berl)* (1997) 75(8):594–602. doi: 10.1007/s001090050144
66. Springer GF, Desai PR, Banatwala I. Blood Group MN Antigens and Precursors in Normal and Malignant Human Breast Glandular Tissue. *J Natl Cancer Inst* (1975) 54(2):335–9.
67. Springer GF, and Tn T. General Carcinoma Autoantigens. *Science* (1984) 224(4654):1198–206. doi: 10.1126/science.6729450
68. Li Q, Anver MR, Butcher DO, Gildersleeve JC. Resolving Conflicting Data on Expression of the Tn Antigen and Implications for Clinical Trials With Cancer Vaccines. *Mol Cancer Ther* (2009) 8(4):971–9. doi: 10.1158/1535-7163.MCT-08-0934
69. Munkley J, Oltean S, Vodak D, Wilson BT, Livermore KE, Zhou Y, et al. The Androgen Receptor Controls Expression of the Cancer-Associated sTn Antigen and Cell Adhesion Through Induction of ST6GalNAc1 in Prostate Cancer. *Oncotarget* (2015) 6(33):34358–74. doi: 10.18632/oncotarget.6024
70. Cozzi PJ, Wang J, Delprado W, Perkins AC, Allen BJ, Russell PJ, et al. MUC1, MUC2, MUC4, MUC5AC and MUC6 Expression in the Progression of Prostate Cancer. *Clin Exp Metastasis* (2005) 22(7):565–73. doi: 10.1007/s10585-005-5376-z
71. Arai T, Fujita K, Fujime M, Irimura T. Expression of Sialylated MUC1 in Prostate Cancer: Relationship to Clinical Stage and Prognosis. *Int J Urol* (2005) 12(7):654–61. doi: 10.1111/j.1442-2042.2005.01112.x
72. Yasumizu Y, Rajabi H, Jin C, Hata T, Pitroda S, Long MD, et al. MUC1-C Regulates Lineage Plasticity Driving Progression to Neuroendocrine Prostate Cancer. *Nat Commun* (2020) 11(1):338. doi: 10.1038/s41467-020-14808-w
73. Hagiwara M, Yasumizu Y, Yamashita N, Rajabi H, Fushimi A, Long MD, et al. MUC1-C Activates the BAF (mSWI/SNF) Complex in Prostate Cancer Stem Cells. *Cancer Res* (2021) 81(4):1111–22. doi: 10.1158/0008-5472.CAN-20-2588
74. Akella NM, Ciraku L, Reginato MJ. Fueling the Fire: Emerging Role of the Hexosamine Biosynthetic Pathway in Cancer. *BMC Biol* (2019) 17(1):52. doi: 10.1186/s12915-019-0671-3
75. Aquino-Gil M, Pierce A, Perez-Cervera Y, Zenteno E, Lefebvre T. OGT: A Short Overview of an Enzyme Standing Out From Usual Glycosyltransferases. *Biochem Soc Trans* (2017) 45(2):365–70. doi: 10.1042/BST20160404

76. Gu Y, Gao J, Han C, Zhang X, Liu H, Ma L, et al. O-GlcNAcylation Is Increased in Prostate Cancer Tissues and Enhances Malignancy of Prostate Cancer Cells. *Mol Med Rep* (2014) 10(2):897–904. doi: 10.3892/mmr.2014.2269
77. Kamigaito T, Okaneya T, Kawakubo M, Shimojo H, Nishizawa, Nakayama J. Overexpression of O-GlcNAc by Prostate Cancer Cells Is Significantly Associated With Poor Prognosis of Patients. *Prostate Cancer Prostatic Dis* (2014) 17(1):18–22. doi: 10.1038/pcan.2013.56
78. Itkonen HM, Minner S, Guldvik IJ, Sandmann MJ, Tsourlakis MC, Berge V, et al. O-GlcNAc Transferase Integrates Metabolic Pathways to Regulate the Stability of C-MYC in Human Prostate Cancer Cells. *Cancer Res* (2013) 73 (16):5277–87. doi: 10.1158/0008-5472.CAN-13-0549
79. Itkonen HM, Urbanucci A, Martin SE, Khan A, Mathelier A, Thiede B, et al. High OGT Activity Is Essential for MYC-Driven Proliferation of Prostate Cancer Cells. *Theranostics* (2019) 9(8):2183–97. doi: 10.7150/thno.30834
80. Itkonen HM, Gorad SS, Duveau DY, Martin SES, Barkovskaya A, Bathen TF, et al. Inhibition of O-GlcNAc Transferase Activity Reprograms Prostate Cancer Cell Metabolism. *Oncotarget* (2016) 7(11):12464–76. doi: 10.18632/oncotarget.7039
81. Ebrahim AH, Alalawi Z, Mirandola L, Rakhshanda R, Dahlbeck S, Nguyen D, et al. Galectins in Cancer: Carcinogenesis, Diagnosis and Therapy. *Ann Transl Med* (2014) 2(9):88. doi: 10.3978/j.issn.2305-5839.2014.09.12
82. Laderach DJ, Gentilini LD, Giribaldi L, Delgado VC, Nugnes L, Croci DO, et al. A Unique Galectin Signature in Human Prostate Cancer Progression Suggests Galectin-1 as a Key Target for Treatment of Advanced Disease. *Cancer Res* (2013) 73(1):86–96. doi: 10.1158/0008-5472.CAN-12-1260
83. Shih TC, Liu R, Wu CT, Li X, Xiao W, Deng X, et al. Targeting Galectin-1 Impairs Castration-Resistant Prostate Cancer Progression and Invasion. *Clin Cancer Res* (2018) 24(17):4319–31. doi: 10.1158/1078-0432.CCR-18-0157
84. Knapp JS, Lokeshwar SD, Vogel U, Hennenlotter J, Schwentner C, Kramer MW, et al. Galectin-3 Expression in Prostate Cancer and Benign Prostate Tissues: Correlation With Biochemical Recurrence. *World J Urol* (2013) 31 (2):351–8. doi: 10.1007/s00345-012-0925-y
85. Gao J, Li T, Mo Z, Hu Y, Yi Q, He R, et al. Overexpression of the Galectin-3 During Tumor Progression in Prostate Cancer and Its Clinical Implications. *Int J Clin Exp Pathol* (2018) 11(2):839–46.
86. Nakajima K, Kho DH, Yanagawa T, Harazono Y, Hogan V, Chen W, et al. Galectin-3 Cleavage Alters Bone Remodeling: Different Outcomes in Breast and Prostate Cancer Skeletal Metastasis. *Cancer Res* (2016) 76(6):1391–402. doi: 10.1158/0008-5472.CAN-15-1793
87. Tzeng SF, Tsai CH, Chao TK, Chou YC, Yang YC, Tsai MH, et al. O-Glycosylation-Mediated Signaling Circuit Drives Metastatic Castration-Resistant Prostate Cancer. *FASEB J* (2018), fj201800687. doi: 10.1096/fj.201800687
88. Tsai CH, Tzeng SF, Chao TK, Tsai CY, Yang YC, Lee MT, et al. Metastatic Progression of Prostate Cancer Is Mediated by Autonomous Binding of Galectin-4-O-Glycan to Cancer Cells. *Cancer Res* (2016) 76(19):5756–67. doi: 10.1158/0008-5472.CAN-16-0641
89. Gentilini LD, Jaworski FM, Tiraboschi C, Perez IG, Kotler ML, Chauchereau A, et al. Stable and High Expression of Galectin-8 Tightly Controls Metastatic Progression of Prostate Cancer. *Oncotarget* (2017) 8(27):44654–68. doi: 10.18632/oncotarget.17963
90. Ricciardelli C, Mayne K, Sykes PJ, Raymond WA, McCaul K, Marshall VR, et al. Elevated Levels of Versican But Not Decorin Predict Disease Progression in Early-Stage Prostate Cancer. *Clin Cancer Res* (1998) 4 (4):963–71.
91. Sakko AJ, Ricciardelli C, Mayne K, Suwiwat S, LeBaron RG, Marshall VR, et al. Modulation of Prostate Cancer Cell Attachment to Matrix by Versican. *Cancer Res* (2003) 63(16):4786–91.
92. Read JT, Rahmani M, Boroomand S, Allahverdian S, McManus BM, Rennie PS. Androgen Receptor Regulation of the Versican Gene Through an Androgen Response Element in the Proximal Promoter. *J Biol Chem* (2007) 282(44):31954–63. doi: 10.1074/jbc.M702099200
93. Jacobsen F, Kraft J, Schroeder C, Hube-Magg C, Kluth M, Lang DS, et al. Up-Regulation of Biglycan is Associated With Poor Prognosis and PTEN Deletion in Patients With Prostate Cancer. *Neoplasia* (2017) 19(9):707–15. doi: 10.1016/j.neo.2017.06.003
94. Datta MW, Hernandez AM, Schlicht MJ, Kahler AJ, DeGueme AM, Dhir R, et al. Perlecan, A Candidate Gene for the CAPB Locus, Regulates Prostate Cancer Cell Growth *via* the Sonic Hedgehog Pathway. *Mol Cancer* (2006) 5:9. doi: 10.1186/1476-4598-5-9
95. Sharpe B, Alghezi DA, Cattermole C, Beresford M, Bowen R, Mitchard J, et al. A Subset of High Gleason Grade Prostate Carcinomas Contain a Large Burden of Prostate Cancer Syndecan-1 Positive Stromal Cells. *Prostate* (2017) 77(13):1312–24. doi: 10.1002/pros.23391
96. Szarvas T, Reis H, Dorp FV, Tschirdewahn S, Niedworok C, Nyirady P, et al. Soluble Syndecan-1 (SDC1) Serum Level as an Independent Pre-Operative Predictor of Cancer-Specific Survival in Prostate Cancer. *Prostate* (2016) 76 (11):977–85. doi: 10.1002/pros.23186
97. Fujii T, Shimada K, Tatsumi Y, Tanaka N, Fujimoto K, Konishi N. Syndecan-1 Up-Regulates microRNA-331-3p and Mediates Epithelial-to-Mesenchymal Transition in Prostate Cancer. *Mol Carcinog* (2016) 55 (9):1378–86. doi: 10.1002/mc.22381
98. Szarvas T, Sevcenco S, Modos O, Keresztes D, Nyirady P, Kubik A, et al. Circulating Syndecan-1 Is Associated With Chemotherapy-Resistance in Castration-Resistant Prostate Cancer. *Urol Oncol* (2018) 36(6):312 e9–312 e15. doi: 10.1016/j.urolonc.2018.03.010
99. Sun Y, Xu K, He M, Fan G, Lu H. Overexpression of Glypican 5 (GPC5) Inhibits Prostate Cancer Cell Proliferation and Invasion *via* Suppressing Sp1-Mediated EMT and Activation of Wnt/beta-Catenin Signaling. *Oncol Res* (2018) 26(4):565–72. doi: 10.3727/096504017X15044461944385
100. Quach ND, Kaur SP, Eggert MW, Ingram L, Ghosh D, Sheth S, et al. Paradoxical Role of Glypican-1 in Prostate Cancer Cell and Tumor Growth. *Sci Rep* (2019) 9(1):11478. doi: 10.1038/s41598-019-47874-2
101. Henke A, Grace OC, Ashley GR, Stewart GD, Riddick ACP, Yeun H, et al. Stromal Expression of Decorin, Semaphorin6D, SPARC, Sprouty1 and Tsukushi in Developing Prostate and Decreased Levels of Decorin in Prostate Cancer. *PloS One* (2012) 7(8):e42516. doi: 10.1371/journal.pone.0042516
102. Hu Y, Sun H, Owens RT, Wu J, Chen YQ, Berquin IM, et al. Decorin Suppresses Prostate Tumor Growth Through Inhibition of Epidermal Growth Factor and Androgen Receptor Pathways. *Neoplasia* (2009) 11 (10):1042–53. doi: 10.1593/neo.09760
103. Coulson-Thomas VJ, Coulson-Thomas YM, Gesteira TF, Andrade de Paula CA, Carneiro CRW, Ortiz V, et al. Lumican Expression, Localization and Antitumor Activity in Prostate Cancer. *Exp Cell Res* (2013) 319(7):967–81. doi: 10.1016/j.yexcr.2013.01.023
104. Zhuo D, Li X, Guan F. Biological Roles of Aberrantly Expressed Glycosphingolipids and Related Enzymes in Human Cancer Development and Progression. *Front Physiol* (2018) 9:466. doi: 10.3389/fphys.2018.00466
105. Shiraishi T, Kinter MT, Mills SE, Lippert MC, Bova GS, Young WW Jr. The Glycosphingolipids of Human Prostate Tissue. *Biochim Biophys Acta* (1988) 961(2):160–9. doi: 10.1016/0005-2760(88)90109-9
106. Ravindranath MH, Muthugounder S, Presser N, Selvan SR, Portoukalian J, Brosman S, et al. Gangliosides of Organ-Confined Versus Metastatic Androgen-Receptor-Negative Prostate Cancer. *Biochem Biophys Res Commun* (2004) 324(1):154–65. doi: 10.1016/j.bbrc.2004.09.029
107. Ravindranath MH, Muthugounder S, Presser N, Ye X, Brosman S, Morton DL. Endogenous Immune Response to Gangliosides in Patients With Confined Prostate Cancer. *Int J Cancer* (2005) 116(3):368–77. doi: 10.1002/ijc.21023
108. Hatano K, Miyamoto Y, Nonomura N, Kaneda Y. Expression of Gangliosides, GD1a, and Sialyl Paragloboside is Regulated by NF-kappaB-Dependent Transcriptional Control of Alpha2,3-Sialyltransferase I, II, and VI in Human Castration-Resistant Prostate Cancer Cells. *Int J Cancer* (2011) 129(8):1838–47. doi: 10.1002/ijc.25860
109. Munkley J, Vodak D, Livermore KE, James K, Wilson BT, Knight B, et al. Glycosylation is an Androgen-Regulated Process Essential for Prostate Cancer Cell Viability. *EBioMedicine* (2016) 8:103–16. doi: 10.1016/j.ebiom.2016.04.018
110. Dalziel M, Crispin M, Scanlan CN, Zitzmann N, Dwek RA. Emerging Principles for the Therapeutic Exploitation of Glycosylation. *Science* (2014) 343(6166):1235681. doi: 10.1126/science.1235681

Conflict of Interest: The authors declare that the research was conducted in the absence of any commercial or financial relationships that could be construed as a potential conflict of interest.

The handling editor declared a past co-authorship with one of the authors JH.

Publisher's Note: All claims expressed in this article are solely those of the authors and do not necessarily represent those of their affiliated organizations, or those of the publisher, the editors and the reviewers. Any product that may be evaluated in this article, or claim that may be made by its manufacturer, is not guaranteed or endorsed by the publisher.

Copyright © 2021 Butler and Huang. This is an open-access article distributed under the terms of the Creative Commons Attribution License (CC BY). The use, distribution or reproduction in other forums is permitted, provided the original author(s) and the copyright owner(s) are credited and that the original publication in this journal is cited, in accordance with accepted academic practice. No use, distribution or reproduction is permitted which does not comply with these terms.

frontiers in Oncology

SYSTEMATIC REVIEW
published: 10 January 2022
doi: 10.3389/fonc.2021.810736

Diagnostic Accuracy of Contemporary Selection Criteria in Prostate Cancer Patients Eligible for Active Surveillance: A Bayesian Network Meta-Analysis

Yu Fan[1,2,3,4*†], *Yelin Mulati*[1,2,3†], *Lingyun Zhai*[5], *Yuke Chen*[1,2,3], *Yu Wang*[1,2,3], *Juefei Feng*[6], *Wei Yu*[1,2,3] *and Qian Zhang*[1,2,3,7*]

[1] Department of Urology, Peking University First Hospital, Beijing, China, [2] Institute of Urology, Peking University, Beijing, China, [3] National Urological Cancer Center, Beijing, China, [4] Department of Urology, Tibet Autonomous Region People's Hospital, Lhasa, China, [5] Department of Urology, The Second Affiliated Hospital of Chongqing Medical University, Chongqing, China, [6] Department of Surgery, Khoo Teck Puat Hospital, Singapore, Singapore, [7] Peking University Binhai Hospital, Tianjin, China

OPEN ACCESS

Edited by:
Andrew Goldstein,
University of California, Los Angeles, United States

Reviewed by:
Gian Maria Busetto,
University of Foggia, Italy
Michele Marchioni,
University of Studies G. d'Annunzio Chieti and Pescara, Italy

***Correspondence:**
Yu Fan
dantefanbmu@pku.edu.cn
Qian Zhang
zhangqianbmu@bjmu.edu.cn

†These authors have contributed equally to this work and share first co-authorship

Specialty section:
This article was submitted to Genitourinary Oncology, a section of the journal Frontiers in Oncology

Received: 07 November 2021
Accepted: 10 December 2021
Published: 10 January 2022

Citation:
Fan Y, Mulati Y, Zhai L, Chen Y, Wang Y, Feng J, Yu W and Zhang Q (2022) Diagnostic Accuracy of Contemporary Selection Criteria in Prostate Cancer Patients Eligible for Active Surveillance: A Bayesian Network Meta-Analysis. Front. Oncol. 11:810736. doi: 10.3389/fonc.2021.810736

Background: Several active surveillance (AS) criteria have been established to screen insignificant prostate cancer (insigPCa, defined as organ confined, low grade and small volume tumors confirmed by postoperative pathology). However, their comparative diagnostic performance varies. The aim of this study was to compare the diagnostic accuracy of contemporary AS criteria and validate the absolute diagnostic odds ratio (DOR) of optimal AS criteria.

Methods: First, we searched Pubmed and performed a Bayesian network meta-analysis (NMA) to compare the diagnostic accuracy of contemporary AS criteria and obtained a relative ranking. Then, we searched Pubmed again to perform another meta-analysis to validate the absolute DOR of the top-ranked AS criteria derived from the NMA with two endpoints: insigPCa and favorable disease (defined as organ confined, low grade tumors). Subgroup and meta-regression analyses were conducted to identify any potential heterogeneity in the results. Publication bias was evaluated.

Results: Seven eligible retrospective studies with 3,336 participants were identified for the NMA. The diagnostic accuracy of AS criteria ranked from best to worst, was as follows: Epstein Criteria (EC), Yonsei criteria, Prostate Cancer Research International: Active Surveillance (PRIAS), University of Miami (UM), University of California-San Francisco (UCSF), Memorial Sloan-Kettering Cancer Center (MSKCC), and University of Toronto (UT). I^2 = 50.5%, and sensitivity analysis with different insigPCa definitions supported the robustness of the results. In the subsequent meta-analysis of DOR of EC, insigPCa and favorable disease were identified as endpoints in ten and twenty-two studies, respectively. The pooled DOR for insigPCa and favorable disease were 0.44 (95%CI, 0.31–0.58) and 0.66 (95%CI, 0.61–0.71), respectively. According to a subgroup analysis, the DOR for favorable disease was significantly higher in US institutions than that in other regions. No significant heterogeneity or evidence of publication bias was identified.

Conclusions: Among the seven AS criteria evaluated in this study, EC was optimal for positively identifying insigPCa patients. The pooled diagnostic accuracy of EC was 0.44 for insigPCa and 0.66 when a more liberal endpoint, favorable disease, was used.

Systematic Review Registration: [https://www.crd.york.ac.uk/prospero/], PROSPERO [CRD42020157048].

Keywords: prostate cancer, active surveillance, selection criteria, diagnostic accuracy, Epstein criteria, network meta-analysis

INTRODUCTION

An estimated 1.28 million new cases of prostate cancer (PCa) occurred in 2018 worldwide (1), and PCa remains the second most commonly diagnosed cancer in men (2). PCa has an indolent natural history in most cases, and most patients die of other causes before disease progression (3). Due to the widespread use of prostate-specific antigen (PSA) screening, many of these cancers are detected when they are in the early stage, low-grade, and localized (4).

With the intention of avoiding overtreatment and preserving quality of life, active surveillance (AS) was originally suggested in 1994 (5), Epstein et al. first introduced the definition of clinically insignificant prostate cancer (insigPCa), which is defined as organ-confined, no Gleason pattern 4/5 and small volume PCa, and the Epstein criteria (EC) was established to predict these insigPCa. Since then, AS has been offered as an alternative to immediate curative intervention in men with favorable-risk PCa. Most patients are monitored on surveillance with PSA and digital rectal examination (DRE) at least biannually, and received surveillance prostate biopsies at a 1–2-year interval. Interventions were taken once high-grade disease was found on surveillance biopsies. The 15-year disease-specific mortality rate of AS is lower than 5% in men with low-risk PCa (6), and AS leads to a better quality-adjusted life experience than is reported by those who undergo curative treatment (7). Consequently, the population considered suitable for AS has rapidly expanded in recent years. The National Comprehensive Cancer Network (NCCN) now recommends AS as the preferred management option for men with very low-risk and low-risk PCa with over a 20-year and 10-year expected survival, respectively, and suggests that AS can even be considered in patients with favorable intermediate-risk cancer (8).

Several eligibility criteria have been established for AS based on published findings from large cohort studies. These criteria include clinical stage, PSA level, PSA density (PSAD = PSA level/prostate volume), Gleason score (GS), number of positive cores, and maximum cancer involved of a single core. However, the eligibility characteristics used to screen patients vary widely across different institutions, and there is currently no consensus on which criteria are optimal (9).

The misclassification rates of AS criteria are controversial. Some research has indicated that AS selection criteria may underestimate disease grade and extent in a small number of cases (10). However, in studies that evaluated upgrading in patients who underwent radical prostatectomy (RP), approximately 30% of men with a Gleason score of 5–6 based on needle biopsy were found to have higher-grade disease during RP (10–12). Meanwhile, several widely-used AS programs noted approximately the same upgrading rate on their first repeat biopsy within 1 year of diagnosis (13–15). These similarities strongly suggest that initial misclassification is the most common reason for reclassification at first-year surveillance biopsy (14, 16).

Variation in the AS selection criteria may result in different diagnostic accuracies (17). As far as we know, no direct comparison of large sample data has been done in this field yet. In this study, we used a Bayesian network meta-analysis (NMA) to indirectly compare the diagnostic accuracy of contemporary AS criteria and provide a diagnostic-accuracy ranking. Then, to further validate the absolute diagnostic odds ratio (DOR, i.e., accurately diagnosed rate) of top-ranked criteria derived from the NMA, another meta-analysis of DOR was performed.

METHODS

This study adhered to the recommendations of the Meta-Analyses of Observational Study in Epidemiology (MOOSE) group (18) and it was pre-registered in PROSPERO (with ID: CRD42020157048).

Search Strategy

First, in order to identify the optimal AS criteria, we systematically reviewed PubMed for articles that were published from January 2008 to May 2019 for our NMA. The following search strategy was used: ((protocols [Title/Abstract]) OR criteria [Title/Abstract])) AND ((active surveillance [Title/Abstract]) AND prostatectomy [Title/Abstract]. Then, to further validate the DOR of the optimal AS criteria, we performed a second systematic search of PubMed articles published before March 2020 using the following search strategy: (((protocol [Title/Abstract]) OR criteria [Title/Abstract])) AND ((Epstein [Title/Abstract]) OR (Hopkins[Title/Abstract])OR (Insignificant[Title/Abstract])) AND prostatectomy [Title/Abstract]).

Inclusion and Exclusion Criteria

The research strategy was framed by PICOS format. The two screening steps shared common inclusion and exclusion criteria. Each study was only included in the analysis if it met the following criteria: (1) the study was retrospective in design; (2) the participants fulfilled the requirements of any AS criteria and were treated with RP without neoadjuvant androgen deprivation treatment; (3) a head-to-head comparison of the diagnostic accuracies of two or more AS criteria was presented (note that

this inclusion criterion was applied only to the NMA); and (4) postsurgical pathology (RP specimen) results were available, especially for cases of pathologically insignificant PCa (insigPCa) or favorable disease. Two definitions of insigPCa were applied: the classical definition (organ-confined Gleason score (GS) ≤6 (no Gleason pattern 4/5, i.e., International Society of Urological Pathology (ISUP) score = 1; and tumor volume <0.5 cm^3) (19); and the updated definition (organ-confined GS ≤6; index and overall tumor volume <1.3 and <2.5 cm^3, respectively) (20). Favorable disease was defined as organ-confined, GS ≤ 6 with a negative surgical margin. The following were defined as exclusion criteria: (1) published in a language other than English; (2) absence of data on insignificant cancer; and (3) reviews, meeting posters, comments, and study criteria. Two researchers independently reviewed the title and abstract of each included study to identify articles for full-text screening. A third author was consulted to resolve any disagreements.

Data Extraction

A predesigned form was used to extract general information and postoperative pathology characteristics for analysis. The following summary data were recorded: first author, year of publication, year of study recruitment, region, total number of patients, mean age, mean preoperative PSA, mean number of biopsy cores, the AS criteria examined, and the number of patients eligible for each protocol, and also the number of insigPCa cases. Our main outcome was diagnostic odds ratio (DOR) = percentage of pathologically insigPCa or favorable disease accurately diagnosed by each criterion.

Statistical Analyses

The network plot of the comparisons among the seven AS criteria was generated using STATA SE 15 software (21). Odds ratios (ORs) with 95% credibility intervals (Crls) were used as summary characteristics to quantify the performance of each AS criterion relative to that of EC (recommended in the AUA \NCCN\EAU guideline) in the NMA. A forest plot was created to compare AS criteria with EC using a Bayesian model and Markov chain Monte Carlo methods in R 3.5.3 (22), random and fixed effects models were created to evaluate reported outcomes; a random effects model was selected if significant heterogeneity was identified. Surface under the cumulative ranking (SUCRA) analysis was then conducted to obtain a hierarchy of the seven AS criteria according to their relative performance (23). Forest plots of diagnostic accuracy were generated for each AS criteria to sketch profiles of the absolute DORs.

Publication bias was tested using funnel plots and Egger's regression test (24), with asymmetrical, skewed and inverted funnels indicating the presence of publication bias (25). Heterogeneity was assessed using forest plots and I2 statistics. I2 values greater than 25, 50, or 75% indicate low, moderate, or high heterogeneity, respectively (26).

Sensitivity analysis was conducted to determine whether the applied definition of insigPCa (classical versus updated) affected the NMA results. First, the NMA included only studies that reported the use of both definitions, to enable us to validate the internal robustness of the results obtained when using each definition individually. Second, we analyzed studies that applied different combinations of insigPCa definitions: InsigPCa1 (6 studies with a classical definition & 1 with an updated definition) and InsigPCa2 (4 studies with a classical definition & 3 with an updated definition). The robustness of the NMA results was validated by comparing the forest plots and ranking plots obtained using different combinations.

A systematic meta-analysis of the DOR was performed for further validation of diagnostic accuracy with the criteria found to achieve the best rank in the SUCRA analysis. Forest plots were generated to estimate the pooled DOR of insigPCa and favorable disease. Heterogeneity was estimated; if significant heterogeneity was found, subgroup analysis and meta-regression were performed to evaluate the potential influencing factors.

RESULTS

Network Meta-Analysis

Three hundred and five articles were identified in the initial database search. Of these, 50 duplicates were excluded, and 167 additional articles were excluded after reviewing their titles and abstracts. Consequently, 88 publications remained for full-text screening. Of these, 7 studies were selected for the final NMA (27–33). Seven criteria were finally identified in this study: EC (5), Prostate Cancer Research International: Active Surveillance (PRIAS) (34), Memorial Sloan-Kettering Cancer Center (MSKCC) (35), University of California, San Francisco (UCSF) (36), University of Miami (UM) (37), University of Toronto (UT) (38), and Yonsei criteria (31); for details of these included critera see **Supplementary Table 1**. **Figure 1** shows the flowchart of the selection procedure.

The baseline characteristics of the patients in the seven included studies are summarized in **Table 1**. All seven were retrospective studies published from January 2008 to May 2019. A total of 3,336 participants were included in this NMA. All these men accepted RP soon after the diagnosis through the AS criteria with TRUS guided biopsy. The EC and PRIAS criteria were analyzed in all 7 included studies (27–33), the MSKCC criteria was analyzed in 6 studies (28–33), the UCSF and UM criteria were analyzed in 5 studies (28–31, 33), the UT protocol was analyzed in 2 studies (30, 32), and the Yonsei protocol was analyzed in only one study, by Lim et al. (31). Four studies used the classical definition of insigPCa as a pathological endpoint (29–32), Iremashvili et al. (28) and Yamada et al. (33) applied both classical and updated definitions (28, 33), and Cantiello et al. used only an updated definition (27).

A network plot was constructed to illustrate the comparisons of the seven AS criteria (**Supplementary Figure 1**). A forest plot showing the comparisons between each AS criteria and the EC is shown in **Figure 2**. Compared to all other criteria except for the Yonsei protocol, the EC was significantly better in predicting pathological insigPCa, and the pooled diagnostic accuracy of EC was 0.45 (95% Crl, 0.28–0.62) (see **Figure 3**). However, only one article reported the diagnostic accuracy of the Yonsei criteria (DOR = 0.25). Diagnostic accuracy of each AS criteria to identify patients with insigPCa is shown in detail in **Supplementary Table 2**. Because the Crl was wide, there was no significant

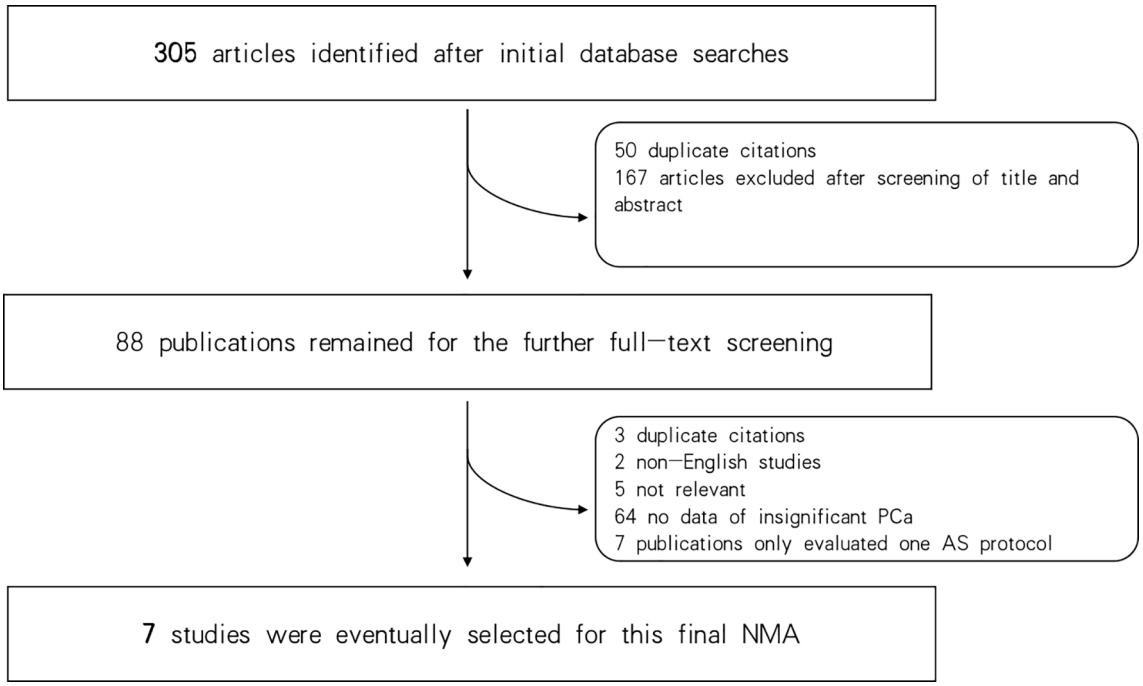

FIGURE 1 | Flowchart of the study selection process and design.

difference between the EC and Yonsei criteria in their ability to predict insigPCa (OR, 0.82; 95% Crl, 0.42–1.50). The Yonsei protocol had no significant advantage over other AS criteria except for the UT protocol (OR, 0.48; Crl, 0.24–0.92) (**Supplementary Figure 2**). A SUCRA plot of these seven AS criteria is presented in **Figure 4**. When the seven AS criteria were ranked from best to worst according to their ability to positively predict insigPCa, their order was as follows: EC, Yonsei, PRIAS, UM, UCSF, MSKCC, and UT.

Moderate heterogeneity was found in the NMA (I^2 = 50.5%, **Supplementary Figure 3**). There was no strong evidence of publication bias, and the funnel plot showed a certain degree of symmetry (**Supplementary Figure 4**).

Sensitivity analysis was carried out in two steps. First, to evaluate the two studies in which both the classical and updated definitions were used, the NMA was conducted on each definition respectively and the results consistently show that among the included criteria, EC was performed best (**Supplementary Figures 5, 6**). Second, the analysis of the InsigPCa1 and InsigPCa2 combinations again showed that EC was the optimal protocol (for InsigPCa1, see **Figure 2**; and for InsigPCa2, see **Supplementary Figure 7**), and the relative ranking of the criteria remained stable (for InsigPCa1, see **Figure 4**; and for InsigPCa2, see **Supplementary Figure 8**).

Meta-Analysis of the DOR of the Optimal AS Criteria Derived From the NMA

After the initial database search, 163 articles were identified in a second search for studies that presented meta-analyses of the DOR achieved by the EC in either insigPCa or favorable disease. After reviewing the titles and abstracts of these articles, 117 were excluded, and 46 remained for further full-text screening. In all, 10 and 22 studies were selected for the meta-analyses of the DOR of the EC in insigPCa and favorable disease, respectively (for the flowchart of this study, see **Supplementary Figure 10**).

A systematic meta-analysis was performed to validate the diagnostic accuracy of the EC for insigPCa. In all, 1,185 men were included from 10 studies (7 studies were same to the NMA with 3 additional studies) (27–33, 39–41), and the pooled DOR was 0.44 (95% Crl, 0.31–0.58, see **Figure 5**), consistent with results of the previously pooled analysis of the original 7 studies. While all 10 of these studies used the classical definition of insigPCa, there was significant heterogeneity (I^2 = 95%). We considered that the region in which the studies were performed (inside or outside the US), the median duration of the study recruitment period, sample size and whether the central pathology was reviewed (yes or no) may represent potential sources of heterogeneity. While the subgroup analysis and meta-regression revealed no statistically significant differences for any of these factors (see **Supplementary Figures 11**, **12** and **Supplementary Table 3**). The funnel plot showed no asymmetry suggestive of publication bias (see **Supplementary Figure 13**), and the P-value of Egger's regression test was 0.7427.

Next, we performed another systematic meta-analysis to validate the diagnostic accuracy of EC in favorable disease. This yielded a total of 5,229 men from 22 studies (4 studies were

TABLE 1 | Baseline characteristics of studies eligible for the network meta-analysis.

Study	Year	Region	Included AS protocols	No. of patients eligible to AS	Median age/years (median;IQR)	Median pre-operative PSA/ng/ml (median;IQR)	Mean No. of biopsy cores (mean; IQR)	Definition of insigPCa
Cantiello et al. (16)	2015	EU	PRIAS	188	66.0 (61.0–67.0)*	4.76 (4.05–7.01)*	NA (≥10)	Updated
			EC	96	65.0 (60.0–68.0)*	5.43 (4.26–7.08)*		
Iremashvili et al. (17)	2012	US	EC	109	60.8 (56.0–64.6)	5.0 (4.0–7.3)	11.3 (10–18)	Classical and update
			MSKCC	246				
			PRIAS	190				
			UCSF	270				
			UM	189				
Kang et al. (18)	2015	Asia	EC	70	62.0 (57.0–67.0)	5.4 (4.3–6.9)	NA(≥10)	Classical
			MSKCC	161				
			PRIAS	109				
			UCSF	141				
			UM	96				
Kim et al. (19)	2014	Asia	EC	137	66.0 (61.0–70.0)	5.5 (4.0–9.0)	NA (≥10)	Classical
			UT	387				
			UCSF	334				
			PRIAS	226				
			UM	222				
			MSKCC	322				
Lim et al. (20)	2013	Asia	EC	31	63.2 ± 7.7**	7.9 ± 0.3**	12.2 ± 1.8**	Classical
			MSKCC	121				
			PRIAS	101				
			UCSF	159				
			UM	88				
			Yonsei	69				
Palisaar et al. (21)	2012	EU	MSKCC	308	65.0 (42.0–77.0)	9.4 (0.6–83)	12.4 (10.0–32.0)	Classical
			EC	99				
			UT	514				
			PRIAS	174				
Yamada et al. (22)	2015	Asia	EC	35	67.0 (48–75)	6.0 (1.05–19.9)	NA	Classical and updated
			PRIAS	55				
			UM	69				
			UCSF	89				
			MSKCC	92				
			UT	118				

**Baseline data of each AS protocol; **Data provided with: mean + SD. IQR, inter quartile range; insigPCa, insignificant Prostate cancer; EC, Epstein Criteria; PRIAS, Prostate Cancer Research International: Active Surveillance; MSKCC, Memorial Sloan-Kettering Cancer Center; UCSF, University of California, San Francisco; UM, University of Miami; UT, University of Toronto.*

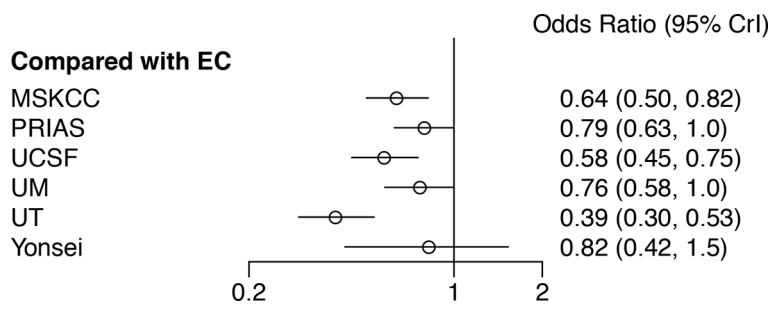

FIGURE 2 | Forest plot showing a comparison of the diagnostic performance of all other included AS criteria in comparison to that of the EC. An OR greater than one represents a benefit relative to EC in terms of diagnostic accuracy for insignificant prostate cancer. EC, Epstein Criteria; PRIAS, Prostate Cancer Research International: Active Surveillance; MSKCC, Memorial Sloan-Kettering Cancer Center; UCSF, University of California, San Francisco; UM, University of Miami; UT, University of Toronto; CrI, Credible interval.

same to the NMA and 18 studies were additional) (28, 30, 40, 42–54), and a pooled DOR of 0.66 (95% CI, 0.61–0.71, see **Figure 6**). There was also significant heterogeneity in this meta-analysis (I^2 = 91%). The subgroup analysis of sample size and meta-regression of region (studies performed inside or outside the USA) produced significant results (see **Supplementary Table 4**): the p-values for sample size and region were 0.049 and 0.013, respectively. The pooled DOR of the EC was

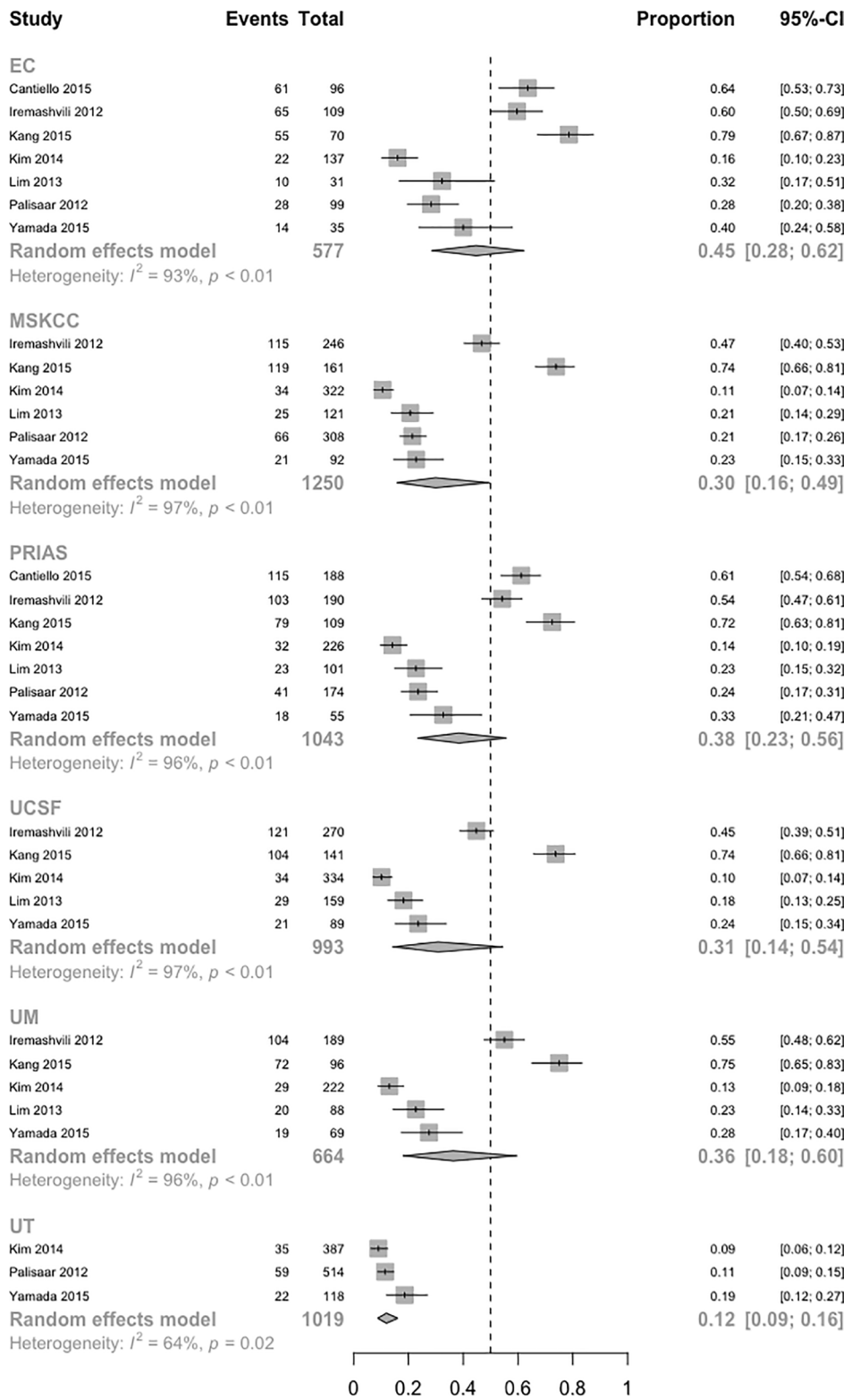

FIGURE 3 | Population-weighted pooled diagnostic accuracy of each AS protocol. (InsigPCa1, including 6 studies with classical definition and 1 study with updated definition of insigPCa). Note: The absolute diagnostic accuracy of the Yonsei protocol was calculated based on only Lim et al, which was 0.25.

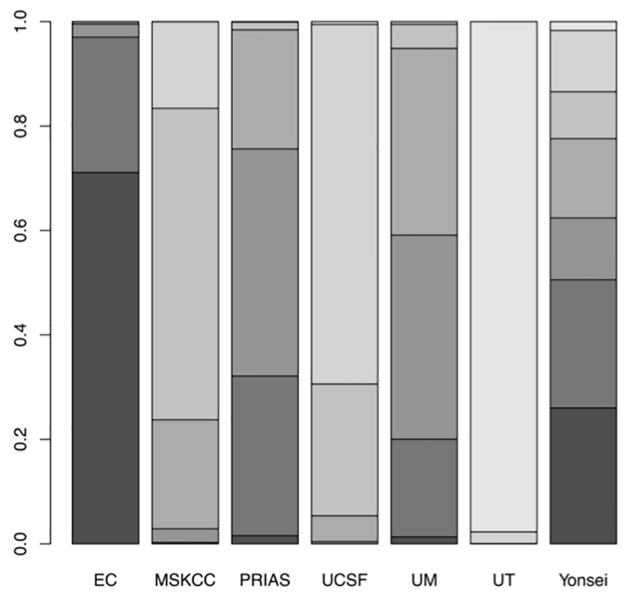

FIGURE 4 | Surface under the cumulative ranking (SUCRA) plot of the 7 included AS protocols. A darker color is proportional to a better performance in predicting insigPCa.

significantly higher in studies performed in the USA than in those performed in other regions (0.73 vs 0.62, p = 0.013; see **Supplementary Figure 14**). While the significant relationship between sample size and the DOR indicated potential publication bias, the funnel plot for publication bias showed a certain degree of symmetry (see **Supplementary Figure 15**), and the p-value of an Egger's regression test for plot symmetry was 0.7585. No evidence of publication bias was found.

DISCUSSION

Identifying patients with purely low-grade prostate cancer is currently problematic because of disease misclassification. The true misclassification rate in these patients is controversial, and the diagnostic abilities of contemporary AS criteria may be overestimated. The diagnostic accuracy of AS criteria can be validated using studies that evaluated pathological outcomes at RP in men who fulfilled AS selection criteria but underwent definitive treatment.

The results of the NMA showed that EC had the best predictive ability for insigPCa, except for the Yonsei criteria, which was evaluated in only 1 study, and sensitivity analysis showed that the results of the NMA were robust regardless of whether a classical or updated definition of insigPCa was used (see **Supplementary Figure 9**). The pooled diagnostic accuracy of the EC for insigPCa was 0.44, indicating that more than half of the cases of prostate cancer that were initially considered clinically "insignificant" were not in fact insignificant. According to the results obtained in previous large AS cohorts, the rate of upgrading at the first repeat biopsy was approximately 30% (14, 55), which is lower than the DOR found for insigPCa using the AS criteria evaluated in this study. Therefore, a separate meta-analysis was performed to validate the DOR of insigPCa using the EC with a more liberal endpoint, favorable disease, which rules out the volume of PCa, which is a restrictive condition. The pooled DOR of the EC for favorable disease was 0.66, which is more consistent with the real-life experience reported in previous large cohorts.

In 2018, the American Urological Association/American Society for Radiation Oncology/Society of Urologic Oncology (AUA/ASTRO/SUO) guidelines announced that given the increase in the number of cores obtained in a systematic biopsy, the definition for a diagnosis of very low-risk PCa should be updated to refer to cases in which no more than

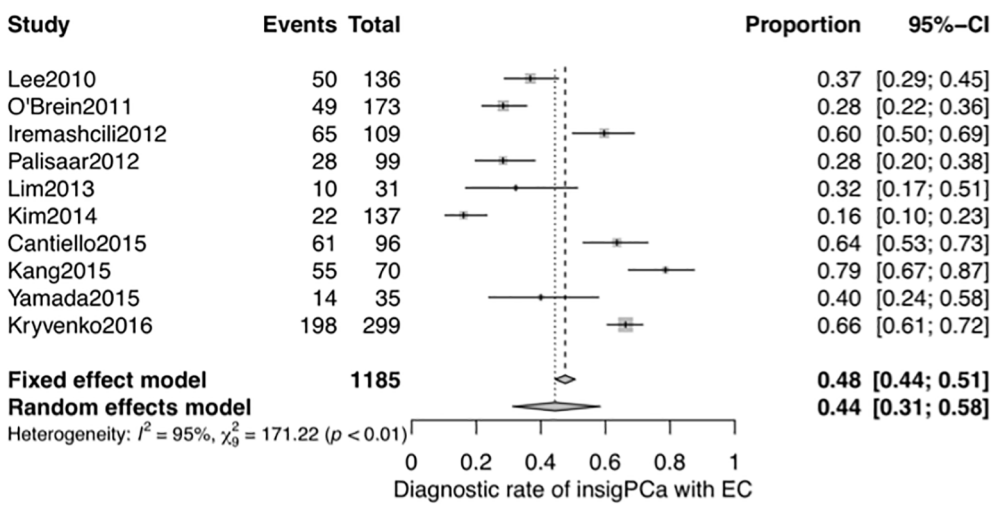

FIGURE 5 | Forest plot of studies that explored the diagnostic accuracy of the EC for insigPCa.

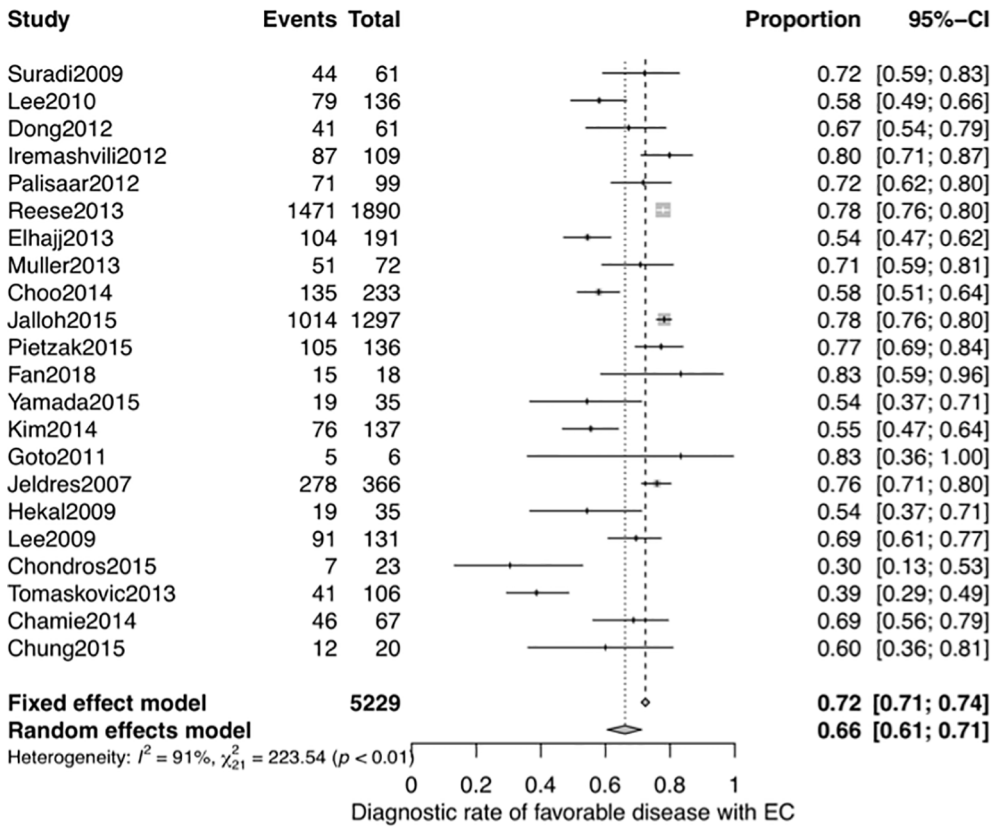

FIGURE 6 | Forest plot of studies that explored the diagnostic accuracy of the EC for favorable disease.

33% of the total cores are positive (instead of those in which no more than two cores are positive, as was stated in the previous version) (56). **Table 1** shows that although the total number of cores obtained during biopsy was more than the traditional six cores in all of the included studies, they all still used "no more than 2 cores" as an eligibility characteristic when applying the EC to diagnose insigPCa. This method may have led to an overestimation of the diagnostic accuracy of the EC, and the true value could therefore be even worse than would be expected based on our results.

Because diagnostic accuracy of criteria designed to identify insigPCa is limited when only a single biopsy is obtained, confirmatory biopsy is recommended as a mandatory step before AS strategy is determined (57). Recently, the ASIST study demonstrated that performing an additional baseline MRI before confirmatory biopsy significantly reduced the rate of upgrading in surveillance biopsies (58). In recent years, multiparametric MRI (mpMRI) has been applied to optimize patient selection and monitoring in AS (59–63). MRI-targeted biopsy showed that confirmatory biopsy did provide additional value in detecting suspicious lesions (64). However, the latest European Urologic Association (EUA) guidelines recommend that men eligible for AS who were diagnosed based on combined systematic and MRI-targeted biopsy do not need a confirmatory biopsy (65). The Prostate Imaging Reporting and Data System (PI-RADS) was established in 2012 (66) and updated in 2015 (v2) (67) and again more recently (v2.1) (68). This approach has minimized the heterogeneity in DOR among different institutions and provided useful supplementary information that may be helpful in preventing incorrect assignment as AS (47, 69). Novel biomarkers, such as PCA3, also urgently need to be incorporated into AS criteria to improve diagnostic accuracy.

Meta-analyses of proportions tend to possess significant heterogeneity (70, 71), and high heterogeneity was also found in the meta-analysis of the individual DOR in this study. We identified the region the study was conducted in (inside or outside the US), the median duration of the study recruitment period, sample size and central review of pathology as potential sources of this heterogeneity. Even so, no publication bias was found in either the NMA or the subsequent meta-analysis of the DOR of the EC.

Institutions in the USA tended to have higher DOR for both insigPCa (0.54 vs 0.40, P-value = 0.32) and favorable disease (0.73 vs 0.62, P-value = 0.013) than was found in those in other regions. Due to a lack of sufficient data, we were unable to further validate the differences between subgroups divided by region. We speculate that the standard measurement of prostate volume (PV) and the use of digital rectal examination (DRE) for clinical T stage in the

USA may contribute to the better performance of those institutions. PV was determined by a variety of methods in the included studies, including transrectal ultrasonography (TRUS), MRI, and CT scan or estimations based on RP specimens using different formulas (e.g., length × width × height × 0.52, tumor area × thickness of specimen × 1.1, weight or weight/1.1), and the PV measurements are known to vary considerably according to the method used (72). Indeed, significant inter-observer variation has been identified in PV measurements obtained with TRUS, and DRE used for PCa clinical staging (73, 74). A detailed and standard operating procedure illustration for DRE and PV measurements in the diagnosis of insigPCa are needed to standardize the selection criteria.

Central pathology review would exclude interobserver variability and eliminate variation in the use of the Gleason score system, potentially improving the quality of the study—as such, we set central pathology review (yes or no) as a potential contributor to heterogeneity. However, no significant outcome was detected for insigPCa or favorable disease (see **Supplementary Figures 12**, **16**). It has also been reported that after the 2005 ISUP modification of the Gleason grading system was introduced, the accuracy of the EC in predicting insigPCa declined (75). In an attempt to validate this decline, we further explored the effect of the median study recruitment duration on the DOR as both a dummy variable (before or after 2005) and a continuous variable, and the results showed there were no significant differences in any variable types or endpoints.

To the best of our knowledge, this is the first NMA to pool contemporary AS criteria together to assess their diagnostic accuracies for insigPCa. While our findings should provide both urologists and AS candidates with valuable information, the present study does have some limitations. First and foremost, we extracted only the positive predictive value (PPV) of each AS criteria; because of our limited access to original data, we could not evaluate negative predictive value, specificity or sensitivity; hence, further studies that evaluate insignificant/significant PCa diagnosed based on any AS criteria are needed. Second, because the number of comparative arms was excessive (≥5) in some of the studies included in the NMA, we were unable to perform a heterogeneity analysis of the NMA. Hence, the heterogeneity assessment of the NMA was conducted using a pairwise meta-analysis, revealing moderate heterogeneity. Third, high heterogeneity was found in the meta-analysis of the DOR; however, subgroup and meta-regression analyses found few factors that could explain the heterogeneity. Forth, limited by available studies, the favourable disease was only used as endpoint in the meta-analysis of DOR of EC.

CONCLUSION

Among the seven contemporary AS criteria evaluated in this study, the EC performed best in positively selecting patients with insigPCa. While the pooled diagnostic accuracy of the EC for the endpoint insigPCa was 0.44, DOR increased to 0.66 when a more liberal endpoint, favorable disease, was used. High heterogeneity was detected in the analysis of individual AS criteria, and subgroup analysis showed that when the EC was used, institutions located in the USA achieved better diagnostic performance than was found for those located in other regions. A further detailed standard operating procedure of screening criteria application in AS is needed in worldwide practice.

DATA AVAILABILITY STATEMENT

The original contributions presented in the study are included in the article/**Supplementary Material**. Further inquiries can be directed to the corresponding authors.

AUTHOR CONTRIBUTIONS

①YF: Concepulation, Methodology, Software, Validation, Writing-Review & Editing, Supervision, Project administration, Funding acquisition; ②YM: Concepulation, Methodology, Software, Investigation, Formal analysis, Writing-original draft, Review & Editing, Visualization; ③LZ: Concepulation, Investigation; ④YC: Methodology, Resources; ⑤YW: Methodology, Resources; ⑥JF: Concepulation, Methodology; ⑦WY: Concepulation, Funding acquisition; ⑧QZ: Supervision, Project administration, Funding acquisition. All authors contributed to the article and approved the submitted version.

FUNDING

This study was supported by grants from the Tibetan Natural Science Foundation of the Medical Group Supporting Program to YF (Grant No. XZ2019ZR-ZY16(Z)) and from the National Natural Science Foundation of China to WY (http://www.nsfc.gov.cn/publish/portal1/) (Grant No. 81870518) and QZ (Grant No. 81872088).

ACKNOWLEDGMENTS

The authors appreciate the advice and practical experience provided by M.S. Sainan Zhu, Department of Statistics, Peking University First Hospital and the methodological suggestions provided by Professor Xiantao Zeng, Center of Evidence Based and Translational Medicine, Zhongnan Hospital of Wuhan University and sincerely thank them both for their help in this work.

SUPPLEMENTARY MATERIAL

The Supplementary Material for this article can be found online at: https://www.frontiersin.org/articles/10.3389/fonc.2021.810736/full#supplementary-material

REFERENCES

1. Bray F, Ferlay J, Soerjomataram I, Siegel RL, Torre LA, Jemal A. Global Cancer Statistics 2018: GLOBOCAN Estimates of Incidence and Mortality Worldwide for 36 Cancers in 185 Countries. *CA Cancer J Clin* (2018) 68 (6):394–424. doi: 10.3322/caac.21492
2. Culp MB, Soerjomataram I, Efstathiou JA, Bray F, Jemal A. Recent Global Patterns in Prostate Cancer Incidence and Mortality Rates. *Eur Urol* (2020) 77 (1):38–52. doi: 10.1016/j.eururo.2019.08.005
3. Bell KJ, Del Mar C, Wright G, Dickinson J, Glasziou P. Prevalence of Incidental Prostate Cancer: A Systematic Review of Autopsy Studies. *Int J Cancer* (2015) 137(7):1749–57. doi: 10.1002/ijc.29538
4. Alberts AR, Schoots IG, Roobol MJ. Prostate-Specific Antigen-Based Prostate Cancer Screening: Past and Future. *Int J Urol* (2015) 22(6):524–32. doi: 10.1111/iju.12750
5. Epstein JI, Walsh PC, Carmichael M, Brendler CB. Pathologic and Clinical Findings to Predict Tumor Extent of Nonpalpable (Stage T1c) Prostate Cancer. *JAMA* (1994) 271(5):368–74. doi: 10.1001/jama.271.5.368
6. Klotz L. Contemporary Approach to Active Surveillance for Favorable Risk Prostate Cancer. *Asian J Urol* (2019) 6(2):146–52. doi: 10.1016/j.ajur.2018.12.003
7. Hayes JH, Ollendorf DA, Pearson SD, Barry MJ, Kantoff PW, Stewart ST, et al. Active Surveillance Compared With Initial Treatment for Men With Low-Risk Prostate Cancer: A Decision Analysis. *JAMA* (2010) 304(21):2373–80. doi: 10.1001/jama.2010.1720
8. Mohler JL, Antonarakis ES, Armstrong AJ, D'Amico AV, Davis BJ, Dorff T, et al. Prostate Cancer, Version 2.2019, NCCN Clinical Practice Guidelines in Oncology. *J Natl Compr Canc Netw* (2019) 17(5):479–505. doi: 10.6004/jnccn.2019.0023
9. Dall'Era MA, Albertsen PC, Bangma C, Carroll PR, Carter HB, Cooperberg MR, et al. Active Surveillance for Prostate Cancer: A Systematic Review of the Literature. *Eur Urol* (2012) 62(6):976–83. doi: 10.1016/j.eururo.2012.05.072
10. Tosoian JJ, JohnBull E, Trock BJ, Landis P, Epstein JI, Partin AW, et al. Pathological Outcomes in Men With Low Risk and Very Low Risk Prostate Cancer: Implications on the Practice of Active Surveillance. *J Urol* (2013) 190 (4):1218–22. doi: 10.1016/j.juro.2013.04.071
11. Epstein JI, Feng Z, Trock BJ, Pierorazio PM. Upgrading and Downgrading of Prostate Cancer From Biopsy to Radical Prostatectomy: Incidence and Predictive Factors Using the Modified Gleason Grading System and Factoring in Tertiary Grades. *Eur Urol* (2012) 61(5):1019–24. doi: 10.1016/j.eururo.2012.01.050
12. Freedland SJ, Kane CJ, Amling CL, Aronson WJ, Terris MK, Presti JCJr., et al. Upgrading and Downgrading of Prostate Needle Biopsy Specimens: Risk Factors and Clinical Implications. *Urology* (2007) 69(3):495–9. doi: 10.1016/j.urology.2006.10.036
13. Bul M, Zhu X, Valdagni R, Pickles T, Kakehi Y, Rannikko A, et al. Active Surveillance for Low-Risk Prostate Cancer Worldwide: The PRIAS Study. *Eur Urol* (2013) 63(4):597–603. doi: 10.1016/j.eururo.2012.11.005
14. Porten SP, Whitson JM, Cowan JE, Cooperberg MR, Shinohara K, Perez N, et al. Changes in Prostate Cancer Grade on Serial Biopsy in Men Undergoing Active Surveillance. *J Clin Oncol* (2011) 29(20):2795–800. doi: 10.1200/JCO.2010.33.0134
15. Van Hemelrijck M, Ji X, Helleman J, Roobol MJ, van der Linden W, Nieboer D, et al. Reasons for Discontinuing Active Surveillance: Assessment of 21 Centres in 12 Countries in the Movember GAP3 Consortium. *Eur Urol* (2019) 75(3):523–31. doi: 10.1016/j.eururo.2018.10.025
16. Inoue LY, Trock BJ, Partin AW, Carter HB, Etzioni R. Modeling Grade Progression in an Active Surveillance Study. *Stat Med* (2014) 33(6):930–9. doi: 10.1002/sim.6003
17. Leyh-Bannurah SR, Karakiewicz PI, Dell'Oglio P, Briganti A, Schiffmann J, Pompe RS, et al. Comparison of 11 Active Surveillance Protocols in Contemporary European Men Treated With Radical Prostatectomy. *Clin Genitourin Cancer* (2017) S1558-7673(17)30246-X. doi: 10.1016/j.clgc.2017.08.005
18. Stroup DF, Berlin JA, Morton SC, Olkin I, Williamson GD, Rennie D, et al. Meta-Analysis of Observational Studies in Epidemiology: A Proposal for Reporting. Meta-Analysis Of Observational Studies in Epidemiology (MOOSE) Group. *JAMA* (2000) 283(15):2008–12. doi: 10.1001/jama.283.15.2008
19. Terris MK, McNeal JE, Stamey TA. Detection of Clinically Significant Prostate Cancer by Transrectal Ultrasound-Guided Systematic Biopsies. *J Urol* (1992) 148(3):829–32. doi: 10.1016/s0022-5347(17)36735-6
20. Wolters T, Roobol MJ, van Leeuwen PJ, van den Bergh RC, Hoedemaeker RF, van Leenders GJ, et al. A Critical Analysis of the Tumor Volume Threshold for Clinically Insignificant Prostate Cancer Using a Data Set of a Randomized Screening Trial. *J Urol* (2011) 185(1):121–5. doi: 10.1016/j.juro.2010.08.082
21. Chaimani A, Higgins JP, Mavridis D, Spyridonos P, Salanti G. Graphical Tools for Network Meta-Analysis in STATA. *PloS One* (2013) 8(10):e76654. doi: 10.1371/journal.pone.0076654
22. Sutton AJ, Abrams KR. Bayesian Methods in Meta-Analysis and Evidence Synthesis. *Stat Methods Med Res* (2001) 10(4):277–303. doi: 10.1177/096228020101000404
23. Salanti G, Ades AE, Ioannidis JP. Graphical Methods and Numerical Summaries for Presenting Results From Multiple-Treatment Meta-Analysis: An Overview and Tutorial. *J Clin Epidemiol* (2011) 64(2):163–71. doi: 10.1016/j.jclinepi.2010.03.016
24. Begg CB, Mazumdar M. Operating Characteristics of a Rank Correlation Test for Publication Bias. *Biometrics* (1994) 50(4):1088–101. doi: 10.2307/2533446
25. Egger M, Davey Smith G, Schneider M, Minder C. Bias in Meta-Analysis Detected by a Simple, Graphical Test. *BMJ* (1997) 315(7109):629–34. doi: 10.1136/bmj.315.7109.629
26. Higgins JP, Thompson SG, Deeks JJ, Altman DG. Measuring Inconsistency in Meta-Analyses. *BMJ* (2003) 327(7414):557–60. doi: 10.1136/bmj.327.7414.557
27. Cantiello F, Russo GI, Cicione A, Ferro M, Cimino S, Favilla V, et al. PHI and PCA3 Improve the Prognostic Performance of PRIAS and Epstein Criteria in Predicting Insignificant Prostate Cancer in Men Eligible for Active Surveillance. *World J Urol* (2016) 34(4):485–93. doi: 10.1007/s00345-015-1643-z
28. Iremashvili V, Pelaez L, Manoharan M, Jorda M, Rosenberg DL, Soloway MS. Pathologic Prostate Cancer Characteristics in Patients Eligible for Active Surveillance: A Head-to-Head Comparison of Contemporary Protocols. *Eur Urol* (2012) 62(3):462–8. doi: 10.1016/j.eururo.2012.03.011
29. Kang HW, Lee JY, Kwon JK, Jeh SU, Jung HD, Cho KS, et al. Pathologic Outcomes in Men With Low-Risk Prostate Cancer Who Are Potential Candidates for Contemporary, Active Surveillance Protocols. *J Korean Med Sci* (2015) 30(7):932–6. doi: 10.3346/jkms.2015.30.7.932
30. Kim TH, Jeon HG, Choo SH, Jeong BC, Seo SI, Jeon SS, et al. Pathological Upgrading and Upstaging of Patients Eligible for Active Surveillance According to Currently Used Protocols. *Int J Urol* (2014) 21(4):377–81. doi: 10.1111/iju.12326
31. Lim SK, Kim KH, Shin TY, Chung BH, Hong SJ, Choi YD, et al. Yonsei Criteria: A New Protocol for Active Surveillance in the Era of Robotic and Local Ablative Surgeries. *Clin Genitourin Cancer* (2013) 11(4):501–7. doi: 10.1016/j.clgc.2013.04.024
32. Palisaar JR, Noldus J, Loppenberg B, von Bodman C, Sommerer F, Eggert T. Comprehensive Report on Prostate Cancer Misclassification by 16 Currently Used Low-Risk and Active Surveillance Criteria. *BJU Int* (2012) 110(6 Pt B): E172–81. doi: 10.1111/j.1464-410X.2012.10935.x
33. Yamada Y, Sakamoto S, Sazuka T, Goto Y, Kawamura K, Imamoto T, et al. Validation of Active Surveillance Criteria for Pathologically Insignificant Prostate Cancer in Asian Men. *Int J Urol* (2016) 23(1):49–54. doi: 10.1111/iju.12952
34. van den Bergh RC, Roemeling S, Roobol MJ, Roobol W, Schroder FH, Bangma CH. Prospective Validation of Active Surveillance in Prostate Cancer: The PRIAS Study. *Eur Urol* (2007) 52(6):1560–3. doi: 10.1016/j.eururo.2007.05.011
35. Adamy A, Yee DS, Matsushita K, Maschino A, Cronin A, Vickers A, et al. Role of Prostate Specific Antigen and Immediate Confirmatory Biopsy in Predicting Progression During Active Surveillance for Low Risk Prostate Cancer. *J Urol* (2011) 185(2):477–82. doi: 10.1016/j.juro.2010.09.095
36. Dall'Era MA, Konety BR, Cowan JE, Shinohara K, Stauf F, Cooperberg MR, et al. Active Surveillance for the Management of Prostate Cancer in a Contemporary Cohort. *Cancer* (2008) 112(12):2664–70. doi: 10.1002/cncr.23502
37. Soloway MS, Soloway CT, Eldefrawy A, Acosta K, Kava B, Manoharan M. Careful Selection and Close Monitoring of Low-Risk Prostate Cancer Patients on Active Surveillance Minimizes the Need for Treatment. *Eur Urol* (2010) 58 (6):831–5. doi: 10.1016/j.eururo.2010.08.027

38. Klotz L, Vesprini D, Sethukavalan P, Jethava V, Zhang L, Jain S, et al. Long-Term Follow-Up of a Large Active Surveillance Cohort of Patients With Prostate Cancer. *J Clin Oncol* (2015) 33(3):272–7. doi: 10.1200/JCO.2014.55.1192
39. Kryvenko ON, Lyapichev K, Chinea FM, Prakash NS, Pollack A, Gonzalgo ML, et al. Radical Prostatectomy Findings in White Hispanic/Latino Men With NCCN Very Low-Risk Prostate Cancer Detected by Template Biopsy. *Am J Surg Pathol* (2016) 40(8):1125–32. doi: 10.1097/PAS.0000000000000656
40. Lee MC, Dong F, Stephenson AJ, Jones JS, Magi-Galluzzi C, Klein EA. The Epstein Criteria Predict for Organ-Confined But Not Insignificant Disease and a High Likelihood of Cure at Radical Prostatectomy. *Eur Urol* (2010) 58 (1):90–5. doi: 10.1016/j.eururo.2009.10.025
41. O'Brien BA, Cohen RJ, Ryan A, Sengupta S, Mills J. A New Preoperative Nomogram to Predict Minimal Prostate Cancer: Accuracy and Error Rates Compared to Other Tools to Select Patients for Active Surveillance. *J Urol* (2011) 186(5):1811–7. doi: 10.1016/j.juro.2011.06.060
42. Chamie K, Sonn GA, Finley DS, Tan N, Margolis DJ, Raman SS, et al. The Role of Magnetic Resonance Imaging in Delineating Clinically Significant Prostate Cancer. *Urology* (2014) 83(2):369–75. doi: 10.1016/j.urology.2013.09.045
43. Chondros K, Karpathakis N, Heretis I, Mavromanolakis E, Chondros N, Sofras F, et al. Validation of Revised Epstein's Criteria for Insignificant Prostate Cancer Prediction in a Greek Subpopulation. *Hippokratia* (2015) 19(1):30–3.
44. Choo SH, Jeon HG, Jeong BC, Seo SI, Jeon SS, Choi HY, et al. Predictive Factors of Unfavorable Prostate Cancer in Patients Who Underwent Prostatectomy But Eligible for Active Surveillance. *Prostate Int* (2014) 2 (2):70–5. doi: 10.12954/PI.14042
45. Chung PH, Darwish OM, Roehrborn CG, Kapur P, Lotan Y. Histologic Upgrading in Patients Eligible for Active Surveillance on Saturation Biopsy. *Can J Urol* (2015) 22(1):7656–60.
46. El Hajj A, Ploussard G, de la Taille A, Allory Y, Vordos D, Hoznek A, et al. Patient Selection and Pathological Outcomes Using Currently Available Active Surveillance Criteria. *BJU Int* (2013) 112(4):471–7. doi: 10.1111/bju.12154
47. Fan Y, Zhai L, Meng Y, Chen Y, Sun S, Wang H, et al. Contemporary Epstein Criteria With Biopsy-Naive Multiparametric Magnetic Resonance Imaging to Prevent Incorrect Assignment to Active Surveillance in the PI-RADS Version 2.0 Era. *Ann Surg Oncol* (2018) 25(12):3510–7. doi: 10.1245/s10434-018-6720-2
48. Goto Y, Nozumi K, Miyazaki K, Matsumoto A, Inoue A, Kito H, et al. Active Surveillance Criteria for Prostate Cancer: Can They be Applied to Japanese Patients? *Int J Urol* (2012) 19(2):163–6. doi: 10.1111/j.1442-2042.2011.02900.x
49. Hekal IA, El-Tabey NA, Nabeeh MA, El-Assmy A, Abd El-Hameed M, Nabeeh A, et al. Validation of Epstein Criteria of Insignificant Prostate Cancer in Middle East Patients. *Int Urol Nephrol* (2010) 42(3):667–71. doi: 10.1007/s11255-009-9670-6
50. Jalloh M, Myers F, Cowan JE, Carroll PR, Cooperberg MR. Racial Variation in Prostate Cancer Upgrading and Upstaging Among Men With Low-Risk Clinical Characteristics. *Eur Urol* (2015) 67(3):451–7. doi: 10.1016/j.eururo.2014.03.026
51. Jeldres C, Suardi N, Walz J, Hutterer GC, Ahyai S, Lattouf JB, et al. Validation of the Contemporary Epstein Criteria for Insignificant Prostate Cancer in European Men. *Eur Urol* (2008) 54(6):1306–13. doi: 10.1016/j.eururo.2007.11.057
52. Lee DH, Jung HB, Lee SH, Rha KH, Choi YD, Hong SJ, et al. Comparison of Pathological Outcomes of Active Surveillance Candidates Who Underwent Radical Prostatectomy Using Contemporary Protocols at a High-Volume Korean Center. *Jpn J Clin Oncol* (2012) 42(11):1079–85. doi: 10.1093/jjco/hys147
53. Lee SE, Kim DS, Lee WK, Park HZ, Lee CJ, Doo SH, et al. Application of the Epstein Criteria for Prediction of Clinically Insignificant Prostate Cancer in Korean Men. *BJU Int* (2010) 105(11):1526–30. doi: 10.1111/j.1464-410X.2009.09070.x
54. . .!!! INVALID CITATION!!!.
55. Eggener SE, Mueller A, Berglund RK, Ayyathurai R, Soloway C, Soloway MS, et al. A Multi-Institutional Evaluation of Active Surveillance for Low Risk Prostate Cancer. *J Urol* (2013) 189(1 Suppl):S19–25; discussion S. doi: 10.1016/j.juro.2012.11.023
56. Sanda MG, Cadeddu JA, Kirkby E, Chen RC, Crispino T, Fontanarosa J, et al. Clinically Localized Prostate Cancer: AUA/ASTRO/SUO Guideline. Part I: Risk Stratification, Shared Decision Making, and Care Options. *J Urol* (2018) 199(3):683–90. doi: 10.1016/j.juro.2017.11.095
57. Klotz L, Loblaw A, Sugar L, Moussa M, Berman DM, van der Kwast T, et al. Active Surveillance Magnetic Resonance Imaging Study (ASIST): Results of a Randomized Multicenter Prospective Trial. *Eur Urol* (2019) 75(2):300–9. doi: 10.1016/j.eururo.2018.06.025
58. Klotz L, Pond G, Loblaw A, Sugar L, Moussa M, Berman D, et al. Randomized Study of Systematic Biopsy Versus Magnetic Resonance Imaging and Targeted and Systematic Biopsy in Men on Active Surveillance (ASIST): 2-Year Postbiopsy Follow-Up. *Eur Urol* (2020) 77(3):311–7. doi: 10.1016/j.eururo.2019.10.007
59. van den Bergh RC, Ahmed HU, Bangma CH, Cooperberg MR, Villers A, Parker CC. Novel Tools to Improve Patient Selection and Monitoring on Active Surveillance for Low-Risk Prostate Cancer: A Systematic Review. *Eur Urol* (2014) 65(6):1023–31. doi: 10.1016/j.eururo.2014.01.027
60. Vargas HA, Akin O, Afaq A, Goldman D, Zheng J, Moskowitz CS, et al. Magnetic Resonance Imaging for Predicting Prostate Biopsy Findings in Patients Considered for Active Surveillance of Clinically Low Risk Prostate Cancer. *J Urol* (2012) 188(5):1732–8. doi: 10.1016/j.juro.2012.07.024
61. Thompson J, Lawrentschuk N, Frydenberg M, Thompson L, Stricker PUsanz. The Role of Magnetic Resonance Imaging in the Diagnosis and Management of Prostate Cancer. *BJU Int* (2013) 112 Suppl 2:6–20. doi: 10.1111/bju.12381
62. Moldovan PC, Van den Broeck T, Sylvester R, Marconi L, Bellmunt J, van den Bergh RCN, et al. What Is the Negative Predictive Value of Multiparametric Magnetic Resonance Imaging in Excluding Prostate Cancer at Biopsy? A Systematic Review and Meta-Analysis From the European Association of Urology Prostate Cancer Guidelines Panel. *Eur Urol* (2017) 72(2):250–66. doi: 10.1016/j.eururo.2017.02.026
63. Guo R, Cai L, Fan Y, Jin J, Zhou L, Zhang K. Magnetic Resonance Imaging on Disease Reclassification Among Active Surveillance Candidates With Low-Risk Prostate Cancer: A Diagnostic Meta-Analysis. *Prostate Cancer P D* (2015) 18(3):221–8. doi: 10.1038/pcan.2015.20
64. Schoots IG, Nieboer D, Giganti F, Moore CM, Bangma CH, Roobol MJ. Is Magnetic Resonance Imaging-Targeted Biopsy a Useful Addition to Systematic Confirmatory Biopsy in Men on Active Surveillance for Low-Risk Prostate Cancer? *A Systematic Rev Meta-analysis BJU Int* (2018) 122 (6):946–58. doi: 10.1111/bju.14358
65. Lam TBL, MacLennan S, Willemse PM, Mason MD, Plass K, Shepherd R, et al. EAU-EANM-ESTRO-ESUR-SIOG Prostate Cancer Guideline Panel Consensus Statements for Deferred Treatment With Curative Intent for Localised Prostate Cancer From an International Collaborative Study (DETECTIVE Study). *Eur Urol* (2019) 76(6):790–813. doi: 10.1016/j.eururo.2019.09.020
66. Barentsz JO, Richenberg J, Clements R, Choyke P, Verma S, Villeirs G, et al. ESUR Prostate MR Guidelines 2012. *Eur Radiol* (2012) 22(4):746–57. doi: 10.1007/s00330-011-2377-y
67. Weinreb JC, Barentsz JO, Choyke PL, Cornud F, Haider MA, Macura KJ, et al. PI-RADS Prostate Imaging - Reporting and Data System: 2015, Version 2. *Eur Urol* (2016) 69(1):16–40. doi: 10.1016/j.eururo.2015.08.052
68. Turkbey B, Rosenkrantz AB, Haider MA, Padhani AR, Villeirs G, Macura KJ, et al. Prostate Imaging Reporting and Data System Version 2.1: 2019 Update of Prostate Imaging Reporting and Data System Version 2. *Eur Urol* (2019) 76 (3):340–51. doi: 10.1016/j.eururo.2019.02.033
69. Zhai LY, Fan Y, Meng YS, Feng XR, Yu W, Jiu J. The Role of Prostate Imaging Reporting and Data System Score in Gleason 3 + 3 Active Surveillance Candidates Enrollment: A Diagnostic Meta-Analysis. *Prostate Cancer P D* (2019) 22(2):235–43. doi: 10.1038/s41391-018-0111-4
70. Ford AC, Marwaha A, Lim A, Moayyedi P. Systematic Review and Meta-Analysis of the Prevalence of Irritable Bowel Syndrome in Individuals With Dyspepsia. *Clin Gastroenterol Hepatol* (2010) 8(5):401–9. doi: 10.1016/j.cgh.2009.07.020
71. Vallely A, Page A, Dias S, Siba P, Lupiwa T, Law G, et al. The Prevalence of Sexually Transmitted Infections in Papua New Guinea: A Systematic Review and Meta-Analysis. *PloS One* (2010) 5(12):e15586. doi: 10.1371/journal.pone.0015586
72. Bezinque A, Moriarity A, Farrell C, Peabody H, Noyes SL, Lane BR. Determination of Prostate Volume: A Comparison of Contemporary Methods. *Acad Radiol* (2018) 25(12):1582–7. doi: 10.1016/j.acra.2018.03.014
73. Evans SM, Murphy DG, Davis ID, Sengupta S, Borzeshi EZ, Sampurno F, et al. Interpolation to Define Clinical Tumor Stage in Prostate Cancer Using

Clinical Description of Digital Rectal Examination. *Asia Pac J Clin Oncol* (2018) 14(5):e412–e9. doi: 10.1111/ajco.12875
74. Smith DS, Catalona WJ. Interexaminer Variability of Digital Rectal Examination in Detecting Prostate Cancer. *Urology* (1995) 45(1):70–4. doi: 10.1016/s0090-4295(95)96812-1
75. Man A, Pickles T, Chi KNBritish Columbia Cancer Agency Prostate Cohort Outcomes I. Asian Race and Impact on Outcomes After Radical Radiotherapy for Localized Prostate Cancer. *J Urol* (2003) 170(3):901–4. doi: 10.1097/01.ju.0000081423.37043.b4

Conflict of Interest: The authors declare that the research was conducted in the absence of any commercial or financial relationships that could be construed as a potential conflict of interest.

Publisher's Note: All claims expressed in this article are solely those of the authors and do not necessarily represent those of their affiliated organizations, or those of the publisher, the editors and the reviewers. Any product that may be evaluated in this article, or claim that may be made by its manufacturer, is not guaranteed or endorsed by the publisher.

Copyright © 2022 Fan, Mulati, Zhai, Chen, Wang, Feng, Yu and Zhang. This is an open-access article distributed under the terms of the Creative Commons Attribution License (CC BY). The use, distribution or reproduction in other forums is permitted, provided the original author(s) and the copyright owner(s) are credited and that the original publication in this journal is cited, in accordance with accepted academic practice. No use, distribution or reproduction is permitted which does not comply with these terms.

frontiers in Oncology

ORIGINAL RESEARCH
published: 21 January 2022
doi: 10.3389/fonc.2021.811866

Construction and Validation of a Clinical Predictive Nomogram for Improving the Cancer Detection of Prostate Naive Biopsy Based on Chinese Multicenter Clinical Data

Tao Tao[1†], Changming Wang[1†], Weiyong Liu[2†], Lei Yuan[3], Qingyu Ge[1], Lang Zhang[4], Biming He[5,6], Lei Wang[1], Ling Wang[1], Caiping Xiang[1], Haifeng Wang[5,6], Shuqiu Chen[4*] and Jun Xiao[1*]*

[1] Department of Urology, The First Affiliated Hospital of USTC, Division of Life Sciences and Medicine, University of Science and Technology of China, Hefei, China, [2] Department of Ultrasound, The First Affiliated Hospital of USTC, Division of Life Sciences and Medicine, University of Science and Technology of China, Hefei, China, [3] Department of Radiology, The First Affiliated Hospital of USTC, Division of Life Sciences and Medicine, University of Science and Technology of China, Hefei, China, [4] Department of Urology, Affiliated Zhongda Hospital of Southeast University, Nanjing, China, [5] Department of Urology, Shanghai East Hospital, Tongji University School of Medicine, Shanghai, China, [6] Department of Urology, Shanghai Changhai Hospital, Second Military Medical University, Shanghai, China

OPEN ACCESS

Edited by:
Antonina Mitrofanova, Rutgers, The State University of New Jersey, United States

Reviewed by:
Ugo Giovanni Falagario, University of Foggia, Italy
Felice Crocetto, Federico II University Hospital, Italy

***Correspondence:**
Jun Xiao
anhuiurology@126.com
Shuqiu Chen
chenshuqiuseu@163.com
Haifeng Wang
a446720864@qq.com

†These authors have contributed equally to this work

Specialty section:
This article was submitted to Genitourinary Oncology, a section of the journal Frontiers in Oncology

Received: *09 November 2021*
Accepted: *28 December 2021*
Published: *21 January 2022*

Citation:
Tao T, Wang C, Liu W, Yuan L, Ge Q, Zhang L, He B, Wang L, Wang L, Xiang C, Wang H, Chen S and Xiao J (2022) Construction and Validation of a Clinical Predictive Nomogram for Improving the Cancer Detection of Prostate Naive Biopsy Based on Chinese Multicenter Clinical Data. Front. Oncol. 11:811866. doi: 10.3389/fonc.2021.811866

Objectives: Prostate biopsy is a common approach for the diagnosis of prostate cancer (PCa) in patients with suspicious PCa. In order to increase the detection rate of prostate naive biopsy, we constructed two effective nomograms for predicting the diagnosis of PCa and clinically significant PCa (csPCa) prior to biopsy.

Materials and Methods: The data of 1,428 patients who underwent prostate biopsy in three Chinese medical centers from January 2018 to June 2021 were used to conduct this retrospective study. The KD cohort, which consisted of 701 patients, was used for model construction and internal validation; the DF cohort, which consisted of 385 patients, and the ZD cohort, which consisted of 342 patients, were used for external validation. Independent predictors were selected by univariate and multivariate binary logistic regression analysis and adopted for establishing the predictive nomogram. The apparent performance of the model was evaluated *via* internal validation and geographically external validation. For assessing the clinical utility of our model, decision curve analysis was also performed.

Results: The results of univariate and multivariate logistic regression analysis showed prostate-specific antigen density (PSAD) (P<0.001, OR:2.102, 95%CI:1.687-2.620) and prostate imaging-reporting and data system (PI-RADS) grade (P<0.001, OR:4.528, 95% CI:2.752-7.453) were independent predictors of PCa before biopsy. Therefore, a nomogram composed of PSAD and PI-RADS grade was constructed. Internal validation in the developed cohort showed that the nomogram had good discrimination (AUC=0.804), and the calibration curve indicated that the predicted incidence was

consistent with the observed incidence of PCa; the brier score was 0.172. External validation was performed in the DF and ZD cohorts. The AUC values were 0.884 and 0.882, in the DF and ZD cohorts, respectively. Calibration curves elucidated greatly predicted the accuracy of PCa in the two validation cohorts; the brier scores were 0.129 in the DF cohort and 0.131 in the ZD cohort. Decision curve analysis showed that our model can add net benefits for patients. A separated predicted model for csPCa was also established and validated. The apparent performance of our nomogram for PCa was also assessed in three different PSA groups, and the results were as good as we expected.

Conclusions: In this study, we put forward two simple and convenient clinical predictive models comprised of PSAD and PI-RADS grade with excellent reproducibility and generalizability. They provide a novel calculator for the prediction of the diagnosis of an individual patient with suspicious PCa.

Keywords: prostate cancer, prostate biopsy, mpMRI, PI-RADS score, PSAD, nomogram

INTRODUCTION

At present, prostate cancer (PCa) is the most common malignancy of aging men worldwide. It has the highest incidence and second mortality despite the fact that the death rate is declining due to early detection of indolent cancers in western countries. Along with economic development and increased early screening tools, the incidence of PCa has also elevated rapidly in China (1, 2). Transrectal ultrasound (TRUS)-guided prostate biopsy is a standard intervention for men with suspicion of PCa (3). This operation can be performed by transrectal or transperineal approach; a few studies have demonstrated that transperineal prostate biopsy is less likely to cause infectious complications, but the cancer detection capacity of these two routes was similar when the same cores were obtained (4). With the development of imaging technology, especially the application of multiparameter magnetic resonance imaging (mpMRI), the technology of prostate biopsy has also been rapidly updated. Some new terminologies such as TRUS-guided cognitive biopsy, MRI-TRUS fusion-guided biopsy, and in-bore MRI targeted biopsy might enhance the detection rates of clinically significant PCa (csPCa) (5). But the positive rate of prostate biopsy is still miserably around 30–70%; that means almost half of the patients are overtreated and received unnecessary biopsies (3).

Apart from mpMRI, the level of serum total prostate-specific antigen (PSA) and the estimate of digital rectal examination (DRE) are two critical indicators when a clinician decides whether a patient needs prostate biopsy initially (6). DRE performed by different examiners was heterogeneous with low specificity and sensitivity (7). PSA is a serine protease, which is specifically expressed in prostate, but the elevation of PSA is not specific in PCa. It exists in benign prostate hyperplasia, prostatitis, elder men, after prostatic examinations, and sexual intercourse, and it can also be affected by taking 5α-reductase inhibitors and antiandrogen drugs (8, 9). PSA density (PSAD) is a PSA derivate, acquired by the ratio of the baseline PSA level to the prostate volume; it is useful when the PSA level is at the gray zone or patients with equivocal imaging (10). PSAD is also useful to identify patients with elevated PSA due to PCa rather than intraprostatic inflammation (11). Indeed, prostatic inflammation is a strong predictor of absence of PCa in the biopsy specimen and is associated with low-grade PCa at radical prostatectomy (12). In addition, other PSA derivates like PSA velocity, PSA rate, PSA double time, and fPSA/tPSA can also be taken into consideration when diagnosing PCa. In recent years, a number of novel molecular markers have also been explored, but their clinical value still needs more evidence before implementing them in a clinic (13, 14). Nevertheless, it is a tragedy that no available variable above can predict the diagnosis of the PCa effectively.

Actually, some risk calculators and factors have been discussed in guidelines for early screening of csPCa for asymptomatic patients with a normal DRE and a PSA value range from 2 to 10 ng/ml, but more effective tools still need to be created (15, 16). In the current study, we conducted a retrospective analysis in three regional medical centers in eastern China. A clinical predictive model was developed and validated by the data of 1,428 prostate biopsy-naive patients. We put forward two risk calculators combining PSAD and prostate imaging—reporting and data system (PI-RADS) grade, which can assess the risk probability of PCa and csPCa. The purpose of our research is to improve the detection rate of prostate cancer and reduce unnecessary prostate biopsy.

MATERIALS AND METHODS

Study Design and Participants

A retrospective multicenter analysis was conducted in 1,428 patients from three independent regional medical centers in China. In the primary cohort, the data of 701 consecutive patients from January 2018 to June 2021 were collected in the Department of Urology at The First Affiliated Hospital of USTC and labeled as the KD cohort; nomogram development and internal validation were performed in this cohort. The data of

385 consecutive patients from January 2018 to January 2020 were collected in the Department of Urology, Affiliated Shanghai East Hospital of Tongji University and labeled as the DF cohort; the data of 342 consecutive patients from January 2018 to March 2020 were collected in the Department of Urology at Affiliated Zhongda Hospital of Southeast University and labeled as the ZD cohort. External validation was performed in these two cohorts. Ethical approval was received from the respective institutional ethics committee, and a signed informed consent was required for every participant before the biopsy.

Baseline Data Collection and Processing

The baseline clinicopathologic information including age, BMI (body mass index) (kg/m^2), serum PSA (ng/ml), mpMRI-based prostate volume (maximum anteroposterior diameter × maximum transverse diameter × maximum longitudinal diameter × 0.52, ml) (17), and PI-RADS score was collected from medical records. PSAD was defined as the ratio of the total PSA value to the prostate volume. A set of inclusion and exclusion criteria was formulated for screening the eligible patients in the three medical centers. ① Only the prostate naive biopsy was considered in this study. ② The enrolled cases must have complete baseline clinicopathologic information; patients with any missing value will be discarded immediately. ③ Laboratory data must be collected within one week before biopsy. ④ Patients with a history of other malignancies or a family history of PCa were excluded. ⑤ None received anti-androgen therapy or took 5α-reductase inhibitors before biopsy. ⑥ Patients with extreme serum PSA values (PSA≥100 ng/ml or PSA<4 ng/ml) were eliminated. The results of the digital rectal examination (DRE) and the fPSA-to-tPSA ratio were not analyzed because the proportion of missing data was >30% in the KD cohort.

MRI Image Acquisition and Interpretation

Patients enrolled in our study underwent a 3.0T MRI scanner with an external 6-channel body array coil (Trio Tim, Siemens Healthineers, Erlangen, Germany) in the KD cohort, a 3.0T system (Magnetom Skyra, Siemens Medical Solutions, Erlangen, Germany) with an 18-channel phased-array coil in the DF cohort, and a 3.0T scanner with an external 8-channel body array coil (PHILIPS, MR Systems Ingenia) in the ZD cohort. The images that required procedure were operated by experienced and professional radiologists within 2 months before biopsy. In order to maintain consistency and authenticity of the data, MRI performed not in the corresponding hospital of the three cohorts or if only a writing report was provided in the medical records was not acceptable. At least axial T2-weighted imaging (T2WI) and diffusion-weighted imaging (DWI) with a quantitative apparent diffusion coefficient (ADC) picture (*b* values were 0, 800, and 1,400 s/mm^2 in the KD cohort; 0, 800, 1,000, and 2,000 s/mm^2 in the DF cohort; and 0, 1,000, and 2,000 s/mm^2 in the ZD cohort) were obtained for the image interpretation according to the PI-RADS v2.1 (18).

Two radiologists who were blinded to histopathological results with more than 3 years of experience in prostate imaging in each medical center were invited to review the images. They first interpreted the MRI images independently and discussed the inconsistent results together subsequently. Finally, an official MRI report with a PIRADS score from 1 to 5 on the basis of PI-RADS v2.1 was obtained for every involved patient. In this study, we divided the PI-RADS scores into three grades: Grade 1 (PI-RADS 1 and 2) represented very low or low probability of PCa; grade 2 (PI-RADS 3) represented intermediate probability of PCa; and grade 3 (PI-RADS 4 and 5) represented high or very high probability of PCa (19).

Prostate Biopsy and Pathology

For all the patients who entered into our study, they underwent TRUS (biplane imaging scan)-guided prostate biopsy operated by professional urologists. A systematic 12-core biopsy was performed first. Next the 0–6 cores of cognitive fusion target biopsy of the suspicious lesions in mpMRI or ultrasound were also performed in all the three medical centers. So, the patient who only underwent target biopsy would be excluded. The primary endpoint of this study is cancer detection of the prostate biopsy. Positive result is defined as PCa with gleason score≥6 (3 + 3). The second endpoint was the detection of csPCa (gleason score≥7). Any other diagnosis like normal prostate gland tissue, benign prostatic hyperplasia, or prostate tissue with inflammation was defined as a negative result.

Model Construction, Validation, and Statistical Analysis

The descriptive statistics means ± standard deviation, interquartile range (IQR), range, number, and proportions were used to depict the baseline characteristics of the patients in primary and validation cohorts. Data in the KD cohort were used for model development. The univariate binary logistic regression analysis method was used to evaluate different variables and calculate the odds ratio (OR) and 95% confidence interval (95%CI). Next, variables with P value<0.05 were entered into the stepwise (forward: conditional) multivariate logistic regression analysis model; variables with P value<0.05 in multivariate analysis were adopted for the establishment of the nomograms. Then, the apparent performance of our nomograms was evaluated *via* internal validation in the KD cohort by the bootstrap (500 resamples) method and geographically external validation in the DF and ZD cohorts. Discrimination and calibration were assessed for model validation, respectively (20). Discrimination was measured by C-statistics, which is equal to the area under the curve (AUC) calculated by plotting the receiver operating characteristic (ROC) curve (21); calibration was measured by drawing calibration curves, and the brier score was calculated by the equation $(Y\text{-}p)^2$, where Y is the actual observed outcome of the dependent variable, and p represents the predicted probability given by our nomogram (22). Statistical analysis was operated by SPSS version 25.0 and R version 4.1.1; statistical significance was considered when P<0.05.

Decision Curve Analysis

Apart from providing a quantitative nomogram for urologists to predict the probability of prostate cancer after biopsy, a decision curve analysis (DCA) was also constructed to estimate the

clinical utility of the nomograms. The clinical net benefits of our model at different threshold probabilities were quantified (23). This was accomplished by using the R software.

RESULTS

Demographic and Clinicopathologic Characteristics of the Patients

All the clinical characteristics of the developed and validated cohorts are summarized in **Table 1**. As for patient selection, it must comply with the aforementioned inclusion and exclusion criteria strictly. Ultimately, 701 patients met the criteria in the KD cohort, 385 patients met the criteria in the DF cohort, and 342 patients were enrolled in the ZD cohort. The average age, BMI, PSA, and PSAD were 68.76 ± 8.97 (years), 23.32 ± 2.55 (kg/m^2), 20.21 ± 17.63 (ng/ml), and 0.62 ± 0.78 in the KD cohort; 66.36 ± 8.35 (years), 23.90 ± 3.11 (kg/m^2), 12.76 ± 10.42 (ng/ml), and 0.41 ± 0.58 in the DF cohort; and 68.65 ± 8.82 (years), 24.39 ± 3.01 (kg/m^2), 16.74 ± 15.67 (ng/ml), and 0.41 ± 0.51 in the ZD cohort, respectively. The proportion in the different PSA group and the PI-RADS score grade of the patients in the three cohorts is also displayed in **Table 1**. The positive rate of prostate biopsy was 43.94%, 51.17%, and 40.06%, and the percentage of csPCa was 34.09%, 42.08%, and 34.21% in the KD, DF, and ZD cohorts, respectively.

Variables Screening, Nomogram Development, and Internal Validation

Binary logistic regression analysis was used for sifting the predictors of PCa in the derivation cohort (the KD cohort). The results of univariate analysis showed that age (P<0.001, OR:1.063, 95%CI:1.043–1.083), BMI (P<0.05, OR:1.071, 95% CI:1.010–1.136), PSA (P<0.01, OR:1.012, 95%CI:1.004–1.021), PSAD (P<0.001, OR:10.906, 95%CI:6.567–18.112), and PI-RADS grade (P<0.001, OR:3.278, 95%CI:2.714–3.959) were significantly associated with the outcome of prostate biopsy. We put these variables into multivariate analysis subsequently, the result indicated that PSAD (P<0.001, OR:2.102, 95% CI:1.687–2.620) and PI-RADS grade (P<0.001, OR:4.528, 95% CI:2.752–7.453) were independent predictors for PCa (**Table 2**). Therefore, a predictive model containing PSAD and PI-RADS grade was established, and a nomogram was also constructed based on our model (**Figure 1**). Internal validation of the KD cohort showed that the predictive nomogram has good discrimination (AUC=0.804) (**Figure 2A**), and the calibration curve indicated that the predicted incidence of PCa was consistent with the observed incidence in the KD cohort (**Figure 2B**); the brier score was 0.172. These results indicated that the modeling process has great reproducibility. A separated predicted nomogram of csPCa was constructed with the same processes; the final variables in the model were also PSAD (P<0.001, OR:2.480, 95%CI:1.947–3.157) and PI-RADS grade (P<0.001, OR:4.769, 95%CI:3.013–7.548) (**Table S1**). Then, the nomogram (**Figure S1**), the ROC curve (AUC=0.848) (**Figure S2A**), the calibration curve (**Figure S2B**), and the brier score (0.138) for internal validation were also received.

External Validation and Clinical Application

External validation was implemented in the DF and ZD cohorts, respectively. Similarly, discrimination and calibration were estimated by the AUC of ROC curves and calibration plots; the brier score was also calculated. For the nomogram of PCa, acceptable results were obtained in both two validation cohorts; the AUC value was 0.884 in the DF cohort and 0.882 in the ZD cohort (**Figures 3A, B**). Calibration plots elucidated greatly predicted the accuracy of PCa in two validation cohorts (**Figures 3C, D**); the brier score was 0.129 in the DF cohort and 0.131 in the ZD cohort. These results indicated a good agreement

TABLE 1 | Demographic characteristics of the patients in development cohort and validation cohorts.

Clinicopathological parameters		KD cohort (n = 701)	DF cohort (n = 385)	ZD cohort (n = 342)
Age (years)		68.76 ± 8.97	66.36 ± 8.35	68.65 ± 8.82
	IQR&Range	12.00 (33.00-90.00)	11.00 (44.00-89.00)	12.25 (34.00-91.00)
BMI (kg/m2)		23.32 ± 2.55	23.90 ± 3.11	24.39 ± 3.01
	IQR&Range	3.65 (14.90-33.50)	3.58 (14.83-32.98)	3.71 (16.56-37.50)
PSA (ng/ml)		20.21 ± 17.63	12.76 ± 10.42	16.74 ± 15.67
	IQR&Range	13.00 (4.28-98.56)	7.47 (4.00-89.72)	11.40 (4.06-99.32)
Group 1 n (%)	4≤PSA<10	204 (29.10%)	195 (50.65%)	143 (41.81%)
Group 2 n (%)	10≤PSA<20	281 (40.09%)	143 (37.14%)	120 (35.09%)
Group 3 n (%)	20≤PSA<100	216 (30.81%)	47 (12.21%)	79 (23.10%)
PSAD		0.62 ± 0.78	0.41 ± 0.58	0.41 ± 0.51
	IQR&Range	0.48 (0.03-5.64)	0.29 (0.05-6.17)	0.32 (0.04-4.95)
PI-RADS score				
Grade 1 n (%)	1-2	346 (49.36%)	141 (36.62%)	104 (30.41%)
Grade 2 n (%)	3	91 (12.98%)	72 (18.70%)	98 (28.65%)
Grade 3 n (%)	4-5	264 (37.66%)	172 (44.68%)	140 (40.94%)
Pathology				
n (%)	positive	308 (43.94%)	197 (51.17%)	137 (40.06%)
	csPCa	239 (34.09%)	162 (42.08%)	117 (34.21%)
n (%)	negative	393 (56.06%)	188 (48.83%)	205 (59.94%)

IQR, interquartile range; BMI, body mass index; PSA, prostate-specific antigen; PSAD, prostate-specific antigen density; PI-RADS, prostate imaging-reporting and data system; csPCa, clinically significant prostate cancer.

TABLE 2 | Univariate and multivariate analysis for screening the predictors of outcomes (PCa) of prostatic biopsy.

Parameters	Univariate model			Multivariate model			
	OR	95%CI	P	B	OR	95%CI	P
Age (years)	1.063	1.043-1.083	<0.001				
BMI (kg/m^2)	1.071	1.010-1.136	0.023				
PSA (ng/ml)	1.012	1.004-1.021	0.006				
PSAD	10.906	6.567-18.112	<0.001	0.743	2.102	1.687-2.620	<0.001
PI-RADS grade	3.278	2.714-3.959	<0.001	1.510	4.528	2.752-7.453	<0.001

PCa, prostate cancer; BMI, body Mass index; PSA, prostate-specific antigen; PSAD, prostate-specific antigen density; PI-RADS, prostate imaging-reporting and data system; OR, odds ratio; CI, confidence interval.

between the predicted risk of PCa and observed outcomes. Meanwhile, similar results obtained for the nomogram of csPCa, AUC values (0.859 in DF cohort and 0.892 in ZD cohort) (**Figures S3A, B**), calibration plots (**Figures S3C, D**), and the brier score (0.149 in DF cohort and 0.119 in ZD cohort) were displayed. All these data demonstrated that our models possessed excellent generalizability.

Decision Curve Analysis

For evaluating the clinical usefulness of our nomograms, the decision curve analysis (DCA) was exhibited (**Figure 4** and **Figure S4**). The DCA curves showed that along with the increase in the probability threshold, making the decision of whether to undergo prostate biopsy while referring to our predicted models can add net benefit compared to intervening all patients or intervening none.

Internal and External Validation in Different PSA Groups

As we all know, PSA is the most commonly used indicator for early screening of PCa in men>50 years old with life expectancy >15 years (15). Although multivariate logistic analysis revealed that PSA was not an independent factor of PCa in the current study, the PSA level is still the most important serum test when urologists decide whether a man should undergo prostate biopsy. Therefore, we divided the patients into 3 groups according to the different PSA level (4≤PSA<10 defined as group 1, 10≤PSA<20 defined as group 2, and 20≤PSA<100 defined as group 3) in the development cohort and two validation cohorts and put our model into these groups for validation. As we expect, our predictive model presented encouraging performance.

For internal validation of the KD cohort, the AUC of ROC was 0.689 in group 1, 0.791 in group 2, and 0.905 in group 3 (**Figures S5A–C**); the brier score was 0.204 in group 1, 0.179 in group 2, and 0.121 in group 3 (**Table 3**). For external validation of the DF cohort, the AUC of ROC was 0.867, 0.909, and 0.885 in groups 1, 2, and 3, respectively (**Figures S6A–C**); the brier score was 0.133, 0.106, and 0.083 in groups 1, 2, and 3, respectively (**Table 3**). For external validation of the ZD cohort, the AUC of ROC was 0.769, 0.906, and 0.914 in groups 1, 2, and 3, respectively (**Figures S7A–C**); the brier score was 0.145 in group 1, 0.118 in group 2, and 0.098 in group 3 (**Table 3**). Calibration curves received acceptable results as well (**Figures S5–S7D–F**). All these results proved that our nomogram has excellent predictive ability in different PSA groups. That means the application of this nomogram can provide reliable evidence

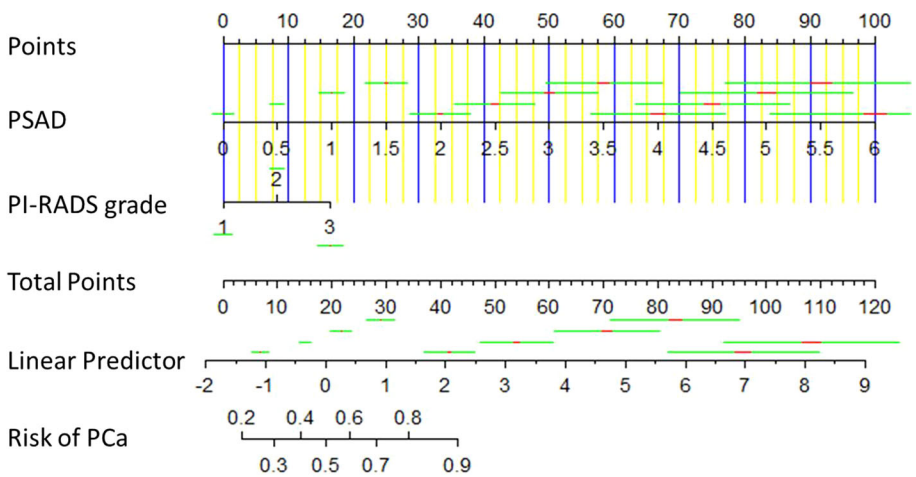

FIGURE 1 | Diagnostic nomogram for predicting the outcome of prostate biopsy. It was established by the development cohort. A total point was calculated by combining PSAD and PI-RADS grade, which parallels to a risk value of PCa.

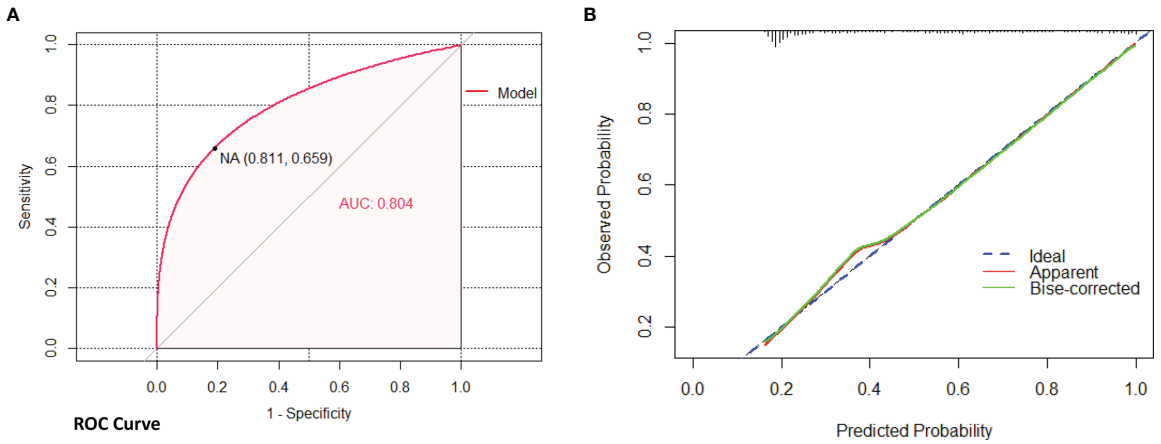

FIGURE 2 | Internal validation of nomogram (PCa) in the KD cohort by bootstrap method (500 resamples). **(A)** Discrimination of the nomogram was evaluated by the ROC curve; AUC=0.804 which is equal to a c-statistic. **(B)** Calibration curves illuminate the agreement between the predicted risks of PCa and the observed incidence of PCa. The blue dotted line represents an ideal flawless model.

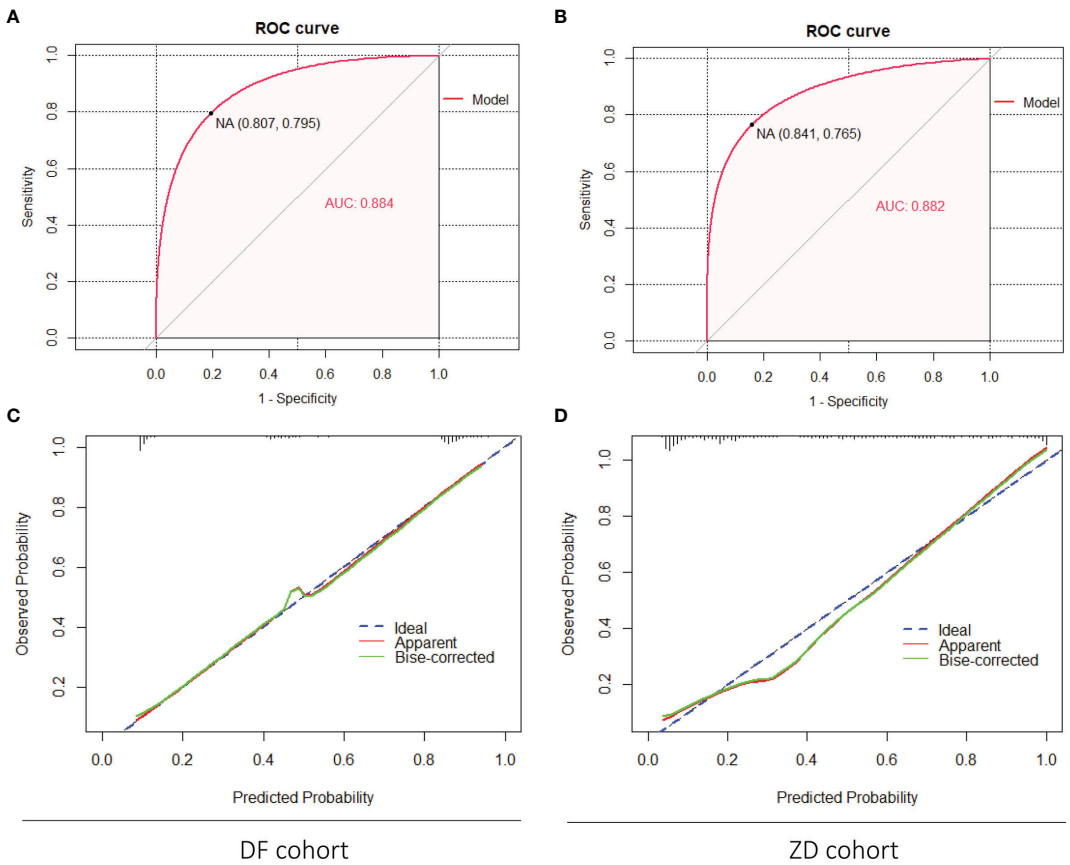

FIGURE 3 | External validation of the nomogram (PCa) in the DF cohort and the ZD cohort. **(A, B)** Discrimination of the nomogram was evaluated by the ROC curve; AUC was 0.884 in the DF cohort and 0.882 in the ZD cohort. Calibration curves of the DF cohort **(C)** and the ZD cohort **(D)** illuminate the great agreement between the predicted risks of PCa and the observed incidence of PCa. The blue dotted line represents an ideal flawless model.

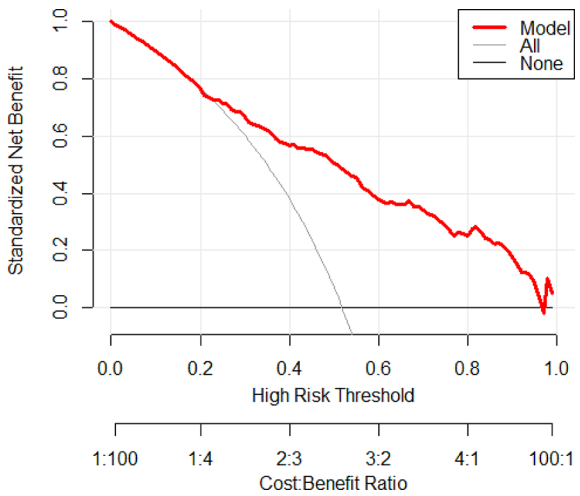

FIGURE 4 | Decision curve analysis was exhibited to estimate the clinical usefulness of the nomogram (PCa). The quantified net benefits can be measured at different threshold probabilities. The y-axis denotes the standardized net benefit, and the x-axis denotes the threshold probabilities. The red line represents our nomogram, the gray line represents the condition that all patients have PCa, and the black line represents the condition that none have PCa.

in clinical decision-making, especially when the PSA is 4–10 ng/ml, which is called the gray zone by urologists.

DISCUSSION

mpMRI is increasingly performed in clinics for the diagnosis of PCa. There are several high-quality studies specifically assessing the efficiency and availability of mpMRI in recent years (24–29). In the PROMIS study (26), they found that mpMRI can be regarded as a triage test before prostate naive biopsy and help a quarter of patients avoid an unnecessary biopsy. For the diagnosis of csPCa in men with PSA up to 15 ng/ml, the sensitivity and specificity of mpMRI and TRUS-biopsy were 93% and 41%, and 48% and 96%, respectively. In the PRECISION study (27), the detection rate of csPCa can increase by 12% by MRI-targeted biopsy (38%) compared to standard biopsy (26%), and less clinically insignificant PCa was detected in the MRI-targeted biopsy group synchronously. But in the MRI-FIRST study (28), they discovered that the positive rate of PCa with MRI-targeted biopsy was adjacent to systematic biopsy. A better outcome can be achieved by combining systematic biopsy with targeted biopsy. In the Trio study (29), they confirmed that MRI-targeted biopsy had lower ability in grade group 1 PCa but showed an outstanding cancer detection rate in higher-grade PCa. Moreover, 8% csPCa would be missed if only MRI-targeted biopsy is performed. A study by Rapisarda et al. (30) also confirmed that mpMRI could improve the diagnostic accuracy of PCa; a combined strategy of fusion targeted and systematic biopsy could reach high concordance rates with histologic result. Collectively, mpMRI has brilliant performance in the detection of csPCa, but it cannot in the case of systematic biopsy completely. In addition, guidelines have recommended mpMRI in patients with suspicion of PCa prior to biopsy (15, 31). It is worth noting that mpMRI cannot be performed as an initial screening tool because the low specificity may lead to false-positive findings and unnecessary biopsies (32). PI-RADS is an interpretation of mpMRI, which can give a quantitative score range from 1 to 5, in which a high score means high probability of PCa. PI-RADS v2.1 is the latest version with enhanced interreader variability and easier PI-RADS assessment procedure compared to PI-RADS v2 (18, 33).

Actually, some predictive models have been set up before for the detection of PCa. Two risk calculators of western patients had been well developed; they are The European Randomized Study of Screening for PCa Risk Calculator and the Prostate Cancer Prevention Trial Risk Calculator. However, it will result in approximately 20% increase in predicted probabilities for PCa in Chinese population on account of the differences of race and region (34, 35). A number of nomograms for the detection of PCa based on Chinese population have been constructed as well recently. Chen et al. (36) constructed the Chinese Prostate Cancer Consortium Risk Calculator (CPCC-RC) based on PSA, age, prostate volume, fPSA-to-tPSA rate, and DRE for forecasting the initial prostate biopsy. This is the largest research of China to date, but the information of mpMRI was not estimated. A clinical nomogram including mpMRI like that of Fang et al. (19) showed that the model that contained mpMRI exhibited higher sensitivity and specificity for the detection of PCa. Niu et al. (37) developed an outperforming model composed of the PI-RADS v2 score and adjusted PSAD. Li et al.

TABLE 3 | The results of internal and external validation of the nomogram in different PSA group.

Cohorts	Parameters	All patients	4≤PSA<10 Group 1	10≤PSA<20 Group 2	20≤PSA<100 Group 3
KD cohort (Internal validation)	AUC	0.804	0.689	0.791	0.905
	Brier score	0.172	0.204	0.179	0.121
DF cohort (External validation 1)	AUC	0.884	0.867	0.909	0.885
	Brier score	0.129	0.133	0.106	0.083
ZD cohort (External validation 2)	AUC	0.882	0.769	0.906	0.914
	Brier score	0.131	0.145	0.118	0.098

PSA, prostate-specific antigen; AUC, area under the curve.

(38) displayed three radiomics prediction models for improving the diagnosis of csPCa on biparametric MRI. Studies including our previous research also verified the prominent diagnostic efficiency of PI-RADS v2. But all these studies were executed in a single center with an insufficient sample size (39–42). To improve the detection of PCa and reduce the needless biopsy procedures, a more accurate diagnostic nomogram and better predictive model is still warranted (43).

In the current study, we performed a retrospective study in three Chinese medical centers. Univariate and multivariate logistic regression analysis revealed that PSAD (P<0.001, OR:2.102, 95%CI:1.687–2.062) and PI-RADS grade (P<0.001, OR:4.528, 95%CI:2.752–7.453) were independent predictors for the diagnosis of PCa and used for establishing the predictive model and the nomogram. Then, model validation in the KD cohort (internal validation) and the DF and ZD cohorts (external validation) was performed. The AUC (0.804) indicated good discrimination; the calibration curve and brier score (0.172) also represent eminent calibration in internal validation. In external validation, AUC was 0.884 in the DF cohort and 0.882 in the ZD cohort, calibration curves elucidated greatly predicted the accuracy of PCa, and the brier score was 0.129 and 0.131 in the DF and ZD cohorts, respectively. Decision curve analysis (DCA) manifested that our nomogram can obviously add the net benefit when forecasting the diagnosis of PCa. Finally, we verified our model in three different PSA groups; acceptable results have also been obtained. In addition to our research, the latest two studies have also demonstrated that the utility of PSAD in addition to MRI PIRADS score can assist in the individualized decision-making process prior to prostate biopsy (44, 45).

Our study also has several limitations. First, our study was enforced in three third-grade class A hospitals in China; it may not be reproducible in less experienced medical centers or other countries. Then, clinicopathological parameters like the results of DRE and the fPSA-to-tPSA rate were not included due to the irretrievably missing value. Third, although the model has excellent performance in our research, it may not be applicable to all the patients, and the dilemma is still going to happen. Combining with different tools such as SelectMDx, 4Kscore can also be considered under special circumstances (46, 47). Finally, although we carried out a set of inclusive and exclusive criteria during the data collection, bias could not be completely avoided. Such as the protocol of biopsy and mpMRI interpretation by different clinicians, inter-institutional outcomes could not be well evaded. In practice, this phenomenon is inevitable because each hospital is independent; it also means our model has good generalizability. Furthermore, a study by Ugo G et al. (48) discovered that the diagnostic accuracy of mpMRI in PCa is not different between races; that means our nomogram can also be applied in other populations.

CONCLUSIONS

We established two simple and convenient clinical predictive nomograms comprised of PSAD and PI-RADS grade with excellent reproducibility and generalizability. They are novel risk calculators for the prediction of the diagnosis of PCa and csPCa in China. But prospective validation and update remain warranted.

DATA AVAILABILITY STATEMENT

The raw data supporting the conclusions of this article will be made available by the authors, without undue reservation.

ETHICS STATEMENT

The studies involving human participants were reviewed and approved by the Ethics Committee of USTC, the Ethics Committee of Southeast University, and the Ethics Committee of Tongji University. The patients/participants provided their written informed consent to participate in this study.

AUTHOR CONTRIBUTIONS

Conception, design, and manuscript reviewing: JX, SC, and HW. Data analysis and manuscript drafting: TT, CW, and WL. Data collection and sorting: LY, QG, LZ, BH, LeW, LiW, and CX. All authors contributed to the article and approved the submitted version.

FUNDING

This study was supported by the National Natural Science Foundation of China (No. 81702540 and No. 82072807), the Natural Science Foundation of Anhui Province (No. 2108085MH293), and Key Research and Development Project of Anhui Province (No. 202004J07020022).

ACKNOWLEDGMENTS

We must express our special thanks to Professor Zhihua Zhang's team at the Department of Epidemiology and Biostatistics, School of Public Health, Anhui Medical University for assisting us in accomplishing the statistical analysis of the study.

SUPPLEMENTARY MATERIAL

The Supplementary Material for this article can be found online at: https://www.frontiersin.org/articles/10.3389/fonc.2021.811866/full#supplementary-material

Supplementary Figure 1 | Diagnostic nomogram for predicting clinically significant prostate cancer(csPCa) of prostate biopsy. It was established by the development cohort. A total point was calculated by combining PSAD and PI-RADS grade which parallels to a risk value of csPCa.

Supplementary Figure 2 | Internal validation of the nomogram (csPCa) in the KD cohort by bootstrap method (500 resamples). (A) Discrimination of the nomogram was evaluated by AUC (0.848). (B) Calibration curves illuminate the agreement

between the predicted risks of csPCa and the observed incidence of csPCa. The blue dotted line represents an ideal flawless model.

Supplementary Figure 3 | External validation of the nomogram (csPCa) in the DF cohort and the ZD cohort. (A, B) Discrimination of the nomogram was evaluated by AUC; it was 0.859 in the DF cohort and 0.892 in the ZD cohort. Calibration curves of the DF cohort (C) and the ZD cohort (D) illuminate the great agreement between the predicted risks of csPCa and the observed incidence of csPCa. The blue dotted line represents an ideal flawless model.

Supplementary Figure 4 | Decision curve analysis was exhibited to estimate the clinical usefulness of the nomogram (csPCa). The quantified net benefits can be measured at different threshold probabilities. The y-axis denotes the standardized net benefit, and the x-axis denotes the threshold probabilities. The red line represents our nomogram, the gray line represents the condition that all patients have csPCa, and the black line represents the condition that none have csPCa.

Supplementary Figure 5 | Internal validation of the nomogram in the KD cohort for three PSA groups. (A, B, and C) ROC curve of the three groups for assessing the discrimination. (D, E, and F) Calibration plots of the three groups for assessing the calibration.

Supplementary Figure 6 | External validation of the nomogram in the DF cohort for three PSA groups. (A, B, and C) The ROC curve of the three groups for assessing the discrimination. (D, E, and F) Calibration plots of the three groups for assessing the calibration.

Supplementary Figure 7 | External validation of the nomogram in the ZD cohort for three PSA groups. (A, B, and C) The ROC curve of the three groups for assessing the discrimination. (D, E, and F) Calibration plots of the three groups for assessing the calibration.

Supplementary Table 1 | Univariate and multivariate analysis for screening the predictors of outcomes (csPCa) of prostatic biopsy. csPCa, clinically significant prostate cancer; BMI, body mass index; PSA, prostate-specific antigen; PSAD, prostate-specific antigen density; PI-RADS, prostate imaging-reporting and data system; OR, odds ratio; CI, confidence interval.

REFERENCES

1. Siegel RL, Miller KD, Fuchs HE, Jemal A. Cancer Statistics, 2021. *CA Cancer J Clin* (2021) 71(1):7–33. doi: 10.3322/caac.21654
2. Chen W, Zheng R, Baade PD, Zhang S, Zeng H, Bray F, et al. Cancer Statistics in China, 2015. *CA Cancer J Clin* (2016) 66(2):115–32. doi: 10.3322/caac.21338
3. Hübner N, Shariat S, Remzi M. Prostate Biopsy: Guidelines and Evidence. *Curr Opin Urol* (2018) 28(4):354–9. doi: 10.1097/mou.0000000000000510
4. Xue J, Qin Z, Cai H, Zhang C, Li X, Xu W, et al. Comparison Between Transrectal and Transperineal Prostate Biopsy for Detection of Prostate Cancer: A Meta-Analysis and Trial Sequential Analysis. *Oncotarget* (2017) 8(14):23322–36. doi: 10.18632/oncotarget.15056
5. Park BK. Image-Guided Prostate Biopsy: Necessity for Terminology Standardization. *J Ultrasound Med* (2020) 39(1):191–6. doi: 10.1002/jum.15083
6. Moul JW. Comparison of DRE and PSA in the Detection of Prostate Cancer. *J Urol* (2017) 197(2s):S208–9. doi: 10.1016/j.juro.2016.11.031
7. Naji L, Randhawa H, Sohani Z, Dennis B, Lautenbach D, Kavanagh O, et al. Digital Rectal Examination for Prostate Cancer Screening in Primary Care: A Systematic Review and Meta-Analysis. *Ann Fam Med* (2018) 16(2):149–54. doi: 10.1370/afm.2205
8. Wang MC, Valenzuela LA, Murphy GP, Chu TM. Purification of a Human Prostate Specific Antigen. *J Urol* (2017) 197(2s):S148–52. doi: 10.1016/j.juro.2016.10.100
9. Catalona WJ, Richie JP, Ahmann FR, Hudson MA, Scardino PT, Flanigan RC, et al. Comparison of Digital Rectal Examination and Serum Prostate Specific Antigen in the Early Detection of Prostate Cancer: Results of a Multicenter Clinical Trial of 6,630 Men. *J Urol* (2017) 197(2s):S200–7. doi: 10.1016/j.juro.2016.10.073
10. Omri N, Kamil M, Alexander K, Alexander K, Edmond S, Ariel Z, et al. Association Between PSA Density and Pathologically Significant Prostate Cancer: The Impact of Prostate Volume. *Prostate* (2020) 80(16):1444–9. doi: 10.1002/pros.24078
11. Bruno SM, Falagario UG, d'Altilia N, Recchia M, Mancini V, Selvaggio O, et al. PSA Density Help to Identify Patients With Elevated PSA Due to Prostate Cancer Rather Than Intraprostatic Inflammation: A Prospective Single Center Study. *Front Oncol* (2021) 11:693684. doi: 10.3389/fonc.2021.693684
12. Sanguedolce F, Falagario UG, Castellan P, Di Nauta M, Silecchia G, Bruno SM, et al. Bioptic Intraprostatic Chronic Inflammation Predicts Adverse Pathology at Radical Prostatectomy in Patients With Low-Grade Prostate Cancer. *Urol Oncol* (2020) 38(10):793.e19–.e25. doi: 10.1016/j.urolonc.2020.02.025
13. Lamy PJ, Allory Y, Gauchez AS, Asselain B, Beuzeboc P, de Cremoux P, et al. Prognostic Biomarkers Used for Localised Prostate Cancer Management: A Systematic Review. *Eur Urol Focus* (2018) 4(6):790–803. doi: 10.1016/j.euf.2017.02.017
14. Yang Z, Yu L, Wang Z. PCA3 and TMPRSS2-ERG Gene Fusions as Diagnostic Biomarkers for Prostate Cancer. *Chin J Cancer Res* (2016) 28(1):65–71. doi: 10.3978/j.issn.1000-9604.2016.01.05
15. Mottet N, van den Bergh RCN, Briers E, Van den Broeck T, Cumberbatch MG, De Santis M, et al. EAU-EANM-ESTRO-ESUR-SIOG Guidelines on Prostate Cancer-2020 Update. Part 1: Screening, Diagnosis, and Local Treatment With Curative Intent. *Eur Urol* (2021) 79(2):243–62. doi: 10.1016/j.eururo.2020.09.042
16. Carroll PH, Mohler JL. NCCN Guidelines Updates: Prostate Cancer and Prostate Cancer Early Detection. *J Natl Compr Canc Netw* (2018) 16(5S):620–3. doi: 10.6004/jnccn.2018.0036
17. Karademir I, Shen DG, Peng YH, Liao S, Jiang YL, Yousuf A, et al. Prostate Volumes Derived From MRI and Volume-Adjusted Serum Prostate-Specific Antigen: Correlation With Gleason Score of Prostate Cancer. *Am J Roentgenol* (2013) 201(5):1041–8. doi: 10.2214/Ajr.13.10591
18. Turkbey B, Rosenkrantz AB, Haider MA, Padhani AR, Villeirs G, Macura KJ, et al. Prostate Imaging Reporting and Data System Version 2.1: 2019 Update of Prostate Imaging Reporting and Data System Version 2. *Eur Urol* (2019) 76(3):340–51. doi: 10.1016/j.eururo.2019.02.033
19. Fang D, Zhao C, Ren D, Yu W, Wang R, Wang H, et al. Could Magnetic Resonance Imaging Help to Identify the Presence of Prostate Cancer Before Initial Biopsy? The Development of Nomogram Predicting the Outcomes of Prostate Biopsy in the Chinese Population. *Ann Surg Oncol* (2016) 23(13):4284–92. doi: 10.1245/s10434-016-5438-2
20. Pabinger I, van Es N, Heinze G, Posch F, Riedl J, Reitter EM, et al. A Clinical Prediction Model for Cancer-Associated Venous Thromboembolism: A Development and Validation Study in Two Independent Prospective Cohorts. *Lancet Haematol* (2018) 5(7):e289–98. doi: 10.1016/s2352-3026(18)30063-2
21. Steyerberg EW, Vergouwe Y. Towards Better Clinical Prediction Models: Seven Steps for Development and an ABCD for Validation. *Eur Heart J* (2014) 35(29):1925–31. doi: 10.1093/eurheartj/ehu207
22. Steyerberg EW, Vickers AJ, Cook NR, Gerds T, Gonen M, Obuchowski N, et al. Assessing the Performance of Prediction Models: A Framework for Traditional and Novel Measures. *Epidemiology* (2010) 21(1):128–38. doi: 10.1097/EDE.0b013e3181c30fb2
23. Huang YQ, Liang CH, He L, Tian J, Liang CS, Chen X, et al. Development and Validation of a Radiomics Nomogram for Preoperative Prediction of Lymph Node Metastasis in Colorectal Cancer. *J Clin Oncol* (2016) 34(18):2157–64. doi: 10.1200/jco.2015.65.9128
24. Drost FH, Osses D, Nieboer D, Bangma CH, Steyerberg EW, Roobol MJ, et al. Prostate Magnetic Resonance Imaging, With or Without Magnetic Resonance Imaging-Targeted Biopsy, and Systematic Biopsy for Detecting Prostate Cancer: A Cochrane Systematic Review and Meta-Analysis. *Eur Urol* (2020) 77(1):78–94. doi: 10.1016/j.eururo.2019.06.023

25. Miah S, Hosking-Jervis F, Connor MJ, Eldred-Evans D, Shah TT, Arya M, et al. A Multicentre Analysis of the Detection of Clinically Significant Prostate Cancer Following Transperineal Image-Fusion Targeted and Nontargeted Systematic Prostate Biopsy in Men at Risk. *Eur Urol Oncol* (2020) 3(3):262–9. doi: 10.1016/j.euo.2019.03.005
26. Ahmed HU, El-Shater Bosaily A, Brown LC, Gabe R, Kaplan R, Parmar MK, et al. Diagnostic Accuracy of Multi-Parametric MRI and TRUS Biopsy in Prostate Cancer (PROMIS): A Paired Validating Confirmatory Study. *Lancet* (2017) 389(10071):815–22. doi: 10.1016/s0140-6736(16)32401-1
27. Kasivisvanathan V, Rannikko AS, Borghi M, Panebianco V, Mynderse LA, Vaarala MH, et al. MRI-Targeted or Standard Biopsy for Prostate-Cancer Diagnosis. *N Engl J Med* (2018) 378(19):1767–77. doi: 10.1056/NEJMoa1801993
28. Rouvière O, Puech P, Renard-Penna R, Claudon M, Roy C, Mège-Lechevallier F, et al. Use of Prostate Systematic and Targeted Biopsy on the Basis of Multiparametric MRI in Biopsy-Naive Patients (MRI-FIRST): A Prospective, Multicentre, Paired Diagnostic Study. *Lancet Oncol* (2019) 20(1):100–9. doi: 10.1016/s1470-2045(18)30569-2
29. Ahdoot M, Wilbur AR, Reese SE, Lebastchi AH, Mehralivand S, Gomella PT, et al. MRI-Targeted, Systematic, and Combined Biopsy for Prostate Cancer Diagnosis. *N Engl J Med* (2020) 382(10):917–28. doi: 10.1056/NEJMoa1910038
30. Rapisarda S, Bada M, Crocetto F, Barone B, Arcaniolo D, Polara A, et al. The Role of Multiparametric Resonance and Biopsy in Prostate Cancer Detection: Comparison With Definitive Histological Report After Laparoscopic/Robotic Radical Prostatectomy. *Abdom Radiol (NY)* (2020) 45(12):4178–84. doi: 10.1007/s00261-020-02798-8
31. Grossman DC, Curry SJ, Owens DK, Bibbins-Domingo K, Caughey AB, Davidson KW, et al. Screening for Prostate Cancer: US Preventive Services Task Force Recommendation Statement. *Jama* (2018) 319(18):1901–13. doi: 10.1001/jama.2018.3710
32. Rouvière O, Schoots IG, Mottet N. Multiparametric Magnetic Resonance Imaging Before Prostate Biopsy: A Chain Is Only as Strong as Its Weakest Link. *Eur Urol* (2019) 75(6):889–90. doi: 10.1016/j.eururo.2019.03.023
33. Rosenkrantz AB, Ginocchio LA, Cornfeld D, Froemming AT, Gupta RT, Turkbey B, et al. Interobserver Reproducibility of the PI-RADS Version 2 Lexicon: A Multicenter Study of Six Experienced Prostate Radiologists. *Radiology* (2016) 280(3):793–804. doi: 10.1148/radiol.2016152542
34. He BM, Chen R, Sun TQ, Yang Y, Zhang CL, Ren SC, et al. Prostate Cancer Risk Prediction Models in Eastern Asian Populations: Current Status, Racial Difference, and Future Directions. *Asian J Androl* (2020) 22(2):158–61. doi: 10.4103/aja.aja_55_19
35. Yoon DK, Park JY, Yoon S, Park MS, Moon du G, Lee JG, et al. Can the Prostate Risk Calculator Based on Western Population be Applied to Asian Population? *Prostate* (2012) 72(7):721–9. doi: 10.1002/pros.21475
36. Chen R, Xie L, Xue W, Ye Z, Ma L, Gao X, et al. Development and External Multicenter Validation of Chinese Prostate Cancer Consortium Prostate Cancer Risk Calculator for Initial Prostate Biopsy. *Urol Oncol* (2016) 34(9):416.e1–7. doi: 10.1016/j.urolonc.2016.04.004
37. Niu XK, He WF, Zhang Y, Das SK, Li J, Xiong Y, et al. Developing a New PI-RADS V2-Based Nomogram for Forecasting High-Grade Prostate Cancer. *Clin Radiol* (2017) 72(6):458–64. doi: 10.1016/j.crad.2016.12.005
38. Li M, Chen T, Zhao W, Wei C, Li X, Duan S, et al. Radiomics Prediction Model for the Improved Diagnosis of Clinically Significant Prostate Cancer on Biparametric MRI. *Quant Imaging Med Surg* (2020) 10(2):368–79. doi: 10.21037/qims.2019.12.06
39. Li X, Pan Y, Huang Y, Wang J, Zhang C, Wu J, et al. Developing a Model for Forecasting Gleason Score ≥7 in Potential Prostate Cancer Patients to Reduce Unnecessary Prostate Biopsies. *Int Urol Nephrol* (2016) 48(4):535–40. doi: 10.1007/s11255-016-1218-y
40. Tao T, Shen D, Yuan L, Zeng A, Xia K, Li B, et al. Establishing a Novel Prediction Model for Improving the Positive Rate of Prostate Biopsy. *Transl Androl Urol* (2020) 9(2):574–82. doi: 10.21037/tau.2019.12.42
41. Liu J, Dong B, Qu W, Wang J, Xu Y, Yu S, et al. Using Clinical Parameters to Predict Prostate Cancer and Reduce the Unnecessary Biopsy Among Patients With PSA in the Gray Zone. *Sci Rep* (2020) 10(1):5157. doi: 10.1038/s41598-020-62015-w
42. Falagario UG, Silecchia G, Bruno SM, Di Nauta M, Auciello M, Sanguedolce F, et al. Does Multiparametric Magnetic Resonance of Prostate Outperform Risk Calculators in Predicting Prostate Cancer in Biopsy Naïve Patients? *Front Oncol* (2020) 10:603384. doi: 10.3389/fonc.2020.603384
43. Alberts AR, Schoots IG, Roobol MJ. Prostate-Specific Antigen-Based Prostate Cancer Screening: Past and Future. *Int J Urol* (2015) 22(6):524–32. doi: 10.1111/iju.12750
44. Falagario UG, Jambor I, Lantz A, Ettala O, Stabile A, Taimen P, et al. Combined Use of Prostate-Specific Antigen Density and Magnetic Resonance Imaging for Prostate Biopsy Decision Planning: A Retrospective Multi-Institutional Study Using the Prostate Magnetic Resonance Imaging Outcome Database (PROMOD). *Eur Urol Oncol* (2020) 4(6):971–9. doi: 10.1016/j.euo.2020.08.014
45. Washino S, Okochi T, Saito K, Konishi T, Hirai M, Kobayashi Y, et al. Combination of Prostate Imaging Reporting and Data System (PI-RADS) Score and Prostate-Specific Antigen (PSA) Density Predicts Biopsy Outcome in Prostate Biopsy Naïve Patients. *BJU Int* (2017) 119(2):225–33. doi: 10.1111/bju.13465
46. Falagario UG, Martini A, Wajswol E, Treacy PJ, Ratnani P, Jambor I, et al. Avoiding Unnecessary Magnetic Resonance Imaging (MRI) and Biopsies: Negative and Positive Predictive Value of MRI According to Prostate-Specific Antigen Density, 4Kscore and Risk Calculators. *Eur Urol Oncol* (2020) 3(5):700–4. doi: 10.1016/j.euo.2019.08.015
47. Maggi M, Del Giudice F, Falagario UG, Cocci A, Russo GI, Di Mauro M, et al. SelectMDx and Multiparametric Magnetic Resonance Imaging of the Prostate for Men Undergoing Primary Prostate Biopsy: A Prospective Assessment in a Multi-Institutional Study. *Cancers (Basel)* (2021) 13(9):2047. doi: 10.3390/cancers13092047
48. Falagario UG, Ratnani P, Lantz A, Jambor I, Dovey Z, Verma A, et al. Staging Accuracy of Multiparametric Magnetic Resonance Imaging in Caucasian and African American Men Undergoing Radical Prostatectomy. *J Urol* (2020) 204(1):82–90. doi: 10.1097/ju.0000000000000774

Conflict of Interest: The authors declare that the research was conducted in the absence of any commercial or financial relationships that could be construed as a potential conflict of interest.

Publisher's Note: All claims expressed in this article are solely those of the authors and do not necessarily represent those of their affiliated organizations, or those of the publisher, the editors and the reviewers. Any product that may be evaluated in this article, or claim that may be made by its manufacturer, is not guaranteed or endorsed by the publisher.

Copyright © 2022 Tao, Wang, Liu, Yuan, Ge, Zhang, He, Wang, Wang, Xiang, Wang, Chen and Xiao. This is an open-access article distributed under the terms of the Creative Commons Attribution License (CC BY). The use, distribution or reproduction in other forums is permitted, provided the original author(s) and the copyright owner(s) are credited and that the original publication in this journal is cited, in accordance with accepted academic practice. No use, distribution or reproduction is permitted which does not comply with these terms.

frontiers in Oncology

ORIGINAL RESEARCH
published: 24 January 2022
doi: 10.3389/fonc.2021.824204

TRUS-Guided Target Biopsy for a PI-RADS 3–5 Index Lesion to Reduce Gleason Score Underestimation: A Propensity Score Matching Analysis

Jae Hoon Chung[1], Byung Kwan Park[2], Wan Song[1], Minyong Kang[1], Hyun Hwan Sung[1], Hwang Gyun Jeon[1], Byong Chang Jeong[1], Seong Il Seo[1], Seong Soo Jeon[1] and Hyun Moo Lee[1]*

[1] Department of Urology, Samsung Medical Center, Sungkyunkwan University School of Medicine, Seoul, South Korea, [2] Department of Radiology, Samsung Medical Center, Sungkyunkwan University School of Medicine, Seoul, South Korea

OPEN ACCESS

Edited by:
Tanya I. Stoyanova, Stanford University, United States

Reviewed by:
Andrea Benedetto Galosi, Marche Polytechnic University, Italy
Francesco Del Giudice, Sapienza University of Rome, Italy

***Correspondence:**
Byung Kwan Park
rapark@skku.edu;
1436park@gmail.com

Specialty section:
This article was submitted to Genitourinary Oncology, a section of the journal Frontiers in Oncology

Received: 29 November 2021
Accepted: 30 December 2021
Published: 24 January 2022

Citation:
Chung JH, Park BK, Song W, Kang M, Sung HH, Jeon HG, Jeong BC, Seo SI, Jeon SS and Lee HM (2022) TRUS-Guided Target Biopsy for a PI-RADS 3–5 Index Lesion to Reduce Gleason Score Underestimation: A Propensity Score Matching Analysis. Front. Oncol. 11:824204. doi: 10.3389/fonc.2021.824204

Background: Magnetic resonance imaging (MRI) and transrectal ultrasound (TRUS)-guided cognitive or image fusion biopsy is performed to target a prostate imaging reporting and data system (PI-RADS) 3–5 lesion. Biopsy Gleason score (GS) is frequently underestimated compared to prostatectomy GS. However, it is still unclear about how many cores on target are necessary to reduce undergrading and if additional cores around the target may improve grade prediction on surgical specimen.

Purpose: To determine the number of target cores and targeting strategy to reduce GS underestimation.

Materials and Methods: Between May 2017 and April 2020, a total of 385 patients undergoing target cognitive or image fusion biopsy of PI-RADS 3–5 index lesions and radical prostatectomies (RP) were 2:1 matched with propensity score using multiple variables and divided into the 1–4 core (n = 242) and 5–6 core (n = 143) groups, which were obtained with multiple logistic regression with restricted cubic spline curve. Target cores of 1–3 and 4–6 were sampled from central and peripheral areas, respectively. Pathologic outcomes and target cores were retrospectively assessed to analyze the GS difference or changes between biopsy and RP with Wilcoxon signed-rank test.

Results: The median of target cores was 3 and 6 in the 1–4 core and 5–6 core groups, respectively ($p < 0.001$). Restricted cubic spline curve showed that GS upgrade was significantly reduced from the 5th core and there was no difference between 5th and 6th cores. Among the matched patients, 35.4% (136/385; 95% confidence interval, 0.305–0.403) had a GS upgrade after RP. The GS upgrades in the 1–4 core and 5–6 core groups were observed in 40.6% (98/242, 0.343–0.470) and 26.6% (38/143, 0.195–0.346), respectively (p = 0.023). Although there was no statistical difference between the matched groups in terms of RP GS (p = 0.092), the 5–6 core group had significantly higher biopsy GS (p = 0.006) and lower GS change from biopsy to RP (p = 0.027).

Conclusion: Five or more target cores sampling from both periphery and center of an index tumor contribute to reduce GS upgrade.

Keywords: prostatic neoplasms, biopsy, Gleason score, prostate imaging and reporting and data system, transrectal ultrasound

INTRODUCTION

Gleason score (GS) can be used to assess the aggressiveness and prognosis of prostate cancer (PCa) (1). However, pathologic discrepancies between pre-operative biopsy and radical prostatectomy (RP) in terms of GS are common (1, 2). GS underestimation is reported to range from 19% to 57% (3–9). The possibility of GS upgrade after RP compared with that after prostate biopsy is well known (10). The low-, intermediate-, and high-risk categories are based on Gleason score as this categorization drives treatment planning. Underestimating Gleason 8 (high risk) as Gleason 6 (low risk) has more clinical impact than underestimating Gleason 10 (high risk) as a Gleason 8 (high risk) (11). Moreover, incorrect GS biopsy can adversely impact treatment for men with PCa (12).

Recently, there has been an increase in usage of multi-parametric magnetic resonance imaging (mpMRI) for prostate-targeted biopsy owing to its significant accuracy for pre-operative PCa diagnosis (13, 14). Many studies reported that mpMRI-targeted biopsy of suspected lesions increases detection of clinically significant PCa (15, 16). Calio et al. reported that saturation target biopsy of an index lesion significantly decreases the risk of upgrading on radical prostatectomy by minimizing the impact of tumor heterogeneity (17). However, there is no consensus on the number of target biopsy cores required per lesion to minimize underestimation of GS during mpMRI-targeted biopsy. Additionally, it is unclear if central sampling of an index tumor is the best strategy for target biopsy. Many radiologists and urologists try to target the center of an index tumor alone. However, this targeting can make it difficult to detect additional significant cancers in the peripheral area of an index tumor, in which tissue heterogeneity is frequent in high GS cancer (17).

However, only a few reports have focused on the strategy of target biopsy and the number of target cores that contribute to reducing GS underestimation (18–22). If prostate biopsy can predict or represent an RP specimen, it would be helpful to determine treatment options and predict prognosis. This study hypothesized that sampling the peripheral and central areas of an index tumor improves GS discrepancies between biopsy and prostatectomy, and that the GS discrepancy is changed according the number of target cores. The purpose of this study was to assess our strategy for target biopsy and to determine the number of target cores to reduce GS underestimation.

MATERIALS AND METHODS

This study was performed in agreement with the applicable laws and regulations, good clinical practices, and ethical principles as described in the Declaration of Helsinki. Our institutional review boards approved the present study (2020-08-137) and waived the need for informed consent.

Patients

We reviewed a total of 2,094 patients who underwent RP between May 2017 and April 2020. Among them, we included patients who were diagnosed with PCa through mpMRI target biopsy by two genitourinary radiologists. Both radiologists were experts in mpMRI target biopsies and had performed more than 250 prostate biopsies per year. Among the 2,094 patients, 998 were excluded because PCa was diagnosed at other institutions. Of the remaining 1,096 patients, 692 were excluded because PCa was diagnosed by systematic biopsy alone. Finally, a total of 404 patients were included in the analysis (**Figure 1**). Of these patients, 22.8% (92/404) had a history of past biopsies. Prostate biopsies were performed in the radiologic department of a single institute. The median time interval between biopsy and RP was 59.0 days [45–81 days]. Pathological reporting was assessed by one genitourinary pathologist who had specialized in genitourinary pathology for 20 years. He examined both biopsy and RP specimens to determine GS, tumor size, and cancer stage based on the 2014 International Society of Urological Pathology Consensus Conference (23). We defined GS upgrade when biopsy GS was upgraded into prostatectomy GS by 1 or more and when biopsy GS 7 (3 + 4) was changed into prostatectomy GS 7 (4 + 3). The entire RP specimen was multi-sectioned, but giant micro-slides that covered both lobes were not created.

Clinico-Pathological Parameters

Baseline characteristics of age at RP, body mass index (BMI), prostate-specific antigen (PSA) level before prostate biopsy, prostate volume (measured on MRI), PSA density (PSAD), alpha-reductase inhibitor, and history of prostate biopsy were evaluated. Pathologic outcomes and number of biopsy cores were compared to analyze the difference between biopsy and RP or GS changes from biopsy to RP. Biopsy complications were recorded to assess whether increasing the number of target biopsy cores influenced post-biopsy complication rates.

MRI Protocol and Interpretation

All MRI examinations were performed with a 3-T scanner (Intera Achieva TX, Philips Healthcare, Best, Netherlands) using a phase-array coil (Philips Healthcare). Standard MRI parameters for both prostate imaging reporting and data system (PI-RADS) versions 2.0 were applied. MR images were interpreted and prostate biopsies were performed by one of two radiologists. MRI protocols included T2-weighted imaging (T2WI), T1-weighted imaging, diffusion-weighted imaging (DWI), apparent diffusion coefficient (ADC) imaging, and dynamic contrast-enhanced imaging (DCEI). The T2WI was

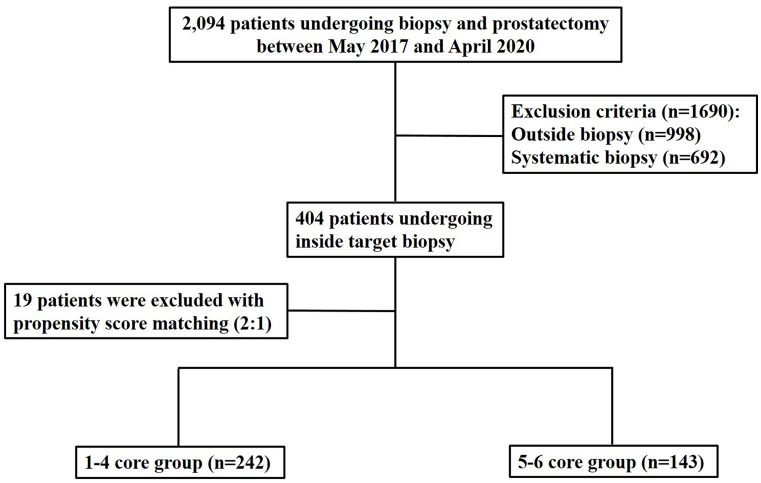

FIGURE 1 | Flow diagram illustrating how to include and to exclude patients.

scanned into axial, sagittal, or coronal planes. The other MR sequences were scanned into only the axial plane. DWI was scanned with *b*-values of 0, 100, 1000, and 1500 s/mm^2. ADC values were calculated with all *b*-values for the DWI, and ADC map images were created. DCEI was obtained with an ultra-fast scan that covered the entire prostate.

Interpretation of MR images was based on PI-RADS version 2.0. Tumor size of a peripheral index lesion was measured on DWI, and that of a transition index lesion was measured on T2WI. Additionally, the size of an index tumor was also measured on the RP specimen to compare between target core groups.

mpMRI-Target Biopsy

Target biopsy (median, 4.00 cores and range, 1–6) was performed on the index tumor, which was categorized as PI-RAD 3–5. Cognitive to image fusion biopsy ratio was 156:248. One of two radiologists performed image fusion biopsy in 156 patients and cognitive biopsy in 29 patients. He obtained mainly three or less target cores from the center of an index lesion. The other performed only cognitive biopsy in 219 patients and he obtained mainly 6 or less target cores from the central and peripheral areas of an index lesion.

The first, second, and third target cores were sampled in the center of an index lesion, and the other (fourth, fifth, and sixth) target cores were sampled in the peripheral area of the index tumor (**Figure 2**). Central sampling was followed by peripheral sampling for target biopsies. Accordingly, number 1–3 target cores indicated central sampling, and number 4–6 target cores indicated peripheral sampling (24). Two radiologists used one of three US scanners including EPIC (Philips Health Care, Bothell, WA, USA), IU22 (Philips Health Care), or Aplio 500 (Toshiba Medical System, Japan). End-fire US probe was introduced into the rectum. Fly Thru and Smart Fusion (Toshiba Medical System) was used for MRI-TRUS fusion imaging. An 18-gauge needle mounted on a spring-loaded commercial biopsy device (ACECUT; TSK Laboratory, Tochigi-shi, Japan) was used for target and systematic biopsies.

Statistical Analysis

Univariate and multivariate analyses were performed to identify what influenced the GS upgrade. Multiple logistic regression was used to determine if there was GS upgrade according to the number of biopsy cores. Also, restricted cubic spline curve was generated to show linearity of the GS upgrade rate as the number of cores increases. It was significantly reduced from the 5th core, but there was no difference between the 5th and 6th cores. Accordingly, we divided the study population into the 1–4 core group and 5–6 core group.

Standardized mean difference (SMD) was assessed to detect how baseline characteristics were changed before and after matching, The cases were matched with 2:1 propensity score using these variables to compare 1–4 core and 5–6 core groups in terms of GS upgrade, GS difference or change, and complication.

Age and BMI, in which these data were in normal distribution, were compared between the groups using *t*-test. Wilcoxon rank sum test was used to compare the other variables in baseline characteristics because these data were not in normal distribution. This statistical test was used to compare GS difference or change from biopsy to RP. Chi-square test was also used to compare percentage data between groups. Data were shown as mean ± standard deviation or median [interquartile range]. Statistical analyses were performed with R version 4.1.0 (2021-05-18) (Vienna, Austria; http://www.R-project.org/). All two-sided *p*-values < 0.05 were considered statistically significant.

RESULTS

Univariate analysis showed that PI-RADS score (p = 0.027–0.003) and number of target cores (p = 0.006) significantly influenced GS upgrade (**Table 1**). Multivariate analysis demonstrated that these variables were also involved in GS

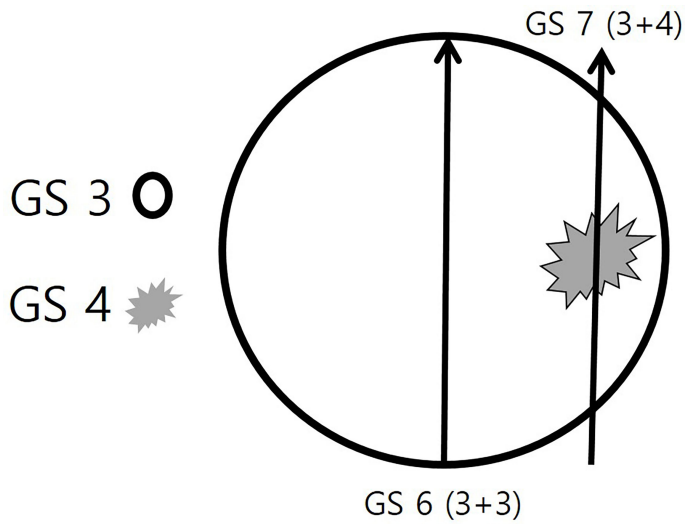

FIGURE 2 | Schematic illustration of the target biopsy strategy. A round prostate cancer consists of two Gleason score (GS) components of GS 3 and GS 4. The GS 3 (black circle) is the major component and the GS 4 (gray spiculation) is the minor component. If a radiologist or urologist targets the central area alone, the histologic diagnosis will be a GS 6 (3 + 3) adenocarcinoma. However, if the periphral area is targeted, the histologic diagnosis will be a GS 7 (3 + 4) adenocarcinoma.

upgrade (**Table 1**). The *p*-values of PI-RADS score and number of target cores were 0.043–0.007 and 0.012, respectively. The odds ratios of these variables ranged from 0.396 to 0.533 (**Table 1**) and thus GS upgrade decreased 0.396–0.533 times as the PI-RADS scores and the number of target cores increased. The other variables such as age, body mass index, previous biopsy history, 5α-reductase inhibitor, PSA, prostate volume, PSAD, and the size of an index lesion did not significantly influence GS upgrade (p = 0.169-0.981).

Spline curve showed that GS upgrade was significantly reduced from the 5th core. However, the decreasing rate of the GS upgrade did not tend to have linearity as the number of target cores increased. Therefore, our study population was divided into the 1–4 core group (n = 260) and the 5–6 core group (n = 144) (**Figure 3**).

However, there was significant difference between the groups in terms of PSA (p = 0.038) (**Table 2**). The SMDs of PSA, prostate volume, and PI-RADS score were significantly reduced from 0.26 to 0.04, from 0.13 to 0.04, and from 0.1 to 0.05 after matching, respectively (**Figure 4**) (**Table 2**). However, the SMDs of baseline characteristics such as age and BMI were not so different after matching (**Figure 4**) (**Table 2**). Therefore, the cases were matched with 2:1 propensity score using PSA, prostate volume, PI-RADS score, age, and BMI (**Table 2**).

TABLE 1 | Clinical variables influencing GS upgrade with univariate and multivariate analyses.

Clinical variables	Simple logistic regression				Multiple logistic regression			
	Odds ratio	Lower limit	Upper limit	*p*-value	Odds ratio	Lower limit	Upper limit	*p*-value
Age	0.996	0.965	1.028	0.807				
Body mass index	1.042	0.966	1.124	0.291				
Number of previous biopsies								
0	Reference							
1	0.694	0.413	1.168	0.169				
2 and 3	1.250	0.275	5.684	0.7727				
Alpha reductase inhibitor	1.482	0.742	2.959	0.265				
Prostate-specific antigen	1.002	0.973	1.032	0.903				
Prostate volume	0.994	0.980	1.009	0.418				
Prostate specific antigen density	1.042	0.442	2.455	0.925				
Size of index lesion	0.957	0.702	1.304	0.781				
PI-RADS								
3	Reference							
4	0.368	0.189	0.714	0.003	0.396	0.202	0.776	0.007
5	0.456	0.227	0.916	0.027	0.483	0.239	0.979	0.043
Number of target cores	0.832	0.729	0.949	0.006	0.533	0.326	0.870	0.012

PI-RADS, prostate imaging and reporting and data system.

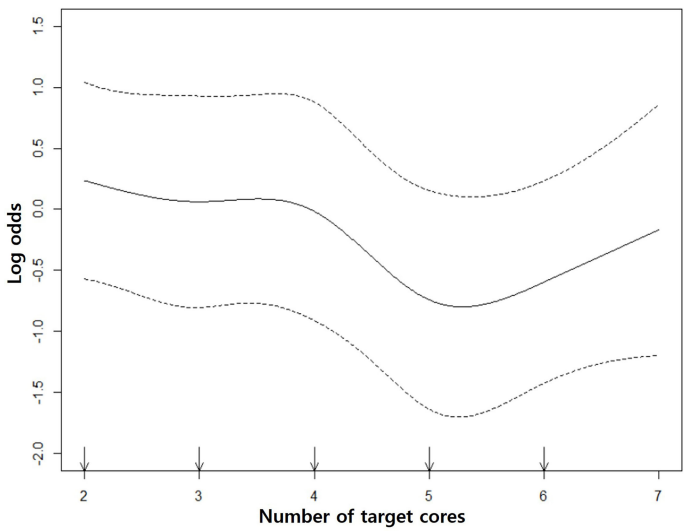

FIGURE 3 | Restricted cubic spline curves. The middle solid curve shows the change of GS upgrade according to the number of target cores. It decreases from the 5th core and there is no significant GS change between 5th and 6th cores. The upper and lower dotted curves indicate the upper and lower limits of log odds.

The number of study population was reduced from 404 to 285 because 19 patients were excluded due to the matching (**Figures 1** and **2**). The numbers of the 1–4 core and 5–6 core groups were reduced to 242 and 143, respectively (**Table 2**). PSA, which was significantly different between the 1–4 core and 5–6 core groups before the matching (p = 0.038), was not significantly different between the groups after the matching (p = 0.433) (**Table 2**). The other variables in baseline characteristics were not significantly different between the matched groups before (p = 0.398–0.806) and after (p = 0.433–0.952) the matching (**Table 2**).

Overall GS upgrade was detected in 35.4% (136/385; 95% confidence interval, 0.305–0.403) in all matched patients. The GS upgrade of the 1–4 core and 5–6 core groups was 40.6% (98/242, 0.343–0.470) and 26.6% (38/143, 0.195–0.346) (**Figure 5**) (**Table 3**). However, no GS change or GS downgrade was not different between the matched groups.

Biopsy GS was significantly different between the 1–4 core and 5–6 core groups before (p = 0.008) and after (p = 0.006) matching even though RP GS was not statistically different before (p = 0.207) or after (p = 0.092) matching (**Table 3**). The changes from biopsy to RP GS were significantly different between the matched groups (p = 0.027). The GS changes were more widely distributed in the 1–4 core group than the 5–6 core group (**Figure 6**).

International Society of Urological Pathology (ISUP) upgrade of the 1–4 core and 5–6 core groups was 36.5% (95/260) and 25.0% (36/144) (p = 0.020), respectively. In ISUP grading, 15.8% (41/260) of the 1–4 core and 8.3%(12/144) of the 5–6 core group was upgraded more than 1 point (p = 0.034). In PI-RADS 5 lesion, 43.8% of patients in the 1–4 core group developed a GS upgrade and 22.2% in the 5–6 core group detected a GS upgrade (**Table 4**).

TABLE 2 | Baseline characteristics before and after propensity score matching.

Pre-biopsy variables	Before matching				After matching			
	1–4 core group	5–6 core group	*p*-value	SMD	1–4 core group	5–6 core group	*p*-value	SMD
No. of pts	260	144			242	143		
Age (years)	65.99 ± 6.44	65.83 ± 6.63	0.806	0.03	65.66 ± 6.45	65.83 ± 6.65	0.814	0.03
BMI	25.15 ± 2.69	25.04 ± 2.72	0.696	0.04	24.99 ± 2.69	25.01 ± 2.70	0.952	0.01
PSA	5.66 [4.04, 8.48]	4.92 [3.86, 7.09]	0.038	0.26	5.31 [3.82, 7.36]	4.88 [3.83, 7.09]	0.433	0.04
Volume	30.10 [24.60, 39.12]	29.55 [24.05, 37.58]	0.463	0.13	30.00 [24.45, 38.10]	29.55 [24.05, 37.58]	0.838	0.04
PSAD	0.17 [0.12, 0.29]	0.17 [0.12, 0.24]	0.398	0.18	0.17 [0.12, 0.24]	0.17 [0.12, 0.24]	0.873	0.01
Index size	1.20 [0.85, 1.70]	1.20 [0.90, 1.60]	0.718	0.04	1.18 [0.85, 1.60]	1.20 [0.90, 1.60]	0.473	0.02
PI-RADS			0.688	0.1			0.871	0.05
3 (%)	29 (11.2)	14 (9.7)			27.1 (11.2)	14.0 (9.8)		
4 (%)	142 (54.6)	85 (59.0)			138.8 (57.3)	85.0 (59.4)		
5 (%)	89 (34.2)	45 (31.2)			76.2 (31.5)	44.0 (30.8)		

[] indicates interquartile range. SMD, standardized mean difference; No. of pts, number of patients; BMI, body mass index (kg/m^2); PSA, prostate-specific antigen (ng/ml); Volume, prostate volume (ml); PSAD, prostate-specific antigen density (ng/ml^2); Index size, the size of an index lesion (cm); PI-RADS, prostate imaging and reporting and data system.

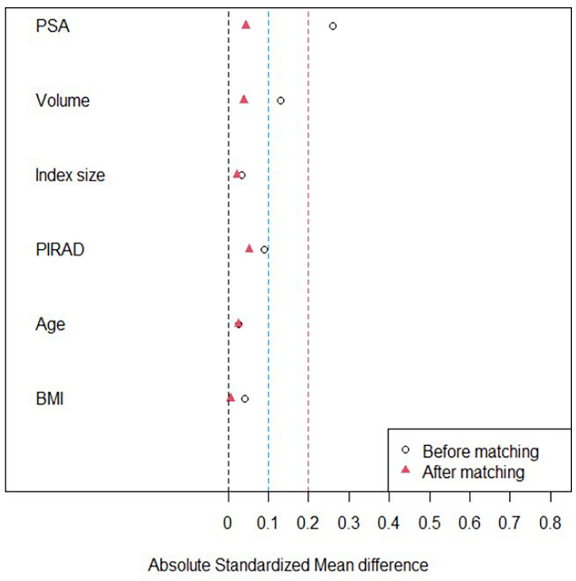

FIGURE 4 | A graph illustrating the change of standardized mean difference (SMD). The SMDs of PSA, prostate volume, and PI-RADS scores are significantly reduced to 0.1 or less after propensity score matching. However, the SMDs of other baseline characteristics such as age, body mass index (BMI), and so on are not siginifcantly different before and after matching.

The complication rate of the 1–4 core group was slightly higher than that of the 5–6 core group, but there was no statistical difference between the groups before and after matching (**Table 3**).

DISCUSSION

This study showed that 5 or more target cores in an index tumor can minimize underestimation of GS score compared with GS in an RP specimen. Moreover, targeting the periphery as well as center of an index tumor allowed detection of additional higher GS and reduced GS discrepancy between biopsy and RP.

With introduction and development of mpMRI to diagnose PCa, a target biopsy approach is being implemented widely due to its effectiveness and accuracy. However, the number of target cores varies across institutions and can vary within an institution, depending on the clinician (25). The American Urological Association recommends a target biopsy of 2 cores or more (26), and the PRECISION trial recommended a target biopsy of 4 cores for PCa (27). Recently, Tu et al. reported that 3–4 cores were better than 1–2 cores, and more than 4 cores showed a better diagnosis of significant PCa than did 4 or fewer cores (28). However, increasing the number of target biopsy cores can increase patient discomfort as well as the potential risk of complications, such as bleeding and acute prostatitis (29). Therefore, many studies have reported the number of target cores to maximize the diagnostic rate without increasing complications.

Previous studies have focused on the saturated target cores for detecting significant PCa (26–28). Diagnosis of significant PCa is important, but accurate diagnosis of GS is equally important in biopsy, as tumor burden and aggressiveness of PCa can be evaluated based on the biopsy results and can help determine a treatment plan and allow prognosis to be assessed. Previous studies reported that high preoperative PSA, high PSAD, obesity, and old age were risk factors for GS upgrade (11, 30, 31), while underlying disease, familial history, and clinical stage were not significantly associated with GS upgrade (32, 33). Our study also showed that PI-RAD classification, clinical stage, number of target cores, biopsy GS, and percentage of tumors in a biopsy core influenced GS upgrade. Therefore, the GS upgrade rate was based on the number of target cores in our study, but a propensity score matching was also used with PSA level, and many clinic-pathologic factors did not differ between the matched groups. As a result, we were able to control possible confounders that can influence GS upgrade.

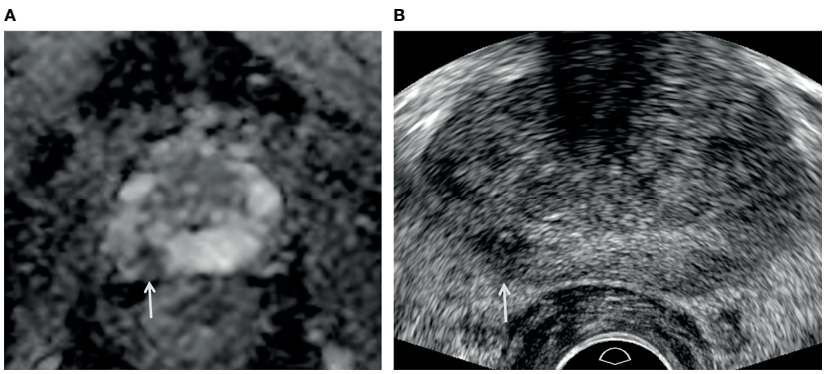

FIGURE 5 | A 73-year-old man with high PSA (3.44 ng/ml). **(A)** Apparent diffusion coefficient map axial image (b = 1,500 s/mm^2) shows a PI-RADS 4 lesion (white arrow) in the right peripheral apex. **(B)** Transrectal-ultrasound transverse image shows a hypoechoic mass (white arrow) well correlated with that on MRI. Target cores of 1–3 and 4–6 were sampled from the center and periphery of the index tumor, respectively. Target cores of 1–4 and 6 were confirmed as GS 6 (3 + 3) adenocarcinoma, but a target core of 5 was GS 7 (3 + 4) adenocarcinoma. A radical prostatectomy specimen demonstrated a final diagnosis of GS 7 (3 + 4) adenocarcinoma.

TABLE 3 | Biopsy and prostatectomy findings before and after propensity score matching.

Post-biopsy variables	Before matching			After matching		
	1–4 core group (*n* = 260)	5–6 core group (*n* = 144)	*p*-value	1–4 core group (*n* = 242)	5–6 core group (*n* = 143)	*p*-value
Positive in DRE	28 (10.7)	13 (9.0)	0.611	24 (9.9)	13 (9.1)	0.859
Previous biopsy	0.25 ± 0.48	0.24 ± 0.49	0.828	0.25 ± 0.48	0.24 ± 0.49	0.914
Biopsy naïve	200 (76.9)	112 (77.8)	0.844	187 (77.3)	111 (77.6)	0.937
Number of target cores	3 [2, 3.25]	6 [5, 6]	<.001	3 [2, 4]	6 [5, 6]	<.001
Detection rate*	79.66 ± 35.33	80.73 ± 27.68	0.755	78.98 ± 35.51	80.59 ± 27.73	0.641
Percentage of malignant tissue within biopsy cores	50 [22.5, 70]	60 [40, 72.5]	0.063	50 [20, 70]	60 [40, 70]	0.019
Biopsy GS	7 [6, 7]	7 [7, 7]	0.008	7 [6, 7]	7 [6.75, 7]	0.006
Prostatectomy GS	7 [7, 7]	7 [7, 7]	0.207	7 [7, 7]	7 [7, 7]	0.092
GS change (%)			0.010			0.023
No change	116 (44.6)	84 (58.3)		113.4 (46.9)	84.0 (58.7)	
Upgrade	107 (41.2)	38 (26.4)		98.2 (40.6)	38.0 (26.6)	
Downgrade	37 (14.2)	22 (15.3)		30.5 (12.6)	21.0 (14.7)	
Complication (%)	13 (5.0)	4 (2.8)	0.420	12.7 (5.2)	4.0 (2.8)	0.196

*[] indicates interquartile range. GS, Gleason score. *number of positive cores/total target cores.*

Although 5ARI increased risk of high-grade PCa (34), in this study, 5ARI did not affect GS upgrading. Among the patients enrolled in this study, only 9 patients (7 in the 1–4 core vs. 2 in the 5–6 core group) had a history of surgery for benign prostatic hyperplasia (BPH) in the past. With a very small number of patients, it was impossible to evaluate the effect of BPH surgery such as TURP on the biopsy method for optimal PCa detection.

In our study, more than 36% of GS upgrades were observed for those with 4 cores or fewer, 24.39% for 5 cores, and 26.51% for 6 cores. It has been previously reported that biopsy of 5 cores or more is recommended for detecting significant PCa (17, 35, 36). These investigations did not determine where target cores were sampled in an index lesion. Therefore, to assess the target location, we obtained 3 cores in the center and the other cores in the periphery of an index lesion. This finding indicates that targeting only the center of an index lesion can miss higher GS for PCa. Additional sampling of the periphery of an index lesion helps to reduce underestimation of GS. The results of previous studies and of this study indicate that the optimal number of target cores in an index lesion is at least 5.

Recently, however, we sampled only two or three cores from PI-RADS 5 with aggressive findings such as extra-capsular extension or seminal vesicle invasion or in patients that were not able to stop medications such as aspirin or anticoagulant therapy. Consequently, our strategy applying target biopsy is not currently recommended in such clinical settings.

Our cases were matched 2:1 but not 1:1 to reduce significant loss of subjects in the 1–4 core group. The number of this group was almost two times greater than that of the 5–6 core group. Several studies have reported that variable ratio matching mostly outperforms 1:1 ratio matching (37, 38).

Downsizing tumor can be related to MRI limitations. That could be also called "MRI undersizing": tumor located at margins of the MR lesion are not visible at MRI (39). That is related to tumor heterogeneity in terms of not-round tumor shape and volume other than histologic sub-type and grading (39).

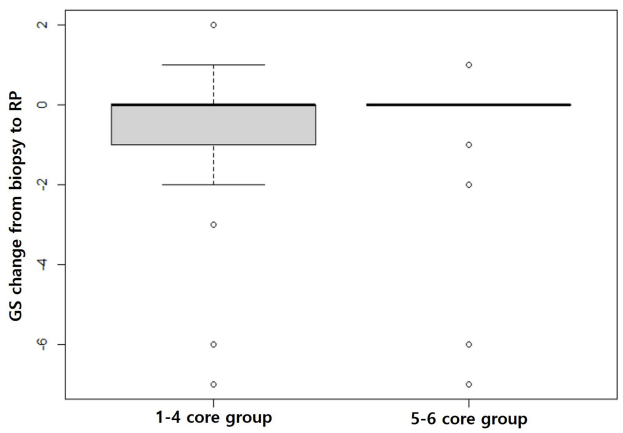

FIGURE 6 | Box plots showing GS changes from biopsy to prostatectomy. The gray box in the 1–4 core group is much larger than that in the 5–6 core group, indicating that the GS changes from biopsy to prostatectomy are significantly greater in the 1–4 core group than the 5–6 core group ($p = 0.027$).

TABLE 4 | Sub-analysis of Gleason score upgrade.

	Gleason score upgrade		*p*-value
	1–4 core group (107/260, 41.15%)	5–6 core group (38/144, 26.39%)	
ISUP upgrade (%)	95 (36.54)	36 (25.00)	0.020
ISUP upgrade (>1 point) (%)	41 (15.77)	12 (8.33)	0.034
PI-RADS 3 (%)	19/29 (65.52)	5/14 (35.71)	0.102
PI-RADS 4 (%)	49/142 (34.51)	23/85 (27.06)	0.302
PI-RADS 5 (%)	39/89 (43.82)	10/45 (22.22)	0.015
Image fusion biopsy (%)	66/154 (42.86)	0/2 (0)	0.509
Cognitive biopsy (%)	41/106 (38.68)	38/142 (26.76)	0.054

ISUP, International Society of Urological Pathology; PI-RADS, prostate imaging and reporting and data system.

Combining these variables, we can imagine how many possible variations could influence final tumor extension and exact location of the most aggressive tumor.

In order to reduce these variables and technical software fusion collimation error: 2-5 mm or cognitive error other than Operator targeting failure (software or cognitive), in 2016, originally Galosi et al. reported the zonal saturation biopsy that overcome bias related to the most important variables (MRI interpretation, collimation, and operator) (40). Recently, in concordance with observation of this study and the former, Tschirdewahn et al. showed that target saturation biopsy detected significantly higher grade disease than Target Biopsy and extended Systematic Biopsy (41).

In the present study, among target biopsy cores, the ratio of the positive cores was 79.6% in the 1–4 core group and 80.7% in the 5–6 core group. The median per-patient percentage of malignant tissue within biopsy cores was 50% (IQR: 22.5–70%) in the 1–4 core group and 60% (IQR: 40–72.5%) in the 5–6 core group. Compared with previous studies, accuracy of the biopsy in this study is reliable (42).

This study had some limitations. First, as it was a retrospective study, the possibility of selection bias cannot be excluded. The cohort was restricted to those treated with prostatectomy, who tend to have smaller tumors at lower stage. Thus, the biopsy sampling strategy may not need to be as aggressive in patients who have larger, more advanced tumors. Second, the optimal number of systematic biopsies was not determined, and systematic biopsy could detect additional significant PCa. Third, there was a lack of analysis according to risk category rather than Gleason score. Underestimation of risk category (i.e., low-, intermediate-, or high-risk histology) rather than simply Gleason score is of more clinical importance and analyzing along those lines would be useful. Montironi et al. (43) showed two relevant issues: the first, ISUP grading is the preferred and easy method to be used compared to Gleason score to evaluate grade difference between biopsy and pathology; the second is that more than 1 ISUP point has a profound impact on disease management rather than 1 point upgrading. In this study, in the 5–6 core group, ISUP upgrade was significantly lower than the 1–4 core group. However, clinical differences, such as biochemical recurrence and adjuvant treatment, between two groups could not be identified according this classification, so further studies will be needed. Fourth, the study population was not uniformly composed. Two radiologists used different techniques: one used cognitive biopsy in all cases and the other did image fusion biopsy in almost all cases.

CONCLUSION

Increasing the number of target cores is useful for minimizing GS underestimation without increasing the complication rate. Based on this analysis, the number of target cores should be five or more. Sampling the periphery as well as center of an index lesion is a key technical step for obtaining higher GS PCa.

DATA AVAILABILITY STATEMENT

The original contributions presented in the study are included in the article/supplementary material. Further inquiries can be directed to the corresponding author.

ETHICS STATEMENT

The studies involving human participants were reviewed and approved by Samsung Medical Center. Written informed consent for participation was not required for this study in accordance with the national legislation and the institutional requirements.

AUTHOR CONTRIBUTIONS

Conceptualization: All authors. Methodology: All authors. Software: JC. Validation: BP. Formal analysis: JC. Investigation: BP. Resources: BP. Data curation: BP. Writing—original draft preparation: JC and BP. Writing—review and editing: All authors. Visualization: BP. Supervision: BP. Project administration: BP. Funding acquisition: none. All authors contributed to the article and approved the submitted version.

ACKNOWLEDGMENTS

We sincerely thank Joong Hyun Ahn, a bio-statistician who is working at Statistical analysis in medical research, Samsung Medical Center. He has contributed to statistical analysis in our study.

REFERENCES

1. Sfoungaristos S, Perimenis P. Clinical and Pathological Variables That Predict Changes in Tumour Grade After Radical Prostatectomy in Patients With Prostate Cancer. *Can Urol Assoc J* (2013) 7(1-2):E93–7. doi: 10.5489/cuaj.270
2. Walker R, Lindner U, Louis A, Kalnin R, Ennis M, Nesbitt M, et al. Concordance Between Transrectal Ultrasound Guided Biopsy Results and Radical Prostatectomy Final Pathology: Are We Getting Better at Predicting Final Pathology? *Can Urol Assoc J* (2014) 8(1-2):47–52. doi: 10.5489/cuaj.751
3. Thickman D, Speers WC, Philpott PJ, Shapiro H. Effect of the Number of Core Biopsies of the Prostate on Predicting Gleason Score of Prostate Cancer. *J Urol* (1996) 156(1):110–3. doi: 10.1016/S0022-5347(01)65956-1
4. Moreira Leite KR, Camara-Lopes LH, Dall'Oglio MF, Cury J, Antunes AA, Sañudo A, et al. Upgrading the Gleason Score in Extended Prostate Biopsy: Implications for Treatment Choice. *Int J Radiat Oncol Biol Phys* (2009) 73 (2):353–6. doi: 10.1016/j.ijrobp.2008.04.039
5. Müntener M, Epstein JI, Hernandez DJ, Gonzalgo ML, Mangold L, Humphreys E, et al. Prognostic Significance of Gleason Score Discrepancies Between Needle Biopsy and Radical Prostatectomy. *Eur Urol* (2008) 53 (4):767–75; discussion 75-6. doi: 10.1016/j.eururo.2007.11.016
6. Pinthus JH, Witkos M, Fleshner NE, Sweet J, Evans A, Jewett MA, et al. Prostate Cancers Scored as Gleason 6 on Prostate Biopsy Are Frequently Gleason 7 Tumors at Radical Prostatectomy: Implication on Outcome. *J Urol* (2006) 176(3):979–84; discussion 84. doi: 10.1016/j.juro.2006.04.102
7. Fitzsimons NJ, Presti JC Jr, Kane CJ, Terris MK, Aronson WJ, Amling CL, et al. Is Biopsy Gleason Score Independently Associated With Biochemical Progression Following Radical Prostatectomy After Adjusting for Pathological Gleason Score? *J Urol* (2006) 176(6 Pt 1):2453–8; discussion 8. doi: 10.1016/j.juro.2006.08.014
8. Grossfeld GD, Chang JJ, Broering JM, Li YP, Lubeck DP, Flanders SC, et al. Under Staging and Under Grading in a Contemporary Series of Patients Undergoing Radical Prostatectomy: Results From the Cancer of the Prostate Strategic Urologic Research Endeavor Database. *J Urol* (2001) 165(3):851–6. doi: 10.1097/00005392-200103000-00028
9. Rajinikanth A, Manoharan M, Soloway CT, Civantos FJ, Soloway MS. Trends in Gleason Score: Concordance Between Biopsy and Prostatectomy Over 15 Years. *Urology* (2008) 72(1):177–82. doi: 10.1016/j.urology.2007.10.022
10. Alchin DR, Murphy D, Lawrentschuk N. Risk Factors for Gleason Score Upgrading Following Radical Prostatectomy. *Minerva Urol Nefrol* (2017) 69 (5):459–65. doi: 10.23736/s0393-2249.16.02684-9
11. Epstein JI, Feng Z, Trock BJ, Pierorazio PM. Upgrading and Downgrading of Prostate Cancer From Biopsy to Radical Prostatectomy: Incidence and Predictive Factors Using the Modified Gleason Grading System and Factoring in Tertiary Grades. *Eur Urol* (2012) 61(5):1019–24. doi: 10.1016/j.eururo.2012.01.050
12. Alchin DR, Murphy D, Lawrentschuk N. What Are the Predictive Factors for Gleason Score Upgrade Following RP? *Urol Int* (2016) 96(1):1–4. doi: 10.1159/000439139
13. Rouvière O, Puech P, Renard-Penna R, Claudon M, Roy C, Mège-Lechevallier F, et al. Use of Prostate Systematic and Targeted Biopsy on the Basis of Multiparametric MRI in Biopsy-Naive Patients (MRI-FIRST): A Prospective, Multicentre, Paired Diagnostic Study. *Lancet Oncol* (2019) 20(1):100–9. doi: 10.1016/s1470-2045(18)30569-2
14. Macura KJ. Multiparametric Magnetic Resonance Imaging of the Prostate: Current Status in Prostate Cancer Detection, Localization, and Staging. *Semin Roentgenol* (2008) 43(4):303–13. doi: 10.1053/j.ro.2008.06.002
15. Haffner J, Lemaitre L, Puech P, Haber GP, Leroy X, Jones JS, et al. Role of Magnetic Resonance Imaging Before Initial Biopsy: Comparison of Magnetic Resonance Imaging-Targeted and Systematic Biopsy for Significant Prostate Cancer Detection. *BJU Int* (2011) 108(8 Pt 2):E171–8. doi: 10.1111/j.1464-410X.2011.10112.x
16. Siddiqui MM, Rais-Bahrami S, Truong H, Stamatakis L, Vourganti S, Nix J, et al. Magnetic Resonance Imaging/Ultrasound-Fusion Biopsy Significantly Upgrades Prostate Cancer Versus Systematic 12-Core Transrectal Ultrasound Biopsy. *Eur Urol* (2013) 64(5):713–9. doi: 10.1016/j.eururo.2013.05.059
17. Calio BP, Sidana A, Sugano D, Gaur S, Maruf M, Jain AL, et al. Risk of Upgrading From Prostate Biopsy to Radical Prostatectomy Pathology-Does Saturation Biopsy of Index Lesion During Multiparametric Magnetic Resonance Imaging-Transrectal Ultrasound Fusion Biopsy Help? *J Urol* (2018) 199(4):976–82. doi: 10.1016/j.juro.2017.10.048
18. An T, Park BK. Validation of New TRUS Biopsy Techniques for PI-RADS 4 or 5. *Precis Future Med* (2020) 4(4):141–8. doi: 10.23838/pfm.2020.00114
19. An T, Park BK. Value of Systematic Biopsy Added to Target Biopsy for Detecting Significant Cancer in Men With Prostate Imaging and Reporting and Data System 5. *Precis Future Med* (2020) 4(3):107–13. doi: 10.23838/pfm.2020.00107
20. Park BK, Park SY. New Biopsy Techniques and Imaging Features of Transrectal Ultrasound for Targeting PI-RADS 4 and 5 Lesions. *J Clin Med* (2020) 9(2):530–41. doi: 10.3390/jcm9020530
21. Kim HS, Park BK. Is Transrectal Ultrasound-Guided Systematic Biopsy Necessary After PI-RADS 4 Is Targeted? *Precis Future Med* (2021) 5 (3):125–32. doi: 10.23838/pfm.2021.00030
22. Chung JH, Park BK. Transrectal Ultrasound Features and Biopsy Outcomes of Transition PI-RADS 5. *Acta Radiol* (2021) 2841851211018775. doi: 10.1177/02841851211018775
23. Epstein JI, Egevad L, Amin MB, Delahunt B, Srigley JR, Humphrey PA. The 2014 International Society of Urological Pathology (ISUP) Consensus Conference on Gleason Grading of Prostatic Carcinoma: Definition of Grading Patterns and Proposal for a New Grading System. *Am J Surg Pathol* (2016) 40(2):244–52. doi: 10.1097/pas.0000000000000530
24. Park BK. How to Improve TRUS-Guided Target Biopsy Following Prostate MRI. *Cancers* (2021) 13(22):5647. doi: 10.3390/cancers13225647
25. Valerio M, Donaldson I, Emberton M, Ehdaie B, Hadaschik BA, Marks LS, et al. Detection of Clinically Significant Prostate Cancer Using Magnetic Resonance Imaging-Ultrasound Fusion Targeted Biopsy: A Systematic Review. *Eur Urol* (2015) 68(1):8–19. doi: 10.1016/j.eururo.2014.10.026
26. Rosenkrantz AB, Verma S, Choyke P, Eberhardt SC, Eggener SE, Gaitonde K, et al. Prostate Magnetic Resonance Imaging and Magnetic Resonance Imaging Targeted Biopsy in Patients With a Prior Negative Biopsy: A Consensus Statement by AUA and SAR. *J Urol* (2016) 196(6):1613–8. doi: 10.1016/j.juro.2016.06.079
27. Kasivisvanathan V, Rannikko AS, Borghi M, Panebianco V, Mynderse LA, Vaarala MH, et al. MRI-Targeted or Standard Biopsy for Prostate-Cancer Diagnosis. *N Engl J Med* (2018) 378(19):1767–77. doi: 10.1056/NEJMoa1801993
28. Tu X, Lin T, Cai D, Liu Z, Yang L, Wei Q. The Optimal Core Number and Site for MRI-Targeted Biopsy of Prostate? A Systematic Review and Pooled Analysis. *Minerva Urol Nefrol* (2020) 72(2):144–51. doi: 10.23736/s0393-2249.20.03639-5
29. Papagiannopoulos D, Abern M, Wilson N, O'Block N, Raff L, Coogan C, et al. Predictors of Infectious Complications After Targeted Prophylaxis for Prostate Needle Biopsy. *J Urol* (2018) 199(1):155–60. doi: 10.1016/j.juro.2017.08.040
30. Vellekoop A, Loeb S, Folkvaljon Y, Stattin P. Population Based Study of Predictors of Adverse Pathology Among Candidates for Active Surveillance With Gleason 6 Prostate Cancer. *J Urol* (2014) 191(2):350–7. doi: 10.1016/j.juro.2013.09.034
31. Seisen T, Roudot-Thoraval F, Bosset PO, Beaugerie A, Allory Y, Vordos D, et al. Predicting the Risk of Harboring High-Grade Disease for Patients Diagnosed With Prostate Cancer Scored as Gleason ≤ 6 on Biopsy Cores. *World J Urol* (2015) 33(6):787–92. doi: 10.1007/s00345-014-1348-8
32. Truong M, Slezak JA, Lin CP, Iremashvili V, Sado M, Razmaria AA, et al. Development and Multi-Institutional Validation of an Upgrading Risk Tool for Gleason 6 Prostate Cancer. *Cancer* (2013) 119(22):3992–4002. doi: 10.1002/cncr.28303
33. Jalloh M, Myers F, Cowan JE, Carroll PR, Cooperberg MR. Racial Variation in Prostate Cancer Upgrading and Upstaging Among Men With Low-Risk Clinical Characteristics. *Eur Urol* (2015) 67(3):451–7. doi: 10.1016/j.eururo.2014.03.026
34. Thompson IM, Goodman PJ, Tangen CM, Lucia MS, Miller GJ, Ford LG, et al. The Influence of Finasteride on the Development of Prostate Cancer. *N Engl J Med* (2003) 349(3):215–24. doi: 10.1056/NEJMoa030660
35. Lu AJ, Syed JS, Ghabili K, Hsiang WR, Nguyen KA, Leapman MS, et al. Role of Core Number and Location in Targeted Magnetic Resonance Imaging-Ultrasound Fusion Prostate Biopsy. *Eur Urol* (2019) 76(1):14–7. doi: 10.1016/j.eururo.2019.04.008

36. Zhang M, Milot L, Khalvati F, Sugar L, Downes M, Baig SM, et al. Value of Increasing Biopsy Cores Per Target With Cognitive MRI-Targeted Transrectal US Prostate Biopsy. *Radiology* (2019) 291(1):83–9. doi: 10.1148/radiol.2019180712
37. Austin PC. The Performance of Different Propensity Score Methods for Estimating Marginal Hazard Ratios. *Stat Med* (2013) 32(16):2837–49. doi: 10.1002/sim.5705
38. Cepeda MS, Boston R, Farrar JT, Strom BL. Optimal Matching With a Variable Number of Controls vs. A Fixed Number of Controls for a Cohort Study. Trade-Offs. *J Clin Epidemiol* (2003) 56(3):230–7. doi: 10.1016/s0895-4356(02)00583-8
39. Galosi AB, Palagonia E, Scarcella S, Cimadamore A, Lacetera V, Delle Fave RF, et al. Detection Limits of Significant Prostate Cancer Using Multiparametric MR and Digital Rectal Examination in Men With Low Serum PSA: Up-Date of the Italian Society of Integrated Diagnostic in Urology. *Arch Ital Urol Androl* (2021) 93(1):92–100. doi: 10.4081/aiua.2021.1.92
40. Galosi AB, Maselli G, Sbrollini G, Donatelli G, Montesi L, Tallè M, et al. Cognitive Zonal Fusion Biopsy of the Prostate: Original Technique Between Target and Saturation. *Arch Ital Urol Androl* (2016) 88(4):292–5. doi: 10.4081/aiua.2016.4.292
41. Tschirdewahn S, Wiesenfarth M, Bonekamp D, Püllen L, Reis H, Panic A, et al. Detection of Significant Prostate Cancer Using Target Saturation in Transperineal Magnetic Resonance Imaging/Transrectal Ultrasonography-Fusion Biopsy. *Eur Urol Focus* (2021) 7(6):1300–7. doi: 10.1016/j.euf.2020.06.020
42. Del Monte M, Cipollari S, Del Giudice F, Pecoraro M, Bicchetti M, Messina E, et al. MRI-Directed Biopsy for Primary Detection of Prostate Cancer in a Population of 223 Men: MRI In-Bore vs MRI-Transrectal Ultrasound Fusion-Targeted Techniques. *Br J Radiol* (2021), 20210528. doi: 10.1259/bjr.20210528
43. Montironi R, Santoni M, Mazzucchelli R, Burattini L, Berardi R, Galosi AB, et al. Prostate Cancer: From Gleason Scoring to Prognostic Grade Grouping. *Expert Rev Anticancer Ther* (2016) 16(4):433–40. doi: 10.1586/14737140.2016.1160780

Conflict of Interest: The authors declare that the research was conducted in the absence of any commercial or financial relationships that could be construed as a potential conflict of interest.

Publisher's Note: All claims expressed in this article are solely those of the authors and do not necessarily represent those of their affiliated organizations, or those of the publisher, the editors and the reviewers. Any product that may be evaluated in this article, or claim that may be made by its manufacturer, is not guaranteed or endorsed by the publisher.

Copyright © 2022 Chung, Park, Song, Kang, Sung, Jeon, Jeong, Seo, Jeon and Lee. This is an open-access article distributed under the terms of the Creative Commons Attribution License (CC BY). The use, distribution or reproduction in other forums is permitted, provided the original author(s) and the copyright owner(s) are credited and that the original publication in this journal is cited, in accordance with accepted academic practice. No use, distribution or reproduction is permitted which does not comply with these terms.

frontiers in Oncology

SYSTEMATIC REVIEW
published: 25 January 2022
doi: 10.3389/fonc.2021.792120

Diagnostic Performance of Extraprostatic Extension Grading System for Detection of Extraprostatic Extension in Prostate Cancer: A Diagnostic Systematic Review and Meta-Analysis

Wei Li[1†], *Wenwen Shang*[1†], *Feng Lu*[2], *Yuan Sun*[3], *Jun Tian*[4*], *Yiman Wu*[1] *and Anding Dong*[1*]

[1] Department of Medical Imaging, Jiangsu Vocational College of Medicine, Yancheng, China, [2] Department of Radiology, Wuxi No. 2 People's Hospital, Wuxi, China, [3] Department of Burn and Plastic Surgery, 71st Group Army Hospital of People's Liberation Army of China, Xuzhou, China, [4] Department of Basic Medicine, Jiangsu Vocational College of Medicine, Yancheng, China

OPEN ACCESS

Edited by:
Tanya I. Stoyanova, Stanford University, United States

Reviewed by:
Helena Vila-Reyes, Columbia University Irving Medical Center, United States
Riccardo Tellini, Careggi University Hospital, Italy

***Correspondence:**
Jun Tian
11368@jsmc.edu.cn
Anding Dong
submitfor_sci@126.com

[†]These authors have contributed equally to this work

Specialty section:
This article was submitted to Genitourinary Oncology, a section of the journal Frontiers in Oncology

Received: 09 October 2021
Accepted: 27 December 2021
Published: 25 January 2022

Citation:
Li W, Shang W, Lu F, Sun Y, Tian J, Wu Y and Dong A (2022) Diagnostic Performance of Extraprostatic Extension Grading System for Detection of Extraprostatic Extension in Prostate Cancer: A Diagnostic Systematic Review and Meta-Analysis. Front. Oncol. 11:792120. doi: 10.3389/fonc.2021.792120

Purpose: To evaluate the diagnostic performance of the extraprostatic extension (EPE) grading system for detection of EPE in patients with prostate cancer (PCa).

Materials and Methods: We performed a literature search of Web of Science, MEDLINE (Ovid and PubMed), Cochrane Library, EMBASE, and Google Scholar to identify eligible articles published before August 31, 2021, with no language restrictions applied. We included studies using the EPE grading system for the prediction of EPE, with histopathological results as the reference standard. The pooled sensitivity, specificity, positive likelihood ratio (LR+), negative likelihood ratio (LR–), and diagnostic odds ratio (DOR) were calculated with the bivariate model. Quality assessment of included studies was performed using the Quality Assessment of Diagnostic Accuracy Studies-2 tool.

Results: A total of 4 studies with 1,294 patients were included in the current systematic review. The pooled sensitivity and specificity were 0.82 (95% CI 0.76–0.87) and 0.63 (95% CI 0.51–0.73), with the area under the hierarchical summary receiver operating characteristic (HSROC) curve of 0.82 (95% CI 0.79–0.85). The pooled LR+, LR–, and DOR were 2.20 (95% CI 1.70–2.86), 0.28 (95% CI 0.22–0.36), and 7.77 (95% CI 5.27–11.44), respectively. Quality assessment for included studies was high, and Deeks's funnel plot indicated that the possibility of publication bias was low ($p = 0.64$).

Conclusion: The EPE grading system demonstrated high sensitivity and moderate specificity, with a good inter-reader agreement. However, this scoring system needs more studies to be validated in clinical practice.

Keywords: prostate neoplasms, magnetic resonance imaging, diagnostic performance, extraprostatic extension, systematic review

INTRODUCTION

Prostate cancer (PCa) is the most common malignancy among males in Northern America and Europe, where one in nine men will be diagnosed with PCa at some point during their lifetime (1, 2). Compared with organ-confined disease (pT2), which can benefit from nerve-sparing surgical procedures, locally advanced disease [pT3, or extraprostatic extension (EPE)] is associated with a higher risk of biochemical recurrence and metastatic disease (3, 4). Despite that patients who underwent radical prostatectomy (RP) have shown high cancer-specific survival, they are suffering from postoperative erectile dysfunction and urinary incontinence (5). On the other hand, preservation of the neurovascular bundles (NVBs) can improve postoperative potency rates; however, increasing the risks of positive surgical margins then leads to biochemical recurrence and treatment failure (6). Thus, preoperative evaluation of EPE plays a crucial role in clinical management and treatment planning. Previously, varied clinical models and grading systems have been proposed for the prediction of EPE, including the Cancer of the Prostate Risk Assessment (CAPRA) score, Memorial Sloan Kettering Cancer Center (MSKCC) nomogram, and Partin tables (PT). Nonetheless, these risk stratification tools are lacking accuracy and are roughly correlated with final histopathologic results in clinical practice, with reported areas under the curve (AUCs) ranging from 0.61 to 0.81 (7–10).

In 2012, the European Society of Urogenital Radiology (ESUR) introduced Prostate Imaging Reporting and Data System (PI-RADS) for performing, interpreting, and reporting the PCa with multiparametric MRI (mpMRI) (11–13), which was widely applied in clinical practice (14–16). However, for localized advantage PCa of EPE, the ESUR PI-RADS demonstrated moderate diagnostic accuracy, mainly depending on radiologists' own experience and short of reproducibility (17). Recently, a new scoring system termed the EPE grade has been proposed by Mehralivand et al. (18), the primary strength of which is simplicity and without needing to cooperate with complex imaging features. According to this grading system, grade 1 is defined as either curvilinear contact length ≥15 mm or capsular bulge and irregularity; grade 2 is defined as both curvilinear contact length ≥15 mm and capsular bulge and irregularity; and grade 3 is defined as visible EPE at MRI. Several studies showed that the EPE grading system has favorable diagnostic performance; however, this new guideline has not been evaluated systematically. Thus, in this study, we aimed to assess the diagnostic accuracy of using the EPE grading system for the prediction of EPE.

METHODS AND MATERIALS

This meta-analysis was in compliance with the Preferred Reporting Items for Systematic Reviews and Meta-Analyses (PRISMA) guidelines (19) and performed with a standardized review and data extraction protocol. A research question was established based on the Patient Index Test Comparator Outcome Study (PICOS) design criteria, as follows: what is the overall diagnostic performance of the EPE grading for prediction of EPE in patients with PCa? Our goal was to pool the sensitivity and specificity based on currently available retrospective and prospective cohort studies.

Search Strategy and Selection Criteria

A computerized literature search of Web of Science, MEDLINE (Ovid and PubMed), Cochrane Library, EMBASE, and Google Scholar for studies applying the EPE grading system from December 2018 to September 2021, with no language restriction, was applied. The terms combined synonyms using for literature search, as follows: [(EPE) or (ECE) or (extracapsular extension) or (extraprostatic extension)] and [(PCa) or (prostate cancer) or (prostate carcinoma)]. Additional papers were identified from the most recent reviews and the reference lists of eligible papers.

Inclusion Criteria

Studies would be included if they met the following eligibility criteria: 1) involved patients underwent MRI for assessment of suspected EPE, 2) with the EPE grading system for prediction of EPE in PCa, 3) reported sufficient information for the reconstruction of 2 × 2 tables to evaluate the diagnostic performance, and 4) with histopathological finding after RP as the reference standard.

Exclusion Criteria

Studies would be excluded if any of the following criteria were satisfied: 1) studies with a too small sample of fewer than 20 participants, 2) studies using other guidelines or risk stratification tools rather than the EPE grading system, 3) not reported sufficient details for assessing the diagnostic performance, 4) studies with overlapping population, and 5) review articles, guidelines, consensus statements, letters, editorials, and conference abstracts. Two reviewers (WL and WS, with 8 and 5 years of experience, respectively, in performing systematic reviews and meta-analyses) independently evaluated all abstracts, subsequently reviewed full texts, and selected potential eligible articles; all disagreements were resolved through consensus in consultation with a third reviewer (AD).

Data Extraction and Quality Assessment

The following information is extracted from each study: 1) demographic characteristics (sample size, patient age, prostate serum antigen (PSA) level, Gleason score or International Society of Urological Pathology (ISUP) classification, and number of patients diagnosed with EPE using histopathology; 2) study characteristics (first author, publication year, affiliation and location, period of patient recruitment duration, study design, cutoff threshold, other scoring systems used, number of readers and corresponding experience, and blinding; 3) technical characteristics (MRI sequences, magnetic field strength, and coil type); and 4) diagnostic accuracy information (number of true positive, false negative, false positive, and true negative findings classified with diagnostic criteria). Data extraction was

performed by one investigator (WL) and confirmed by a second investigator (WS), with disagreements resolved by consensus after discussion with another one (AD). The methodologic quality of included studies was assessed with the Diagnostic Accuracy Studies-2 tool (20).

Data Synthesis and Analysis

Heterogeneity among included studies was summarized with the inconsistency index (I^2) and Q test: for value between 0% and 40%, unimportant; between 30% and 60%, moderate; between 50% and 90%, substantial; and between 75% and 100%, considerable (21). Pooled sensitivity, specificity, positive likelihood ratio (LR+), negative likelihood ratio (LR−), diagnostic odds ratio (DOR), and their 95% CI were calculated with the bivariate model (22, 23) and then graphically presented in the forest plots; the area under the hierarchical summary receiver operating characteristic (HSROC) curve was calculated as well. In addition, we constructed an HSROC curve with a 95% confidence region and prediction region to demonstrate the results (22, 23). Publication bias was evaluated using Deeks' funnel plot and determined with Deeks' asymmetry test (24). All analyses were conducted using STATA 16.0, and statistical significance was set at a p-value <0.05.

RESULTS

Literature Search and Data Extraction

Figure 1 shows the flowchart of the publication selection process. Our searches generated 137 relevant articles, of which 39 records were excluded for duplicates. After abstract inspection, 65 records were excluded, and a full-text examination was performed in the remaining 13 potentially eligible studies. A total of 29 studies were excluded due to insufficient data to

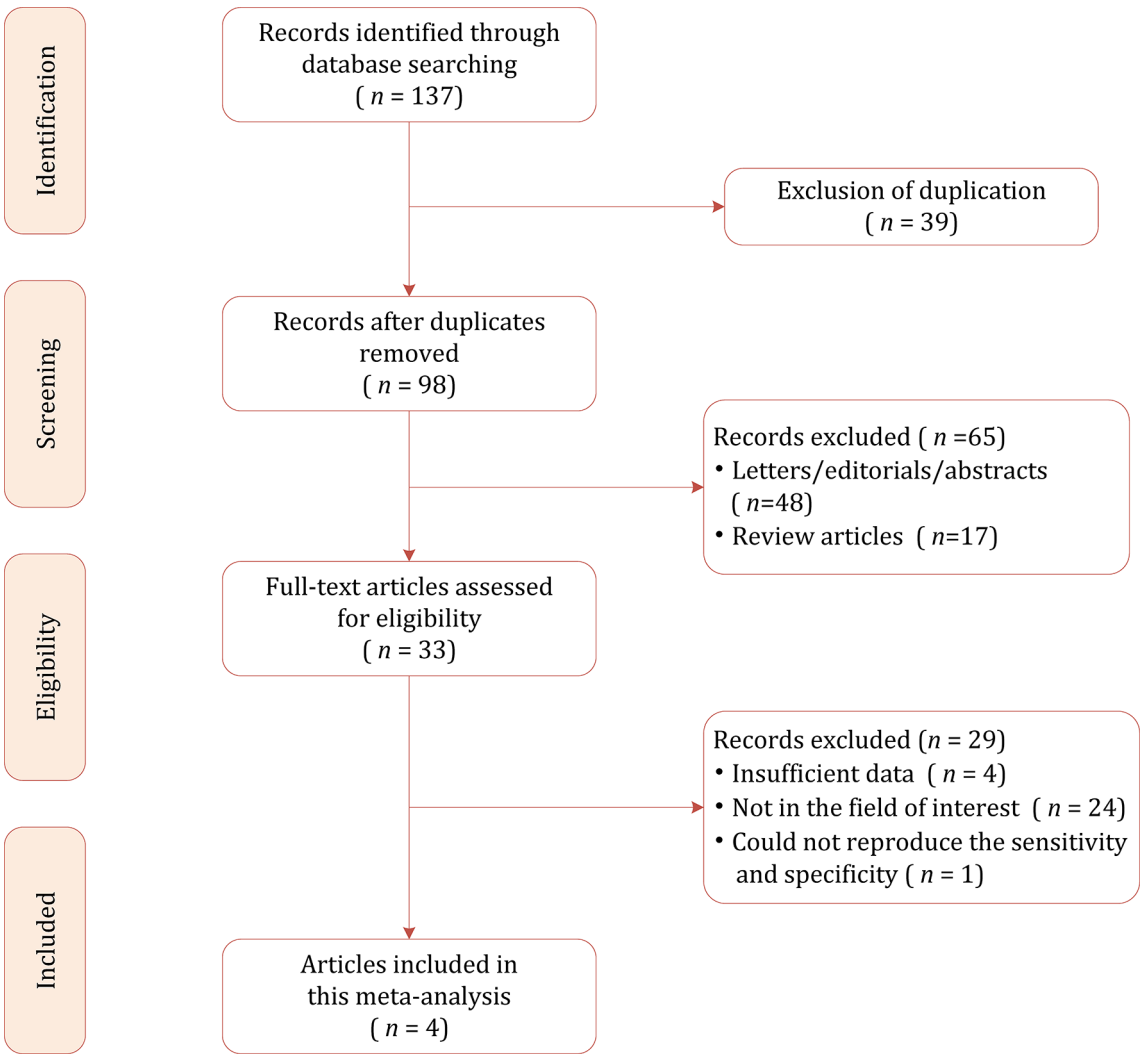

FIGURE 1 | Study selection process for this systematic review and meta-analysis.

reconstruct 2 × 2 tables, not in the field of interest, and could not reproduce the sensitivity and specificity. Consequently, a total of 4 studies comprising 1,294 participants were included in the present meta-analysis (18, 25–27).

Characteristics of the Included Studies

The demographic characteristics are presented in **Table 1**. The sample size of the study population ranged from 130 to 553 patients, with a mean age of 60–65 years. Histopathological results after RP revealed that EPE was presented in 22.6%–48.5% of patients. The mean PSA levels of participants ranged from 6.28 to 9.95 ng/ml, with an ISUP category of 1–5. Concerning study design, only 1 was prospective, and all the remaining 3 were retrospective in nature. In all studies, MRI sequences of T2-weighted imaging (T2WI), dynamic contrast enhanced (DCE), and diffusion-weighted imaging (DWI) sequences were used. Regarding the cutoff, 1 study reported the outcomes of 3 thresholds (EPE grades ≥1, ≥2, and ≥3) (18), whereas the remaining studies only reported the outcome of a cutoff threshold ≥1. Aside from the EPE grading system, diagnostic accuracy of a quantitative assessment of the length of capsular contact (LCC) and in-house Likert scale were reported by 2 studies (18, 25, 26). In all studies, the MRI images were interpreted by 2 radiologists independently with experience of 2–15 years. The inter-reader agreement calculated with kappa values was reported by 3 studies, which ranged from 0.47 to 0.88 (25–27). In 1 study, the MRI was performed with a 1.5-T scanner (25), whereas all the remaining 3 studies used 3.0-T scanners. In 3 studies, the readers were blinded to final pathology results; however, 1 study reported that the readers were aware that patients had PCa (26). The study characteristics are summarized in **Table 2**, and the key points of the included studies are summarized in **Table 3**.

Quality Assessment

Generally, quality assessment for included studies was high (**Figure 2**). However, concerning the patient selection domain, 3 of 4 studies were retrospective in study design (25–27). For the index test domain, one study reported that the radiologists were aware that patients were diagnosed with PCa and had undergone RP but were unaware of the final histopathologic finding (26). Concerning the two other domains, all studies were considered as low risk of bias.

Diagnostic Accuracy of the Extraprostatic Extension Grading System

The sensitivity and specificity for individual studies were 0.75–0.89 and 0.47–0.76. Pooled sensitivity and specificity of 4 included studies combined were 0.82 (95% CI 0.76–0.87) and 0.63 (95% CI 0.51–0.73), respectively; the coupled forest plots are presented in **Figure 3**. Higgins's I^2 statistics revealed moderate heterogeneity regarding sensitivity (I^2 = 55.87%) and considerable heterogeneity regarding specificity (I^2 = 93.05%). The pooled LR+ and LR− were 2.20 (95% CI 1.70–2.86) and 0.28 (95% CI 0.22–0.36), respectively, with a DOR of 7.77 (95% CI 5.27–11.44; **Figure 4**). The calculated area under the HSROC curve was 0.82 (95% CI 0.79–0.85). The large difference between the 95% confidence region and the 95% prediction region in the HSROC curve revealed heterogeneity between the studies, which is demonstrated in **Figure 5**. Deeks' funnel plot and asymmetry test showed that there was no significant probability of publication bias among included studies, with a *p*-value of 0.64 (**Figure 6**).

TABLE 1 | Demographic characteristics of the included studies.

First author	Country	Year	Period	Patient number	Malignancy	Age (year, mean ± SD)	PSA (ng/ml, mean or median)	ISUP
Mehralivand	USA	2019	Jun. 2007/Mar. 2017	553	125	60 ± 8	6.28 (0.21–170)	1–5
Reisæter	Norway	2020	Jan. 2010/Dec. 2012	310	80	63.6 (60–67)*	8.8 (6–13)	1–5
Xu	China	2021	Jan. 2015/Jan. 2020	130	63	64.21 ± 8.10	9.95 (2.78–83.02)	1–5
Park	Korea	2020	Jul. 2016/Mar. 2017	301	129	65 ± 7	7.55 ± 5.62	1–5

NA, not available; PSA, prostate serum antigen; ISUP, International Society of Urological Pathology.
**Median, interquartile range.*

TABLE 2 | Study characteristics of included studies.

First author	Study design	No. of readers	Experience (years)	Magnet field strength	*b* values (mm^2/s)	Coil	Blinded	Other guidelines	κ	Cutoff threshold
Mehralivand	Prospective	2	9/15	3.0 T	1,500/2,000	ERC	Yes	LLC	NA	≥1/≥2/≥3
Reisæter	Retrospective	2	≥10	1.5 T	0/50/400/800/1,200	ERC	Yes	Likert	0.47	≥1
Xu	Retrospective	3	2/4/7	3.0 T	0–2,000	NA	Yes	CAPRA score MSKCC	0.88	≥1
Park	Retrospective	2	3/15	3.0 T	0/50/500/1,000	Surface	Yes*	Tumor size/LLC/ESUR score/Likert scale	0.71	≥1

ADC, apparent diffusion coefficient; CAPRA, Cancer of the Prostate Risk Assessment; ERC, endorectal coil; EUSR, the European Society of Urogenital Radiology; LCC, length of capsular contact; MSKCC, Memorial Sloan Kettering Cancer Center nomogram; NA, not available.
**Aware that all patients had prostate cancer.*

TABLE 3 | Key points of the included studies.

Study	Key points
Mehralivand	Proposed a standardized grading system for the detection of EPE at mpMRI, which provides a graded quantifiable risk assessment of EPE. It is based on only a few imaging features, making it easy to teach, and it should be relatively easy to implement.
Reisæter	Compared with Likert, the EPE grade showed a trend toward increased sensitivity at the cost of decreased specificity, and there was no significant difference in AUC for predicting EPE. The EPE grade showed moderate inter-reader agreement.
Xu	Comparing the EPE grade with the CAPRA score and MSKCCn, the results showed that the AUCs were comparable among these 3 models. Compared with using CAPRA score and MSKCCn alone, the combination of EPE grades significantly improved their diagnostic performance. Nevertheless, there was no statistically significant difference between the three combined models and EPE grade by itself (all $p > 0.05$). The EPE grade showed perfect inter-reader agreement between radiologists;
Park	Compared the EPE grade with Likert scale, ESUR, and length of capsular contact. The EPE grade showed substantial inter-reader agreement and good diagnostic performance, and association with histopathologic tumor extension.

EPE, extraprostatic extension; mpMRI, multiparametric MRI; AUC, area under the curve; CAPRA, Cancer of the Prostate Risk Assessment; MSKCCn, Memorial Sloan Kettering Cancer Center nomogram.

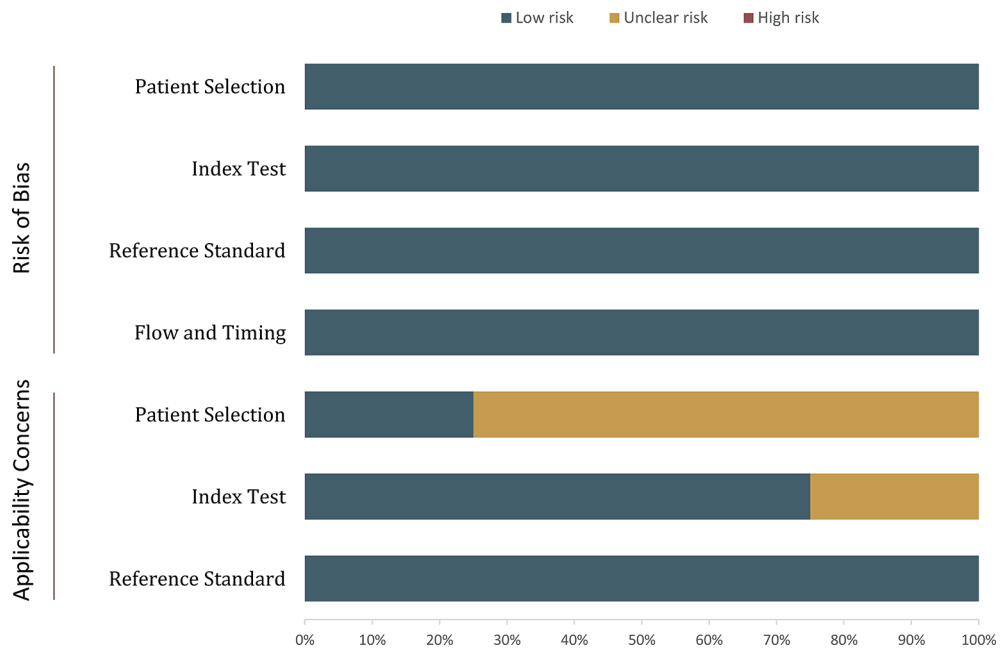

FIGURE 2 | Grouped bar charts show the risk of bias and concerns for applicability of included studies.

Discussion

In the current study, we assessed the diagnostic performance of the EPE grading system for predicting EPE in patients with PCa. Based on 4 studies, the pooled sensitivity and specificity were 0.82 (95% CI 0.76–0.87) and 0.63 (95% CI 0.51–0.73), with an area under HSROC of 0.82 (95% CI 0.79–0.85). Because of insufficient data, it is unfeasible to pool the summary estimates of inter-reader agreement; however, 3 studies reported that the κ values ranged from 0.47 to 0.88, indicating a moderate to substantial reproducibility among radiologists.

Previous conventional assessment of the 5-point EPE Likert scale (1 = highly unlikely, 2 = unlikely, 3 = equivocal or indeterminate, 4 = likely, and 5 = highly likely) have been employed widely in clinical practice, in which radiologists assign a score for the likelihood of EPE during MRI interpretation. However, the Likert scale primarily depends on radiologists' personal patterns and experience and then lacks objective criteria, resulting in widely varied accuracy (28–30). A prior meta-analysis showed that the pooled sensitivity and specificity were 0.57 and 0.91 for detection of EPE with mpMRI (31); by contrast, the EPE grading system yielded higher sensitivity but lower specificity and with overall similar diagnostic performance. However, compared with previous MRI grading methods, the EPE grading system provided a standardized and simplified scoring system for the prediction of EPE, because it is based on only a few imaging features and is easy to teach and learn. Moreover, Xu et al. and Park et al. reported good inter-reader agreement while using

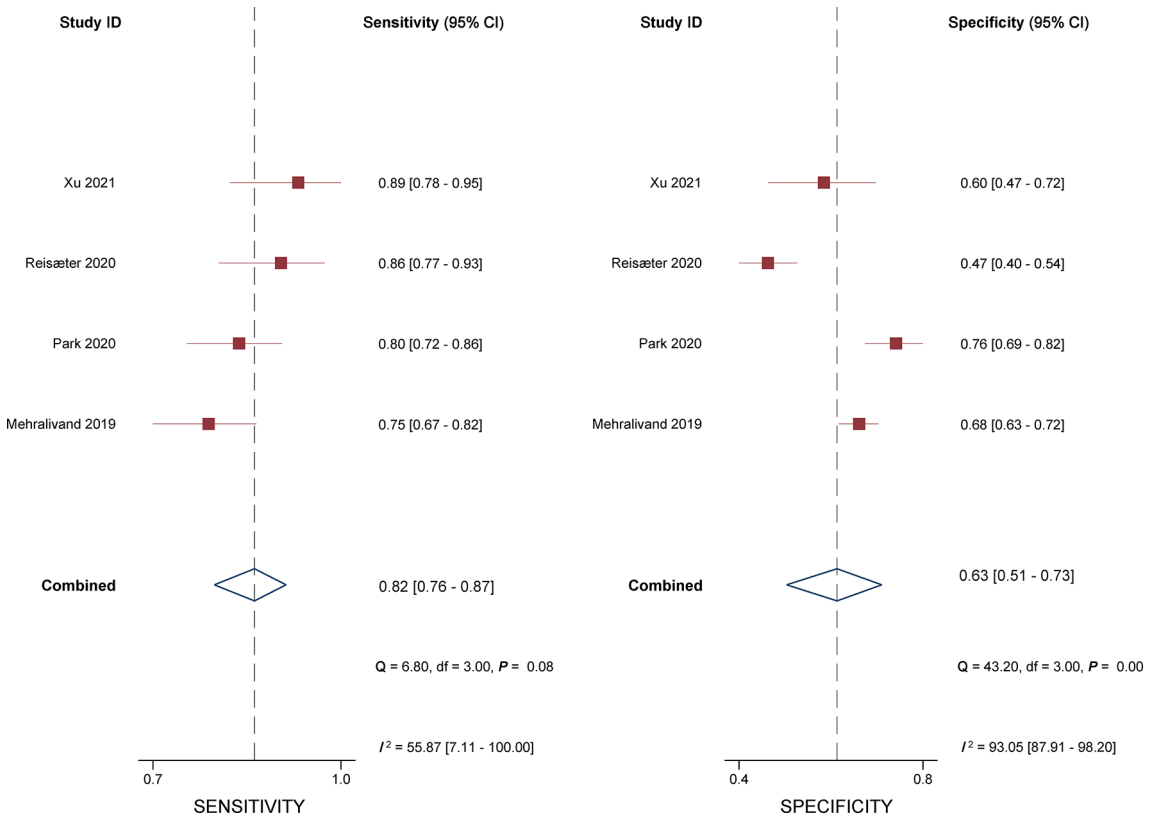

FIGURE 3 | Coupled forest plot of pooled sensitivity and specificity.

the EPE grading system, and less experienced radiologists could benefit from this guideline and yield good diagnostic accuracy (26, 27). Nonetheless, the EPE grading system is still burdened with a subjective bias between radiologists due to some qualitative analyses (25).

For patients with EPE, aggressive surgery led to high cancer-specific survival but at the cost of a higher rate of urinary incontinence and erectile dysfunction, whereas preservation of the NVBs leads to a higher risk of positive surgical margin and biochemical recurrence, which then leads to treatment failure after RP. The optimal clinical decision is a trade-off, which needs accurate preoperative assessment of histopathologic EPE. An ideal scoring system should be based on precise definitions, is easy to apply in clinical practice, is robust, and has a high level of inter-reader agreement. For prediction of EPE, it should include both quantitative measures (apparent diffusion coefficient, tumor size, tumor volume, and LLC) and the qualitative criteria. The ESUR PI-RADS recommends reporting these features when evaluating mpMRI prostate examinations; however, it does not assign a likelihood of EPE based on a combination of these findings (11–13). Although the ESUR PI-RADS includes a discontinuous scale (1 = capsular abutment; 2 = not specified; 3 = capsular irregularity; 4 = NVB thickening, bulge, or loss of capsule; and 5 = measurable extracapsular disease) for prediction of EPE, only a few studies assessed its diagnostic performance. A recent meta-analysis showed that the pooled sensitivity and specificity were 0.71 and 0.76 (17). Nevertheless, the diagnostic results were extracted from more experienced readers or more accurate outcomes.

In recent years, quantitative metrics are intensively investigated for assisting the prediction of EPE, which includes LCC, ADC, tumor volume, and tumor size. These mpMRI quantitative metrics showed moderate-to-high diagnostic accuracy as an independent predictor for the detection of EPE. Nonetheless, various measurement approaches and tools, along with MRI techniques and sequences, result in widely varied optimal cutoff thresholds (32, 33). The EPE grading system recommends the quantitative metric of 15-mm curvilinear contact length as a threshold for evaluation of EPE; however, it was unclear how such threshold was derived. According to current evidence, the reported optimal threshold varied from 6 to 20 mm, with sensitivity of 0.59–0.91 and specificity of 0.44–0.88 (34). The lower cutoff value for predicting EPE will lead to higher sensitivity but at the cost of decreased specificity, and vice versa. In PI-RADS v2, a tumor size of 15 mm was recommended as the cutoff for the prediction of EPE, while some studies demonstrated that the optimal threshold was 16–18 mm (35, 36). Nevertheless, this quantitative assessment was not included in the EPE grading system.

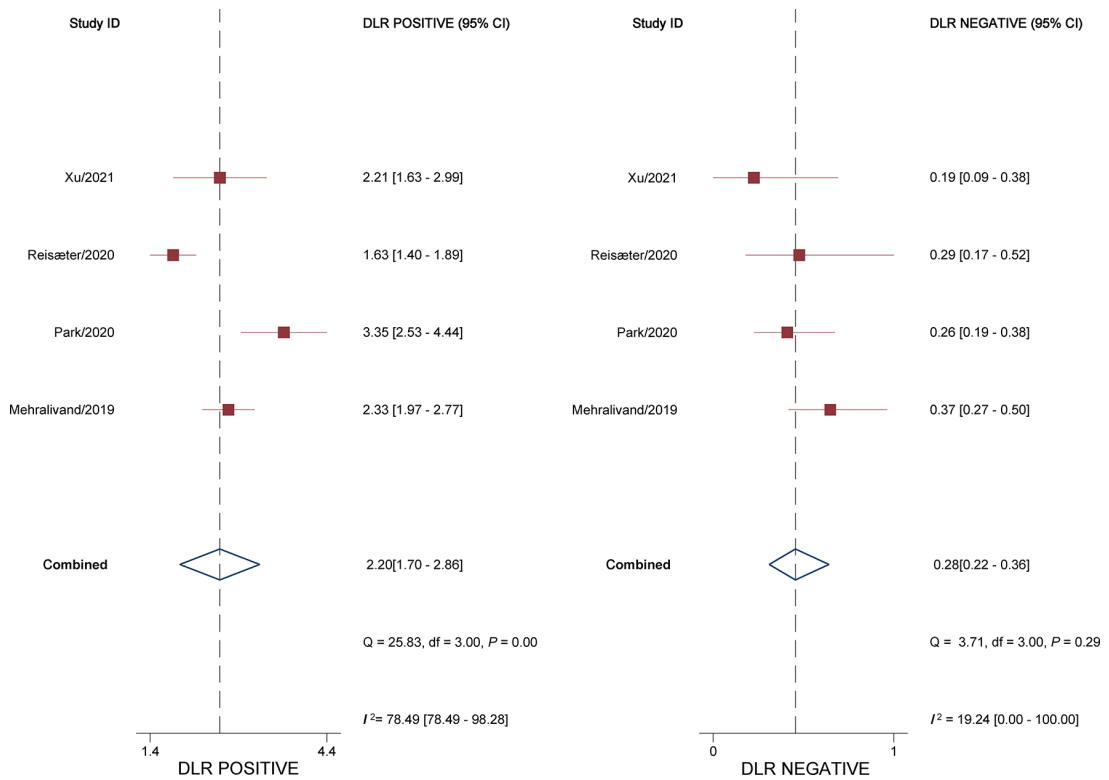

FIGURE 4 | Coupled forest plot of pooled negative and positive likelihood ratios.

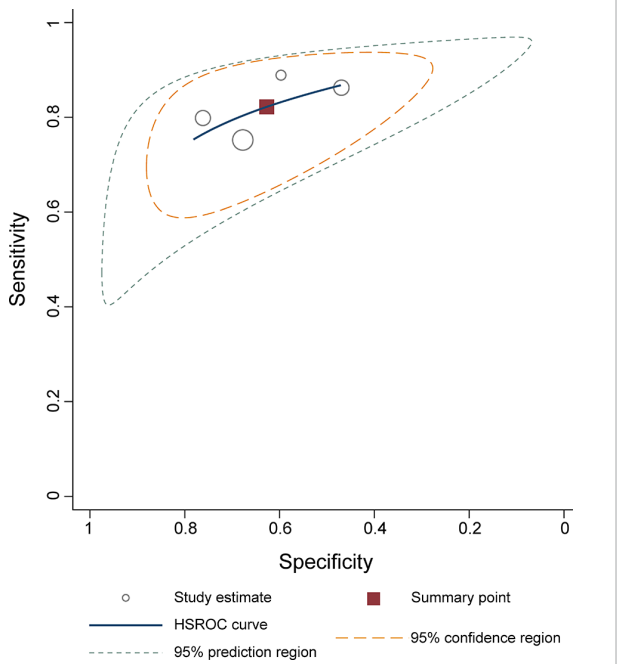

FIGURE 5 | Hierarchical summary receiver operating characteristic plots with summary point and 95% confidence area for the overall.

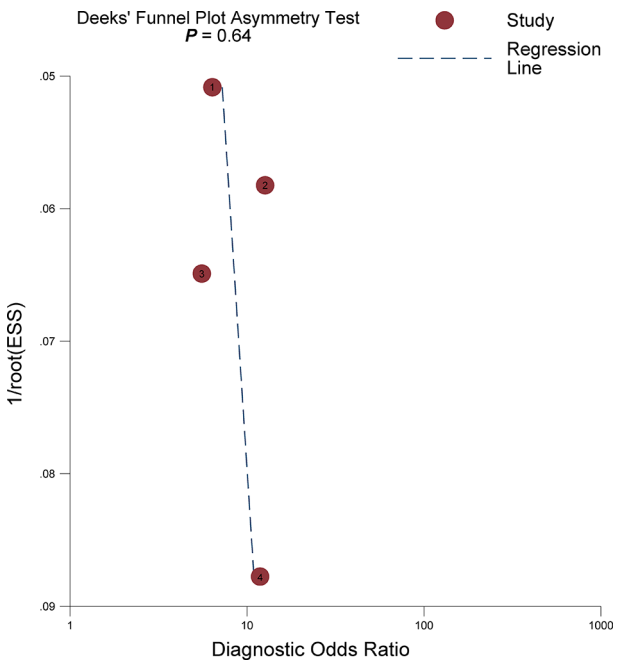

FIGURE 6 | Deeks's funnel plot. A *p*-value of 0.64 suggests that the likelihood of publication bias is low.

There are some limitations to our study. First, the majority of studies included were retrospective in study design, leading to high risk regarding patient selection domain. Nevertheless, it is unfeasible to pool the summary estimates from prospective studies. Second, substantial heterogeneity was found across included studies, which affected the general applicability of our meta-analysis. However, it is impossible to perform meta-regression and subgroup analyses to investigate the source because there are merely 4 studies in total. Nevertheless, we applied a solid and robust methodology for this meta-analysis using the guidelines published by the Cochrane Collaboration. Third, our analysis was based on only 4 studies; therefore, the results should be regarded with caution, and large prospective studies are needed to validate this guideline in the future. In addition, because of insufficient information, we cannot perform direct comparisons between the EPE grades with other scoring systems.

CONCLUSIONS

The EPE grading system demonstrated high sensitivity and moderate specificity, with a good inter-reader agreement. However, this scoring system needs more large prospective studies to be validated in clinical practice.

DATA AVAILABILITY STATEMENT

The original contributions presented in the study are included in the article/supplementary material. Further inquiries can be directed to the corresponding authors.

AUTHOR CONTRIBUTIONS

Guarantor of the article: JT. Conception and design: WL and WWS. Collection and assembly of data: FL and YS. Data analysis and interpretation: YMW, JT, and ADD. All authors contributed to the article and approved the submitted version.

FUNDING

This study was supported by the Natural Science Foundation of Jiangsu Vocational College of Medicine (No. 20204112).

REFERENCES

1. Ferlay J, Colombet M, Soerjomataram I, Dyba T, Randi G, Bettio M, et al. Cancer Incidence and Mortality Patterns in Europe: Estimates for 40 Countries and 25 Major Cancers in 2018. *Eur J Cancer Oxf Engl 1990* (2018) 103:356–87. doi: 10.1016/j.ejca.2018.07.005
2. Siegel RL, Miller KD, Jemal A. Cancer Statistics, 2020. *CA Cancer J Clin* (2020) 70:7–30. doi: 10.3322/caac.21590
3. Tollefson MK, Karnes RJ, Rangel LJ, Bergstralh EJ, Boorjian SA. The Impact of Clinical Stage on Prostate Cancer Survival Following Radical Prostatectomy. *J Urol* (2013) 189:1707–12. doi: 10.1016/j.juro.2012.11.065
4. Mikel Hubanks J, Boorjian SA, Frank I, Gettman MT, Houston Thompson R, Rangel LJ, et al. The Presence of Extracapsular Extension is Associated With an Increased Risk of Death From Prostate Cancer After Radical Prostatectomy for Patients With Seminal Vesicle Invasion and Negative Lymph Nodes. *Urol Oncol* (2014) 32:26.e1–7. doi: 10.1016/j.urolonc.2012.09.002
5. Quinlan DM, Epstein JI, Carter BS, Walsh PC. Sexual Function Following Radical Prostatectomy: Influence of Preservation of Neurovascular Bundles. *J Urol* (1991) 145:998–1002. doi: 10.1016/s0022-5347(17)38512-9
6. Swindle P, Eastham JA, Ohori M, Kattan MW, Wheeler T, Maru N, et al. Do Margins Matter? The Prognostic Significance of Positive Surgical Margins in Radical Prostatectomy Specimens. *J Urol* (2008) 179:S47–51. doi: 10.1016/j.juro.2008.03.137
7. Rayn KN, Bloom JB, Gold SA, Hale GR, Baiocco JA, Mehralivand S, et al. Added Value of Multiparametric Magnetic Resonance Imaging to Clinical Nomograms for Predicting Adverse Pathology in Prostate Cancer. *J Urol* (2018) 200:1041–7. doi: 10.1016/j.juro.2018.05.094
8. Ohori M, Kattan MW, Koh H, Maru N, Slawin KM, Shariat S, et al. Predicting the Presence and Side of Extracapsular Extension: A Nomogram for Staging Prostate Cancer. *J Urol* (2004) 171:1844–9; discussion 1849. doi: 10.1097/01.ju.0000121693.05077.3d
9. Eifler JB, Feng Z, Lin BM, Partin MT, Humphreys EB, Han M, et al. An Updated Prostate Cancer Staging Nomogram (Partin Tables) Based on Cases From 2006 to 2011. *BJU Int* (2013) 111:22–9. doi: 10.1111/j.1464-410X.2012.11324.x
10. Morlacco A, Sharma V, Viers BR, Rangel LJ, Carlson RE, Froemming AT, et al. The Incremental Role of Magnetic Resonance Imaging for Prostate Cancer Staging Before Radical Prostatectomy. *Eur Urol* (2017) 71:701–4. doi: 10.1016/j.eururo.2016.08.015
11. Barentsz JO, Richenberg J, Clements R, Choyke P, Verma S, Villeirs G, et al. ESUR Prostate MR Guidelines 2012. *Eur Radiol* (2012) 22:746–57. doi: 10.1007/s00330-011-2377-y
12. Weinreb JC, Barentsz JO, Choyke PL, Cornud F, Haider MA, Macura KJ, et al. PI-RADS Prostate Imaging – Reporting and Data System: 2015, Version 2. *Eur Urol* (2016) 69:16–40. doi: 10.1016/j.eururo.2015.08.052
13. Turkbey B, Rosenkrantz AB, Haider MA, Padhani AR, Villeirs G, Macura KJ, et al. Prostate Imaging Reporting and Data System Version 2.1: 2019 Update of Prostate Imaging Reporting and Data System Version 2. *Eur Urol* (2019) 76:340–51. doi: 10.1016/j.eururo.2019.02.033
14. Hamoen EHJ, Rooij M, Witjes JA, Barentsz JO, Rovers MM. Use of the Prostate Imaging Reporting and Data System (PI-RADS) for Prostate Cancer Detection With Multiparametric Magnetic Resonance Imaging: A Diagnostic Meta-Analysis. *Eur Urol* (2015) 67:1112–21. doi: 10.1016/j.eururo.2014.10.033
15. Woo S, Suh CH, Kim SY, Cho JY, Kim SH. Diagnostic Performance of Prostate Imaging Reporting and Data System Version 2 for Detection of Prostate Cancer: A Systematic Review and Diagnostic Meta-Analysis. *Eur Urol* (2017) 72:177–88. doi: 10.1016/j.eururo.2017.01.042
16. Park KJ, Choi SH, Kim M-H, Kim JK, Jeong IG. Performance of Prostate Imaging Reporting and Data System Version 2.1 for Diagnosis of Prostate Cancer: A Systematic Review and Meta-Analysis. *J Magn Reson Imaging JMRI* (2021) 54:103–12. doi: 10.1002/jmri.27546
17. Li W, Dong A, Hong G, Shang W, Shen X. Diagnostic Performance of ESUR Scoring System for Extraprostatic Prostate Cancer Extension: A Meta-Analysis. *Eur J Radiol* (2021) 143:109896. doi: 10.1016/j.ejrad.2021.109896
18. Mehralivand S, Shih JH, Harmon S, Smith C, Bloom J, Czarniecki M, et al. A Grading System for the Assessment of Risk of Extraprostatic Extension of Prostate Cancer at Multiparametric MRI. *Radiology* (2019) 290:709–19. doi: 10.1148/radiol.2018181278
19. Liberati A, Altman DG, Tetzlaff J, Mulrow C, Gøtzsche PC, Ioannidis JPA, et al. The PRISMA Statement for Reporting Systematic Reviews and Meta-Analyses of Studies That Evaluate Healthcare Interventions: Explanation and Elaboration. *Epidemiol Biostat Public Health* (2009) 6:e1–34. doi: 10.1016/j.jclinepi.2009.06.006

20. Whiting PF. QUADAS-2: A Revised Tool for the Quality Assessment of Diagnostic Accuracy Studies. *Ann Intern Med* (2011) 155:529. doi: 10.7326/0003-4819-155-8-201110180-00009
21. Higgins JPT, Altman DG, Gøtzsche PC, Jüni P, Moher D, Oxman AD, et al. The Cochrane Collaboration's Tool for Assessing Risk of Bias in Randomised Trials. *BMJ* (2011) 343:889–93. doi: 10.1136/bmj.d5928
22. Reitsma JB, Glas AS, Rutjes AWS, Scholten RJPM, Bossuyt PM, Zwinderman AH. Bivariate Analysis of Sensitivity and Specificity Produces Informative Summary Measures in Diagnostic Reviews. *J Clin Epidemiol* (2005) 58:982–90. doi: 10.1016/j.jclinepi.2005.02.022
23. Rutter CM, Gatsonis CA. A Hierarchical Regression Approach to Meta-Analysis of Diagnostic Test Accuracy Evaluations. *Stat Med* (2001) 20:2865–84. doi: 10.1002/sim.942
24. Deeks JJ. Systematic Reviews of Evaluations of Diagnostic and Screening Tests. *BMJ* (2001) 323:157–62. doi: 10.1136/bmj.323.7305.157
25. Reisæter LAR, Halvorsen OJ, Beisland C, Honoré A, Gravdal K, Losnegård A, et al. Assessing Extraprostatic Extension With Multiparametric MRI of the Prostate: Mehralivand Extraprostatic Extension Grade or Extraprostatic Extension Likert Scale? *Radiol Imaging Cancer* (2020) 2:e190071. doi: 10.1148/rycan.2019190071
26. Park KJ, Kim M, Kim JK. Extraprostatic Tumor Extension: Comparison of Preoperative Multiparametric MRI Criteria and Histopathologic Correlation After Radical Prostatectomy. *Radiology* (2020) 296:87–95. doi: 10.1148/radiol.2020192133
27. Xu L, Zhang G, Zhang X, Bai X, Yan W, Xiao Y, et al. External Validation of the Extraprostatic Extension Grade on MRI and Its Incremental Value to Clinical Models for Assessing Extraprostatic Cancer. *Front Oncol* (2021) 11:655093. doi: 10.3389/fonc.2021.655093
28. Costa DN, Passoni NM, Leyendecker JR, de Leon AD, Lotan Y, Roehrborn CG, et al. Diagnostic Utility of a Likert Scale Versus Qualitative Descriptors and Length of Capsular Contact for Determining Extraprostatic Tumor Extension at Multiparametric Prostate MRI. *Am J Roentgenol* (2018) 210:1066–72. doi: 10.2214/AJR.17.18849
29. Freifeld Y, Diaz de Leon A, Xi Y, Pedrosa I, Roehrborn CG, Lotan Y, et al. Diagnostic Performance of Prospectively Assigned Likert Scale Scores to Determine Extraprostatic Extension and Seminal Vesicle Invasion With Multiparametric MRI of the Prostate. *AJR Am J Roentgenol* (2019) 212:576–81. doi: 10.2214/AJR.18.20320
30. Fütterer JJ, Engelbrecht MR, Huisman HJ, Jager GJ, Hulsbergen-van De Kaa CA, Witjes JA, et al. Staging Prostate Cancer With Dynamic Contrast-Enhanced Endorectal MR Imaging Prior to Radical Prostatectomy: Experienced Versus Less Experienced Readers. *Radiology* (2005) 237:541–9. doi: 10.1148/radiol.2372041724
31. de Rooij M, Hamoen EHJ, Witjes JA, Barentsz JO, Rovers MM. Accuracy of Magnetic Resonance Imaging for Local Staging of Prostate Cancer: A Diagnostic Meta-Analysis. *Eur Urol* (2016) 70:233–45. doi: 10.1016/j.eururo.2015.07.029
32. Shieh AC, Guler E, Ojili V, Paspulati RM, Elliott R, Ramaiya NH, et al. Extraprostatic Extension in Prostate Cancer: Primer for Radiologists. *Abdom Radiol NY* (2020) 45:4040–51. doi: 10.1007/s00261-020-02555-x
33. Schieda N, Lim CS, Zabihollahy F, Abreu-Gomez J, Krishna S, Woo S, et al. Quantitative Prostate MRI. *J Magn Reson Imaging JMRI* (2020) 53:1632–45. doi: 10.1002/jmri.27191
34. Kim T-H, Woo S, Han S, Suh CH, Ghafoor S, Hricak H, et al. The Diagnostic Performance of the Length of Tumor Capsular Contact on MRI for Detecting Prostate Cancer Extraprostatic Extension: A Systematic Review and Meta-Analysis. *Korean J Radiol* (2020) 21:684–94. doi: 10.3348/kjr.2019.0842
35. Ahn H, Hwang SI, Lee HJ, Suh HS, Choe G, Byun S-S, et al. Prediction of Extraprostatic Extension on Multi-Parametric Magnetic Resonance Imaging in Patients With Anterior Prostate Cancer. *Eur Radiol* (2020) 30:26–37. doi: 10.1007/s00330-019-06340-3
36. Schieda N, Lim CS, Idris M, Lim RS, Morash C, Breau RH, et al. MRI Assessment of Pathological Stage and Surgical Margins in Anterior Prostate Cancer (APC) Using Subjective and Quantitative Analysis. *J Magn Reson Imaging JMRI* (2017) 45:1296–303. doi: 10.1002/jmri.25510

Conflict of Interest: The authors declare that the research was conducted in the absence of any commercial or financial relationships that could be construed as a potential conflict of interest.

Publisher's Note: All claims expressed in this article are solely those of the authors and do not necessarily represent those of their affiliated organizations, or those of the publisher, the editors and the reviewers. Any product that may be evaluated in this article, or claim that may be made by its manufacturer, is not guaranteed or endorsed by the publisher.

Copyright © 2022 Li, Shang, Lu, Sun, Tian, Wu and Dong. This is an open-access article distributed under the terms of the Creative Commons Attribution License (CC BY). The use, distribution or reproduction in other forums is permitted, provided the original author(s) and the copyright owner(s) are credited and that the original publication in this journal is cited, in accordance with accepted academic practice. No use, distribution or reproduction is permitted which does not comply with these terms.

frontiers in Oncology

ORIGINAL RESEARCH
published: 14 February 2022
doi: 10.3389/fonc.2021.831603

Establishment of an Individualized Predictive Model to Reduce the Core Number for Systematic Prostate Biopsy: A Dual Center Study Based on Stratification of the Disease Risk Score

Zeyu Chen[1†], Min Qu[1†], Xianqi Shen[1†], Shaoqin Jiang[1,2†], Wenhui Zhang[1†], Jin Ji[1†], Yan Wang[1], Jili Zhang[1], Zhenlin Chen[2], Lu Lin[1], Mengqiang Li[2‡], Cheng Wu[3‡] and Xu Gao[1]*

[1] Department of Urology, Shanghai Changhai Hospital, Second Military Medical University, Shanghai, China, [2] Department of Urology, Fujian Union Hospital, Fujian Medical University, Fuzhou, China, [3] Department of Health Statistics, Second Military Medical University, Shanghai, China

Purpose: To establish an individualized prostate biopsy model that reduces unnecessary biopsy cores based on multiparameter MRI (mpMRI).

Materials and Methods: This retrospective, non-inferiority dual-center study retrospectively included 609 patients from the Changhai Hospital from June 2017 to November 2020 and 431 patients from the Fujian Union Hospital between 2014 and 2019. Clinical, radiological, and pathological data were analyzed. Data from the Changhai Hospital were used for modeling by calculating the patients' disease risk scores. Data from the Fujian Union Hospital were used for external verification.

Results: Based on the data of 609 patients from the Changhai Hospital, we divided the patients evenly into five layers according to the disease risk score. The area under the receiver operating characteristic (ROC) curve (AUC) with 95% confidence intervals (CI) was analyzed. Twelve-core systemic biopsy (12-SBx) was used as the reference standard. The SBx cores from each layer were reduced to 9, 6, 5, 4, and 4. The data of 279 patients with benign pathological results from the Fujian Union Hospital were incorporated into the model. No patients were in the first layer. The accuracies of the models for the other layers were 88, 96.43, 94.87, and 94.59%. The accuracy of each layer would be increased to 96, 100, 100, and 97.30% if the diagnosis of non-clinically significant prostate cancer was excluded.

Conclusions: In this study, we established an individualized biopsy model using data from a dual center. The results showed great accuracy of the model, indicating its future clinical application.

Keywords: prostate biopsy, multiparameter MRI, PI-RADS, multicenter study, predictive models

OPEN ACCESS

Edited by:
Tanya I. Stoyanova, Stanford University, United States

Reviewed by:
Enrico Checcucci, IRCCS Candiolo Cancer Institute, Italy
Matteo Droghetti, University of Bologna, Italy

***Correspondence:**
Xu Gao
gaoxu.changhai@foxmail.com

[†]These authors have contributed equally to this work and share first authorship

[‡]These authors have contributed equally to this work and share senior authorship

Specialty section:
This article was submitted to Genitourinary Oncology, a section of the journal Frontiers in Oncology

Received: *08 December 2021*
Accepted: *27 December 2021*
Published: *14 February 2022*

Citation:
Chen Z, Qu M, Shen X, Jiang S, Zhang W, Ji J, Wang Y, Zhang J, Chen Z, Lin L, Li M, Wu C and Gao X (2022) Establishment of an Individualized Predictive Model to Reduce the Core Number for Systematic Prostate Biopsy: A Dual Center Study Based on Stratification of the Disease Risk Score. Front. Oncol. 11:831603. doi: 10.3389/fonc.2021.831603

INTRODUCTION

Prostate biopsy is the standard procedure for tissue acquisition for pathological diagnosis. Since the 1980s, when TRUS-guided 6-core systematic biopsy was proposed by Hodge et al. (1), it was found to have a 33% misdiagnosis rate for Pca (2). Thus, 8-, 10-, or 12-core and even saturation biopsies are recommended to improve the detection rate, even though they increase the risk of rectal bleeding, urinary tract infection, erectile dysfunction, and other complications (3, 4).

Since MRI-guided prostate biopsy was first performed by D'Amico in 2000 (5), it has been proven to detect more csPCa with fewer biopsy cores than system biopsy by high-quality research (6). It is still unclear how to decrease the number of cores under the condition that more csPCa is diagnosed (7, 8). Because mpMRI inter-reader reproducibility remains moderate at best (9, 10), the accuracy and reproducibility of targeted biopsy still need to be improved (11), and the optimal core number and site for MRI-targeted biopsy have not been clearly elucidated (12). Furthermore, the NVP of MRI-guided prostate biopsy is unstable (13). Thus, the EAU Guidelines recommend combining targeted and systematic biopsy in patients who are naïve in biopsy when mpMRI is positive (i.e., PI-RADS ≥3) (14), which will increase the risk of complications (15).

Based on the existence of many unstable factors in MRI-guided prostate biopsy, an alternative approach is to reduce the number of cores on systemic biopsy. Current research has focused on specific factors, such as prostate volume or PSA level, to reduce the cores of systematic biopsy (16), or analyzed different hypothetical sampling schemes when compared with targeted biopsy plus 12-SBx (17). Fewer studies have reported the reduction of cores after individualization of patients according to the location of suspicious lesions on MRI, and a variety of factors are not yet sufficient.

Therefore, we performed a dual-center, non-inferiority study to establish an individualized predictive model to optimize prostate biopsy. The model can plan the biopsy location by reducing the cores after comprehensively incorporating the basic information, tumor indicators, mpMRI, and other related patient factors. We circumvented the deficiencies of similar research, and for the first time combined multiple factors into one completed individualized analysis of basic patient information. On the other hand, we made a website for model use, which is convenient for clinics. At the same time, this website can input information about the nodule position of the patient, which completes the individualized analysis of mpMRI information.

Abbreviations: TPSA, total prostate-specific antigen; 12-SBx,12-core systematic biopsy; TBx, targeted biopsy; csPCa, clinically significant prostate cancer; mpMRI, multiparametric magnetic resonance imaging; TRUS, transrectal ultrasound guided; AUC, Area Under the ROC Curve; BMI, Body Mass Index; PCa, Prostate Cancer; PSA, Prostate Specific Antigen; DRS, Disease Risk Score; CI, confidence intervals; NPV, negative prediction value.

MATERIALS AND METHODS

Participants

This study retrospectively analyzed patients who underwent 12-core (or 13-core) transrectal US-guided prostate biopsy for suspected PCa with a PI-RADS score ≥3 at the Changhai Hospital and the Fujian Union Hospital. Diagram for inclusion of patients in the study are shown in **Figure 1**.

The inclusion criteria were: (1) indications for biopsy and (2) abnormal nodules revealed on mpMRI (PI-RADS score ≥3).

The exclusion criteria were: (1) previous biopsy; (2) inability to complete the standard 12-core system biopsy; (3) cases with antiandrogen therapy; (4) negative 12-core system biopsy and positive MRI-guided prostate biopsy; and (5) incomplete or obviously wrong data.

A total of 609 patients were enrolled in the Changhai Hospital to establish the model and 279 patients with positive biopsy in the Fujian Union Hospital were enrolled as an external independent validation group.

Patients in the Changhai Hospital underwent 12-SBx (as shown in **Figure 2A**), and some patients underwent MRI-guided prostate biopsy. Patients in the Fujian Union Hospital underwent 13-SBx (as shown in **Figure 2B**), and some patients underwent MRI-guided prostate biopsy.

mpMRI and Scan Protocol

mpMRI examinations were performed using a 3.0-T system (Magnetom Skyra, Siemens Medical Solutions, Erlangen, Germany) with an 18-channel phased-array coil, before biopsy. The sequences of examination mainly included T2-weighted imaging (T2WI), diffusion-weighted imaging (DWI), and dynamic contrast-enhanced imaging. Two radiologists with >10 years of experience in MRI evaluated and scored the images according to the Prostate Imaging Reporting and Data System version 2 criteria (18). Next, three diameters of the prostate and the smallest diameter of the suspicious lesion were measured and calculated using mpMRI on the T2WI sequence.

Prostate Biopsy Method

The entire prostate biopsy processes were completed by a surgeon with more than five years of experience. Preoperative routine examinations included routine blood tests, coagulation function, liver and kidney function, urine routine, fecal routine, and serum PSA concentration. If patients used aspirin, warfarin, and other anticoagulants, they were requested to stop using the drugs for 2 weeks. A cleansing enema was also performed on patients in the lithotomy position, and the perineum and perianal region were disinfected with 0.5% iodophor. A novel perineal nerve block approach (19) was adopted with 5% lidocaine.

An ultrasound probe was inserted through the anus to measure the three diameters of the prostate followed by a 12-needle system biopsy. A biopsy point distribution diagram for the two centers is shown in **Figure 2**. Patients in the Changhai Hospital underwent 12-SBx (as shown in **Figure 2A**), and some patients underwent

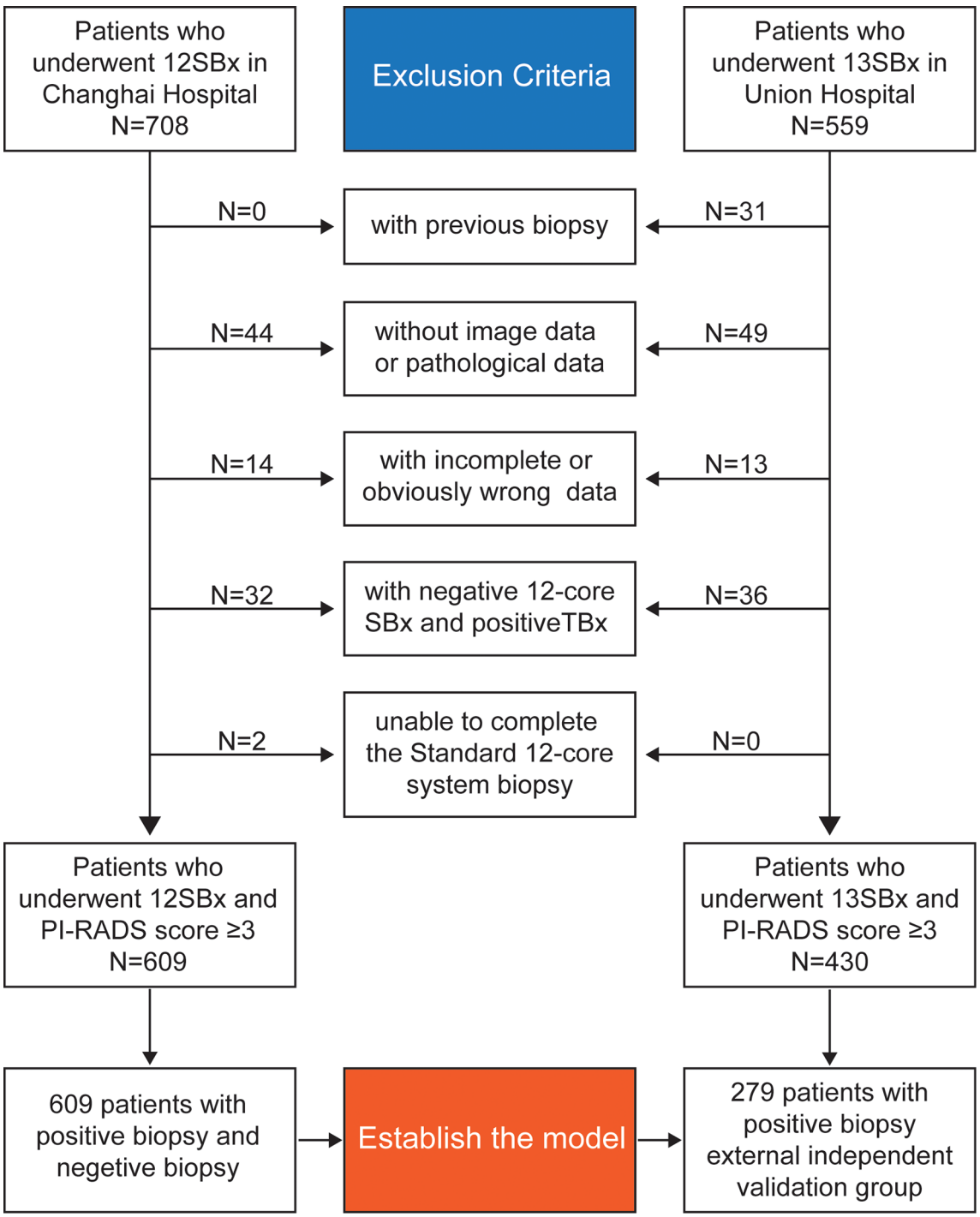

FIGURE 1 | Diagram for inclusion of patients in the study.

MRI-guided prostate biopsy. Patients in the Fujian Union Hospital underwent 13-SBx (as shown in **Figure 2B**), and some patients underwent MRI-guided prostate biopsy.

After the biopsy, for bleeding patients, an iodophor gauze was placed around the perineum. The tissues were fixed in 10% formalin.

The Simulated Process of Reducing the Number of Cores

Two clinicians (Doctors A and B) with >5 years of experience in mpMRI complete the simulated process of reducing the number of cores. Doctor A knew the pathological results of each patient (accurate

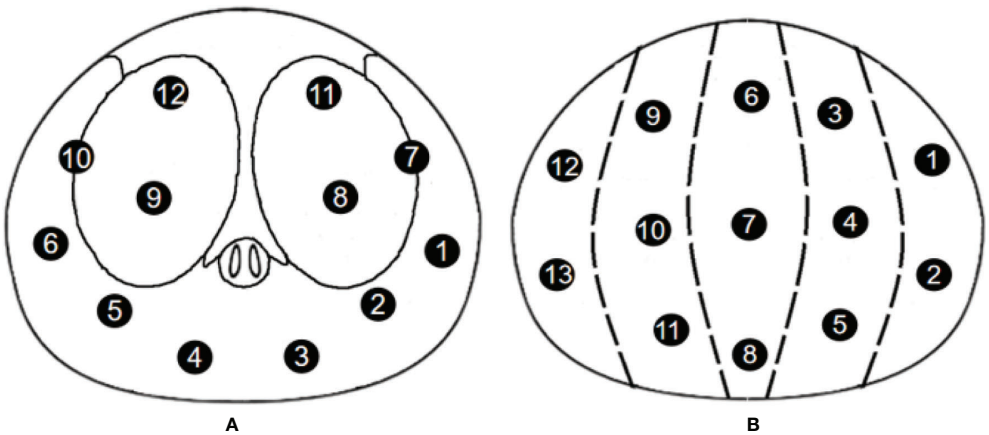

FIGURE 2 | Biopsy point distribution diagram for the two centers **(A)** 12-core, Changhai Hospital; **(B)** 13-core, Fujian Union Hospital).

to the pathology of each core), and Doctor B knew the mpMRI data of each patient, and the biopsy point distribution diagram.

Doctor B judged the location of the most suspicious lesion based on the mpMRI based on the distance between the center of the lesion location and each systemic biopsy core. When one core was taken, the closest core to the lesion was recorded; when two cores were taken, the two cores closest to the lesion were recorded; this simulated process was restored to 12 cores. For example, if the lesion was located in the right peripheral zone of the base zone (as shown in **Figure 3**), the simulated system biopsy process was restored 12 times (**Figure 4**).

Doctor B did not know the pathological results of each simulated system biopsy process; if there were two or more suspicious lesions, Doctor B independently determined the location of the most suspicious lesions based on clinical experience, and Doctor A recorded the negative or positive result of simulated biopsy under different numbers of biopsy cores.

Statistical Analysis

Measurement data were tested whether they followed normal distribution. Measurement data with normal distribution and equal variance was described by mean ± standard deviation (SD), and independent samples t-test was used for comparison between two independent samples; measurement data with non-normal distribution or unequal variance was described by Median (Q1–Q3), and Mann–Whitney test was used. The categorical data was described by n (%), and Pearson chi-square test or Fisher's exact test was used to test the difference between the two groups.

We used a Disease Risk Score (DRS) to measure the risk of prostate cancer for each participation. DRS is a comprehensive index based on all covariates, which is defined as the probability of occurrence of final events under the condition of certain covariates in the model. Logistic regression was used to calculate the DRS. Then the participation were equally divided into 5 layers according to the percentiles of their DRS, that is,

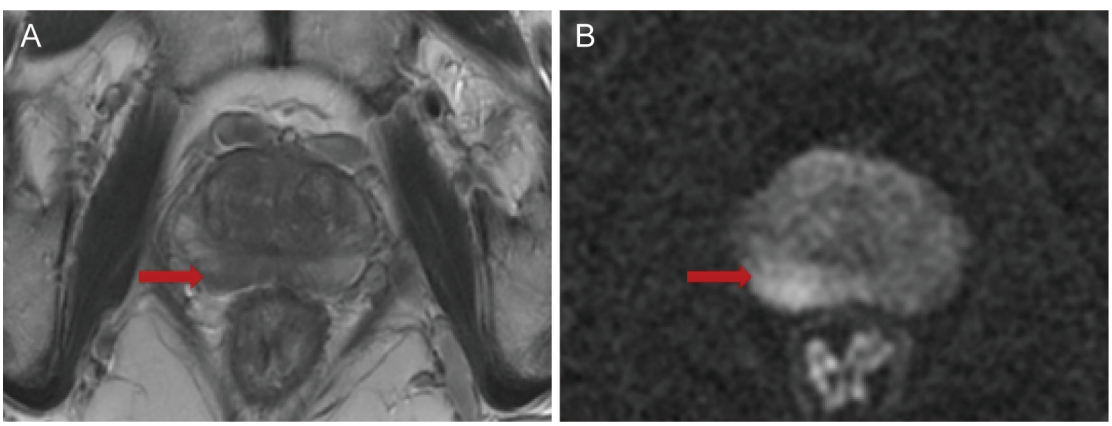

FIGURE 3 | **(A)** T2-weighted imaging (T2WI); **(B)** diffusion-weighted imaging (DWI).

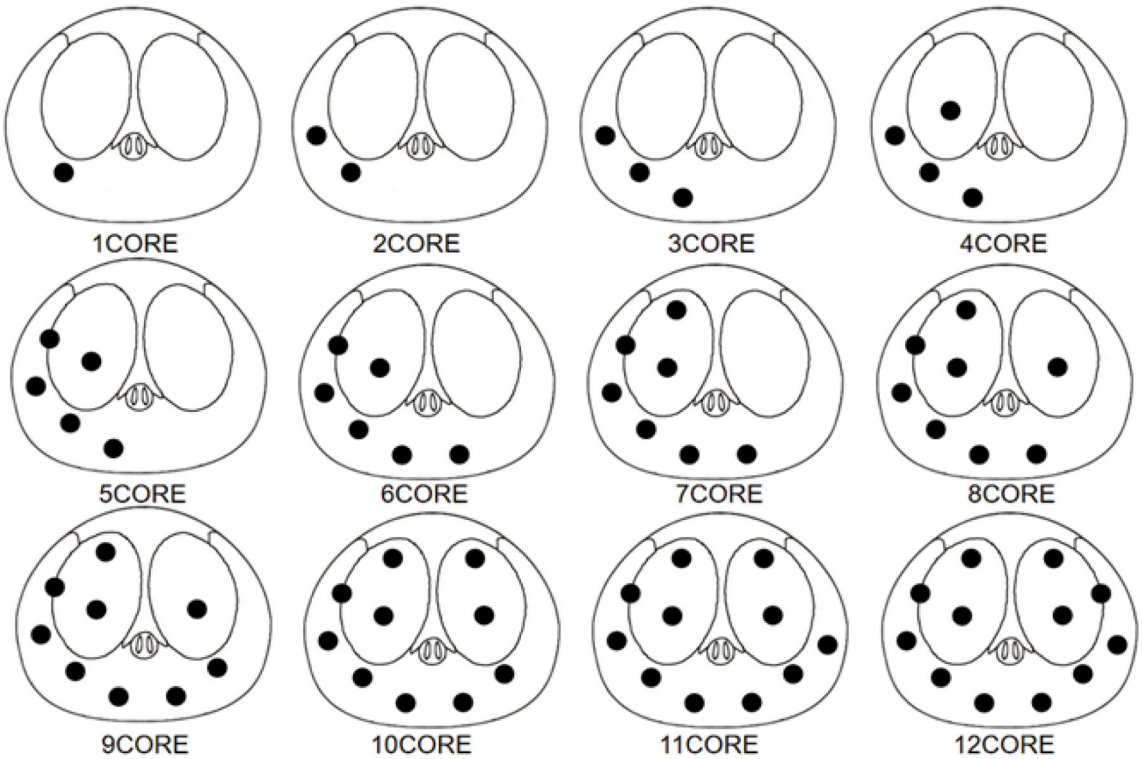

FIGURE 4 | Biopsy point distribution diagram for the 1-core to 12-core methods.

Min–P20, P20–P40, P40–P60, P60–P80, and P80–Max. [Distribution range of Disease Risk Score (DRS) is shown in the **Supplementary Table 14**].

We calculated the detection rate of prostate cancer in different layers. Moreover, the sensitivity, negative prediction value, accuracy and area under the ROC curve (AUC) with 95%CI were analyzed, and the values were compared with those of the 12-core systematic biopsy results to get the most suitable number of biopsy cores for each layer(the lower boundary of the two-sided 95%CI ≥95%). McNemar's test was used to compare the detection rate between 12-core systematic biopsy and 1-core to 11-core method.

We validate the constructed DRS layers and their most suitable number of biopsy cores with external data. We used the disease risk score model of Changhai Hospital to calculate the DRS of patients with positive prostate puncture in the Fujian Union Hospital, then, stratified the patients into 5 layers according to the stratification method of Changhai Hospital. The detection rate of prostate cancer of the patients and its 95% CI in each layer was calculated.

After validation, we also developed a web-based visualization tool for clinical application (website: https://daringsky.shinyapps.io/prediction_v2/).

Statistical significance was defined as two-sided p-value of <0.05. Statistical analyses were performed using SPSS v24.0 (SPSS Inc., Chicago, IL, USA).

RESULTS

Predictive Model Using the Disease Risk Score Based on Data From the Changhai Cohort

Patients' Baseline Characteristics

There was no significant statistical difference in the BMI of the patients (p = 0.482) and longest diameter of lesions (p = 0.138), while patients with PCa were older, had higher PSA, larger prostate volume, and higher PI-RADS scores (all p <0.05) (as shown in **Table 1**).

Divide the Patient Evenly Into 5 Layers by DRS

The formula for calculating the disease risk score by the model is as follows:

$$DRS = \frac{1}{e^{-(-5.57+0.062X1+0.055X2+0.015X3-0.531X4-0.171X5-0.374X6-0.301X7+1.680X8)}}$$

X1 = AGE (year), X2 = BMI (kg/m^2), X3 = TPSA (ng/ml), X4 = transverse diameter (cm), X5 = anteroposterior diameter (cm), X6 = cephalocaudal diameter (cm), X7 = Lesion's longest diameter (cm), X8 = PI-RADS v2 score(number).

We included the following seven factors (X1-X7) because we conducted the paired chi-square test on these factors and found that these seven factors were meaningful to our study. The results

TABLE 1 | Characteristics of patients in Changhai Hospital.

	total	Biopsy positive group	Biopsy negative group	P
N	609	454	155	
age, year	68.32 ± 8.01	69.09 ± 8.06	66.07 ± 7.45	<0.01
BMI, kg/m²	24.22 (22.49–26.14)	24.22 (22.49–26.30)	24.24 (22.49–25.86)	0.482
TPSA, ng/ml	10.8 (87.36–17.45)	10.85 (7.26–17.19)	9.4 (6.22–14.04)	<0.001
transverse diameter, cm	4.9 (4.5–5.3)	4.8 (4.4–5.2)	5.2 (4.8–5.7)	<0.001
anteroposterior diameter, cm	3.4 (2.9–4.0)	3.3 (2.9–3.8)	3.9 (3.3–4.5)	<0.001
cephalocaudal diameter, cm	4.0 (3.5–4.7)	3.9 (3.4–4.425)	4.5 (3.8–5.2)	<0.001
Lesion's longest diameter, cm	1.5 (1–2)	1.5 (1–2)	1.44 (1–1.97)	0.138
PI-RADS v2 score, number (percent)				
3	197 (32.35)	86 (18.94)	111 (71.61)	
4	241 (39.57)	204 (44.93)	37 (23.87)	<0.001
5	171 (27.97)	164 (36.12)	7 (4.52)	

are shown in the supplementary table (**Supplementary Tables 6–13**). Then the participation were equally divided into 5 layers according to the percentiles of their DRS, that is, Min–P20, P20–P40, P40–P60, P60–P80, and P80–Max.

Simulation and Model Establishment

The pathologic outcomes according to different sampling scheme from 1 core to 12 cores, sensitivities, NPV, accuracy and AUC with 95%CI are shown in **Table 2** (We only display the statistical results of the first layer, and the statistical results of the remaining 4 layers are displayed in the **Supplement Tables 1–4**). We analyzed AUC, when the lower boundary of the two-sided 95%CI was ≥95%, the number of cores is the most suitable. According to this standard, we chose 9 cores for layer 1, 6 cores for layer 2, 5 cores for layer 3, 4 cores for layer 4, and 4 cores for layer 5.At the same time, these selected number of cores also show a very high accuracy (layer 1: 99.18%; layer 2: 97.52%; layer 3: 97.56%; layer 4: 97.52%; layer 5: 95.90%). In addition, the first level missed 3 patients (3 csPCa), the second level missed 3 patients (3 csPCa), the third level missed 3 patients (2 csPCa), the fourth level missed 3 patients (3 csPCa), the fifth level missed 5 patients (5 csPCa). The data did not change significantly after including the concept of clinically significant prostate cancer.

Verification of the Model Using Data From the Fujian Union Hospital Cohort

A total of 279 patients with positive pathological results from the Fujian Union were included and stratified according to the method established by the Changhai cohort. Based on this principle, re-simulation was carried out for core reduction in patients in the Fujian Union cohort (**Table 3**). No patients were in the first layer. In the other layers, except for the second layer

TABLE 2 | Detection rate of prostate cancer by different biopsy sampling schemes compared with that of 12-core systematic biopsy as the reference standard in layer 1.

The number of layers	CORE	12SBx (POSITIVE)		P (McNemar's test)	Sensitivity (%)	NPV (%)	Accuracy (%)	AUC (95% CI)	P (AUC)
1	1	POSITIVE	17	0	48.57	82.86	85.25	0.743 (0.631–0.855)	<0.001
		NEGATIVE	18						
	2	POSITIVE	25	0	71.43	89.69	91.80	0.857 (0.765–0.95)	<0.001
		NEGATIVE	10						
	3	POSITIVE	NA	NA	NA	NA	NA	NA	NA
		NEGATIVE	NA						
	4	POSITIVE	27	0	77.14	91.58	93.44	0.886 (0.801–0.970)	<0.001
		NEGATIVE	8						
	5	POSITIVE	28	0.008	80.00	92.55	94.26	0.900 (0.820–0.980)	<0.001
		NEGATIVE	7						
	6	POSITIVE	30	0.063	85.71	94.57	95.90	0.929 (0.860–0.998)	<0.001
		NEGATIVE	5						
	7	POSITIVE	31	0.125	88.57	95.60	96.72	0.943 (0.880–1.000)	<0.001
		NEGATIVE	4						
	8	POSITIVE	NA	NA	NA	NA	NA	NA	NA
		NEGATIVE	NA						
	9	POSITIVE	34	1	97.14	98.86	99.18	0.986 (0.954–1.000)	<0.001
		NEGATIVE	1						
	10	POSITIVE	35	1	100	100	100	1.000 (1.000–1.000)	<0.001
		NEGATIVE	0						
	11	POSITIVE	35	1	100	100	100	1.000 (1.000–1.000)	<0.001
		NEGATIVE	0						

NA, NO ANSWER.

TABLE 3 | Analysis of External Validation Data of Fujian Union Hospital.

The number of layer	Core number	Total number	Number of positives after core reduction	Accuracy (ISUP ≥1)	Accuracy (ISUP ≥2)
2	6	25	22	88%	96.00%
3	5	28	27	96.43%	100%
4	4	78	74	94.87%	100%
5	4	148	140	94.59%	97.30%

(88%), the accuracy rate were very considerable (The second-layer patients have a lower disease risk score than the other 3 layers, indicating that these patients have a relatively low risk of disease. More cores were needed to be taken for such patients, so the core reduction showed a relatively low accuracy, but the value of 88% we think is also ideal). However, the accuracy of each layer would be greatly improved, especially the third and fourth and even reaching 100%, when ignoring the non-clinically significant PCa.

Establishment of the Website for Clinical Application

As shown in **Figure 5**, the biopsy point distribution diagram of Changhai Hospital was adopted, and the relevant data of patients with PI-RADS score 3 and above reported by mpMRI was entered into the website. Among these, the lesion location website adopts the prostate division method used in PI-RADSV2.0 (18) and V2.1. The operator judges the possible positions of the lesion based on mpMRI. The position of the nodule location is divided into three areas: in the prostate BAES/MID/APEX, on the left or right side of the prostate, and the cross-sectional area of the prostate (divided according to PI-RADS V2.1). The website then outputs the DRS of the patient and the optimal number of cores, and our recommended biopsy point distribution diagram (The logic of website creation appendix in **Supplementary Table 5**).

DISCUSSION

The PRECISION study (6) showed that MRI-targeted biopsy could be minimally invasive, have few side effects, identify a high

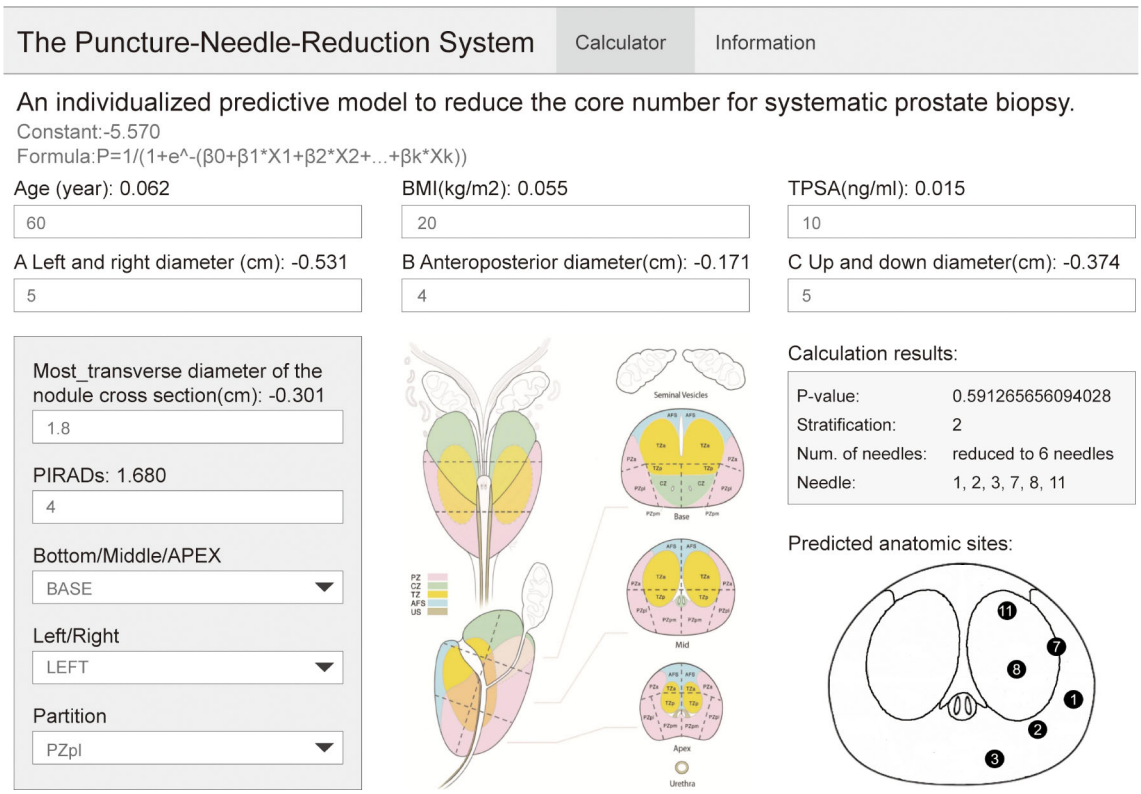

FIGURE 5 | Website application display example.

proportion of men who would benefit from treatment, and minimize the identification of men with clinically insignificant cancer in order to prevent overtreatment. The MRI-FIRST study (20) also pointed out that there is no significant difference between simple MRI-targeted biopsy and simple systematic biopsy for the detection of clinically significant prostate cancer (32.3% vs. 29.9%, p = 0.38); however, if the two methods are combined, the positive rate of clinically significant prostate cancer can reach 66%. In another multicenter prospective study 4M (21), the diagnostic efficacy of simple MRI-targeted biopsy and simple systematic biopsy for clinically significant prostate cancer was also compared; there was no significant difference between the two (23% vs. 25%, p = 0.17). However, systematic puncture can increase the positive rate of clinically insignificant prostate cancer (25% vs. 14%, p <0.0001).

Over the past few years many new technologies have become available for the management of Pca (22), but research on whether MRI-targeted biopsy can replace systematic biopsy has plateaued. Therefore, many compromised core reduction methods have also been studied and compared with similar studies; our research has two major advantages.

First, our research included as much mpMRI data as possible. In a recent Cochrane meta-analysis (23), mpMRI had a pooled sensitivity of 0.91 (95%CI: 0.83–0.95) and a pooled specificity of 0.37 (95%CI: 0.29–0.46) for ISUP grade >2 cancers. Several studies found that the PI-RADS score was a significant independent predictor of csPCa at biopsy (24, 25). In studies such as that of Hu et al. (16), this type of research did not include mpMRI data and only included tumor-related factors, and found that for patients with a PSA concentration of 20 ng/ml or higher, a 6-core systematic biopsy is preferred. However, we obtained fewer biopsy cores (5 cores and 4 cores) under stricter statistical conditions; therefore, we included the mpMRI data, especially the PI-RADS score, which is an important factor for core reduction. We included not only the scores for the lesions (PI-RADS score), but also the location of the lesions reported by mpMRI, which is a very important reason for the reduction in the number of cores.

Second, our research is the first to use modeling methods to combine basic patient information such as age, BMI, PSA, and indicators involved in mpMRI (transverse diameter, anteroposterior diameter, cephalocaudal diameter, lesion longest diameter, and PI-RADS v2 score). In a study by Shen (17), the biopsy point distribution diagram can be reduced to TBx + lateral 6-SBx based on TBx + 12-SBx, which means that the systematic biopsy core number can be reduced to 6 based on 12. The results of this study were also not satisfactory for the reduction of the core number (6 cores vs. 5/4 cores) because it did not achieve individualization; it did not include the age, PSA, BMI of the patient and other factors, or did not integrate these factors for individualized analysis. Age (26), BMI (27), PSA (28), three diameters of prostate, etc., have been confirmed as having a strong correlation factor with prostate cancer, and have their own significance in the impact on core number. However, if analyzed separately, they will often produce the opposite result. For example, if a patient has a higher PSA indicator (indicating fewer cores) but a smaller cancer lesion (indicating more puncture needles). However, studies that comprehensively consider these indicators are still insufficient.

This study is the first to introduce the concept of DRS value into model establishment for the comprehensive treatment of patients with a relatively comprehensive stratification of various factors. Through this processing method, more factors are integrated, and the layered processing makes the core number reduction more gradual, making it possible to reduce more biopsy cores, enabling us to achieve individualization in the true sense for the first time. Moreover, our study is also the first to consider the position of the lesion and perform personalized core reduction for each patient based on the position of the lesion through the website.

We successfully established an individualized model and established a website. Using this model, patients were equally divided into five layers. To ensure the detection rate, the number of cores can be reduced to less than 6 cores for more than half of the patients with lesions (PI-RADS ≥3 points). The website can directly provide the recommended number of systematic biopsy cores and recommended biopsy point distribution diagram, which is convenient for the promotion of the model among multiple centers and the development of follow-up prospective studies. After the patient is admitted to the hospital, the clinician will need to input patient information into the website, and then, with the assistance of the imaging doctor or the clinician's own judgment of mpMRI, select the location of the lesion; the recommended core numbers and biopsy point distribution diagram will then be obtained. The surgeon can choose to use or not to use targeted biopsy according to the situation of the center and the patient.

This study has some limitations: First, the small sample size resulted in too few patients included in the first two layers in the external verification, which has a great impact on the result. Similarly, the inclusion of fewer patients in the first and second layers and more patients in the last three layers in the external verification reflects the imbalance of regional medical standards when China conducts multi-center research; screening levels in Shanghai and other regions are much higher than those in other regions (29), screening for prostate cancer remains inadequate in other regions. Second, the simulated process of reducing the number of cores is a human operation, and there is the influence of human subjective bias leading to instability of the model. Finally, this study adopts the method of grouping by DRS, resulting in a large difference in the number of pathologically negative and pathologically positive patients in each layer, especially the fifth layer. The statistical test efficiency will be affected by this, which requires us to perform follow-up prospective randomized research.

In conclusion, we are the first to propose a practical and feasible model of core reduction that considers the individual factors of each patient. Through the establishment of the website, the clinical application of the model becomes possible. For patients with suspicious lesions reported by mpMRI, we successfully reduced the number of cores to a minimum of 4.

DATA AVAILABILITY STATEMENT

The raw data supporting the conclusions of this article will be made available by the authors, without undue reservation.

ETHICS STATEMENT

Ethical review and approval was not required for the study on human participants in accordance with the local legislation and institutional requirements. Written informed consent for participation was not required for this study in accordance with the national legislation and the institutional requirements.

AUTHOR CONTRIBUTIONS

XG, ZeC, MQ, ML, and CW contributed to conception and design of the study. ZeC, MQ, SJ, ZhC, and XS organized the database. CW, ZeC, SJ, and XS performed the statistical analysis. ZeC wrote the first draft of the manuscript. MQ, JJ, WZ, YW, SJ, JZ, and LL wrote sections of the manuscript. WZ and JJ established the website. All authors contributed to the article and approved the submitted version.

FUNDING

The study was supported by the Promote Clinical Skills and Innovation Ability of Municipal Hospitals Project (Grant number: SHDC2020CR6007).

ACKNOWLEDGMENTS

We also would like to thank Editage (https://www.editage.com/) for English language editing.

SUPPLEMENTARY MATERIAL

The Supplementary Material for this article can be found online at: https://www.frontiersin.org/articles/10.3389/fonc.2021.831603/full#supplementary-material

REFERENCES

1. Hodge KK, McNeal JE, Terris MK, Stamey TA. Random Systematic Versus Directed Ultrasound Guided Transrectal Core Biopsies of the Prostate. *J Urol* (1989) 142:71–4. doi: 10.1016/S0022-5347(17)38664-0
2. Babaian RJ, Toi A, Kamoi K, Troncoso P, Sweet J, Evans R, et al. A Comparative Analysis of Sextant and an Extended 11-Core Multisite Directed Biopsy Strategy. *J Urol* (2000) 163:152–7. doi: 10.1016/S0022-5347(05)67993-1
3. Seles M, Gutschi T, Mayrhofer K, Fischereder K, Ehrlich G, Galle G, et al. Sampling of the Anterior Apical Region Results in Increased Cancer Detection and Upgrading in Transrectal Repeat Saturation Biopsy of the Prostate. *BJU Int* (2016) 117:592–7. doi: 10.1111/bju.13108
4. Smeenge M, de la Rosette J, Wijkstra H. Current Status of Transrectal Ultrasound Techniques in Prostate Cancer. *Curr Opin Urol* (2012) 22:297–302. doi: 10.1097/MOU.0b013e3283548154
5. D'Amico A, Tempany C, Cormack R, Hata N, Jinzaki M, Tuncali K, et al. Transperineal Magnetic Resonance Image Guided Prostate Biopsy. *AUA J* (2000) 164:385–7. doi: 10.1016/S0022-5347(05)67366-1
6. Kasivisvanathan V, Rannikko AS, Borghi M, Panebianco V, Mynderse LA, Vaarala MH, et al. MRI-Targeted or Standard Biopsy for Prostate-Cancer Diagnosis. *N Engl J Med* (2018) 378:1767–77. doi: 10.1056/NEJMoa1801993
7. Baco E, Rud E, Eri LM, Moen G, Vlatkovic L, Svindland A, et al. A Randomized Controlled Trial To Assess and Compare the Outcomes of Two-Core Prostate Biopsy Guided by Fused Magnetic Resonance and Transrectal Ultrasound Images and Traditional 12-Core Systematic Biopsy. *Eur Urol* (2016) 69:149–56. doi: 10.1016/j.eururo.2015.03.041
8. Siddiqui MM, Rais-Bahrami S, Turkbey B, George AK, Rothwax J, Shakir N, et al. Comparison of MR/ultrasound Fusion-Guided Biopsy With Ultrasound-Guided Biopsy for the Diagnosis of Prostate Cancer. *JAMA* (2015) 313:390–7. doi: 10.1001/jama.2014.17942
9. Richenberg J, Logager V, Panebianco V, Rouviere O, Villeirs G, Schoots IG. The Primacy of Multiparametric MRI in Men With Suspected Prostate Cancer. *Eur Radiol* (2019) 29:6940–52. doi: 10.1007/s00330-019-06166-z
10. Sonn GA, Fan RE, Ghanouni P, Wang NN, Brooks JD, Loening AM, et al. Prostate Magnetic Resonance Imaging Interpretation Varies Substantially Across Radiologists. *Eur Urol Focus* (2019) 5:592–9. doi: 10.1016/j.euf.2017.11.010
11. Lu AJ, Syed JS, Ghabili K, Hsiang WR, Nguyen KA, Leapman MS, et al. Role of Core Number and Location in Targeted Magnetic Resonance Imaging-Ultrasound Fusion Prostate Biopsy. *Eur Urol* (2019) 76:14–7. doi: 10.1016/j.eururo.2019.04.008
12. Tu X, Lin T, Cai D, Liu Z, Yang L, Wei Q. The Optimal Core Number and Site for MRI-Targeted Biopsy of Prostate? A Systematic Review and Pooled Analysis. *Minerva Urol e Nefrologica = Ital J Urol Nephrol* (2020) 72:144–51. doi: 10.23736/S0393-2249.20.03639-5
13. Sathianathen N, Omer A, Harriss E, Davies L, Kasivisvanathan V, Punwani S, et al. Negative Predictive Value of Multiparametric Magnetic Resonance Imaging in the Detection of Clinically Significant Prostate Cancer in the Prostate Imaging Reporting and Data System Era: A Systematic Review and Meta-Analysis. *Europ Urol* (2020) 78:402–14. doi: 10.1016/j.eururo.2020.03.048
14. Cornford P, van den Bergh RCN, Briers E, Van den Broeck T, Cumberbatch MG, De Santis M, et al. EAU-EANM-ESTRO-ESUR-SIOG Guidelines on Prostate Cancer. Part II—2020 Update: Treatment of Relapsing and Metastatic Prostate Cancer. *Eur Urol* (2021) 79:263–82. doi: 10.1016/j.eururo.2020.09.046
15. Merriel SWD, Funston G, Hamilton W. Prostate Cancer in Primary Care. *Adv Ther* (2018) 35:1285–94. doi: 10.1007/s12325-018-0766-1
16. Hu Z, Wang J, Sun D, Cui L, Ran W. How Many Cores Does Systematic Prostate Biopsy Need?: A Large-Sample Retrospective Analysis. *J Ultrasound Med* (2019) 38:1491–9. doi: 10.1002/jum.14834
17. Shen WW, Cui LG, Ran WQ, Sun Y, Jiang J, Pei XL, et al. Targeted Biopsy With Reduced Number of Cores: Optimal Sampling Scheme in Patients Undergoing Magnetic Resonance Imaging/Transrectal Ultrasound Fusion Prostate Biopsy. *Ultrasound Med Biol* (2020) 46:1197–207. doi: 10.1016/j.ultrasmedbio.2020.01.017
18. Weinreb JC, Barentsz JO, Choyke PL, Cornud F, Haider MA, Macura KJ, et al. PI-RADS Prostate Imaging - Reporting and Data System: 2015, Version 2. *Eur Urol* (2016) 69:16–40. doi: 10.1016/j.eururo.2015.08.052
19. Wang H, Lin H, He B, Guo X, Zhou Y, Xi P, et al. A Novel Perineal Nerve Block Approach for Transperineal Prostate Biopsy: An Anatomical Analysis-Based Randomized Single-Blind Controlled Trial. *Urology* (2020) 146:25–31. doi: 10.1016/j.urology.2020.01.058
20. Rouvière O, Puech P, Renard-Penna R, Claudon M, Roy C, Mège-Lechevallier F, et al. Use of Prostate Systematic and Targeted Biopsy on the Basis of Multiparametric MRI in Biopsy-Naive Patients (MRI-FIRST): A Prospective, Multicentre, Paired Diagnostic Study. *Lancet Oncol* (2019) 20:100–9. doi: 10.1016/s1470-2045(18)30569-2
21. van der Leest M, Cornel E, Israël B, Hendriks R, Padhani A, Hoogenboom M, et al. Head-To-Head Comparison of Transrectal Ultrasound-Guided Prostate Biopsy Versus Multiparametric Prostate Resonance Imaging With Subsequent Magnetic Resonance-Guided Biopsy in Biopsy-Naïve Men With Elevated

Prostate-Specific Antigen: A Large Prospective Multicenter Clinical Study. *European Urology* (2019) 75:570–8. doi: 10.1016/j.eururo.2018.11.023
22. Checcucci E, Amparore D, De Luca S, Autorino R, Fiori C, Porpiglia F. Precision Prostate Cancer Surgery: An Overview of New Technologies and Techniques. *Minerva Urol e Nefrologica = Ital J Urol Nephrol* (2019) 71:487–501. doi: 10.23736/S0393-2249.19.03365-4
23. Drost FH, Osses DF, Nieboer D, Steyerberg EW, Bangma CH, Roobol MJ, et al. Prostate MRI, With or Without MRI-Targeted Biopsy, and Systematic Biopsy for Detecting Prostate Cancer. *Cochrane Database Syst Rev* (2019) 4: CD012663. doi: 10.1002/14651858.CD012663.pub2
24. Distler FA, Radtke JP, Bonekamp D, Kesch C, Schlemmer HP, Wieczorek K, et al. The Value of PSA Density in Combination With PI-RADS™ for the Accuracy of Prostate Cancer Prediction. *J Urol* (2017) 198:575–82. doi: 10.1016/j.juro.2017.03.130
25. Washino S, Okochi T, Saito K, Konishi T, Hirai M, Kobayashi Y, et al. Combination of Prostate Imaging Reporting and Data System (PI-RADS) Score and Prostate-Specific Antigen (PSA) Density Predicts Biopsy Outcome in Prostate Biopsy Naïve Patients. *BJU Int* (2017) 119:225–33. doi: 10.1111/bju.13465
26. Vinjamoori AH, Jagannathan JP, Shinagare AB, Taplin ME, Oh WK, Van den Abbeele AD, et al. Atypical Metastases From Prostate Cancer: 10-Year Experience at a Single Institution. *AJR. Am J Roentgenol* (2012) 199:367–72. doi: 10.2214/AJR.11.7533
27. He B, Chen R, Gao X, Ren S, Yang B, Hou J, et al. Nomograms for Predicting Gleason Upgrading in a Contemporary Chinese Cohort Receiving Radical Prostatectomy After Extended Prostate Biopsy: Development and Internal Validation. *Oncotarget* (2016) 7:17275–85. doi: 10.18632/oncotarget.7787
28. Welch H, Albertsen P. Reconsidering Prostate Cancer Mortality - The Future of PSA Screening. *N Engl J Med* (2020) 382:1557–63. doi: 10.1056/NEJMms1914228
29. Fu Z, Guo X, Zhang S, Zheng R, Zeng H, Chen R, et al. Statistical Analysis of Incidence and Mortality of Prostate Cancer in China, 2015. *Chinese J Onco* (2020) 42:718–22. doi: 10.3760/cma.j.cn112152-20200313-00200

Conflict of Interest: The authors declare that the research was conducted in the absence of any commercial or financial relationships that could be construed as a potential conflict of interest.

Publisher's Note: All claims expressed in this article are solely those of the authors and do not necessarily represent those of their affiliated organizations, or those of the publisher, the editors and the reviewers. Any product that may be evaluated in this article, or claim that may be made by its manufacturer, is not guaranteed or endorsed by the publisher.

Copyright © 2022 Chen, Qu, Shen, Jiang, Zhang, Ji, Wang, Zhang, Chen, Lin, Li, Wu and Gao. This is an open-access article distributed under the terms of the Creative Commons Attribution License (CC BY). The use, distribution or reproduction in other forums is permitted, provided the original author(s) and the copyright owner(s) are credited and that the original publication in this journal is cited, in accordance with accepted academic practice. No use, distribution or reproduction is permitted which does not comply with these terms.

frontiers in Oncology

ORIGINAL RESEARCH
published: 24 February 2022
doi: 10.3389/fonc.2022.840786

Utility of Clinical–Radiomic Model to Identify Clinically Significant Prostate Cancer in Biparametric MRI PI-RADS V2.1 Category 3 Lesions

Pengfei Jin[1,2†], *Liqin Yang*[1,2†], *Xiaomeng Qiao*[1,2], *Chunhong Hu*[1,2], *Chenhan Hu*[1,2], *Ximing Wang*[1,2*] *and Jie Bao*[1,2*]

[1] Department of Radiology, The First Affifiliated Hospital of Soochow University, Suzhou, China, [2] Institute of Medical Imaging, Soochow University, Suzhou, China

OPEN ACCESS

Edited by:
Antonina Mitrofanova, Rutgers, The State University of New Jersey, United States

Reviewed by:
Ugo Giovanni Falagario, University of Foggia, Italy
Andrea Benedetto Galosi, Marche Polytechnic University, Italy

***Correspondence:**
Ximing Wang
wangximing1998@163.com
Jie Bao
baojie7346@sina.com

[†]These authors have contributed equally to this work and share first authorship

Specialty section:
This article was submitted to Genitourinary Oncology, a section of the journal Frontiers in Oncology

Received: 21 December 2021
Accepted: 01 February 2022
Published: 24 February 2022

Citation:
Jin P, Yang L, Qiao X, Hu C, Hu C, Wang X and Bao J (2022) Utility of Clinical–Radiomic Model to Identify Clinically Significant Prostate Cancer in Biparametric MRI PI-RADS V2.1 Category 3 Lesions. Front. Oncol. 12:840786. doi: 10.3389/fonc.2022.840786

Purpose: To determine the predictive performance of the integrated model based on clinical factors and radiomic features for the accurate identification of clinically significant prostate cancer (csPCa) among Prostate Imaging Reporting and Data System (PI-RADS) 3 lesions.

Materials and Methods: A retrospective study of 103 patients with PI-RADS 3 lesions who underwent pre-operative 3.0-T MRI was performed. Patients were randomly divided into the training set and the testing set at a ratio of 7:3. Radiomic features were extracted from axial T2WI, diffusion-weighted imaging (DWI), and apparent diffusion coefficient (ADC) images of each patient. The minimum redundancy maximum relevance (mRMR) and least absolute shrinkage and selection operator (LASSO) feature selection methods were used to identify the radiomic features and construct a radiomic model for csPCa identification. Moreover, multivariable logistic regression analysis was used to integrate the clinical factors with radiomic feature model to further improve the accuracy of csPCa identification, and the two are presented in the form of normogram. The performance of the integrated model was compared with radiomic model and clinical model on testing set.

Results: A total of four radiomic features were selected and used for radiomic model construction producing a radiomic score (Radscore). Radscore was significantly different between the csPCa and the non-csPCa patients (training set: $p < 0.001$; testing set: $p = 0.035$). Multivariable logistic regression analysis showed that age and PSA could be used as independent predictors for csPCa identification. The clinical–radiomic model produced the receiver operating characteristic (ROC) curve (AUC) in the testing set was 0.88 (95% CI, 0.75–1.00), which was similar to clinical model (AUC = 0.85; 95%CI, 0.52–0.90) ($p = 0.048$) and higher than the radiomic model (AUC = 0.71; 95%CI, 0.68–1.00) ($p < 0.001$).

The decision curve analysis implies that the clinical–radiomic model could be beneficial in identifying csPCa among PI-RADS 3 lesions.

Conclusion: The clinical–radiomic model could effectively identify csPCa among biparametric PI-RADS 3 lesions and thus could help avoid unnecessary biopsy and improve the life quality of patients.

Keywords: radiomics, clinically significant prostate cancer, PI-RADS score 3, nomogram, biparametric MRI (Bp-MRI)

INTRODUCTION

Prostate cancer (PCa) is one of the most common cancer and the second leading cause of cancer deaths among men (1). The Prostate Imaging Reporting and Data System (PI-RADS) aims to standardize the interpretation and reporting of prostate MRI, which develop a 5-point assessment to assist in identifying suspicious lesions and reflect their relative possibility of a clinically significant prostatic cancer (csPCa) (2). Despite offering valuable information in predicting csPCa on a population level, one of the main limitations of PI-RADS is the high inter-reader variability impacting on cancer detection (3). Additionally, the PI-RADS has an inability to resolve some ambiguity and uncertainty associated with some reporting criteria and lesion descriptors.

Currently, the classification of PI-RADS category 3 lesions has not been clearly defined, which represents a "gray zone" that contains benign, indolent, and invasive lesions. Since considered as positive MRI finding, PI-RADS 3 lesion should always be biopsied according to European Association of Urology guidelines, which results in a diagnosis of csPCa in 3%–50% of the patients (4, 5). However, other studies have reported that cancer diagnosis rates range from 2% to 23% in PI-RADS 3 lesions and suggested that mostly they are benign lesions or non-significative cancers (6–8). Due to the uncertainty and lack of clear management recommendations of undetermined lesions, it is still under debate whether a biopsy should be performed or not. Therefore, determining which lesions are csPCa will help improve patients' quality of life *via* avoiding unnecessary biopsies and overtreatment.

Recent studies have shown that patient age, high prostate-specific antigen density (PSAD), PSA velocity, low apparent diffusion coefficient (ADC) signal, and even genetic risk are associated with the existence of csPCa (5, 7, 9). Furthermore, it has been illustrated that in radiomics, a large number of quantitative features, extracted from MRI images, have been employed in detecting PCa, evaluating PCa aggressiveness, and clinical decision-making (10). However, the potential role of MRI radiomics in identifying csPCa among PI-RADS 3 lesions has not been determined. A recent study suggested that texture analysis based on machine learning could help to identify csPCa in PI-RADS 3 lesions (11). In 2019, PI-RADS V2.1 proposed the concept of biparametric magnetic resonance imaging (bpMRI), which only includes T2WI, diffusion-weighted imaging (DWI), and ADC sequences to simplify the process of prostate MRI scanning (2). The diagnostic accuracy and performance of bpMRI are comparable to multi-parameter magnetic resonance imaging (mpMRI), which also covers dynamic contrast enhancement (DCE), and the former is less expensive, rapid, and well tolerated by patients (12).

Therefore, the objective of this study was to construct a nomogram that integrate radiomics based on bpMRI and clinical information to identify csPCa in PI-RADS 3 lesions.

MATERIALS AND METHODS

Study Cohort

The Institutional Review Board approved this retrospective study performed at a single medical institution and waived the requirement of informed consent (2021; Approval No. 262). A retrospective collection of 1,675 patients who underwent prostate MRI examination due to PSA elevation in our hospital from January 2016 to January 2019 was conducted. All MRI images were assigned PI-RADS V2.1 score by two genitourinary radiologists experienced in urological diagnosis (3- and 6-year experience). Screened out lesions identified as PI-RADS 3 and sent to another experienced genitourinary radiologist (more than 10-year experience) for review. All the radiologists were blind to the histopathological results at the time of reading. If there is a disagreement on the diagnosis, the three radiologists will discuss it until a consensus is reached. PI-RADS V2.1 defined the score 3 lesion as the focal low signal of ADC and/or high signal of DWI with high b-value in the peripheral zone (PZ) or the uneven signal of T2WI sequence in the transitional zone (TZ) with blurred edges. In the course of the discussion, 25 cases were downgraded to PI-RADS 1–2, and 39 cases were upgraded to PI-RADS 4–5. The final scoring results showed that 859 patients (51.3%) had PI-RADS scores of 1 and 2, and 153 patients (9.1%) had PI-RADS scores of 3; the other 663 cases (39.6%) had PI-RADS scores of 4 and 5.

Exclusion criteria were as follows: (1) PI-RADS 1–2, PI-RADS 4–5, or PI-RADS 3 coexisted with other types of lesions (N = 1,529); (2) poor image quality (N = 8); (3) MRI findings were not confirmed by histopathological results(N = 11); (4) intervention prior to MRI examination, such as biopsy, surgery, or hormone therapy (N = 24) (**Figure 1**). In addition, clinical data, such as the International Society of Urological Pathology (ISUP) grade, pathological stage, age, and PSA value, were obtained by querying electronic records in PACS system. A total of 103 patients meeting above criteria were included in this study, with an average age of 67.5 ± 9.4 years and a mean PSA level of 14.9 ± 13.8 ng/ml.

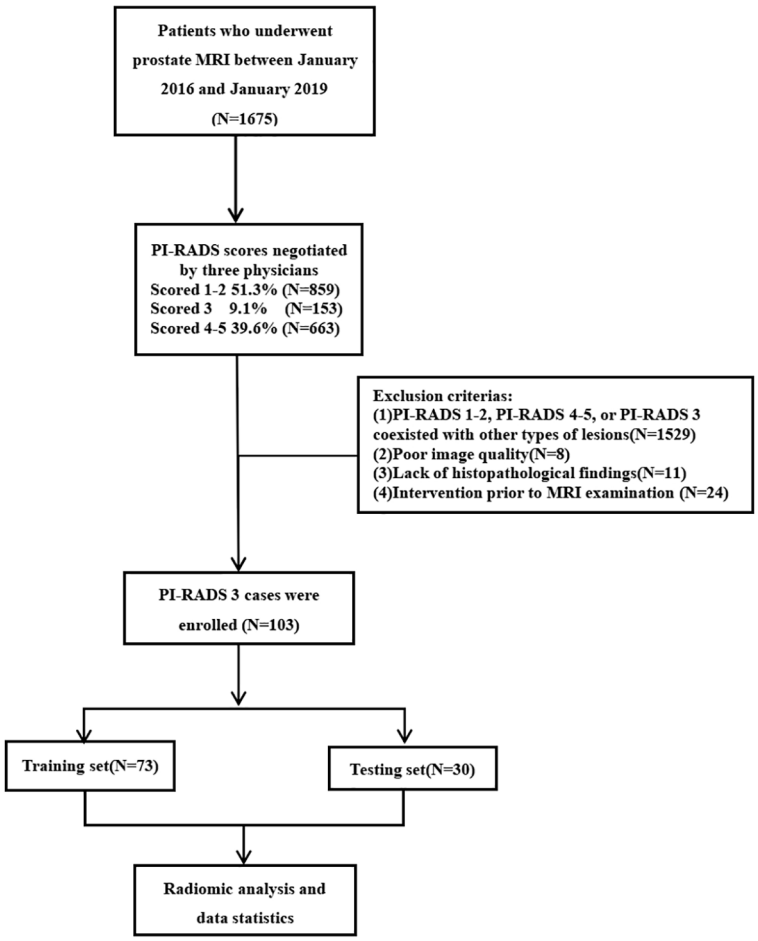

FIGURE 1 | Patient recruitment flowchart.

Scanning Equipment and Parameters

A 3.0-T superconducting MR scanner (Skyra; Siemens, Munich, Germany) with 32-channel body phased line coil was adopted. The scanning sequence included T1WI, axial T2WI (no fat-saturated), sagittal T2WI, coronal T2WI, DWI (b = 100, 800, 1 500 s/mm^2) and/or dynamic-contrast-enhanced T1WI. Based on the DWI images of 1,500 b-values, the ADC icons were calculated by extended single exponential fitting model. The specific scanning parameters were recommended by PI-RADS V2.1 (**Table 1**) (2).

Biopsy and Histopathology

All identified patients underwent MRI-transrectal ultrasound (MRI-TRUS) fusion-guided prostate biopsy with a navigation system (HIVISION Noblus/TopicPath). At least two biopsy samples were obtained from each targeted lesion. The 12-core systematic biopsies were routinely performed following the targeted biopsy procedure. If patients underwent radical prostatectomy, their pathological ISUP grades, instead of biopsy ISUP grades, were used to define csPCa. The pathological results

TABLE 1 | Multi-parameter MRI scan sequence and parameters.

Sequence	Repetition time (ms)	Echo time (ms)	Layer thickness (mm)	Interlayer spacing (mm)	Field of view (mm × mm)
T1WI	680.0	13.00	5	0.50	380 × 380
Axial T2WI	6,980.0	104.00	3	0	200 × 200
Sagittal T2WI	3,900.0	89.00	3	0.45	200×200
Coronal T2WI	3,500.0	85.00	3	0.60	220 × 220
DWI	5,000.0	72.00	3	0	288 × 288
DCE-MRI	4.2	1.34	3	0	260 × 260

T2WI, T2-weighted imaging; DWI, diffusion-weighted imaging; ADC, apparent diffusion coefficient; DCE, dynamic contrast enhancement.

were evaluated by expert urologists, and the location of the lesions were recorded to ensure the correspondence to the suspicious lesions on MRI. csPCa was defined as ISUP Class 2 or higher (Gleason = 3 + 4 or higher). Lesions with GS = 3 + 3 were defined as clinically insignificant prostate cancer (ciPCa), which were categorized in the same group as benign lesions (13).

MRI Image Preprocessing and Focus Segmentation

First, histogram-based intensity standardization method was used to standardize the bpMRI, and the voxel size of image was resampled to 1 mm × 1 mm × 1 mm. Then, the axial T2WI, high b-value (1,500 mm/s^2) DWI, and ADC were co-registered using Elastix software package (v.4.10) to ensure that DWI and ADC images have the same resolution, field of view (FOV), and orientation as T2WI. The two radiologists involved in the image evaluation used Insight Segmentation and Registration Toolkit (ITK, v. 4.7.2; https://itk.org/) to manually draw the region of interest (ROI) on the T2WI image layer by layer, then copy it to DWI and ADC images to ensure the consistency of volume of interest (VOI) sketches in different sequences. To ensure the stability and repeatability of the annotations, the same radiologists repeated the annotation procedure after a week, and all the annotations were re-examined by another senior radiologist with 15 years of experience in prostate MRI diagnosis.

Feature Extraction and Consistency Agreement

The radiomics software FeAture Explorer (FAE v0.4.0) was used to extract and select the features of each mode with reference to VOI (14). A total of 2,553 radiomic features were extracted, including (1) 54 first-order gray statistics, (2) 42 features of shape-based, (3) 72 gray-level co-occurrence matrixes (GLCM), (4) 48 gray-level run length matrixes (GLRLM), (5) 48 gray-level size zone matrixes (GLSZM), (6) 42 gray-level dependence matrixes (GLDM), and (7) 15 neighborhood gray tone difference matrixes (NGTDM). In addition, 2,232 wavelet features were extracted in three spatial directions. The inter- and intra-observer reproducibility of tumor segmentation and feature extraction was evaluated by intraclass correlation coefficients (ICCs), and radiomic features with ICCs values >0.75 were retained.

Radiomics Model Development

All samples were randomly divided into the training set and the testing set at a ratio of 7:3. First of all, most of the features were excluded by using the mRMR method, and only 30 features with the least redundancy and the greatest correlation with the target label were retained. The radiomic signature was constructed based on the features selected from the training set. Due to the large number of features extracted, there was redundancy between features, and some features had little or no correlation with the modeling object. Then, least absolute shrinkage and selection operator (LASSO) was used to select the most useful features. Finally, a logistic regression was trained using the remaining features, and a radiomic score was calculated as the linear combination of the selected radiomic features and corresponding coefficients.

In addition, we have employed the multivariate logistic regression analysis to combine clinical characteristics, including age, PSA value, zone of the lesion, prostate volume, with radiomic features, and identify the independent predictors of csPCa among PI-RADS V2.1 category 3 lesions in the training set. Furthermore, a clinical–radiomic nomogram was built to provide clinicians with a quantitative tool for csPCa identification. The area under receiver operating characteristic (ROC) curve (AUC) was adopted to evaluate the accuracy of the nomogram in identifying csPCa.

Model Evaluation

AUCs of clinical, radiomic, and clinical–radiomic model were basically evaluated with histopathological manifestations in both training and testing set. Moreover, DeLong's test was used to compare the ROC curves of the nomogram, radiomic, and clinical model, and Hosmer–Lemeshow test was performed to evaluate the goodness-of-fit of the calibration curve between nomogram and the pathological results. Furthermore, decision curve analysis (DCA) was used to quantify the net benefit of each predictive model.

Statistical Analysis

To identify csPCa among PI-RADS 3 lesions on bpMRI, we trained the binary classification models by labeling csPCa as 1 and both ciPCa and benign lesions as 0. R language software (version 4.1.0, www.Rproject.org) was used for quantitative feature analysis. The Shapiro–Wilk test was performed to evaluate the normality of data. According to the results of normality test, independent sample t-test or Mann–Whitney U-test was used to detect the difference of clinical characteristics between non-csPCa group and csPCa group. Multivariable logistic regression was performed using "rms" package to construct the clinical–radiomic nomogram. ROC curves and AUCs were established using "PROC" package to evaluate the diagnostic accuracy of each predictive model. Calibration curve and Hosmer–Lemeshow test were performed with "ModelGood" and "DescTools" packages, respectively. Finally, the "rmda" software package was used for decision curve analysis. $p < 0.05$ indicated that the difference was statistically significant.

RESULTS

Baseline Characteristics

Among the 103 lesions with a score of PI-RADS 3 were 28 cases of csPCa (27.2%), 70 cases of benign hyperplasia (67.9%), and 5 cases of ciPCa (4.9%); 44.7% (46/103) lesions were located in TZ, and 55.3% (57/103) lesions were located in PZ. The prevalence of csPCa located in TZ and PZ was 11.7% (12/103) and 15.5% (16/103), respectively. Among the 28 patients with csPCa, 13 cases were ISUP grade 2 (GS = 3 + 4), 6 cases were ISUP grade 3 (GS =

4 + 3), 7 cases were ISUP grade 4 (GS = 4 + 4, 5 + 3), and 2 cases were ISUP grade 5 (GS = 5 + 4). The diameter of lesions ranged from 5.2 to 18.6 mm, with an average diameter of 9.5 mm ± 3.4 mm (**Table 2**).

Performance of Prediction Models

Clinical Model

Univariate logistic analysis showed that age and PSA value were significant factors for predicting csPCa. Multivariate logistic regression analysis showed that the odd ratio of PSA level to detect csPCa was 1.04; the difference was statistically significant ($p = 0.041$). Therefore, these two clinical factors can be used as independent predictors (**Table 3**). Finally, a logistic regression classifier was established according to the selected clinical features. The performance of clinical model in identifying csPCa is listed in **Table 4**.

TABLE 2 | Demographic and disease characteristics.

	Training set	Testing set	*p*-value
Ages	64.7 ± 9.2	66.8 ± 8.3	0.326
PSA (ng/ml)	14.8 ± 10.1	17.5 ± 5.7	0.518
Lesion type			–
Benign	48 (46.6%)	22 (21.4%)	
csPCa	22 (21.4%)	6 (5.8%)	
ciPCa	3 (2.9%)	2 (1.9%)	
Zone			
PZ	41	16	
TZ	32	14	
Total	73	30	

PSA, prostate-specific antigen; csPCa, clinically significant prostate cancer; ciPCa, clinically insignificant prostate cancer; PZ, peripheral zone; TZ, transitional zone.
The p-values are derived from the comparison between training set and testing set.

Prediction Model Based on Radiomic Features

A total of four radiomic features were selected and used to build a logistic regression model based in the training cohort (**Figures 2** and **3**). Radscore was significantly different between the csPCa group and the non-csPCa group (training set: $p < 0.001$; testing set: $p = 0.035$), which indicated that the probability of csPCa was positively correlated with Radscore. The radiomics feature model has an above-average predictive efficiency for csPCa in PI-RADS 3 lesions, with an AUC of 0.71 (**Table 4**).

Clinical–Radiomic Model

The nomogram that combined age, PSA, and Radscore is shown in **Figure 4**. Compared with the radiomics model, the clinical–radiomic nomogram showed an improved performance in predicting csPCa among PI-RADS category 3 lesions. The AUC values of the training group and the validation group were 0.90 (95%CI: 0.83–0.97) and 0.88 (95%CI: 0.75–1.00),

TABLE 3 | Univariate and multivariate logistic analyses results of clinical factors.

Baseline characteristics	Non-clinically significant cancer (n = 75)	Clinically significant cancer (n = 28)	Univariate logistic regression		Multivariate logistic regression	
			Odds ratio (95%CI)	*p*-value	Odds ratio(95%CI)	*p*-value
Age	65.6 ± 9.1	72.5 ± 8.3	1.06 (1.00–1.13)	0.042	1.09 (1.00–1.13)	0.046
PSA (ng/ml)	12.3 ± 10	21.8 ± 19.4	1.04 (1.00–1.09)	0.034	1.04 (1.00–1.08)	0.041
Lesion location			1.01 (1.00–1.07)	0.063	1.03 (1.02–1.10)	0.052
Peripheral zone	41 (39.8%)	16 (15.5%)				
Transition zone	34 (33.0%)	12 (11.7%)				
Gland volume	43.8 ± 24.3	40.7 ± 15.8	1.02 (0.97–1.06)	0.074	1.01 (0.99–1.05)	0.097

PSA, prostate-specific antigen; 95%CI, 95% confidence interval.

TABLE 4 | The AUC outcomes of clinical, radiomic, and combined model in prediction of csPCa in category 3 lesions.

	Clinics		Radiomics		Nomogram	
Index	Training set	Testing set	Training set	Testing set	Training set	Testing set
Cutoff	–0.77		–0.84		–1.54	
Accuracy	0.74	0.57	0.75	0.57	0.78	0.70
(95%CI)	(0.62–0.84)	(0.54–0.88)	(0.64–0.85)	(0.37–0.75)	(0.67–0.87)	(0.45–0.82)
Sensitivity	0.68	0.67	1.00	1.00	0.91	0.83
Specificity	0.76	0.75	0.65	0.46	0.73	0.65
PPV	0.56	0.40	0.55	1.00	0.59	0.47
NPV	0.85	0.90	0.46	0.32	0.95	0.91
AUC	0.70	0.85	0.85	0.71	0.90	0.88
(95%CI)	(0.55–0.84)	(0.68–1.00)	(0.76–0.93)	(0.52–0.90)	(0.83–0.97)	(0.75–1.00)
p-value (vs nomogram)	$p = 0.001$	$p = 0.048$	$p < 0.001$	$p < 0.001$	–	–

95%CI, 95% confidence interval; PPV, positive predict value; NPV, negative predictive value. The p-values from Delong tests compared with nomogram.

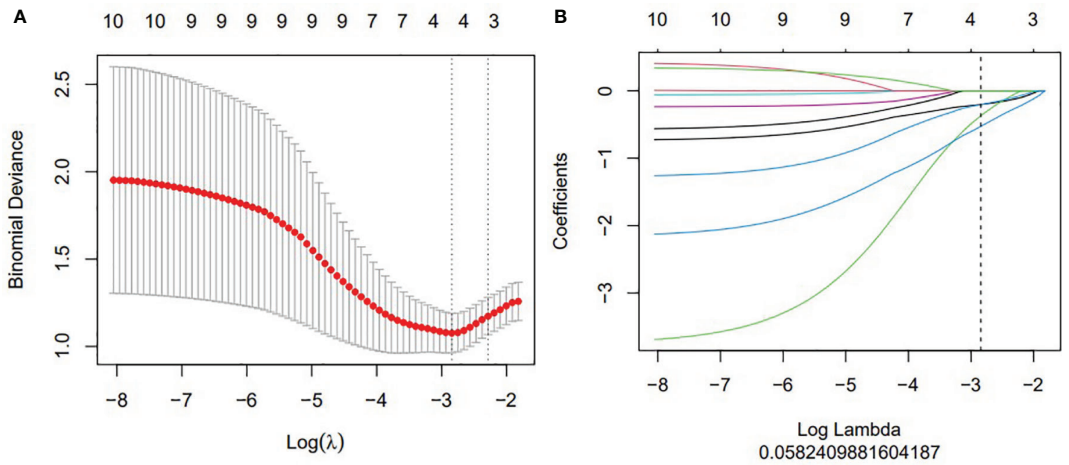

FIGURE 2 | The construction of LASSO regression model. **(A)** Curve of binomial deviation of biparameter MR radiomics model varying with parameter λ. The horizontal axis is the log (λ) value. The vertical axis represents binomial deviation. The number above represents the number of selected features, and the λ at the minimum binomial deviation of the model is the optimal value (vertical dotted line). **(B)** Biparameter MRI model changing with λ. The number above indicates the number of features filtered out.

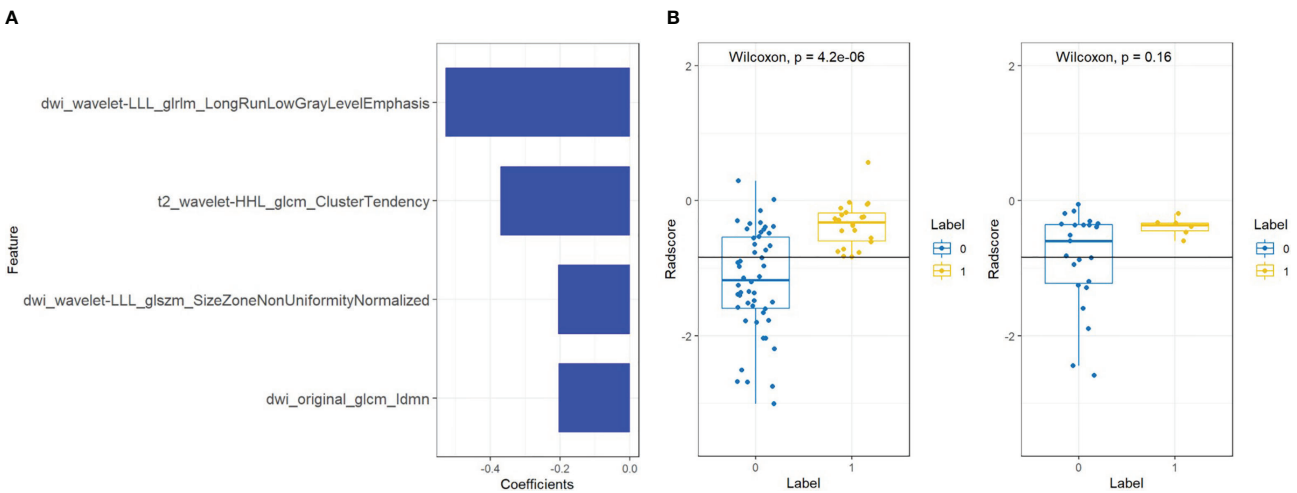

FIGURE 3 | Features and radiomics labels used in bpMRI model. **(A)** Imaging characteristics screened by bpMRI model. **(B)** comparison of Radscore between training set (left) and testing set (right). The blue label represents benign lesions or ciPCa, and the yellow label is csPCa.

respectively. The calibration curve showed that the nomogram had a higher pathological coincidence rate. The p-value of the nomogram prediction ability obtained by the Hosmer–Lemeshow test was 0.740 in the training cohort and 0.503 in the testing cohort (**Figure 5**). The AUC, accuracy, sensitivity, and specificity of the three models are listed in **Table 4**. Our results showed that the ability of nomogram to distinguish csPCa from non-csPCa in PI-RADS category 3 lesions was higher than that of clinical model and radiomic model. Furthermore, nomogram had the highest net benefit compared to clinical and radiology (**Figures 6** and **7**).

DISCUSSION

Radiomics is a technique for extracting and analyzing quantitative features from medical images. It can capture sub-visual signatures, such as the change of gray level and spatial distribution of the intensity. It has been shown that radiomics was of great potentials in PCa classification, risk stratification, and thus help with the clinical diagnostic workflow. The correlation between multi-parameter MRI radiomic features and Gleason grading also showed that the radiomic model could predict Gleason score and distinguish between invasive PCa (GS ≥ 4 + 3) and inert PCa (GS < 4 + 3).

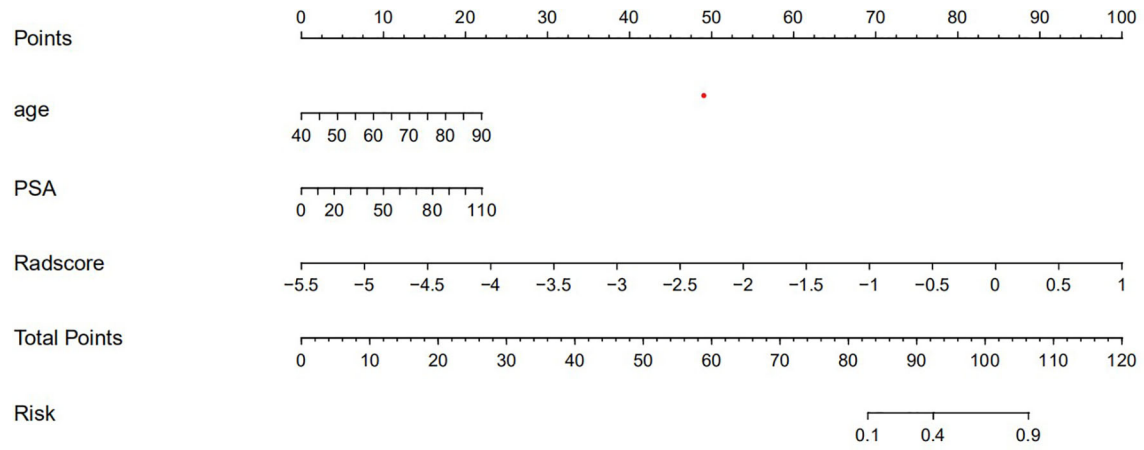

FIGURE 4 | Clinical–radiomic nomogram.

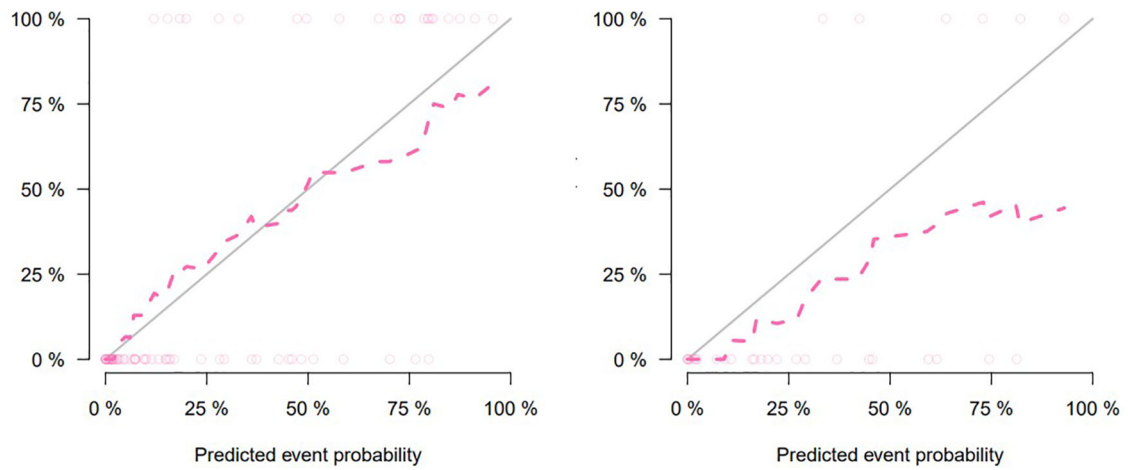

FIGURE 5 | Calibration curve for clinical–radiomic nomogram prediction of the consistency between the predicted results and pathological results (training set on the left, testing set on the right).

Zhang et al. developed and verified a non-invasive radiomic model based on MRI to distinguish between inert and invasive PCa before treatment. They finally selected nine radiomic features to construct imaging tags with 0.944 for sensitivity, 0.786 for specificity, and 0.901 for AUC in the validation set (15). Radiomic not only can assist PCa detection and grading but also can be used to evaluate tumor extracapsular invasion, which is conducive to accurate preoperative staging. Ma et al. selected 17 imaging features extracted from T2WI images to predict extracapsular invasion in PCa patients, showing great recognition ability and excellent calibration performance in training and verification sets (16).

Giambeluca et al. introduced the concept of texture analysis into the study of PI-RADS 3 lesions for the first time (11). They found that nine and six independent texture features on T2WI and ADC maps were significantly correlated with the final histopathological results, and the derived model predicted that the AUC of csPCa was 0.82 and 0.74, respectively. However, the sample size of their study is too small (only 46 PI-RADS 3 lesions) and has not been verified by the test set, which affects the reliability of the results. In this study, we constructed and validated a comprehensive diagnostic model combining clinical variables and radiomic features, which was used to identify csPCa lesions in PI-RADS 3 lesions on biparameter MRI, and compared with separate clinical model and radiomic model (Radscore). As demonstrated by DeLong's test, the clinical–radiomic model was significantly superior to both clinical and Radscore in identifying csPCa. In the testing set, compared with 33% (2/6) in the clinical model, only 17% (1/6) csPCa were missed using the combined model, which helped reducing the rate of missed diagnosis greatly without significantly decreasing

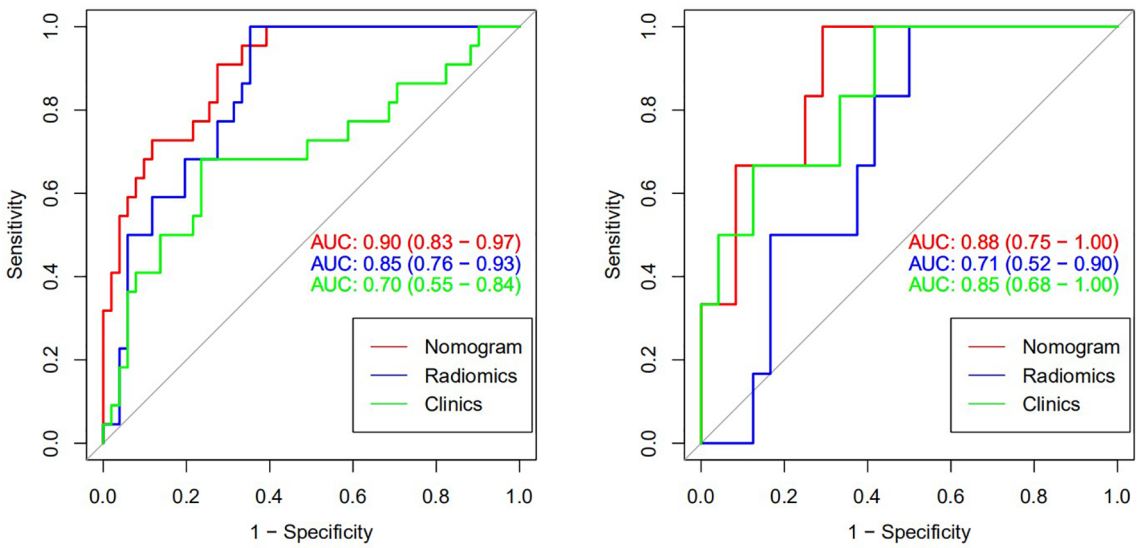

FIGURE 6 | Receiver operating characteristic (ROC) curve of csPCa predicted by three models (training set on the left and verification set on the right).

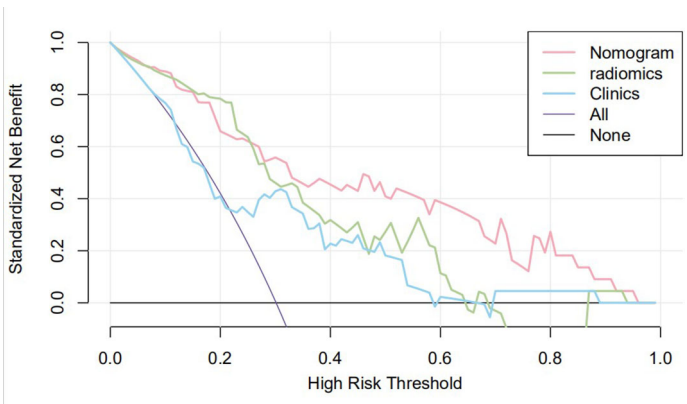

FIGURE 7 | Clinical decision curve of the three models. The X-axis represents the threshold probability, and the Y-axis represents the net benefit. The decision curve showed that if the threshold probability of a patient was within the range from 25% to 95%, using the joint nomogram to predict csPCa occurrences added more benefit than the biopsy-all-patients scheme or the surveil-all-patients scheme.

the specificity (75% vs. 65%). It is worth noting that although the radiomic model has a high sensitivity (100%), its specificity is very low (46%), which may lead to unnecessary biopsies. The combined model has the advantages of both clinical and radiomic model, and the output results have higher stability. In order to more intuitively show the risk probability of the comprehensive model for predicting csPCa, this study presents it in the form of nomogram. This clinical–radiomic nomogram provides an easy-to-use, quantifiable, and individualized screening tool for PCa, helping to avoid unnecessary treatment and invasive examination in men with PCa patients and preventing and delaying the progression of low-grade PCa. In recent years, the nomogram prediction model has been widely used in clinical medicine, using risk scores to represent the risk factors of a variety of diseases and predict the prognosis of patients. The expression of this model is clear, concise, easy to understand, and conducive to doctor–patient communication.

Previous studies on intelligent diagnosis of PI-RADS 3 lesions were limited to simple imaging features (17–19), without considering the additional diagnostic value of clinical indicators. Compared with these similar studies, this study fused clinical indicators and imaging features when designing the model and proved that the two are complementary in the differentiation of benign and malignant prostate lesions. Univariate and multivariate analyses showed that radiomic features, age, and PSA could be used as independent predictors

for the differential diagnosis of benign and malignant prostate lesions. In this study, the AUC (0.85) of the radiomics model in the training set was higher than that of the clinical model (0.70), but in the testing set, the AUC of the radiomic model in the diagnosis of csPCa was lower than that of the clinical model (0.71 vs. 0.85, $p < 0.05$). In our opinion, the reason may be that the sample size of csPCa in the testing set was too small (only six cases) to accept comprehensive verification, thus caused a certain randomness in the result. In addition, malignant epithelial cells of sectional csPCa in PI-RADS 3 lesions were sparsely arranged and distributed along the acinar, which overlapped greatly with some benign diseases such as inflammation, hyperplasia, and fibrosis, resulting in insignificant changes in MRI signal. Age was associated with Gleason score, and the older the age, the higher the risk of poor histology. Studies have shown that the ORs and 95%CI of poor histological prognosis of prostate were 2.21 (1.30–3.76) and 1.58 (0.90–2.76) in men over 80 years old compared with those under 70 years old, respectively (20). Although this study did not prove a positive correlation between prostate volume and the occurrence of csPCa, several studies have confirmed that PSAD (PSA value/gland volume) was independently correlated to csPCa even in patients with serum PSA slightly above limits or even within normal limits, which was observed in every clinical scenario early diagnosis, repeat biopsy, and active surveillance (21). For example, Roscigno et al. found that higher PSAD was associated with higher risk of reclassification at confirmatory or follow-up biopsy using 0.20 as cutoff (22). Pagniez et al. increased the negative predictive value of PI-RADS from 84.4% to 90.4% by using the PSAD with a cutoff of 0.15 ng/ml/cc (23). PSAD is also useful to identify patients with elevated PSA due to PCa rather than intraprostatic inflammation, which is indeed a strong predictor of the absence of PCa in biopsy specimen (24). As a rule, compared with TZ, the risk of developing PCa tends to appear on PZ; therefore, the anatomical location of lesions is helpful for the differential diagnosis of equivocal lesions (defined as PI-RADS 3). Yang et al. analyzed cancer detection rate in 683 patients with PI-RADS 3 lesions of the PZ and TZ and reported 18.7% of csPCa in the PZ, while in the TZ, the rate of csPCa was 6.0% (25). However, the results of this study suggest that the zone of the lesions cannot be an independent predictor to refine classification of PI-RADS 3 lesions. The reason may be that the T2WI scoring criteria of PI-RADS 3 lesion in TZ is too vague to grasp for inexperienced evaluators; more TZ lesions were selected while building the study cohort, and the probability of csPCa increased accordingly. In addition, the clinical variables used to construct nomogram were not comprehensive enough, such as palpable nodule, correlation between PSA, and prostate volume, which were not analyzed. Studies have shown that despite low PSA levels, the incidence of csPCa is higher in patients with positive digital rectal examination (DRE) (26). PSA density and DRE could be analyzed in the nomogram as the next step to improve selection of PI-RADS 3 lesions. The decision curve also indicates that if the patient's threshold probability is 25%–95%, patients can benefit more from using the radiomic feature-based nomogram in this study to predict the identification of benign and malignant nodules, and the combined model has better predictive performance than individual clinical risk factors or radiomics features.

In the construction of radiomics model, the feature subsets extracted from DWI images were the most relevant factor for classification of PI-RADS category 3 lesions, while the contribution of ADC feature subsets was the least, which was different from the previous research results of Bonekamp et al. They believe that the effectiveness of radiomic model based on bpMRI in distinguishing benign and malignant prostate lesions is comparable to that of single ADC model (27). The reason for the inconsistent results may be that the PI-RADS category 3 refers to the lesions with mild or moderate low signal on the ADC maps, excluding those obvious benign and malignant lesions in advance. In addition, the transitional zone lesions included in this study accounted for 44.7%, while the TZ lesions were mainly based on the definition of T2WI manifestations, and ADC had little reference significance in the diagnosis of TZ lesions.

For the generalization ability of the model across different populations, studies have shown that the performance of MRI to predict the presence of extraprostatic extension and high-grade PCa is unaffected in Caucasian and African American men, and no difference was found between races in pathological outcomes after radical prostatectomy (28). These findings suggest that access to and use of advanced diagnostic tests may help mitigate PCa racial disparities; thus, the present model may be valid also in other populations. In subsequent studies, independent external validation sets can be set up to evaluate the stability of the predicted results of the model in different cohorts.

There are some limitations in this study. First of all, this study was a retrospective analysis of a relatively small group of patients from a unitary institution and a single scanner, and our predictive model needs to be prospectively validated in a larger scale of patients from other medical units using different MRI scanners prior to wider clinical application. Second, clinical factors only analyzed PSA and age; rather, they may be used to discover a population at higher risk to have a csPCa. Therefore, increase probability of favorable results independently of imaging interpretation. Third, subjects were not followed up, so the number of cancers diagnosed in the months after baseline is not available. Finally, in this study, there was no separate analysis of PZ and TZ lesions.

CONCLUSION

We have developed a nomogram based on radiomics and clinical indicators, which has excellent predictive performance for csPCa in biparametric PI-RADS 3 lesions, and provide an intuitive and quantitative method for radiologists to diagnose PCa more confidently and reduce unnecessary biopsies.

DATA AVAILABILITY STATEMENT

The raw data supporting the conclusions of this article will be made available by the authors, without undue reservation.

ETHICS STATEMENT

The studies involving human participants were reviewed and approved by Institutional Review Board of the First Affiliated Hospital of Soochow University. Written informed consent for participation was not required for this study in accordance with the national legislation and the institutional requirements.

AUTHOR CONTRIBUTIONS

XW and JB created the study design. PJ collected the data and processed the data. PJ and LY conducted data analysis. PJ and LY wrote the manuscript. All authors contributed to the article and approved the submitted version.

FUNDING

This study was supported by (1) Special Program for Diagnosis and Treatment Technology of Clinical Key Diseases in Suzhou (LCZX202001), (2) Gusu Health Talent Project of Suzhou (GSWS2020003), (3) Suzhou Key Laboratory of Health Information Technology (SZS201818).

REFERENCES

1. Siegel RL, Miller KD, Jemal A. Cancer Statistics, 2020. *CA Cancer J Clin* (2020) 70(1):7–30. doi: 10.3322/caac.21590
2. Turkbey B, Rosenkrantz AB, Haider MA, Padhani AR, Villeirs G, Macura KJ, et al. Prostate Imaging Reporting and Data System Version 2.1: 2019 Update of Prostate Imaging Reporting and Data System Version 2. *Eur Urol* (2019) 76 (3):340–51. doi: 10.1016/j.eururo.2019.02.033
3. Wajswol E, Winoker JS, Anastos H, Falagario U, Okhawere K, Martini A, et al. A Cohort of Transperineal Electromagnetically Tracked Magnetic Resonance Imaging/Ultrasonography Fusion-Guided Biopsy: Assessing the Impact of Inter-Reader Variability on Cancer Detection. *BJU Int* (2020) 125 (4):531–40. doi: 10.1111/bju.14957
4. Mottet N, van den Bergh RCN, Briers E, Van den Broeck T, Cumberbatch MG, De Santis M, et al. EAU-EANM-ESTRO-ESUR-SIOG Guidelines on Prostate Cancer-2020 Update. Part 1: Screening, Diagnosis, and Local Treatment With Curative Intent. *Eur Urol* (2021) 79(2):243–62. doi: 10.1016/j.eururo.2020.09.042
5. Hermie I, Van Besien J, De Visschere P, Lumen N, Decaestecker K. Which Clinical and Radiological Characteristics Can Predict Clinically Significant Prostate Cancer in PI-RADS 3 Lesions? A Retrospective Study in a High-Volume Academic Center. *Eur J Radiol* (2019) 114:92–8. doi: 10.1016/j.ejrad.2019.02.031
6. Schoots IG. MRI in Early Prostate Cancer Detection: How to Manage Indeterminate or Equivocal PI-RADS 3 Lesions? *Trans Androl Urol* (2018) 7:70–82. doi: 10.21037/tau.2017.12.31
7. Kan Y, Zhang Q, Hao J, Wang W, Zhuang J, Gao J, et al. Clinico-Radiological Characteristic-Based Machine Learning in Reducing Unnecessary Prostate Biopsies of PI-RADS 3 Lesions With Dual Validation. *Eur Radiol* (2020) 30 (11):6274–84. doi: 10.1007/s00330-020-06958-8
8. Padhani AR, Barentsz J, Villeirs G, Rosenkrantz AB, Margolis DJ, Turkbey B, et al. PI-RADS Steering Committee: The PI-RADS Multiparametric MRI and MRI-Directed Biopsy Pathway. *Radiology* (2019) 292(2):464–74. doi: 10.1148/radiol.2019182946
9. Al Hussein Al Awamlh B, Marks LS, Sonn GA, Natarajan S, Fan RE, Gross MD, et al. Multicenter Analysis of Clinical and MRI Characteristics Associated With Detecting Clinically Significant Prostate Cancer in PI-RADS (V2.0) Category 3 Lesions. *Urol Oncol* (2020) 38(7):637. doi: 10.1016/j.urolonc.2020.03.019
10. Cutaia G, La Tona G, Comelli A, Vernuccio F, Agnello F, Gagliardo C, et al. Radiomics and Prostate MRI: Current Role and Future Applications. *J Imaging* (2021) 7(2):34. doi: 10.3390/jimaging7020034
11. Giambelluca D, Cannella R, Vernuccio F, Comelli A, Pavone A, Salvaggio L, et al. PI-RADS 3 Lesions: Role of Prostate MRI Texture Analysis in the Identification of Prostate Cancer. *Curr Probl Diagn Radiol* (2021) 50(2):175–85. doi: 10.1067/j.cpradiol.2019.10.009
12. Tamada T, Kido A, Yamamoto A, Takeuchi M, Miyaji Y, Moriya T, et al. Comparison of Biparametric and Multiparametric MRI for Clinically Significant Prostate Cancer Detection With PI-RADS Version 2.1. *J Magn Reson Imaging* (2021) 53(1):283–91. doi: 10.1002/jmri.27283
13. Epstein JI, Egevad L, Amin MB, Delahunt B, Srigley JR, Humphrey PA, et al. The 2014 International Society of Urological Pathology (ISUP) Consensus Conference on Gleason Grading of Prostatic Carcinoma: Definition of Grading Patterns and Proposal for a New Grading System. *Am J Surg Pathol* (2016) 40(2):244–52. doi: 10.1097/PAS.0000000000000530
14. Song Y, Zhang J, Zhang YD, Hou Y, Yan X, Wang Y, et al. FeAture Explorer (FAE): A Tool for Developing and Comparing Radiomics Models. *PLoS One* (2020) 15(8):e0237587. doi: 10.1371/journal.pone.0237587
15. Zhang L, Jiang D, Chen C, Yang X, Lei H, Kang Z, et al. Development and Validation of a Multiparametric MRI-Based Radiomics Signature for Distinguishing Between Indolent and Aggressive Prostate Cancer. *Br J Radiol* (2021) 29:20210191. doi: 10.1259/bjr.20210191
16. Ma S, Xie H, Wang H, Yang J, Han C, Wang X, et al. Preoperative Prediction of Extracapsular Extension: Radiomics Signature Based on Magnetic Resonance Imaging to Stage Prostate Cancer. *Mol Imaging Biol* (2020) 22 (3):711–21. doi: 10.1007/s11307-019-01405-7
17. Hou Y, Bao ML, Wu CJ, Zhang J, Zhang YD, Shi HB. A Radiomics Machine Learning-Based Redefining Score Robustly Identifies Clinically Significant Prostate Cancer in Equivocal PI-RADS Score 3 Lesions. *Abdom Radiol (NY)* (2020) 45(12):4223–34. doi: 10.1007/s00261-020-02678-1
18. Hectors SJ, Chen C, Chen J, Wang J, Gordon S, Yu M, et al. Magnetic Resonance Imaging Radiomics-Based Machine Learning Prediction of Clinically Significant Prostate Cancer in Equivocal PI-RADS 3 Lesions. *J Magn Reson Imaging* (2021) 54(5):1466–73. doi: 10.1002/jmri.27692
19. Lim CS, Abreu-Gomez J, Thornhill R, James N, Al Kindi A, Lim AS, et al. Utility of Machine Learning of Apparent Diffusion Coefficient (ADC) and T2-Weighted (T2W) Radiomic Features in PI-RADS Version 2.1 Category 3 Lesions to Predict Prostate Cancer Diagnosis. *Abdom Radiol (NY)* (2021) 46 (12):5647–58. doi: 10.1007/s00261-021-03235-0
20. Calvocoressi L, Uchio E, Ko J, Radhakrishnan K, Aslan M, Concato J. Prostate Cancer Aggressiveness and Age: Impact of P53, BCL-2 and Microvessel Density. *J Investig Med* (2018) 66(8):1142–6. doi: 10.1136/jim-2018-000804
21. Galosi AB, Palagonia E, Scarcella S, Cimadamore A, Lacetera V, Delle Fave RF, et al. Detection Limits of Significant Prostate Cancer Using Multiparametric MR and Digital Rectal Examination in Men With Low Serum PSA: Up-Date of the Italian Society of Integrated Diagnostic in Urology. *Arch Ital Urol Androl* (2021) 93(1):92–100. doi: 10.4081/aiua.2021.1.92
22. Roscigno M, Stabile A, Lughezzani G, Pepe P, Galosi AB, Naselli A, et al. The Use of Multiparametric Magnetic Resonance Imaging for Follow-Up of Patients Included in Active Surveillance Protocol. Can PSA Density Discriminate Patients at Different Risk of Reclassification? *Clin Genitourin Cancer* (2020) 18(6):e698–704. doi: 10.1016/j.clgc.2020.04.006
23. Pagniez MA, Kasivisvanathan V, Puech P, Drumez E, Villers A, Olivier J. Predictive Factors of Missed Clinically Significant Prostate Cancers in Men With Negative Magnetic Resonance Imaging: A Systematic Review and Meta-Analysis. *J Urol* (2020) 204(1):24–32. doi: 10.1097/JU.0000000000000757
24. Sanguedolce F, Falagario UG, Castellan P, Di Nauta M, Silecchia G, Bruno SM, et al. Bioptic Intraprostatic Chronic Inflammation Predicts Adverse Pathology at

Radical Prostatectomy in Patients With Low-Grade Prostate Cancer. *Urol Oncol* (2020) 38(10):793.e19–25. doi: 10.1016/j.urolonc.2020.02.025
25. Yang S, Zhao W, Tan S, Zhang Y, Wei C, Chen T, et al. Combining Clinical and MRI Data to Manage PI-RADS 3 Lesions and Reduce Excessive Biopsy. *Transl Androl Urol* (2020) 9(3):1252–61. doi: 10.21037/tau-19-755
26. Halpern JA, Oromendia C, Shoag JE, Mittal S, Cosiano MF, Ballman KV, et al. Use of Digital Rectal Examination as an Adjunct to Prostate Specific Antigen in the Detection of Clinically Significant Prostate Cancer. *J Urol* (2018) 199 (4):947–53. doi: 10.1016/j.juro.2017.10.021
27. Bonekamp D, Kohl S, Wiesenfarth M, Schelb P, Radtke JP, Götz M, et al. Radiomic Machine Learning for Characterization of Prostate Lesions With MRI: Comparison to ADC Values. *Radiology* (2018) 289(1):128–37. doi: 10.1148/radiol.2018173064
28. Falagario UG, Ratnani P, Lantz A, Jambor I, Dovey Z, Verma A, et al. Staging Accuracy of Multiparametric Magnetic Resonance Imaging in Caucasian and African American Men Undergoing Radical Prostatectomy. *J Urol* (2020) 204 (1):82–90. doi: 10.1097/JU.0000000000000774

Conflict of Interest: The authors declare that the research was conducted in the absence of any commercial or financial relationships that could be construed as a potential conflict of interest.

Publisher's Note: All claims expressed in this article are solely those of the authors and do not necessarily represent those of their affiliated organizations, or those of the publisher, the editors and the reviewers. Any product that may be evaluated in this article, or claim that may be made by its manufacturer, is not guaranteed or endorsed by the publisher.

Copyright © 2022 Jin, Yang, Qiao, Hu, Hu, Wang and Bao. This is an open-access article distributed under the terms of the Creative Commons Attribution License (CC BY). The use, distribution or reproduction in other forums is permitted, provided the original author(s) and the copyright owner(s) are credited and that the original publication in this journal is cited, in accordance with accepted academic practice. No use, distribution or reproduction is permitted which does not comply with these terms.

frontiers in Oncology

MINI REVIEW
published: 31 March 2022
doi: 10.3389/fonc.2022.864723

Harnessing the Utility of *Ex Vivo* Patient Prostate Tissue Slice Cultures

Lillian M. Perez[1,2] *and Larisa Nonn*[1,2*]

[1] University of Illinois at Chicago Pathology Department, Chicago, IL, United States, [2] University of Illinois Cancer Center, Chicago, IL, United States

Patient-derived prostate tissue explant cultures are powerful research tools that offer the potential for personalized medicine. These cultures preserve the local microenvironment of the surrounding stroma but are not without limitations and challenges. There are several methods and processing techniques to culture tissue *ex vivo*, that include explant tissue chunks and precision-cut tissue slices. Precision-cut tissue slices provide a consistent distribution of nutrients and gases to the explant. Herein we summarize the prostate tissue slice method, its limitations and discuss the utility of this model, to investigate prostate biology and therapeutic treatment responses.

Keywords: prostate, *ex vivo* culture, precision medicine, prostate cancer, androgens

OPEN ACCESS

Edited by:
Andrew Goldstein, University of California, Los Angeles, United States

Reviewed by:
Xiuping Yu, Louisiana State University Health Shreveport, United States
Douglas Strand, University of Texas Southwestern Medical Center, United States

***Correspondence:**
Larisa Nonn
lnonn@uic.edu

Specialty section:
This article was submitted to Genitourinary Oncology, a section of the journal Frontiers in Oncology

Received: *28 January 2022*
Accepted: *28 February 2022*
Published: *31 March 2022*

Citation:
Perez LM and Nonn L (2022) Harnessing the Utility of Ex Vivo Patient Prostate Tissue Slice Cultures. Front. Oncol. 12:864723. doi: 10.3389/fonc.2022.864723

INTRODUCTION

Ex vivo tissue culture retains the local microenvironment and is potentially a powerful tool to examine prostate responses to treatment and/or genetic manipulation. This technique is particularly relevant to prostate, which contains several cell types including glandular epithelium, fibromuscular stroma, neuroendocrine cells, and immune cells. The crosstalk between these cell types may influence experimental responses between patients. Several methods for *ex vivo* prostate tissue culture have been reported, which have some similarities, but there is no established gold standard method. Briefly, prostate tissue, benign or cancer, is cultured in media within a culture vessel over the course of 2-5 days. The patient-derived explant (PDE) model typically refers to prostate tissue that is chopped, minced, or sliced with surgical tools whereas tissue slice culture (TS) utilizes a precision slicing method to cut slices into an exact thickness. These methods are also useful for *ex vivo* patient-derived xenografts (PDXs) from mice. This review focuses on the prostate TS method, utilization, challenges and opportunities.

EX VIVO RADICAL PROSTATECTOMY TISSUES CULTURED AS PRECISION CUT SLICES

Precision cut slices from fresh tissues enable consistent diffusion of gases across the tissue and rely on capillary action to bring culture medium into the tissues. Slices were initially developed using liver and kidney for use in pharmacology metabolism studies (1). Parrish et al. were the first to extend this method to other tissues, including prostate (2). The *ex vivo* culture of prostate TSs was further refined to preserve the secretory epithelium and reduce basal cell hyperplasia (3).

Androgen responsiveness is essential for any *ex vivo* model and the Peehl Lab showed that TS respond to androgens and androgen ablation both *ex vivo* and when grafted under the renal capsule of mice (3, 4).

TS relies on precise sectioning of a core of fresh radical prostatectomy tissue using a specialized tissue slicing instrument. The uniform thickness of the slices enables even nutrient and oxygen diffusion through the tissue to avoid necrosis (3). Diseases of the prostate, such as cancer, are often multi-focal and challenging to identify on gross specimens, thus it is essential to collect slices for histological examination. Culture length is variable and has been reported between one day and five days, dependent on endpoints.

TISSUE SLICE CULTURE METHOD

Patient radical prostatectomy specimens or PDXs (5) have been used for prostate TS cultures (**Figure 1**). The detailed method has been reported by others (2, 4, 6, 7). Briefly, a 5 or 10 mm core of fresh tissue is stabilized in agar and mounted in a precision slicer, generating ~300 μm slices, which are quickly placed into culture. The majority of studies utilize titanium mesh inserts to mount slices within 6-well tissue culture plates (3, 6, 8–12). The TS on a titanium mesh rotates on an angle to dip the TS in and out of media, driving capillary action for equivalent distribution of media and exposure to gases. However, earlier tissue cultures have utilized titanium mesh within scintillation vials (2). Alternative to mounting TS on titanium mesh, Blauer et al. demonstrated retention of androgen responsiveness and luminal epithelium by culturing the TS completely submerged (7).

Optimization of primary culture medium can be challenging and TS cultures have been tested in different mediums including KSFM, M199, MCD105, and PFMR, with additives of supplements, serum, and androgens. One of the earliest studies used KSFM on titanium mesh within scintillation vials and varied supplementation with bovine pituitary extract, EGF, DHT, and FBS (10%) (2). They concluded that DHT promotes tissue slice viability, as the medium containing DHT prevented the loss of luminal epithelial cells, and that media containing 10% FBS promotes hyper-proliferation of basal cells. This proliferation of basal cells was also observed by Maund et al., who found low levels of androgen resulted in the basal hyper-proliferation (3). Maund et al. systematically tested many conditions for TS cultures. The first condition contained a mixture of KSFM and M199 [the 1:1 ratio as reported by (7)] with 1 nM DHT and resulted in luminal cell degeneration and basal cell hyperplasia. The second media contained PFMR-4A with 10 nM R1881 and resulted in less cell loss and viability for up to two days, after-which tissue slices exhibited luminal cell degeneration and basal cell hyperplasia. The third media contained PFMR-4A with 50 nM R1881 and resulted in the most cell viability at two days, with histology, proliferation, and apoptosis that was most similar to day zero TS. In summary, assessment of viability, toxicity, proliferation, and apoptosis resulted with the media composition containing PFMR-4A and 50 nM R1881 being optimal for TS culture media and concentration of testosterone (3). However, PFMR-4A is not commercially available and others have found success using PrEGM supplemented with 50 nM R1881 (12) or serum-free aDMEM/F12 K medium with R1881 (13).

TS from patient derived xenograft models (PDX-TS), has been used in several studies. Zhang et al. did a systematic analysis on PDX-TS culture method and the effects of media composition (13). They used 3 PDX-TS and found that rocking on a cell strainer (very similar to titanium grids rotating) in serum-free aDMEM/F12 K medium with R1881 was optimal to preserve proliferation and prevent apoptosis. Proof of concept studies in PDX-TS have developed a method to examine many tissues at once in 96-well format by a method they call micro-dissected tissue (MDT) (14, 15). MDT are 500 μm in diameter, compared to normal TS which are 3-5 mm, thus MDT permits more precise tissue acquisition and potentially many more experimental endpoints. Dorrigiv et al. optimized this by using cell line xenografts as the tissue source (15). They also developed a method to create an FFPE microarray from the MDT

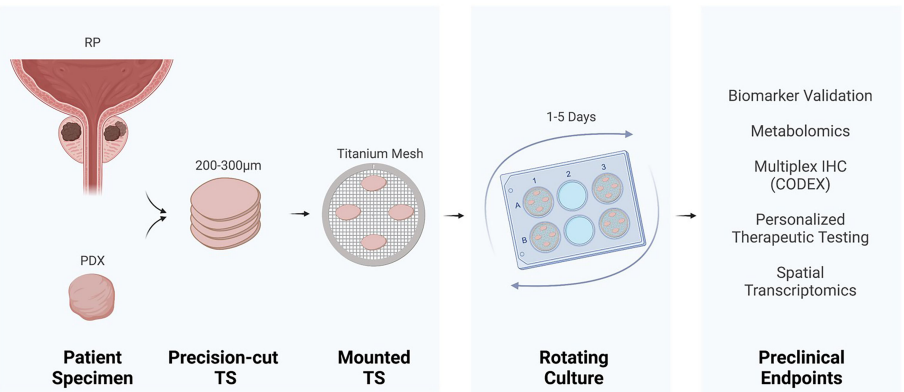

FIGURE 1 | Tissue slice culture workflow and preclinical endpoints. Precision cut tissue slices (TS) derived from radical prostatectomy (RP) or a patient-derived xenograft (PDX) incubate on titanium mesh grids at a 45° angle within a rotating tissue culture plate.

(MDTMA) (14). The small MDT appeared to be free of the challenges with larger tissue pieces and preserved cell morphology, viability, and proliferation throughout 15 days of culture.

INVESTIGATION OF PROSTATE BIOLOGICAL RESPONSES USING TISSUE SLICE CULTURES

TS cultures have been utilized to target key developmental signaling pathways and validate prior findings from *in vitro* studies in human prostate. TS retain expression of the hormone receptors and are shown to be responsive to the hormones vitamin D (12, 16) and androgen (2, 3, 7, 9, 13, 16, 17). McCray et al. analyzed TSs treated with 25-hydroxyvitamin D and analyzed epithelial and stromal gene expression *via* spatial transcriptomics (12). Among a panel of genes, the Wnt pathway and DKK3 were identified as downregulated by 25-hydroxyvitamin D. In another study, TS responded to both 25-hydroxyvitamin D and testosterone in regulation of target genes (16). The TS also retained expression of the endocytic membrane receptor, megalin, which imports hormones into the cells (16). Importantly, in both vitamin D studies, the TS data corroborated evidence from patient-derived organoids and relationships in patient specimens, demonstrating consistency and reproducibility between models to investigate developmental pathways *ex vivo*.

Several studies have utilized TS cultures to investigate DNA damage responses. DNA damage response of benign radical prostatectomy-derived TS was monitored following ionizing radiation (IR) (6). They found that IR did not elicit Tyr (15) and p53 responses in TS and they suggest that absence of these DNA damage response pathways may contribute to carcinogenesis (6).

TS AND BIOMARKER DISCOVERY

TS from prostate cancer (PCa) are suited for biomarker discovery since the amount of tissue of each pathology can be controlled; matched benign/PCa tissues are available from each patient, and specimens from multiple patients can be used to account for inter-patient heterogeneity. Spichiarich et al. identified glycoproteins, specifically sialylated glycans, associated with PCa using bio-orthogonal labeling (10). They used paired benign and PCa TS from eight different patients and identified 21 proteins unique to all PCa samples and undetected in the benign tissue, including VDAC1 and the sialoglycoprotein, legumain. The unique metabolic state of PCa compared to benign tissue is preserved in TS and a source for biomarkers. The Kurhanewicz group used intracellular labeling of [$^{3\text{-}13}$C] pyruvate in TS (7 benign and 4 PCa) to identify hyperpolarized ^{13}C lactate as a PCa biomarker (8). They further examined lactate by TS of various Gleason Grade and showed that high-grade PCa (N=4) has higher lactate than low grade (N=11) or benign tissue (N=15) (11).

THERAPEUTIC RESPONSES IN *EX VIVO* PDE AND TS

Research advancements in anti-androgen therapies, alternative therapeutics for CRPC models, and other experimental therapeutics have been made with *ex vivo* TS or PDEs (**Table 1**). PDE cultures of tissue chunks have been used more frequently than TS for these studies. Although there are limited reports that use TS to measure treatment outcomes, these reports have demonstrated responses that may inform treatments in the clinic. PDEs are described as the *ex vivo* culture of prostate tissue as small pieces on sponges with conditions that promote or maintain tumor microenvironment and tissue architecture. *Ex vivo* PCa tumor cultures have demonstrated the tumor microenvironment remains intact using established methods (21). Both low and high tumor grades (Gleason 3-5) have been cultured successfully and remain viable for up to five days (3, 8, 10, 11). The methodology for PDE cultures and the promise of their preclinical utility has been previously reviewed by others (20, 28, 29) and is only briefly discussed here.

TS and PDEs are highly responsive to androgens and have been used to examine several anti-androgen therapies. Zhao et al. revealed that the castration response of TS grafted into mice mimicked the expression of proteins in prostate specimens from patients with androgen deprivation therapies (9). The patient heterogeneity of anti-proliferation responses to bicalutamide and enzalutamide was demonstrated in PDE (17, 18). Butler et al. further showed tumor areas resistant to enzalutamide also had aberrations in their lipid profiles (18), which lead to discovery of ELOVL5, a fatty acid elongase, as a new metabolic target of androgens (24). The potential to predict patient response to combination therapy with enzalutamide and docetaxel was shown in PDE, reflecting individual treatment outcomes observed in the clinic (21). Shafi et al. also identified heterogeneous responses to experimental therapeutics, including veliparib, palbociclib, and NU7441 (21), emphasizing that patient-specific responses may be tested in PDEs. The antiandrogen therapy, apalutamide, was shown to radiosensitize PDX-TS PCa demonstrating a possible therapeutic treatment for AR-dependent PCa (19). Explants are also useful for studying resident immune cells and PDEs were recently used to show an increase in CD163+/CD68+ macrophages after enzalutamide (23).

PDEs from PDXs have been used to test therapeutics. Galiellalactone, a STAT3 inhibitor, reduced AR activity in PDEs of thin tissue pieces (cut by a razor blade) (27). Bray et al. showed in 5 human prostatectomy-derived tumors that combination treatment with BCL-2 inhibitor, ABT-737, and cisplatin yielded a synergistic therapeutic response more than either treatment alone using *ex vivo* PCa TS (200 μm) (25). PDEs from PDX of CRPC demonstrated sensitivity of CRPC to BRET inhibitors (22), and PARP inhibitors (26). Zhang at al. used PDXs from 3 patients for TS cultures and observed the expected

TABLE 1 | Therapeutics tested in *ex vivo* prostate cultures.

Target	Therapeutic	*Ex Vivo* Model	Reference
ACC1/2	PF-05175157 (10 μM, 25 μM, 50 μM)	PDE	Butler et al., 2021 (18)
AR	Apalutamide (1 μM) + EBRT (2Gy)	PDX (TS, 300 μm)	Zhang et al., 2019a (19)
	Bicalutamide (10 μM)	PDE	Centenera et al., 2013 (20)
	Castration	TS grafts, 300 μm	Zhao et al, 2013 (9)
	Enzalutamide (1 μM)	PDE	Shafi et al., 2018 (21)
	Enzalutamide (1 μM)	PDX (TS, 300 μm)	Zhang et al., 2019b (13)
	Enzalutamide (1 μM) + Docetaxel (50 nM)	PDE	Shafi et al., 2018 (21)
	Enzalutamide (10 μM, 50 μM)	PDE	Butler et al., 2021 (18)
	Enzalutamide (10 μM)	CRPC-PDX (PDE)	Lawrence et al., 2018 (22)
	Enzalutamide (10 μM)	PDE	Boibessot et al., 2021 (23)
	Enzalutamide (10 μM)	PDE	Centenera et al., 2013 (20)
	Enzalutamide (10 μM)	PDE	Centenera et al., 2021 (24)
	Galeterone (10 μM)	CRPC-PDX (PDE)	Lawrence et al., 2018 (22)
BCL-2	Cisplatin + ABT-737 (10 μM)	TS, 200 μm	Bray et al., 2009 (25)
BRET	iBET151 (1 μM) and JQ1 (1 μM)	CRPC-PDX (PDE)	Lawrence et al., 2018 (22)
CDK4 and CDK6	Palbociclib (1 μM)	PDE	Shafi et al., 2018 (21)
	Ribociclib (1 μM)	CRPC-PDX (PDE)	Lawrence et al., 2018 (22)
DNAPK	NU7441 (1 μM)	PDE	Shafi et al., 2018 (21)
HSP90	NVP-AUY922 (100-1000 nM)	PDE	Centenera et al., 2013 (20)
	NVP-HSP990 (100-1000 nM)	PDE	Centenera et al., 2013 (20)
pan-PIM	CX-6258 (5 μM)	CRPC-PDX (PDE)	Lawrence et al., 2018 (22)
PARP	Talazoparib (1 μM)	CRPC-PDX (PDE)	Lawrence et al., 2018 (22)
	ABT888 (2.5 μM)	PDE	Schiewer et al., 2012 (26)
	Olaparib (10 μM)	PDX (TS, 300 μm)	Zhang et al., 2019 (19)
	Veliparib (2.5 μM)	PDE	Shafi et al., 2018 (21)
RNA polymerase I	CX-5461 (1 μM)	CRPC-PDX (PDE)	Lawrence et al., 2018 (22)
STAT3	Galiellalactone (5 μM)	PDE	Handle et al., 2018 (27)

TS, tissue slice culture; EBRT, external beam radiation therapy; PDX, patient-derived xenograft; PDE, patientderived explant; CRPC, castration resistance prostate cancer.

responses to enzalutamide and olaparib, based on the AR expression and BRCA2 mutations, respectively (13).

LIMITATIONS AND CHALLENGES OF PROSTATE TS AND *EX VIVO* CULTURES

There are challenges that are common between all *ex vivo* culture methods and those unique to TS. The primary challenge to *ex vivo* cultures for TS (or PDEs) is rapid accessibility to fresh surgical specimens. This requires close collaboration and cooperation between research and clinical staff as well as pre-surgical consent of the patient to utilize excess tissue not needed for diagnosis. The size of the specimen further limits the amount of TS or PDE that can be made from it. These challenges contribute to the rarity of *ex vivo* CRPC cultures and underscore the importance of PDX-CRPC. To date, neuroendocrine prostate cancer (NEPC) has yet to be reported for TS studies, likely owing to limited access. Identification of cancer areas on gross radical prostatectomy specimens is a challenge. Furthermore, fresh tissue pieces are never one cell type. Benign areas will contain varied amounts of glandular epithelium and stroma. PCa often presents multi-focal lesions that are not fully encapsulated in a sample. Thus, samples for *ex vivo* culture may contain mixed pathologies that will bias endpoints that homogenize the entire piece of tissue. The TS method preserves histological features and allows for spatial examination of endpoints such as immunohistochemistry, *in situ* hybridization, ISH or spatial transcriptomics. The method of MDT (described above) (14) and pathology guided micropunching (PGM) (30) sample smaller areas (260-500 μM), reducing heterogeneity of the specimens, but also provide limited tissue for endpoint analyses. The relatively short length of culture for androgen adaptation studies is a limitation to both PDEs and TS. However, several studies grafted TS under in the renal capsule of nude mice, rather than *in vitro* culture, and were able to predict androgen sensitivity (4, 9). Finally, while TS are optimal for assessing therapeutic responses, overexpression and knockdown tools needed for mechanistic studies need to be carefully optimized to penetrate into explant tissue cultures. This includes delivery of siRNAs, as reported in localized PCa PDE cultures by Tieu et al. (31).

TS have several additional limitations. The main one is that specialized equipment is required to prepare and culture the precision slices. Secondly, as PCa tumors are small, the pathology of the specimen often drifts through the slices, requiring additional collection of slices for pathology if the endpoint doesn't facilitate visualization of the histology. Lastly, preparing frozen or FFPE sections from the TS is challenging and requires a trained technician to obtain high quality sections from a TS that is only about 200 μM thick after fixation.

OPPORTUNITIES FOR PROSTATE TS *EX VIVO* CULTURE

Despite the challenges, TS cultures provide spatial examination of inter and intra-patient heterogeneity not possible by other

methods. The rapid advancement and increased resolution of spatial transcriptomic methods (32, 33) offers the ability to compare transcriptomic differences (RNAseq) between areas of the tissue and between patients. Co-detection by indexing (CODEX) tissue imaging with DNA-barcoded antibodies has the potential to examine up to 60 markers in one sample (34), which would greatly expand the data available from a TS experiment. Localized prostate tumors are often under hypoxia and Figiel at al recently showed that localized PCa TS respond to hypoxic culture conditions (35), which support use of TS in therapeutic response studies.

In summary, although *ex vivo* culture of prostate TS was first described two decades ago, it remains an emerging model that holds promise for both research questions and for precision medicine. TS are primed and amenable to recent technologic breakthroughs in single cell sequencing and spatial data collection.

AUTHOR CONTRIBUTIONS

LMP and LN jointly wrote and edited this manuscript. All authors contributed to the article and approved the submitted version.

FUNDING

This work was supported by Department of Defense Prostate Cancer Research Program Cancer Health Disparities Grant PC190699 (LN) and University of Illinois Cancer Center Cancer Biology Training Program Pilot Funding (LP).

ACKNOWLEDGMENTS

Figure 1 was created with Biorender.com.

REFERENCES

1. Parrish AR, Gandolfi AJ, Brendel K. Precision-Cut Tissue Slices: Applications in Pharmacology and Toxicology. *Life Sci* (1995) 57:1887–901. doi: 10.1016/0024-3205(95)02176-j
2. Parrish AR, Sallam K, Nyman DW, Orozco J, Cress AE, Dalkin BL, et al. Culturing Precision-Cut Human Prostate Slices as an *In Vitro* Model of Prostate Pathobiology. *Cell Biol Toxicol* (2002) 18:205–19. doi: 10.1023/a:1015567805460
3. Maund SL, Nolley R, Peehl DM. Optimization and Comprehensive Characterization of a Faithful Tissue Culture Model of the Benign and Malignant Human Prostate. *Lab Invest* (2014) 94:208–21. doi: 10.1038/labinvest.2013.141
4. Zhao H, Nolley R, Chen Z, Peehl DM. Tissue Slice Grafts: An *In Vivo* Model of Human Prostate Androgen Signaling. *Am J Pathol* (2010) 177:229–39. doi: 10.2353/ajpath.2010.090821
5. Kocher S, Beyer B, Lange T, Nordquist L, Volquardsen J, Burdak-Rothkamm S, et al. A Functional *Ex Vivo* Assay to Detect PARP1-EJ Repair and Radiosensitization by PARP-Inhibitor in Prostate Cancer. *Int J Cancer* (2019) 144:1685–96. doi: 10.1002/ijc.32018
6. Kiviharju-af Hallstrom TM, Jaamaa S, Monkkonen M, Peltonen K, Andersson LC, Medema RH, et al. Human Prostate Epithelium Lacks Wee1A-Mediated DNA Damage-Induced Checkpoint Enforcement. *Proc Natl Acad Sci USA* (2007) 104:7211–6. doi: 10.1073/pnas.0609299104
7. Blauer M, Tammela TL, Ylikomi T. A Novel Tissue-Slice Culture Model for non-Malignant Human Prostate. *Cell Tissue Res* (2008) 332:489–98. doi: 10.1007/s00441-008-0602-z
8. Keshari KR, Sriram R, Van Criekinge M, Wilson DM, Wang ZJ, Vigneron DB, et al. Metabolic Reprogramming and Validation of Hyperpolarized 13C Lactate as a Prostate Cancer Biomarker Using a Human Prostate Tissue Slice Culture Bioreactor. *Prostate* (2013) 73:1171–81. doi: 10.1002/pros.22665
9. Zhao H, Thong A, Nolley R, Reese SW, Santos J, Ingels A, et al. Patient-Derived Tissue Slice Grafts Accurately Depict Response of High-Risk Primary Prostate Cancer to Androgen Deprivation Therapy. *J Transl Med* (2013) 11:199. doi: 10.1186/1479-5876-11-199
10. Spiciarich DR, Nolley R, Maund SL, Purcell SC, Herschel J, Iavarone AT, et al. Bioorthogonal Labeling of Human Prostate Cancer Tissue Slice Cultures for Glycoproteomics. *Angew Chem Int Ed Engl* (2017) 56:8992–7. doi: 10.1002/anie.201701424
11. Sriram R, Van Criekinge M, DeLos Santos J, Ahamed F, Qin H, Nolley R, et al. Elevated Tumor Lactate and Efflux in High-Grade Prostate Cancer Demonstrated by Hyperpolarized (13)C Magnetic Resonance Spectroscopy of Prostate Tissue Slice Cultures. *Cancers (Basel)* (2020) 12. doi: 10.3390/cancers12030537
12. McCray T, Pacheco JV, Loitz CC, Garcia J, Baumann B, Schlicht MJ, et al. Vitamin D Sufficiency Enhances Differentiation of Patient-Derived Prostate Epithelial Organoids. *iScience* (2021) 24:101974. doi: 10.1016/j.isci.2020.101974
13. Zhang W, van Weerden WM, de Ridder CMA, Erkens-Schulze S, Schonfeld E, Meijer TG, et al. *Ex Vivo* Treatment of Prostate Tumor Tissue Recapitulates *In Vivo* Therapy Response. *Prostate* (2019) 79:390–402. doi: 10.1002/pros.23745
14. Simeone K, Guay-Lord R, Lateef MA, Peant B, Kendall-Dupont J, Orimoto AM, et al. Paraffin-Embedding Lithography and Micro-Dissected Tissue Micro-Arrays: Tools for Biological and Pharmacological Analysis of *Ex Vivo* Solid Tumors. *Lab Chip* (2019) 19:693–705. doi: 10.1039/c8lc00982a
15. Dorrigiv D, Simeone K, Communal L, Kendall-Dupont J, St-Georges-Robillard A, Peant B, et al. Microdissected Tissue vs Tissue Slices-a Comparative Study of Tumor Explant Models Cultured On-Chip and Off-Chip. *Cancers (Basel)* (2021) 13. doi: 10.3390/cancers13164208
16. Garcia J, Krieger KD, Loitz C, Perez L, Richards ZA, Helou Y, et al. Vitamin D Deficiency Increases Prostatic Megalin Expression and Globulin-Bound Testosterone Import, Increasing Prostatic Androgens in African American Men. *bioRxiv* (2021) 2011:2009:467567. doi: 10.1101/2021.11.09.467567
17. Centenera MM, Hickey TE, Jindal S, Ryan NK, Ravindranathan P, Mohammed H, et al. A Patient-Derived Explant (PDE) Model of Hormone-Dependent Cancer. *Mol Oncol* (2018) 12:1608–22. doi: 10.1002/1878-0261.12354
18. Butler LM, Mah CY, Machiels J, Vincent AD, Irani S, Mutuku SM, et al. Lipidomic Profiling of Clinical Prostate Cancer Reveals Targetable Alterations in Membrane Lipid Composition. *Cancer Res* (2021) 81:4981–93. doi: 10.1158/0008-5472.CAN-20-3863
19. Zhang W, Liao CY, Chtatou H, Incrocci L, van Gent DC, van Weerden WM, et al. Apalutamide Sensitizes Prostate Cancer to Ionizing Radiation *via* Inhibition of non-Homologous End-Joining DNA Repair. *Cancers (Basel)* (2019) 11. doi: 10.3390/cancers11101593
20. Centenera MM, Raj GV, Knudsen KE, Tilley WD, Butler LM. *Ex Vivo* Culture of Human Prostate Tissue and Drug Development. *Nat Rev Urol* (2013) 10:483–7. doi: 10.1038/nrurol.2013.126
21. Shafi AA, Schiewer MJ, de Leeuw R, Dylgjeri E, McCue PA, Shah N, et al. Patient-Derived Models Reveal Impact of the Tumor Microenvironment on Therapeutic Response. *Eur Urol Oncol* (2018) 1:325–37. doi: 10.1016/j.euo.2018.04.019
22. Lawrence MG, Obinata D, Sandhu S, Selth LA, Wong SQ, Porter LH, et al. Patient-Derived Models of Abiraterone- and Enzalutamide-Resistant Prostate Cancer Reveal Sensitivity to Ribosome-Directed Therapy. *Eur Urol* (2018) 74:562–72. doi: 10.1016/j.eururo.2018.06.020
23. Boibessot C, Joncas FH, Park A, Berrehail Z, Pelletier JF, Gris T, et al. Using *Ex Vivo* Culture to Assess Dynamic Phenotype Changes in Human Prostate Macrophages Following Exposure to Therapeutic Drugs. *Sci Rep* (2021) 11:19299. doi: 10.1038/s41598-021-98903-y
24. Centenera MM, Scott JS, Machiels J, Nassar ZD, Miller DC, Zinonos I, et al. ELOVL5 is a Critical and Targetable Fatty Acid Elongase in Prostate Cancer. *Cancer Res* (2021) 81:1704–18. doi: 10.1158/0008-5472.CAN-20-2511
25. Bray K, Chen HY, Karp CM, May M, Ganesan S, Karantza-Wadsworth V, et al. Bcl-2 Modulation to Activate Apoptosis in Prostate Cancer. *Mol Cancer Res* (2009) 7:1487–96. doi: 10.1158/1541-7786.MCR-09-0166

26. Schiewer MJ, Goodwin JF, Han S, Brenner JC, Augello MA, Dean JL, et al. Dual Roles of PARP-1 Promote Cancer Growth and Progression. *Cancer Discov* (2012) 2:1134–49. doi: 10.1158/2159-8290.CD-12-0120
27. Handle F, Puhr M, Schaefer G, Lorito N, Hoefer J, Gruber M, et al. The STAT3 Inhibitor Galiellalactone Reduces IL6-Mediated AR Activity in Benign and Malignant Prostate Models. *Mol Cancer Ther* (2018) 17:2722–31. doi: 10.1158/1535-7163.MCT-18-0508
28. Templeton AR, Jeffery PL, Thomas PB, Perera MPJ, Ng G, Calabrese AR, et al. Patient-Derived Explants as a Precision Medicine Patient-Proximal Testing Platform Informing Cancer Management. *Front Oncol* (2021) 11:767697. doi: 10.3389/fonc.2021.767697
29. van de Merbel AF, van der Horst G, van der Pluijm G. Patient-Derived Tumour Models for Personalized Therapeutics in Urological Cancers. *Nat Rev Urol* (2021) 18:33–45. doi: 10.1038/s41585-020-00389-2
30. Johnson BP, Vitek RA, Geiger PG, Huang W, Jarrard DF, Lang JM, et al. Vital *Ex Vivo* Tissue Labeling and Pathology-Guided Micropunching to Characterize Cellular Heterogeneity in the Tissue Microenvironment. *Biotechniques* (2018) 64:13–9. doi: 10.2144/000114626
31. Tieu T, Irani S, Bremert KL, Ryan NK, Wojnilowicz M, Helm M, et al. Patient-Derived Prostate Cancer Explants: A Clinically Relevant Model to Assess Sirna-Based Nanomedicines. *Adv Healthc Mater* (2021) 10:e2001594. doi: 10.1002/adhm.202001594
32. Brady L, Kriner M, Coleman I, Morrissey C, Roudier M, True LD, et al. Inter- and Intra-Tumor Heterogeneity of Metastatic Prostate Cancer Determined by Digital Spatial Gene Expression Profiling. *Nat Commun* (2021) 12:1426. doi: 10.1038/s41467-021-21615-4
33. Pachynski RK, Kim EH, Miheecheva N, Kotlov N, Ramachandran A, Postovalova E, et al. Single-Cell Spatial Proteomic Revelations on the Multiparametric MRI Heterogeneity of Clinically Significant Prostate Cancer. *Clin Cancer Res* (2021) 27:3478–90. doi: 10.1158/1078-0432.CCR-20-4217
34. Black S, Phillips D, Hickey JW, Kennedy-Darling J, Venkataraaman VG, Samusik N, et al. CODEX Multiplexed Tissue Imaging With DNA-Conjugated Antibodies. *Nat Protoc* (2021) 16:3802–35. doi: 10.1038/s41596-021-00556-8
35. Figiel S, Pasqualin C, Bery F, Maupoil V, Vandier C, Potier-Cartereau M, et al. Functional Organotypic Cultures of Prostate Tissues: A Relevant Preclinical Model That Preserves Hypoxia Sensitivity and Calcium Signaling. *Am J Pathol* (2019) 189:1268–75. doi: 10.1016/j.ajpath.2019.02.017

Conflict of Interest: The authors declare that the research was conducted in the absence of any commercial or financial relationships that could be construed as a potential conflict of interest.

Publisher's Note: All claims expressed in this article are solely those of the authors and do not necessarily represent those of their affiliated organizations, or those of the publisher, the editors and the reviewers. Any product that may be evaluated in this article, or claim that may be made by its manufacturer, is not guaranteed or endorsed by the publisher.

Copyright © 2022 Perez and Nonn. This is an open-access article distributed under the terms of the Creative Commons Attribution License (CC BY). The use, distribution or reproduction in other forums is permitted, provided the original author(s) and the copyright owner(s) are credited and that the original publication in this journal is cited, in accordance with accepted academic practice. No use, distribution or reproduction is permitted which does not comply with these terms.

frontiers | Frontiers in Oncology

ORIGINAL RESEARCH
published: 07 April 2022
doi: 10.3389/fonc.2022.785684

Machine Learning-Based Prediction of Pathological Upgrade From Combined Transperineal Systematic and MRI-Targeted Prostate Biopsy to Final Pathology: A Multicenter Retrospective Study

Junlong Zhuang[1,2†], Yansheng Kan[1†], Yuwen Wang[1,2,3†], Alessandro Marquis[4], Xuefeng Qiu[1,2], Marco Oderda[4], Haifeng Huang[1,2], Marco Gatti[5], Fan Zhang[1,2], Paolo Gontero[4], Linfeng Xu[1,2], Giorgio Calleris[4], Yao Fu[6], Bing Zhang[7], Giancarlo Marra[4,8] and Hongqian Guo[1,2*]*

[1] Department of Urology, Affiliated Drum Tower Hospital, Medical School of Nanjing University, Nanjing, China, [2] Institute of Urology, Nanjing University, Nanjing, China, [3] Medical School of Southeast University, Nanjing Drum Tower Hospital, Nanjing, China, [4] Department of Urology, San Giovanni Battista Hospital, Città della Salute e della Scienza and University of Turin, Turin, Italy, [5] Department of Radiology, San Giovanni Battista Hospital, Città della Salute e della Scienza and University of Turin, Turin, Italy, [6] Department of Pathology, Affiliated Drum Tower Hospital, Medical School of Nanjing University, Nanjing, China, [7] Department of Radiology, Affiliated Drum Tower Hospital, Medical School of Nanjing University, Nanjing, China, [8] Department of Urology and Clinical Research Group on Predictive Onco-Urology, APHP, Sorbonne University, Paris, France

Objective: This study aimed to evaluate the pathological concordance from combined systematic and MRI-targeted prostate biopsy to final pathology and to verify the effectiveness of a machine learning-based model with targeted biopsy (TB) features in predicting pathological upgrade.

Materials and Methods: All patients in this study underwent prostate multiparametric MRI (mpMRI), transperineal systematic plus transperineal targeted prostate biopsy under local anesthesia, and robot-assisted laparoscopic radical prostatectomy (RARP) for prostate cancer (PCa) sequentially from October 2016 to February 2020 in two referral centers. For cores with cancer, grade group (GG) and Gleason score were determined by using the 2014 International Society of Urological Pathology (ISUP) guidelines. Four supervised machine learning methods were employed, including two base classifiers and two ensemble learning-based classifiers. In all classifiers, the training set was 395 of 565 (70%) patients, and the test set was the remaining 170 patients. The prediction performance of each model was evaluated by area under the receiver operating characteristic curve (AUC). The Gini index was used to evaluate the importance of all features and to figure out the most contributed features. A nomogram was established to visually predict the risk of upgrading. Predicted probability was a prevalence rate calculated by a proposed nomogram.

OPEN ACCESS

Edited by:
Antonina Mitrofanova, Rutgers, The State University of New Jersey, United States

Reviewed by:
Ning Li, Fourth Affiliated Hospital of China Medical University, China
Pietro Pepe, Cannizzaro Hospital, Italy
Jose Eduardo Tavora, Faculdade de Ciências Médicas de Minas Gerais (FCMMG), Brazil

***Correspondence:**
Giancarlo Marra
drgiancarlomarra@gmail.com
Hongqian Guo
dr.ghq@nju.edu.cn

†These authors have contributed equally to this work

Specialty section:
This article was submitted to Genitourinary Oncology, a section of the journal Frontiers in Oncology

Received: *29 September 2021*
Accepted: *01 March 2022*
Published: *07 April 2022*

Citation:
Zhuang J, Kan Y, Wang Y, Marquis A, Qiu X, Oderda M, Huang H, Gatti M, Zhang F, Gontero P, Xu L, Calleris G, Fu Y, Zhang B, Marra G and Guo H (2022) Machine Learning-Based Prediction of Pathological Upgrade From Combined Transperineal Systematic and MRI-Targeted Prostate Biopsy to Final Pathology: A Multicenter Retrospective Study. Front. Oncol. 12:785684. doi: 10.3389/fonc.2022.785684

Results: A total of 515 patients were included in our cohort. The combined biopsy had a better concordance of postoperative histopathology than a systematic biopsy (SB) only (48.15% vs. 40.19%, $p = 0.012$). The combined biopsy could significantly reduce the upgrading rate of postoperative pathology, in comparison to SB only (23.30% vs. 39.61%, $p < 0.0001$) or TB only (23.30% vs. 40.19%, $p < 0.0001$). The most common pathological upgrade occurred in ISUP GG1 and GG2, accounting for 53.28% and 20.42%, respectively. All machine learning methods had satisfactory predictive efficacy. The overall accuracy was 0.703, 0.768, 0.794, and 0.761 for logistic regression, random forest, eXtreme Gradient Boosting, and support vector machine, respectively. TB-related features were among the most contributed features of a prediction model for upgrade prediction.

Conclusion: The combined effect of SB plus TB led to a better pathological concordance rate and less upgrading from biopsy to RP. Machine learning models with features of TB to predict PCa GG upgrading have a satisfactory predictive efficacy.

Keywords: prostate cancer, biopsy, upgrade, prostatectomy, prediction, machine learning

INTRODUCTION

Biopsy-derived tumor grade is currently used for risk stratification and clinical decision-making of prostate cancer (PCa) (1). However, up to 36% of patients with low-grade biopsy upgrade after radical prostatectomy (RP) (2, 3), leading to the potential risk of underestimation and following undertreatment. The risk of the pathological upgrade has been historically predicted using multivariable tools based on clinical parameters (4–6).

In recent years, multiparametric MRI (mpMRI) and mpMRI-targeted biopsy (mpMRI-TB) have been shown to improve the detection of clinically significant PCa (csPCa) (7, 8). Currently, the guideline recommends mpMRI before biopsy and mpMRI-TB combined with 12-core systematic biopsy (SB) for patients with positive mpMRI results (2021). Several models have been developed to predict pathological upgrading using final pathology as the reference (9). A significant added value of mpMRI and mpMRI-TB to the clinical parameters in predicting the risk of upgrading as well as reducing the number of unnecessary repeat prostate biopsies has been previously investigated (9, 10).

Machine learning techniques have been increasingly used in the medical field due to their high accuracy. Compared to the traditional predictive models, machine learning-based models can incorporate a larger number of variables (11). Liu et al. developed a risk model to predict upgrading from biopsy to RP using learning machine-assisted decision-support models (12). However, this tool was developed in patients undergoing transrectal ultrasound (TRUS)-guided SB, with big concerns about its applicability in the era of mpMRI and mpMRI-TB.

Therefore, based on a previous multicenter prospective cohort study of mpMRI-TB (13, 14), we aimed to develop a machine learning-based model for the identification of patients at high risk of upgrading from combined SB and mpMRI-TB to RP.

MATERIAL AND METHODS

Study Design

The institutional review board of two hospitals approved this retrospective study from a prospective cohort of mpMRI fusion-targeted biopsies (14) and waived the requirement for informed consent. All patients in this study underwent prostate mpMRI and transperineal systematic plus targeted prostate biopsy under local anesthesia sequentially from October 2016 to February 2020 in Drum Tower Hospital and Molinette Hospital, as previously described (13, 14). Those who were diagnosed with PCa and subsequently treated with robot-assisted laparoscopic RP (RARP) were included. More details about the criteria are shown in **Figure 1**.

Multiparametric MRI Technique

All patients underwent mpMRI performed with a 1.5- or 3-Tesla system (details shown in **Supplementary Table 1**) (15, 16). Two radiologists with over 10-year experience in urology image analyses supervised the results using the Prostate Imaging-Reporting and Data System (PI-RADS) v2 standards (17). All radiologists had at least 1,000 prostate MRI images of reading experience. The protocol consisted of T2-weighted (T2W) imaging in three planes, diffusion-weighted imaging (DWI) with the calculation of apparent diffusion coefficient (ADC) maps, high b-value images ($b > 1{,}500$ s/mm^2), and dynamic contrast-enhanced imaging (18). In case there was disagreement over the outcome of the image, the radiologists would discuss it until they reached a consensus.

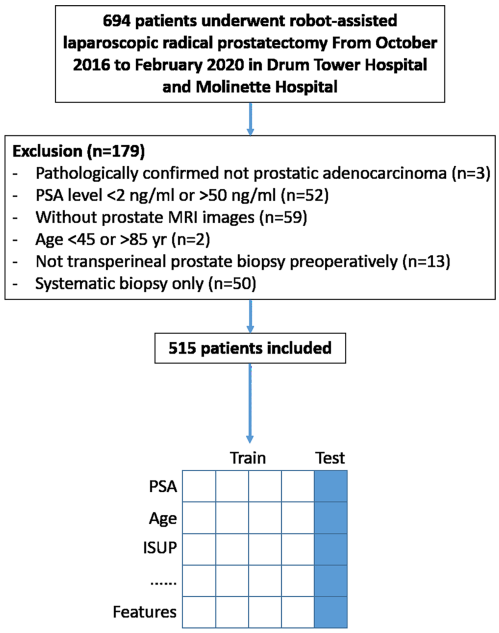

FIGURE 1 | Study flowchart. Data from four out of five included patients were trained for prediction model building and the rest for model validation.

Biopsy

Biopsy targets were defined as regions of interest (ROIs), which were lesions with PI-RADS score ≥ 3. Before the biopsy, operators annotated targets using an ultrasound system (Esaote Real Time Virtual Sonography, Hitachi Medical Corporation, Tokyo, Japan) with reference to the reports from the two radiologists. All patients underwent transperineal MRI–ultrasonography (MRI-US) fusion biopsy (18G needles with sampling length 17 mm) with a US diagnostic system (MyLab Twice, Esaote S.p.A., Genoa, Italy) consisting of 12-core SB and 2- to 4-core targeted biopsies for each ROI under local anesthesia, as previously described (13, 14).

Histopathology

Histopathology of prostate biopsies was performed by specialized urological pathologists independent of MRI results. For cores with cancer, grade group (GG) and Gleason score (GS) were determined by using the 2014 International Society of Urological Pathology (ISUP) guidelines (19). csPCa was defined as different criteria according to MRI-FIRST study (csPCa-1, ISUP GG 2 or higher tumors; csPCa-2, ISUP GG 3 or higher tumors) (20).

Data Collection

Retrospective collection of urology, radiology, and histopathology data for all patients included the following clinical characteristics: histopathology result of biopsy and RP, age, height, weight, body mass index (BMI), pre-biopsy serum prostate-specific antigen (PSA) value (ng/ml), prostate volume, the maximum diameter of lesion, gap days between biopsy and RP, number of cores, and PI-RADS. The length of the prostate on anterior–posterior (AP), head–foot (HF), and right–left (RL) directions were also calculated on T2W mpMRI images.

Data Visualization and Machine Learning Classifiers

"Upgrade" was defined as ISUP in RP pathology higher than ISUP in biopsy pathology, while "downgrade" was defined as ISUP in RP pathology lower than ISUP in biopsy pathology. These data were visualized under different biopsy situations including SB only, TB only, and SB combined with TB. At the same time, the upgrading and downgrading of different ISUP scores were also visualized. All the visualizations were conducted in Python v3.6.5 (Python Software Foundation) along with the machine learning classifiers with 10-fold cross-validation.

The machine learning algorithms were written using the Python SciKit-learn library except for eXtreme Gradient Boosting (XGBoost), which was written in an individual library called "XgBoost" (21). The logistic regression implemented in SciKit-Learn library was regularized logistic regression. Four classifiers were used including two base classifiers and two ensemble learning-based classifiers. In all classifiers, the training set was 395 of 565 (70%) patients, and the test set was the remaining 170 patients in the two institutions. Among the whole dataset, discrete variables were input to the one-hot encoder, denoting values taken on by categorical (discrete) features. The output would be a sparse matrix where each column corresponded to one possible value of one feature.

Firstly, logistic regression, one of the most classic classifiers to estimate the probability that a patient would have a particular outcome on the basis of related information or clinical

characteristics, was used (22). Secondly, a support vector machine (SVM), a mathematical entity for maximizing a particular mathematical function with respect to a given collection of data, was used. The kernel function was used to "space up" the data to higher dimensions, which allowed the data to be linearly separated (23).

A scalable end-to-end tree-boosting system called XGBoost was then used, which could be built with a smaller sample size than most existing systems for ensemble learning-based classifiers. XGBoost is based on gradient tree boosting, an algorithm with which new models are created that predict the residuals of prior models and are then added together for the final prediction (24).

Finally, a random forest within a multiple decision tree model was used (25). Each tree was developed from a bootstrap sample of the training dataset, and each node was the part that was the best among a haphazardly chosen subset of features. The class predictions created by each tree within the forest were amassed, and the ultimate prediction was based on the lion's share vote (26).

Parameter Tuning

For all classifiers, we needed to choose optimal parameters based on the training set. A grid search was applied to iterate through each parameter combination. The best parameter set was confirmed by first plotting the receiver operating characteristic (ROC) curve and then selecting the one with the maximum area under the ROC curve (AUC). All classifiers were used to make predictions on the test set.

Model Evaluation

The performance of these classifiers was mainly evaluated by using overall accuracy, sensitivity, specificity, and AUC. Overall accuracy was the total correct ratio on all test sets. Sensitivity, similar to recall, indicated the proportion of upgraded PCa patients correctly identified by the classifier. Specificity indicated the proportion of patients who were correctly classified as "no-upgrade." AUC indicated the probability that the classifier would have a higher prediction between "upgrade" and "no-upgrade" cases. All randomizations involved a random seed number of 0.

Feature Importance

To evaluate the importance of these features and to figure out the most contributed features, the Gini index was leveraged. In the random-forest classifier, every time a node was split on a single feature, the Gini impurity criterion for the two descendent nodes was less than that of the parent node. Adding up the Gini decreases for each feature over all trees in the forest gives fast feature importance, defined as follows:

$$Gini(p) = \sum_{k=1}^{K} p_k(1 - p_k)$$

In the formula, K represents the total number of categories and p_k the probability that a case is divided into k categories in the case of a single feature (16). Our study was a binary classification, so K was equal to 2.

Nomogram and Evaluation

A nomogram was proposed to visually predict the risk of upgrading. A nomogram was composed of graphical lines of risk factors, points, total points, and upgrading probability. A calibration plot was used to validate how well the nomogram was calibrated. The x-axis of the calibration plot was defined as predicted probability, and the y-axis was defined as the actual probability (27).

Predicted probability was a prevalence rate calculated by a proposed nomogram. Actual probability could be calculated by dividing the number of patients with the same predicted probability by the total number of patients. An ideal line was drawn at a 45° angle in the calibration plot. The nomogram and calibration plot were plotted with R version 3.6.0 in package "rms" version 5.1-4.

RESULTS

Baseline Information

From October 2016 to February 2020, a total of 694 patients underwent RARP after prostate biopsy in Drum Tower Hospital and Molinette Hospital. Of these patients, 179 were excluded because they did not meet the criteria. The remaining 515 were included (**Figure 1**). Clinical characteristics of patients are summarized in **Table 1**.

Upgrading and Downgrading Under Different Biopsy Methods

Regardless of the combination of SB and TB, of these 515 patients, only 245 (48.15%) cases were in accord with postoperative whole-mount histopathology, accompanied by 120 (23.30%) cases upgrading and 147 (27.18%) cases downgrading (**Figure 2** and **Table 2**).

The combined biopsy had a better concordance of postoperative histopathology than SB only (48.15% vs. 40.19%, $p = 0.012$). But there was no difference between the combined biopsy and TB only (48.15% vs. 42.33%, $p = 0.069$). The combined biopsy could significantly reduce the upgrading rate of postoperative pathology, in comparison to SB only (23.30% vs. 39.61%, $p < 0.0001$) or TB only (23.30% vs. 40.19%, $p < 0.0001$). Meanwhile, the combined biopsy would lead to a higher postoperative pathology downgrade rate (27.18% vs. 20.19% in SB, $p = 0.002$; and 27.18% vs. 17.48% in TB, $p < 0.0001$) (**Table 2** and **Supplementary Figures 1, 2**). The pathology detail of primary and secondary Gleason patterns from SB and TB to RP is shown in **Supplementary Table 2**.

Upgrading and Downgrading Under Different International Society of Urological Pathology

Under different ISUP guidelines, 65 (53.28%), 29 (20.42%), 14 (11.29%), and 12 (10.81%) patients with ISUP1, ISUP2, ISUP3, and ISUP4, respectively, had upgrades as compared with postoperative whole-mount histopathology. At the same time, ISUP2, ISUP3, ISUP4, and ISUP5 had 8 (5.63%), 54 (43.54%), 74

TABLE 1 | Clinical characteristics of patients.

Characteristics	N = 515
Age (years)	68.0 (63.0–74.0)
Height (cm)	170.0 (167.0–175.0)
Weight (kg)	72.0 (68.0–77.0)
BMI (kg/m^2)	24.7 (22.9–27.1)
Pre-biopsy serum PSA value (ng/ml)	8.3 (6.0–12.0)
Anterior-posterior (AP) length (cm)	4.2 (3.9–4.8)
Right–left (RL) length (cm)	4.8 (4.3–5.0)
Head–foot (HF) length (cm)	3.8 (3.4–4.5)
Prostate volume (ml)	35.2 (26.0–48.1)
Maximum diameter of lesion (cm)	1.3 (1.0–1.8)
Number of cores (n)	14.0 (14.0–16.0)
Gap days (d)	18.0 (15.0–25.0)
PI-RADS (n)	
3	85 (16.50%)
4	260 (50.49%)
5	170 (33.01%)

All features except PI-RADS are represented by median (IQR). PI-RADS is represented by n (%).
BMI, body mass index; PI-RADS, Prostate Imaging-Reporting and Data System; PSA, prostate-specific antigen; IQR, interquartile range.

(66.67%), and 10 (62.50%) patients with histopathological downgrades, respectively. One patient with confirmed ISUP1 by biopsy was found to have no PCa in the final histopathology (**Figure 2** and **Supplementary Table 3**).

For different levels of upgrading and downgrading, most patients would upgrade to ISUP2 from ISUP1, regardless of the biopsy method. Very few patients upgrade (1.55%) or downgrade (9.13%) two levels or more (**Supplementary Table 3**).

When we identified clinically significant PCa using different ISUP levels (csPC-1: ISUP > 1; csPCa-2: ISUP > 2), there were 65 (53.28%) or 34 (12.88%) cases of clinically significant upgrading and 14 (3.56%) or 85 (33.86%) cases of clinically significant downgrading (**Figure 3**).

Different Classifier Results

We used several supervised machine learning algorithms to predict pathology upgrades at RP. We established some dichotomous models in which the label was set to be an upgrade or otherwise. The overall accuracy was 0.703, 0.768, 0.794, and 0.761 for logistic regression, random forest, XGBoost, and SVM, respectively, adjusted for optimal parameters. Their AUC values were 0.674, 0.670, 0.711, and 0.679, respectively. The detailed parameters are described in **Table 3**, and the ROC curve is shown in **Figure 4**.

Subsequently, the feature importance calculated using the Gini index was demonstrated, as shown in **Supplementary Figure 3**. The top four important features were ISUP score in a TB, primary Gleason pattern (G1) score in a TB, ISUP score in an SB, and G1 score in an SB. These features were later used in the construction of nomograms.

Nomogram Construction for Upgrade

We constructed the nomogram to predict the risk of upgrading using 10 risk factors including the top four important features, shown in **Figure 5A**. The longer the line for each feature, the higher the score. When these scores were summed, the higher the total points, the greater the probability of pathology upgrading. When the total points were below 520, the probability of

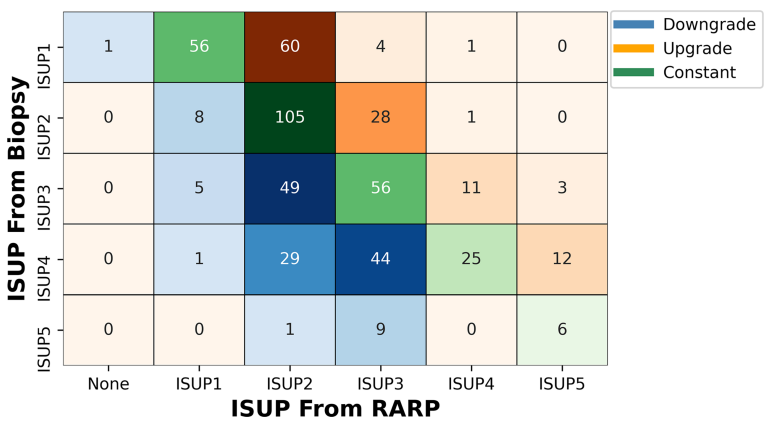

FIGURE 2 | Volume plot of pathological results from combined biopsy to final RARP according to ISUP grade group. The shade of color reflects the number. ISUP, International Society of Urological Pathology; RARP, robot-assisted laparoscopic radical prostatectomy.

TABLE 2 | Concordance, upgrade, and downgrade of Gleason score according to different biopsy methods.

	Combined biopsy (A)	Systematic biopsy (B)	Targeted biopsy (C)	*p*A vs. B	*p*A vs. C	*p*B vs. C
Concordance	248 (48.15%)	207 (40.19%)	218 (42.3%)	0.012	0.069	0.528
Upgrade	120 (23.3%)	204 (39.61%)	207 (40.19%)	<0.0001	<0.0001	0.899
Downgrade	147 (27.18%)	104 (20.19%)	90 (17.48%)	<0.0001	<0.0001	0.300

pathology upgrading was less than 10%, while when the total points were above 650, the probability of pathology upgrading would rise to about 0.7.

A calibration plot was created with 1,000 repetitions boot in **Figure 5B**. The mean absolute error was 0.04 in these 515 patients.

DISCUSSION

Accurate GS is still the strongest decision factor of PCa management and predictor of oncologic outcomes. However, overall pathological characteristics of the prostate cannot be presented by biopsy sampling, as the GG in needle biopsies has poor reproducibility and lack correlation with corresponding RP specimens (28). Approximately 30%–50% of cases will be misled by the biopsy grading system (5, 29). In our multicenter cohort, we found that the overall concordance rate of GG was 48.15% from biopsy to RP.

In recent decades, a relatively growing number of men with PCa are opting for therapies other than RP, such as focal therapy, radiation therapy, or active surveillance, which made biopsy grade more important in therapeutic choices (30). Clinicians are more concerned about the upgrade rates, as the only tissue sampled is from the needle biopsy. The confirmatory biopsy setting was upgraded with a range of 18%–30% of cases, who are previously detected to have PCa and were on active surveillance (31).

Pre-biopsy MRI scan and MRI-guided TB have been widely recommended for men with naïve biopsy or repeat biopsy, as several studies have been proven the improvement of detective rates of PCa or clinically significant PCa (8, 20, 32). Moreover, after RP, pathological upgrade is less likely to occur with MRI-guided TB as previously described (33, 34). Our results showed a significantly lower upgrade rate in the combined biopsy, versus SB or TB alone (both $p < 0.0001$). There was no difference in GG upgrade between SB (39.61%) and TB (40.19%). Some studies indicated that TB alone had better results in pathologic disease upgrade than SB. A possible explanation is in these cohorts of four to six cores, or even saturated biopsy for each lesion was taken (35, 36). Conversely, only two to four cores were performed for each lesion in our protocol.

Similar to other studies (29, 37, 38), the most common pathological upgrade occurred in ISUP GG1 and GG2, accounting for 53.28% and 20.42%, respectively. And these are the two populations of PCa who were potentially selected for active surveillance and/or focal therapy. When we identified csPCa with criteria of ISUP GG3 or higher tumors (csPCa-2 in our study) as previously reported (20), the upgrade rate was 12.88%. But when we made use of other definition criteria, being ISUP GG2 or higher tumors (csPCa-1), the upgrade rate was as high as 53.28%. All these data suggest that upgrading GG may have consequences on clinical outcomes from clinically non-significant PCa to csPCa.

To solve these discrepancies, researchers have sought to predict this pathological upgrade in order to identify patients who are more suitable for active surveillance or needed better and earlier intervention. Several predictive models or analyses of

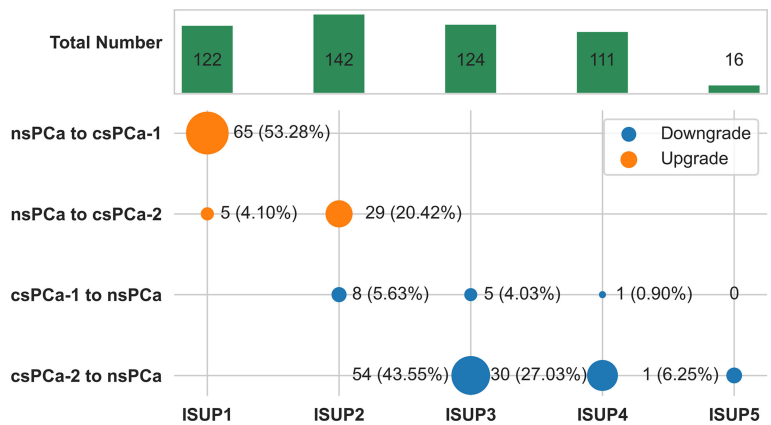

FIGURE 3 | Change plot of clinically significant pathological upgrade or downgrade from combined biopsy to final radical prostatectomy according to ISUP grade group. csPCa-1 was defined as ISUP grade group 2 or higher tumors. csPCa-2 was defined as ISUP grade group 3 or higher tumors. The size of dot reflects the number.csPCa, clinically significant prostate cancer; nsPCa, non-significant prostate cancer; ISUP, International Society of Urological Pathology.

TABLE 3 | Parameters and performance of machine learning algorithms.

Algorithms	Parameters	Overall accuracy	AUC
Logistics regression	C=0.01, penalty='l2'	0.703	0.674
Random forest	n_estimators=400, criterion=gini, max_depth=3	0.768	0.670
XGBoost	n_estimators=100, learning_rate=0.01, max_depth=6	0.794	0.711
SVM	C=0.001, kernel='linear', gamma=$1*10^{-10}$	0.761	0.679

XGboost, eXtreme Gradient Boosting; SVM, support vector machine; AUC, area under the receiver operating characteristic curve.

adverse factors were reported, but almost all of them are based on MRI and using PI-RADS (6, 9, 39). Several investigators have included quantitative histologic features to better predict the stage and risk of disease recurrence (40, 41). However, the methods previously used are mainly regression analysis.

Along with the improvement of computer technology, machine learning-based analysis has become better at processing existing data more comprehensively and eliminating more errors (12). Moreover, machine learning methods can construct classifiers with good predictive efficacy. Recently, others combined texture features of mpMRI and machine learning methods to predict GG upgrading (42). They suggested that ADC maps of mpMRI could predict PCa GG upgrading from biopsy to RP non-invasively with satisfactory predictive efficacy. However, their analysis was carried out on a retrospective study of a small group of patients from a single center. Moreover, only TRUS-guided systemic biopsies were included.

To our knowledge, this is the first study to use machine learning to predict pathological GG upgrading including TB. Our transperineal TB cohort was derived from a prospective data collection (13, 14). We used four kinds of supervised machine learning algorithms to predict pathological upgrades from biopsy to RP. Not logistic regression, but XGBoost, was the most accurate algorithm in our cohort. Moreover, we analyzed almost all the relevant characteristics, including TB ISUP score and primary Gleason pattern (G1) score. The top four important features were the ISUP score and G1 score in TB and SB, respectively. We constructed the nomogram to predict the risk of upgrading using 10 risk factors including the top four important features. Similar to another study (6), PI-RADS was one of the most significant predictors, but we demonstrated that the ISUP score and G1 score from TB played a more important role in the prediction model. We hold the opinion that adding features of TB to the prediction model is a notable advance in the selection of candidates for active surveillance. Moreover, the results of the relatively high upgrade rate of ISUP 1 (53.28%) and ISUP2 (20.42%) group might explain the fact that patients with relatively low risk at biopsy suffer from metastasis or even death from PCa. It might suggest that the ISUP 1 and ISUP 2 population, who normally tend to receive active surveillance or focal therapy, might not be suitable candidates.

Some limitations need to be highlighted. Firstly, our study was performed on a retrospective analysis. More prospective data are needed to validate our findings. Secondly, the relatively high

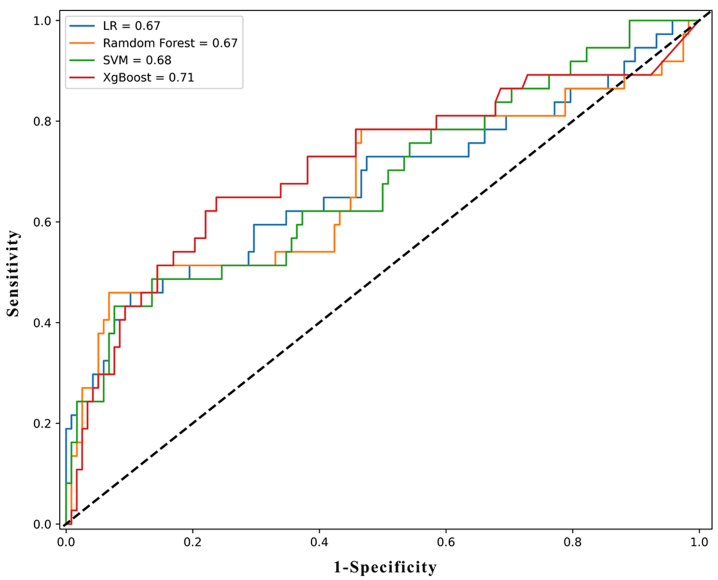

FIGURE 4 | The ROC results of machine learning models. ROC, receiver operating characteristic curve; LR, logistic regression; XGboost, eXtreme Gradient Boosting; SVM, support vector machine.

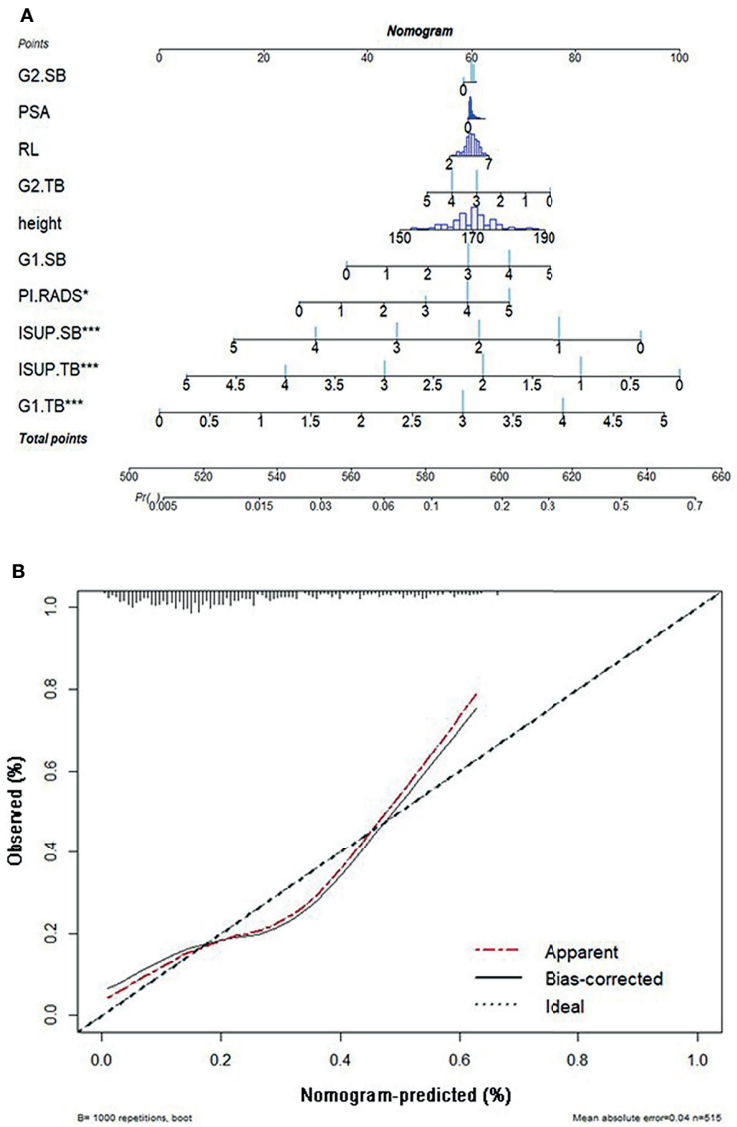

FIGURE 5 | **(A)** The nomogram of pathological upgrade prediction. **(B)** Calibration plots of observed and predicted probability of pathological upgrade. ISUP, International Society of Urological Pathology; TB, targeted biopsy; G1, primary Gleason pattern; SB, systematic biopsy; G2, secondary Gleason pattern; RL, right–left diameter; PSA, prostate-specific antigen; PI-RADS, Prostate Imaging-Reporting and Data System.

number of different operators performed the procedure. Likely, results would have even improved if performed by experienced operators only. In our opinion, the use of multiple operators, together with the multicenter nature, reinforces our results in terms of reproducibility. Despite the limitations, we firmly believe that the principal results of our preliminary study are sufficiently valid.

In conclusion, the combined effect of SB plus TB led to a better pathological concordance rate and the less upgrading rate from biopsy to RP. Machine learning models to predict PCa GG upgrading had satisfactory predictive efficacy. Adding features of TB to the prediction model is a notable advance in the selection of appropriate therapeutic strategies.

DATA AVAILABILITY STATEMENT

The original contributions presented in the study are included in the article/**Supplementary Material**. Further inquiries can be directed to the corresponding authors.

ETHICS STATEMENT

Written informed consent was obtained from the individual(s) for the publication of any potentially identifiable images or data included in this article.

AUTHOR CONTRIBUTIONS

JZ, HG, and GM conceived the study and revised the paper. AM, MO, HH, MG, FZ, LX, YF, and BZ performed the project. YK, YW, GC, and PG collected and analyzed data. JZ, YK, and XQ wrote the draft. JZ, YW, GM, and XQ interpreted the data.

FUNDING

This study was supported by grants from the National Natural Science Foundation of China (81602232, 81802535, and 81974394), Natural Science Foundation of Jiangsu Province for Excellent Young Scholars (BK20200051), and Nanjing Medical Science and technique Development Foundation (GRX17127).

SUPPLEMENTARY MATERIAL

The Supplementary Material for this article can be found online at: https://www.frontiersin.org/articles/10.3389/fonc.2022.785684/full#supplementary-material

REFERENCES

1. Mottet M, Cornford P, van den Bergh RCN, Briers E, De Santis M, Gillessen S, et al. EAU - ESTRO ESUR - SIOG Guidelines on Prostate Cancer 2021. Arnhem, The Netherlands: European Association of Urology Guidelines Office. (2021).
2. Gearman DJ, Morlacco A, Cheville JC, Rangel LJ, Karnes RJ. Comparison of Pathological and Oncologic Outcomes of Favorable Risk Gleason Score 3 + 4 and Low Risk Gleason Score 6 Prostate Cancer: Considerations for Active Surveillance. *J Urol* (2018) 199(5):1188–95. doi: 10.1016/j.juro.2017.11.116
3. Yang DD, Mahal BA, Muralidhar V, Nezolosky MD, Vastola ME, Labe SA, et al. Risk of Upgrading and Upstaging Among 10 000 Patients With Gleason 3+4 Favorable Intermediate-Risk Prostate Cancer. *Eur Urol Focus* (2019) 5 (1):69–76. doi: 10.1016/j.euf.2017.05.011
4. Le JD, Stephenson S, Brugger M, Lu DY, Lieu P, Sonn GA, et al. Magnetic Resonance Imaging-Ultrasound Fusion Biopsy for Prediction of Final Prostate Pathology. *J Urol* (2014) 192(5):1367–73. doi: 10.1016/j.juro.2014.04.094
5. Audenet F, Rozet F, Resche-Rigon M, Bernard R, Ingels A, Prapotnich D, et al. Grade Group Underestimation in Prostate Biopsy: Predictive Factors and Outcomes in Candidates for Active Surveillance. *Clin Genitourin Cancer* (2017) 15(6):e907–13. doi: 10.1016/j.clgc.2017.04.024
6. Alqahtani S, Wei C, Zhang Y, Szewczyk-Bieda M, Wilson J, Huang Z, et al. Prediction of Prostate Cancer Gleason Score Upgrading From Biopsy to Radical Prostatectomy Using Pre-Biopsy Multiparametric MRI PIRADS Scoring System. *Sci Rep* (2020) 10(1):7722. doi: 10.1038/s41598-020-64693-y
7. Ahmed HU, El-Shater Bosaily A, Brown LC, Gabe R, Kaplan R, Parmar MK, et al. Diagnostic Accuracy of Multi-Parametric MRI and TRUS Biopsy in Prostate Cancer (PROMIS): A Paired Validating Confirmatory Study. *Lancet* (2017) 389(10071):815–22. doi: 10.1016/s0140-6736(16)32401-1
8. Kasivisvanathan V, Rannikko AS, Borghi M, Panebianco V, Mynderse LA, Vaarala MH, et al. MRI-Targeted or Standard Biopsy for Prostate-Cancer Diagnosis. *N Engl J Med* (2018) 378(19):1767–77. doi: 10.1056/NEJMoa1801993
9. Gandaglia G, Ploussard G, Valerio M, Mattei A, Fiori C, Roumiguie M, et al. The Key Combined Value of Multiparametric Magnetic Resonance Imaging, and Magnetic Resonance Imaging-Targeted and Concomitant Systematic Biopsies for the Prediction of Adverse Pathological Features in Prostate Cancer Patients Undergoing Radical Prostatectomy. *Eur Urol* (2020) 77 (6):733–41. doi: 10.1016/j.eururo.2019.09.005
10. Pepe P, Garufi A, Priolo GD, Galia A, Fraggetta F, Pennisi M. Is it Time to Perform Only Magnetic Resonance Imaging Targeted Cores? Our Experience With 1,032 Men Who Underwent Prostate Biopsy. *J Urol* (2018) 200(4):774–8. doi: 10.1016/j.juro.2018.04.061
11. LeCun Y, Bengio Y, Hinton G. Deep Learning. *Nature* (2015) 521(7553):436–44. doi: 10.1038/nature14539
12. Liu H, Tang K, Peng E, Wang L, Xia D, Chen Z. Predicting Prostate Cancer Upgrading of Biopsy Gleason Grade Group at Radical Prostatectomy Using Machine Learning-Assisted Decision-Support Models. *Cancer Manag Res* (2020) 12:13099–110. doi: 10.2147/CMAR.S286167
13. Marra G, Zhuang J, Marquis A, Zhao X, Calleris G, Kan Y, et al. Pain in Men Undergoing Transperineal Free-Hand Multiparametric Magnetic Resonance Imaging Fusion Targeted Biopsies Under Local Anesthesia: Outcomes and Predictors From a Multicenter Study of 1,008 Patients. *J Urol* (2020) 204 (6):1209–15. doi: 10.1097/ju.0000000000001234
14. Marra G, Zhuang J, Beltrami M, Calleris G, Zhao X, Marquis A, et al. Transperineal Freehand Multiparametric MRI Fusion Targeted Biopsies Under Local Anaesthesia for Prostate Cancer Diagnosis: A Multicentre Prospective Study of 1014 Cases. *BJU Int* (2021) 127(1):122–30. doi: 10.1111/bju.15121
15. Huang H, Wang W, Lin T, Zhang Q, Zhao X, Lian H, et al. Comparison of the Complications of Traditional 12 Cores Transrectal Prostate Biopsy With Image Fusion Guided Transperineal Prostate Biopsy. *BMC Urol* (2016) 16 (1):68. doi: 10.1186/s12894-016-0185-z
16. Kan Y, Zhang Q, Hao J, Wang W, Zhuang J, Gao J, et al. Clinico-Radiological Characteristic-Based Machine Learning in Reducing Unnecessary Prostate Biopsies of PI-RADS 3 Lesions With Dual Validation. *Eur Radiol* (2020) 30 (11):6274–84. doi: 10.1007/s00330-020-06958-8
17. Barentsz JO, Weinreb JC, Verma S, Thoeny HC, Tempany CM, Shtern F, et al. Synopsis of the PI-RADS V2 Guidelines for Multiparametric Prostate Magnetic Resonance Imaging and Recommendations for Use. *Eur Urol* (2016) 69(1):41–9. doi: 10.1016/j.eururo.2015.08.038
18. van der Leest M, Cornel E, Israel B, Hendriks R, Padhani AR, Hoogenboom M, et al. Head-To-Head Comparison of Transrectal Ultrasound-Guided Prostate Biopsy Versus Multiparametric Prostate Resonance Imaging With Subsequent Magnetic Resonance-Guided Biopsy in Biopsy-Naive Men With Elevated Prostate-Specific Antigen: A Large Prospective Multicenter Clinical Study. *Eur Urol* (2019) 75(4):570–8. doi: 10.1016/j.eururo.2018.11.023
19. Epstein JI, Egevad L, Amin MB, Delahunt B, Srigley JR, Humphrey PA, et al. The 2014 International Society of Urological Pathology (ISUP) Consensus Conference on Gleason Grading of Prostatic Carcinoma: Definition of Grading Patterns and Proposal for a New Grading System. *Am J Surg Pathol* (2016) 40(2):244–52. doi: 10.1097/PAS.0000000000000530
20. Rouvière O, Puech P, Renard-Penna R, Claudon M, Roy C, Mège-Lechevallier F, et al. Use of Prostate Systematic and Targeted Biopsy on the Basis of Multiparametric MRI in Biopsy-Naive Patients (MRI-FIRST): A Prospective, Multicentre, Paired Diagnostic Study. *Lancet Oncol* (2019) 20(1):100–9. doi: 10.1016/s1470-2045(18)30569-2
21. Abraham A, Pedregosa F, Eickenberg M, Gervais P, Mueller A, Kossaifi J, et al. Machine Learning for Neuroimaging With Scikit-Learn. *Front Neuroinform* (2014) 8:14. doi: 10.3389/fninf.2014.00014
22. Tolles J, Meurer WJ. Logistic Regression: Relating Patient Characteristics to Outcomes. *JAMA* (2016) 316(5):533–4. doi: 10.1001/jama.2016.7653
23. Huang S, Cai N, Pacheco PP, Narrandes S, Wang Y, Xu W. Applications of Support Vector Machine (SVM) Learning in Cancer Genomics. *Cancer Genomics Proteomics* (2018) 15(1):41–51. doi: 10.21873/cgp.20063
24. Ogunleye A, Wang QG. XGBoost Model for Chronic Kidney Disease Diagnosis. *IEEE/ACM Trans Comput Biol Bioinform* (2020) 17(6):2131–40. doi: 10.1109/TCBB.2019.2911071
25. Yang L, Wu H, Jin X, Zheng P, Hu S, Xu X, et al. Study of Cardiovascular Disease Prediction Model Based on Random Forest in Eastern China. *Sci Rep* (2020) 10(1):5245. doi: 10.1038/s41598-020-62133-5
26. Pavey TG, Gilson ND, Gomersall SR, Clark B, Trost SG. Field Evaluation of a Random Forest Activity Classifier for Wrist-Worn Accelerometer Data. *J Sci Med Sport* (2017) 20(1):75–80. doi: 10.1016/j.jsams.2016.06.003

27. Iasonos A, Schrag D, Raj GV, Panageas KS. How to Build and Interpret a Nomogram for Cancer Prognosis. *J Clin Oncol* (2008) 26(8):1364–70. doi: 10.1200/JCO.2007.12.9791
28. Epstein JI, Feng Z, Trock BJ, Pierorazio PM. Upgrading and Downgrading of Prostate Cancer From Biopsy to Radical Prostatectomy: Incidence and Predictive Factors Using the Modified Gleason Grading System and Factoring in Tertiary Grades. *Eur Urol* (2012) 61(5):1019–24. doi: 10.1016/j.eururo.2012.01.050
29. Athanazio D, Gotto G, Shea-Budgell M, Yilmaz A, Trpkov K. Global Gleason Grade Groups in Prostate Cancer: Concordance of Biopsy and Radical Prostatectomy Grades and Predictors of Upgrade and Downgrade. *Histopathology* (2017) 70(7):1098–106. doi: 10.1111/his.13179
30. Marra G, Ploussard G, Ost P, De Visschere PJL, Briganti A, Gandaglia G, et al. Focal Therapy in Localised Prostate Cancer: Real-World Urological Perspective Explored in a Cross-Sectional European Survey. *Urol Oncol* (2018) 36(12):529.e511–529.e522. doi: 10.1016/j.urolonc.2018.08.013
31. Shapiro DD, Gregg JR, Lim AH, Nogueras-González GM, Choi H, Kang HC, et al. Comparing Confirmatory Biopsy Outcomes Between MRI-Targeted Biopsy and Standard Systematic Biopsy Among Men Being Enrolled in Prostate Cancer Active Surveillance. *BJU Int* (2021) 127(3):340–8. doi: 10.1111/bju.15100
32. Ahdoot M, Wilbur AR, Reese SE, Lebastchi AH, Mehralivand S, Gomella PT, et al. MRI-Targeted, Systematic, and Combined Biopsy for Prostate Cancer Diagnosis. *N Engl J Med* (2020) 382(10):917–28. doi: 10.1056/NEJMoa1910038
33. Goel S, Shoag JE, Gross MD, Al Hussein Al Awamlh B, Robinson B, Khani F, et al. Concordance Between Biopsy and Radical Prostatectomy Pathology in the Era of Targeted Biopsy: A Systematic Review and Meta-Analysis. *Eur Urol Oncol* (2020) 3(1):10–20. doi: 10.1016/j.euo.2019.08.001
34. Wenzel M, Preisser F, Wittler C, Hoeh B, Wild PJ, Tschabunin A, et al. Correlation of MRI-Lesion Targeted Biopsy vs. Systematic Biopsy Gleason Score With Final Pathological Gleason Score After Radical Prostatectomy. *Diagn (Basel)* (2021) 11(5):882. doi: 10.3390/diagnostics11050882
35. Porpiglia F, Passera R, Manfredi M, Mele F, Bollito E, De Pascale A, et al. Multiparametric-Magnetic Resonance/Ultrasound Fusion Targeted Prostate Biopsy Improves Agreement Between Biopsy and Radical Prostatectomy Gleason Score. *Anticancer Res* (2016) 36(9):4833–9. doi: 10.21873/anticanres.11045
36. Calio BP, Sidana A, Sugano D, Gaur S, Maruf M, Jain AL, et al. Risk of Upgrading From Prostate Biopsy to Radical Prostatectomy Pathology-Does Saturation Biopsy of Index Lesion During Multiparametric Magnetic Resonance Imaging-Transrectal Ultrasound Fusion Biopsy Help? *J Urol* (2018) 199(4):976–82. doi: 10.1016/j.juro.2017.10.048
37. Demirtaş A, Sönmez G, Tombul Ş T, Demirtaş T, Akgün H. Comparison of the Upgrading Rates of International Society of Urological Pathology Grades and Tumor Laterality in Patients Undergoing Standard 12-Core Prostate Biopsy Versus Fusion Prostate Biopsy for Prostate Cancer. *Urol Int* (2019) 103(3):256–61. doi: 10.1159/000501528
38. Shoag JE, Cai PY, Gross MD, Gaffney C, Li D, Mao J, et al. Impact of Prebiopsy Magnetic Resonance Imaging on Biopsy and Radical Prostatectomy Grade Concordance. *Cancer* (2020) 126(13):2986–90. doi: 10.1002/cncr.32821
39. Liu H, Tang K, Xia D, Wang X, Zhu W, Wang L, et al. Added Value of Biparametric MRI and TRUS-Guided Systematic Biopsies to Clinical Parameters in Predicting Adverse Pathology in Prostate Cancer. *Cancer Manag Res* (2020) 12:7761–70. doi: 10.2147/CMAR.S260986
40. Freedland SJ, Terris MK, Csathy GS, Kane CJ, Amling CL, Presti JCJr., et al. Preoperative Model for Predicting Prostate Specific Antigen Recurrence After Radical Prostatectomy Using Percent of Biopsy Tissue With Cancer, Biopsy Gleason Grade and Serum Prostate Specific Antigen. *J Urol* (2004) 171(6 Pt 1):2215–20. doi: 10.1097/01.ju.0000124463.13319.0a
41. Pepe P, Fraggetta F, Galia A, Grasso G, Piccolo S, Aragona F. Is Quantitative Histologic Examination Useful to Predict Nonorgan-Confined Prostate Cancer When Saturation Biopsy is Performed? *Urology* (2008) 72(6):1198–202. doi: 10.1016/j.urology.2008.05.045
42. Xie J, Li B, Min X, Zhang P, Fan C, Li Q, et al. Prediction of Pathological Upgrading at Radical Prostatectomy in Prostate Cancer Eligible for Active Surveillance: A Texture Features and Machine Learning-Based Analysis of Apparent Diffusion Coefficient Maps. *Front Oncol* (2020) 10:604266. doi: 10.3389/fonc.2020.604266

Conflict of Interest: The authors declare that the research was conducted in the absence of any commercial or financial relationships that could be construed as a potential conflict of interest.

Publisher's Note: All claims expressed in this article are solely those of the authors and do not necessarily represent those of their affiliated organizations, or those of the publisher, the editors and the reviewers. Any product that may be evaluated in this article, or claim that may be made by its manufacturer, is not guaranteed or endorsed by the publisher.

Copyright © 2022 Zhuang, Kan, Wang, Marquis, Qiu, Oderda, Huang, Gatti, Zhang, Gontero, Xu, Calleris, Fu, Zhang, Marra and Guo. This is an open-access article distributed under the terms of the Creative Commons Attribution License (CC BY). The use, distribution or reproduction in other forums is permitted, provided the original author(s) and the copyright owner(s) are credited and that the original publication in this journal is cited, in accordance with accepted academic practice. No use, distribution or reproduction is permitted which does not comply with these terms.

frontiers | Frontiers in Oncology

ORIGINAL RESEARCH
published: 08 April 2022
doi: 10.3389/fonc.2022.772403

Automatic Prostate Gleason Grading Using Pyramid Semantic Parsing Network in Digital Histopathology

*Yali Qiu[1], Yujin Hu[1], Peiyao Kong[1], Hai Xie[1], Xiaoliu Zhang[1], Jiuwen Cao[2], Tianfu Wang[1] and Baiying Lei[1]**

[1] School of Biomedical Engineering, Health Science Center, Shenzhen University, National-Regional Key Technology Engineering Laboratory for Medical Ultrasound, Guangdong Key Laboratory for Biomedical Measurements and Ultrasound Imaging, Shenzhen, China, [2] Key Lab for Internet of Things (IOT) and Information Fusion Technology of Zhejiang, Hangzhou Dianzi University, Hangzhou, China

Purpose: Prostate biopsy histopathology and immunohistochemistry are important in the differential diagnosis of the disease and can be used to assess the degree of prostate cancer differentiation. Today, prostate biopsy is increasing the demand for experienced uropathologists, which puts a lot of pressure on pathologists. In addition, the grades of different observations had an indicating effect on the treatment of the patients with cancer, but the grades were highly changeable, and excessive treatment and insufficient treatment often occurred. To alleviate these problems, an artificial intelligence system with clinically acceptable prostate cancer detection and Gleason grade accuracy was developed.

Methods: Deep learning algorithms have been proved to outperform other algorithms in the analysis of large data and show great potential with respect to the analysis of pathological sections. Inspired by the classical semantic segmentation network, we propose a pyramid semantic parsing network (PSPNet) for automatic prostate Gleason grading. To boost the segmentation performance, we get an auxiliary prediction output, which is mainly the optimization of auxiliary objective function in the process of network training. The network not only includes effective global prior representations but also achieves good results in tissue micro-array (TMA) image segmentation.

Results: Our method is validated using 321 biopsies from the Vancouver Prostate Centre and ranks the first on the MICCAI 2019 prostate segmentation and classification benchmark and the Vancouver Prostate Centre data. To prove the reliability of the proposed method, we also conduct an experiment to test the consistency with the diagnosis of pathologists. It demonstrates that the well-designed method in our study can achieve good results. The experiment also focused on the distinction between high-risk cancer (Gleason pattern 4, 5) and low-risk cancer (Gleason pattern 3). Our proposed method also achieves the best performance with respect to various evaluation metrics for distinguishing benign from malignant.

OPEN ACCESS

Edited by:
Antonina Mitrofanova, Rutgers, The State University of New Jersey, United States

Reviewed by:
Jose Eduardo Tavora, Faculdade de Ciências Médicas de Minas Gerais (FCMMG), Brazil
Jiayun Li, Google, United States

****Correspondence:***
Baiying Lei
leiby@szu.edu.cn

Specialty section:
This article was submitted to Genitourinary Oncology, a section of the journal Frontiers in Oncology

Received: *08 September 2021*
Accepted: *22 February 2022*
Published: *08 April 2022*

Citation:
Qiu Y, Hu Y, Kong P, Xie H, Zhang X, Cao J, Wang T and Lei B (2022) Automatic Prostate Gleason Grading Using Pyramid Semantic Parsing Network in Digital Histopathology. Front. Oncol. 12:772403. doi: 10.3389/fonc.2022.772403

Availability: The Python source code of the proposed method is publicly available at https://github.com/hubutui/Gleason. All implementation details are presented in this paper.

Conclusion: These works prove that the Gleason grading results obtained from our method are effective and accurate.

Keywords: prostate, gleason grading, histopathology, PSPNet, prostate - pathology

INTRODUCTION

The incidence and mortality of prostate cancer have been increasing over the past decades (1). With the high risk of overdiagnosis and overtreatment, there is an urgent need to accurately assess patient prognosis (2–4). Currently, the effective diagnostic index of histopathological biopsy of prostate cancer is still the Gleason grade (5). The Gleason grading system for prostate cancer refers to observing and scoring the cancer cells according to the similarity between the normal tissue and cancer cells (6–9). Pathologists recognize that the prognosis of prostate cancer is between its primary structure and secondary structure (10–12). In 2016, pathologists updated the grading system and redefined the grading criteria 1–5 (13). Although its clinical value has been widely recognized, the grading system is very complex and highly subjective. Moreover, the number of the qualified pathologists is insufficient to meet the global demand for pathological detection of prostate cancer. Therefore, how to use the Gleason grading system effectively to realize early automatic diagnosis and treatment has become an important research topic (14, 15).

Automatic segmentation has the potential to decrease lag time between diagnostic tests and treatment by providing a strong and standardized report of tissue location in a fraction of the time, which would take a pathologist to do so (16). However, the diagnostic process highly relies on the pathologist's rich personal experience, which is not only time-consuming and labor-intensive but also suffering from high subjective errors (17, 18). Moreover, the diagnostic process is also affected by high interobserver variability from different pathologists and limits its effect on individual patients. In order to solve the above problems, doctors often use computer science and technology to assist diagnosis. Among them, the deep learning method has been successfully introduced into the field of medical image analysis (19–21).

Deep learning algorithms have shown their potential for pathological diagnosis at the expert level in other tasks, such as diagnosing skin tissue lesions and identifying breast cancer metastasis. Long et al. (22) proposed a full convolutional network (FCN), which created a new chapter of semantic segmentation and improved the generalization of dynamic objects with an end-to-end way. Liu et al. (23) proved that FCN with the global average pooling module can enhance the segmentation performance. Subsequently, Noh et al. (24) proposed a coarse-to-fine deconvolution network structure for image segmentation. However, FCN only forecasts on a single scale, which cannot effectively deal with the change of size. Due to the significant variations in appearances of prostate cancers, the automatic grading of prostate tissue segmentation is tedious and troublesome. As histopathology image segmentation and classification images are usually of high resolution, it is challenging for the deep learning model to train and learn discriminative features due to the limited computing resources (25, 26). The blurred boundaries of some histopathological tissue may make this task more challenging.

Apart from the existing problems, there are three main challenges in extracting information from digital histopathology of prostate cancer. The first challenge is the high heterogeneity of cells and tissues. The grading of pathological images is complex. It may have several grades in a histopathology image. The second challenge is high interobserver variability. Under the huge data requirements, experts may have different opinions on the annotation of pictures. The third challenge is to learn features from high-resolution images. Considering the high heterogeneity of data and the difference of expert annotation, it is difficult to extract features in network training. Thus, how to efficiently extract useful features is quite critical.

To address the above challenges, we propose a new system to automatically identify prostate histopathology images in this article. In order to obtain data annotation with high interpretability and good robustness, we use the Simultaneous Truth and Performance Level Estimation algorithm (STAPLE) (27) to synthesize different expert annotations. The STAPLE algorithm can alleviate the heavy task of experts and deal with different expert annotations. The proposed system has the potential to improve prostate cancer prognostics and achieves a high agreement with the reference standard. The established benchmark can assess and compare the state of image analysis and machine learning-based algorithms. It will also help assess the robustness and accuracy of these computerized methods against the suggestion of numerous experts. Given the importance of prostate cancer and challenges of the Gleason grade system to detect and diagnose prostate cancer, the promising results can be quite beneficial in the medical community.

Our main contributions are three-fold:

1. A systematic framework is presented, which is beneficial for providing pathologists with an adequate and effective alternative prostate Gleason grading system.
2. An effective feature extraction strategy is proposed based on the pyramid semantic parsing network, which can extract

more effective information and improve the accuracy of disease diagnosis.
3. Our method is validated *via* the Vancouver Prostate Centre and ranks first on the MICCAI 2019 prostate segmentation benchmark, which is consistent with the diagnosis of pathologists.

METHODOLOGY

Overview of the Proposed Method

In this paper, we utilize the pyramid semantic parsing network (PSPNet) to extract features and then refine those features from different scales *via* the pyramid pooling module. To boost the segmentation performance, we get an auxiliary prediction output, which is mainly the optimization of auxiliary objective function in the process of network training. The network not only includes effective global prior representations but also achieves good results in tissue micro-array (TMA) image segmentation.

STAPLE Algorithm

For different segmentation tasks, the expert segmentation is achieved independently, but with the same real segmentation goal. The STAPLE algorithm is used to compare the differences of the final segmentation results based on a rapid interactive level set and hand contours for tumor segmentation (28). The algorithm segments images and calculates the probability of true segmentation simultaneously. The STAPLE algorithm not only takes the systematic deviation caused by the difference of different experts' annotations into account but also evaluates the annotation quality of each expert. The algorithm can balance the two aspects well and then generate a fuzzy real annotation. We can extract more critical information with different weights of each part of the input, which makes the model to have more accurate judgments and reduces the calculation and storage of the model. The flowchart of the detailed annotation of TMA core images provided by different pathologists is shown in **Figure 1**.

The output of the STAPLE algorithm is a picture with floating point values from 0 to 1, which represents the probability that the pixel point belongs to a specific segmentation target. The picture has the same size as the original image. Further, we want to extend it to multi-category situations. If each pixel has the maximum probability of belonging to a different category, the category label of the point is uncertain. At this point, we take the label of the most experienced expert as the true category label of the point. After preprocessing, the merged labels can be used for subsequent network training and verification.

Feature Extraction

Feature extraction is a key step in the field of computer vision and image processing, which can be used to extract image information and determine whether the points of each image belong to the useful features. The purpose of feature extraction is to divide the points on the image into different subsets, which are often represented as isolated points, continuous curves, or continuous regions. The quality of extracted features has a crucial impact on the performance of the training network (29).

In recent years, the way of feature extraction has developed from manual design to automatic extraction by the convolution neural network. Since AlexNet was proposed, researchers have devised a variety of convolutional neural network architectures to achieve automatic learning and extraction of features, such as VGG network (30), residual network (ResNet) (31), and densely connected network (DenseNet) (32). Different from classic convolutional neural networks, FCN can handle original input images from an arbitrary dimension and reserve spatial information. It classifies the original image pixel by pixel from the upper sampling and ignores the adjacent information when unpooling the low-resolution feature images. However, the main problem of FCN is that it cannot make good use of category information from a global scene. For the image classification task, the increase in network depth may bring additional optimization difficulties.

The residual block can solve this problem by using the long skip connection in each block and bring good performance. In the deep residual network, the latter layer mainly learns the residual thrown from the previous layer. Influenced by the most widely residual network, our research also uses ResNet as the skeleton network for feature extraction. ResNet is mainly composed of residual modules. Unlike the direct use of convolutional stacking, the residual module introduces residual

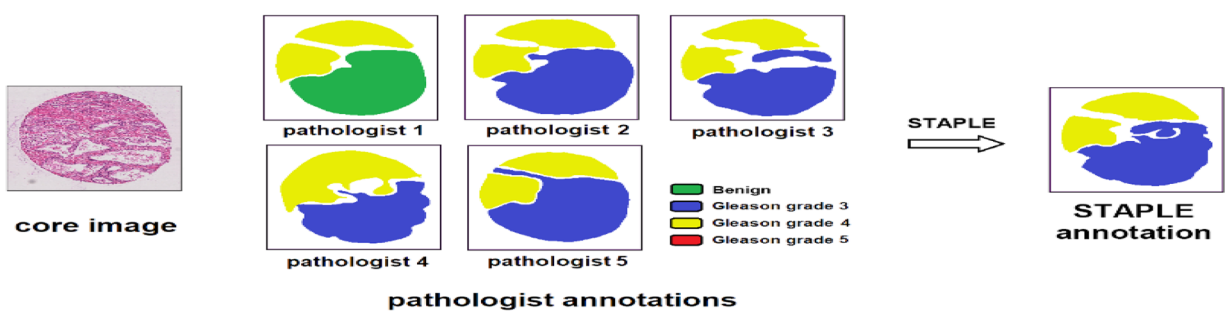

FIGURE 1 | Image processing of pathologist annotations of TMA core images. The STAPLE algorithm, the same as pixel-wise majority voting, fuses the annotations of different pathologists to build the "ground truth label".

learning, and hence the network can be made deeper and have more powerful capabilities of feature extraction. The skeleton network can effectively extract the tissue structure features using the prostate cancer pathological slice images and prepare for the next step of feature learning.

Pyramid Pooling Module

Global pooling has been widely used in the classical complex digital tissue pathological sections to get global image-level features (33). The pyramid pooling module (PPM) is a comparatively good way to fully utilize global information. To reduce the impact of the loss of contextual information between different subregions in the stage of training, some researchers proposed a hierarchical global prior, which contains variations among different subregions and numerous information with different scales (34, 35). Different levels of feature mapping created by the pyramid pool module are ultimately flattened and then connected to the full connection layer as input. We can utilize the global prior technique to eliminate the negative effects of fixed size constraints for the training of the convolutional network (36). The PPM collects different scales of information, which is more typical than global pooling (37). This multi-scale pooling can intuitively maintain global context information and global information of different scales better than single pooling.

After using the residual network as the feature extractor to extract the features, we need to further learn and process the extracted features to different sizes. These feature maps can be stacked into spatial pyramid feature maps. The pyramid feature map is subjected to different convolutions for feature learning and then resampled to restore the size of the input feature map. Then, these feature maps are combined with the input feature maps in a splicing manner. PPM can overcome the problems such as many parameters, difficult training, information loss, and overfitting and integrate features from four different pyramid scales. The gray module in PPM represents the feature map obtained after network training and continues to extract features with blocks having sizes of 1 × 1, 2 × 2, 3 × 3, and 6 × 6 pixels. We put these three grids on the feature map and can get 12 different blocks, and extract a feature from each block. Thus, 12 groups of features can be obtained. Obviously, the PPM can effectively combine features of different scales, including both deep-level high-level semantic features and low-level structural features. Accordingly, it can better learn and merge features.

In **Figure 2**, different levels of output in the PPM contain different sizes of feature maps. The bold red highlight represents a single bin output. When the size of the pyramid layers set by the network is N, the corresponding global size decreases to $1/N$ of the initial size, which is sampled to the same size as the original feature map after low-dimensional feature mapping by bilinear interpolation. To better weigh the global feature weights, we add a 1 × 1 convolution layer after the pyramidal pooling layer. Finally, different levels of features are connected at different levels as the final global feature.

Auxiliary Branch Network

This auxiliary branch network undergoes operations such as convolution and upsampling to output a prediction result. Note that the loss function of the backbone network is L_1 and the loss function of the auxiliary branch network is L_2, where the loss function L of the entire PSPNet network can then be expressed as:

$$L = L_1 + \alpha \cdot L_2 \tag{1}$$

where α is a weight coefficient that balances the 0two loss functions, and both L_1 and L_2 are cross-entropy loss functions. Finally, we set $\alpha = 0.5$.

Unlike the traditional backpropagation loss of its auxiliary blocking relays to the shallow layer of the network, we use two different loss mechanisms that can pass through all convolution layers for network calculation. The auxiliary loss can optimize the network learning without affecting the learning of the main branch. The combination of local and global information can

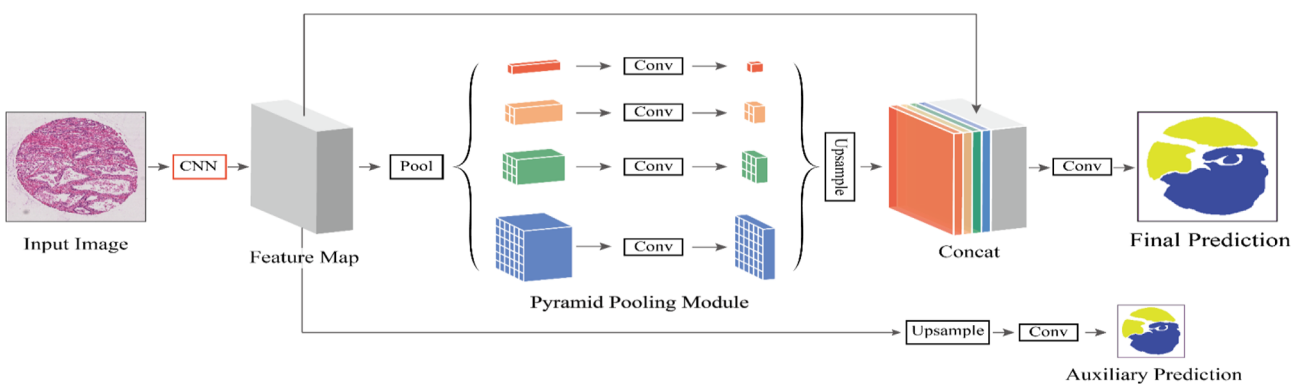

FIGURE 2 | The flowchart of our proposed method. We define CNN as the basic feature extraction layer of our proposed network. By giving the original image, we first obtain the feature mapping of the last network convolution layer using CNN and then make an auxiliary prediction for the feature mapping by upsampling and concatenation layers. Next, we obtain the final feature representation with local and global information through different subregion representations in the PPM after upsampling and connection layers. Finally, these representations are fed into a convolution layer to get the final per-pixel prediction.

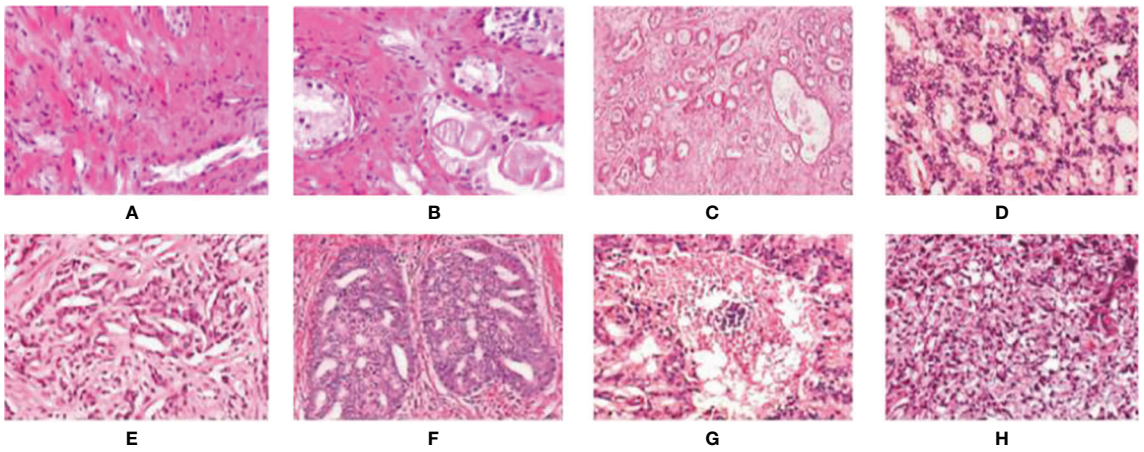

FIGURE 3 | Examples of digital histopathology images for Prostate Gleason Grading. We list four different Gleason grade groups: **(A, B)** Benign; **(C, D)** Grade 3; **(E, F)** Grade4; and **(G, H)** Grade 5. It can be observed that each level has a variety of sizes, shapes, and irregular object boundaries. Gleason Grade 3 consists of well-formed and well-defined glands with varying sizes but which are smaller and tighter than non-cancerous prostatic tissue. While Gleason Grade 4 is associated with poorly formed glands, gland fusion is no longer separated by the matrix, even related to a pattern known as cribriform. Gleason Grade 5 includes the worst differentiated glands.

effectively avoid information loss and make the diagnosis and prediction of diseases more reliable. During testing, we use the main branch with better optimization for final prediction. Specifically, we obtain the feature map by feeding the pathological slice image of prostate cancer into ResNet101. Subsequently, the feature map is fed into the PPM for multi-scale feature learning, and then the learned features pass through several convolution layers. Finally, we can get the final prediction result.

By constructing a feature pyramid to extract features of different sizes, each feature has rich image information, which improves the reliability of network feature extraction. The network model reveals the tradeoff between memory and accuracy and achieves good segmentation performance. Aiming at solving the problem of digital histopathological segmentation of prostate cancer, this method has high accuracy and robustness. Our method helps us get the champion of automatic prostate Gleason grading challenge 2019 which placed 1st on the MICCAI 2019 prostate segmentation benchmark, as well as the Vancouver Prostate Centre dataset.

EXPERIMENTAL SETUP AND RESULTS

Dataset

In **Figure 3**, we can see the differences at each gleason grade groups in detail. The histopathological data in this article are provided by the Vancouver Prostate Center, which are collected from different medical institutions and process tissue microarray blocks. It should be noted that the prostate tissue microarray is gained from patients with a suspicion of having prostate cancer. For the training dataset, the Gleason-level determination of the core image of each tissue microarray is associated with the most prevalent and second prevalent Gleason grading of expert annotations.

Data Processing

The 2019 MICCAI Gleason Competition provides annotations from six experts, and the annotations provided by each expert are not necessarily complete. Fortunately, the annotation by all annotators completely covers all the data. Therefore, using these annotations becomes a primary challenge. All TMA core images are annotated as benign and Gleason patterns 3, 4, and 5. Six pathologists drew regions (closed contours) on pathological images and labeled each area with grades. Although all of the TMA core images are annotated in detail by pathologists, none of them is complete. There are even two images in the expert's annotation without a corresponding image in the training set. However, one real tag is needed for network training; we need to merge the tags of six experts to enhance the robustness. Only four of the six pathologists label all the images, while the other two pathologists label only 191 and 92 images. To make better use of all expert annotations, we use the STAPLE algorithm to build the finally "ground truth label" *via* merging the annotations provided by multiple annotators.

Implementation and Data Augmentation

To demonstrate the effectiveness of our method, we participate the MICCAI Gleason 2019 Challenge[1]. A total of 331 images (including 224 train images and 87 test images) are used from tissue microarray blocks. These images are manually annotated by professional dermatologists.

We use PyTorch for the distributed parallel training of algorithmic models on an Ubuntu high-performance graphic workstation. The learning rate decay strategy is $\eta = \eta_0(1 - \frac{n}{N})^{\beta}$,

[1]Competition website: https://Gleason2019.grand-challenge.org/Home/

where $\eta_0 = 0.002$ is the initial learning rate, n is the current training rounds, $N = 200$ is the total training rounds, and $\beta = 0.9$.

Due to the large size of the prostate pathological slice image, it cannot be directly input to the network for learning. In this paper, we directly scale the short side of the input image to a size of 1,024 pixels and then randomly crop an 800×800 image patch as the input of the network. All samples are divided into five parts (each subset has an approximately equal number of samples). We repeat the entire process five times to avoid possible deviation of dataset partition during cross-validation. The final results are calculated by averaging five group results. To avoid network overfitting caused by insufficient data, we propose a data augmentation technique by randomly resizing and mirror training datasets.

Evaluation Metrics

Performance metrics such as accuracy, mean, entropy, and standard deviation were used to evaluate performance. In this article, we evaluate the network performance through the evaluation metrics such as the distance similarity coefficient (DSC), Jaccard Index (JA), Hausdorff distance (HD), Cohen's kappa coefficient, and F1 score.

The distance similarity coefficient (DSC) is defined as follows:

$$\mathrm{DSC} = \frac{2|A \cap B|}{|A| + |B|} \tag{2}$$

where $|\cdot|$ represents a set of pixels, and A and B represent the real label and segmentation result, respectively. The Hausdorff distance (HD) is defined as follows:

$$\mathrm{HD}\,(X_S, Y_S) = \max\left(h(X_S, Y_S),\ h(Y_S, X_S)\right) \tag{3}$$

where X_S and Y_S represent the point set of the real label and the segmentation result, respectively. $h(X_S, Y_S)$ and $h(Y_S, X_S)$ can be calculated as follows:

$$h(X_S, Y_S) = \max_{x_i \in X_S} \min_{y_j \in Y_S} ||x_i - y_j|| \tag{4}$$

$$h(Y_S, X_S) = \max_{y_j \in Y_S} \min_{x_i \in X_S} ||y_j - x_i|| \tag{5}$$

where $\|\cdot\|$ represents Euclidean distance. The average surface distance is another distance evaluation index. The lower the HD value, the better the network performance. Cohen's kappa efficient k is defined as follows:

$$\kappa = \frac{p_0 - p_e}{1 - p_e} \tag{6}$$

Where p_0 is the relative scoring consistency of raters, and p_e refers to the observed data used to calculate the hypothetical probability. If the scores of the two scores are the same, then $\kappa = 1$.

$$\mathrm{Precision} = \frac{\mathrm{TP}}{\mathrm{TP} + \mathrm{FP}} \tag{7}$$

$$\mathrm{Recall} = \frac{\mathrm{TP}}{\mathrm{TP} + \mathrm{FN}} \tag{8}$$

$$\mathrm{JA} = \frac{\mathrm{TP}}{\mathrm{TP} + \mathrm{FN} + \mathrm{FP}} \tag{9}$$

$$F_1 = 2\frac{precision \times recall}{precision + recall} \tag{10}$$

where TN, TP, FN, and FP represent true negative, true positive, false negative, and false positive, respectively.

2019 MICCAI Automatic Prostate Gleason Grading Challenge

The 2019 MICCAI prostate grading challenge provides a unique dataset and strict evaluation conditions of Gleason grading for the challenging task. During the experiment, each region in the pathological section is mapped to the Gleason's mode, and the low-level mode corresponds to the nearly normal prostate tumor. The differentiation level with the largest area is registered as the most important differentiation value, while the differentiation level with the second largest area is registered as the secondary differentiation value. The third largest or less than 5% minority is ignored. The prostate grading challenge includes two different tasks. One is the prediction of pixel-level Gleason grade, the other one is the prediction of core-level Gleason grade. Task 1 is regarded as a segmentation task, and we utilize PSPNet to accomplish this task. For task 2, we do not train a different network but provide a prediction of task 1 according to the Gleason grading system.

1) Pixel-Level Gleason Grade Prediction

In the first task of this competition, the content is segmented into four pathological sections of different Gleason patterns. The evaluation metrics in this task provided by the competition-organizing committee are a combination of F1 scores and Cohen's kappa coefficient. The coefficient is considered as an agreement to evaluate reliability and generally accepted to be a more robust measure rather than simple percent calculation. We use this combination score formula to calculate the final score on each test image. **Table 1** shows the predicted results of the pixel-level Gleason grade (note that the data in **Table 1** can be found on the official website of the competition). **Figure 4** shows T-SNE visualization with four-Gleason grading using our proposed method.

2) Core-Level Gleason Grade Prediction

In the second task of this competition, the content is transformed from the segmentation of pathological sections to the classification of different Gleason patterns. To achieve automatic Gleason classification of prostate pathological images, we focus on not only segmentation but also the effect of network grading. We are interested in screening benign plaques from all biopsy pathological tissues. In addition, we focus more on distinguishing between high-grade cancers (Grades 4, 5) and low-grade cancers (Grade 3). Task 2 classifies and grades Gleason according to the results of task 1. Its classification effect is far more than that of the direct classification of pathological sections. Ignoring the background part of the image in the pixel-level Gleason grading result, we get the Gleason grading

TABLE 1 | Task 1: pixel-level Gleason grade prediction.

Rank	Team	Score
10	qq604395564	0.643761
9	jpviguerasguillen	0.649812
8	AlirezaFatemi	0.712537
7	XiaHua	0.716059
6	cvblab	0.757838
5	sdsy888	0.759776
4	zhangjingmri	0.778061
3	ternaus	0.789663
2	nitinsinghal	0.792585
1	Ours	0.845152

result with the largest proportion in the image. By comparing the predicted results with the direct calculation of the image-level Gleason grading results, we can analyze the image-level Gleason grading performance of each network. To verify the superiority of automatic grading of our network, we list the confusion matrix results of the top four contests. **Figure 5** lists the confusion matrix results for different teams. Note that the confusion matrix is derived from the whole training and test dataset on the Gleason grade group.

In **Figure 5**, the first line of the confusion matrix provided by group (a) shows that 95.94% of benign pixels are classified correctly; 0.07% of benign pixels are wrongly classified to grade 3, 0.98% to grade 4, and 3.00% to grade 5. From **Table 1** and **Figure 5**, we can see that our method consistently obtains good results in terms of the listed evaluation metrics and achieves the best segmentation results. Given the validity and reliability of the Gleason grading system in the detection and diagnosis of prostate cancer, our results are useful to the medical community in prostate cancer diagnosis.

Comparison of Different Methods

For the training of the deep neural network, the amount of image information is associated with the size and number of input images. However, in the process of network training, the increase in network depth may bring additional optimization problems. According to the previous literature (38), FCN based on the residual network solves this problem *via* skipping connection in each block. We compare the four proposed different classical semantic segmentation networks, i.e., FCN (22), SegNet (39), U-Net (40), and DeepLabv3 (41), to verify the segmentation performance. The results are reported in **Table 2**.

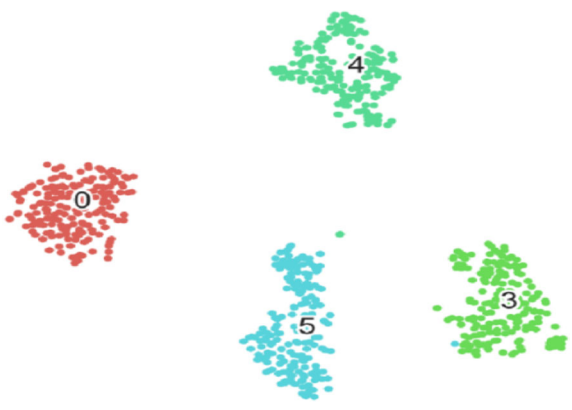

FIGURE 4 | Our proposed method for T-SNE visualization with four-Gleason grading, where 0 represents benignity and 3, 4, and 5 represent Gleason grading 3, 4, and 5, respectively.

To maintain consistency, we compare the three networks based on ResNet or with a network structure like ResNet in our prediction of pixel-level Gleason grade and core-level Gleason grades. During the experiment, we quantify Cohen's quadratic kappa statistics to compare the consistency among pathologists, and the annotator consistency between models and pathologists. The comparison of pixel-level grade prediction of different methods is shown in **Table 3**.

As the doctors are concerned about the benignity and the malignancy of tumors at actual clinical practice, they are interested to make the distinction between high-risk cancer (Gleason patterns 4, 5) and low-risk cancer (Gleason pattern 3). Also, the classification results are based on high and low scores. Comparing the prediction results with the real labels, the core-level Gleason classification performance of each network is shown in **Table 4**. The comparative results of the proposed method with several recently proposed methods are reported in **Table 5**.

From **Table 3**, we can know that the PSPNet used in this study is superior to other comparative methods, which is consistent with the scores of six experts (calculated by Cohen's kappa coefficient k) or the macro-average and micro-average F1 scores. On the test cohort, the minimum and maximum k of each of the six experts respectively scored by PSPNet are 0.23 and 0.62, while the minimum and maximum k between the six experts are 0.38 and 0.70. Therefore, the consistency of the PSPNet score between each expert and Gleason grade at the pixel level is within the consistency range of these six experts' scores.

As is shown in **Tables 4**, **5**, the proposed PSPNet achieves the best performance with respect to various evaluation metrics for distinguishing benign from malignant. For distinguishing high and low score tumors, most performance metrics of the methods listed in the table are reduced, indicating that more difficulty existed to identify the high and low score tumors. However, PSPNet still acquires the best result, which further illustrates the stability and reliability of the method.

DISCUSSION

There may be numerous ways to improve this model, ranging from the overall architecture to the sampling of data. Despite the promising results of our model, it is not guaranteed that the application of this model in actual disease diagnosis leaves no room for errors. In this case, the tumor must be removed as far as possible without damaging other healthy tissue.

Regarding task 2 core level prediction, we have not directly calculated it. The final predicted results will be submitted to the evaluation platform, and the competition organizers will conduct

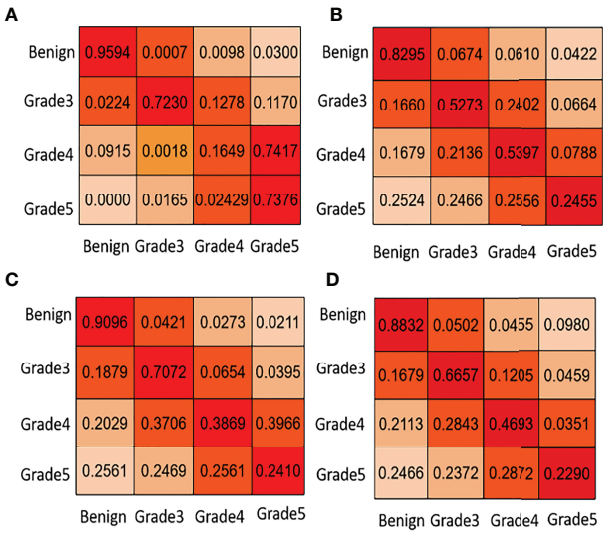

FIGURE 5 | Task 2: core-level Gleason grade prediction. We list some confusion matrix results for different teams in this figure. **(A)** PSPNet (Our), **(B)** U-net++ (Ni), **(C)** U-net++ (Ternaus), **(D)** U-net (Zhang).

experimental evaluation. From **Figure 5**, other participants have poor predictions on Gleason 5 and miss many high-scoring tumors, while the PSPNet method we use could detect Gleason 5 tumors well, but the discrimination between Gleason 3 and 4 is not good enough.

We also discuss the poor results of Gleason grade 4 with many experts and scholars and draw a conclusion that there is a certain randomness in the testing data selected in the experimental evaluation (Gleason grade 4 and Gleason grade 5 are very similar in shape), and the error rate of estimation is very high. However, pathologists believed that Gleason grade 4 and Gleason grade 5 are high-risk grades, which threatens the health and prognosis of patients. Although PSPNet achieves the lowest prediction accuracy of Gleason grade 4 at the core level, the automatic grading of prostate pathological images is not affected.

To effectively improve the diagnostic accuracy of the disease, we use a novel model to automatically grade digital prostate cancer histopathology. To prove the superiority of the proposed network, we extract feature maps from the residuals and visualize them, as shown in **Figure 6**; we can observe that our method effectively preserves the original input image information.

Compared to other teams, PSPNet performs the best among the submissions in MICCAI Automatic Prostate Gleason Grading Challenge 2019. All dynamic selections are automatically determined by PSPNet. The overall static design and dynamic selection are based on rules determined by our expertise in the field. These segmentation results of some challenging and representative samples are shown in **Figure 7**.

TABLE 2 | Results of different network models (boldface denotes best performance).

Model	DSC	kappa	JA	Score	HD
FCN (22)	0.784	0.753	0.728	0.717	0.312
U-Net (40)	0.812	0.774	0.742	0.757	0.266
SegNet (39)	0.833	0.788	0.751	0.732	0.242
DeepLabv3 (41)	0.859	0.814	0.821	0.798	0.213
PSPNet (ours)	**0.871**	**0.847**	**0.836**	**0.827**	**0.190**

Bold values represents the best performance.

TABLE 3 | Pixel-level Gleason grade prediction of different methods.

Method	κ	F_{macro}	F_{micro}
FCN (22)	0.504 ± 0.128	0.605 ± 0.185	0.835 ± 0.126
DeepLabv3 (41)	0.438 ± 0.119	0.549 ± 0.188	0.773 ± 0.165
PSPNet (ours)	**0.524 ± 0.135**	**0.634 ± 0.198**	**0.839 ± 0.133**

Bold values represents the best performance.

TABLE 4 | Core-level Gleason grade prediction of different methods.

Method	Benign VS. malignant				Gleason 3 VS. Gleason 4 and 5			
	Accuracy	Precision	Sensitivity	Specificity	Accuracy	Precision	Sensitivity	Specificity
FCN (39)	0.925	0.963	0.954	0.714	0.813	0.904	0.801	0.835
DeepLabv3 (41)	0.902	0.944	0.944	0.600	0.729	0.840	0.734	0.718
PSPNet (ours)	**0.934**	**0.972**	**0.954**	**0.869**	**0.836**	**0.904**	**0.831**	**0.846**

Bold values represents the best performance.

TABLE 5 | Comparison of the proposed method with several recently proposed methods.

Method	Benign VS. malignant			Gleason 3 VS. Gleason 4 and 5		
	Accuracy	Sensitivity	Specificity	Accuracy	Sensitivity	Specificity
Arvaniti et al. (42)	0.82	0.85	0.79	0.77	0.81	0.74
Nagpal et al. (43)	0.81	0.81	0.79	0.76	0.77	0.74
Davood et al. (44)	0.85	0.86	0.85	0.82	0.82	0.82
Ours	**0.94**	**0.96**	**0.87**	**0.84**	**0.83**	**0.85**

Bold values represents the best performance.

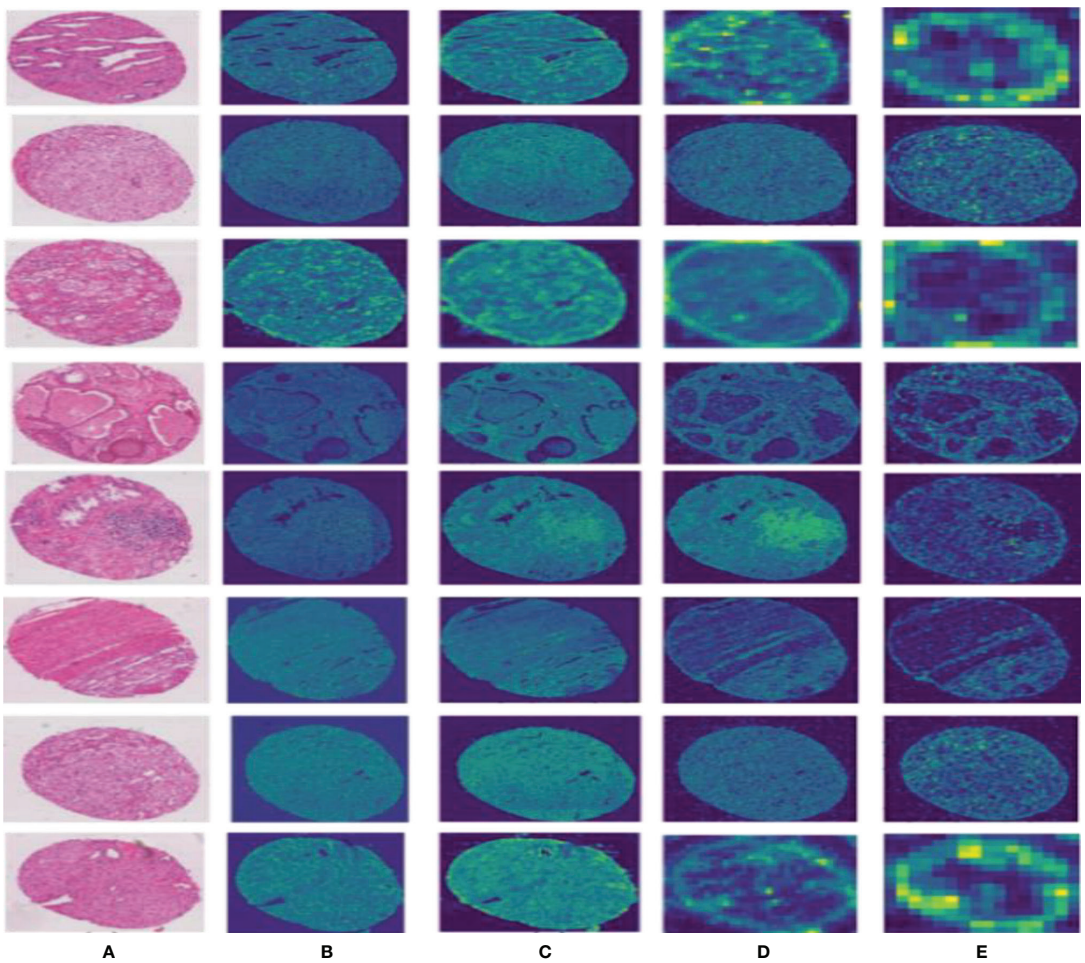

FIGURE 6 | Results of the feature map visualization. Column **(A)** is the input image; columns **(B–E)** show that feature maps are obtained *via* four convolutional layers in PPM, respectively.

PSPNet can effectively learn multi-scale features to accurately classify prostate pathological images automatically. Even though this method has achieved good segmentation results, it still has some shortcomings. The main drawback of our method is that our training dataset is not enough for disease diagnosis for medical image analysis. Although the original data set has been increased 5-fold by data enhancement technology, we are still unable to guarantee its complete application to feature learning of deep neural networks. What is more, our method cannot segment some images well, as shown in **Figure 8**. We can observe that the three categories of Grade 3, Grade 4, and Grade 5 are easily confused.

Our proposed network can easily distinguish benign from malignant, but the differentiation of Gleason grades 3, 4, and 5 is insufficient. We consider that this may be related to the imbalance of the data distribution of each score in the dataset. In our training data, Gleason 5 has a small amount of data, so there are some errors in the results of network learning.

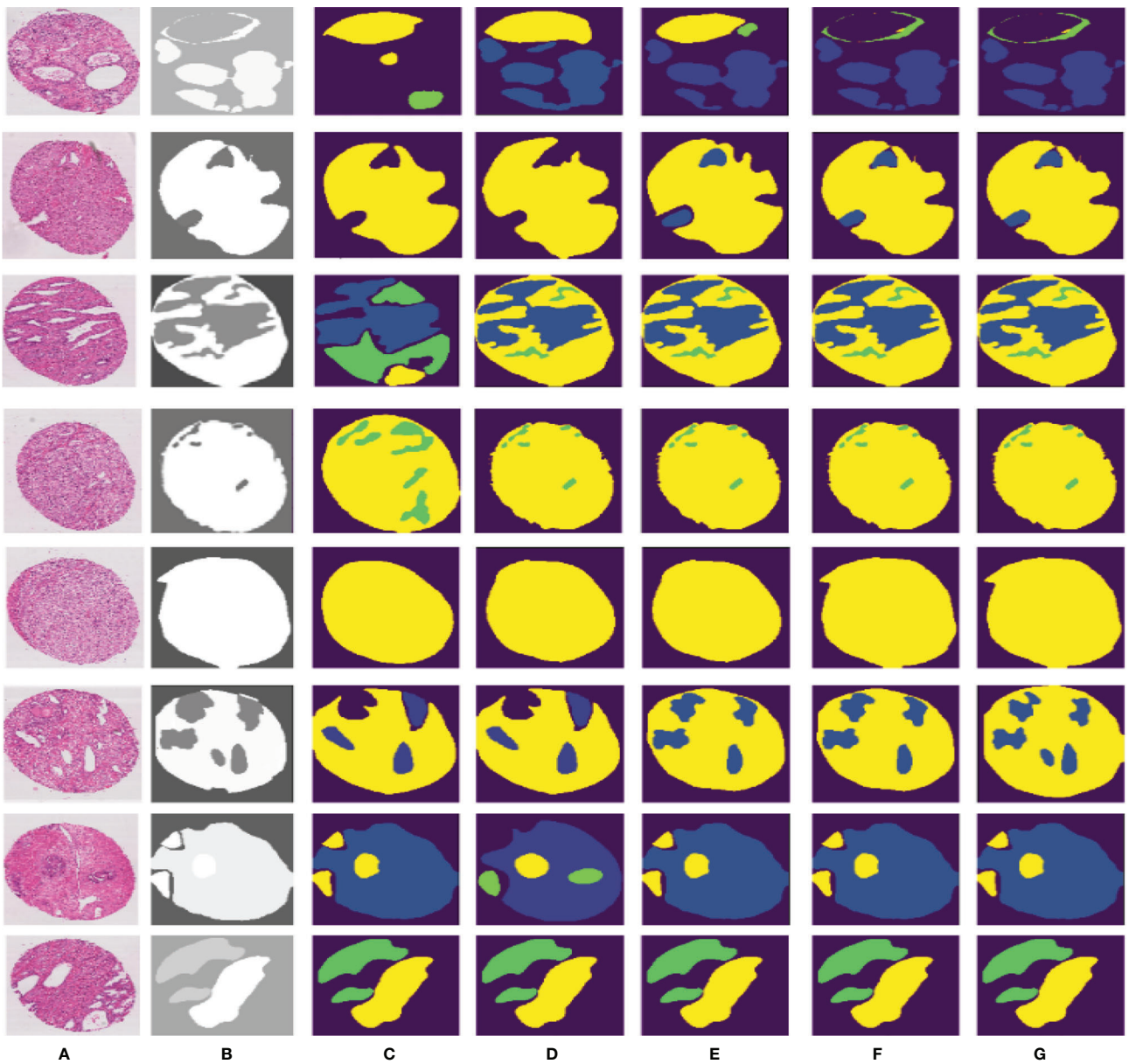

FIGURE 7 | Different segmentation results from FCN, SegNet, U-Net, DeepLabv3, and our proposed method. Column **(A)** is the input image, column **(B)** is the final expert annotation used by the sample algorithm, and columns **(C–G)** indicate the final segmentation results of FCN, SegNet, U-Net, DeepLabv3, and PSPNet, respectively.

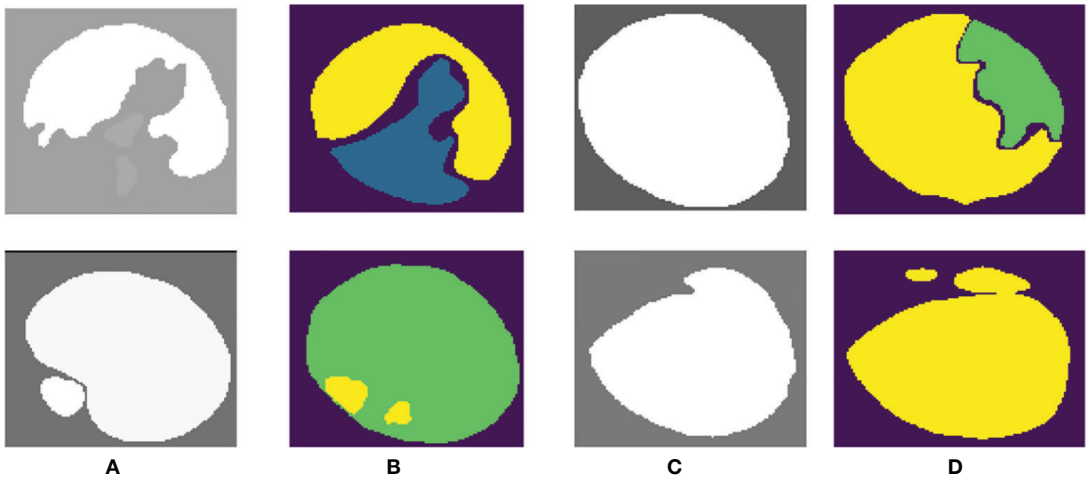

FIGURE 8 | Poor-performing images using our method. Columns **(A, C)** are the "ground truth", and columns **(B, D)** are the final segmentation result.

CONCLUSION

In this paper, we propose a new automatic identification system for prostate biopsy tissues and use the STAPLE algorithm to synthesize different expert labels. The results based on cross validation show that our method achieves promising results in classification performance. The system could potentially improve the prognosis of prostate cancer and is highly consistent with the reference standard.

In the future work, some improvements could be taken into account from several sides. First, our approach puts particular emphasis on using image features as input to the network model. However, this handcrafted feature limits the richness of image structure information. To make the most of the power of the convolutional network model to acquire image features, fusing the hand-crafted features from original data and using more advanced network models to devise our framework could be tried. Second, we can bring other sophisticated factors into the proposed framework to potentially improve performance. Finally, we need to suggest to better integrate deep learning systems with the diagnosis processes of pathologists, and the impact of this artificial intelligence-based auxiliary method on the overall efficiency, accuracy, and prognosis of Gleason's score in clinical practice.

DATA AVAILABILITY STATEMENT

Publicly available datasets were analyzed in this study. These data can be found in the following competition website: https://Gleason2019.grand-challenge.org/Home/.

AUTHOR CONTRIBUTIONS

YQ and YH wrote the programs, performed the data analysis, and drafted the manuscript. PK, HX, and XZ helped to check the contours. TW, JC, and BL guided the study and participated in the discussions and preparation of the manuscript. All authors read, discussed, and approved the final manuscript, and conceived the study design.

FUNDING

This work was partly supported by National Natural Science Foundation of China (Nos.81771922, 62071309, 61801305, 62006160, 81971585, 62106153 and 61871274), National Natural Science Foundation of Guangdong Province (No.2019A1515111205), Shenzhen Key Basic Research Project (Nos. JCYJ20170818094109846, JCYJ20180507184647636, JCYJ20190808155618806, GJHZ20190822095414576, and JCYJ20190808145011259).

ACKNOWLEDGMENTS

Thanks are given to the Organizing Committee for providing an excellent platform.

REFERENCES

1. Allsbrook WC Jr, Mangold KA, Johnson MH, Lane RB, Lane CG, Epstein JI, et al. Interobserver Reproducibility of Gleason Grading of Prostatic Carcinoma: Urologic Pathologists. *Hum Pathol* (2001) 32(1):81–8. doi: 10.1053/hupa.2001.21135
2. Schröder FH, Hugosson J, Roobol MJ, Tammela TLJ, Auvinen A. Prostate-Cancer Mortality at 11 Years of Follow-Up. *N Engl J Med* (2012) 366(11):981–90. doi: 10.1056/NEJMoa1113135
3. Freddie BJF, Isabelle S. Global Cancer Statistics 2018: GLOBOCAN Estimates of Incidence and Mortality Worldwide for 36 Cancers in 185 Countries. *CA: A Cancer J Clin* (2018) 68:394–424. doi: 10.3322/caac.21492

4. Cooperberg MR, Broering JM, Carroll PR. Time Trends and Local Variation in Primary Treatment of Localized Prostate Cancer. *J Clin Oncol Off J Am Soc Clin Oncol* (2010) 28(7):1117–23. doi: 10.1200/JCO.2009.26.0133
5. Bulten W, Pinckaers H, Hulsbergen-van de Kaa C, Litjens G. Automated Gleason Grading of Prostate Biopsies Using Deep Learning. *Modern Pathol* (2020) 21:233–41. doi: 10.1016/S1470-2045(19)30739-9
6. Bailar JCI, Mellinger G, Gleason D. Survival Rates of Patients With Prostatic Cancer, Tumor Stage, and Differentiation-Preliminary Report. *Cancer Chemother Rep Part* (1966) 50(3):129–36.
7. Gleason DF. Classification of Prostatic Carcinomas. *Cancer Chemother Rep* (1966) 50:125–8.
8. Mellinger GT, Gleason D, Rd BJ. The Histology and Prognosis of Prostatic Cancer. *J Urol* (1967) 97(2):331–7. doi: 10.1016/S0022-5347(17)63039-8
9. Ornstein David K. *Pathology and Genetics: Tumours of the Urinary System and Male Genital Organs*. Hagerstown, MD, USA:Wolters Kluwer Health Inc. (2004).
10. Bjartell A. The 2005 International Society of Urological Pathology (ISUP) Consensus Conference on Gleason Grading of Prostatic Carcinoma. *Am J Surg Pathol* (2006) 29(9):1228–42. doi: 10.1097/01.pas.0000173646.99337.b1
11. Hossfeld DK. World Health Organization Classification of Tumors: Pathology and Genetics of Tumors of Haematopoietic and Lymphoid Tissues. *Ann Oncol* (2002) 13(3):490. doi: 10.1093/annonc/mdf146
12. Berg KD, Thomsen FB, Nerstrøm C, Røder MA, Iversen P, Toft BG, et al. The Impact of the 2005 International Society of Urological Pathology Consensus Guidelines on Gleason Grading - A Matched-Pair Analysis. *BJU Int* (2016) 117(6):883–9. doi: 10.1111/bju.13439
13. Epstein JI, Egevad L, Amin MB, Delahunt B, Rodrigues G. The 2014 International Society of Urological Pathology (ISUP) Consensus Conference on Gleason Grading of Prostatic Carcinoma. *Am J Surg Pathol* (2015) 40:758–9. doi: 10.1097/PAS.0000000000000530
14. Wang Y, Dou H, Hu X, Zhu L, Yang X, Xu M, et al. Deep Attentive Features for Prostate Segmentation in 3D Transrectal Ultrasound. *IEEE Trans Med Imaging* (2019) 38:2768–78. doi: 10.1109/TMI.2019.2913184
15. Bulten W, Balkenhol M, Belinga J-JA, Brilhante A, Çakır A, Egevad L, et al. Artificial Intelligence Assistance Significantly Improves Gleason Grading of Prostate Biopsies by Pathologists. *Modern Pathol* (2021) 34(3):660–71. doi: 10.1038/s41379-020-0640-y
16. Nagpal K, Foote D, Tan F, Liu Y, Chen P-HC, Steiner DF, et al. Development and Validation of a Deep Learning Algorithm for Gleason Grading of Prostate Cancer From Biopsy Specimens. *JAMA Oncol* (2020) 6(9):1372–80. doi: 10.1001/jamaoncol.2020.2485
17. Yuan Y, Wang J, Li B, Meng MQ-H. Saliency Based Ulcer Detection for Wireless Capsule Endoscopy Diagnosis. *IEEE Trans Med Imaging* (2015) 34 (10):2046–57. doi: 10.1109/TMI.2015.2418534
18. Li Y, Huang M, Zhang Y, Chen J, Xu H, Wang G, et al. Automated Gleason Grading and Gleason Pattern Region Segmentation Based on Deep Learning for Pathological Images of Prostate Cancer. *IEEE Access* (2020) 8:117714–25. doi: 10.1109/ACCESS.2020.3005180
19. Yang X, Yu L, Li S, Wen H, Luo D, Bian C, et al. Towards Automated Semantic Segmentation in Prenatal Volumetric Ultrasound. *IEEE Trans Med Imaging* (2018) 38(1):180–93. doi: 10.1109/TMI.2018.2858779
20. Dou Q, Chen H, Yu L, Zhao L, Qin J, Wang D, et al. Automatic Detection of Cerebral Microbleeds From MR Images via 3D Convolutional Neural Networks. *IEEE Trans Med Imaging* (2016) 35(5):1182–95. doi: 10.1109/TMI.2016.2528129
21. Liu J, Xu B, Chi Z, Gong Y, Jon G, Daniele S, et al. An End-To-End Deep Learning Histochemical Scoring System for Breast Cancer TMA. *IEEE Trans Med Imaging* (2018) 38:617–28.
22. Long J, Shelhamer E, Darrell T. Fully Convolutional Networks for Semantic Segmentation. In: *Proceedings of the IEEE Conference on Computer Vision and Pattern Recognition*. Boston, MA, USA: IEEE (2015). p. 3431–40. doi: 10.1109/TMI.2018.2868333
23. Liu W, Rabinovich A, Berg AC. ParseNet: Looking Wider to See Better. *Comput Sci*. Boston, MA, USA (2015). doi: 10.48550/arXiv.1506.04579
24. Noh H, Hong S, Han B. Learning Deconvolution Network for Semantic Segmentation. In: *2015 IEEE International Conference on Computer Vision (ICCV)*. Santiago, Chile: IEEE Computer Society (2015). doi: 10.1109/iccv.2015.178.
25. Gandomkar Z, Brennan PC, Mello-Thoms C. MuDeRN: Multi-Category Classification of Breast Histopathological Image Using Deep Residual Networks. *Artif Intell Med* (2018) 88:14–24. doi: 10.1016/j.artmed.2018.04.005
26. Talo M. Automated Classification of Histopathology Images Using Transfer Learning. *Artif Intell Med* (2019) 101:101743–. doi: 10.1016/j.artmed.2019.101743
27. Vaswani A, Shazeer N, Parmar N, Uszkoreit J, Jones L, Gomez AN, et al. Attention Is All You Need. In: *Advances in Neural Information Processing Systems*. Long Beach, CA, USA:MIT Press (2017). p. 5998–6008.
28. Warfield SK, Zou KH, Wells WM. Simultaneous Truth and Performance Level Estimation (STAPLE): An Algorithm for the Validation of Image Segmentation. *IEEE Trans Med Imaging* (2004) 23(7):903. doi: 10.1109/TMI.2004.828354
29. Jung H, Choi M-K, Jung J, Lee J-H, Kwon S, Young Jung W. ResNet-Based Vehicle Classification and Localization in Traffic Surveillance Systems. In: *Proceedings of the IEEE Conference on Computer Vision and Pattern Recognition Workshops*. Honolulu, HI, USA: IEEE (2017). p. 61–7.
30. Simonyan K, Zisserman A. Very Deep Convolutional Networks for Large-Scale Image Recognition. In: *Proceedings of the IEEE Conference on Computer Vision and Pattern Recognition*. Columbus, OH, USA: IEEE (2014).
31. He K, Zhang X, Ren S, Sun J. Deep Residual Learning for Image Recognition. In: *Proceedings of the IEEE Conference on Computer Vision and Pattern Recognition*. Las Vegas, Nevada: IEEE (2016). p. 770–8.
32. Huang G, Liu Z, van der Maaten L, Weinberger KQ. Densely Connected Convolutional Networks. In: *Proceedings of the IEEE Conference on Computer Vision and Pattern Recognition*. Honolulu, HI, USA: IEEE (2017). p. 4700–8.
33. Lee CY, Gallagher PW, Tu Z. Generalizing Pooling Functions in Convolutional Neural Networks: Mixed, Gated, and Tree. *Comput Sci* (2015) 3:464–72.
34. Betro B, Guglielmi A. Methods for Global Prior Robustness Under Generalized Moment Conditions. In: *Robust Bayesian Analysis*. Springer (2000). p. 273–93.
35. Polson NG, Scott JG. On the Half-Cauchy Prior for a Global Scale Parameter. *Bayesian Anal* (2012) 7(4):887–902. doi: 10.1214/12-BA730
36. Zhao H, Shi J, Qi X, Wang X, Jia J. Pyramid Scene Parsing Network. In: *Proceedings of the IEEE Conference on Computer Vision and Pattern Recognition*. Honolulu, HI, USA: IEEE (2017). p. 2881–90.
37. Yu B, Yang L, Chen F. Semantic Segmentation for High Spatial Resolution Remote Sensing Images Based on Convolution Neural Network and Pyramid Pooling Module. *IEEE J Selected Topics Appl Earth Observations Remote Sens* (2018) 11(9):3252–61. doi: 10.1109/JSTARS.2018.2860989
38. Garcia-Garcia A, Orts-Escolano S, Oprea S, Villena-Martinez V, Garcia-Rodriguez J. A Review on Deep Learning Techniques Applied to Semantic Segmentation. In: *Proceedings of the IEEE Conference on Computer Vision and Pattern Recognition*. Honolulu, HI, USA: IEEE (2017).
39. Badrinarayanan V, Kendall A, Cipolla R. Segnet: A Deep Convolutional Encoder-Decoder Architecture for Image Segmentation. *IEEE Trans Pattern Anal Mach Intell* (2017) 39(12):2481–95. doi: 10.1109/TPAMI.2016.2644615
40. Ronneberger O, Fischer P, Brox T. U-Net: Convolutional Networks for Biomedical Image Segmentation. In: *International Conference on Medical Image Computing and Computer-Assisted Intervention*. Springer (2015). p. 234–41.
41. Chen L-C, Papandreou G, Schroff F, Adam H. Rethinking Atrous Convolution for Semantic Image Segmentation. *arXiv preprint arXiv:.05587*. Honolulu, HI, USA: IEEE (2017). doi: 10.48550/arXiv.1706.05587
42. Arvaniti E, Fricker KS, Moret M, Rupp N, Hermanns T, Frankhauser C, et al. Automated Gleason Grading of Prostate Cancer Tissue Microarrays via Deep Learning. *Sci Rep* (2018) 8(1):1–11. doi: 10.1038/s41598-018-30535-1
43. Nagpal K, Foote D, Liu Y, Chen P-HC, Wulczyn E, Tan F, et al. Development and Validation of a Deep Learning Algorithm for Improving Gleason Scoring of Prostate Cancer. *NPJ Digital Med* (2019) 2(1):1–10. doi: 10.1038/s41746-019-0112-2
44. Karimi D, Nir G, Fazli L, Black PC, Goldenberg L, Salcudean SE. Deep Learning-Based Gleason Grading of Prostate Cancer From Histopathology Images-Role of Multiscale Decision Aggregation and Data Augmentation. *IEEE J Biomed Health Inf* (2019) 2:1–10. doi: 10.1109/JBHI.2019.2944643

Conflict of Interest: The authors declare that the research was conducted in the absence of any commercial or financial relationships that could be construed as a potential conflict of interest.

Publisher's Note: All claims expressed in this article are solely those of the authors and do not necessarily represent those of their affiliated organizations, or those of the publisher, the editors and the reviewers. Any product that may be evaluated in

this article, or claim that may be made by its manufacturer, is not guaranteed or endorsed by the publisher.

Copyright © 2022 Qiu, Hu, Kong, Xie, Zhang, Cao, Wang and Lei. This is an open-access article distributed under the terms of the Creative Commons Attribution License (CC BY). The use, distribution or reproduction in other forums is permitted, provided the original author(s) and the copyright owner(s) are credited and that the original publication in this journal is cited, in accordance with accepted academic practice. No use, distribution or reproduction is permitted which does not comply with these terms.

frontiers | Frontiers in Oncology

ORIGINAL RESEARCH
published: 19 April 2022
doi: 10.3389/fonc.2022.855188

Bone Marrow-Derived Stem Cell Factor Regulates Prostate Cancer-Induced Shifts in Pre-Metastatic Niche Composition

*Brittni M. Foster[1], Lihong Shi[1], Koran S. Harris[1], Chirayu Patel[1], Victoria E. Surratt[1], Kendall L. Langsten[1] and Bethany A. Kerr[1,2]**

[1] Department of Cancer Biology, Wake Forest School of Medicine, Winston-Salem, NC, United States, [2] Wake Forest Baptist Comprehensive Cancer Center, Winston-Salem, NC, United States

Skeletal metastasis is the leading cause of morbidity and mortality in prostate cancer, with 80% of advanced prostate cancer patients developing bone metastases. Before metastasis, bone remodeling occurs, stimulating pre-metastatic niche formation and bone turnover, and platelets govern this process. Stem cell factor (SCF, Kit Ligand) is increased in advanced prostate cancer patient platelet releasates. Further, SCF and its receptor, CD117/c-kit, correlate with metastatic prostate cancer severity. We hypothesized that bone-derived SCF plays an important role in prostate cancer tumor communication with the bone inducing pre-metastatic niche formation. We generated two cell-specific SCF knockout mouse models deleting SCF in either mature osteoblasts or megakaryocytes and platelets. Using two syngeneic androgen-insensitive murine prostate cancer cell lines, RM1 (*Ras* and *Myc* co-activation) and mPC3 (*Pten* and *Trp53* deletion), we examined the role of bone marrow-derived SCF in primary tumor growth and bone microenvironment alterations. Platelet-derived SCF was required for mPC3, but not RM1, tumor growth, while osteoblast-derived SCF played no role in tumor size in either cell line. While exogenous SCF induced proangiogenic protein secretion by RM1 and mPC3 prostate cancer cells, no significant changes in tumor angiogenesis were measured by immunohistochemistry. Like our previous studies, tumor-induced bone formation occurred in mice bearing RM1 or mPC3 neoplasms, demonstrated by bone histomorphometry. RM1 tumor-bearing osteoblast SCF knockout mice did not display tumor-induced bone formation. Bone stromal cell composition analysis by flow cytometry showed significant shifts in hematopoietic stem cell (HSC), mesenchymal stem cell (MSC), and osteoblast cell percentages in mice bearing RM1 or mPC3 tumors. There were no significant changes in the percentage of macrophages, osteoclasts, or osteocytes. Our study demonstrates that megakaryocyte/platelet-derived SCF regulates primary mPC3 tumor growth, while SCF originating from osteoblasts plays a role in bone marrow-derived progenitor cell composition and pre-metastatic niche formation. Further, we show that both the source of SCF and the genetic profile of prostate cancer determine the effects of SCF. Thus, targeting the SCF/CD117 signaling axis with tyrosine kinase inhibitors could

OPEN ACCESS

Edited by:
Tanya I. Stoyanova, Stanford University, United States

Reviewed by:
Shiqin Liu, Stanford University, United States
Natasha Kyprianou, Icahn School of Medicine at Mount Sinai, United States

***Correspondence:**
Bethany A. Kerr
bkerr@wakehealth.edu

Specialty section:
This article was submitted to Genitourinary Oncology, a section of the journal Frontiers in Oncology

Received: *14 January 2022*
Accepted: *18 March 2022*
Published: *19 April 2022*

Citation:
Foster BM, Shi L, Harris KS, Patel C, Surratt VE, Langsten KL and Kerr BA (2022) Bone Marrow-Derived Stem Cell Factor Regulates Prostate Cancer-Induced Shifts in Pre-Metastatic Niche Composition. Front. Oncol. 12:855188. doi: 10.3389/fonc.2022.855188

affect primary prostate carcinomas or play a role in reducing bone metastasis dependent on the gene deletions or mutations driving the patients' prostate cancer.

Keywords: stem cell factor, CD117/c-kit, prostate cancer, bone microenvironment, platelet, osteoblast

INTRODUCTION

Skeletal metastasis is the leading cause of prostate cancer patient morbidity and mortality (1). Once the primary tumor has mobilized to the bone, the patient survival rate drops to less than 30% (2, 3). Most advanced prostate cancer patients experience complications with skeletal metastases such as bone pain, fractures, and spinal cord compression. Bone metastasis remains incurable; therefore, finding molecular targets to prevent and treat metastasis is urgently needed. The mechanism of prostate cancer metastasis to the bone is still unknown. However, active communication between the tumor and bone microenvironment is demonstrated by an increased bone formation that occurs prior to metastasis (4, 5).

The bone formation that occurs before the identification of measurable prostate cancer metastatic lesions results in the stimulation of osteoblasts and inhibition of osteoclasts. During homeostasis within the bone niche, there exists a balance between activation of the bone-forming cells, osteoblasts, and bone-resorbing cells, osteoclasts (6). Imbalances such as those occurring during prostate cancer progression result in altered bone metabolism, with prostate cancer stimulating an increase in bone formation. Platelets regulate this tumor-induced bone formation. Depletion of platelets in both xenograft and murine allograft models inhibited bone formation (7). Coupled with prostate cancer-induced osteoblast activation and bone formation, platelet production increases in response to tumor growth (8–12). Further, tumor-induced bone formation requires platelet secretion and can be regulated by several tumor-derived proteins sequestered in platelets (13, 14). Defining the platelet-derived proteins controlling communication between the primary tumor and the bone prior to metastasis is key to fighting metastatic disease.

Platelet-derived stem cell factor (SCF, Kit Ligand, Steel Factor) correlated with prostate cancer severity (15). SCF is expressed in both the primary tumor and bone metastases, while its sole ligand CD117/c-kit demonstrates increased expression in bone metastases compared with primary tumors (16). CD117 expression is also found on prostate cancer circulating tumor cells and is associated with a stem cell-like phenotype (15, 17). Thus, the SCF/CD117 signaling axis may play a role in platelet-regulated prostate cancer bone formation and metastatic spread.

Platelet SCF is likely packaged by megakaryocytes or may be sequestered from stromal cells in the bone microenvironment. Many bone marrow cell types express SCF, including perivascular cells, endothelial cells, pericytes, mesenchymal stem cells (MSCs), osteoblasts, and stromal cells (18–21). SCF in the bone microenvironment functions as a hematopoietic cytokine maintaining hematopoietic stem cell (HSC) proliferation and enhancing the differentiation of megakaryocytes and osteoclasts (22). This intercommunication between osteoblasts, osteoclasts, and megakaryocytes through SCF regulates HSC homing, bone formation, and platelet production. Thus, the platelet-derived SCF found in prostate cancer patients could originate from osteoblasts or megakaryocytes to control tumor-induced bone formation and prostate cancer spread.

To ascertain whether osteoblast or megakaryocyte/platelet-derived SCF played a role in prostate cancer progression, we depleted SCF in osteoblasts *via* the osteocalcin promoter and in megakaryocytes/platelets *via* the platelet factor 4 promoter using a conditional knockout murine model. Using two syngeneic tumor allografts, we examined the effect of SCF depletion on primary tumor growth, angiogenesis, and bone pre-metastatic niche formation. We found that SCF from megakaryocytes/platelets affects primary tumor growth, while SCF from osteoblasts plays a role in stem cell mobilization and pre-metastatic niche formation.

MATERIALS AND METHODS

Cell Culture

Two murine prostate cancer cell lines, mPC3 and RM1, were used to study the effects of SCF. mPC3-luc (mPC3) murine prostate cancer cells were gifted by Dr. Zongbing You (Tulane University) and were generated by Dr. Zhenbang Chen (Meharry Medical College) (23, 24). The mPC3 cell line was generated from spontaneous tumors in probasin4-driven *Pten*$^{-/-}$;*Trp53*$^{-/-}$ mice. These cells are grown in DMEM with 200 μg/mL hygromycin B and 10% FBS. RM1-luc-effly-eGFP (RM1) cells were gifted by Dr. Yusuke Shiozawa (Wake Forest School of Medicine). The parental RM1 cells (RRID: CVCL_B459) were obtained from ATCC prior to transfection with the luciferase/eGFP construct. The RM1 cells were initially derived from spontaneous prostate tumors that developed in *Ras* and *Myc* mice. These cells are grown in DMEM, 10% FBS, and penicillin/streptomycin (100 U/mL and 100 μg/mL, respectively). All cell lines are tested regularly for mycoplasma.

2D Confluence Assay

To examine proliferation, cell confluence was tracked by live-cell imaging. RM1 or mPC3 cells were seeded in a 96 well plate in complete media at 1,000 cells/well. At the time of seeding, 50 ng/mL of murine recombinant SCF (STEMCELL, #78064) was added. The cells were incubated at 37°C. Bright-field images were taken using the IncuCyte ZOOM live-cell imaging and analysis platform (Sartorius) in the Cell Engineering Shared Resource every 2 hours until confluent. Media was changed every three days. Percent confluence over 74 hours was analyzed using the IncuCyte Software (Version 2016A).

Conditional Knockout Mouse Generation

Bone marrow SCF conditional knockout mice were generated in-house under approved Institutional Animal Care and Use Committee Protocols (A18-127, A15-194) at Wake Forest School of Medicine. To delete SCF (*Kitlg*) in megakaryocytes and platelets, the platelet factor 4 promoter (Cre-PF4) was used. To delete SCF in mature osteoblasts, the osteocalcin promoter (Cre-OC) was used. SCF floxed (RRID: IMSR_JAX:017861), Cre-PF4 (RRID: IMSR_JAX:008535), and Cre-OC (RRID: IMSR_JAX:019509) mice were purchased from Jackson Laboratory (Bar Harbor, MI) on a C57BL/6J background. Both conditional knockouts were generated by crossing $Cre^{+/-}$ mice with the SCF floxed mice to generate the F0 generation of $Cre^{+/-}SCF^{fl/-}$. This F0 generation was again crossed with $SCF^{fl/fl}$ to generate the F1 $Cre^{+/-}SCF^{fl/fl}$. Finally, to generate our knockout models, F1 was intercrossed to generate the $Cre\text{-}PF4^{-/-};SCF^{fl/fl}$ (PLT-WT), $Cre\text{-}OC^{-/-};SCF^{fl/fl}$ (OB-WT), $Cre\text{-}PF4^{+/-};SCF^{fl/fl}$ (PLTΔSCF), and $Cre\text{-}OC^{+/-};SCF^{fl/fl}$ (OBΔSCF) mice.

Tumor Growth

Male, 8-12-week-old knockout mice were bred and housed in the animal facilities at Wake Forest School of Medicine, fed a standard diet, and were on a standard light/dark cycle. All animal studies were approved by the Institutional Animal Care and Use Committee (Protocols A18-127, A15-221) at Wake Forest School of Medicine. Mice were anesthetized with isoflurane, and RM1 ($4x10^5$ cells) or mPC3 cells ($1x10^6$ cells) were injected subcutaneously on day 0. On day 11, mice were intraperitoneally injected with luciferin (150 mg/kg) to visualize tumor luciferase signal and then imaged using Perkin Elmer *In Vitro* Imaging System (IVIS) maintained by the Cell Engineering Shared Resource. Average radiance was analyzed using Living Image Software (Perkin Elmer). Tumors were allowed to grow for 12 days before sacrifice, and tumor weight and dimensions were measured. Tumor volume was calculated from caliper measurements using $V = (W^2 \times L)/2$ as the formula (25)

Angiogenesis Protein Array

To measure the secretion of angiogenesis-related proteins, conditioned media was collected from prostate cancer cells treated with SCF. RM1 or mPC3 cells were grown on 10 cm tissue culture dishes and incubated at 37°C until they reached 70-80% confluence. The cells were then washed with serum-free media and treated with 50 ng/mL murine recombinant SCF for 24 hours. The cell culture supernatant was collected and centrifuged at 300 g for 10 min to remove cell debris. The conditioned media was stored at -80°C until further use. The Proteome Profiler Mouse Angiogenesis Array (R&D Systems, RRID: AB_1655573) was used in accordance with the manufacturer's protocol with 700 µL of thawed supernatant. The array was analyzed by densitometry using Bio-Rad ImageLab. Proteins were normalized and compared to cells grown without SCF to calculate fold-change.

Hindlimb and Tumor Tissue Processing

After 12 days, mice were humanely euthanized, and tumors and long bones were collected in 10% neutral, buffered formalin or PBS. After fixation, hindlimbs were cleaned by removing skin and muscle around the tibia and femur and decalcified in 14% neutral buffered EDTA for 2-3 weeks or until bones became soft. Tumors were fixed for 24-48 hours in 10% neutral, buffered formalin. All tissues were processed and embedded in-house using the following protocol. Dehydration from 50%-100% ethanol at 1 hour each was followed by two incubations in xylene for 1 hour each and two incubations in paraffin for 6 hours each. Tissues were then embedded in paraffin and sectioned at a thickness of 5 µm onto charged slides.

Tumor Immunohistochemistry

To assess angiogenesis, tumors were stained for new vessel formation (CD31) and smooth muscle cell recruitment (αSMA). Tumors were sectioned and baked at 58°C for 1 hour. Antigen unmasking was performed by heat-induced epitope retrieval using 0.05% citraconic anhydride solution (PH 7.4) for 45 minutes at 98°C. Samples were blocked with 1% BSA for 30 minutes at room temperature then incubated with antibodies against CD31 (1:300, Abcam, RRID: AB_726362) or αSMA (1:2000, Abcam, RRID: AB_2223021) overnight at 4°C. The sections were visualized with ImmPACT NovaRED (HRP) Substrate (Vector Laboratories) and counterstained with hematoxylin Gill Method 1 (Fisher Scientific). Slides were scanned at 20X with a Hamamatsu Photonics Nanozoomer Slide Scanner in the Virtual Pathology Core. Visiopharm digital pathology analysis software (Version 2020.08, Visiopharm, RRID: SCR_021711) and custom-designed applications were used to quantify the percent of positive immunostained areas. A region of interest was drawn around the tissue, the area of the positive staining was identified and measured within the region of interest, and the ratios of the positive staining area to the total area were calculated.

TRAP Staining and Bone Histomorphometry Analysis

To assess the bone structure and osteoclast presence, long bone sections were stained for tartrate-resistant acid phosphatase (TRAP), and bone histomorphometry was analyzed. TRAP buffer was prepared in-house with 0.1 M acetate buffer, 0.3 M sodium tartrate, 10 mg/mL naphthol solution, triton x-100, and Fast Red Violet at pH 5.0. Sections were baked onto positively charged slides for 1 hour at 58°C. Slides were deparaffinized 3x in xylene and rehydrated from 100%-70% ethanol with a final wash in water. Slides were incubated in TRAP solution at 37°C for 1 hour. Slides were rinsed with water, counterstained with hematoxylin for 1 min, and washed with deionized water before dehydrating. To dehydrate, slides were incubated in increasing ethanol (70%-100%) then incubated in xylene 3x for 2 min. Images were scanned at 20X using the Hamamatsu Photonics Nanozoomer Slide Scanner in the Virtual Pathology Core and analyzed in-house using the BioQuant Osteo software (BioQuant Osteo 2016 v16.1.60, RRID: SCR_016423). Images were analyzed by drawing a region of interest in the diaphysis starting 150 microns distal to the growth plate of the tibia at 1500 µm length by width. Measurements generated using the software

were Bone Volume normalized by Tissue Volume (BV/TV, Bone Fraction, %), Bone Surface normalized by Bone Volume (BS/BV, 1/mm), Number of Osteoclasts per millimeter of Bone Surface (Oc.S/BS). Trabecular Thickness (Tb.Th) was calculated using Tb.Th =2/(BV/BS)*1000.

Bone Stromal Cell Flow Cytometry

To measure bone marrow cell composition changes, bone stromal and bone-residing cells were isolated and profiled by flow cytometry (26). Hind limbs were collected from mice after sacrifice and marrow extruded in PBS to collect HSCs, MSCs, and macrophages. The remaining bone underwent partial collagenase digestion (1 mg/mL) to release bone-residing cells: osteoblasts, osteoclasts, and osteocytes. Cells were resuspended in fluorescence-activated cell sorting buffer (BM-FACS buffer) and blocked with FcR mouse blocking reagent (2 μL/1x10^7 cells, Miltenyi Biotec, 130-092-575). BM-FACS buffer was composed of 3% bovine serum albumin (BSA, A3059-100g), 2 mM EDTA (Fisher, S311-100), and 10 mM HEPES (Gibco,15-630-080) in 1x PBS. The cells were then stained with ZombieAqua™ live/dead stain (1:1000, BioLegend, 423102). The sample was divided into 1x10^6 cells/100 μL and stained with the appropriate cell identification antibody mix described below using the antibodies listed in **Supplementary Table 1**. Bone marrow was analyzed for HSCs (CD34+, CD45+, Sca1+) MSCs (Sca1+, CD146+, CD29+, CD90+), Osteoblasts (Alkaline Phosphatase+, CD90+), Osteoclasts (CD11b-, CD115+, CD68+, RANKL+), Osteocytes (GP38+, SPARC+), and Macrophages (CD11b+, CD115+, CD68+, RANKL-). Each sample was then fixed in 1% methanol-free paraformaldehyde (Polysciences INC, 04018-1) in PBS. Samples were analyzed using the BD FACSCanto™ II (BD Biosciences), maintained by the Flow Cytometry Shared Resource, and FlowJo analysis software (RRID: SCR_008520).

Statistical Analysis

Comparisons of means among more than two groups were analyzed using analysis of variance (ANOVA) with Tukey post-testing. Between two groups, analysis was performed using a two-tailed unpaired Student's t-test. For proliferation rates, a two-tailed nonparametric t-test was performed with the Mann-Whitney test to compare ranks. Data were analyzed using Prism 9 (GraphPad Software, RRID: SCR_002798). Error bars represent the experimental standard error of the mean (SEM). * represents $p<0.05$, ** represents $p<0.005$, *** represents $p<0.0005$, and **** represents $p<0.0001$.

RESULTS

SCF Has No Effect on *In Vitro* Proliferation

Our prior study indicated that exogenous SCF induced proliferation of human prostate cancer cells expressing the tyrosine kinase receptor CD117 (17). Like human prostate cancer cells, both the *Ras/Myc* overexpressing RM1 and the *Pten*$^{-/-}$;*Trp53*$^{-/-}$ mPC3 murine prostate cancer cell lines contain a subpopulation of CD117 expressing cells: 10-15% and 20-40%, respectively (data not shown). Thus, we performed live-cell imaging-based proliferation assays to assess the effect of SCF on prostate cancer growth. There was no change in percent confluence after treatment with 50 ng/mL of SCF for either mPC3-luc (mPC3) or RM1-luc-effly-eGFP (RM1) cells over 60 hours (**Figures 1A, B**). Thus, exogenous SCF did not affect the proliferation of the murine prostate cancer cells *in vitro*.

PLTΔSCF mPC3-luc Tumor-Bearing Mice Have Decreased Tumor Volume

To examine the effects of bone marrow-derived SCF on primary tumor growth, we generated conditional SCF knockout mice with SCF deleted in megakaryocytes and platelets (PLTΔSCF) or mature osteoblasts (OBΔSCF) using a Cre-lox system. In these mice, both the membrane and soluble form of SCF are deleted from the target cells. To implant primary tumors, syngeneic mPC3 or RM1 cells were injected subcutaneously into the left flank of control (PLT-WT, OB-WT), megakaryocyte and platelet SCF deleted PLTΔSCF, or mature osteoblast SCF deficient OBΔSCF mice (**Figures 1C–F**). The tumors were allowed to grow for 12 days post-injection. Since both cell lines expressed luciferase, bioluminescent imaging was performed one day before sacrifice. No significant change was measured for the average radiance for mPC3 or RM1 tumors in both genotypes (**Figures 1C, D**; **Supplementary Figure 1**). However, radiance for mPC3 tumors was 2.7-fold higher in PLT-WT tumors compared with PLTΔSCF tumors ($p=0.08$) and 4.3-fold higher in OBΔSCF tumors compared with OB-WT tumors ($p=0.11$). Tumors were then collected on day 12, and tumor volume was calculated to determine the effect of SCF on primary tumor growth. Deletion of SCF in platelets and megakaryocytes (PLTΔSCF) caused a significant decrease ($p<0.05$) in mPC3 tumor volume (**Figure 1E**) compared to PLT-WT. The average mPC3 tumor volume for PLTΔSCF was decreased 3.6-fold compared with PLT-WT tumors (41.04 mm^3 and 145.85 mm^3, respectively). In fact, many of the mPC3 tumors in PLTΔSCF mice did not develop. No difference was measured in tumor volume for mPC3 tumors between OBΔSCF and OB-WT mice (**Figure 1E**). The average mPC3 tumor volume for OBΔSCF was 209.25 mm^3 compared to OB-WT at 141.55 mm^3. As well, there was no difference in tumor volume for RM1 tumor-bearing mice for PLTΔSCF or OBΔSCF compared with their WT controls (**Figure 1F**). These data demonstrate that platelet-derived SCF was important for mPC3 tumor growth.

SCF Causes an Increase in Proangiogenic Protein Secretion

SCF is known to stimulate angiogenesis (27), an essential process for tumor growth. To determine which proangiogenic factors SCF regulated, prostate cancer conditioned media were analyzed using an angiogenesis protein profiler array after treatment with 50 ng/mL SCF for 24 hours. For mPC3 cells, four angiogenic proteins were increased more than 1.2-fold after SCF treatment (**Figure 2A**) compared to the untreated control group. Increased proangiogenic proteins were monocyte chemoattractant protein-1 (1.2-fold increase), nephroblastoma overexpressed (1.2-fold increase), proliferin (1.3-fold increase), and stromal cell-derived

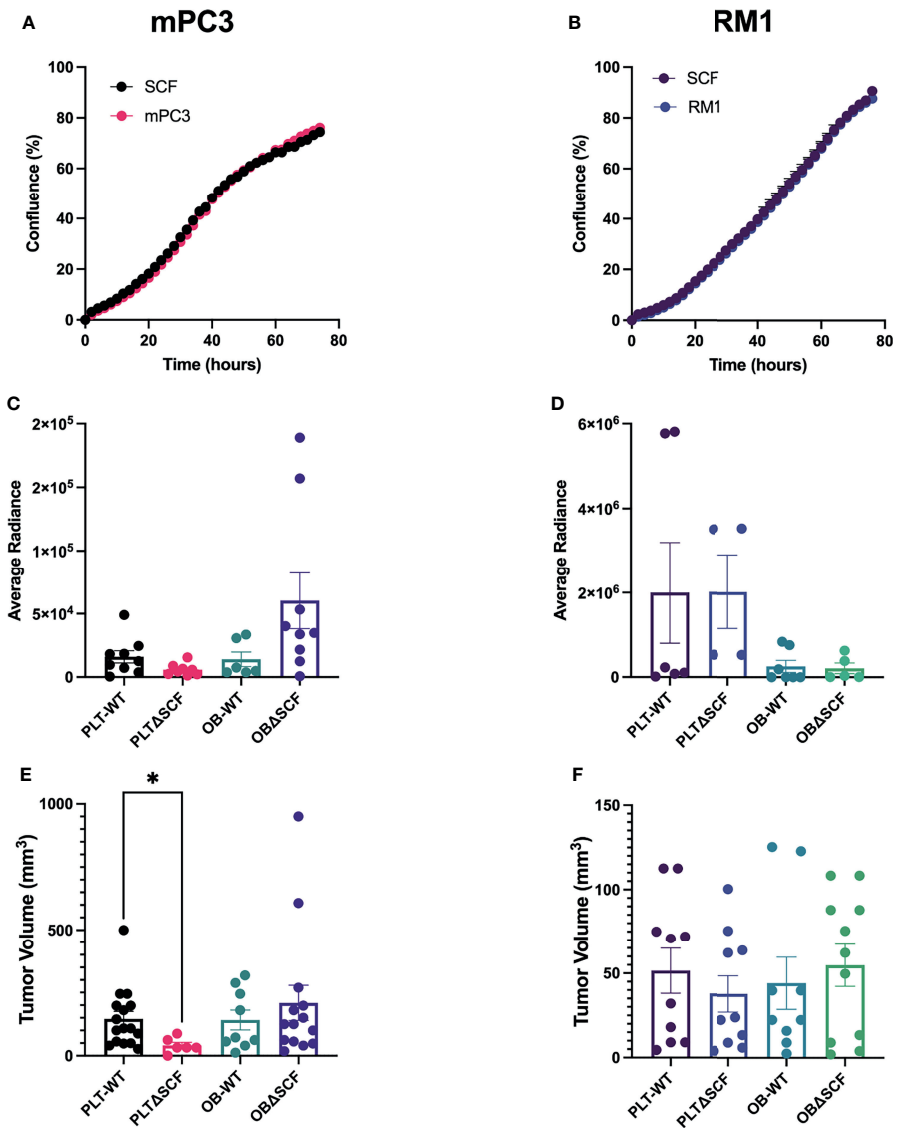

FIGURE 1 | Platelet deletion of SCF reduces mPC3 tumor growth. mPC3 **(A)** and RM1 cells **(B)** were treated with 50 ng/mL of SCF, and proliferation measured over 74 hours represented as mean percent confluence ± SEM (n=3). **(C–F)** mPC3 and RM1 cells were injected subcutaneously into PLT-WT, PLTΔSCF, OB-WT, or OBΔSCF mice. Tumors were allowed to grow for 12 days and imaged *via* IVIS on day 11 for average radiance **(C, D)**. Tumor volume **(E, F)** and average radiance are represented by mean ± SEM (n = 4-9). * represents $p < 0.05$ by unpaired t-test between mice of the same background.

factor-1/CXCL12 (SDF-1; 1.5-fold increase). The other angiogenic proteins had unchanged or decreased expression compared to mPC3 cells without treatment. SCF stimulated a 1.2-fold or higher release of 12 angiogenic proteins from RM1 cells (**Figure 2B**), which included amphiregulin (1.6-fold increase), angiogenin (1.9-fold increase), cysteine-rich angiogenic inducer 61 (2.0-fold increase), delta-like canonical notch ligand 4 (1.5-fold increase), endothelin-1 (1.2-fold increase), granulocyte-macrophage colony-stimulating factor (1.3-fold increase), interleukin-1 alpha (1.2-fold increase), CXCL10/IP-10 (1.2-fold increase), CXCL1/KC (1.3-fold increase), matrix metalloproteinase 9 (1.2-fold increase), SDF-1 (1.3-fold increase), and Serpin F1 (1.3-fold increase). The other proangiogenic proteins had decreased expression or no change in RM1 cells treated with SCF. These data demonstrate that SCF induces different proangiogenic signaling pathways in RM1 and mPC3 cells, with only SDF-1 increasing in both cell lines.

Bone-Derived SCF Did Not Affect Tumor Angiogenesis

To examine angiogenesis and vascular maturation, immunohistochemistry was performed on tumor tissues. Staining for the endothelial cell marker CD31 was performed to measure blood vessel coverage in tumors, while smooth

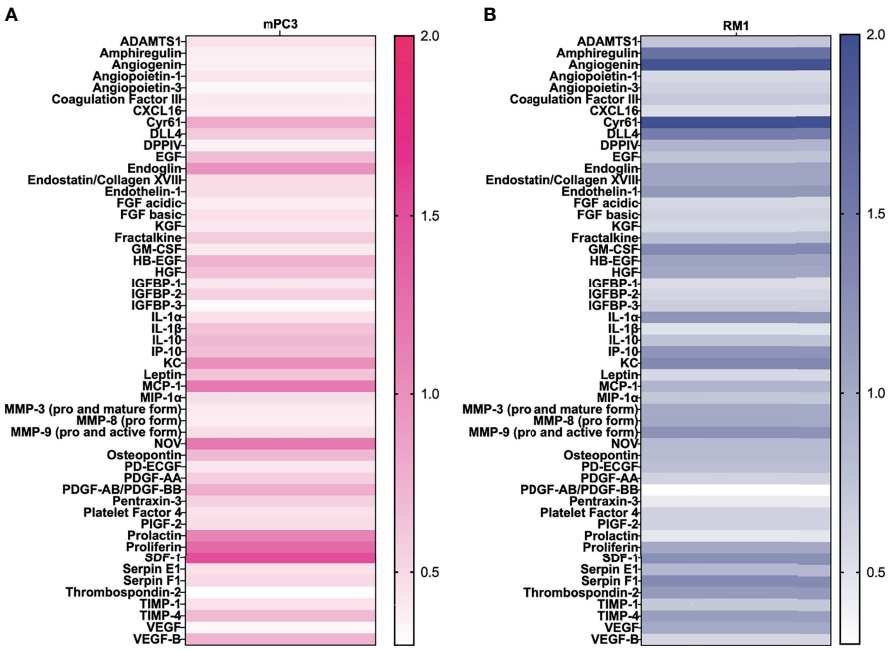

FIGURE 2 | SCF causes an increase in angiogenic factors in vitro. mPC3 **(A)** and RM1 **(B)** cells were treated with 50 ng/mL SCF for 24 hours. Conditioned media was collected and analyzed using an angiogenesis protein array. Densitometry values were normalized to conditioned media from untreated cells.

muscle actin (αSMA) staining was used to differentiate mature blood vessels (28). Tumors from PLTΔSCF mice injected with mPC3 cells were too small for downstream analysis, and thus, we were unable to compare angiogenesis in mPC3 tumors from PLTΔSCF with PLT-WT tumors. While not significant, OBΔSCF mPC3 tumors tended to have increased percentage of αSMA positive cells (2.1-fold, p=0.077) and CD31-positive vessel coverage (1.9-fold, p=0.22) compared with OB-WT mPC3 tumors (**Figures 3A, B**). These data align with the higher tumor volumes seen in **Figure 1** for mPC3 tumors, although the effects did not reach significance. For mice injected with RM1 tumors, PLTΔSCF and OBΔSCF had no significant difference in percent αSMA positive area or CD31-positive blood vessel coverage compared to the PLT-WT and OB-WT tumors (**Figures 3C–F**). Thus, SCF deletion had no significant effect on tumor angiogenesis.

Bone Marrow Deletion of SCF Did Not Affect the Bone Structure in Tumor-Bearing Mice

Our prior studies demonstrated that subcutaneous RM1 tumor growth induced bone formation and that platelets governed this pre-metastatic communication with the bone microenvironment (7, 29). To examine whether deletion of bone marrow-derived SCF would alter the bone microenvironment, bone sections from tumor-bearing mice were stained for tartrate-resistant acid phosphatase (TRAP) positive osteoclasts to determine osteoclast number and measure bone histomorphometry. mPC3 tumor growth stimulated bone formation in PLTΔSCF (3.2-fold, p<0.0001), PLT-WT (3.9-fold, p<0.0001), OBΔSCF (1.8-fold, p=0.036), and OB-WT (2.4-fold, p=0.0003) mice (**Figures 4A, B**). Interestingly, RM1 tumor growth induced bone formation in PLTΔSCF (1.8-fold, p=0.005) and PLT-WT (2.1-fold, p=0.005) but not in OBΔSCF or OB-WT mice (**Figures 4C, D**). Further, there was no difference in tumor-induced bone formation with SCF deletion in either osteoblasts or megakaryocytes and platelets. Neither bone fraction (BV/TV), osteoclast surface fraction (OC.s/BS), nor trabecular thickness (Tb.Th) was altered between groups (**Table 1**). No significant differences in bone histomorphometry were seen between PLTΔSCF and PLT-WT or OBΔSCF and OB-WT in mice without tumors (**Figure 4**). Thus, tumor-induced bone formation still occurred in most mice and was not affected by SCF deletion.

Osteoblast-Derived SCF Plays a Role in Bone Stem Cell Populations

Alterations in the bone structure result in changes in the composition of the bone microenvironment with shifts in the numbers of osteoclasts and osteoblasts. Further, the bone marrow HSC niche is the colonization site for disseminated cancer cells in murine bone (30, 31). These cells then compete for space in the bone marrow with metastatic lesions, causing a decrease in the HSC population in the bone (32). Once these cancer cells have disseminated and metastasized to the bone, osteoblasts act as an anchor and play a role in dormancy (33, 34). Thus, the bone niche cellular composition plays a vital role in tumor metastasis and creating the pre-metastatic niche.

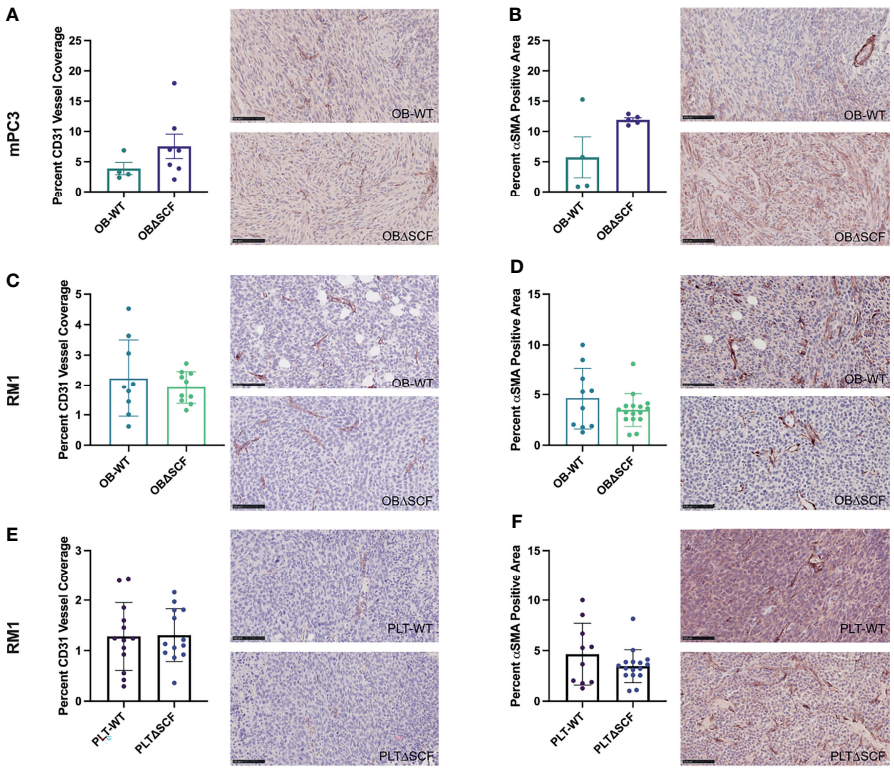

FIGURE 3 | Bone marrow derived-SCF loss does not affect tumor angiogenesis. mPC3 **(A, B)** and RM1 **(C–F)** tumors from PLT-WT, PLTΔSCF, OB-WT, or OBΔSCF mice were collected and stained for CD31 **(A, C, E)** or α-SMA **(B, D, F)**. CD31 was measured as percent CD31 vessel coverage, and α-SMA was calculated as percent α-SMA positive area and represented as mean ± SEM (n = 4-9). Scale bars represent 100 μm.

To determine how SCF from osteoblasts or platelets and megakaryocytes affects the pre-metastatic bone niche, bone marrow and bone-residing cells after partial collagenase digestion were collected from tumor-bearing mice, and flow cytometry was performed to analyze different bone cell progenitor and stromal cell populations. We used specific cell surface markers to differentiate HSCs, MSCs, macrophages, osteoblasts, osteoclasts, and osteocyte populations. While not significant, macrophage (2.0-fold, p=0.056) and osteoclast (2.3-fold, p=0.12) populations were decreased in PLTΔSCF compared to PLT-WT mPC3 tumor-bearing mice (**Supplementary Figures 2A, B**). No difference was seen in HSCs, MSCs, osteoblasts, or osteocyte populations in these mice (**Figures 5A–C**; **Supplementary Figure 2C**). Conversely, osteoblast-derived SCF played a significant role in mPC3 tumor-bearing bone progenitor cell populations. HSC numbers were significantly decreased (2.6-fold decrease, p=0.007) in OBΔSCF mPC3 tumor-bearing mice compared to OB-WT (**Figure 5D**). In contrast, the MSC population significantly increased (1.9-fold, p=0.04) in the OBΔSCF compared to the OB-WT mice (**Figure 5E**). In addition, OBΔSCF mPC3 tumor-bearing mice had a significant increase (1.5-fold increase, p=0.038) in osteoblast numbers (**Figure 5F**) compared to OB-WT tumor-bearing mice. While not significant, macrophages tended to be increased (1.9-fold, p=0.095), and osteoclasts (3.6-fold, p=0.087) were decreased in OBΔSCF mPC3 tumor-bearing mice compared to OB-WT. There was no difference in the osteocyte population (**Supplementary Figures 2D–F**). These data indicated that for mPC3 tumors, osteoblast-derived SCF might alter the colonization and dormancy niches in the bone microenvironment for metastatic cells.

The effects of bone marrow-derived SCF were different for RM1 tumors. PLTΔSCF RM1 tumor-bearing mice showed a significant increase in HSC (4.8-fold increase, p=0.046) and MSC (12.3-fold increase, p=0.02) populations as shown in **Figures 5H, I**. There was no difference in osteoblast, macrophage, osteoclasts, or osteocyte populations (**Figure 5J**, **Supplementary Figures 2H–J**). OBΔSCF RM1 tumor-bearing mice demonstrated a similar, but not significant, increase in HSC (1.8-fold, p=0.45) and MSC (1.2-fold, p=0.74) numbers (**Figures 5K, L**). However, osteoblast numbers were significantly decreased in OBΔSCF mice compared to OB-WT (2.8-fold, p=0.002, **Figure 5M**), which directly contrasts the data seen for mPC3 tumors. OBΔSCF RM1 tumor-bearing mice had a non-significant increase in osteoclast numbers (4.5-fold, p=0.087) but no difference in macrophage or osteocyte populations compared with OB-WT (**Supplementary Figures 2K–M**). There was no significant difference in bone cell populations in mice without tumors between PLTΔSCF and PLT-WT or OBΔSCF and OB-WT (data not shown). Thus, the effects on the bone microenvironment progenitor cell population and metastatic niche composition can

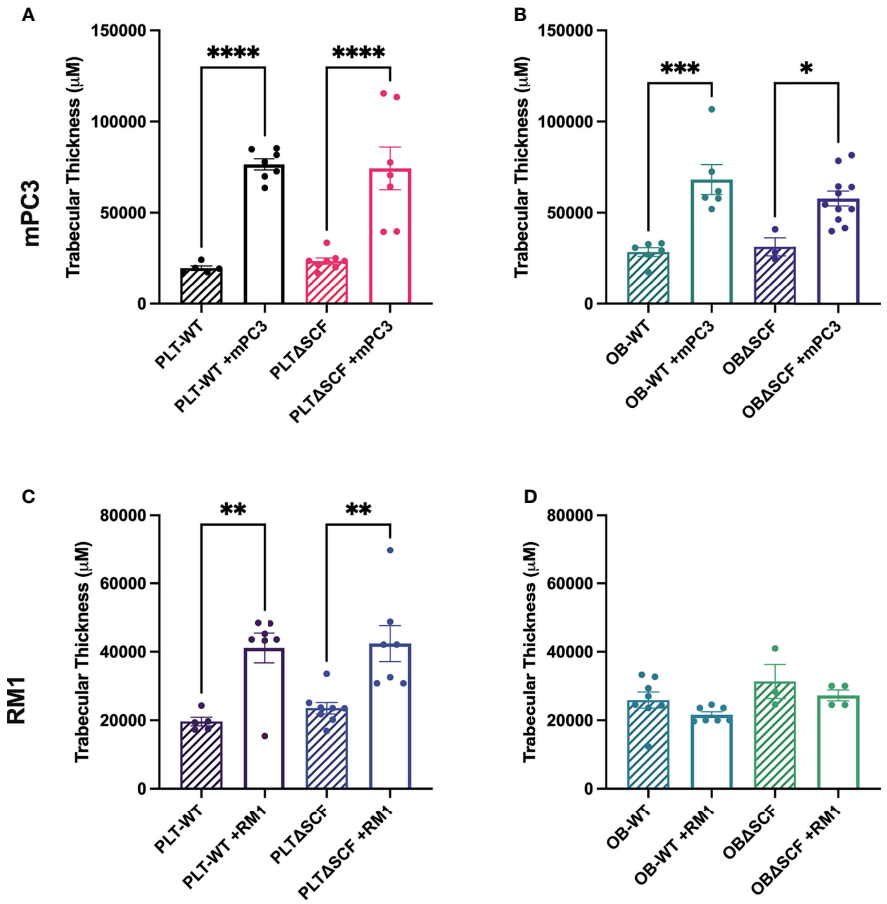

FIGURE 4 | Osteoblast-derived SCF regulates RM1 tumor-induced bone formation. Tibiae from mPC3 **(A, B)** and RM1 **(C–F)** tumor-injected mice were compared with tibiae from non-tumor bearing control PLT-WT and PLTΔSCF **(A, C)** or OB-WT and OBΔSCF **(B, D)** mice. Trabecular thickness measured by bone histomorphometry is represented as mean ± SEM (n=4-9). * represents $p < 0.05$, ** represents $p < 0.005$, *** represents $p < 0.0005$ and **** represents $p < 0.0001$ by one-way ANOVA.

be altered by bone marrow-derived SCF, but the result is dependent on the tumor cell line studied.

DISCUSSION

This study aimed to characterize the role of bone marrow-derived SCF in primary tumor growth, angiogenesis, and the pre-metastatic bone niche. We found that the source of SCF and the prostate cancer's genetic background both played a role in disease progression. SCF originating from megakaryocytes and platelets caused significantly decreased mPC3 tumor growth, while there was no effect in RM1 tumors. Osteoblast-derived SCF did not affect tumor growth. Angiogenesis and tumor-induced bone formation were not affected by SCF deletion in either genetic background. However, there were significant shifts in bone marrow composition. Osteoblast-derived SCF loss decreased HSCs and increased MSCs and osteoblasts in mPC3 tumor-bearing mice, while platelet deletion had no effect. For RM1 tumor-bearing mice, platelet depletion of SCF increased HSC and MSC progenitor cell populations with the loss of SCF in osteoblasts resulting in reduced osteoblast numbers. Thus, our data demonstrate that megakaryocyte and platelet-derived SCF regulates primary mPC3 tumor growth, while SCF originating from osteoblasts plays a role in bone marrow progenitor cell mobilization and pre-metastatic niche formation.

The role of SCF in prostate cancer tumor growth differed based on the model tested. Platelet and megakaryocyte depletion of SCF dramatically reduced mPC3 tumor volume, which could be due to alterations in proliferation, angiogenesis, or other cell survival pathways. Proliferation *in vitro* was not affected by exogenous SCF for either the mPC3 or RM1 cells, indicating that this mechanism is unlikely to be the main reason for reduced mPC3 tumor growth. RM1 tumors in platelet SCF depleted mice did not have significantly reduced tumor size. This may be due to fewer CD117 receptors on the RM1 cells. The mPC3 cells have a higher CD117 subpopulation, so they

TABLE 1 | Average relative search volume (RSV) and information prevalence from Google search and trends.

Parameter	WT Mean	SEM	ΔSCF Mean	SEM	p-value	n
mPC3 PLT						
BV/TV	0.21	0.034	0.22	0.031	0.83	7
OC.S/BS	0.14	0.15	0.19	0.34	0.20	7
Tb.Th	76,582	3,087	74,392	11,697	0.86	7
mPC3 OB						
BV/TV	0.20	0.031	0.25	0.026	0.94	6-11
OC.S/BS	0.19	0.031	0.11	0.012	0.14	6-11
Tb.Th	82,540	8,182	62,179	4,135	0.22	6-11
RM1 PLT						
BV/TV	0.31	0.025	0.28	0.029	0.44	8-10
OC.S/BS	0.14	0.031	0.12	0.022	0.70	8-10
Tb.Th	41,126	4,366	42,411	5,240	0.85	8-10
RM1 OB						
BV/TV	0.22	0.024	0.28	0.037	0.24	8-10
OC.S/BS	0.19	0.043	0.16	0.021	0.86	8-10
Tb.Th	21,154	1,430	24,264	1,258	0.26	8-10

Bone fraction (BV/TV); Osteoclast surface fraction (OC.S/BS); Trabecular thickness (Tb.Th).

may be more reliant on CD117 activation for tumor growth and angiogenesis. Our prior data demonstrate that CD117 expression on prostate cancer stem-like cells is associated with tumor initiation (17). The loss of CD117 activation in a subpopulation of mPC3 cells could also reduce tumor formation and growth in mice after platelet SCF depletion. The effect of SCF on other pathways supporting mPC3 tumor growth, including hypoxia and apoptosis resistance warrants further study.

Platelets regulate angiogenesis (9, 34–37), and SCF binding to CD117 activates a signaling cascade stimulating angiogenesis (38, 39). Due to the size of mPC3 tumors after platelet SCF deletion, blood vessel formation could not be examined and remains a potential mechanism by which platelet SCF controls mPC3 tumor growth. Treatment of prostate cancer cells with SCF *in vitro* resulted in the secretion of proangiogenic proteins that may be required for blood vessel development or stabilization but only SDF-1 was common between the two prostate cancer cell lines. Tumor-derived SDF-1 is upregulated in platelets of RM1 tumor-bearing mice (13) and increased circulating SDF-1 is associated with enhanced homing of CXCR4-positive bone marrow-derived progenitor cells to tumors driving angiogenesis (14). Thus, reduced SDF-1 secretion by prostate cancer cells after depletion of platelet SCF could result in diminished mPC3 tumor growth due to inhibition of angiogenesis through effects on the SDF-1/CXCR4 pathway.

Osteoblast secretion of SCF was not necessary for either RM1 or mPC3 tumor growth or angiogenesis. This lack of response is not surprising as SCF deletion occurs in the bone microenvironment distal to the primary tumor. Platelets circulating between the osteoblast microenvironment and primary tumors would be exposed to many potential sources of SCF, including endothelial cells (19–21). In the bone microenvironment, osteoblast SCF regulates megakaryocyte function (40, 41), and a negative feedback loop could result in an upregulation of megakaryocyte SCF production (42). This could increase the amount of SCF in platelets in mice with osteoblast SCF deletion.

Bone stromal cells such as osteoblasts, osteoclasts, MSCs, HSCs, and megakaryocytes can accelerate or impede skeletal metastasis (43, 44). The ratio and activation status of osteoblasts and osteoclasts directly affect bone remodeling and the overall pre-metastatic niche. Prostate cancer can cause an osteoblastic, osteolytic, or mixed phenotype before and after a metastatic lesion has formed (7) and prostate cancer is more likely to metastasize during bone remodeling (45). Like our prior studies, both RM1 and mPC3 tumor growth induced bone formation. However, this was not affected by either megakaryocyte and platelet or osteoblast SCF deletion. Beyond changes in the bone structure, tumors can cause alterations in the bone marrow cell composition. For example, tumor growth stimulates bone marrow-derived progenitor cell mobilization (14, 46–48). Osteoblast deletion of SCF reduced hematopoietic lineage cells (HSCs and osteoclasts) and increased mesenchymal lineage cells (MSCs and osteoblasts) in mice bearing mPC3 tumors. The MSC population was also increased in mice after osteoblast deletion of SCF and in RM1-bearing megakaryocyte and platelet-depleted SCF mice. SCF does not affect the proliferation of MSCs but increases expression of adhesion molecules and matrix metalloproteinases controlling migration (49). Thus, the loss of SCF in the bone microenvironment may be preventing MSC mobilization. In contrast, osteoblast percentages depended on the prostate cancer's genetic background. mPC3 tumor growth increased osteoblast

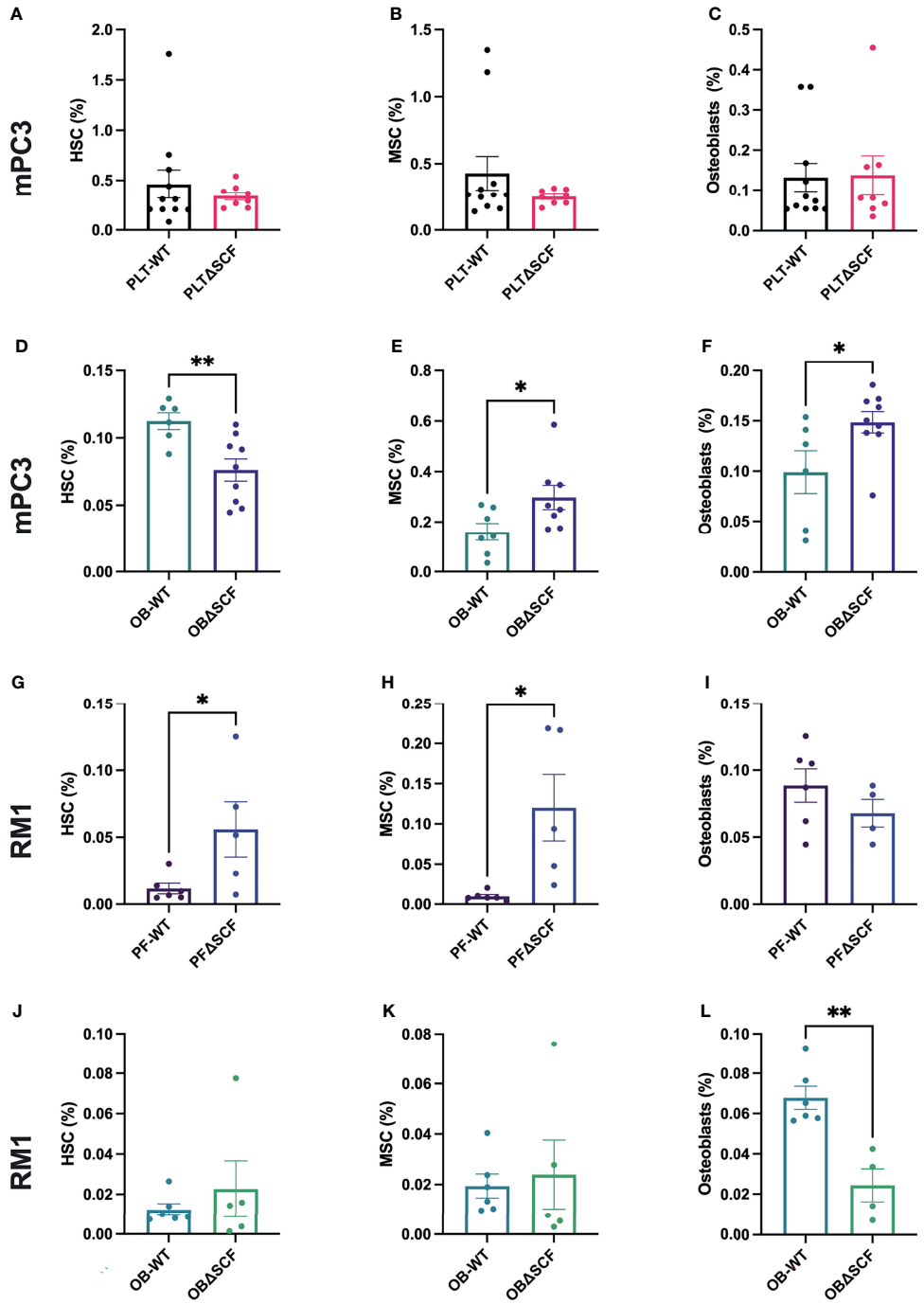

FIGURE 5 | SCF mediated alterations of the bone niche composition. Tibiae were isolated from PLT-WT, PLTΔSCF **(A–C, H–J)**, OB-WT, or OBΔSCF **(D–F, K–M)** mice after tumor implantation with mPC3 **(A–F)** or RM1 **(H–M)** prostate cancer cells. Bone marrow was isolated and stained for HSCs **(A, D, H, K)**, MSCs **(B, E, I, L)**, and osteoblasts **(C, F, J, M)**. Flow cytometry was performed to calculate the percent cell population represented as mean ± SEM (n = 6-9). * represents $p < 0.05$ and ** represents $p < 0.005$ by unpaired t-test.

numbers, while RM1 tumor growth reduced osteoblast numbers in mice with osteoblast deletion of SCF. This alteration in osteoblast numbers could affect the dormancy of disseminated prostate cancer cells. In addition, quiescent, bone-lining osteoblasts secrete undetectable SCF, while activated bone-forming osteoblasts along the mineralization front have higher SCF production (50). Thus, tumor-induced bone formation could increase SCF production through osteoblast

activation which may have subsequent effects on prostate cancer cell homing to the bone microenvironment.

Counterbalancing the mesenchymal lineage, the hematopoietic lineage cells were also altered in response to tumor growth. Mice bearing RM1 tumors demonstrated an increase in HSC numbers in the bone marrow, although this was only statistically significant with megakaryocyte and platelet depletion of SCF. Conversely, osteoblast deletion of SCF reduced HSC numbers in mPC3 tumor-bearing mice. These alterations in the HSC counts could either be through altered HSC mobilization or proliferation. In prior studies, the reductions in HSCs seen with perivascular and mesenchymal SCF deletion were not due to proliferation differences (51), indicating that proliferation is likely not the mechanism controlling HSC populations in our SCF deletion models. Thus, the reduction in HSCs may be due to altered mobilization into the circulation. Studies suggest that membrane-bound SCF in the bone is an important adhesion molecule for HSCs and a decrease in SCF causes an increase in HSC mobilization (52). Further studies demonstrated that the effect of SCF on HSCs is dependent on the source. SCF deletion in perivascular stromal cells or mesenchymal lineage cells (osteocytes, chondrocytes, and adipocytes) led to reduced HSC numbers in the bone marrow (53). While studies show that osteoblast-derived SCF does not affect HSCs (21, 51), the differentiation status of the osteoblast may alter its crosstalk with HSCs. More differentiated, bone-forming osteoblasts increase HSC renewal through membrane-bound SCF and cell-cell interaction, while less differentiated, more mesenchymal osteoblasts secrete more cytokines capable of signaling to HSCs (50, 54). Our genetic deletion removed both the membrane and soluble forms of SCF and only in terminally differentiated osteoblasts, unlike prior studies that deleted SCF earlier in osteoblast differentiation. In addition, membrane-bound SCF binding to CD117 on bone stromal cells stimulates megakaryocyte DNA synthesis and proliferation (55). Approximately 20% of HSCs can be found directly adjacent to megakaryocytes along bone marrow sinusoids, with 50% of HSCs being within two cell diameters of megakaryocytes (56, 57). Megakaryocyte depletion increases HSC proliferation and cell numbers (56). Further, platelet depletion induces membrane localization of SCF on megakaryocytes and stimulates nearby HSC proliferation (58). The number megakaryocytes increase with age leading to higher platelet counts (59) and higher numbers of HSCs in the bone marrow. Since most men develop prostate cancer at an advanced age, megakaryocyte and platelet SCF may play a more prominent role in older patients, which was not studied here. The effects of SCF loss on prostate cancer progression depended not only on the source of SCF but also on the genetic background of the prostate cancer cell lines.

Our study examined murine prostate cancer cell lines developed to mimic the common genetic mutations in prostate cancer patients with castration-resistant disease: *MYC, RAS, PTEN*, and *TP53*. The proto-oncogene *MYC* is expressed in approximately 40% of primary adenocarcinomas and 90% of metastases, with metastases often displaying gene amplification (60, 61). The tumor suppressor *TP53* is frequently mutated or deleted in cancers, with mutations in 8% of primary prostate adenocarcinomas and 47% of metastatic prostate cancers (62, 63). Deletions of *PTEN* are often associated with aggressive prostate cancer and can be found in up to 17% of primary prostate cancer patients and in 41% of metastatic cancers (60, 63). The oncogenes encoding the Ras protein are activated in many prostate cancers (up to 24%) and are associated with higher staged prostate carcinomas (60). Our data demonstrate that the genetic background of the cells played a significant role in the study outcomes. *Myc/Ras* co-activation is associated with prostate cancer bone metastasis in mice with a prostate-specific *Pten* deletion background and in patient bone biopsies (64). Further, *Myc/Ras* co-activation does not play a role in prostate cancer patient primary tumors. Thus, the lack of response to SCF depletion in RM1 (*Ras* and *Myc* co-activation) primary tumor growth and angiogenesis in our study is less surprising. Ras pathway activation stimulates angiogenesis in tumors (65), and thus, the overactivation of the Ras pathway may be why there were no significant differences in vessel formation in the RM1 tumors. In contrast, mPC3 (*Pten* and *Trp53* deletion) tumor growth was significantly reduced by platelet and megakaryocyte SCF loss and may increase with osteoblast SCF deletion. *TP53* and *PTEN* coalterations are found in 17% of localized prostate cancer and 16% of metastatic castration-sensitive prostate cancer, increasing to 56% for metastatic castration-resistant prostate cancers (66). Thus, the effects of SCF deletion on mPC3 tumor growth may be dependent on the source of SCF and the site of the tumor. The gene encoding SCF's ligand CD117, *KIT*, is the most prevalently mutated gene in prostate cancer patients, in addition to *RAS* and *TP53*, and is associated with aggressive prostate cancer (67). Thus, SCF may play a greater role in prostate cancer colonization and engraftment in the bone microenvironment during metastasis which will be the subject of future studies.

In summary, we determined that SCF from megakaryocytes and platelets is important for primary tumor growth in mPC3 tumor-bearing mice. While in RM1 tumor-bearing mice, SCF from platelets affects HSC and MSC pre-metastatic niche populations. SCF from osteoblasts alters bone marrow progenitor cell composition and pre-metastatic niche formation for both RM1 and mPC3 tumor-bearing mice. We demonstrate that the origin of bone marrow-derived SCF and the genetic background of the prostate cancer have differential effects on primary growth and pre-metastatic niche formation. Thus, treating patients with tyrosine kinase inhibitors targeting the SCF/CD117 pathway requires consideration of the patient's genetic profile. Further, the effects of SCF pathway intervention will likely differ based on the stage of the prostate cancer.

DATA AVAILABILITY STATEMENT

The raw data supporting the conclusions of this article will be made available by the authors, without undue reservation.

ETHICS STATEMENT

The animal study was reviewed and approved by Wake Forest School of Medicine Institutional Animal Care and Use Committee.

AUTHOR CONTRIBUTIONS

Conceptualization: BK. Formal Analysis: BF and LS. Funding Acquisition: BK. Investigation: BF, LS, KH, CP, VS, and KL. Project Administration: BK. Supervision: BK. Visualization: BF. Writing – Original Draft: BF. Writing – Review and Editing: BF, LS, KH, CP, VS, KL, and BK.

FUNDING

This work was supported by research funding from the National Cancer Institute at the National Institutes of Health (R00 CA175291 to BK). The use of the core services: Cell Engineering Shared Resource and Flow Cytometry Shared Resource, were partially subsidized by the Wake Forest Baptist Comprehensive Cancer Center Shared Resources grant (NIH/NCI CCSG P30 CA012197). This research was additionally supported by a Wake Forest CTSI grant (NIH/NCATS UL1 TR001420) which supports the Virtual Pathology Core.

ACKNOWLEDGMENTS

The authors would like to thank Dr. Zongbing You (Tulane University), Dr. Zhenbang Chen (Meharry Medical College), and Dr. Yusuke Shiozawa (Wake Forest School of Medicine) for the kind gift of the cell lines used in this study. We would also like to acknowledge the contributions and assistance of Mary Mobley and the undergraduate research assistants who assisted with tissue collections: Phyllis Elliot, Conner Song, Jessica Dean, Stephen Sokolosky, Lexie Skeen, and Shamon Mercier.

SUPPLEMENTARY MATERIAL

The Supplementary Material for this article can be found online at: https://www.frontiersin.org/articles/10.3389/fonc.2022.855188/full#supplementary-material

REFERENCES

1. Bubendorf L, Schöpfer A, Wagner U, Sauter G, Moch H, Willi N, et al. Metastatic Patterns of Prostate Cancer: An Autopsy Study of 1,589 Patients. *Hum Pathol* (2000) 31:578–83. doi: 10.1053/hp.2000.6698
2. Liu D, Kuai Y, Zhu R, Zhou C, Tao Y, Han W, et al. Prognosis of Prostate Cancer and Bone Metastasis Pattern of Patients: A SEER-Based Study and a Local Hospital Based Study From China. *Sci Rep* (2020) 10:1–11. doi: 10.1038/s41598-020-64073-6
3. Hensel J, Thalmann GN. Biology of Bone Metastases in Prostate Cancer. *Urology* (2016) 92:6–13. doi: 10.1016/j.urology.2015.12.039
4. Rucci N, Angelucci A. Prostate Cancer and Bone: The Elective Affinities. *BioMed Res Int* (2014) 2014:1–14. doi: 10.1155/2014/167035
5. Logothetis CJ, Lin SH. Osteoblasts in Prostate Cancer Metastasis to Bone. *Nat Rev Cancer* (2005) 5:21–8. doi: 10.1038/nrc1528
6. Ottewell PD. The Role of Osteoblasts in Bone Metastasis. *J Bone Oncol* (2016) 5:124–7. doi: 10.1016/j.jbo.2016.03.007
7. Kerr BA, McCabe NP, Feng W, Byzova TV. Platelets Govern Pre-Metastatic Tumor Communication to Bone. *Oncogene* (2013) 32:4319–24. doi: 10.1038/onc.2012.447
8. Lin SC, Yu-Lee LY, Lin SH. Osteoblastic Factors in Prostate Cancer Bone Metastasis. *Curr Osteoporosis Rep* (2018) 16:642–7. doi: 10.1007/s11914-018-0480-6
9. Quiroz-Munoz M, Izadmehr S, Arumugam D, Wong B, Kirschenbaum A, Levine AC. Mechanisms of Osteoblastic Bone Metastasis in Prostate Cancer: Role of Prostatic Acid Phosphatase. *J Endocrine Soc* (2019) 3:655–64. doi: 10.1210/JS.2018-00425
10. Fizazi K, Yang J, Peleg S, Sikes CR, Kreimann EL, Daliani D, et al. Prostate Cancer Cells-Osteoblast Interaction Shifts Expression of Growth/Survival-Related Genes in Prostate Cancer and Reduces Expression of Osteoprotegerin in Osteoblasts. *Clin Cancer Res* (2003) 9:2587–97.
11. Sylman JL, Boyce HB, Mitrugno A, Tormoen GW, Thomas I-C, Wagner TH, et al. A Temporal Examination of Platelet Counts as a Predictor of Prognosis in Lung, Prostate, and Colon Cancer Patients. *Sci Rep* (2018) 8:1–11. doi: 10.1038/s41598-018-25019-1. 2018 8:1.
12. Leblanc R, Peyruchaud O. The Role of Platelets and Megakaryocytes in Bone Metastasis. *J Bone Oncol* (2016) 5:109–11. doi: 10.1016/j.jbo.2016.02.007
13. Kerr BA, Miocinovic R, Smith AK, Klein EA, Byzova TV. Comparison of Tumor and Microenvironment Secretomes in Plasma and in Platelets During Prostate Cancer Growth in a Xenograft Model. *Neoplasia (New York NY)* (2010) 12:388–96. doi: 10.1593/neo.10166
14. Feng W, Madajka M, Kerr BA, Mahabeleshwar GH, Whiteheart SW, Byzova TC. A Novel Role for Platelet Secretion in Angiogenesis: Mediating Bone Marrow-Derived Cell Mobilization and Homing. *Blood* (2011) 117:3893–902. doi: 10.1182/blood-2010-08-304808
15. Kerr BA, Miocinovic R, Smith AK, West XZ, Watts KE, Alzayed AW, et al. $CD117^+$ Cells in the Circulation Are Predictive of Advanced Prostate Cancer. *Oncotarget* (2015) 6:1889–97. doi: 10.18632/oncotarget.2796
16. Wiesner C, Nabha SM, dos Santos EB, Yamamoto H, Meng H, Melchior SW, et al. C-Kit and Its Ligand Stem Cell Factor: Potential Contribution to Prostate Cancer Bone Metastasis. *Neoplasia (New York NY)* (2008) 10:996–1003. doi: 10.1593/neo.08618
17. Harris KS, Shi L, Foster BM, Mobley ME, Elliott PL, Song CJ, et al. CD117/c-Kit Defines a Prostate CSC-Like Subpopulation Driving Progression and TKI Resistance. *Sci Rep* (2021) 11:1465. doi: 10.1038/s41598-021-81126-6
18. Asada N, Takeishi S, Frenette PS. Complexity of Bone Marrow Hematopoietic Stem Cell Niche. *Int J Hematol* (2017) 106:45–54. doi: 10.1007/s12185-017-2262-9
19. Broudy VC. Stem Cell Factor and Hematopoiesis. *Blood* (1997) 90:1345–64. doi: 10.1182/blood.V90.4.1345
20. Foster BM, Langsten KL, Mansour A, Shi L, Kerr BA. Tissue Distribution of Stem Cell Factor in Adults. *Exp Mol Pathol* (2021) 122:104678. doi: 10.1016/j.yexmp.2021.104678
21. Ding L, Saunders TL, Enikolopov G, Morrison SJ. Endothelial and Perivascular Cells Maintain Haematopoietic Stem Cells. *Nature* (2012) 481:457–62. doi: 10.1038/nature10783
22. Kacena MA, Gundberg CM, Horowitz MC. A Reciprocal Regulatory Interaction Between Megakaryocytes, Bone Cells, and Hematopoietic Stem Cells. *Bone* (2006) 39:978–84. doi: 10.1016/j.bone.2006.05.019
23. Zhong L, Miller HD, Zhang Y, Jin B, Ge D, You Z. Intra-Arterial Injection to Create Bone Metastasis of Prostate Cancer in Mice. *Am J Clin Exp Urol* (2020) 8:93–100.

24. Chen Z, Trotman LC, Shaffer D, Lin H-K, Dotan ZA, Niki M, et al. Crucial Role of P53-Dependent Cellular Senescence in Suppression of Pten-Deficient Tumorigenesis. *Nature* (2005) 436:725–30. doi: 10.1038/nature03918
25. Faustino-Rocha A, Oliveira PA, Pinho-Oliveira J, Teixeira-Guedes C, Soares-Maia R, da Costa RG, et al. Estimation of Rat Mammary Tumor Volume Using Caliper and Ultrasonography Measurements. *Lab Anim* (2013) 42:217–24. doi: 10.1038/LABAN.254
26. Patel C, Shi L, Whitesides JF, Foster BM, Fajardo RJ, Quillen EE, et al. A New Method of Bone Stromal Cell Characterization by Flow Cytometry. *Curr Protoc* (2022) 4:1–26. doi: 10.1002/cpz1.400
27. Kim JY, Choi JS, Song SH, Im JE, Kim JM, Kim K, et al. Stem Cell Factor Is a Potent Endothelial Permeability Factor. *Arteriosclerosis Thrombosis Vasc Biol* (2014) 34:1459–67. doi: 10.1161/ATVBAHA.114.303575
28. Kerr BA, West XZ, Kim Y-W, Zhao Y, Tischenko M, Cull RM, et al. Stability and Function of Adult Vasculature Is Sustained by Akt/Jagged1 Signalling Axis in Endothelium. *Nat Commun* (2016) 7:10960. doi: 10.1038/ncomms10960
29. Kerr BA, Harris KS, Shi L, Willey JS, Soto-Pantoja DR, Byzova TV. Platelet TSP-1 Controls Prostate Cancer-Induced Osteoclast Differentiation and Bone Marrow-Derived Cell Mobilization Through Tgfβ-1. *Am J Clin Exp Urol* (2021) 9:18.
30. Rossnag S, Ghura H, Groth C, Altrock E, Jakob F, Schott S, et al. A Subpopulation of Stromal Cells Controls Cancer Cell Homing to the Bone Marrow. *Cancer Res* (2018) 78:129–42. doi: 10.1158/0008-5472.CAN-16-3507
31. Müller A, Homey B, Soto H, Ge N, Catron D, Buchanan ME, et al. Involvement of Chemokine Receptors in Breast Cancer Metastasis. *Nature* (2001) 410:50–6. doi: 10.1038/35065016
32. Shiozawa Y, Pedersen EA, Havens AM, Jung Y, Mishra A, Joseph J, et al. Human Prostate Cancer Metastases Target the Hematopoietic Stem Cell Niche to Establish Footholds in Mouse Bone Marrow. *J Clin Invest* (2011) 121:1298–312. doi: 10.1172/JCI43414
33. Byrne NM, Summers MA, McDonald MM. Tumor Cell Dormancy and Reactivation in Bone: Skeletal Biology and Therapeutic Opportunities. *JBMR Plus* (2019) 3:e10125. doi: 10.1002/JBM4.10125
34. Jung Y, Shiozawa Y, Wang J, Patel LR, Havens AM, Song J, et al. Annexin-2 Is a Regulator of Stromal Cell-Derived Factor-1/CXCL12 Function in the Hematopoietic Stem Cell Endosteal Niche. *Exp Hematol* (2011) 39 4:151–66.e1. doi: 10.1016/J.EXPHEM.2010.11.007
35. Wojtukiewicz MZ, Sierko E, Hempel D, Tucker SC, Honn KV. Platelets and Cancer Angiogenesis Nexus. *Cancer Metastasis Rev* (2017) 36:249–62. doi: 10.1007/s10555-017-9673-1
36. Pilatova K, Zdrazilova-Dubska L, Klement GL. The Role of Platelets in Tumour Growth. *Klinicka Onkologie: Casopis Ceske Slovenske Onkologicke Spolecnosti* (2012) 25:2S50.
37. Sierko E, Wojtukiewicz MZ. Platelets and Angiogenesis in Malignancy. *Semin Thromb Hemost* (2004) 30:95–108. doi: 10.1055/s-2004-822974
38. Foster B, Zaidi D, Young T, Mobley M, Kerr B. CD117/c-Kit in Cancer Stem Cell-Mediated Progression and Therapeutic Resistance. *Biomedicines* (2018) 6:31. doi: 10.3390/biomedicines6010031
39. Walsh TG, Metharom P, Berndt MC. The Functional Role of Platelets in the Regulation of Angiogenesis. *Platelets* (2015) 26:199–211. doi: 10.3109/09537104.2014.909022
40. Li TS, Hamano K, Nishida M, Hayashi M, Ito H, Mikamo A, et al. CD117+ Stem Cells Play a Key Role in Therapeutic Angiogenesis Induced by Bone Marrow Cell Implantation. *Am J Physiol Heart Circulatory Physiol* (2003) 285 4:H931–7. doi: 10.1152/AJPHEART.01146.2002
41. Leblanc R, Peyruchaud O. Metastasis: New Functional Implications of Platelets and Megakaryocytes. *Blood* (2016) 128:24–31. doi: 10.1182/blood-2016-01-636399
42. Erickson-Miller CL, Murphy MJ. Megakaryocytopoiesis and Platelet Production: Does Stem Cell Factor Play a Role? *Stem Cells (Dayton Ohio)* (1993) 11(Suppl 2):163–9. doi: 10.1002/STEM.5530110826
43. Ren G, Esposito M, Kang Y. Bone Metastasis and the Metastatic Niche. *J Mol Med* (2015) 93:1203–12. doi: 10.1007/s00109-015-1329-4
44. Jackson W, Sosnoski DM, Ohanessian SE, Chandler P, Mobley A, Meisel KD, et al. Role of Megakaryocytes in Breast Cancer Metastasis to Bone. *Cancer Res* (2017) 77:1942–54. doi: 10.1158/0008-5472.CAN-16-1084
45. Zheng Y, Zhou H, Dunstan CR, Sutherland RL, Seibel MJ. The Role of the Bone Microenvironment in Skeletal Metastasis. *J Bone Oncol* (2013) 2:47–57. doi: 10.1016/j.jbo.2012.11.002
46. Cuiffo BG, Karnoub AE. Mesenchymal Stem Cells in Tumor Development: Emerging Roles and Concepts. *Cell Adhesion Migration* (2012) 6:220. doi: 10.4161/CAM.20875
47. Furesi G, Rauner M, Hofbauer LC. Emerging Players in Prostate Cancer–Bone Niche Communication. *Trends Cancer* (2021) 7:112–21. doi: 10.1016/j.trecan.2020.09.006
48. Hoggatt J, Pelus LM. Mobilization of Hematopoietic Stem Cells From the Bone Marrow Niche to the Blood Compartment. *Stem Cell Res Ther* (2011) 2:13. doi: 10.1186/SCRT54
49. Enciso N, Ostronoff LLK, Mejías G, León LG, Fermín ML, Merino E, et al. Stem Cell Factor Supports Migration in Canine Mesenchymal Stem Cells. *Veterinary Res Commun* (2018) 42:29–38. doi: 10.1007/S11259-017-9705-X. 2018 42:1.
50. Blair HC, Dong SS, Julian BA. Expression of Stem Cell Factor by Osteoblasts in Normal and Hyperparathyroid Bone: Relation to Ectopic Mast Cell Differentiation. *Virchows Archiv: an Int J Pathol* (1999) 435:50–7. doi: 10.1007/S004280050394
51. Le PM, Andreeff M, Battula VL. Osteogenic Niche in the Regulation of Normal Hematopoiesis and Leukemogenesis. *Haematologica* (2018) 103:1945–55. doi: 10.3324/HAEMATOL.2018.197004
52. Zhang CC, Lodish HF. Cytokines Regulating Hematopoietic Stem Cell Function. *Curr Opin Hematol* (2008) 15:307. doi: 10.1097/MOH.0B013E3283007DB5
53. Asada N, Kunisaki Y, Pierce H, Wang Z, Fernandez NF, Birbrair A, et al. Differential Cytokine Contributions of Perivascular Haematopoietic Stem Cell Niches. *Nat Cell Biol* (2017) 19:214–23. doi: 10.1038/ncb3475
54. Nakamura Y, Arai F, Iwasaki H, Hosokawa K, Kobayashi I, Gomei Y, et al. Isolation and Characterization of Endosteal Niche Cell Populations That Regulate Hematopoietic Stem Cells. *Blood* (2010) 116:1422–32. doi: 10.1182/BLOOD-2009-08-239194
55. Avraham H, Scadden DT, Chi S, Broudy VC, Zsebo KM, Groopman JE. Interaction of Human Bone Marrow Fibroblasts With Megakaryocytes: Role of the C-Kit Ligand. *Blood* (1992) 80:1679–84. doi: 10.1182/BLOOD.V80.7.1679.1679
56. Bruns I, Lucas D, Pinho S, Ahmed J, Lambert MP, Kunisaki Y, et al. Megakaryocytes Regulate Hematopoietic Stem Cell Quiescence Through CXCL4 Secretion. *Nat Med* (2014) 20:1315–20. doi: 10.1038/nm.3707
57. Zhao M, Perry JM, Marshall H, Venkatraman A, Qian P, He XC, et al. Megakaryocytes Maintain Homeostatic Quiescence and Promote Post-Injury Regeneration of Hematopoietic Stem Cells. *Nat Med* (2014) 20:1321–6. doi: 10.1038/nm.3706
58. Ramasz B, Krüger A, Reinhardt J, Sinha A, Gerlach M, Gerbaulet A, et al. Hematopoietic Stem Cell Response to Acute Thrombocytopenia Requires Signaling Through Distinct Receptor Tyrosine Kinases. *Blood* (2019) 134:1046–58. doi: 10.1182/blood.2019000721
59. Poscablo DM, Worthington AK, Smith-Berdan S, Forsberg EC. Megakaryocyte Progenitor Cell Function Is Enhanced Upon Aging Despite the Functional Decline of Aged Hematopoietic Stem Cells. *Stem Cell Rep* (2021) 16:1598–613. doi: 10.1016/j.stemcr.2021.04.016
60. Dong JT. Prevalent Mutations in Prostate Cancer. *J Cell Biochem* (2006) 97:433–47. doi: 10.1002/JCB.20696
61. Carneiro A, Barbosa ÁRG, Takemura LS, Kayano PP, Moran NKS, Chen CK, et al. The Role of Immunohistochemical Analysis as a Tool for the Diagnosis, Prognostic Evaluation and Treatment of Prostate Cancer: A Systematic Review of the Literature. *Front Oncol* (2018) 8:377. doi: 10.3389/fonc.2018.00377
62. Meyers FJ, Gumerlock PH, Chi SG, Borchers H, Deitch AD, DeVere White RW. Very Frequent P53 Mutations in Metastatic Prostate Carcinoma and in Matched Primary Tumors. *Cancer* (1998) 83:2534–9. doi: 10.1002/(SICI)1097-0142(19981215)83:12<2534::AID-CNCR19>3.0.CO;2-V
63. Frank S, Nelson P, Vasioukhin V. Recent Advances in Prostate Cancer Research: Large-Scale Genomic Analyses Reveal Novel Driver Mutations

and DNA Repair Defects. *F1000Research* (2018) 7:1173. doi: 10.12688/f1000research.14499.1
64. Arriaga JM, Panja S, Alshalalfa M, Zhao J, Zou M, Giacobbe A, et al. A MYC and RAS Co-Activation Signature in Localized Prostate Cancer Drives Bone Metastasis and Castration Resistance. *Nat Cancer* (2020) 1:1082–96. doi: 10.1038/s43018-020-00125-0
65. Rak J, Filmus J, Finkenzeller G, Grugel S, Marmé D, Kerbel RS. Oncogenes as Inducers of Tumor Angiogenesis. *Cancer metastasis Rev* (1995) 14:263–77. doi: 10.1007/BF00690598
66. Hamid AA, Gray KP, Shaw G, MacConaill LE, Evan C, Bernard B, et al. Compound Genomic Alterations of TP53, PTEN, and RB1 Tumor Suppressors in Localized and Metastatic Prostate Cancer. *Eur Urol* (2019) 76:89–97. doi: 10.1016/j.eururo.2018.11.045
67. Martinez-Gonzalez LJ, Pascual Geler M, Robles Fernandez I, Cozar JM, Lorente JA, Alvarez Cubero MJ. Improving the Genetic Signature of Prostate Cancer, the Somatic Mutations. *Urologic Oncol* (2018) 36:312.e17–23. doi: 10.1016/j.urolonc.2018.03.012

Conflict of Interest: The authors declare that the research was conducted in the absence of any commercial or financial relationships that could be construed as a potential conflict of interest.

Publisher's Note: All claims expressed in this article are solely those of the authors and do not necessarily represent those of their affiliated organizations, or those of the publisher, the editors and the reviewers. Any product that may be evaluated in this article, or claim that may be made by its manufacturer, is not guaranteed or endorsed by the publisher.

Copyright © 2022 Foster, Shi, Harris, Patel, Surratt, Langsten and Kerr. This is an open-access article distributed under the terms of the Creative Commons Attribution License (CC BY). The use, distribution or reproduction in other forums is permitted, provided the original author(s) and the copyright owner(s) are credited and that the original publication in this journal is cited, in accordance with accepted academic practice. No use, distribution or reproduction is permitted which does not comply with these terms.

frontiers | Frontiers in Oncology

ORIGINAL RESEARCH
published: 19 May 2022
doi: 10.3389/fonc.2022.837127

A Novel Combination of Serum Markers in a Multivariate Model to Help Triage Patients Into "Low-" and "High-Risk" Categories for Prostate Cancer

Christopher J. McNally[1], Joanne Watt[2], Mary Jo Kurth[2], John V. Lamont[2], Tara Moore[1], Peter Fitzgerald[2], Hardev Pandha[3,4], Declan J. McKenna[1†] and Mark W. Ruddock[2†]*

[1] Genomic Medicine Research Group, Ulster University, Coleraine, United Kingdom, [2] Clinical Studies Group, Randox Laboratories Ltd., Crumlin, United Kingdom, [3] Royal Surrey County Hospital NHS Foundation Trust, Research Development and Innovations Department, The Royal Surrey County Hospital, Guildford, United Kingdom, [4] School of Biosciences and Medicine, Faculty of Health and Medical Sciences, University of Surrey, Guildford, United Kingdom

OPEN ACCESS

Edited by:
Antonina Mitrofanova, The State University of New Jersey, United States

Reviewed by:
Gian Maria Busetto, University of Foggia, Italy
Andrea Benedetto Galosi, Marche Polytechnic University, Italy

***Correspondence:**
Mark W. Ruddock
mark.ruddock@randox.com

†These authors share senior authorship

Specialty section:
This article was submitted to Genitourinary Oncology, a section of the journal Frontiers in Oncology

Received: *16 December 2021*
Accepted: *14 April 2022*
Published: *19 May 2022*

Citation:
McNally CJ, Watt J, Kurth MJ, Lamont JV, Moore T, Fitzgerald P, Pandha H, McKenna DJ and Ruddock MW (2022) A Novel Combination of Serum Markers in a Multivariate Model to Help Triage Patients Into "Low-" and "High-Risk" Categories for Prostate Cancer. Front. Oncol. 12:837127. doi: 10.3389/fonc.2022.837127

Background: Almost 50,000 men in the United Kingdom (UK) are diagnosed each year with prostate cancer (PCa). Secondary referrals for investigations rely on serum prostate-specific antigen (PSA) levels and digital rectal examination. However, both tests lack sensitivity and specificity, resulting in unnecessary referrals to secondary care for costly and invasive biopsies.

Materials and Methods: Serum samples and clinical information were collected from *N* = 125 age-matched patients (*n* = 61 non-PCa and *n* = 64 PCa) and analyzed using Biochip Array Technology on high-sensitivity cytokine array I (IL-2, IL-4, IL-6, IL-8, IL-10, IL-1α, IL-1β, TNFα, MCP-1, INFγ, EGF, and VEGF), cerebral array II (CRP, D-dimer, neuron-specific enolase, and sTNFR1), and tumor PSA oncology array (fPSA, tPSA, and CEA).

Results: The data showed that 11/19 (68.8%) markers were significantly different between the non-PCa and the PCa patients. A combination of EGF, $\log_{10}$ IL-8, $\log_{10}$ MCP-1, and $\log_{10}$ tPSA significantly improved the predictive potential of tPSA alone to identify patients with PCa (DeLong, $p < 0.001$). This marker combination had an increased area under the receiver operator characteristic (0.860 *vs*. 0.700), sensitivity (78.7 *vs*. 68.9%), specificity (76.5 *vs*. 67.2%), PPV (76.2 *vs*. 66.7%), and NPV (79.0 *vs*. 69.4%) compared with tPSA.

Conclusions: The novel combination of serum markers identified in this study could be employed to help triage patients into "low-" and "high-risk" categories, allowing general practitioners to improve the management of patients in primary care settings and potentially reducing the number of referrals for unnecessary, invasive, and costly treatments.

Keywords: algorithm, EGF, fPSA, IL-8, marker, MCP-1, prostate cancer, tPSA

INTRODUCTION

Prostate cancer (PCa) is very common, with almost 50,000 men diagnosed each year in the UK (1) and 240,000 in the US (2). Annually, PCa kills almost 35,000 men in the US (2). Tumors of the prostate are likely to be localized, clinically unapparent, and with International Society of Urological Pathology (ISUP) grade grouping 1 (3, 4). Slow-growing, non-significant PCa may not cause serious harm (5) and often does not require any intervention. However, clinically significant prostate cancers require urgent treatment, as they have the potential to metastasize and cause a serious disease.

Patients with PCa are usually asymptomatic, and the presenting symptoms are not specific and are often observed in men with benign prostate enlargement (BPE), one of the most frequently reported age-related diseases in men over 60 years. The symptoms include painful or burning sensation during urination, frequent urination (particularly at night—nocturia), difficulty stopping and starting urination, sudden erectile dysfunction, blood in the urine (hematuria) or semen, bone pain, and weight loss.

The risk factors for PCa include patient age (>50 years), ethnicity (African-American ethnicity and other minority ethnicities have a greater risk of progression and are more likely to develop aggressive cancer than Caucasian men), obesity (patients who are obese have a higher risk of PCa), and family history (blood relative, *e.g.*, parent) (6). The complications of PCa and subsequent treatment include metastatic spread of the disease, urinary incontinence, and erectile dysfunction (7).

The gold standard for diagnosing PCa is histological assessment of prostate tissue obtained by transrectal ultrasound-guided systematic (TRUS) core needle biopsy. The most common scale used to evaluate the grade of PCa is the Gleason score (8). The higher the Gleason score, the more likely that the cancer will grow and spread quickly (9).

Screening patients for PCa remains controversial and is not recommended due to the potential for overtreatment (10). Data presented by the Surveillance, Epidemiological, and End Results registry have estimated that screening for PCa, using prostate-specific antigen (PSA) alone, resulted in an increase of 28% of patients being over-diagnosed in the US (11). Furthermore, the European Randomised Study of Screening for Prostate Cancer trial also estimated that, when PSA is used alone as a screening tool for PCa, almost 50% of patients were over-diagnosed (12).

Although advances in PCa management have been made, an elevated PSA and/or abnormal digital rectal examination (DRE; nodular, indurated, and/or asymmetry) would still normally warrant a referral for investigation (13). An abnormal DRE is the second most common finding that initiates further investigation for malignancy (14–16). As a result, many patients with elevated PSA/abnormal DRE are referred to secondary care for invasive and costly procedures (17). These are often unnecessary as almost 75% of patients who are referred for further investigation have a negative biopsy (18). In addition, some 2.5 to 3% of patients are admitted to a hospital within a week of their TRUS procedure with a serious infection (urinary tract infections and/or bacterial prostatitis). This could be avoided with better decision-making in primary care but requires more biological information on the patient's disease to be available to their GP.

Currently, no biomarker or biomarker combinations that have the sensitivity and specificity to replace PSA have been identified (19). Therefore, improved approaches are required to differentiate between men who have a prostate disease that require treatment or surveillance and those who do not. The symptoms and PSA results are not an accurate indicator of disease. Indeed no level of PSA is truly diagnostic (20)—for example, a patient could have a PSA >10 ng/ml and not have any cancer, whereas another patient with a PSA <1 ng/ml could have aggressive cancer. Therefore, there is an urgent need for new tests which can at least stratify patients and, if possible, be diagnostic. However, it is very unlikely, given the heterogeneous nature of PCa, that a single biomarker will prove to be diagnostic.

The effective management of PCa requires an accurate diagnosis. However, the challenge for the clinician is to differentiate benign conditions (BPE) from PCa, which presents with similar symptoms. The PSA test exhibits a negative benefit-to-harm ratio based on population estimates (12). Therefore, biomarkers that would contribute to the sensitivity and specificity of PSA could offer the clinician additional information so that a more informed management decision could be made on whether to refer a patient to secondary care for further investigations or to manage the patient in primary care.

The aim of the study was to investigate the levels of serum markers in patients who present to primary care with PCa-like symptoms so as to identify markers that could be used to improve the triage of patients into low- and high-risk categories, thereby enhancing patient management.

MATERIALS AND METHODS

Patient Cohort and Sample Collection

One hundred twenty-five patients were included in the study. The patient cohort consisted of two independent patient sample sets.

The first set of patients ($N = 33$; $n = 10$ non-PCa and $n = 23$ PCa) were recruited by Royal Surrey County Hospital (NHS Foundation Trust) between 2015 and 2018 (Diagnosis of Clinically Significant Prostate Cancer; Royal Surrey County Hospital, Research Development and Innovations Department, The Royal Surrey County Hospital, Leggett Building, Daphne Jackson Road, Guildford, Surrey GU2 7WG, 15/LO/0218). The inclusion criteria included (i) men >18 years referred by their GP to investigate the cause of (ii) an abnormal PSA test. The exclusion criteria included (i) an active urine infection, confirmed by urine dipstick testing or midstream urine microscopy, (ii) men with a PSA <4 and >20 ng/ml, (iii) men already diagnosed with PCa, (iv) men with a prior or concurrent malignancy (apart from basal cell carcinoma of the skin), and (v) men who cannot give informed consent (**Supplementary 1**). Blood (24 ml) and urine (20–30 ml) were collected after a prostatic examination, along with a detailed clinical history.

The study complied with the Declaration of Helsinki, and written informed consent was obtained from all participants.

The second patient cohort ($N = 92$; $n = 54$ non-PCa and $n = 38$ PCa) was obtained from Discovery Life Sciences (DLS; CA, USA). The patient samples were de-identified and publicly available and were thus exempt from the requirement of the Institutional Review Board (IRB) approval (exempt category 4, IRB/EC). However, the DLS samples were procured pursuant to informed consent provided by the individual under approved protocols 45 CFR 46.116. Serum (1 ml) with clinical history was obtained for each DLS patient. The samples were selected from treatment-naive patients based on ICD-10 codes for prostate-related conditions.

Pathological Examination of Prostate Biopsies

Prostate cancer was confirmed by a histological examination of prostate biopsies from both sample sets. The Gleason scores assigned by the pathologists are described in **Table 1**. The non-PCa group included patients with confirmed benign prostatic hyperplasia (BPH; $n = 30/61$, 49.2%). All patients were treatment-naïve at the time of prostate biopsy.

Both patient cohorts were combined ($N = 125$) and separated into two groups, depending on the pathology reports: non-PCa ($n = 64/125$, 51.2%) and PCa ($n = 61/125$, 48.8%).

Clinical Factors and Behaviors

Clinical factors were not available for all patients. However, where data was available, the most common presenting symptoms included the following: lower urinary tract symptoms (LUTS), urine retention, urgency, nocturia, lower back pain, and microscopic hematuria. For many of the patients, there was no previous history of benign disease prior to their PCa diagnosis.

Smoking history and details on alcohol consumption (units/week) were also available for a limited number of patients. Many PCa patients were former smokers. Where data was available, the number of cigarettes smoked per day ranged from 10 to 25. Pack-year data was not available. The alcohol consumption ranged from 1 to 48 units/week (where data was available).

Medications were also noted for a limited number of patients; where data was available, the most common drugs that the patients were prescribed with included sertraline, loratadine, omeprazole, aspirin, tamsulosin, simvastatin, losartan, atorvastatin, imvastatin, bendroflumethiazide, citalopram, sildenafil, fluoxetine, ranitidine, metformin, and bisoprolol.

Biomarker Analysis

Patient blood and urine samples were stored in duplicate at -80°C prior to analysis by Randox Laboratory Clinical Services, Antrim, UK, by scientists blinded to the patients' data. In total, 19 biomarkers were investigated by Biochip Array Technology (BAT) (Randox Laboratories Ltd., Crumlin, UK) (21) using the Evidence Investigator analyzer (Randox Laboratories Ltd., Crumlin, UK) and following the manufacturer's instructions. The limits of detection (LOD) for the markers on the biochip arrays were as follows: EGF, 2.5 pg/ml; IFNγ, 2.1 pg/ml; IL-1α 0.9, pg/ml; IL-1β, 1.3 pg/ml; IL-2, 4.9 pg/ml; IL-4, 3.5 pg/ml; IL-6, 0.4 pg/ml; IL-8, 2.3 pg/ml; IL-10, 1.1 pg/ml; MCP-1, 25.5 pg/ml; TNFα, 3.7 pg/ml; VEGF, 10.8 pg/ml; CRP, 0.67 mg/L; D-dimer, 2.1 ng/ml; neuron-specific enolase (NSE), 0.26 ng/ml; sTNFR1, 0.24 ng/ml; CEA, 0.29 ng/ml; fPSA, 0.02 ng/ml; and tPSA, 0.045 ng/ml. The biomarkers below the LOD were recorded as 90% of the LOD (22).

Statistical Analyses

Statistical analyses were undertaken using R version 4.0.5 (23). Wilcoxon rank-sum test was used to identify differentially expressed markers. Markers with $p < 0.05$ were considered significant. The ability of the markers to predict PCa was further investigated using logistic LASSO regression following a cross-validation testing of several models. For marker and marker combinations, areas under the receiver operator characteristic (AUROC) (and 95% CI), sensitivity (and 95% CI), specificity (and 95% CI), positive predictive value (PPV), and negative predictive value (NPV) were calculated to identify models that differentiated between the two diagnostic groups (non PCa *vs.* PCa). DeLong test was used to compare AUROCs for the model and tPSA; $p < 0.05$ was considered significant.

RESULTS

The clinical and pathological characteristics of the patients involved in the study are described in **Table 1**. Both tPSA and

TABLE 1 | Clinical and pathological characteristics of the patients. Data shown as mean ± SD or *n*/total (%), Wilcoxon rank-sum test; $p < 0.05$ was considered significant.

Clinical characteristics	Non-PCa ($n = 64$)	PCa ($n = 61$)	*p*-value
Age (years)	62.7 ± 10.4	64.4 ± 8.3	0.439
BPH	30/64 (46.9%)		
Gleason score			
6		11/60 (18.3%)	
7		31/60 (51.7%)	
8		12/60 (20%)	
9		6/60 (10%)	
tPSA (ng/ml)	4.2 ± 3.7	20.8 ± 58.2	<0.001
fPSA (ng/ml)	0.8 ± 0.9	3.6 ± 9.5	0.005
CEA (ng/ml)	2.4 ± 3.0	4.4 ± 16.5	0.158

PCa, prostate cancer; BPH, benign prostatic hyperplasia; tPSA, total prostate-specific antigen; fPSA, free prostate-specific antigen; CEA, carcinoembryonic antigen.

fPSA were significantly elevated in the PCa group. However, CEA was not significantly different.

Biochip Array Technology

From the marker results obtained using the biochip arrays, 11/16 (68.8%) markers were significantly different between the non-PCa and the PCa patient groups (**Table 2**). Of these, 7/16 (43.8%) markers were elevated in the PCa patients *vs*. non-PCa, 4/16 (25%) were lower in the PCa *vs*. non-PCa, and 5/16 (31.2%) were not significantly different between either group.

Regression Analysis

Logistic LASSO regression identified a model for a combination of markers that demonstrated higher sensitivity and specificity *vs*. tPSA alone (**Table 3**). The four markers selected by LASSO regression to identify patients with PCa included EGF, IL-8, MCP-1, and tPSA (**Figure 1A**). As some of the data was not normally distributed, $\log_{10}$ transformation was applied to IL-8, MCP-1, and tPSA in the model.

When comparing the new model identified by LASSO to tPSA on its own, the number of false positives was reduced from 21/64 (32.8%) to 15/64 (23.4%), and the number of false negatives increased from 11/61 (18.0%) to 13/61 (21.3%) (**Table 4**).

Calculating the Patient Risk Score

The risk of PCa was based on the following marker combination: EGF, $\log_{10}$ IL-8, $\log_{10}$ MCP-1, and $\log_{10}$ tPSA. In this dataset, a cutoff of 0.054 (as shown in **Figure 1B**) was applied to achieve the highest sensitivity and specificity for identifying patients with PCa; PRS <0.054—patients are negative for PCa, whereas PRS ≥0.054—patients would be positive for PCa. It should be noted that the PRS would be used in combination with clinical risk factors when triaging patients. Thus, patients with a positive risk score and positive clinical risk factors (*e.g*., painful or burning sensation during urination, frequent urination, difficulty starting or stopping urination, sudden erectile dysfunction, and blood in urine or semen) could be prioritized for urgent referral for further investigations. Patients who were positive for clinical risk factors and negative for marker risk (PRS) could potentially be managed in primary care or referred for investigation as necessary. Importantly, this type of combined measurement approach is recommended for risk stratification methods by the National Institute for Health and Care Excellence (NICE 2019) guidelines for PCa.

To test the linearity of the model, predicted probability was plotted against patient score (**Figure 1C**). The high correlation between the predicted probability and patient score (r = 0.95) would suggest confidence in the model.

TABLE 2 | The analysis showed that 11/16 (68.8%) serum markers were significantly different between the non-PCa and the PCa patient groups.

Marker	non-PCa (n = 64)	PCa (n = 61)	p-value
IL-8 (pg/ml)	175.3 ± 261.5	28.4 ± 42.4	<0.001
IL-10 (pg/ml)	1.8 ± 2.0	3.2 ± 9.0	<0.001
MCP-1 (pg/ml)	189.9 ± 106.9	291.1 ± 148.0	<0.001
VEGF (pg/ml)	69.1 ± 68.5	145.5 ± 132.9	<0.001
IL-1β (pg/ml)	11.6 ± 44.1	1.9 ± 1.2	0.001
NSE (ng/ml)	15.3 ± 11.3	7.8 ± 5.3	0.001
EGF (pg/ml)	87.1 ± 54.7	129.5 ± 81.8	0.002
IL-6 (pg/ml)	37.8 ± 148.2	19.9 ± 42.1	0.004
sTNFRI (ng/ml)	1.2 ± 1.3	1.5 ± 1.1	0.009
CRP (μg/ml)	45.5 ± 41.0	73.8 ± 49.6	0.012
D-dimer (ng/ml)	173.6 ± 194.2	331.0 ± 382.9	0.014
IL-1α (pg/ml)	0.8 ± 0.1	0.8 ± 0.0	0.090
TNFα (pg/ml)	4.2 ± 3.1	3.9 ± 1.4	0.130
IL-2 (pg/ml)	4.7 ± 1.6	4.4 ± 0.1	0.327
IFNγ (pg/ml)	1.9 ± 0.2	1.9 ± 0.2	0.606
IL-4 (pg/ml)	3.2 ± 0.4	3.2 ± 0.4	0.608

Data shown as mean ± SD. Wilcoxon rank-sum test; p < 0.05 was considered significant.

PCa, prostate cancer; IL-8, interleukin-8; IL-10, interleukin-10; MCP-1, monocyte chemoattractant protein-1; VEGF, vascular endothelial growth factor; IL-1β, interleukin-1β; NSE, neuron-specific enolase; EGF, endothelial growth factor; IL-6, interleukin-6; sTNFR1, soluble tumor necrosis factor receptor-1; CRP, C-reactive protein; IL-1α, interleukin-1α; TNFα, tumor necrosis factor-α; IL-2, interleukin-2; IFNγ, interferon γ; IL-4, interleukin-4.

TABLE 3 | Individual analytes and model EGF, IL-8, MCP-1, and tPSA AUROC, sensitivity, specificity, PPV, and NPV for non-PCa *vs*. PCa.

Markers and marker combination	AUROC (95% CI)	Sensitivity (95% CI)	Specificity (95% CI)	PPV (%)	NPV (%)
EGF	0.658 (0.562–0.754)	0.656 (0.541–0.770)	0.609 (0.500–0.734)	61.5	65.0
IL-8	0.703 (0.612–0.794)	0.738 (0.623–0.836)	0.563 (0.438–0.688)	61.6	69.2
MCP-1	0.739 (0.651–0.826)	0.738 (0.623–0.836)	0.703 (0.594–0.813)	70.3	73.8
tPSA	0.700 (0.606–0.793)	0.689 (0.574–0.803)	0.672 (0.563–0.781)	66.7	69.4
EGF + $\log_{10}$ IL-8 + $\log_{10}$ MCP-1 + $\log_{10}$ tPSA	0.860 (0.796–0.923)	0.787 (0.688–0.885)	0.765 (0.656–0.875)	76.2	79.0

PCa, prostate cancer; IL-8, interleukin-8; MCP-1, monocyte chemoattractant protein-1; EGF, endothelial growth factor; tPSA, total prostate-specific antigen; AUROC, area under receiver operating characteristic curve; CI, confidence interval (95%); PPV, positive predictive value; NPV, negative predictive value.

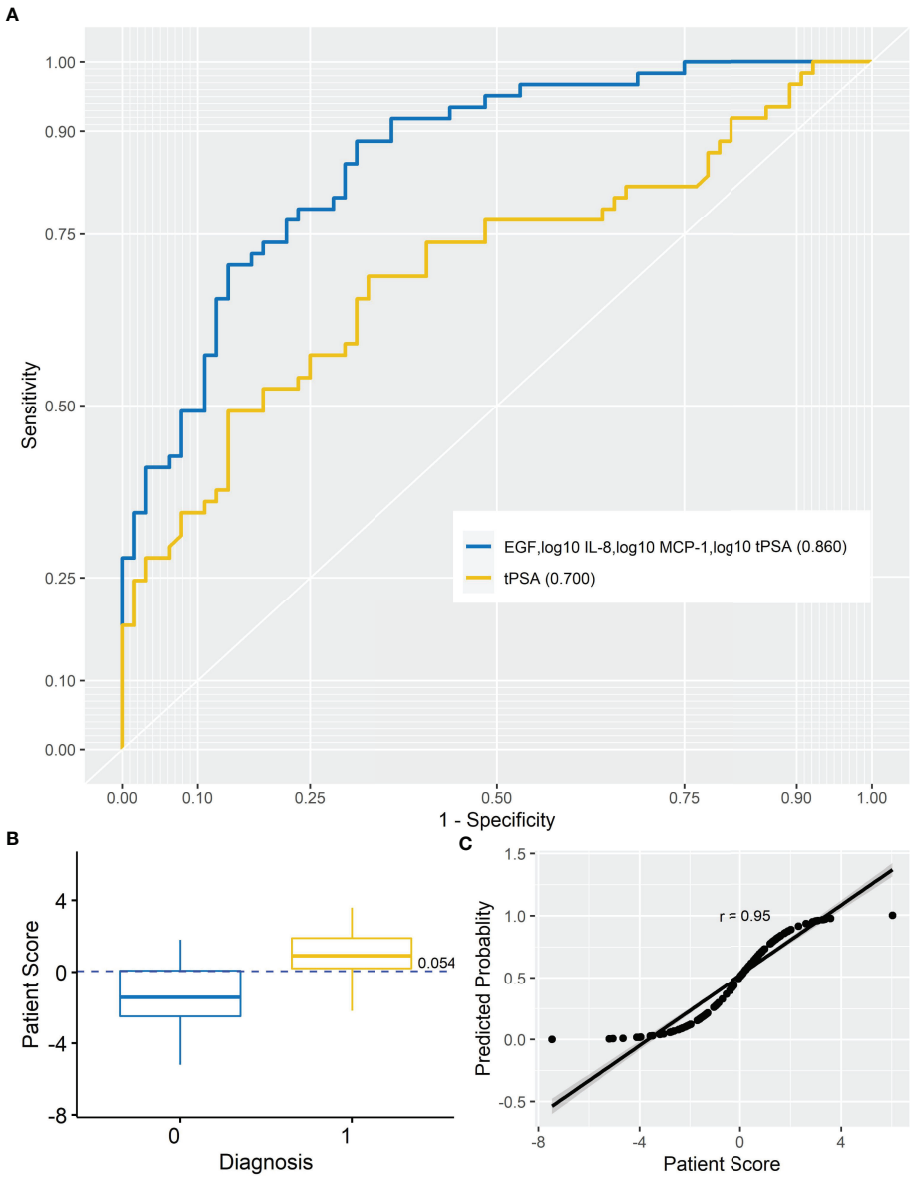

FIGURE 1 | Prostate cancer model. **(A)** AUROC for analyte model (AUROC, 0.860) and tPSA (AUROC, 0.700). When the AUROC for the model (EGF, log_{10} IL-8, log_{10} MCP-1, and log_{10} tPSA) was compared with the AUROC for tPSA, the model significantly improved upon tPSA alone (DeLong, $p < 0.001$) at differentiating non-PCa from PCa patients. **(B)** Simple box plot of patient score by diagnosis [non-PCa (0) and PCa (1); mean ± SD] for the model at a cutoff of 0.054. **(C)** Simple scatter with fit line for predicted probability by patient score for the marker model ($r = 0.95$). AUROC, area under receiver operating characteristic; IL-8, interleukin-8; MCP-1, monocyte chemoattractant protein-1; EGF, endothelial growth factor; tPSA, total prostate-specific antigen.

DISCUSSION

In this study, we investigated 19 serum markers involved in PCa (**Supplementary 2**). The results showed 11/16 (68.8%) cytokines that were significantly different between the non-PCa *vs.* PCa groups. Seven of these markers were elevated in the PCa group, whereas 4 markers were elevated in the non-PCa group. In the PCa group, 2/3 (66.6%) cancer markers (fPSA and tPSA) were also elevated.

The serum levels of IL-10, EGF, VEGF, MCP-1, sTNFR1, CRP, and D-dimer were significantly higher in the PCa patients. Of these serum markers, MCP-1 had the highest AUROC for detecting PCa (MCP-1 0.739 *vs.* tPSA 0.700). MCP-1 (CCL2) is a member of the chemokine family that acts as a paracrine and autocrine factor to promote PCa growth and invasion (24). MCP-1 is also a potent chemotactic factor regulating stromal–epithelial cells in PCa (25). Unsurprisingly, the angiogenic factors VEGF and EGF were also elevated in patients with

TABLE 4 | Confusion matrices comparing tPSA and the model EGF, IL-8, MCP-1, and tPSA.

		tPSA		Model	
		Predicted		Predicted	
		No PCa	PCa	No PCa	PCa
Actual	No PCa	43	19	49	13
	PCa	21	42	15	48

For each matrix, the figure in the top left represents the true number of negatives, the top right figure represents the number of false positives, the bottom left figure represents the number of false negatives, and the bottom right figure represents the number of true positives.
PCa, prostate cancer; IL-8, interleukin-8; MCP-1, monocyte chemoattractant protein-1; EGF, endothelial growth factor; tPSA, total prostate-specific antigen.

PCa. However, in other studies, VEGF has been shown to have no significant prognostic or predictive value for expression for localized or advanced PCa (26). In contrast, EGF modulates PCa invasiveness by regulating the urokinase-type plasminogen activity (27). Inhibition of the EGF receptor may prevent tumor cell dissemination (28).

CRP is a general marker for inflammation, although it does not differentiate benign from malignant disease (29). However, IL-10, which was also elevated in our PCa patients, has anti-inflammatory and anti-angiogenic properties (30). Therefore, it was unsurprising that both markers were elevated in the PCa patients.

The thrombotic factor D-dimer has been detected in patients with PCa. However, the relationship between PCa and the coagulation disorder remains unknown (31). Nonetheless, high plasma levels of D-dimer are associated with an increased risk of PCa mortality (32). Similarly, sTNFR1 has been identified in men with PCa. Furthermore, sTNFR1 has been shown to be a potential biomarker for identifying PCa when compared with PSA alone (AUROC 0.97) (33). However, as this was a small study, the authors acknowledged that the results need to be assessed in a much larger patient cohort. In our study, sTNFR1 had an AUROC of 0.635 for PCa.

Prostate cancer is an inflammatory disease; however, we found that 4/11 (36.4%) inflammatory markers (IL-8, IL-1β, NSE, and IL-6 levels) were significantly lower in the PCa patients.

The circulating IL-8 serum levels have not been shown to be a significant predictor of diagnosis, aggressiveness, or prognosis for PCa (34). However, increased circulating IL-8 serum levels have been detected in patients with an underlying inflammatory disease (34). In our study, IL-8 was identified as a marker that could differentiate non-PCa from PCa, potentially by identifying patients with inflammatory disease, *i.e.*, BPH. In addition, IL-1β is elevated in patients with chronic prostatitis, chronic pelvic pain syndrome, and BPH (35, 36). Furthermore, elevated IL-6 has also been reported in men with BPH, LUTS, and erectile disfunction (37). Therefore, it was not surprising that these three markers were elevated in the non-PCa patient group; almost 50% of non-PCa patients had a diagnosis of BPH.

Higher levels of NSE have been observed in non-PCa patients (38), albeit higher levels of NSE have also been observed in patients with metastatic disease (39). In our study, 42/64 (65.6%) PCa patients had a Gleason score ≤7; no information was available on metastatic disease, and there was no significant difference in the NSE levels by Gleason score (data not shown). However, elevated serum NSE has been suggested to correlate with prognosis in advanced PCa (38). The PCa patients in our study were treatment-naïve, and only 6/64 (9.4%) patients presented with a Gleason score ≥9.

In our study, the serum levels of IL-1α, TNFα, IL-2, IL-4, and IFNγ were not significantly different between the non-PCa and the PCa groups.

Combination Model

The results demonstrated that no single marker significantly outperformed tPSA. However, a combination of EGF, $\log_{10}$ IL-8, $\log_{10}$ MCP-1, and $\log_{10}$ tPSA significantly improved the predictive potential of tPSA alone to identify patients with PCa. This marker combination had an increased AUROC (0.860 *vs.* 0.700), sensitivity (78.7 *vs.* 68.9%), specificity (76.5 *vs.* 67.2%), PPV (76.2 *vs.* 66.7%), and NPV (79.0 *vs.* 69.4%) compared with tPSA.

Using this marker combination in this patient dataset reduced the number of false positives from 21/64 (32.8%) to 15/64 (23.4%); however, the number of false negatives increased from 11/61 (18.0%) to 13/61 (21.3%) compared with tPSA. Thus, an additional 9.4% (6/64) of patients were correctly assigned as non-PCa using the marker combination. If the management of these patients was based solely on their tPSA results, $n = 7$ patients could have potentially undergone unnecessary and invasive investigations. An additional 3.3% (2/61) of patients were incorrectly assigned as PCa.

Evidence suggests that the use of multiple markers to differentiate non-clinically significant from clinically significant disease is an important strategy for reducing unnecessary referrals for further investigation (40). Integrating inflammatory serum biomarkers into a risk calculator may provide additional information for detecting and managing PCa risk (40). The predictive value of inflammatory markers for PCa diagnosis has been evaluated in primary care (41). Our data demonstrate the value of measuring multiple markers in this heterogenous pathophysiology in combination with tPSA. The main limitations of this feasibility study included the following: (1) the small number of participants in each patient cohort and (2) the limited patient information [demographics, behaviors, medications, socioeconomic data, and clinicopathological data (*e.g.*, DRE)]. Nevertheless, these results warrant further

investigation in a larger cohort, and this will help validate the model.

It is worth noting that other combination models are being investigated elsewhere, including the Stockholm-3 risk-based model (42), the 4kscore (43), the European Randomised Study of Screening for Prostate Cancer risk calculator (44), the Prostate Cancer Prevention Trial (45), and the Irish Prostate Cancer Risk Calculator (46). The work described in this study is therefore an important addition to the global research effort to identify combinations of biological and clinical measurements to inform evidence-based decision-making in PCa patients.

CONCLUSION

This study demonstrated that a novel serum marker combination of EGF, $\log_{10}$ IL-8, $\log_{10}$ MCP-1, and $\log_{10}$ tPSA significantly improved the predictive potential of tPSA alone to identify patients with PCa. Application of this serum marker combination could provide clinicians with valuable information to help triage their patients into low- and high-risk categories. Improved risk category stratification of patients would enable better management of men who present at primary care with prostate-cancer-like symptoms. In turn, the utilization of this novel combination of markers could potentially reduce the number of patients that are referred to secondary care for unnecessary, costly, and invasive procedures. However, it should be noted that this is a preliminary study and the markers identified would need to be validated in a larger patient cohort.

DATA AVAILABILITY STATEMENT

The raw data supporting the conclusions of this article will be made available by the authors without undue reservation.

ETHICS STATEMENT

The studies involving human participants were reviewed and approved by cohort (1): Ethics was granted by the NHS, Health Research Authority, NRES Committee South East Coast—Brighton and Sussex, Health Research Authority, Skipton House, 80 London Road, London SE1 6LH, UK (REC Reference 15/LO/0218). The second patient cohort was obtained from Discovery Life Sciences (DLS), California, USA. The patient samples are de-identified and publicly available and are thus exempt from the requirement of the Institutional Review Board Ethics Committee (IRB/EC) approval (Exempt Category 4, IRB/EC). All DLS biospecimens are collected under IRB/EC-approved protocols. The samples are procured pursuant to the informed consent provided by the individual, following the general guidelines for informed consent found in the Code of Federal Regulations 45 CFR 46.116. The patients/participants provided their written informed consent to participate in this study.

AUTHOR CONTRIBUTIONS

The authors confirm contribution to the paper as follows: study conception and design: CM, MJK, JL, TM, PF, DM, and MR; data collection: CM, JW, HP, DM, and MR; analysis and interpretation of results: CM, JW, MJK, JL, PF, HP, DM, and MR; and draft manuscript preparation: CM, JW, MJK, TM, HP, DM, and MR. All authors contributed to the article and approved the submitted version.

SUPPLEMENTARY MATERIAL

The Supplementary Material for this article can be found online at: https://www.frontiersin.org/articles/10.3389/fonc.2022.837127/full#supplementary-material

REFERENCES

1. Cancer Research UK. *Prostate Cancer Statistics* . Available at: https://www.cancerresearchuk.org/health-professional/cancer-statistics/statistics-by-cancer-type/prostate-cancer.
2. Cancer.Net. *Prostate Cancer: Statistics* (2019). Available at: https://www.cancer.net/cancer-types/prostate-cancer/statistics.
3. Popiolek M, Rider JR, Andrén O, Andersson SO, Holmberg L, Adami HO, et al. Natural History of Early, Localized Prostate Cancer: A Final Report From Three Decades of Follow-Up. *Eur Urol* (2013) 63(3):428–35. doi: 10.1016/j.eururo.2012.10.002
4. Montironi R, Santoni M, Mazzucchelli R, Burattini L, Berardi R, Galosi AB, et al. Prostate Cancer: From Gleason Scoring to Prognostic Grade Grouping. *Expert Rev Anticancer Ther* (2016) 16(4):433–40. doi: 10.1586/14737140.2016.1160780
5. *Prostate Cancer - Symptoms and Causes - Mayo Clinic* . Available at: https://www.mayoclinic.org/diseases-conditions/prostate-cancer/symptoms-causes/syc-20353087 (Accessed June 10, 2021).
6. Hamilton W, Sharp DJ, Peters TJ, Round AP. Clinical Features of Prostate Cancer Before Diagnosis: A Population-Based, Case-Control Study. *Br J Gen Pract* (2006) 56(531):756–62.
7. Simoneau AR. Treatment- and Disease-Related Complications of Prostate Cancer. *Rev Urol* (2006) 8 Suppl 2(Suppl 2):S56–67.
8. Rubin MA, Dunn R, Kambham N, Misick CP, O'Toole KM. Should a Gleason Score be Assigned to a Minute Focus of Carcinoma on Prostate Biopsy? *Am J Surg Pathol* (2000) 24(12):1634–40. doi: 10.1097/00000478-200012000-00007
9. Epstein JI. Prostate Cancer Grading: A Decade After the 2005 Modified System. *Mod Pathol* (2018) 31(S1):47–63. doi: 10.1038/modpathol.2017.133
10. Stark JR, Mucci L, Rothman KJ, Adami HO. Screening for Prostate Cancer Remains Controversial. *BMJ* (2009) b3601: 339. doi: 10.1136/bmj.b3601
11. Etzioni R, Gulati R, Cooperberg M, Penson D, Weiss N, Thompson I. Limitations of Basing Screening Policies on Screening Trials: The US Preventive Services Task Force and Prostate Cancer Screening. *Med Care* (2013) 51(4):295–300. doi: 10.1097/MLR.0b013e31827da979
12. Alberts AR, Schoots IG, Roobol MJ. Prostate-Specific Antigen-Based Prostate Cancer Screening: Past and Future. *Int J Urol* (2015) 22(6):524–32. doi: 10.1111/iju.12750
13. Palmerola R, Smith P, Elliot V, Reese CT, Mahon FB, Harpster LE, et al. The Digital Rectal Examination (DRE) Remains Important-Outcomes From a Contemporary Cohort of Men Undergoing an Initial 12-18 Core Prostate Needle Biopsy. *Can J Urol* (2012) 19(6):6542–7.
14. Izawa JI, Babaian RJ. Prostate Cancer: Detection and Biopsy Strategies. *Prostate Cancer Sci Clin Pract* (2003) 2003:129–36. doi: 10.1016/B978-012286981-5/50016-1
15. Galosi AB, Palagonia E, Scarcella S, Cimadamore A, Lacetera V, Delle Fave RF, et al. Detection Limits of Significant Prostate Cancer Using Multiparametric MR

and Digital Rectal Examination in Men With Low Serum PSA: Up-Date of the Italian Society of Integrated Diagnostic in Urology. *Arch Ital Di Urol E Androl* (2021) 93(1):92–100. doi: 10.4081/aiua.2021.1.92
16. Fandella A, Scattoni V, Galosi A, Pepe P, Fiorentino M, Gaudiano C, et al. Italian Prostate Biopsies Group: 2016 Updated Guidelines Insights. *Anticancer Res* (2017) 37(2):413–24. doi: 10.21873/ANTICANRES.11333
17. Young SM, Bansal P, Vella ET, Finelli A, Levitt C, Loblaw A. Guideline for Referral of Patients With Suspected Prostate Cancer by Family Physicians and Other Primary Care Providers. *Can Fam Physician* (2015) 61(1):33–9.
18. *Prostate Cancer Diagnosis and Management Guidance NICE* . Available at: https://www.nice.org.uk/guidance/ng131/chapter/Recommendations#assessment-and-diagnosis.
19. Mcnally CJ, Ruddock MW, Moore T, Mckenna DJ. Biomarkers That Differentiate Benign Prostatic Hyperplasia From Prostate Cancer: A Literature Review. *Cancer Manag Res* (2020) 12:5225–41. doi: 10.2147/CMAR.S250829
20. Duffy MJ. Biomarkers for Prostate Cancer: Prostate-Specific Antigen and Beyond. *Clin Chem Lab Med* (2020) 58(3):326–39. doi: 10.1515/cclm-2019-0693
21. FitzGerald SP, Lamont JV, McConnell RI, Benchikh EO. Development of a High-Throughput Automated Analyzer Using Biochip Array Technology. *Clin Chem* (2005) 51(7):1165–76. doi: 10.1373/clinchem.2005.049429
22. Kurth MJ, McBride WT, McLean G, Watt MJ, Domanska A, Lamont JV, et al. Acute Kidney Injury Risk in Orthopaedic Trauma Patients Pre and Post Surgery Using a Biomarker Algorithm and Clinical Risk Score. *Sci Rep* (2020) 10(1):20005–5. doi: 10.1038/s41598-020-76929-y
23. R Core Team. (2018).
24. Lu Y, Cai Z, Galson DL, Xiao G, Liu Y, George DE, et al. Monocyte Chemotactic Protein-1 (MCP-1) Acts as a Paracrine and Autocrine Factor for Prostate Cancer Growth and Invasion. *Prostate* (2006) 66(12):1311–8. doi: 10.1002/pros.20464
25. Loberg RD, Day LL. Lauren N St. MCP-1 is a Potent Regulator of Prostate Cancer Cell Chemoaxataxis and Growth. *Via Stimulation CCR2 CCRL1 Cancer Res* (2006) 66(8 Supplement):578–86. doi: 10.1593/neo.06280
26. Pan L, Baek S, Edmonds PR, Roach M, Wolkov H, Shah S, et al. Vascular Endothelial Growth Factor (VEGF) Expression in Locally Advanced Prostate Cancer: Secondary Analysis of Radiation Therapy Oncology Group (RTOG) 8610. *Radiat Oncol* (2013) 8(1):1–11. doi: 10.1186/1748-717X-8-100
27. Festuccia C, Angelucci A, Gravina GL, Biordi L, Millimaggi D, Muzi P, et al. Epidermal Growth Factor Modulates Prostate Cancer Cell Invasiveness Regulating Urokinase-Type Plasminogen Activator Activity. *EGF-receptor Inhibition May Prevent Tumor Cell Dissemination Thromb Haemost* (2005) 93 (5):964–75. doi: 10.1160/TH04-09-0637
28. Sigismund S, Avanzato D, Lanzetti L. Emerging Functions of the EGFR in Cancer. *Mol Oncol* (2018) 12(1):3–20. doi: 10.1002/1878-0261.12155
29. Santotoribio JD, Jimenez-Romero ME. Serum Biomarkers of Inflammation for Diagnosis of Prostate Cancer in Patients With Nonspecific Elevations of Serum Prostate Specific Antigen Levels. *Transl Cancer Res* (2019) 8(1):273–8. doi: 10.21037/tcr.2019.01.31
30. Shao N, Xu B, Mi YY, Hua LX. IL-10 Polymorphisms and Prostate Cancer Risk: A Meta-Analysis. *Prostate Cancer Prostatic Dis* (2011) 14(2):129–35. doi: 10.1038/pcan.2011.6
31. Çalışkan S, Sungur M. Fibrinogen and D-Dimer Levels in Prostate Cancer: Preliminary Results. *Prostate Int* (2017) 5(3):110–2. doi: 10.1016/j.prnil.2017.05.001
32. Ay C, Dunkler D, Pirker R, Thaler J, Quehenberger P, Wagner O, et al. High D-Dimer Levels are Associated With Poor Prognosis in Cancer Patients. *Haematologica* (2012) 97(8):1158–64. doi: 10.3324/haematol.2011.054718
33. Chadha K, Miller A, Nair B, Schwartz S, Trump D, Underwood W. New Serum Biomarkers for Prostate Cancer Diagnosis. *Clin Cancer Investig J* (2014) 4(1):72. doi: 10.4103/2278-0513.125802
34. Roumeguère T, Legrand F, El RE, Kaitouni MI, Albisinni S, Rousseau A, et al. A Prospective Clinical Study of the Implications of IL-8 in the Diagnosis, Aggressiveness and Prognosis of Prostate Cancer. *Futur Sci OA* (2018) 4 (2):266. doi: 10.4155/fsoa-2017-0084
35. Nadler RB, Koch AE, Calhoun EA, Campbell PL, Pruden DL, Bennett CL, et al. IL-1β and TNF-α in Prostatic Secretions Are Indicators in the Evaluation of Men With Chronic Prostatitis. *J Urol* (2000) 164(1):214–8. doi: 10.1016/S0022-5347(05)67497-6
36. Ashok A, Keener R, Rubenstein M, Stookey S, Bajpai S, Hicks J, et al. Consequences of Interleukin 1β-Triggered Chronic Inflammation in the Mouse Prostate Gland: Altered Architecture Associated With Prolonged CD4+ Infiltration Mimics Human Proliferative Inflammatory Atrophy. *Prostate* (2019) 79(7):732–45. doi: 10.1002/pros.23784
37. Urios A, Ordoño F, García-García R, Mangas-Losada A, Leone P, José Gallego J, et al. Tadalafil Treatment Improves Inflammation, Cognitive Function, And Mismatch Negativity Of Patients With Low Urinary Tract Symptoms And Erectile Dysfunction. *Sci Rep* (2019) 9(1):1–9. doi: 10.1038/s41598-019-53136-y
38. Kamiya N, Akakura K, Suzuki H, Isshiki S, Komiya A, Ueda T, et al. Pretreatment Serum Level of Neuron Specific Enolase (NSE) as a Prognostic Factor in Metastatic Prostate Cancer Patients Treated With Endocrine Therapy. *Eur Urol* (2003) 44 (3):309–14. doi: 10.1016/S0302-2838(03)00303-8
39. Muoio B, Pascale M, Roggero E. The Role of Serum Neuron-Specific Enolase in Patients With Prostate Cancer: A Systematic Review of the Recent Literature. *Int J Biol Markers* (2018) 33(1):10–21. doi: 10.5301/ijbm.5000286
40. Jalali A, Kitching M, Martin K, Richardson C, Murphy TB, FitzGerald SP, et al. Integrating Inflammatory Serum Biomarkers Into a Risk Calculator for Prostate Cancer Detection. *Sci Rep* (2021) 11(1):2525. doi: 10.1038/S41598-021-81965-3
41. Watson J, Salisbury C, Banks J, Whiting P, Hamilton W. Predictive Value of Inflammatory Markers for Cancer Diagnosis in Primary Care: A Prospective Cohort Study Using Electronic Health Records. *Br J Cancer* (2019) 120 (11):1045–51. doi: 10.1038/S41416-019-0458-X
42. Eklund M, Nordström T, Aly M, Adolfsson J, Wiklund P, Brandberg Y, et al. The Stockholm-3 (STHLM3) Model can Improve Prostate Cancer Diagnostics in Men Aged 50-69 Yr Compared With Current Prostate Cancer Testing. *Eur Urol Focus* (2018) 4(5):707–10. doi: 10.1016/J.EUF.2016.10.009
43. Punnen S, Pavan N, Parekh DJ. Finding the Wolf in Sheep's Clothing: The 4kscore Is a Novel Blood Test That Can Accurately Identify the Risk of Aggressive Prostate Cancer. *Rev Urol* (2015) 17(1):3.
44. Schröder FH, Hugosson J, Roobol MJ, Tammela TLJ, Ciatto S, Nelen V, et al. Screening and Prostate-Cancer Mortality in a Randomized European Study. *N Engl J Med* (2009) 18:1320–8. doi: 10.1056/NEJMoa0810084
45. Thompson IM, Ankerst DP, Chi C, Goodman PJ, Tangen CM, Lucia MS, et al. Assessing Prostate Cancer Risk: Results From the Prostate Cancer Prevention Trial. *JNCI J Natl Cancer Inst* (2006) 98(8):529–34. doi: 10.1093/JNCI/DJJ131
46. Jalali A, Foley RW, Maweni RM, Murphy K, Lundon DJ, Lynch T, et al. A Risk Calculator to Inform the Need for a Prostate Biopsy: A Rapid Access Clinic Cohort. *BMC Med Inf Decis Mak* (2020) 20(1):1–11. doi: 10.1186/S12911-020-01174-2

Conflict of Interest: The authors declare that this study received funding from Randox Laboratories Ltd as part of the Randox Laboratories Ltd – Ulster University PhD Academy Studentship. Randox had the following involvement in the study: analysis of patient samples, statistical analysis, supervision of the project, preparation of the manuscript, and the decision to publish.

JW, MJK, JL, and MR are employees of Randox Laboratories Ltd. but hold no shares in the company. PF is the managing director and owner of Randox Laboratories Ltd. A patent has been filed to protect the biomarker combination disclosed in the manuscript.

The remaining authors declare that the research was conducted in the absence of any commercial or financial relationships that could be construed as a potential conflict of interest.

Publisher's Note: All claims expressed in this article are solely those of the authors and do not necessarily represent those of their affiliated organizations, or those of the publisher, the editors and the reviewers. Any product that may be evaluated in this article, or claim that may be made by its manufacturer, is not guaranteed or endorsed by the publisher.

Copyright © 2022 McNally, Watt, Kurth, Lamont, Moore, Fitzgerald, Pandha, McKenna and Ruddock. This is an open-access article distributed under the terms of the Creative Commons Attribution License (CC BY). The use, distribution or reproduction in other forums is permitted, provided the original author(s) and the copyright owner(s) are credited and that the original publication in this journal is cited, in accordance with accepted academic practice. No use, distribution or reproduction is permitted which does not comply with these terms.

Advantages of publishing in Frontiers

OPEN ACCESS
Articles are free to read for greatest visibility and readership

FAST PUBLICATION
Around 90 days from submission to decision

HIGH QUALITY PEER-REVIEW
Rigorous, collaborative, and constructive peer-review

TRANSPARENT PEER-REVIEW
Editors and reviewers acknowledged by name on published articles

Frontiers
Avenue du Tribunal-Fédéral 34
1005 Lausanne | Switzerland

Visit us: www.frontiersin.org
Contact us: frontiersin.org/about/contact

REPRODUCIBILITY OF RESEARCH
Support open data and methods to enhance research reproducibility

DIGITAL PUBLISHING
Articles designed for optimal readership across devices

FOLLOW US
@frontiersin

IMPACT METRICS
Advanced article metrics track visibility across digital media

EXTENSIVE PROMOTION
Marketing and promotion of impactful research

LOOP RESEARCH NETWORK
Our network increases your article's readership